PHYSI
VOLUME 85

Published by the American
for the

AMERICAN PHYSI

Officers

President

J. H. Van Vleck
Harvard University
Cambridge, Mass.

Vice-President

Enrico Fermi
University of Ch
Chicago, Illinois

Secretary

K. K. Darrow
Bell Telephone
Office:
Columbia Univ
New York 27, N

Treasurer

G. B. Pegram
Columbia Univ
New York 27, N

Local Secretaries for the Pacific

J. Kaplan
University of
Angeles
Los Angeles, Ca

Managing Editor

S. A. Goudsmit
Brookhaven Nati
Upton, Long Isl
New York

The

Entered as

Acceptance for mailing at

VIEW

ed by S. L. Hoisington

OF REVIEWS

Associate Editors

L. Goldhaber
Hofstadter
W. Lawson
Pais
Serber
C. H. Townes

should be submitted to
Laboratory, Upton, Long Island,
to pay a publication
them as 100 free reprints.

controversial papers in the
Publication Manager, Am
York 27, New York.

Subscription Rates

and Canada

Back Numbers

volume while complete sets are available:

$20.00
$22.00

prior to July, 1929:
July, 1929–December, 1941:
January, 1942–December, 1946:
January, 1947–December, 1948:
hereafter.
$2.00.

numbers for back numbers should be
, 57 East 55 Street, New York

of members of the American
; in the case of other

Business Manager, Ogden, Minnesota.

Lancaster, Pennsylvania, under the Act of
of 1948, as

THE
PHYSICAL REVIEW

A journal of experimental and theoretical physics established by E. L. Nichols in 1893

SECOND SERIES, VOL. 85, NO. 4 FEBRUARY 15, 1952

Mesonic Proper-Field*

HIROOMI UMEZAWA, YASUSHI TAKAHASHI, AND SUSUMU KAMEFUCHI
Institute of Theoretical Physics, Nagoya University, Nagoya, Japan
(Received May 21, 1951)

A method is presented of treating the meson cloud around the nucleon. The meson cloud is described in terms of the free field operators which coincide, on the world point on the space-like surface, with the usual field operators in the Heisenberg representation. In the second and the third sections, the relation between the field and its source on an arbitrary space-like surface is studied. The fourth and fifth sections are concerned with the method of the phenomenological investigation of the meson cloud in our formalism and with the treatment of the problem of the multiple production of mesons and the magnetic moment of the nucleon-meson system. This treatment of the multiple production of mesons is shown to be the covariant generalization of Bloch-Nordsiecks' method for the multiple production of low energy photons.

1. INTRODUCTION

IT is well known that the meson theory, based on the quantum field theory, has been a foundation for the study of models of elementary particles, namely the kinds of actual particles and their mutual interactions. The experimental evidence of the creation of π-mesons by nucleon-nucleon or γ-nucleon collisions seems to afford testimony of the existence of the meson field interacting with the nucleon. This meson field gives the effect of the field reaction on the nucleon. Some of the difficulties in meson theory have been resolved by modifying the model into a two-meson theory, but the problem of the field reaction still remains an important problem to be investigated.

In quantum electrodynamics the problem of the field reaction has been studied in detail in Tomonaga-Schwinger's covariant formalism, and it has become clear that the effect of the field reaction plays an indispensable role in the explanation of experimental results (Lamb-Retherford-shift, etc.).

In the field of the meson theory not only are there many problems which cannot be solved by renormalization, but also various results depend on the method of treating divergences.[1] This is probably due to the meson having a heavier mass than the electron, the coupling between nucleon and meson not being invariably weak, the meson cloud having a greater singularity in the vicinity of a nucleon, and so on. Therefore, in the meson theory, it is probable that the "structure" of the elementary particle will present a problem in the investigation of its model, and that one of the most important problems in the theory of the "structure" of elementary particles may consist in the clarification of the relation between the nucleon and the meson field (meson cloud) attached to it.

In this respect, Heisenberg[2] has attempted, using the results of Bloch and Nordsieck,[3] to consider the spectrum of multiple production of mesons as the difference between the proper fields of the nucleon as it is and as it should be after the scattering process; and further he has assumed that:

(I) the "spectrum" of meson cloud can be obtained on the classical basis, and

(II) the probability of the emission of mesons is subject to the Poisson distribution.

In this paper we shall attempt a general formulation of the quantum theoretical treatment of the meson cloud. To this end we introduce an operator which denotes the "spectrum" of the meson field around a nucleon, i.e., the meson cloud. Without making any restrictions on the magnitude of the coupling strength,

* The contents of this paper were briefly reported in Prog. Theoret. Phys. 6, 426, 628 (1951), but the publication of the paper has been delayed.

[1] For example, the C-meson introduced by Sakata in order to construct a stable electron model does not show any observable effects in the region of quantum electrodynamics, but it does have an observable effect in the case of heavy particles. S. Sakata and H. Umezawa, Prog. Theoret. Phys. 5, 682 (1950).

[2] W. Heisenberg, Z. Physik 101, 533 (1936); 113, 61 (1939).

[3] F. Bloch and A. Nordsieck, Phys. Rev. 52, 54 (1937).

the discussions are developed exactly by a method based on the quantum theory.

To express this meson spectrum in terms of time-dependent operators of the meson field, we shall use the Heisenberg representation. The various characteristics of the meson cloud will be discussed in Secs. 2, 3, and 4. The discussion of the relation between the meson cloud and certain phenomena (the multiple production of mesons and the magnetic moment of nucleons) is given in Sec. 5.

This treatment of the multiple production of mesons is the covariant generalization of Bloch-Nordsiecks' method for the multiple production of low energy photons (and so of Heisenberg's semiclassical method).

A detailed consideration of the spectrum, i.e., comparing the various theoretical spectra with experimental results and looking for their actual forms suitable to the explanation of the latter, etc., are problems for further investigation.

2. SPECTRUM OF THE MESON FIELD[4]

In this paper we shall discuss, for simplicity, a zero-spin meson field, i.e., a scalar or pseudoscalar field.

The Lagrange function (in Heisenberg representation) is given by

$$L=\int\{L^m+L^n+L^{mn}-\bar{\psi}V\psi\}dv, \tag{2.1}$$

where L^m, L^n are the free parts of the Lagrange densities of the meson and the nucleon fields, respectively, and L^{mn} is the interaction part between them, which takes the following forms:

$$L^{mn}=\begin{cases}-g^\nu\bar{\psi}O^\nu\psi U^\nu & \text{(scalar type)}, \quad (2.2)\\ -g^\nu\bar{\psi}O_\mu{}^\nu\psi\partial U^\nu/\partial x_\mu & \text{(vector type)}. \quad (2.2')\end{cases}$$

V is an external potential and ψ, U^ν are field operators of the nucleon and the meson, respectively.

From (2.1) we get the following equations of motion:

$$\left.\begin{aligned}(\Box-\kappa^2)U^\nu&=g^\nu\bar{\psi}O^\nu\psi\equiv g^\nu O^\nu(x),\\ (\gamma_\mu\partial/\partial x_\mu+\mu)\psi&=-(g^\nu O^\nu U^\nu+V)\psi.\end{aligned}\right\} \tag{2.3}$$

Firstly we shall consider, for brevity, the case of scalar coupling. If there is no interaction in the remote past, the solutions of (2.3) will be as follows:

$$U^\nu(x)=U_{\text{in}}{}^\nu(x)+g^\nu\int\Delta_{\text{ret}}(x-x')O^\nu(x')d^4x', \tag{2.4}$$

$$\psi(x)=\psi_{\text{in}}(x)-\int S_{\text{ret}}(x-x')\{g^\nu O^\nu U^\nu(x')+V(x')\}\psi(x')d^4x', \tag{2.5}$$

where $U_{\text{in}}{}^\nu(x)$ and $\psi_{\text{in}}(x)$ are incoming fields which coincide in the infinite past with $U^\nu(x)$ and $\psi(x)$, respectively, and satisfy respective homogeneous free field equations. Therefore, they satisfy the following commutation relations:

$$\left.\begin{aligned}[\psi_{\text{in}}{}^\alpha(x),\bar{\psi}_{\text{in}}{}^\beta(x')]_+&=-iS_{\alpha\beta}(x-x'),\\ [U_{\text{in}}{}^\nu(x),U_{\text{in}}{}^\mu(x')]&=i\delta_{\mu\nu}\Delta(x-x').\end{aligned}\right\} \tag{2.6}$$

Furthermore:

$$\left.\begin{aligned}\Delta_{\text{ret}}(x-x')&=\tfrac{1}{2}\{1+\epsilon(x,x')\}\Delta(x-x'),\\ S_{\text{ret}}(x-x')&=\tfrac{1}{2}\{1+\epsilon(x,x')\}S(x-x'),\\ \epsilon(x,x')&=\begin{cases}+1 & \text{for}\quad \sigma(x)>\sigma'(x'),\\ -1 & \text{for}\quad \sigma(x)<\sigma'(x').\end{cases}\end{aligned}\right\} \tag{2.7}$$

A given free meson field $U_f(x)$ can be decomposed into the positive frequency part ${}^+U_f(x)$ and the negative frequency part ${}^-U_f(x)$ in the same way as in Schwinger's paper.[5] The Fourier components of $U_f(x)$, are introduced in

$$U_f(x)=\int U_f(k)\delta(k^2+\kappa^2)e^{ik_\mu x_\mu}d^4k, \tag{2.8}$$

and $U(k)(-k_\mu\epsilon_\mu>0)$ and $U(k)(k_\mu\epsilon_\mu>0)$ are written with ${}^+U(k)$ and ${}^-U(k)$, respectively, where ϵ is a unit time-like vector. As the magnitude of the vector ${}^+U_f(k)$, i.e., ${}^+U_f{}^*(k){}^+U_f(k)$, represents the number of mesons with momentum k_μ, it is convenient to use the positive frequency parts of the free meson fields $U^\nu(x,\sigma)$, which coincide with $U^\nu(x)$ of (2.4) on a space-like surface σ, in order to express the number of mesons on the surface σ. From (2.4), we obtain such free meson fields $U^\nu(x,\sigma)$ as follows:

$$U^\nu(x,\sigma)=U_{\text{in}}{}^\nu(x)+g^\nu\int_{-\infty}^{\sigma}\Delta(x-x')O^\nu(x')d^4x'. \tag{2.9}$$

$U^\nu(x,\sigma)$ satisfies the homogeneous free equation for fixed σ and

$$\left.\begin{aligned}[\psi^\alpha(x,\sigma),\bar{\psi}^\beta(x',\sigma)]_+&=-iS_{\alpha\beta}(x-x'),\\ [U^\nu(x,\sigma),U^\mu(x',\sigma)]&=i\delta_{\mu\nu}\Delta(x-x').\end{aligned}\right\} \tag{2.10}$$

$$U^\nu(x/\sigma)\equiv[U^\nu(x,\sigma)]_{x\text{ on }\sigma}=U^\nu(x), \tag{2.11}$$

using the notation x/σ for x on σ. Yang and Feldman[6] have shown that $U^\nu(x,\sigma)$ can be obtained by the unitary transformation S from $U^\nu(x,\sigma')$:

$$U^\nu(x,\sigma)=S^{-1}(\sigma,\sigma')U^\nu(x,\sigma')S(\sigma,\sigma'). \tag{2.12}$$

It follows from (2.12) that

$$U^\nu(x/\sigma)=[S^{-1}(\sigma)U_{\text{in}}{}^\nu(x)S(\sigma)]_{x/\sigma}, \tag{2.13}$$

[4] Throughout this paper natural units are used, i.e., $\hbar=C=1$. and κ and μ represent the rest mass of the meson and the nucleon, respectively. A^* is the hermite conjugate operator of A. A_μ is A_1, A_2, A_3 and $A_4=iA_0$. In particular we may write $x_0=t$. The formulation in this section is closely related to Heisenberg's theory appearing in Ann. Physik **5**, 339 (1931).

[5] J. Schwinger, Phys. Rev. **75**, 651 (1949).

[6] C. N. Yang and D. Feldman, Phys. Rev. **79**, 972 (1950).

with

$$S(\sigma)=S(\sigma,-\infty). \tag{2.14}$$

Furthermore, they have shown that

$$i\delta S(\sigma)/\delta\sigma(x)=H^{i}(x)S(\sigma) \tag{2.15}$$

and that, for various types of meson fields, $H^{i}(x)$ coincides with the interaction Hamiltonian in the interaction representation in which $U^{r}(x)$ and $\psi(x)$ are replaced by $U_{\text{in}}{}^{r}(x)$ and $\psi_{\text{in}}(x)$, respectively.[6]

Since $U^{r}(x,\sigma)$ satisfies the homogeneous free field equation, we can split it into two parts, and from (2.12), for the positive frequency part, we get

$${}^{+}U^{r}(x,\sigma)=S^{-1}(\sigma){}^{+}U_{\text{in}}{}^{r}(x)S(\sigma), \tag{2.16}$$

which can be written, by (2.9), as follows:

$${}^{+}U^{r}(x,\sigma)={}^{+}U_{\text{in}}{}^{r}(x)+g^{r}\int_{-\infty}^{\sigma}{}^{+}\Delta(x-x')O^{r}(x')d^{4}x' \quad \text{(scalar type)}, \tag{2.17}$$

$$O^{r}(x')=[S^{-1}(\sigma)\bar{\psi}_{\text{in}}(x')O^{r}\psi_{\text{in}}(x')S(\sigma)]_{x'/\sigma}, \tag{2.17'}$$

where ${}^{+}\Delta(x)$ is the positive frequency part of $\Delta(x)$. We call this ${}^{+}U(x,\sigma)$ "the cloud spectrum in the Heisenberg representation" (c-spectrum), by which one can express the number of mesons at x/σ.[7]

As is evident from the definition, $O(x)$ denotes the change of the nucleon spin density due to the interaction H^{i} between meson and nucleon. This will be called, in the following pages, the "effective spin" (e-spin) of a nucleon in the meson cloud. It describes the nucleon states in the meson cloud and, therefore, plays an important role in the treatment of the meson cloud. Now, we introduce ${}^{+}u$ as follows:

$${}^{+}U^{r}(x,\sigma)\equiv{}^{+}U_{\text{in}}{}^{r}(x)+(-i)\int_{-\infty}^{\infty}{}^{+}u^{r}(x,\sigma;x')d^{4}x'. \tag{2.18}$$

Here ${}^{+}u$ is an operator in the Heisenberg representation and is called the "spectrum density" (d-spectrum) with respect to x' contributing to the meson field at σ.

Equation (2.18) means that the c-spectrum at x/σ is the sum of the contributions of the d-spectrum at all the points denoted by x' and ${}^{+}U_{\text{in}}$.

In the absence of an external potential we shall denote $S(\sigma)$, the e-spin and the spectra by $S_{0}(\sigma)$, $\bar{O}(x)$, and $({}^{+}U_{0},{}^{+}u_{0})$, respectively. These spectra are related to the mesonic proper-field.

$({}^{+}U_{0},{}^{+}u_{0})$ are obtained by replacing $S(\sigma)$ by $S_{0}(\sigma)$ respectively in (2.16) and (2.17). When we restrict ourselves to the case in which one nucleon and no mesons exist in the remote past, the c-spectrum at a definite time is called the "c-spectrum of the single nucleon." In this case, there is the following relation:

$${}^{+}U_{\text{in}}{}^{r}(x)\rangle_{\sigma=0}=0$$

and so from (2.18) we have:

$${}^{+}U_{0}{}^{r}(x,\sigma)\rangle_{\sigma=0}=(-i)\int_{-\infty}^{\infty}{}^{+}u_{0}{}^{r}(x,\sigma;x')\rangle_{\sigma=0}d^{4}x'. \tag{2.19}$$

Operators ${}^{+}U^{r}$ and ${}^{+}u^{r}$ have forms of nonlinear interactions containing many operators $\bar{\psi}_{\text{in}}$, ψ_{in}, and $U_{\text{in}}{}^{r}$. From (2.18) and (2.17) we obtain

$${}^{+}u^{r}(x,\sigma;x')=ig^{r}\left(\frac{1+\epsilon(\sigma,x')}{2}\right){}^{+}\Delta(x-x')O^{r}(x'). \tag{2.20}$$

Similarly, in the case of the vector coupling (2.2′), we can obtain the corresponding d-spectrum:

$${}^{+}u^{r}(x,\sigma;x')=ig^{r}\left(\frac{1+\epsilon(\sigma,x')}{2}\right)\frac{\partial^{+}\Delta(x-x')}{\partial x_{\mu}}O_{\mu}{}^{r}(x') \tag{2.20'}$$

with

$$O_{\mu}{}^{r}(x)\equiv[S^{-1}(\sigma)\bar{\psi}_{\text{in}}(x)O_{\mu}{}^{r}\psi_{\text{in}}(x)S(\sigma)]_{x/\sigma}. \tag{2.20''}$$

$\bar{O}(x)$ is uniquely determined from ${}^{+}U_{0}(x,\sigma)$ as will be pointed out in Sec. 4.

Now, we shall proceed to define the "e-spin with the forced vibration $\bar{O}(x)F[\sigma(x)]$" of the nucleon, the oscillation of which is forced by the effect of its past processes that is described by $F[\sigma(x)]$. Such a forced vibration of the nucleon may be possible when the external disturbance is present. (See Sec. 5.) We shall define "the c-spectrum of a nucleon with the forced vibration" as follows:

$$[{}^{+}U_{0}{}^{r}F\}(x_{0},\sigma)\equiv\begin{cases}{}^{+}U_{\text{in}}{}^{r}(x_{0})+g^{r}\int^{\sigma}{}^{+}\Delta(x_{0}-x)\bar{O}^{r}(x)F[\sigma(x)]d^{4}x & \text{(scalar coupling)}, \quad (2.21)\\ {}^{+}U_{\text{in}}{}^{r}(x_{0})+g^{r}\int^{\sigma}\frac{\partial^{+}\Delta(x_{0}-x)}{\partial x_{\mu}}\bar{O}_{\mu}{}^{r}(x)F[\sigma(x)]d^{4}x & \text{(vector coupling)}. \quad (2.21')\end{cases}$$

(2.21), (2.21′) also satisfy the homogeneous free equation of the meson field. From (2.19), we obtain

$$[{}^{+}U_{0}F\}(x_{0},\sigma)\rangle_{\sigma=0}=(-i)\int_{-\infty}^{\infty}{}^{+}u_{0}{}^{r}(x_{0},\sigma;x)F[\sigma(x)]d^{4}x\rangle_{\sigma=0}. \tag{2.22}$$

More generally we use the notation $[AF\}$ for the operator in which the e-spin $\bar{O}(x)$ of the nucleon with the meson cloud contained in the operator A is replaced by $\bar{O}(x)F[\sigma(x)]$. Making the surface σ flat, and using

[7] We can expect that when the interaction between the meson and the nucleon is switched off on a surface σ, mesons are emitted according to the spectrum amplitude ${}^{+}U(x/\sigma)$. This was pointed out by Professor Tomonaga.

the relations

$$\left.\begin{aligned}\bar{O}^r(x)&\equiv\int\bar{O}^r(k)e^{ikx}d^4k,\\ F[\sigma(x)]&=\int F(b)e^{ibt}db,\\ K&\equiv(\mathbf{k}^2+\kappa^2)^{\frac{1}{2}},\\ k_\mu&\equiv(k_1,k_2,k_3,k_4=ik_0),\\ K_\mu&\equiv(k_1,k_2,k_3,iK),\end{aligned}\right\}\tag{2.23}$$

we find after some calculations the following relations:

$$[{}^+U_0{}^rF](x_0,\sigma)={}^+U_{\text{in}}{}^r(x_0)+\frac{g}{2}\int\frac{\bar{O}^r(k)F(b)}{K[b(k)+b]}$$
$$\times e^{iKx_0}e^{i[b(k)+b]t}d^4kdb\quad\text{(scalar coupling)},\tag{2.24}$$

$$[{}^+U_0{}^rF](x_0,\sigma)={}^+U_{\text{in}}{}^r(x_0)+\frac{g}{2}\int\frac{(iK_\mu)\bar{O}_\mu{}^r(k)F(b)}{K[b(k)+b]}$$
$$\times e^{iKx_0}e^{i[b(k)+b]t}d^4kdb\quad\text{(vector coupling)},\tag{2.24'}$$

where t is the time of the flat surface σ and

$$b(k)\equiv k_0-K.\tag{2.25}$$

As seen in (2.24) and (2.24'), k_0 is the energy transfer on σ of the nucleon with the meson cloud, and so $\bar{O}(\mathbf{k},k_0)$ and $b(k)$ depend on the state of the nucleon on the surface σ through the variable k_0. Now, ${}^+U_0{}^r(x_0,\sigma)$ can be obtained as the particular case of (2.24), (2.24') in which $F(x)=1$ and so $F(b)=\delta(b)$. It will then be

$${}^+U_0{}^r(x_0,\sigma)={}^+U_{\text{in}}{}^r(x_0)-\frac{g}{2}\int\frac{\bar{O}^r(k)}{K(K-k_0)}$$
$$\times e^{iKx_0}e^{-i(K-k_0)t}d^4k\quad\text{(scalar coupling)},\tag{2.26}$$

or

$${}^+U_0{}^r(x_0,\sigma)={}^+U_{\text{in}}{}^r(x_0)-\frac{g}{2}\int\frac{iK_\mu\bar{O}_\mu{}^r(k)}{K(K-k_0)}$$
$$\times e^{iKx_0}e^{-i(K-k_0)t}d^4k\quad\text{(vector coupling)}.\tag{2.26'}$$

Here, let us introduce the number operator of mesons. Since $U(x_0,\sigma)$ satisfies the homogeneous free field equation, the "number operator" $N(\sigma)$ of this meson field on the surface σ is defined as follows:

$$N^r(\sigma)\equiv\frac{2}{i}\left[\int_\sigma({}^+U(x,\sigma))^*\frac{\partial{}^+U^r(x,\sigma)}{\partial x_\mu}d\sigma_\mu\right]_{x/\sigma}$$
$$\equiv\int N_\sigma{}^r(k)d^4k.\tag{2.27}$$

Using (2.26) and (2.26'), the expectation value of (2.27) for the state of a nucleon can be written in the following forms (making the surface σ flat):

$$\langle N(\sigma)\rangle_{\substack{n=1\\m=0}}=\frac{g^2}{2}\int\frac{\langle O^r(k)^*O^r(k)\rangle_{\substack{n=1\\m=0}}}{K(K-k_0)^2}d^4k$$
$$\text{(scalar coupling)},\tag{2.28}$$

$$\langle N(\sigma)\rangle_{\substack{n=1\\m=0}}=\frac{g^2}{2}\int\frac{K_\mu K_\rho}{K(K-k_0)^2}\langle O_\mu{}^r(k)^*O_\rho{}^r(k)\rangle_{\substack{n=1\\m=0}}d^4k$$
$$\text{(vector coupling)},\tag{2.28'}$$

which implicitly depend on σ through the variable k_0.

Finally we will examine the relation between $S(\sigma)$ and $S_0(\sigma)$, when an external field $\bar{\psi}V\psi$ is present. When we denote $S(\sigma)$ as follows as the power series of $V(x)$:

$$S(\sigma)=S_0(\sigma)+S_1(\sigma)+\cdots\tag{2.29}$$

then it is easily seen that

$$S_m(\sigma)=S_0(\sigma)\int_{-\infty}^{\infty}dx_1\int_{-\infty}^{\infty}dx_2\cdots\int_{-\infty}^{\infty}dx_m(-i)^m$$
$$\times V(\sigma,x_1/\sigma_1)V(\sigma_1,x_2/\sigma_2)\cdots V(\sigma_{m-1},x_m/\sigma_m),\tag{2.30}$$

where

$$V(\sigma;x/\sigma')$$
$$\equiv\tfrac{1}{2}[1+\epsilon(\sigma,x)]S_0{}^{-1}(\sigma')\bar{\psi}_{\text{in}}(x)V(x)\psi_{\text{in}}(x)S_0(\sigma')\tag{2.31}$$

is the external disturbance acting on the nucleon with the meson cloud. Using these relations, we can obtain the connection between ${}^+U^r(x,\sigma)$ and ${}^+U_0{}^r(x,\sigma)$.

Here we remark that for the state Ψ_0 in which there exist one nucleon and no mesons, we have the relation

$$S_0(\infty)\Psi_0\doteqdot\Psi_0,\tag{2.32}$$

(where the notation $\doteqdot$ means the equality of both sides except for a constant phase factor) under the assumption that the interaction between the meson and the nucleon is adiabatically switched on and switched off at $\sigma=-\infty$ and $\sigma=+\infty$, respectively.[8]†

In our formalism which constantly makes use of the Heisenberg operator, the transition probabilities are

[8] κ and μ are the masses of the bare meson and the bare nucleon respectively, and so they differ from the observable masses κ_{ob} and μ_{ob}:

$$\kappa=\kappa_{\text{ob}}-\delta_m,\qquad\mu=\mu_{\text{ob}}-\delta_n.$$

δ_n and δ_m are the self-energies of a nucleon and a meson, respectively, which are obtained in Sec. 3. Their values are infinite in the usual quantum field theory. Masses appearing in the Δ-functions and the spectrum ${}^+u$ are not $(\kappa_{\text{ob}},\mu_{\text{ob}})$ but (κ,μ) in the present formalism, which differs from the usual renormalization formalism in which masses appearing in the Δ-functions are $(\kappa_{\text{ob}},\mu_{\text{ob}})$, and in which (δ_m,δ_n) appears in the interaction terms. Considering the success of the usual mass renormalization in perturbation procedure, it is expected that the (δ_m,δ_n) of the (κ,μ) appearing in the Δ-functions cancels the infinities which originate from the self-energies, although a general proof independent of the perturbation procedure has not yet been given. If so, the infinities of the constant phase factor in (2.32) will be calcelled. Such a renormalization procedure with the use of (δ_m,δ_n) in the Δ-functions is now being investigated.

† *Note added in proof.*—This problem will be discussed in detail by H. Umezawa and S. Kamefuchi, Prog. Theoret. Phys. (to be published).

obtained in the following way. In general, the state of the system can be represented by the numbers $n_1, n_2, \cdots$ of the mesons with the momenta $\mathbf{k}_1, \mathbf{k}_2, \cdots$. Then, the average number of mesons is given by

$$\bar{N}(\sigma)=\langle i|N(\sigma)|i\rangle = \sum\langle i|S^{-1}(\sigma)|v\rangle\langle v|S(\sigma)|i\rangle N_{\text{in}}(\sigma, v) \quad \langle 2.33\rangle$$

with

$$N_{\text{in}}(a)=-2i\int {}^{+}U_{\text{in}}{}^{*}(x)[\partial^{+}U_{\text{in}}(x)/\partial x_{\mu}]d\sigma_{\mu}$$

and

$$\langle v'|N_{\text{in}}(\sigma)|v\rangle=N_{\text{in}}(\sigma, v')\delta_{vv'},$$

because $N_{\text{in}}(\sigma)$ is diagonal in this representation. The coefficient $|\langle v|S(\sigma)|i\rangle|^2$ of $N_{\text{in}}(\sigma, v)$ in $\langle 2.33\rangle$ is to be interpreted as the probability that the state on the surface σ is found in v. Thus, we find that the transition matrix between the states i and v is given by

$$\langle v|S(\sigma)|i\rangle. \quad \langle 2.34\rangle$$

3. RELATION BETWEEN THE MESONIC PROPER-FIELD AND THE SPECTRUM

We shall discuss in more detail the relation between the mesonic proper-field and the c-spectrum as defined above.

First, we consider intuitively the energy of the interacting meson and nucleon to be composed of the following three parts:

(1) The kinetic energy E^{m} of the free meson field (meson cloud) which is given by

$$E^{m}(\sigma)=\left\langle\int\left[\frac{\partial^{+}U^{*}(x,\sigma)}{\partial x_i}\frac{\partial^{+}U(x,\sigma)}{\partial x_i}+\frac{\partial^{+}U^{*}(x,\sigma)}{\partial t}\frac{\partial^{+}U(x,\sigma)}{\partial t}+\kappa^{2}{}^{+}U^{*}(x,\sigma)^{+}U(x,\sigma)\right]dv\right\rangle_{x/\sigma} \quad (3.1)$$

$$=\left\langle\int KN_{\sigma}(k)d^{4}k\right\rangle. \quad (3.2)$$

(2) The interaction energy E^{mn} between a nucleon, the meson cloud ${}^{+}U(x,\sigma)$, and the fluctuation field ${}^{-}U(x,\sigma)$, which, taking account of the Hermitian character of $O(x)$, is given by

$$E^{mn}(\sigma)=\left\langle g\int O(x)\{{}^{+}U(x,\sigma)+{}^{+}U^{*}(x,\sigma)\}dv\right\rangle_{x/\sigma}$$

(scalar coupling), (3.3)

$$E^{mn}(\sigma)=\left\langle g\int O_{\mu}(x)\frac{\partial}{\partial x_{\mu}}\{{}^{+}U(x,\sigma)+{}^{+}U^{*}(x,\sigma)\}dv - \tfrac{1}{2}g^{2}\int O_{4}{}^{*}(x)O_{4}(x)dv\right\rangle_{x/\sigma}$$

(vector coupling). (3.3′)

Taking account of the properties ${}^{+}U_{\text{in}}\rangle_{m=0}=0$, we see that the term $U_{\text{in}}(x)$ in $U(x,\sigma)$ does not contribute to $E^{mn}(\sigma)$ for the state $\Psi(m=0)$. From (3.3), we obtain, by means of commutability of $O(x)$ and ${}^{+}U(x,\sigma)$ for x/σ;

$$\langle E^{mn}(\sigma)\rangle_{m=0}=-\left\langle\int\frac{g^{2}O^{*}(k)O(k)}{K(K-k_0)}d^{4}k\right\rangle_{m=0},$$

(scalar coupling). (3.3″)

(3) The kinetic-energy $E^{n}(\sigma)$ of a free nucleon $\psi(x,\sigma)$, which is

$$E^{n}(\sigma)=\left\langle\int\left[\bar{\psi}(x,\sigma)\gamma_i\frac{\partial}{\partial x_i}\psi(x,\sigma)+\mu\bar{\psi}(x,\sigma)\psi(x,\sigma)\right]dv\right\rangle_{x/\sigma}, \quad (3.4)$$

where $\psi(x,\sigma)=S^{-1}(\sigma)\psi_{\text{in}}(x)S(\sigma)$ and $\bar{\psi}(x,\sigma)$ satisfies the individual free field equations.

We shall first discuss, under the approximation of Bloch-Nordsieck, the total energy obtained by the above intuitional consideration. The approximation that σ-spin and τ-spin matrices are regarded as c-number unit vectors and $O(k)$ is treated as the change of these classical vectors corresponds to the treatment of Bloch-Nordsieck[3] and Lewis-Oppenheimer-Wouthuysen.[9]

In this case it is easily seen from (2.23) and (2.24) that k_0 is equal to the energy transfer E_p-E_q of the nucleon. Introducing the nucleon mean velocity $\mathbf{v}=(\mathbf{v}_p+\mathbf{v}_q)/2$, as in the Bloch-Nordsieck paper, we may write

$$k_0=E_p-E_q\approx(\mathbf{v},\ \mathbf{p}-\mathbf{q})=(\mathbf{v}\cdot\mathbf{k}),$$

and, therefore,

$$N(\sigma)\simeq\frac{1}{2}\int\frac{|g(\mathbf{q}|O(\mathbf{k})|\mathbf{p})|^{2}}{K(K-(\mathbf{v}\cdot\mathbf{k}))^{2}}d\mathbf{k}\simeq\int N(\mathbf{k})d^{3}\mathbf{k}$$

(scalar coupling). (3.5)

Thus, we obtain

$$E^{m}(\sigma)\simeq\frac{1}{2}\int\frac{|g(\mathbf{q}|O(\mathbf{k})|\mathbf{p})|^{2}}{(K-(\mathbf{v}\cdot\mathbf{k}))^{2}}d^{3}\mathbf{k}\ \text{(scalar coupling)}. \quad (3.6)$$

Now, in the nonrelativistic and classical approximation, as the nucleon suffers the recoil $-\mathbf{k}$ from the meson of momentum $\mathbf{k}$, we obtain the following kinetic energy:

$$E^{n}(\sigma)\simeq-\int(\mathbf{v}\cdot\mathbf{k})N(\mathbf{k})d\mathbf{k}=-\frac{1}{2}\int\frac{|g(\mathbf{q}|O(\mathbf{k})|\mathbf{p})|^{2}}{K(K-(\mathbf{v}/\mathbf{k}))^{2}}(\mathbf{v}\mathbf{k})d\mathbf{k}. \quad (3.7)$$

[9] Lewis, Oppenheimer, and Wouthuysen, Phys. Rev. **73**, 127 (1948).

Adding to this the interaction energy $E^{mn}(\sigma)$ and free meson energy $E^{m}(\sigma)$, the total energy $E(\sigma)$ will be as follows:

$$E=E^{n}+E^{m}+E^{mn}=-\frac{1}{2}\int\frac{|g(\mathbf{p}+\mathbf{k}|O(\mathbf{k})|\mathbf{p})|^{2}}{K(K-(\mathbf{v}\cdot\mathbf{k}))}d\mathbf{k}$$

(scalar coupling). (3.8)

Equation (3.8) agrees exactly with the self-energy obtained by Bloch-Nordsieck[8] and Pauli-Fierz[10] by a canonical transformation.

It can easily be seen that the energy of the meson-nucleon system is given exactly by $E=E^{n}+E^{m}+E^{mn}$.

The total energy of the meson-nucleon system is, in the Heisenberg representation,

$$-\int T_{44}(x)dv=-\int T_{44}{}^{m}(x)dv-\int T_{44}{}^{n}(x)dv, \quad (3.9)$$

where

$$T_{44}{}^{m}(x)=\begin{cases}\dfrac{\partial U^{\nu}(x)}{\partial x_{4}}\dfrac{\partial U^{\nu}(x)}{\partial x_{4}}+L^{m}(x) & \text{(scalar coupling),}\quad (3.10)\\ \left(\dfrac{\partial U^{\nu}(x)}{\partial x_{4}}+g^{\nu}\bar{\psi}O_{4}{}^{\nu}\psi\right)\dfrac{\partial U^{\nu}(x)}{\partial x_{4}}+L^{m}(x) & \text{(vector coupling),}\quad (3.11)\end{cases}$$

$$T_{44}{}^{n}(x)=-\frac{1}{2}\left\{\bar{\psi}(x)\gamma_{4}\frac{\partial}{\partial x_{4}}\psi(x)+\bar{\psi}'(x)\gamma_{4}\frac{\partial}{\partial x_{4}}\psi'(x)\right\}, \quad (3.12)$$

$$L^{m}=-\frac{1}{2}\left\{\frac{\partial U^{\nu}(x)}{\partial x_{\mu}}\frac{\partial U^{\nu}(x)}{\partial x_{\mu}}+\kappa^{2}U^{\nu}(x)U^{\nu}(x)\right\}. \quad (3.13)$$

On the other hand, the canonical transformation $S(\sigma)$ requires the following replacement:

$$\frac{\partial U(x/\sigma)}{\partial x_{\mu}}=\begin{cases}\left[\dfrac{\partial U(x,\sigma)}{\partial x_{\mu}}\right]_{x/\sigma} & \text{(scalar coupling),}\\ \left[\dfrac{\partial U(x,\sigma)}{\partial x_{\mu}}+n_{\mu}n_{\nu}g\bar{\psi}(x,\sigma)O_{\nu}\psi(x,\sigma)\right]_{x/\sigma} & \text{(vector coupling),}\end{cases} \quad (3.14)$$

$$\frac{\partial\psi(x/\sigma)}{\partial x_{\mu}}=\begin{cases}\left[\dfrac{\partial\psi(x,\sigma)}{\partial x_{\mu}}+gn_{\mu}(n\gamma)U(x,\sigma)O\psi(x,\sigma)\right]_{x/\sigma} & \text{(scalar coupling),}\\ gn_{\mu}(n\gamma)\dfrac{\partial U(x,\sigma)}{\partial x_{\nu}}O_{\nu}\psi(x,\sigma)\Big] & \text{(vector coupling).}\end{cases} \quad (3.15)$$

From (3.14) and (3.15), it is clear that $-\{\int T_{44}{}^{n}(x)dv\}$ is equal to $E^{mn}+E^{n}$. Using the zero-point energy E_{0}, it is easily shown that

$$-\{T_{44}{}^{m}(x)dv\}=E^{m}+E_{0}, \quad (3.16)$$

where

$$E_{0}=-i\int_{\sigma}\left[\frac{\partial^{2}}{\partial x_{4}{}^{2}}{}^{+}\Delta(x-x')\right]_{x=x'}dv=\frac{1}{2}\int Kd\mathbf{k}. \quad (3.17)$$

If the zero-point energy is subtracted by the vacuum-subtraction method, $-\int T_{44}(x)dv$, (3.9), coincides with $E^{m}+E^{n}+E^{mn}$ obtained by intuitional consideration.[11] The fact that we must not neglect E^{mn} means that the cloud and the nucleon cannot be considered separately. (The usual intuitive picture of the meson cloud is not valid in this sense.)

It is noteworthy that E^{m} and E^{mn} are determined only by the c-spectrum, since $O(x)$ is calculated from a given spectrum ${}^{+}U(x,\sigma)$ as shown in the next section.

So far we have considered only the real field operator ${}^{+}U^{\nu}(x,\sigma)$, but the charged meson field with complex field operators U and U^{*} can also be treated in a similar manner.

${}^{+}U^{\pm}$ (positive frequency parts of $\pm$ charged meson fields $U^{\pm}(x_{0},\sigma)$) are introduced as follows:

$${}^{+}U^{\pm}(x_{0},\sigma)={}^{+}U_{\text{in}}{}^{\pm}(x_{0})+(-i)\int_{\infty}^{\infty}{}^{+}u^{\pm}(x_{0},\sigma;x)d^{4}x. \quad (3.18)$$

When the interaction is of the form $g(\bar{\psi}O^{+}\psi U+\bar{\psi}O^{-}\psi U^{*})$, we get

$$\left.\begin{aligned}{}^{+}u^{+}(x_{0}/\sigma;x)&=ig^{+}\Delta_{\text{ret}}(x_{0}-x)O^{-}(x),\\ {}^{+}u^{-}(x_{0}/\sigma;x)&=ig^{+}\Delta_{\text{ret}}(x_{0}-x)O^{+}(x).\end{aligned}\right\} \quad (3.19)$$

4. AN EXAMPLE OF THE SPECTRUM

Since it is very difficult actually to calculate the exact c-spectrum from the present quantum field theory, we must solve the problem by using suitable methods of approximation in various cases.

Here we shall give an example in which the d-spectrum and the e-spin of a nucleon in the meson cloud can be obtained from the given c-spectrum.

Let us consider the pseudoscalar meson with pseudovector coupling under the strong coupling approxima-

[10] W. Pauli and M. Fierz, Nuovo cimento **15**, No. 3 (1938).

[11] Thus, strictly speaking, in order to determine the binding energy of the stationary state of the A nucleons system, we must take into account not only the kinetic energy $E^{n}(A)$ of the A nucleons and the interaction energy $E^{mn}(A)$, but also the kinetic energy $E^{m}(A)$ of the meson cloud.

tion. In this case the interaction is given by:

$$L^{\text{int}}=-g(\tau^{+}U+\tau^{-}U^{*}+2^{-\frac{1}{2}}\tau^{3})D(x), \tag{4.1}$$

where $D(x)$ is a spherical symmetric function representing the extended source. The Fourier component of $D(x)$ is

$$F(k)=\int D(x)e^{-ikx}dv, \tag{4.2}$$

and if we use r_0, as the radius of the source, then we may write as follows:

$$\left.\begin{aligned} F(k)&=1 \quad \text{for} \quad k\lesssim 1/(4\pi)^{\frac{1}{2}}r_0,\\ F(k)&=0 \quad \text{for} \quad k\gtrsim 1/(4\pi)^{\frac{1}{2}}r_0. \end{aligned}\right\} \tag{4.3}$$

Under the condition of the strong coupling ($\kappa g\gg r_0\kappa$, $r_0\kappa\ll 1$) we get in the zeroth-order approximation the following meson field:[12]

$$\left.\begin{aligned} U^{\pm}(x/\sigma)\rangle_{m=0}&=(g/8\pi)(\mathbf{e}^{1}\pm i\mathbf{e}^{2})\text{grad}K(x)e^{-ik_0t}\\ U^{3}(x/\sigma)\rangle_{m=0}&=(g/4\pi 2^{\frac{1}{2}})\mathbf{e}^{3}\,\text{grad}K(x)e^{-ik_0t}, \end{aligned}\right\} \tag{4.4}$$

where

$$K(x)=\int D(x')\exp\{-\kappa|\mathbf{r}-\mathbf{r}'|\}/|\mathbf{r}-\mathbf{r}'|\cdot dv.$$

We can obtain the source $\bar{O}(x)$ by means of (4.7):

$$\left.\begin{aligned} O^{\pm}(x)\rangle_{m=0}&=-\frac{\mathbf{e}^{1}\pm i\mathbf{e}^{2}}{2}\int\frac{(K^2-k_0^2)}{2K^2}F(k)e^{ik_\mu x_\mu}\frac{d\mathbf{k}}{(2\pi)^3}\\ O^{3}(x)\rangle_{m=0}&=-\frac{\mathbf{e}^{3}}{2^{\frac{1}{2}}}\int\frac{(K^2-k_0^2)}{2K^2}F(k)e^{ik_\mu x_\mu}\frac{d\mathbf{k}}{(2\pi)^3} \end{aligned}\right\} \tag{4.5}$$

where $\mathbf{e}^{i}(i=1,2,3)$ is such a q-number as to make the interaction Hamiltonian diagonal.

${}^{+}U_0(x,\sigma)$ can be obtained from (2.26′) as follows:

$$\left.\begin{aligned} &{}^{+}U_0{}^{\pm}(x,\sigma)\rangle_{m=0}\\ &=\frac{i}{2}g\int\frac{(\mathbf{e}^{1}\mp i\mathbf{e}^{2},\mathbf{k})}{2}\frac{(K^2-k_0^2)}{K^2}\frac{F(k)}{2K(K-k_0)}\\ &\qquad\times e^{i(K_\mu x_\mu+i(K-k_0)t_0}\frac{d\mathbf{k}}{(2\pi)^3}\\ &{}^{+}U_0{}^{3}(x,\sigma)\rangle_{m=0}\\ &=\frac{i}{2}g\int\frac{(\mathbf{e}^{3},\mathbf{k})}{2^{\frac{1}{2}}}\frac{(K^2-k_0^2)}{K^2}\frac{F(k)}{2K(K-k_0)}\\ &\qquad\times e^{i(K_\mu x_\mu+i(K-k_0)t_0}\frac{d\mathbf{k}}{(2\pi)^3}. \end{aligned}\right\} \tag{4.6}$$

Thus, if the meson field $U_0(x/\sigma)$ is obtained, by whatever means it may be, the e-spins of the nucleon in the meson cloud are uniquely determined by the following relations:

$$\left.\begin{aligned} g\bar{O}(x)&=(\Box-\kappa^2)U_0(x/\sigma)\\ &\qquad\qquad\text{(scalar coupling)}\\ -g\partial\bar{O}_\mu(x)/\partial x_\mu&=(\Box-\kappa^2)U_0(x/\sigma)\\ &\qquad\qquad\text{(vector coupling)} \end{aligned}\right\} \tag{4.7}$$

${}^{+}U_0(x,\sigma)$ can be determined by means of (2.26), (2.26′), and the Fourier representation of $\bar{O}(x)$ and $\bar{O}_\mu(x)$. Such ${}^{+}U_0(x,\sigma)$ is obtained by replacing $\exp(ik_0t)$ and $k_\mu\exp(ik_0t)$ in the Fourier representation of $U(x/\sigma)$ by $(K^2-k_0^2)/2K(K-k_0)\cdot\exp\{iKx_0-i(K-k_0)t\}$ (for the scalar coupling case) and $K_\mu(K^2-k_0^2)/2K(K-k_0)\cdot\exp\{iKx_0-i(K-k_0)t\}$ (for the vector coupling case), respectively, where t is the time on the flat surface σ.

5. TREATMENT OF SOME PHENOMENA BY THE SPECTRUM

It is, of course, not possible to observe directly the meson cloud, and so its physical properties must be found in the correlated phenomena. In this connection we have considered, in Sec. 3, the self-energy of the nucleon, which is rather an inadequate phenomenon for our consideration in spite of its immediate relation to the cloud, since its contribution is already contained in the experimental mass. To find out the nature of the proper field experimentally, therefore, we must put it under the disturbance of external fields. We may take up here the multiple production of mesons and the anomalous magnetic moment of the nucleon, discuss the relations between the spectrum of the proper field and these two phenomena, and re-examine along these lines the various theoretical results so far presented.

(1) Multiple Production of Mesons (Covariant Generalization of the Bloch-Nordsieck Method)[13]

The process of the production of mesons is described by the transition from the mesonic vacuum state Ψ_0 to the state $\Psi(n)$ with n mesons. Introducing an operator

$$W^{n}(x_0)\equiv[{}^{+}U_{\text{in}}(x_0)]^{n}/n!,^{14} \tag{5.1}$$

the state $\Psi(m=n)$ is given by $W_n{}^{*}(x_0)\Psi_0$. (Taking into account the change of the normalization factor[15] $\Pi_i(2K_i)$ in (5.8)).

[12] W. Pauli and S. M. Dancoff, Phys. Rev. **62**, 85 (1942).

[13] After completion of the work, we have received Phil. Mag. **42**, 244 (1951) in which W. Thirring and B. Touschek describe a method of treatment of this problem, similar to the method of this paper.

[14] $\psi(\mathbf{k}_1,\cdots,\mathbf{k}_n)$, in which there are n mesons with momenta $\mathbf{k}_i(i=1,\cdots,n)$ is equivalent, apart from the constant phase factor $\exp(i\Sigma\mathbf{k}_ix_0)$ (x_0 is a given space-time point), to

$$(\mathbf{k}_1,\cdots,\mathbf{k}_n|\Pi_i(2K_i)^{\frac{1}{2}}W(x_0)^{*}\Psi_0.$$

This fact is taken into consideration when we use (5.1) and (5.8) below.

[15] Of course, the Fourier transformation of $W^{n}(x_0)$ with respect to x_0 corresponds to the creation operators of final mesons with the given momenta $\mathbf{k}_1,\cdots,\mathbf{k}_n$.

Then, the transition matrix element for the production of n mesons on the surface σ is equivalent to the following matrix element between Ψ_0^* and Ψ_0. [See (2.34)]:

$$S^n(x_0/\sigma)=\langle W^n(x_0)S(\sigma)\rangle_{m=0}. \tag{5.2}$$

We have the following relation:

$$\begin{aligned} i\frac{\delta}{\delta\sigma(x)}&S_0^{-1}(\sigma)W^n(x_0)S(\sigma)\\ &={}^+u_0(x_0,\sigma';x)S_0^{-1}(\sigma)W^{n-1}(x_0)S(\sigma)\\ &\quad+V(\sigma';x)S_0^{-1}(\sigma)W^n(x_0)S(\sigma), \end{aligned} \tag{5.3}$$

where σ' is a certain surface later than σ, $V(\sigma';x)$ is

$$\tfrac{1}{2}\{1+\epsilon(\sigma,x)\}[S_0^{-1}(\sigma)\psi_{\text{in}}(x)V(x)\psi_{\text{in}}(x)S_0(\sigma)]_{x/\sigma}.$$

$V(\sigma';x)$ means the external interaction acting on the nucleon accompanied by the meson cloud.

The solution of (5.3), which has the zero initial value for $\sigma=-\infty$ $(n>0)$, is given as follows:

$$\begin{aligned} &S_0^{-1}(\sigma)W^n(x_0)S(\sigma)\rangle_{m=0}\\ &=\sum_{j=0}^{\infty}\sum_{m_1=0}^{m_2}\cdots\sum_{m_j=0}^{n}\int_{-\infty}^{\sigma}\cdots\int_{-\infty}^{\sigma}dx_1\cdots\\ &\times dx_{m_1}dy_1dx_{m_1+1}\cdots dx_{m_j}dy_jdx_{m_j+1}\cdots dx_n\\ &\times{}^+u_0(x_0,\sigma;x_1)^+u_0(x_0,\sigma_1;x_2)\cdots{}^+u_0(x_0,\sigma_{m_1-1};x_{m_1})\\ &\times V(\sigma_{m_1};y_1)^+u_0(x_0,\sigma_{y_1};x_{m_1+1})\cdots\\ &\times{}^+u_0(x_0,\sigma_{m_j-1};x_{m_j})V(\sigma_{m_j};y_j)^+u_0(x_0,\sigma_{y_j};x_{m_j+1})\cdots\\ &\qquad\times{}^+u_0(x_0,\sigma_{n-1};x_n)\rangle_{m=0}. \end{aligned} \tag{5.3'}$$

This solution can be easily obtained by the following consideration: From (5.3), we can get[16]

$$\left.\begin{aligned} i\frac{\delta}{\delta\sigma(x)}T&=\{a^+u(x_0,\sigma';x)+V(\sigma';x)\}T,\\ T&=\sum_{n=0}^{\infty}a^nS_0^{-1}(\sigma)W^n(x_0)S(\sigma)\rangle,\\ T(\sigma\to-\infty)&=1. \end{aligned}\right\} \tag{5.4}$$

Thus, we get $S_0^{-1}(\sigma)W^nS(\sigma)$ as the nth-order term with respect to $a^+u_0(x_0,\sigma;x)$ in T. We may also see, from (5.4), that T has the form of the S-matrix with the interaction a^+u_0+V. Of course, we can see directly, without using (5.4), that (5.3′) satisfies Eq. (5.3). Thus, when we restrict ourselves to the approximation of the first order with respect to $V(x)$ (though we can also treat similarly the case of the higher order), we obtain $S^n(x_0/\sigma)$ from T:

$$\begin{aligned} S^n(x_0/\sigma)=(-i)^{n+1}\Big\langle&\int_{-\infty}^{\sigma}\cdots\int_{-\infty}^{\sigma}dx_1\cdots dx_mdydx_{m+1}\cdots\\ &\times dx_m{}^+u_0(x_0/\sigma;x_1)^+u_0(x_0,\sigma_1;x_2)\cdots\\ &\times{}^+u_0(x_0,\sigma_{m-1};x_m)V(\sigma_m;y)^+u_0(x_0,\sigma_y;x_{m+1})\cdots\\ &\times{}^+u_0(x_0,\sigma_{n-1};x_n)\Big\rangle_{m=0}, \end{aligned} \tag{5.5}$$

where we have eliminated $S_0(\infty)$ by the use of the relation (2.32). By means of (2.22), we obtain, therefore, from (5.5),

$$\begin{aligned} &S^n(x_0/\infty)\\ &=\Big\langle\sum_{m=0}^{n}(-i)^{n+1}[(+U_0)^mV(+U_0)^{n-m}\}(x_0/\infty)\Big\rangle_{m=0}, \end{aligned} \tag{5.6}$$

where we have used the notation $[A_1A_2\cdots A_n\}\equiv[A_1[A_2[\cdots[A_{n-1},A_n\}\}\cdots\}$. Equations (5.5) and (5.6) show that the production of mesons is described by the iteration of the spectra, the vibration of which is influenced by the effect of the meson-production in the preceding processes. Equation (5.5) shows that ${}^+u_0(x_0/\sigma,x')$ has a physical meaning which may correspond to that of Heisenberg's η-matrix.[17] Moreover, we may say that (5.6) is the quantum theoretical relation which corresponds to the Heisenberg's classical treatment of the multiple production of mesons[4] based on the classical meson spectrum which has been briefly explained in Sec. 1.

The probability that n mesons are produced is given by

$$dw_n=\{\prod_{i=1}^{n}(2K_id\mathbf{k}_i)\}\,|S(\mathbf{k}_1,\cdots,\mathbf{k}_n)|^2, \tag{5.7}$$

$$S^n(x_0/\infty)\equiv\int S(\mathbf{k}_1,\cdots,\mathbf{k}_n)e^{i\Sigma\mathbf{k}_i\mathbf{x}}d\mathbf{k}_1\cdots d\mathbf{k}_n, \tag{5.8}$$

where $S(\mathbf{k}_1,\cdots,\mathbf{k}_n)$ is the matrix element of $S^n(x_0/\infty)$ responsible for the process under consideration.

Equations (5.5), (5.7), and (5.8) will afford a starting-point for our discussion of the multiple production of mesons. This is an exact relation obtained by the quantum field theory and is valid for any magnitude of the coupling strength between meson and nucleon fields.

Now, we shall investigate the relation (5.5) in detail. We introduce $v(l)$ as follows:

$$\psi(y)V(y)\psi(y)\equiv\int v(l)e^{ily}d^4l. \tag{5.9}$$

[16] a is a constant introduced from the dimensional consideration.

[17] W. Heisenberg, Z. Physik **120**, 673 (1943).

Then, using (2.24) and (2.24'), we obtain, from (5.6):

$$S(\mathbf{k}_1, \cdots, \mathbf{k}_n)=\left\{\prod_{i=1}^{n}\frac{1}{(2K_i)}\right\}\sum_{a=0}^{n}\times\sum_{(\text{perm})}^{(1,\cdots,n)}\langle\bar{O}(k_1)\bar{O}(k_2)\cdots\bar{O}(k_a)v(l)\bar{O}(k_{a+1})\cdots\bar{O}(k_n)\rangle_{m=0}$$
$$\times\frac{(-1)^{n-a}\delta(b_1+\cdots+b_n+l_0)d^4l}{b_n\cdots(b_{a+1}+\cdots+b_n)(b_1+b_2+\cdots+b_a)\cdots(b_1+b_2)b_1}, \quad (5.10)$$

where $\sum_{(\text{perm})}^{(1,\cdots,n)}$ means the summation over all permutations of the group $(\mathbf{k}_1, \cdots, \mathbf{k}_n)$ and $b_i\equiv b(k_i)$. From (5.9) it is seen that $l_\mu=(\mathbf{l}, il_0)$ is the energy-momentum transfer of the nucleon accompanying the meson cloud during the scattering process by the external potential $V(y)$.

In (5.10), $\bar{O}(k)$ is defined by

$$\bar{O}(k)\equiv\begin{cases}\bar{O}(k) & \text{(scalar coupling)}, \quad (5.11)\\ iK_\mu\bar{O}_\mu(k) & \text{(vector coupling)}. \quad (5.12)\end{cases}$$

Equation (5.10) gives the intuitive picture of the multiple production of mesons: the meson-production is caused by the oscillation of the e-spin of the nucleon with the meson cloud in the external potential. Now, in order to compare the exact formulas (5.5) and (5.10) with the approximate result of Bloch and Nordsieck, we examine (5.10) under the following conditions, which are satisfied in the Bloch-Nordsieck case:

(1) $O(k_i)(i=1, 2, \cdots, n)$ and $v(l)$ are commutable with one another.

(2) The nucleon with the meson cloud before and after the scattering due to the external potential $v(l)$ can be assumed to be in the states $(\ )''$ and $(\ )'$, respectively. We denote $O(k)$, $b(k)$ in the states $(\ )'$ and $(\ )''$ as $O(k)'$, $b(k)'$, $O(k)''$, and $b(k)''$, respectively.

Under these approximations it is shown below that mesons are produced according to the Poisson distribution.

In rewriting (5.10) it is convenient to use the following relation:

$$\sum_{(\text{perm})}^{(1,2,\cdots,n)}1/b_1(b_1+b_2)\cdots(b_1+\cdots+b_n)$$
$$=1/b_1b_2\cdots b_n, \quad (5.13)$$

and so we obtain

$$\left\langle\sum_{a=0}^{n}\sum_{(\text{perm})}^{(1,2,\cdots,n)}\frac{\bar{O}(k_1)'\cdots\bar{O}(k_a)'v(l)\bar{O}(k_{a+1})''\cdots\bar{O}(k_{n-1})''\bar{O}(k_n)''(-1)^{n-a}}{b_1'(b_1'+b_2')\cdots(b_1'+\cdots+b_a')(b_{a+1}''+\cdots+b_n'')\cdots(b_{n-1}''+b_n'')b_n''}\right\rangle_{m=0}$$
$$=\left[\frac{\bar{O}(k_1)'\cdots\bar{O}(k_n)'}{b_1'b_2'\cdots b_n'}-\left(\frac{\bar{O}(k_1)''\bar{O}(k_2)'\cdots\bar{O}(k_n')}{b_1''b_2'\cdots b_n'}+\cdots\right)+\left(\frac{\bar{O}(k_1)''\bar{O}(k_2)''\bar{O}(k_3)'\cdots\bar{O}(k_n)'}{b_1''b_2''b_3'\cdots b_n'}+\cdots\right)\right.$$
$$\left.+\cdots+(-1)^n\frac{\bar{O}(k_1)''\bar{O}(k_2)''\cdots\bar{O}(k_n)''}{b_1''b_2''\cdots b_n''}\right]v(l) \quad (5.14)$$
$$=\left\{\prod_{i=1}^{n}\Delta\frac{\bar{O}(k_i)}{b_i}\right\}v(l),$$

where

$$\Delta\frac{\bar{O}(k_i)}{b_i}\equiv\frac{\bar{O}(k_i)'}{b_i'}-\frac{\bar{O}(k_i)''}{b_i''}, \quad (5.16)$$

which denotes the momentum distribution of the difference of two spectra in states $(\ )'$ and $(\ )''$, and so is equivalent to $(\sigma_{s\lambda}-\tau_{s\lambda})$ appearing in Bloch and Nordsieck's paper.

Then we obtain from (5.15) and (5.8),

$$dw_n=\left\{\prod_{i=1}^{n}\frac{d\mathbf{k}_i}{2K_i}\left(\Delta\frac{\bar{O}(k_i)}{b_i}\right)^2\right\}|v(l)|^2, \quad (5.17)$$

which is integrated over $\mathbf{k}_i(i=1, 2, \cdots)$ to give

$$w_n=(1/n!)\left\{\int\Delta N(\mathbf{k})d\mathbf{k}\right\}^n|v(l)|^2, \quad (5.18)$$

with

$$\Delta N(\mathbf{k})\equiv\frac{g^2}{2}\frac{1}{K}\left(\Delta\frac{O(k)}{b(k)}\right)^2=N(k)'-N(k)''. \quad (5.19)$$

In (5.18) the three-fold integration in momentum space is to be performed in such a way as to satisfy the energy momentum conservation law. (5.17) and (5.18) show that the multiple production of mesons is caused by the change of the state of the nucleon accompanying the meson cloud (spin, τ-spin states, etc.). (5.18), which has been obtained under the conditions (1) and (2), agrees with the Bloch-Nordsieck and Lewis-Oppenheimer-Wouthuysen formulas for multiple pro-

duction of bosons. In fact, by substituting the approximate spectra[18] into (5.19) we can show that in the case of scalar or pseudoscalar meson fields (5.18) gives the same results as obtained by Lewis, Oppenheimer, and Wouthuysen[10] (see Appendix). Therefore, (5.5) and (5.11), from which (5.18) has been obtained, can be regarded as the generalized formulas of the Bloch-Nordsieck result.

According to (5.18), the probability for the production of n mesons due to a nucleon (a)-nucleon (b) collision is found to be, under the conditions (1) and (2) (Poisson distribution),

$$w_n=\sum_{n_a=0}^{n}\binom{n}{n_a}\frac{1}{n_a!}\left\{\int\Delta N_a(\mathbf{k})d\mathbf{k}\right\}^{n_a}\times\frac{1}{n_b!}\left\{\int\Delta N_b(\mathbf{k})d\mathbf{k}\right\}^{n_b}. \quad (5.18')$$

A detailed account of this case, in which the conditions (1) and (2) (Poisson distribution) are fulfilled, (the relation between the energy spectrum of produced mesons and the c-spectrum of the meson field around a nucleon) will be given in the Appendix.

(2) Magnetic Moment of the Nucleon

The magnetic moment of the nucleon may also be interpreted as a phenomenon which expresses the effect of the meson cloud around it.[19] It is obtained by computing the corrections due to the mesonic interaction of the operator

$$\mathbf{M}=\frac{1}{2}\int[\mathbf{r}\times\mathbf{J}]dv,$$

and for the case of a charged spinless meson field, $\mathbf{J}$ is given by

$$\begin{aligned}&J_\mu=J_\mu{}^{\mathrm{n}}+J_\mu{}^{\mathrm{m}}+J_\mu{}^{\mathrm{mn}},\\&J_\mu{}^{\mathrm{n}}=-\tfrac{1}{2}ie\bar{\psi}\gamma_\mu(1-\tau_3)\psi,\\&J_\mu{}^{\mathrm{m}}=ie\{(\partial U^*/\partial x_\mu)U-(\partial U/\partial x_\mu)U^*\}, \quad (5.20)\\&J_\mu{}^{\mathrm{mn}}=-eg\bar{\psi}O_\mu{}^{+}\psi U-eg\bar{\psi}O_\mu{}^{-}\psi U^*\\&\qquad\mu=1,2,3. \qquad \text{(vector coupling)}\end{aligned}$$

The mesonic correction of the moment $\mathbf{M}$ arising from the mesonic current $\mathbf{J}^{\mathrm{m}}$ is given by

$$\langle\mathbf{M}^{\mathrm{m}}\rangle=\frac{1}{2}\int[\mathbf{r}\times\langle\mathbf{J}^{\mathrm{m}}(x)\rangle]dv. \quad (5.21)$$

The external magnetic field exerts on the meson cloud the following effects: (1) the scattering of mesons, and (2) the pair creation and annihilation of mesons, by which the current due to the meson cloud is disturbed and then returns to its original stationary state. In a manner similar to the self-energy case, $\mathbf{J}^{\mathrm{m}}$ can be written in terms of the free meson field, i.e.,

$$\langle J_\mu{}^{\mathrm{m}}(x)\rangle=ie\langle\partial U^*(x,\sigma)/\partial x_\mu\cdot U(x,\sigma)-\partial U(x,\sigma)/\partial x_\mu\cdot U^*(x,\sigma)\rangle_{x/\sigma}, \quad (5.21)'$$

where the terms $-U^{++}U^{+}$, $-U^{-+}U^{-}$ denote the scattering effects, and $-U^{+-}U^{-}$, $+U^{++}U^{-}$ denote the pair creation and annihilation, respectively. Actually, $\mathbf{M}^{\mathrm{m}}$ has a nonvanishing value even for the spinless meson, due to the fact that the positively and negatively charged parts of the meson cloud have their respective angular momenta. In the weak coupling theory, for instance, the perturbation calculations show that the contribution from $\mathbf{M}^{\mathrm{m}}$ and, $\mathbf{M}^{\mathrm{mn}}$ is of the same order of magnitude as the nucleon current.[20]

By the same argument as in the derivation of (3.3), the magnetic moment due to the current $\mathbf{J}^{\mathrm{mn}}$ is found to be

$$\langle\mathbf{M}^{\mathrm{mn}}\rangle=\tfrac{1}{2}eg^2\left\langle\int[\mathbf{r}\times(\mathbf{O}^{+}(x)U(x,\sigma)-\mathbf{O}^{-}(x)U^*(x,\sigma))]dv\right\rangle_{x/\sigma}. \quad (5.22)$$

It is worth noticing that $\mathbf{M}^{\mathrm{m}}$ and $\mathbf{M}^{\mathrm{mn}}$ can be uniquely determined in this way by the given c-spectrum ${}^{+}U(x,\sigma)$.

$(\mathbf{M}^{\mathrm{m}}+\mathbf{M}^{\mathrm{mn}})$ has the same magnitude but opposite signs for proton and neutron, due to the different signs of electric charge of the meson cloud.[21] Remembering that the existence of a small difference in the anomalous magnetic moments of the proton and the neutron has been experimentally confirmed, we may say that the nucleon current contributes slightly to its magnetic moment.

The magnetic moment $\mathbf{M}^{\mathrm{n}}$ due to the current $\mathbf{J}^{\mathrm{n}}$ is determined by the behavior of τ_3- and σ-spins in the meson cloud; that is, it is given by the expectation

[18] Such an approximation leads to the erroneous nuclear forces, i.e., the ratio of exchange to ordinary forces becomes very small. R. Serber and S. M. Dancoff, Phys. Rev. **63**, 143 (1943).

[19] While, by expressing the charge distribution ρ around the nucleon in terms of the spectrum, the problem of neutron-electron interaction is more easily treated than that of the magnetic moment, the information obtained from the former is restricted; i.e., it gives only the depth of the equivalent square well (symmetric static part of the cloud).

[20] From the Case's results for the anomalous magnetic moment of the nucleon, the meson cloud is supposed to spread over a considerably wide region around the nucleon. According to Brueckner, on the contrary, to explain the isotropic angular distribution of the mesons produced by γ-rays it is desirable that the cloud should be closely bound to the nucleon. In the problem of the meson cloud, therefore, it is very important to look for a consistent model which satisfies the above two requirements. Recently, an example of such a model has been suggested by Y. Fujimoto and H. Miyazawa, who attempted to explain the isotropic angular distribution of produced mesons by assuming the existence of isobar energy levels of the cloud, an extension of which satisfies the requirement of the magnetic moment. Y. Fujimoto and H. Miyazawa, Prog. Theoret. Phys. **5**, 1052 (1950).

[21] This point has been proved, including the cases of higher order approximation, in the perturbation calculation. Y. Takahashi, Prog. Theoret. Phys. **6**, 624 (1951).

values of[22]

$$\int[\mathbf{r}\times\Delta\{\tfrac{1}{2}(1-\tau_3)\boldsymbol{\gamma}\}]dv.$$

But, in general, it is not always possible to calculate $\Delta\{\frac{1}{2}(1-\tau_3)\boldsymbol{\gamma}\}$ from a given spectrum. Therefore, we have to be content with the following intuitive and rough estimation: From an intuitive model, we shall estimate $\mathbf{M}^n$ as follows.

$$\mathbf{M}^n\sim(e/2\mu)P,$$

where eP is the average value of the charge of a nucleon in the meson cloud. Making a transformation (3.14), (3.15) and calculating in the same way as in the self-energy case, we get

$$e_m=\left\langle\int\rho dv\right\rangle_{\substack{m=0\\n=1}}=\left\langle e\int[\{\partial^-U^+(x,\sigma)/\partial x_4\cdot{}^+U^+(x,\sigma)-\partial^+U^+(x,\sigma)/\partial x_4\cdot{}^-U^+(x,\sigma)\}-\{\partial^-U^-(x,\sigma)/\partial x_4\cdot{}^+U^-(x,\sigma)-\partial^+U^-(x,\sigma)/\partial x_4\cdot{}^-U^-(x,\sigma)\}]_{x^4=\sigma}d\mathbf{v}\right\rangle_{\substack{m=0\\n=1}}. \quad (5.23)$$

Further rewriting gives the expression

$$e_m=e\left\langle\int(N^+(\mathbf{k})-N^-(\mathbf{k}))d\mathbf{k}\right\rangle. \quad (5.24)$$

The average value of the charge of a nucleon in the meson cloud is obtained by the relation

$$eP=e_t-e_m \quad (5.25)$$

where e_t is the total charge of the nucleon-meson system. ($e_t=e$ for an apparent proton and $e_t=0$ for an apparent neutron).

For the spectrum (4.5) given in Sec. IV, we can calculate $\mathbf{M}^m$ from (5.21) and obtain the result, for the system of a nucleon and no meson,

$$\langle\mathbf{M}^m\rangle_{\substack{m=0\\n=1}}=-2eg^2\mathbf{e}_3/12(4\pi r_0),\qquad[\mathbf{e}_1\times\mathbf{e}_2]=\mathbf{e}_3. \quad (5.26)$$

For the spectrum (4.5), we get, from (4.6) and (5.22),

$$\langle\mathbf{M}^{mn}\rangle_{\substack{m=0\\n=1}}=eg^2\mathbf{e}_3/12(4\pi r_0). \quad (5.27)$$

Adding (5.26) to the above expression (5.27) we obtain

$$\langle\mathbf{M}^{mn}+\mathbf{M}^m\rangle_{\substack{m=0\\n=1}}=-eg^2\mathbf{e}_3/12(4\pi r_0)\quad\text{(for (4.5))}, \quad (5.28)$$

which is exactly the result obtained by Pauli and Dancoff. Equation (5.28) has opposite signs for proton and neutron since the vector $\mathbf{e}_3$ has opposite signs for them. For the spectrum (4.5), we find $e_m=0$ and $P=1$ for an apparent proton and $P=0$ for an apparent neutron and so $\mathbf{M}^n\approx0$. Here it is to be remembered that, since (4.5) is merely a leading term in the strong coupling theory, e_m does not vanish in the higher approximations. Therefore, we expect that the next approximation may give a nonvanishing and small $\mathbf{M}^n$.[23]

[22] $\Delta\{\frac{1}{2}(1-\tau_3)\boldsymbol{\gamma}\}$ means $\mathbf{O}(x)$, where $\mathbf{O}=\frac{1}{2}(1-\tau_3)\boldsymbol{\gamma}$.

ACKNOWLEDGMENTS

We wish to express our cordial thanks to Professor S. Sakata and Mr. R. Kawabe for their continual encouragement and valuable discussions. We are also deeply indebted to Professor S. Tomonaga for his constructive criticism. This work was supported by the fund of the "Chubu-Nippon Press."

APPENDIX

Under the conditions (1) and (2), the relation between the most probable number of mesons and the c-spectrum of the meson field around a nucleon can be obtained from (5.18′).

If we make the assumptions

$$K\Delta N_a(\mathbf{k})=f(a)g(\mathbf{k}),\qquad K\Delta N_b(\mathbf{k})=f(b)g(\mathbf{k}), \quad (A.1)$$

where the function f depends on the nucleon variables only and g on the meson variables only, w_n will be

$$w_n=\sum_{n_a=0}^{n}n!/(n_a!)^2(n_b!)^2\cdot(f(a))^{n_a}(f(b))^{n_b}\left\{\int\frac{d\mathbf{k}}{K}g(\mathbf{k})\right\}^n. \quad (A.2)$$

For the large value of n, the above expression with the summation over n_a can be replaced by

$$w_n\sim\frac{(2\pi)^n}{n!}\left\{\frac{f(a)+f(b)}{d_1^{d_1}d_2^{d_2}}\right\}^n\left\{\int\frac{d\mathbf{k}}{K}g(\mathbf{k})\right\}^n, \quad (A.3)$$

with

$$d_1=f(a)/[f(a)+f(b)],\qquad d_2=f(b)/[f(a)+f(b)]. \quad (A.4)$$

The most probable number $\bar{n}$ of emitted mesons is determined by the following relation

$$\frac{w_{n+1}}{w_n}=\frac{2\pi}{\bar{n}}\frac{f(a)+f(b)}{d_1^{d_1}d_2^{d_2}}\left\{\int\frac{d\mathbf{k}}{K}g(\mathbf{k})\right\}^{\bar{n}+1}\Big/\left\{\int\frac{d\mathbf{k}}{K}g(\mathbf{k})\right\}^{\bar{n}}\sim1. \quad (A.5)$$

Now, let us consider the case in which the spectrum ${}^+U$ has the asymptotic form

$${}^+U(\mathbf{k})\sim K^q/K^3 \quad (A.6)$$

[23] In fact, Pauli and Dancoff obtained $-e\mathbf{e}_3/2\mu$ for $\mathbf{M}^n$ (see reference 12).

in the high energy region. Then

$$N(\mathbf{k}) \propto K^{2q}, \quad g(\mathbf{k}) \propto K^{2q+1}. \tag{A.7}$$

Therefore, it follows from Dirichlet's formula that

$$\left\{\int \frac{d\mathbf{k}}{K} g(\mathbf{k})\right\}^n \propto \left\{4\pi \int K^{2q+2} dK\right\}^n_{\Sigma K_i \leqq \epsilon_{\max}}$$

$$= (4\pi)^n \frac{\{\Gamma(2q+3)\}^n}{\Gamma(2nq+3n+1)} \epsilon_{\max}{}^{2nq+3n}, \tag{A.8}$$

where $\epsilon_{\max}$ is the maximum energy transfer from the nucleons to the emitted mesons and $\bar{n}$ will be

$$\bar{n} \sim 2\pi \frac{f(a)+f(b)}{d_1{}^{d_1} d_2{}^{d_2}} \left\{\int \frac{d\mathbf{k}}{K} g(\mathbf{k})\right\}^{\bar{n}} \Big/ \left\{\int \frac{d\mathbf{k}}{K} g(\mathbf{k})\right\}^{\bar{n}-1}. \tag{A.9}$$

When $f(a)$ behaves as

$$f(a) \propto (\epsilon_{\max})^p, \tag{A.10}$$

from (A.8), (A.9), (A.4), and (A.1), we get the result

$$\bar{n} \propto \begin{cases} \epsilon_{\max}{}^{(2q+3+p)/(2q+1)} & \text{for } q > -\frac{3}{2}, \\ \epsilon_{\max}{}^p \log \epsilon_{\max} & \text{for } q = -\frac{3}{2}. \end{cases} \tag{A.11}$$

Under these approximations, the spectrum ($p=0$, $q=-\frac{3}{2}$) gives

$$\bar{n} \propto \log \epsilon_{\max},$$

which agrees with the result obtained by Lewis *et al.* in the case of the scalar meson with scalar coupling. The spectrum ($p=0$, $q=-\frac{1}{2}$) gives

$$\bar{n} \propto \epsilon_{\max}{}^{\frac{1}{2}},$$

which is the result obtained by them in the case of pseudoscalar meson with pseudovector coupling. Further, from the spectrum

$${}^{+}U(\mathbf{k}) = F(\mathbf{k})(\boldsymbol{\sigma}\cdot\mathbf{k})/K^2 (p=0, q=-\tfrac{1}{2}) \tag{A.12}$$

obtained in Sec. 4 from the strong coupling theory of pseudoscalar meson with pseudovector coupling, it follows

$$\bar{n} \propto \epsilon_{\max}{}^{\frac{1}{2}}. \tag{A.13}$$

Recently, Fermi[24] has presented a new theory of the multiple production of mesons based on statistical considerations. His method consists in assuming that the meson cloud is so rigidly attached to the nucleon that an external disturbance is rapidly transferred to the whole cloud. As a result of this assumption, the probabilities for multiple production of mesons are determined only by the statistical weight, i.e., the magnitude of volume in phase space. Fermi's idea is, therefore, essentially different from our theory in which probabilities are determined essentially by the cloud spectrum itself. However, the result of his theory is reinterpreted in terms of the c-spectrum theory in the following way. Translating his theory into ours, it is easily found that Fermi's assumption

$$w_n \propto \text{volume in phase space}$$

is equivalent, in our theory, to assuming that

$$N(\mathbf{k}) \text{ is independent of } K,$$

i.e.,

$$q=0, \tag{A.14}$$

and

$$\Omega \propto (\epsilon_{\max})^{-1}, \tag{A.15}$$

i.e.,

$$f(a) \propto (\epsilon_{\max})^{-1}. \tag{A.16}$$

From (5.34) and (5.36) we obtain, by means of (5.29),

$$\bar{n} \propto \epsilon_{\max}{}^{\frac{1}{2}}, \tag{A.17}$$

which is Fermi's result.

Apart from the above assumption, it may also be interesting to discuss the statistical probability factor in connection with its Lorentz invariancy. Assuming that the number of mesons in the Lorentz invariant volume element $d\mathbf{k}/K$ of phase space is independent of momentum $\mathbf{k}$, i.e.,

$$N(\mathbf{k}) d\mathbf{k} \propto d\mathbf{k}/K, \quad (q=-\tfrac{1}{2}), \tag{A.18}$$

we obtain, in high energy region, the following result:

$$\bar{n} \propto \epsilon_{\max}{}^{\frac{1}{2}}. \tag{A.19}$$

[24] E. Fermi, Prog. Theoret. Phys. **5**, 570 (1950).

The Nuclear Scattering of 1-Mev Electrons and Positrons

HARRY J. LIPKIN
Palmer Physical Laboratory, Princeton University, Princeton, New Jersey
(Received June 18, 1951)

The scattering of 1-Mev electrons and positrons by thin foils has been investigated from two points of view: (1) to compare the cross section for elastic nuclear scattering of positrons with that of electrons, and (2) to look for evidence of inelastically scattered electrons which have suffered large energy losses. The first experiment is of interest because theory predicts a large difference between electron and positron scattering as a result of spin-orbit coupling, and thus involves the magnetic moment of the electron. The second experiment is of importance because there have been many conflicting reports on the existence of inelastic scattering whereas theoretically one expects almost no inelastic scattering.

Electrons and positrons from artificially radioactive sources were energy selected by a solenoidal spectrometer before being scattered by various foils. After being scattered, the particles entered a second, analyzer, magnetic field and were then detected by a Geiger counter. To study inelastic scattering of electrons the analyzer field was varied. To study the e^-/e^+ scattering ratio, various scatterers could be employed without changing the equipment in any way except to replace the electron source by a positron source. Thus the e^-/e^+ scattering ratio could be measured with greater accuracy than the scattering of either particle separately.

The observed e^-/e^+ scattering ratio 2–3 is consistent with a rather rough theory which does not take into account screening. No inelastic scattering was found in foils of copper, aluminum, or platinum.

INTRODUCTION

IT is perhaps surprising that there have not been any measurements of positron scattering by nuclei more precise than those of Fowler and Oppenheimer,[1] Lasich,[2] and Seliger,[3] especially since Massey[4] has predicted a large effect due to spin-orbit coupling in such a scattering experiment. There have been no other investigations of the magnetic interactions of positrons; in fact there have been surprisingly few attempts to study their behavior directly and verify the assumption that they act as Dirac particles of positive charge.

Another aspect of electron-nuclear scattering which bears further investigation is inelastic scattering. A number of experimenters[5–10] have reported the observation of much more inelastic scattering than is predicted by theory. A typical result is that of Klarmann and Bothe, who report that 48 percent of the observed scattered particles lost over 20 percent, and 21 percent had lost over 50 percent of their initial energy. All these experimenters used cloud chambers in magnetic fields measuring track curvatures to obtain energy values. Bothe,[11] using a Geiger counter with magnetic beta-ray spectrograph to measure energies of electrons, failed to observe any anomalous inelastic scattering at 210 and 370 kev.

The present work attempts to study the elastic scattering of 1-Mev positrons and electrons in copper and platinum with greater precision than that of the previous investigations. This is achieved by use of Geiger counters, rather than cloud chambers to obtain better statistics. By using the same apparatus with positron and electron sources, the ratio of electron scattering to positron scattering can be determined directly to a precision much greater than could be obtained in an absolute measure of either cross section independently, and with less possibility of errors.

The apparatus used to study elastic scattering is then also used to look for anomalous inelastic scattering in aluminum, copper, platinum, and lead.

THEORY

The scattering of charged particles by a Coulomb field is independent of the sign of the charge only in the nonrelativistic region. The relativistic corrections to the sign-independent Rutherford formula are sign-dependent and appreciable. Thus, in the 1-Mev region, the scattering at 60° of positrons by heavy nuclei differs from that of electrons by a factor of three![12]

This effect can be interpreted as a result of spin-orbit coupling and has been considered in detail by Mott,[12] using the Dirac equation. Similar qualitative results are obtained from a more naive approach, treating the Dirac electron classically as a combination point charge and magnetic dipole, giving a simple physical picture of the phenomenon.

Consider an electron passing the nucleus at a large distance, so that the deflection is small, and the undeflected path can be used to consider the effect of the magnetic interaction. The moving dipole sees the nuclear Coulomb field as a magnetic field **H** which

[1] W. A. Fowler and J. Oppenheimer, Phys. Rev. **54**, 320 (1938).
[2] W. B. Lasich, Australian J. Sci. **A1**, 249 (1948).
[3] H. H. Seliger, Phys. Rev. **78**, 491 (1950).
[4] H. W. S. Massey, Proc. Roy. Soc. (London) **A181**, 14 (1942).
[5] H. Klarmann and W. Bothe, Z. Physik **101**, 489 (1936).
[6] D. Skobeltzyn and E. Stephanowa, Nature **137**, 456 (1936).
[7] A. Barber and F. C. Champion, Proc. Roy. Soc. (London) **A168**, 159 (1938).
[8] R. L. Sen Gupta, Proc. Phys. Soc. (London) **51**, 355 (1939).
[9] L. Le Prince Ringuet, Ann. Phys. (11), **7**, 5 (1937).
[10] L. J. Laslett and D. G. Hurst, Phys. Rev. **52**, 1035 (1937).
[11] W. Bothe, Z. Naturforsch. **4a**, 88 (1949).
[12] N. Mott and H. W. S. Massey, *Theory of Atomic Collisions* (Oxford University Press, Oxford, 1950), 2nd Edition, p. 74.

exerts a force

$$\mathbf{F}=(\boldsymbol{\mu}\cdot\nabla)\mathbf{H}=-(\mathbf{v}/c)\times(\boldsymbol{\mu}\cdot\nabla)\mathbf{E} \qquad (1)$$

where $\boldsymbol{\mu}$ is the magnetic moment of the electron, $\mathbf{v}$ the velocity, and $\mathbf{E}$ the electric field at the position of the electron.

If the electron is polarized parallel or antiparallel to the direction of motion, the first-order effect is a force perpendicular to the plane of the motion, which reverses sign as the electron passes the nucleus, and therefore gives the electron path a small deviation but no angular deflection. The second-order effect results in an angular deflection which is always toward the nucleus and is independent of the sign of the charge or the spin direction. The second-order force can be calculated from Eq. (1) by using for $\mathbf{v}$ the transverse component of velocity given by the first-order effect. This force is found to be of order of magnitude

$$F\sim(Ze^2/r)[(Ze^2/\hbar c)(\hbar/mcr)^2]$$

where Z is the atomic number of the scattering nucleus, and r is the distance of the electron from the nucleus.

Comparing this with the Coulomb force Ze^2/r^2, it is evident that the spin-orbit force is significant for heavy nuclei where $Ze^2/\hbar c\sim 1$, and for electrons which come closer to the nucleus than the Compton wavelength $(\hbar/mc)$ of the electron.

From this naive picture, the following qualitative results are obtained which are confirmed by the rigorous calculation: (1) The scattering of negative electrons is increased, that of positrons is decreased, since the spin-orbit force is always attractive. (2) The effect is greater for nuclei of high atomic number. (3) The effect is greater for electrons than for positrons, since the former pass closer to the nucleus.

The exact quantum-mechanical calculation is laborious and complicated because of the screening of the nucleus by the atomic electrons. Barlett and Watson[13] and Massey[4] have calculated the scattering of electrons and positrons by unscreened mercury nuclei, and McKinley and Feshbach[14] give a series for light and medium nuclei. Calculations for a screened Coulomb field[15–17] have been made only for electrons, but not for positrons. These show that the effect of screening is appreciable; being 10 percent for 1-Mev electrons scattered at 60°.

For the present work, the unscreened theory is used for comparison with experiment, since there is no complete screened theory. A discrepancy between experiment and the unscreened theory of the order of 10 percent should be expected, and greater precision in the experimental result cannot be interpreted using present theory. Since such precision is easily obtainable, it is hoped that a calculation of the scattering of positrons by a screened Coulomb field will be undertaken in the near future.

For light nuclei, polystyrene and copper, the approximate formula of McKinley and Feshbach is used:

$$r=1-\beta^2\sin^2\tfrac{1}{2}\theta+\pi\alpha\beta(\sin\tfrac{1}{2}\theta)\cdot(1-\sin\tfrac{1}{2}\theta).$$

r is the ratio of the relativistic electron scattering to Rutherford scattering, θ is the angle of scattering, α is $Ze^2/\hbar c$, and β is v/c.

The value of r for positrons is obtained by replacing α by $-\alpha$.

The validity of this approximation for light nuclei was checked by noting that the screening terms in the McKinley and Feshbach expansion had a negligible effect on the ratio of electron to positron scattering.

For platinum, the results of Bartlett and Watson and Massey were used. Although these were calculated for mercury, it is assumed that the error introduced thereby is small compared to that due to the neglect of screening.

MULTIPLE SCATTERING

Nearly all electron scattering experiments are affected to an appreciable degree by multiple scattering in the scattering medium, and many of the older experiments are seriously in error because of failure to make the proper corrections. Consequently, considerable effort has been made in the present work to reduce multiple scattering and to compute the necessary corrections. The details of the calculations are extremely laborious and are reported in the author's doctorate thesis and in an AEC technical report by Dr. T. Teichmann. I am deeply indebted to Dr. Teichmann for a very careful analysis of the problem.

A particle, emerging from a scatterer at a given angle θ with respect to the undeflected beam, may have suffered one or more collisions in passing through the scatterer. To determine the contribution of multiple scattering, it is convenient to divide it into two types: (1) scattering by an angle nearly equal to θ plus one or more small angle scatterings, (2) scattering by two or more large angles.

The first type of scattering is best calculated by an extension of the method of Butler[18] to the case of large angles ($\sim$60°). Much of the idea of this method seems to have been given first, albeit heuristically, by Chase and Cox.[19] After laborious calculations, a good deal more complicated than those given by Butler, one finds that the additional correction to the single scattering probability $P_1(\theta)$ (normalized to unity) is given by the following expression:

$$\Delta P(\theta)=t^{-2}e^{-\theta^2/4t}C(\theta,t)+tM_2(\theta)+\tfrac{1}{2}t^2M_4(\theta)+\tfrac{1}{6}t^3M_6(\theta)+\cdots$$

[13] J. H. Bartlett, Jr., and R. E. Watson, Proc. Am. Acad. Arts Sci. **74**, 53 (1940).
[14] W. A. McKinley, Jr., and H. Feshbach, Phys. Rev. **74**, 1759 (1948).
[15] J. H. Bartlett, Jr., and T. A. Welton, Phys. Rev. **59**, 281 (1941).
[16] H. W. S. Massey and C. B. O. Mohr, Proc. Roy Soc. (London) **A177**, 341 (1940).
[17] C. B. O. Mohr, Proc. Roy. Soc. (London) **A182**, 189 (1943).
[18] S. T. Butler, Proc. Phys. Soc. (London) **A63**, 599 (1950).
[19] C. T. Chase and R. T. Cox, Phys. Rev. **58**, 243 (1940).

where

$$t=2(\pi/0.00765)^2(e^2/mc^2)^2NsZ^{4/3}(w^2/(w^2-1))\times\int_0^{\theta_1}\sin\vartheta\,\sin^2\tfrac{1}{2}\theta\cdot P_1(\theta)d\theta$$

[N = number of scatterers per cm.^{3}
w = energy of electrons in units mc^2]

while $C(\theta, t)$, and $M_{2k}(\theta)$ are, respectively, rather nasty power series in θ and t, and complicated trigonometric functions of θ times derivatives of $P_1(\theta)$ up to the $2k$th. They are listed elsewhere. θ_1 is an angle rather larger than the cut-off angle (see Mott and Massey) and determined roughly so as to minimize $C(\theta, t)$ without making the remainder of ΔP (*viz.* the series in the M_k) too large.

The second type of scattering is principally double scattering, i.e., scattering by two angles greater than θ. This type of scattering can be calculated directly if the Rutherford formula is assumed for the single scattering formula. For the case where the scattered beam emerges normally from the foil, the fractional correction to single scattering due to double scattering by angles greater than θ_1 is approximately

$$\frac{\Delta P_2(\theta)}{P(\theta)}\approx\pi As\left\{\left(8+\left[\frac{1-\cos\theta}{\cos\theta}\right]^2\right)(1-\cos\theta)^{-1}\times\log\left(\frac{\csc^2\frac{1}{2}\theta_1-\csc^2\frac{1}{2}\theta}{\csc^2\frac{1}{4}\theta-\csc^2\frac{1}{2}\theta}\right)\right\}$$

where s is the foil thickness.

If this contribution of double scattering is small, that due to triple and higher order scattering involving more than two large angles can be considered to be negligible.

One particular type of double scattering of interest is the case where the first scattering is nearly in the plane of the foil.[20–22] The long path-length traversed by such a particle in the foil results in an appreciable probability for a second scattering. The energy loss due to ionization in the long-path length can be misinterpreted as inelastic scattering. For the case where the scattered beam emerges normal to the foil, the fractional contribution to the total scattering due to particles which traversed a path length in the foil between l_1 and l_2 is given by

$$\Delta P/P_1(\theta)=[2\pi P_1(\theta)(1-\cos\theta)^4/(1+\cos^2\theta)]\times[L/(L-l)+\log(l/(L-l))]_{l_1}^{l_2}$$

where $P_1(\theta)$ is the probability of single scattering by an angle θ, as given by the Rutherford formula, and L is the range of the particle in the scattering materials.

[20] V. A. Petukhov and I. A. Vishinsky, J. Physiol. U.S.S.R. **5**, 137 (1940).
[21] Shull, Chase, and Myers, Phys. Rev. **63**, 29 (1943).
[22] G. Goertzel and R. T. Cox, Phys. Rev. **63**, 37 (1943).

This effect is particularly large when the scattered beam emerges on the same side of the foil as the incident beam. For the case where both beams make equal angles with the normal,

$$\Delta P/P_1(\theta)=\{\pi P_1(\theta)[1-\cos\theta]^4[5-3\sin^2\tfrac{1}{2}\theta]\csc^4\tfrac{1}{2}\theta\}\times\{L/(L-l)+\log(l/(L-l))\}_{l_1}^{l_2}.$$

This may well account for the large energy losses observed by Le Prince Ringuet[9] in lead and silver foils of 0.1 mm. For 1-Mev electrons scattered by 120° in a 0.1-mm lead foil, this effect results in a large number of "inelastically" scattered particles. The probability of an energy loss between $\frac{1}{3}$ and $\frac{2}{3}$ of the original energy is twice the probability of elastic scattering!

EXPERIMENTAL PROCEDURE

A diagram of the apparatus is shown in Fig. 1. The scattering chamber is within a long solenoid, which is used to select a small energy band from the continuous spectrum of particles emitted from the source. Those which are selected by this solenoid spectrograph are incident upon the scattering foil along the elements of a cone, making an angle of 57.9°±2.7° with the axis,

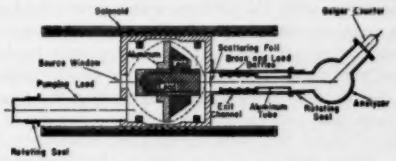

FIG. 1. Scattering apparatus.

and have a momentum spread of ±8 percent. Those particles scattered along the axis emerge from the solenoid through the exit channel and enter the analyzer, where they are deflected by a transverse magnetic field into the thin window Geiger counter. The apparatus was evacuated to a pressure of between 10 and 50 microns, using a Cenco Hyvac pump.

The sources used for this experiment were Ce^{144} and Ga^{66}. A 300 millicurie source of Ce^{144} with radioactive daughter Pr^{144} was obtained from Oak Ridge and was a very satisfactory electron source, having an upper energy limit of 2.99 Mev and a half-life of 375 days. A high energy, long-lived source of positrons being unavailable, 9.4-hr Ga^{66} was used, made by α-particle bombardment of copper in the cyclotron at the Carnegie Institution of Washington.

The short half-life of the positron source and the necessity of transporting it from Washington to Princeton were the principal limitations of the elastic scattering experiment. Thus instead of studying the scattering over a wide range of angles, incident energies, and scattering materials, one angle was chosen (57.9°), three energies (0.7, 1.0, and 1.3 Mev), and three scattering materials (polystyrene, copper and plati-

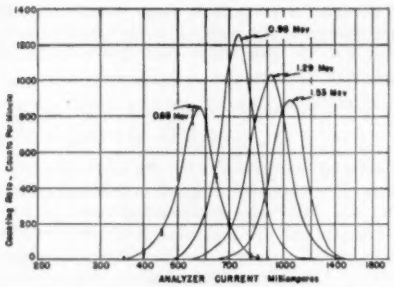

FIG. 2. Spectra of electrons scattered from 1-mil lead foil for incident energies of 0.68, 0.98, 1.29, and 1.53 Mev.

num). At these points the difference between positron and electron scattering is considerable, and the effects of spin-orbit coupling therefore quite noticeable.

Data were taken by inserting the source in the chamber and observing the counting rates of scattered particles for each energy and for each scattering material. Background counting rates, taken by removing the scattering foil, were subtracted. The complete data were taken using the electron source some time before the positron source arrived. The positron source was then continuously used until it was too weak to obtain significant data. Foils were changed at regular intervals so that the data at each point was the sum of a number of runs taken at various times during the life of the source. These data were checked for consistency with the known half-life of the source. After the positron run was completed, the electron run was repeated to reveal any possible changes in the apparatus between electron and positron runs.

The energy range of incident particles used was set by the solenoid field. The analyzer was set accordingly, and separated out the soft component of the scattered beam (inelastically scattered particles, knock-ons, etc.). Both fields were reversed in direction when changing from electrons to positrons.

The theory of McKinley and Feshbach predicts a difference of only 8 percent between the scattering of electrons and positrons from polystyrene. This value was accepted and the data from the polystyrene foil was used to normalize the electron and positron source strengths. Ratios of electron to positron scattering were then obtained for copper and platinum. The foil thicknesses used (15-mil polystyrene, 0.68-mil Cu, and 0.1- and 0.2-mil Pt), were the minimum possible to give reasonable statistics with the weak positron source used. They were still too thick to make multiple scattering as small as desired, but the corrections in most cases were of reasonable magnitude. The use of two thicknesses of platinum served as a check on the validity of the multiple scattering corrections.

The counting rates obtained with the cerium source were of the order of 300–400 counts per minute, depending on the scattering foil used, as compared with a background of 175–215 counts per minute. The gallium source gave counting rates initially of the order of 30–130 counts per minute, with a constant background of 40 counts per minute and a decaying background starting at about 60 counts per minute. Thus the data from the thinnest foils were well down in the background and long counts were required.

The investigation of inelastic scattering consisted simply of analyzing the beam of scattered particles into a momentum spectrum by varying the current in the analyzer magnet and recording the counting rate. A plot of the counting rate against the analyzer magnet current then gives a peaked curve, having a width

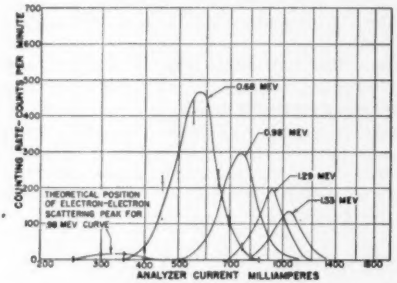

FIG. 3. Spectra of electrons scattered from 1-mil copper foil for incident energies of 0.68, 0.98, 1.29, and 1.53 Mev.

corresponding to the energy resolution of the apparatus. Any inelastic scattering present should appear as a tail on the curve in the direction of decreasing analyzer current.

Spectra of scattered particles were taken at four incident energies from 0.68 to 1.53 Mev for foils of copper and lead. Spectra were also taken at 1 Mev for three different thicknesses of aluminum and platinum foils. These spectra represent attempts to search for inelastic scattering over a moderate energy range in representative light, medium, and heavy nuclei, and to observe, using the variation of foil thickness, any multiple effects which might otherwise be misinterpreted. Background spectra were taken with no scattering foil and subtracted from the corresponding spectra of scattered particles.

The spectra were plotted on semilogarithmic paper, as shown in Figs. 2, 3, 4, and 5. The logarithmic scale was used for analyzer current because the fractional rather than the absolute momentum resolution of the analyzer remains constant as the analyzer current is varied. On a semi-log plot, the measured counting rates can be plotted directly, with no correction factor for the resolution variation, and the area under the curve between any two abcissas is proportional to the number of scattered particles in that corresponding momentum interval.

SOURCES OF ERROR

In this experiment, the final data are counting rates in a Geiger counter. It is important to establish that these counts actually represent the phenomena to be investigated and are not due to any spurious effects. Background runs, taken with no scattering foil and subtracted, insure that the net data represent events occurring in the scattering foil. The analyzer magnet insures that all particles counted are in the desired energy range. But there are other effects, not excluded by these experimental precautions, which must be considered separately.

The principal source of error in this experiment is multiple scattering. In order to obtain reasonable counting rates with the available positron sources, foil thickness giving appreciable multiple scattering were required. Because the scattering cross section varies rapidly with energy, the amount of multiple scattering does also. Since it was not possible to change foil thicknesses for each energy measurement, a compromise value was chosen which is reasonable for mean energy. At the lower energy the multiple scattering was greater.

Calculations of multiple scattering of electrons and positrons were made using for the single scattering formulas the appropriate theoretical values of McKinley and Feshbach,[16] Mohr,[17] and Massey.[4] Table I shows the correction factors to the 4th and 6th order. It is clear from this table that the 6th-order correction to the e^-/e^+ ratio does not differ much from the 4th order except for the thickest foils of platinum at the lowest

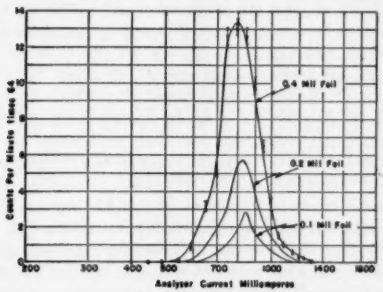

FIG. 4. Spectra of electrons scattered from platinum foils of various thicknesses. Incident energy 0.98 Mev.

energy. In general the e^-/e^+ ratio correction factor is smaller and more constant than either of the single scattering corrections. An experimental check on the validity of the corrections is given by the comparison of two different thicknesses of platinum at the three energies used. Aside from the lowest energy, when the correction factor is large, it is gratifying that the agreement in corrected e^-/e^+ ratio is about as good as the statistical errors would allow.

Another possible source of error is scattering by the atomic electrons in the foil. Single electron scattering is easily distinguished from nuclear scattering because of the energy loss which is a unique function of the scattering angle. Multiple scattering destroys this uniqueness and results in a distribution of energy loss which can be confused with inelastic nuclear scattering. This effect is most significant in light elements, and can be eliminated by using thinner foils.

Scattering from chamber walls and gas atoms, annihilation of positrons, and the various possible interactions of the gamma-rays were all calculated roughly and found to have a negligible effect upon the results of this experiment.

RESULTS—INELASTIC SCATTERING

Figure 2 shows the spectra of scattered particles at four energies from a 1-mil lead foil. The experimental points and their standard deviations are shown for one curve, and are similar for the others.

These curves show no evidence for inelastic scattering in which the electron has lost more than 20 percent of its energy. Their breadth can be attributed completely to the energy resolution of the apparatus and to the variation of ionization energy loss due to the variable path lengths traversed in the material, as previously discussed.

It is clear from these spectra that the number of particles losing over 40 percent of their energy is extremely small, certainly less than 1 percent of the number of elastically scattered particles. There is no indication of any particles losing more than 20 percent of their energy, but these might conceivably be missed, due to the width of the spectrum. One can safely say that the total number of particles losing more than 20 percent of their energy is less than 5 percent of the total distribution.

Figure 3 shows similar results for copper, and the same conclusions can be drawn here as for the case of lead. Note that there is a subsidiary peak shown for the 0.98-Mev curve, which can be attributed to electron-electron scattering. The theoretical position of this peak is indicated on the graph and agrees very well with the curve. The magnitude of this peak is difficult

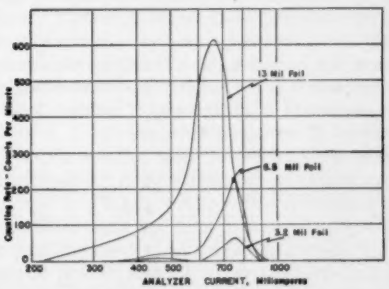

FIG. 5. Spectra of electrons scattered from aluminum foils of various thicknesses. Incident energy 0.98 Mev.

TABLE I. Summary of observed and corrected scattering of electrons and positrons by polystyrene, copper, and platinum.

Col. 1	2	3	4	5	6	7	8	9	10	11	12	13
Foil	Kinetic energy of $e^{\pm}$	Corr. factor to single e^- scattering		Corr. factor to single e^+ scattering		Inverse Corr. factor to ratio of single e^-/e^+ scattering		Meas. value of e^-/e^+ ratio	Corrected value of e^-/e^+ ratio (Corrected to single scat.)		Theoretical value	Statistical error %
	(Mev)	4th order	6th order	4th order	6th order	4th order	6th order		4th order	6th order		
15-mil polystyrene	0.68	1.11	1.15	1.09	1.12	0.978	0.970					
	0.98	1.06	1.06	1.04	1.05	0.988	0.987					
	1.29	1.05	1.05	1.04	1.04	0.988	0.987					
0.68-mil copper	0.68[a]	1.23	1.52	1.23	1.53	0.995	1.001	1.73	1.72	1.73	1.46	4
	0.98	1.12	1.14	1.12	1.15	1.002	1.003	1.93	1.93	1.93	1.49	5
	1.29	1.06	1.07	1.06	1.07	0.997	0.997	2.07	2.06	2.06	1.51	11
0.2-mil platinum	0.68[b]	1.42	2.63	1.57	3.66	1.103	1.395	2.27	2.50	3.17	2.74	4
	0.98[a]	1.17	1.31	1.24	1.50	1.060	1.145	2.88	3.05	3.30	2.90	5
	1.29	1.18	1.21	1.43	1.49	1.211	1.228	3.00	3.63	3.68	2.98	11
0.1-mil platinum	0.68[a]	1.60	1.64	2.61	2.70	1.638	1.641	3.13	5.13	5.14	2.74	5
	0.98	1.06	1.07	1.08	1.10	1.022	1.028	3.13	3.20	3.22	2.90	4
	1.29	1.06	1.07	1.08	1.10	1.025	1.029	3.60	3.69	3.70	2.98	10

[a] In these cases the sixth-order correction is appreciable compared to the total up to the fourth order, but the relative correction for positrons and electrons remains nearly the same, and it is therefore felt that the corrections are reliable.
[b] For obvious reasons this correction cannot be regarded as reliable.
[a] The correction here could be applied in such a way that the bulk of it came from the central (Gaussian) distribution, rather than from the tail. Hence, the contributions from orders higher than the fourth could be made small, even though the correction up to the fourth order was large. It was not possible to do this for the other points with large fourth-order corrections.

to determine accurately because of the statistical error, but it is the right order of magnitude, approximately $1/Z$ times the elastic peak, the curves of other energies do not show the electron-electron peak, either because it is at too low an energy, or because its magnitude is not appreciably greater than the statistical error.

The same absence of inelastic scattering is shown on the curves for platinum at 0.98 Mev. There is no significant difference between the three foil thicknesses. The displacement of the peak toward lower energies and the broadening of the distribution with increasing foil thickness is the result of the ionization energy loss.

A definite indication of inelastic scattering appears in the spectrum of scattered particles from the 13-mil aluminum foil. A large tail is present at the low energy end of the spectrum. However, the tail is greatly diminished in the curve for the 6.5-mil foil, and it is hardly observable in the curve for the 3.2-mil foil. One concludes therefore that the tail is due to a multiple effect, probably a combination of nuclear and electron-electron scattering, which for heavy nuclei is much less probable in comparison with elastic nuclear scattering.

From the curve for the 3.2-mil aluminum foil, one can conclude that the number of particles losing more than 20 percent of their energy is certainly less than 10 percent of the total distribution.

Thus the experimental data indicate that in light nuclei electron-electron scattering in combination with multiple nuclear scattering can give rise to large numbers of electrons which have lost appreciable energy. On the other hand, there is no evidence, as claimed by previous investigators, for inelastic nuclear scattering of electrons in the 1-Mev energy region from aluminum, copper, platinum, or lead.

e^-/e^+ ELASTIC SCATTERING RATIO—DISCUSSION

Table I, columns 9, 10, 11, 12, contains the final comparison of experiment and theory on the elastic scattering of electrons and positrons by nuclei. In this table it is assumed that for a light material such as polystyrene the theory is correct and that consequently the relative electron and positron source strength can be obtained from the observed e^-/e^+ scattering ratio. The data in column 9 were obtained by multiplying the actually observed ratios by the reciprocal of the observed, corrected polystyrene e^-/e^+ ratio. Since the theory of McKinley and Feshbach predicts an e^-/e^+ ratio for polystyrene of approximately 1.08, and since the multiple scattering corrections in columns 7 and 8 are small, we have considerable confidence in this method of normalizing the radioactive source strengths.

It will be seen in columns 11 and 12 that in a rough way theory and experiment are in agreement. The discrepancy is, however, well outside our experimental error and in a direction of giving a higher e^-/e^+ ratio than expected. This may be due to the effects of screening, for the calculations of Mohr show that the effect for electrons is of comparable magnitude and is in the proper direction. However, no calculations have been made on the effect of screening on positron scattering; so no definite conclusions can be drawn until a more accurate theory is available.

Note also that if the effect of screening is appreciable, the multiple scattering corrections will be altered. The multiple scattering formula requires a knowledge of the single scattering law, and in particular of the derivatives of the angular distribution at the angle of measurement. The contribution of screening to the values of these derivatives may produce noticeable

changes in the multiple scattering correction, especially if the diffraction maxima and minima discussed by Mohr are appreciable.

From these results it can be concluded that the effect predicted by theory of spin-orbit coupling on scattering of electrons and positrons is certainly present, and that the experimental data are in rough quantitative agreement with the theory which assumes that the magnetic moments of electron and positron are equal. More cannot be said at this point because of the lack of an adequate theoretical treatment of the scattering of positrons by a screened Coulomb field.

The author wishes to express his appreciation to Professor M. G. White for his suggestion of the problem, and for his many valuable suggestions and discussions during the course of the experimental work and the preparation of this article. The author is also very grateful to Dr. H. W. Fulbright, Dr. R. A. Goeckermann, and Dr. J. A. T. Odencrantz for their assistance in the handling and preparation of sources, to Dr. M. P. Peisakoff of the Princeton Mathematics Department for his generous assistance with statistical problems. The important work of Dr. T. Teichmann on multiple scattering has been acknowledged earlier.

It is a pleasure to acknowledge the help of the Oak Ridge National Laboratory, and in particular Mr. J. A. Cox, in providing the Ce^{144} and in developing the techniques necessary for depositing it upon our holder. The author is particularly indebted to Mr. Dean Cowie and the Department of Terrestrial Magnetism of the Carnegie Institution of Washington for so kindly providing the Ga^{66}. Their generosity in devoting an appreciable portion of their cyclotron time to these bombardments, at a time shortly after the destruction by fire of the Princeton cyclotron, is appreciated by all concerned.

The author is indebted to the du Pont Company and the Hercules Powder Company for fellowships early in the course of this work, and to Princeton University for a Proctor Fellowship. The research was supported in part by the office of Naval Research, the Atomic Energy Commission, and the Higgins Scientific Trust Fund.

PHYSICAL REVIEW VOLUME 85, NUMBER 4 FEBRUARY 15, 1952

Disintegration of the Deuteron by π^+ Mesons and the Spin of the π^+ Meson*

DONALD L. CLARK, ARTHUR ROBERTS, AND RICHARD WILSON†
University of Rochester, Rochester, New York

(Received August 9, 1951)

The total cross section for the reaction $\pi^+ + d \rightarrow p + p$ has been measured for an average incident meson energy of 23 Mev. This corresponds to a proton energy of 340 Mev in the inverse reaction $p + p \rightarrow \pi^+ + d$, for which the total cross section has been measured by Richman, Cartwright, Peterson, and others. Comparison of these two cross sections, using the theorem of detailed balancing, leads to a determination of the statistical weight, and hence the spin, of the π^+ meson. The spin turns out to be zero.

INTRODUCTION

OF the various methods which might be used for an experimental determination of the spin of the π^+ meson, the most promising is the possibility of application of the principle of detailed balancing. This method resembles that of the measurement of the alternation of intensities in rotation-vibration spectra of homonuclear diatomic molecules, in its ability to determine unambiguously a spin of zero, and in maximum sensitivity for small values of the spin.

In order to apply the principle of detailed balancing, it is necessary to measure the ratio of the cross sections for a reaction and its inverse at the same energy in the center-of-mass system. For practical purposes one must use a reaction with only two particles participating on each side. The only nuclear reaction to which detailed balancing has been successfully applied to date is the photodisintegration of the deuteron

$$h\nu + d \rightleftarrows n + p, \tag{1}$$

and its inverse, the radiative capture of neutrons by protons. Unfortunately, the comparison has not been made at the same center-of-mass energy; the n-p capture cross section has been measured at low energies and the photodisintegration at energies 200 kev or more above threshold. It is therefore necessary to use the theoretical energy dependence of the cross sections. The comparison has recently been reviewed by Salpeter.[1] Agreement is obtained within the experimental error of 20 percent, if we assume the neutron spin to be $\frac{1}{2}$. This result may be taken as a more direct measurement (at least in principle) of the neutron spin than the results given by neutron scattering in *ortho-* and *para*-hydrogen; more generally it is used to verify the theoretical cross sections.

* This work was assisted by the AEC.
† Now at Stanford University.

[1] E. E. Salpeter, Phys. Rev. **82**, 60 (1951).

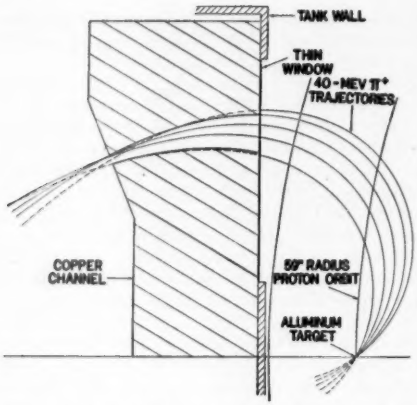

FIG. 1. The 40-Mev meson channel. Mesons leaving the aluminum target in a 30-degree wide interval about a direction of 150° to the incident proton beam are brought to an approximate focus by the fringing field and selected by a channel placed outside a thin window. The channel selects 40±1 Mev mesons.

The discovery[2] of the reaction

$$p+p \rightleftarrows \pi^+ + d - 137 \text{ Mev}, \qquad (2)$$

brings up the possibility of the application of detailed balancing to obtain the spin of the π^+ meson. This possibility was first pointed out by Johnson,[3] and independently by Marshak and Cheston.[4] If we denote by σ_{prod} the cross section for the reaction (2) proceeding to the right, producing mesons, and by σ_{abs} the cross section for the inverse reaction, then the theorem of detailed balancing[5] tells us that

$$\sigma_{\text{abs}}/\sigma_{\text{prod}} = [2/3(2I+1)](p^2/\mu^2), \qquad (3)$$

where p and μ are, respectively, the proton and meson momenta; all quantities are in the center-of-mass system, 2 is the statistical weight of the two protons, 3 the statistical weight of the deuteron, and $2I+1$ the statistical weight of the meson, I being the meson spin. The statistical weight of the protons is 2 rather than 4 because of the occurrence of 2 identical particles. The cross sections to be used may be either total or differential cross sections, at the same energy in the center-of-mass system.

Differential cross sections for the meson-production reaction have been obtained by several experimenters at 340 Mev; their results will be discussed later. We have now measured the total cross section for the meson-absorption inverse reaction at the corresponding bombarding meson energy of 22.7 Mev, and thus found the statistical weight of the π^+ meson. The spin turns out to be zero.[6]

In measuring the statistical weight, it is necessary only to distinguish among integral spins, since it is clear that reaction (2) cannot otherwise conserve angular momentum. That the spin of the π^- meson is integral has been demonstrated by numerous previous experiments.[7]

APPARATUS AND PROCEDURE

It was not possible, with the limited meson beam at our disposal, to measure the absorption cross section at a unique energy and angle. In order to obtain a reasonable counting rate, we measured the reaction averaged over meson energies from 0 to 33 Mev, and over angles from about 20° to 160°. An auxiliary experiment was performed to show that the cross section does not change sufficiently with energy to invalidate the averaging over meson energy, and estimates of the angular dependence have been obtained from the data on the production cross section.

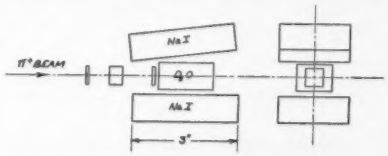

FIG. 2. Counter arrangement. The incident meson beam traverses a threefold anthracene counter telescope; each crystal is ½ inch square. The mesons then enter a D_2O or H_2O target, ¾ by 1 inch in cross section, 4 cm long, in a thin Lucite box. Emergent protons are detected by NaI crystals 2×3×¾ inches. Since the entire apparatus is in a strong magnetic field, 4-foot Lucite rods conduct the light to shielded photomultipliers. 1P21's are used for the meson telescope, 5819's for the NaI counters.

Production of π^+ Meson Beam

Protons are accelerated to 240 Mev in the 130-in. Rochester synchrocyclotron; they strike an aluminum target, 1 in. thick in the direction of the beam, and 0.1 in. transverse to the beam. π^+ mesons produced in this target and emerging in a generally backward direction escape from the cyclotron vacuum tank through a thin, 0.03-in. aluminum window (see Fig. 1). In front of the window, a collimating channel in a large copper block selects mesons of 40±1 Mev. The fringing field of the cyclotron brings the mesons to an approximate focus.

The mesons are detected by three ½-inch square anthracene scintillation counters in coincidence.[8] The

[3] Cartwright, Richman, Whitehead, and Wilcox, Phys. Rev. **78**, 823 (1951).
[3] M. H. Johnson, private communication.
[4] R. E. Marshak, Rochester High Energy Physics Conference, December, 1950 (unpublished). W. Cheston, Phys. Rev. **83**, 1118 (1951).
[5] See, e.g., H. A. Bethe, *Elementary Nuclear Physics* (John Wiley and Sons, Inc., New York, 1947), p. 61.
[6] Results of this work have been briefly reported previously: Clark, Roberts, and Wilson, Phys. Rev. **83**, 649 (1951).
[7] W. Cheston and L. Goldfarb, Phys. Rev. **78**, 683 (1950); F. Adelman, University of California Radiation Laboratory 1005; Menon, Muirhead, and Rochat, Phil. Mag. Ser. 7, **51**, 583 (1950).
[8] D. L. Clark, Phys. Rev. **81**, 313 (1951).

amplifier for the second scintillation counter in the telescope is arranged to reject pulses which are below a given threshold or above a predetermined ceiling. Thus the detected particles are selected both in momentum and rate of energy loss.

Arrangement of Counters

The mesons lose 7 Mev in the three anthracene crystals. The emergent 33-Mev beam strikes a target either of D_2O or H_2O, enclosed in thin Lucite boxes. Each is 4 cm thick, just enough to stop 33-Mev mesons.

The two fast protons resulting from disintegration of the deuteron proceed in almost opposite directions, and are detected by two NaI scintillation counters above and below the target (see Fig. 2). The five counters are place in fivefold coincidence to detect events in which two fast protons accompany a π^+ meson (see Fig. 3). Backgrounds from oxygen and chance coincidences are measured by replacing the D_2O by H_2O and taking the difference count.

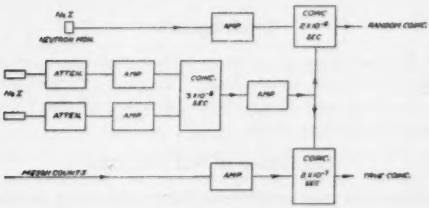

FIG. 3. Circuit arrangement. The meson telescope uses a three-fold addition coincidence circuit with a resolving time of about 2.5×10^{-8} sec. The circuit is provided with an additional discriminator so that pulses above a predetermined height in one channel actuate an anticoincidence circuit, thus setting a pulse-height "ceiling." The NaI counter amplifiers each comprise two cascaded Spencer-Kennedy model 202 200-mc wide chain amplifier. The extra NaI monitor provides a coincidence rate proportional to the random background in the true coincidence channel.

This procedure does not require that all mesons traversing the telescope be recorded; it requires that the triple coincidences be caused by mesons and that all disintegration protons (or a known fraction) be recorded. Thus, the arrangement is designed to measure the fraction of incident mesons that produce two fast protons.

To assist in evaluating random background, an extra NaI counter was used, which monitored the fast neutrons produced in the Al target. Experimentally, this counter gave a counting rate proportional to that recorded by the meson telescope. Thus, in coincidence with the two NaI proton counters, a rate proportional to the random background in the fivefold coincidence channel is produced and used to correct the observed rate in the event of variations in beam intensity.

The large light efficiency of the NaI counters made it possible to use a coincidence circuit[9] of resolving time

[9] R. L. Garwin, Rev. Sci. Instr. **21**, 569 (1950).

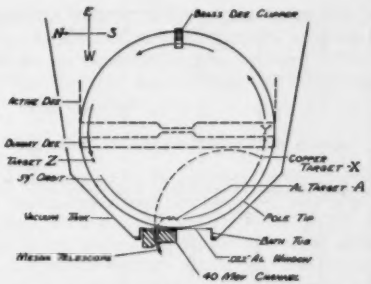

FIG. 4. Sources of contamination of the meson beam. The only region of the cyclotron which can provide fast positive particles that might emerge from the meson channel is that near X, Y. The beam clipper reduces the number of protons scattered in the target A which strike the dee.

3×10^{-8} sec, despite the fact that the light flashes from the crystals last about 0.5 μsec. This is possible only by sacrificing most of the light output and is feasible because the pulses counted represent 30 Mev or more spent in the crystal.

The coincidences between meson-telescope triple coincidences and NaI double coincidences were obtained from a 0.25 μsec resolving time 6AS6 mixer. The delays in all circuits were adjusted by using artificial pulses. The NaI monitor pulses were mixed with the meson telescope triples in an Atomic Instrument Company model 502 coincidence analyzer, using a 2.0 μsec resolving time to increase the random rate.

Meson Purity

As far as particles coming from the aluminum target are concerned, the combined selection of momentum and rate of energy loss is sufficient to distinguish mesons from all other particles. In fact, protons and deuterons from the target will be of such low energy that they will not traverse the telescope. However, the channel is not a sufficiently good collimator to prevent the emergence from it of fast particles originating from other parts of the cyclotron and the pulse-height selection has only fair resolution. It is therefore important to evaluate the contamination of the meson beam under the experimental conditions used.

From Fig. 4, we may consider the following sources of particles which may come down the channel: the target, the dee and dummy dee at the south side of the cyclotron, and neutron recoils. It was found, by placing a target in position X in Fig. 4, that large numbers of protons and deuterons could penetrate the meson channel and produce triple coincidences. No particles can appear from the spot X when the meson-producing target A is in use, but protons scattered through small angles from target A can strike the copper edges of the dee and dummy dee near the point Y. Consequently, an investigation was made of the counts to be expected from a copper target near this position—namely, at X.

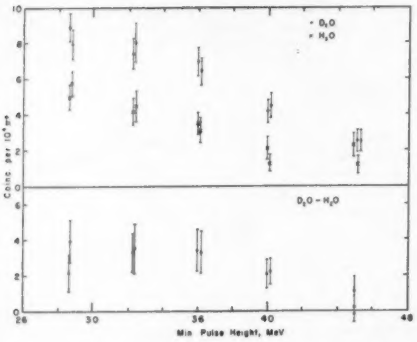

FIG. 5. Upper part: Fivefold coincidence rates observed with H_2O and D_2O targets as a function of minimum energy loss in each NaI crystal. These data are taken by changing the calibrated attenuator settings in both channels. Random background has not been subtracted. The results of two independent runs are shown. There is an uncertainty of about 10 percent in the absolute values of the energy loss (pulse height). Lower part: D_2O-H_2O differences, showing the "plateau" below 40 Mev and the disappearance of the difference at 50 Mev, in agreement with the expectations for the geometry used.

It was found from a range measurement, that high energy protons and deuterons were counted in approximately equal numbers, with a total counting rate 4 times the normal meson counting rate. It was shown further, that the ratio of fivefold to threefold coincidences with protons and deuterons being detected was approximately the same as with mesons being detected; but there was no significant difference (-0.000015 ± 0.00007 count per meson) between D_2O and H_2O. The only possible effect of any contamination, therefore, is to make us measure a spuriously low cross section.

Therefore, before each experimental run, a test was made on the threefold coincidences in the meson telescope. When absorbers are placed between the second and third crystals, the counting rate is not much affected until the meson range is reached. About 6 percent of the counts remain for a thick absorber; at least 4 percent of all counts are because of random coincidences, as estimated by placing a delay in one of the counters. This gives an upper limit of 2 percent of fast protons. The absorption curves show no sign of deuterons, but since the deuteron range expected is nearly the same as the meson range, we can only rule out a contamination of about 8 percent or more on this basis. The data taken with the copper target X indicate roughly equal numbers of protons and deuterons counted, and accordingly, we can reduce the upper limit on deuteron contamination to 2 percent on this basis.

A correction of 6 percent has therefore been applied to the observed data, to take into account both the random background of triple coincidences and any possible heavy particle contamination. This number may be slightly too small if any heavy particle contamination exists, but probably cannot exceed 8 percent since the proton and deuteron contamination should be about equal.

Neutron recoils were minimized by extensive lead shielding between the target and the counters. Also, at 180° to the target a beam clipper of 1-in. aperture was placed, which should absorb 80 percent of the protons scattered through small angles by the target. Only a fraction of the remaining 20 percent can strike the dee to produce neutrons in the forward direction to hit our counters, and extensive shielding is placed inside and outside the tank to reduce this effect still further. It is found that when a target at the position Z, Fig. 4, is inserted, the count in the meson telescope is many times its normal value, largely a result of random counts which represent at least a hundredfold increase in the fast neutron intensity. This indicates that with the normal targets, a negligible effect is to be expected from neutron recoils, as is verified by the meson absorption curves.

Counting Rate

In operation, an average meson counting rate of about 1000 min was available. This gave a fivefold true coincidence rate (D_2O-H_2O difference) of about one count in three minutes.

Calibration of NaI Counters

The NaI counters were calibrated by using protons recoiling from neutron collisions with paraffin; the fourfold recoil proton scintillation counter telescope used[10] was adjusted so that only protons losing a known minimum amount of energy in the last crystal were counted. Each NaI crystal in turn was inserted between the third and last crystals of the proton telescope and coincidences between the NaI counter and the recoil proton telescope recorded. By this means the attenuator setting was determined at which essentially all the protons of given energy loss in the NaI crystal were counted. The NaI crystals were quite uniform in sensitivity over their whole volume, and their efficiency exceeded 90 percent; it was assumed to be 100 percent.

It was found that despite all efforts at stabilization there was a slow drift in gain of the SKL model 202 amplifiers for the NaI counters. However, it was discovered that when the NaI counters were in the normal position, no pulses greater than about 200 Mev were obtained and that the pulse-height cutoff was sharp and could be reproduced to 5 percent or better. This served as a secondary calibration, to allow for the amplifier drifts.

Measurement of Disintegration Proton Energy

The ratio of fivefold to threefold coincidences was determined for several attenuator settings. D_2O and H_2O

[10] Guernsey, Mott, and Nelson, Phys. Rev. **83**, 873 (1951).

targets were interchanged frequently to compensate for amplifier and cyclotron drifts. A correction was made to the counting rates for the random coincidences, by observation of the random coincidence channel. This had been calibrated with faster counting rates in all channels. This correction for randoms always had only a small effect (less than 10 percent) on the D_2O-H_2O difference. The results are shown in Fig. 5. It is seen that a pleateau is to be found for the D_2O-H_2O difference effect and that the difference disappears at proton energies of 50 Mev and above. With 70–85-Mev protons incident normally on the NaI crystals, only 40 to 45 Mev are lost. Not many protons pass through the crystals with sufficient obliqueness to lose appreciably more energy. This cut-off value is therefore in agreement with expectation and serves as a check that the proper reaction is being observed.

Scattering and Crossfire of the Meson Beam

Not all the mesons which count in the threefold coincidence telescope traverse the entire D_2O target. Some are scattered out by multiple Coulomb scattering in the crystals and the target itself, and some are traveling in oblique directions originally. To investigate this effect, a fourth crystal was placed in coincidence with the three other crystals. Its dimensions, 1 in.$\times\frac{3}{4}$ in., were the same as the cross section of the D_2O target. The ratio of fourfold coincidences to threefold coincidences was measured for the crystal at various distances behind the telescope, and also with varying thicknesses of H_2O absorber in place. The resultant difference between the coincidence rates was integrated to give an over-all cross section correction of 11 percent.

Calculation of Effective Solid Angle

The fraction of deuterium disintegrations observed in our experiment depends upon the solid angle subtended at the target by the NaI counters, and also on the angular distribution of the disintegration protons with respect to the meson beam. To obtain this fraction, one must calculate the effective solid angle, as weighted by the angular distribution.

In making the calculation, we first assume an angular distribution of the form $A+\cos^2\theta$; this is in accord with the experimental data on the inverse reaction, as discussed below. For the isotropic portion of the distribution, the calculation is made by averaging the solid angle subtended by the crystals over the target volume, taking into account the requirement that both protons must traverse a minimum path in the crystals (enough to lose 30 Mev). The integration is performed numerically. The deviations from 180° in the angle between the protons, which never exceed 12°, are neglected, as are also the facts that the solid angle varies somewhat with the energy of the meson in the target, and the obliquity and scattering of the meson beam which somewhat increase the target volume and tend to increase the isotropy of the protons in the laboratory system. All these effects are estimated to be small.

For the $\cos^2\theta$ distribution, the averaging of the solid angle over the target volume is repeated with an appropriate weighting factor.

Variation of Cross Section with Energy

In order to ascertain the nature of the variation of the cross section with energy, we made two targets of H_2O and D_2O, each one-half the thickness of the usual target. An experiment was performed in which the D_2O and H_2O were alternately placed first and last in the meson beam. This difference between these two positions gives a measure of the difference between the yield averaged over meson energies from 33 to 23 Mev, and the yield averaged from 23 to 0 Mev. The result was 0.00004 ± 0.00005 disintegration per meson. This figure has to be corrected because some of the mesons scatter out of the targets before traversing the second target; the corrected figure becomes 0.00002 ± 0.00005.

If we assume that the variation of the cross section with energy is monotonic and of the form $\sigma\sim E^n$, we find $n=0.2\pm0.5$. If we compute the ratio of the cross section at the desired energy of 23 Mev to the cross section averaged over the range, as measured, we find, under the assumption of a dependence as E^n, that a correction factor of $[1+0.1n]$ must be applied. (This simple formula is valid for $-0.7\leqslant n\leqslant 1$.) It is thus clear that no appreciable correction is applicable and that the cross section as observed for the average over 33 to 0 Mev is essentially the same as the cross section at 23 Mev. This conclusion would be invalid if the variation of cross section with energy is not monotonic, e.g., if resonances occur. This seems quite unlikely on theoretical grounds, and our conclusion as to the nature of the yield curve has recently been verified.[11] The meson intensity available was not sufficient for us to attempt this verification.

RESULTS

In calculating the value of our experimental cross section, we have used all the data corresponding to the "plateau" of Fig. 4; the result follows from the equation

$$\sigma=P/(N\Omega S), \tag{4}$$

where P is the ratio of observed proton coincidences (D_2O-H_2O difference) to the number of mesons incident on the target, corrected for background and purity; N is the number of deuterium atoms per cm^2 in the target; Ω is the fraction of the total solid angle subtended by the NaI counters; and S is the correction for scattering of mesons out of the target. We found P was $3.55\pm0.49\times10^{-4}$, S was 0.89, and $N=2.67\times10^{23}$ cm^{-2}. Ω depends on the angular distribution assumed; the value of Ω is 0.30 for a pure $\cos^2\theta$ angular distribution, and 0.47 for an isotropic distribution. We have

[11] Durbin, Loar, and Steinberger, Phys. Rev. 83, 646 (1951).

assumed the NaI crystals 100 percent efficient; the true value is certainly close to this. A correction would tend to raise the calculated cross section.

The resulting cross sections are shown in Table I, for various values of A in the angular distribution function $A+\cos^2\theta$. Also shown are the computed values to be expected from the detailed balancing theorem [Eq. (3)] on the basis of the Berkeley data on the inverse reaction. The errors in Table I are probable errors. They include 10 percent in computation of the solid angle; 2 percent in the scattering measurement; a possibility that up to 10 percent of the proton coincidences are being missed; and 3 percent in the meson purity estimate. The last two errors could only raise the cross section.

Results for Inverse Reaction

The reaction $p+p\rightarrow\pi^++d$ has been studied by Richman, Cartwright, Peterson, and others.[12] The determination of the cross section is complicated by the presence of a competing reaction, $p+p\rightarrow n+p+\pi^+$. The yield of π^+ mesons has been measured at various angles,

TABLE I. Comparison of predicted and observed total cross sections for $\pi^++d\rightarrow p+p$, for various assumed angular distribution functions.

Angular dependence c. m. system	Predicted total cross section, mb Spin 0	Spin 1	Measured total cross section, mb
$\cos^2\theta$	2.55±0.6	0.85±0.2	5.0±0.9
$0.1+\cos^2\theta$	3.0 ±0.7	1.0 ±0.24	4.7±0.9
$0.5+\cos^2\theta$	4.2 ±1.0	1.4 ±0.35	4.2±0.8
$0.2\pm0.1+\cos^2\theta$	3.4 ±0.9	1.1 ±0.3	4.5±0.8

by different groups of experimenters, using different techniques, with generally concordant results.

In comparing these results with our value for the cross section of the inverse reaction, one must first separate out the part of the cross section caused by the reaction $p+p\rightarrow\pi^++d$, which yields monoenergetic mesons at any given angle. We must then evaluate the angular distribution, so that it can be used in the computation of the effective solid angle, and also integrate to obtain the total cross section. For the comparison of Table I we have used Richman's estimate[13] of the angular distribution $0.2\pm0.1+\cos^2\theta$ and Cartwright's value $1.3\pm0.26\times10^{-28}$ cm^2/sterad for the differential cross section at 0° in the laboratory system as obtained by analyzing the total meson spectrum into a continuum and a superposed monoenergetic line.[14]

CONCLUSION

We conclude from the comparison of Table I that the spin of the π^+ meson is zero.[11] The conclusion depends on certain assumptions: that we are in fact measuring the reaction we think we are, that the variation of cross section with energy is a monotonic function, and that the theorem of detailed balancing is applicable, so that the angular distribution can be correctly assumed from the inverse reaction. Further experiments which would definitely settle the last two points would certainly be desirable; however, we believe a spin of zero to be rather firmly established by the present results.

Statistically, the ability to distinguish between spin 1 and spin 0 is somewhat better than the quoted errors might suggest. If the true value of the cross section were the spin one value, we must consider the probability that in the time of observation we should observe the large number of counts that we did. We then must consider the probable error of the expected number of counts, not the probable error of the actual number of counts. The nonstatistical errors appear only as factors. This makes the likelihood that the spin is one equal to the likelihood that we have a deviation 5× the probable error. The odds against this exceed 1000:1. Thus, the result appears secure as far as statistics are concerned.

DISCUSSION

Meson Polarization

It has been pointed out to us by Kaplon[15] that the detailed balancing operation might not hold in the form of Eq. (3) if the meson has e.g., spin 1, and the mesons in both experiments are polarized, for this might disturb the averaging over all the spin states in the absorption experiment.

Let us suppose the mesons used in the present absorption experiment are polarized; they will then have preferred spin orientations relative to a specified direction, e.g., direction of incident proton beam. They strike and disintegrate deuterons which are unpolarized, having random spin orientations. With respect to any arbitrary direction, say the direction of the incident proton beam, the deuterons occupy in equal numbers states with $m_s=1, 0$, and -1. For each of these states we must now add the cross sections for the three possible polarizations of the meson. If the cross sections or angular distributions are orientation-dependent, the total cross section observed will depend upon the state of meson polarization even though the deuterons are unpolarized; it will be a suitable average over all polarization states.

Now it might happen that in the production reaction, all cross sections were negligible except that for the production of one state of polarization of the mesons; the total cross section observed for production would then be a result of this state alone. This would not matter in the application of detailed balancing, provided the meson beam used in the absorption reaction were unpolarized; the absorption reaction would then

[12] Cartwright, Richman, Whitehead, and Wilcox, Phys. Rev. **81**, 652 (1951); Crawford, Crowe, and Stevenson, Phys. Rev. **82**, 97 (1951).

[13] C. Richman, private communication.

[14] Richman, Cartwright, and Whitehead (quoted by K. M. Watson and K. A. Brueckner), Phys. Rev. **83**, 1 (1951).

[15] M. Kaplon, private communication.

take place for the mesons in this particular polarization state, and the correct spin value of 1 would be observed. However, if the meson beam is completely polarized in this unique favorable state, all the mesons contribute to the absorption reaction, and an effective statistical weight of 1, or spin zero, is observed.

Now if this has in fact happened, and spin zero is being counterfeited by spin 1 mesons, we can estimate how complete the polarization must be. If the polarization were 75 percent complete in one and the same spin state in both the production and absorption experiments, and the cross sections for this spin state greatly exceed those for the other spin states, a predicted cross section only two probable errors less than the observed cross section would result. In view of the fact that our meson beam consists of mesons coming off nearly backwards from an aluminum target (which mean) they have probably made collisions within the nucleuss it is difficult to suppose that they are 75 percent polarized, and in just such a direction as to correspond to the production case. We therefore think it highly unlikely that polarization effects can modify the conclusion of zero spin.

All these arguments are quite independent of the additional theoretical arguments against the existence of considerable polarization in either the production experiment or the inverse reaction. Thus, the mesons produced in a p-p collision are expected to be polarized in a vector meson model, but only at energies just above threshold. Theory[15] predicts negligible polarization for pseudovector mesons even at threshold.

Background from Oxygen

It is of some interest to consider the probability of two high energy protons coming from meson bombardment of an oxygen nucleus. These protons, by momentum considerations, would have to travel in approximately opposite directions, and so would be detected in our counters. When chance background has been subtracted, we find $2.5\pm1\times10^{-4}$ count per meson for protons above 30 Mev in our geometry. If the cross section for this process were geometrical and the angular distribution isotropic, we would expect 2.5×10^{-2} per meson. The small number we observe is not consistent with the two-nucleon hypothesis of Levinger,[16] according to which one might expect 1/10 geometrical cross section for such a process.

[16] J. S. Levinger, Phys. Rev. **82**, 300 (1951).

Meson Parity

If we consider the results of the experiment on π^- absorption in deuterium,[17] we conclude[18] that the π^- meson has odd parity if it has spin 0. If we now assume the same parity and spin for π^+ and π^- mesons, we must conclude that the π^+ and π^- mesons are pseudoscalar.

It ought to be pointed out that it is normally assumed that both the proton and neutron have even intrinsic parity, although there is, as far as we are aware, no evidence for such a belief. The intrinsic parities of the proton and neutron enter into consideration only in reactions in which a proton is transformed into a neutron or vice versa; thus, they are not important in ordinary nuclear combinations, becoming only a sign convention in nuclear models and ordinary nuclear reactions. However, in beta-decay or meson reactions, the intrinsic parities do indeed enter. Thus, in concluding that π-mesons are pseudoscalar, we assume that protons and neutrons have the same parity, if their parity type[19] is real; or opposite parities if it is imaginary.

ACKNOWLEDGMENTS

We are much indebted to the members of the cyclotron shops under E. Chandler, R. Mortenson, and H. Logemann for their assistance in the construction of the apparatus, and to the operating crew under F. Palmer for the smooth operation of the cyclotron. We are grateful to G. Guernsey, G. Mott, and B. Nelson for the use of their proton recoil telescope for calibrating our NaI crystals, and to many of the staff members of the cyclotron project for continued assistances and encouragement. We owe much to Professor Robert E. Marshak for his unfailing encouragement, especially at moments when the experiment appeared quite hopeless. The D_2O was allocated by the Atomic Energy Commission.

[17] Panofsky, Aamodt, and Hadley, Phys. Rev. **81**, 565 (1951).
[18] S. Tamor and R. E. Marshak, Phys. Rev. **80**, 766 (1950).
[19] C. N. Yang and J. Tiomno, Phys. Rev. **79**, 495 (1950).

The Pairing Effect in Nuclei and the Beta-Labile Elements*

TRUMAN P. KOHMAN
Department of Chemistry, Carnegie Institute of Technology, Pittsburgh, Pennsylvania
(Received September 5, 1951)

It has been shown previously that in certain regions of nuclides the pairing energy of protons exceeds that of neutrons. Statistical examination of the beta-stable odd-mass nuclides shows that this situation is probably fairly general except for light elements. Theoretical explanations of the effect are suggested. Its bearing on the beta-lability of technetium and promethium and the possible beta-lability of astatine and indium is discussed.

I. EMPIRICAL EVIDENCE

FROM an analysis of alpha- and beta-disintegration energies of the heavy nuclides, Glueckauf[1] has shown that the pairing energy of protons exceeds that of neutrons in heavy nuclei. Thus the masses of odd-A nuclides in this region do not lie on a single smooth surface, but on two parallel surfaces separated by about 0.2 Mev, with even-Z nuclides on the lower surface and odd-Z nuclides on the upper. The effect is similar to but much less pronounced than the well-known even-odd effect for even-A nuclides. By a somewhat different method of analysis for which more experimental data were available, this finding has been substantiated.[2]

Kowarski[3] has postulated that such a situation exists in regions of open-shell neutrons, in order to explain the occurrence of the beta-labile elements $_{43}$Tc and $_{61}$Pm beyond closed neutron shells. Suess[4] has adduced experimental evidence for this from beta-disintegration energies.

A classification of the beta-stable odd-A nuclides according to parity of Z, Table I, shows a greater frequency of even values than of odd, everywhere except in the region of light nuclei. The inequality seems too great to be a matter of chance and strongly suggests that the effect in question is fairly general for medium-weight as well as heavy nuclei.

TABLE I. Classification of beta-stable odd-A nuclides.

Range of A	Number of beta-stable odd-A nuclides with Even Z	Odd Z
1–39	8	11
41–79	9	11
81–119	13	7
121–159	11	8
161–199	12	8
201–243	9	7
Total	62	52

The apparent generality of this effect suggests that the pairing energy term of atomic mass equations based on statistical concepts, such as those of Bethe and Bacher[5] and of Bohr and Wheeler,[6] should be modified as follows:

$-\frac{1}{2}\delta_A$ for even A, even Z,
$-\frac{1}{2}\epsilon_A$ for odd A, even Z,
$+\frac{1}{2}\epsilon_A$ for odd A, odd Z,
$+\frac{1}{2}\delta_A$ for even A, odd Z.

If π_A is the excess energy associated with an unpaired proton and ν_A that for an unpaired neutron in nuclei of mass number $\sim A$, then $\delta_A=\pi_A+\nu_A$ and $\epsilon_A=\pi_A-\nu_A$.

II. THEORETICAL CONSIDERATIONS

An explanation of this inequality in pairing energy of protons and neutrons has been sought in terms of several possible contributions to the pairing energy:

1. Exclusion Principle

Consider an independent-particle nuclear model in which protons and neutrons move freely in the same potential well, with nondegenerate energy levels fairly evenly spaced. Since the Pauli exclusion principle allows two nucleons of each kind to a level, in the ground state of a nucleus with $N>Z$ the levels are occupied by neutrons to a higher energy than by protons (the difference being approximately the electrostatic energy of a proton in the field of the other protons). In any such potential, the average spacing between levels decreases with increasing energy, so that the spacing at the top of the proton distribution, S_p, is greater than that at the top of the neutron distribution, S_n. It can be shown from simple considerations that in this model $\pi_A=\frac{1}{4}S_p$ and $\nu_A=\frac{1}{4}S_n$, so that $\delta_A=\frac{1}{4}(S_p+S_n)$ and $\epsilon_A=\frac{1}{4}(S_p-S_n)$. Using the statistical mechanical formula[7] for average level spacings of noninteracting particles of mass m and twofold spin degeneracy confined to a sphere of radius r:

$$S_p=\tfrac{1}{3}(3/4\pi)^{4/3}(h^2/mr^2)(\tfrac{1}{2}Z)^{-\frac{1}{3}},$$
$$S_n=\tfrac{1}{3}(3/4\pi)^{4/3}(h^2/mr^2)(\tfrac{1}{2}N)^{-\frac{1}{3}}$$

* This work was assisted by the AEC. A part of it was done at the Radiation Laboratory, University of California at Berkeley. I am indebted to Professor G. C. Wick for advice on several points.
[1] E. Glueckauf, Proc. Phys. Soc. (London) **61**, 25 (1948).
[2] Unpublished work with G. T. Seaborg.
[3] L. Kowarski, Phys. Rev. **78**, 477 (1950).
[4] H. E. Suess, Phys. Rev. **81**, 1071 (1951).
[5] H. A. Bethe and R. F. Bacher, Revs. Modern Phys. **8**, 82 (1936).
[6] N. Bohr and J. A. Wheeler, Phys. Rev. **56**, 426 (1939).
[7] E. Feenberg, Revs. Modern Phys. **19**, 239 (1947).

there results for a typical heavy nucleus:

$$S_p = 0.28 \text{ Mev}, \quad \delta_A = 0.13 \text{ Mev},$$
$$S_n = 0.24 \text{ Mev}, \quad \epsilon_A = 0.01 \text{ Mev}.$$

A more realistic (tapering) nuclear potential would give a more rapid decrease of level spacing with increasing energy, but this could hardly more than double ϵ_A. Thus the exclusion principle accounts for only about a tenth of the experimentally observed values of both δ_A and ϵ_A.

2. Electromagnetic Interaction

Besides the electrostatic interaction between two protons, there should be an electromagnetic interaction between any two nucleons due to their magnetic dipole moments, which approximates the coupling between two permanent magnets having the same moments and orientation and separated by a distance of the order of nuclear dimensions. If the measured moment of an odd-nucleon nucleus can be attributed entirely to the odd particle, the observation that odd-proton nuclei usually have larger moments than odd-neutron nuclei can be considered as evidence for larger moments for protons than for neutrons in general. This results from the fact that the orbital charge motion of a proton can make an important contribution to its net moment. The paired nucleons are assumed to have magnetic moments equal in magnitude and opposite in direction. The coupling energy is given roughly by $\xi \sim \mu^2/d^3$, where d is an appropriate distance. Taking as representative values $\mu_p = 3$ and $\mu_n = 1$ in nuclear magnetons and $d \sim 3 \times 10^{-13}$ cm, there results $\xi_p \sim 0.005$ Mev and $\xi_n \sim 0.0006$ Mev, so that the contribution to $\epsilon_A = \xi_p - \xi_n \sim 0.004$ Mev. Again the contribution is in the right direction but is only a small part of the observed magnitude.

3. Overlap Effect

The main part of the pairing energy is presumably due to the similarity of the spatial parts of the wave functions of the pairing nucleons and the consequent extensive overlap.[8] Thus the mutual attraction of the pairing nucleons is greater than the average for two random nucleons in the same nucleus. In nuclei having considerably more particles of one kind than the other, the general character of the orbitals at the tops of the two distributions will be different, so it is quite plausible that there might be a difference in the magnitude of the overlap energy for the two types of particles. Unfortunately, there is no simple way of estimating the magnitude of this effect, nor is any reason apparent why the effect should be consistently greater for protons than for neutrons. In fact Suess[4] suggests that in certain regions of nuclides the neutron pairing energy exceeds that of protons; in such regions ϵ_A would take on negative values.

[8] E. Feenberg, Phys. Rev. **76**, 1275 (1949).

III. THE BETA-LABILE ELEMENTS

A favoring of even values of Z for odd-A nuclides can help to explain the complete beta-lability of the odd-Z elements mentioned, as noted by Kowarski[3] and Suess.[4] However, from the evidence cited above it appears that this effect is not limited to the regions in which these elements occur, but is fairly general. Therefore it alone could hardly be the whole explanation, or there would presumably be a considerable number of such beta-labile elements.

On the other hand, it has been noted on several occasions[8, 9–12] that both of these beta-labile elements occur near closed neutron shells, with $N = 50$ and $N = 82$. Aten[10] has explained how the closing of a shell perturbs the normal mass valley so that the line of maximum beta-stability[6, 13] tends to run more nearly parallel to the line joining the closed-shell isotopes or isotones at the point of crossing. Its slope is thus decreased near closed proton shells and increased near closed neutron shells, and in the latter case the possibility of beta-stable odd-A isotones is enhanced. However, only right at the point of crossing is the increase in the slope ever sufficiently great to stabilize a pair of odd-A isotones unassisted. This does occur at $N = 20$ and $N = 82$, but here the labilized nuclides have even Z, so beta-labile elements do not result.

In the combination of these two effects, individually insufficient, probably lies the explanation of the beta-lability of technetium and promethium. It is not necessary, however, that such an occurrence should be associated with every pronounced neutron shell closure, since other, seemingly accidental, factors are also involved. There is a distinct possibility on experimental grounds that $_{85}$At is completely beta-labile,[12] but this is not necessarily to be expected as has been postulated.[12]

It seems likely that $_{49}$In is also beta-labile. In^{115} is known[14–16] to be unstable with respect to Sn^{115}. Evidence has been obtained[15] for cadmium L x-rays associated with electron-capture decay of In^{113} to Cd^{113}, and the anomalously high absorption half-thickness found[16] for the In^{115} β-rays might be accounted for by an admixture of cadmium K x-rays. The beta-lability of this element may likewise be explained by a combination of two effects. The stronger pairing of protons, as compared to neutrons, helps to stabilize Cd^{113} relative to In^{113}, but this is certainly insufficient to make both indium isotopes unstable in a region where the beta-stability curve has such a low slope. The lability of In^{115} relative to Sn^{115} is attributable to the especial stability of 50-proton configurations.

[8] A. Broniewski, Compt. rend. **228**, 916 (1949).
[10] A. H. W. Aten, Science **110**, 260 (1949).
[11] W. D. Harkins, Phys. Rev. **76**, 1538 (1949).
[12] Perlman, Ghiorso, and Seaborg, Phys. Rev. **77**, 26 (1950).
[13] T. P. Kohman, Phys. Rev. **73**, 16 (1948).
[14] Bell, Ketelle, and Cassidy, Phys. Rev. **76**, 574 (1949).
[15] S. G. Cohen, Nature **167**, 779 (1951).
[16] E. A. Martell and W. F. Libby, Phys. Rev. **80**, 977 (1950).

The Nuclear Magnetic Moment of S^{33} from Microwave Spectroscopy*

J. R. Eshbach,† R. E. Hillger,‡ and M. W. P. Strandberg
Research Laboratory of Electronics, Massachusetts Institute of Technology, Cambridge, Massachusetts
(Received October 15, 1951)

The magnetic dipole moment of the S^{33} nucleus was determined by means of the Zeeman effect on the hyperfine pattern of the $J=1\rightarrow 2$ rotational absorption of the molecule $O^{16}C^{12}S^{33}$ at about 24,020 Mc/sec. The result is

$$\mu(S^{33}) = +0.633 \pm 0.010 \text{ nuclear magneton.}$$

The sign of this moment was determined by using circularly polarized microwave radiation with σ-type Zeeman observations.

The frequencies of all of the components of the hyperfine pattern were measured. They all fit the nuclear electric quadrupole coupling theory to within ± 0.01 Mc/sec. The measured value for eqQ of the S^{33} nucleus in $O^{16}C^{12}S^{33}$ is

$$eqQ(O^{16}C^{12}S^{33}) = -29.07 \pm 0.01 \text{ Mc/sec.}$$

I. INTRODUCTION

THE INTERACTION OF NUCLEI WITH MOLECULAR ROTATION

MOST molecules have $^1\Sigma$ electronic ground states, which means that these molecules have zero electronic orbital and spin angular momenta. Thus, the total angular momentum, which is a constant of the motion of the system of particles comprising the molecule, is instantaneously the vector sum of the angular momentum of molecular-rotation and the spin-angular-momenta of the nuclei. These component angular momenta are not constant in time, since in general there are interaction forces between them. The magnetic dipole moment of the total molecule is therefore some combination of the rotational magnetic moment, discussed elsewhere,[1,2] and the nuclear magnetic moments. Since one can observe different known combinations of the nuclear moments with the rotational moment, they can be deduced separately. The results given in reference 1 show that the rotational magnetic moments are of the same order of magnitude as nuclear moments.

Usually the interaction energies between the nuclear spins and the molecular rotation are very small compared to the rotational energy of the molecule. In the limit of no interaction the orientation of the nuclear spins with respect to molecule fixed axes cannot affect the molecular energy and the energy levels may be labeled with the rotational quantum numbers alone. For a linear molecule let J be the rotational quantum number and I the spin quantum number of one of its nuclei. Then, if there is no interaction, the rotational levels may be specified by J alone, since the various permitted combinations of I with a given value of J will all result in the same energy. In this case the rotational angular momentum and the nuclear spin are separate constants of the motion as well as the total angular momentum.

If a small interaction between I and J exists, then the rotational energy level labeled by a given value of J will become a group of closely spaced levels each of which must now be labeled with a value of the total angular momentum quantum number, F. F takes on all integrally spaced values from $J+I$ to $|J-I|$. A rotational absorption, which resulted in a single line in the absence of interaction, becomes a group of closely spaced lines when the interaction is present. Such a group is called a hyperfine pattern. The allowed rotational transitions (molecular electric dipole transitions are normally observed in microwave spectroscopy) which give rise to the hyperfine pattern are given by the selection rules $\Delta F=0, \pm 1$ (but $F=0\rightarrow 0$ is not allowed), and $\Delta M_F=0, \pm 1$. The relative spacings between the lines of a hyperfine pattern depend on the type of interaction causing the splitting, while the magnitude of the spacings depends, of course, on the strength of the interaction.

Two types of interactions between a nucleus and molecular rotation have been important in microwave spectroscopy up to now. Of greatest importance is the interaction of the nuclear electric quadrupole moment with the gradient of a component of the electric field at the nucleus due to the remainder of the molecule.[3,4] Of secondary importance is the energy of the nuclear magnetic dipole moment in the weak magnetic field due to molecular rotation. This magnetic dipole-dipole energy alone is usually too small to cause a hyperfine pattern resolvable by present-microwave spectroscopic methods, but its importance must be recognized in some cases as a small correction to the electric quadrupole type of splitting in order to account for experimental data.[5,6]

* This work has been supported in part by the Signal Corps, the Air Materiel Command, and the ONR.
† Now at General Electric Research Laboratory, Schenectady, New York.
‡ Now at Snow and Schule, Cambridge, Massachusetts.
[1] J. R. Eshbach and M. W. P. Strandberg, Phys. Rev. **85**, 24 (1952).
[2] C. K. Jen, Phys. Rev. **81**, 197 (1951).
[3] Daily, Kyhl, Strandberg, Van Vleck, and Wilson, Phys. Rev. **70**, 984 (1946).
[4] J. Bardeen and C. H. Townes, Phys. Rev. **73**, 97 (1948).
[5] H. M. Foley, Phys. Rev. **72**, 504 (1947).
[6] J. M. Jauch, Phys. Rev. **74**, 1262 (1948).

A well-resolved hyperfine pattern is essential for the measurement of a nuclear magnetic moment by the Zeeman effect on a rotational absorption line. Let eqQ be the quadrupolar interactions energy, where Q is the nuclear electric quadrupole moment and $q=(\partial^2V)/(\partial z^2)$, the second derivative along the molecular axis of the electrostatic potential at the nucleus; and let the energy of the molecule in an externally applied magnetic field be $-\mu H$, where μ is an effective magnetic dipole moment for the total molecule. Two limiting cases are evident, $|\mu H|\ll|eqQ|$ and $|\mu H|\gg|eqQ|$. In the first, or weak field case, the nuclear spin and the molecular rotation combine in the same way as when no field was present and the permitted transitions are given by the same selection rules as before. In the strong field case the nuclear moment and the rotational magnetic moment tend to orient themselves in the applied field independent of each other and the proper magnetic quantum numbers become M_I and M_J, instead of M_F. Also, the selection rules for the rotational transitions observed by the microwave absorption method become $\Delta M_J=0, \pm1$ and $\Delta M_I=0$. These considerations show that in order to determine the nuclear magnetic moment a resolved Zeeman pattern must be obtained under weak field conditions, since the selection rule $\Delta M_I=0$ means that the nuclear moment does enter into the observed strong field transitions. This is the same as saying that a well-resolved quadrupole hyperfine pattern is required, since in the case of an unresolved hyperfine pattern a strong field condition is necessary to produce resolved Zeeman components. This more or less intuitive picture is substantiated by the quantitative expressions given below.

II. THEORETICAL BACKGROUND

The effect of nuclear electric quadrupole coupling in the case of atomic spectra was first investigated quantum-mechanically by Casimir.[7] Casimir's results have subsequently been applied to nuclear quadrupole interaction with molecular rotation.[3,4,8,9] For a symmetric top molecule the diagonal quadrupole energy, which must be added to the unperturbed rotational energy, is

$$E_q(I,J,K,F)=eqQ\left[\frac{3K^2}{J(J+1)}-1\right]G(I,J,F), \quad (1)$$

where

$$G(I,J,F)=\frac{\frac{3}{4}C(C+1)-I(I+1)J(J+1)}{2(2J+3)(2J-1)I(2I-1)},$$

$$C=F(F+1)-I(I+1)-J(J+1).$$

In the case of a linear molecule this becomes simply

$$E_q(I,J,F)=-eqQG(I,J,F). \quad (2)$$

The Zeeman effect on the resulting hyperfine pattern has been treated theoretically by Jen[10,11] and Coester[12] following the procedure used in atomic spectra.[13] If the resolved hyperfine splitting is caused by the interaction of a single nucleus of the molecule, the others having $I<1$ or negligible interaction, then the total Hamiltonian for the rotating molecule in a magnetic field, $\mathbf{H}$, may be written

$$\mathcal{H}=\mathcal{H}_0+\mathcal{H}_q+\mathcal{H}_m, \quad (3)$$

where $\mathcal{H}_0$ is the rotational energy; $\mathcal{H}_q$ is the quadrupole interaction energy; and

$$\mathcal{H}_m=-\mu_0[g_{\text{mole}}(\mathbf{J}\cdot\mathbf{H})+g_{\text{nuc}}(\mathbf{I}\cdot\mathbf{H})], \quad (4)$$

where $\mu_0=e\hbar/2M_pc$, the nuclear magnetron (M_p= the proton mass), g_{mole} is the molecular rotational g-factor and may depend on the rotational quantum numbers as explained in reference 1, and g_{nuc} is the nuclear g-factor.

In a weak magnetic field, $|\mathcal{H}_m|\ll|\mathcal{H}_q|$, the $IJKFM_F$ representation is suitable. The energy levels are given by

$$E=E_0(J,K)+E_q(I,J,K,F)+E_m(I,J,K,F,M_F), \quad (5)$$

where $E_0(J,K)=BJ(J+1)+(A-B)K^2$ for a symmetric top and is diagonal in this representation. (A and B are the rotational constants for the molecule.) $\mathcal{H}_q$ has the diagonal elements given in Eq. (1). There are also off-diagonal elements of $\mathcal{H}_q$ with respect to J, but these are usually negligible since they represent an interaction with levels remote with respect to $\mathcal{H}_q$; they do not affect the Zeeman splittings in this case anyway. $\mathcal{H}_m$ has the diagonal elements

$$E_m(I,J,K,F,M_F)=-M_F\mu_0H[\alpha_Jg_{\text{mole}}+\alpha_Ig_{\text{nuc}}], \quad (6)$$

where

$$\alpha_J=[F(F+1)-I(I+1)+J(J+1)]/[2F(F+1)],$$

$$\alpha_I=[F(F+1)-J(J+1)+I(I+1)]/[2F(F+1)],$$

and $M_F=F, F-1, \cdots, -F$ so that each hyperfine level splits into $2F+1$ levels in the presence of a magnetic field. These expressions are identical with those of Back and Goudsmit[13] for the Zeeman effect on the hyperfine structure of atomic levels. The off-diagonal elements of $\mathcal{H}_m$ will be discussed shortly.

In the strong field case, $|\mathcal{H}_m|\gg|\mathcal{H}_q|$, the $IJKM_IM_J$ representation is proper. $\mathcal{H}_m$ is diagonal and its elements are

$$E_m=-\mu_0H[M_Jg_{\text{mole}}+M_Ig_{\text{nuc}}]. \quad (7)$$

The quadrupole energy expression in the strong field is given by Coester,[12] but it is quite complicated and is not needed for the following discussion.

The selection rules are affected by the presence of a magnetic field. In the weak field case $\Delta M_F=0$ transitions occur when the electric vector of the incident microwave radiation is parallel to the applied magnetic

[7] H. B. G. Casimir, *On the Interaction Between Atomic Nuclei and Electrons* (Teyler's Tweede Genootschap, De Erren F. Bohn, Haarlen, 1936).
[8] Kellogg, Rabi, Ramsey, Jr., and Zacharias, Phys. Rev. **57**, 677 (1940).
[9] J. H. Van Vleck, Phys. Rev. **71**, 468 (A) (1947).
[10] C. K. Jen, Phys. Rev. **74**, 1396 (1948).
[11] C. K. Jen, Phys. Rev. **76**, 1494 (1949).
[12] F. Coester, Phys. Rev. **77**, 454 (1950).
[13] E. Back and S. Goudsmit, Z. Phys. **47**, 174 (1928).

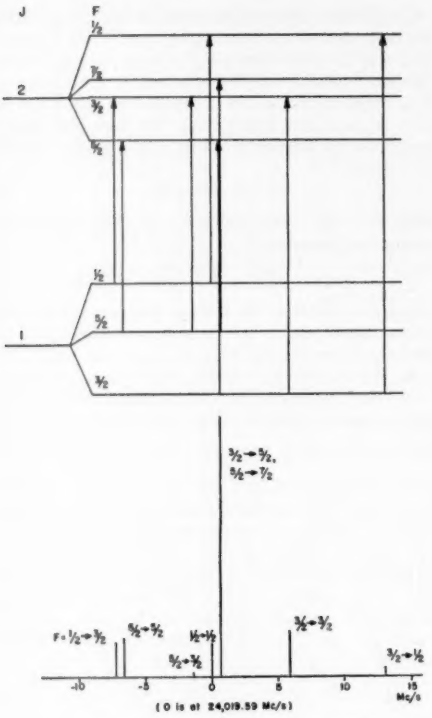

FIG. 1. The $J=1\rightarrow2$ hyperfine pattern of $O^{16}C^{12}S^{32}$.

field (π-transitions) and $\Delta M_F=\pm1$ transitions occur if it is perpendicular to the applied field (σ-transitions). For a strong field condition the selection rules become $\Delta M_J=0$, $\Delta M_I=0$ for π-transitions and $\Delta M_J=\pm1$, $\Delta M_I=0$ for σ transitions.

Using these selection rules and expression for the first-order Zeeman effect, Eq. (6), the expression for the transition frequencies under weak field conditions for a linear molecule (g_{mol} is the same for both the initial and final levels) is found to be:

For π transitions ($\Delta M_F=0$)

$$\Delta\nu_m=M_F(\mu_0/\hbar)H(g_{\text{mol}}-g_{\text{nuc}})(\alpha_{J1}-\alpha_{J2}). \quad (8)$$

For σ transitions ($M_F\rightarrow M_F\pm1$)

$$\Delta\nu_m=(\mu_0/\hbar)H\{g_{\text{mol}}[M_F(\alpha_{J1}-\alpha_{J2})\pm\alpha_{J2}] +g_{\text{nuc}}[M_F(\alpha_{I1}-\alpha_{I2})\pm\alpha_{I2}]\}, \quad (9)$$

where α_{J1} and α_{J2} are the α_J's of the initial and final levels respectively, and α_{I1} and α_{I2} are the α_I's of the initial and final levels.

As has been pointed out, the weak field case is of greatest interest for the purpose of measuring nuclear moments. However, a resolved Zeeman effect under true weak field conditions, in the sense that the off-diagonal elements of $\mathcal{H}_m$ are negligibly small, is often not fully realized experimentally. In particular, for the OCS[33] experiment described below it was found that even the second order correction, as given in Coester's paper, was not always sufficient to satisfy the experimental data; but, as shown in the following, the matrix of $\mathcal{H}_m$ is sometimes simple enough to permit exact diagonalization at any given intermediate field strength rather than relying on perturbation approximations.

In the $IJKFM_F$ representation $\mathcal{H}_m$ is diagonal with respect to M_F so that only states with the same M_F can mix with each other, and for a given M_F matrix the only off-diagonal elements are between F and $F\pm1$ levels. Only the off-diagonal elements for levels of the same J need be considered since the energy difference between levels of different J is large enough to make the perturbation between J and $J\pm1$ levels truly negligible except in extremely strong fields. Thus, the energy matrix for a given M_F under consideration is of the form

$F\diagdown F$	$I+J$	$I+J-1$	·	$\lvert M_F\rvert+1$	$\lvert M_F\rvert$
$I+J$	X	X	0	0	0
$I+J-1$	X	X	X	0	0
·	0	X	X	X	0
$\lvert M_F\rvert+1$	0	0	X	X	X
$\lvert M_F\rvert$	0	0	0	X	X

where the X's indicate the nonzero elements. It is to be noted that only states for which $|M_F|\leqslant F$ exist. The diagonal elements of this matrix are given in Eqs. (5), (1), and (6). The off-diagonal elements are given by Coester[12] and are

$$(F, M_F|\mathcal{H}_m|F-1, M_F) =\mu_0H(g_{\text{nuc}}-g_{\text{mole}})[(F^2-M_F^2)R(F)]^{\frac{1}{2}}, \quad (10)$$

where

$$R(F)=[F^2-(I-J)^2][(I+J+1)^2-F^2]/[4F^2(2F-1)(2F+1)]$$

and $\mathcal{H}_m$ is given in Eq. (4).

TABLE I. Measured frequencies for the $J=1\rightarrow2$ hyperfine pattern of $O^{16}C^{12}S^{32}$.

Transition $F_1\rightarrow F_2$	Intensity[a] ($\alpha\times10^6$)	Measured frequency present Work[b] (Mc/sec)	Measured frequency Townes and Geschwind[c] (Mc/sec)
1/2→3/2	3.2	24,012.33	24,013.04
5/2→5/2	3.4	24,012.94	
5/2→3/2	0.4	24,018.13	
1/2→1/2	3.2	24,019.59	24,020.21
3/2→5/2, 5/2→7/2	23.3	24,020.23	
3/2→3/2	4.1	24,025.42	24,025.39
3/2→1/2	0.7	24,032.68	24,032.75

[a] α is the absorption coefficient in cm^{-1} for an OCS sample with all the component atoms occurring in their natural abundance.
[b] All frequencies are measured to ±0.02 Mc/sec.
[c] See reference 15.

The exact diagonalization of these matrices was used in the analysis of the OCS^{33} experiment. A convenient method of solution for the roots of such a matrix is the continued fraction scheme described by Crawford and Cross.[14]

III. ELECTRIC QUADRUPOLE COUPLING OF THE S^{33} NUCLEUS IN $O^{16}C^{12}S^{33}$

The nuclear spin of the sulfur isotope of mass number 33 was determined by Townes and Geschwind[15] by measuring the relative splittings in the hyperfine pattern of the $J=1\rightarrow2$ transition of carbonyl sulfide ($O^{16}C^{12}S^{33}$) at about 24,020 Mc/sec. Carbonyl sulfide is a linear molecule[16,17] and the spins of both O^{16} and C^{12} were known to be zero.[18] The observed frequencies were found to best fit the nuclear quadrupole coupling expression, Eq. (2), if $I(S^{33})=3/2$ and $eqQ(OCS^{33})=-28.5\pm0.7$ Mc/sec. In their experiment, because of low resolution, they did not observe the complete pattern which should occur for $I=3/2$ but the observed pattern and line shapes were compared with those for several possible values of I.

In the present work this quadrupole hyperfine pattern was remeasured preliminary to the Zeeman effect experiment [determination of the nuclear magnetic dipole moment $\mu(S^{33})$].

A sample of carbonyl sulfide, prepared from sulfur enriched in S^{33} to 5.54 percent (about 7.5 times the natural abundance), was used for this experiment.[19] This enrichment provided a corresponding increase in the absorption intensities. The increased intensities and the use of a high sensitivity spectrograph to be described in a future report afforded the opportunity of measuring the entire pattern and of completely resolving all the hyperfine components.

TABLE II. Comparison of measured and theoretical hyperfine splittings for $eqQ(OCS^{33})=-29.07$ Mc/sec.

Transition $F_1\rightarrow F_2$	$\Delta\nu$ measured[a] (Mc/sec)	$\Delta\nu$ calculated[a] (Mc/sec)	Discrepancy (measured-calculated) (Mc/sec)
1/2→3/2	−7.27	−7.27	0.00
5/2→5/2	−6.66	−6.65	−0.01
5/2→3/2	−1.47	−1.46	−0.01
1/2→1/2	−0.01	0.00	−0.01
3/2→5/2, 5/2→7/2	0.63	0.62	+0.01
3/2→3/2	5.82	5.81	+0.01
3/2→1/2	13.08	13.08	0.00

[a] The calculated $\Delta\nu$'s are taken from the $F=1/2\rightarrow1/2$ frequency and the measured $\Delta\nu$'s are taken so as to give a least square fit.

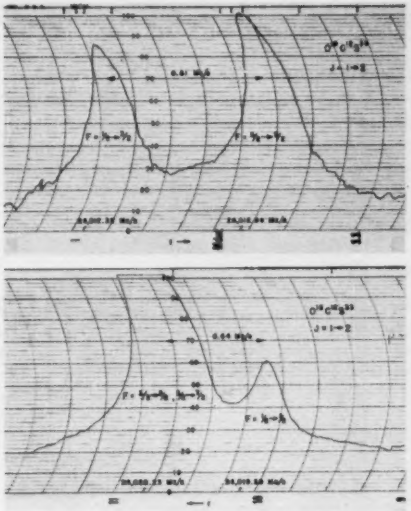

FIG. 2. Part of the $O^{16}C^{12}S^{33}$ hyperfine pattern.

The allowed transitions and the resulting hyperfine patterns are displayed in Fig. 1.

The measured frequencies for these transitions are given in Table I. All of the relative frequency splittings are in agreement with the quadrupole coupling theory to within ±0.01 Mc/sec if $I(S^{33})=3/2$ and $eqQ(OCS^{33})=-29.07$ Mc/sec. The calculated splittings using these values are compared with the measured splittings in Table II. The frequencies reported by Townes and Geschwind are also given in Table I. Their frequency for the unresolved $F=1/2\rightarrow3/2$, $5/2\rightarrow5/2$ transitions is apparently in error since it falls outside of the frequencies of the resolved lines (which are of nearly equal intensity) as measured in the present experiment. Also their value for eqQ does not fit their measured individual relative splittings too well, although it represents an average fit of their data.

Since the fit obtained in the present experiment with the quadrupole coupling expression, Eq. (2), was exact to within the capability of the experiment, it is presumed that the coupling of the S^{33} nucleus through its magnetic dipole interaction with the molecular magnetic field is less than 0.01 Mc/sec and also that the effects of off-diagonal elements of the quadrupole energy matrix are correspondingly small, as was previously pointed out. In the analysis of the Zeeman effect data the value

$$eqQ(OCS^{33})=-29.07\pm0.01 \text{ Mc/sec}, \qquad (11)$$

was therefore used.

[14] B. L. Crawford and P. C. Cross, Jr., J. Chem. Phys. **5**, 621 (1937).
[15] C. H. Townes and S. Geschwind, Phys. Rev. **71**, 562 (1947).
[16] G. Herzberg, *Molecular Spectra and Molecular Structure II: Infrared and Raman Spectra of Polyatomic Molecules* (D. Van Nostrand Company, Inc., New York, 1950).
[17] Strandberg, Wentink, and Kyhl, Phys. Rev. **75**, 270 (1949).
[18] H. L. Poss, Brookhaven National Laboratory Report 26 (T-10), October 1, 1949.
[19] The authors are indebted to C. K. Jen for the loan of this OCS sample. Then enhanced S^{33} was initially obtained from the Isotopes Division of the Atomic Energy Commission.

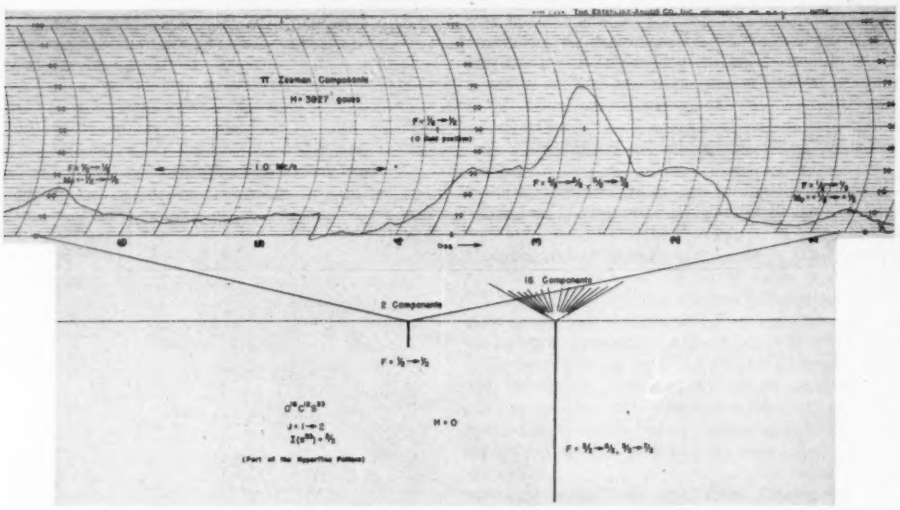

FIG. 3. π Zeeman components of the $F=3/2\rightarrow5/2$, $5/2\rightarrow7/2$ and the $F=1/2\rightarrow1/2$ lines.

Spectrograms of some of the lines of this hyperfine pattern are shown in Fig. 2.[20]

IV. THE ZEEMAN EFFECT EXPERIMENT AND RESULTS

Previous attempts to measure the nuclear magnetic moment of S^{33} by means of the Zeeman effect on the $J=1\rightarrow2$ rotational transition of $O^{16}C^{12}S^{32}$ have not been in agreement in spite of the large uncertainties assigned.[18,21] The difficulties lay in the low intensities of these lines with the natural abundance of S^{33} (0.74 percent) and the sensitivity of the spectroscopes used. A high sensitivity spectrograph ($\alpha_{\min}\simeq3\times10^{-9}$ cm^{-1}) and the OCS sample previously mentioned were used in the present experiments to determine $\mu(S^{33})$ by the method outlined in Part II. Both π- and σ-transitions were observed using linearly polarized microwave radiation. As is seen from the theory reviewed in Part II, the absolute values of both g_{nuc} and g_{mole} and their relative sign may be obtained from such measurements. A σ transition observation using circularly polarized radiation then served to fix the absolute sign of the g-factors. Actually g_{mole} may be obtained from a separate experiment. $g_{\text{mole}}(O^{16}C^{12}S^{32})$ is easily obtained from σ type Zeeman measurements on the $O^{16}C^{12}S^{32}$ rotational spectrum since all the nuclear spins involved are zero. According to the theory of rotational magnetic moments, $g_{\text{mole}}(O^{16}C^{12}S^{33})$ may then be found by multiplying by the ratio of the molecular moments of inertia. Since $g_{\text{mole}}(OCS^{32})$ had been previously determined,[1,2] its value was used as a check on the analysis of the data

TABLE III. π-transition Zeeman measurements on the $J=1\rightarrow2$ hyperfine pattern of $O^{16}C^{12}S^{33}$. ($H=3912$ gauss.)

Transition $F_1\rightarrow F_2$ (M_F)	$\Delta\nu$ measured (Mc/sec)	$\Delta\nu_{\text{calc}}$ exact diagonalization (Mc/sec)		Discrepancy with measured $\Delta\nu$	$\Delta\nu_{\text{calc}}$ 1st order theory only (Mc/sec)	Discrepancy with measured $\Delta\nu$
1/2→1/2	3.530					
(±1/2)	3.530					
	3.515					
	3.509					
	——	3.521	3.513	+0.008	3.567	−0.046
3/2→1/2		2.286	2.275	+0.011	2.320	−0.034
(±1/2)						
1/2→3/2	2.005					
(±1/2)	2.002					
	1.995					
	1.985					
	2.014					
	2.018					
	——	2.003	1.999	+0.004	1.963	+0.040
5/2→5/2	1.537					
(±5/2)	1.521					
	1.516					
	1.505					
	1.523					
	1.525					
	——	1.521	1.528	−0.007	1.527	−0.006

[20] After completion of the present work the following frequencies have been reported by Geschwind and Gunther-Mohr [referred to by Wentink, Koski, and Cohen, Phys. Rev. **81**, 948 (1951)], for some of the hyperfine components of the transition under consideration.

$F_1\rightarrow F_2$	Frequency (Mc/sec)
1/2→3/2	24,012.292
5/2→5/2	24,012.974
1/2→1/2	24,019.641
3/2→5/2, 5/2→7/2	24,020.264
3/2→3/2	24,025.467

[21] J. E. Mack, Revs. Modern Phys. **22**, 65 (1950).

TABLE IV. σ-transition measurements on the $J=1\rightarrow2$ hyperfine pattern of $O^{16}C^{12}S^{33}$.

(a) $F=1/2\rightarrow1/2$	$\Delta\nu$ measured (Mc/sec)	$\Delta\nu_{\text{calc}}$ $g_{\text{nuc}}=+0.424$ $g_{\text{mole}}=-0.025$	$\Delta\nu_{\text{calc}}$ $g_{\text{nuc}}=-0.474$ $g_{\text{mole}}=-0.025$
Total splittings between $M_F=+1/2\rightarrow-1/2$ and $M_F=-1/2\rightarrow+1/2$ components ($H=1486$ gauss).	0.276 0.259 0.264 0.257		
	0.264	0.287	0.398
Splitting of low frequency component from zero field position ($H=3019$ gauss).	0.183 0.179		
	0.181	0.197	0.311
(b) $F=3/2\rightarrow1/2$			
Total splitting between $M_F=-3/2\rightarrow-1/2$ and $M_F=+3/2\rightarrow+1/2$ components. ($H=1486$ gauss).	1.559	1.564	1.678

of the present experiment. Once g_{nuc} is established, the nuclear magnetic dipole moment in nuclear magnetons is given by

$$\mu=g_{\text{nuc}}I. \tag{12}$$

From Eq. (8) it is seen that π-type Zeeman measurements give the quantity $|g_{\text{nuc}}-g_{\text{mole}}|$ directly. This is actually true to even better than first order since in the off-diagonal elements for the Zeeman perturbation, Eq. (10), the g-factors also appear only in the combination $|g_{\text{nuc}}-g_{\text{mole}}|$. Because of this, considerable effort was placed on the π-transition measurements. The π-measurements were made on five of the seven lines of the hyperfine pattern (Fig. 1). The coincident $F=3/2\rightarrow5/2$, $5/2\rightarrow7/2$ transitions were not used because the multitude of Zeeman components, many of which had low splitting factors, $(\alpha_{J1}-\alpha_{J2})$, [see Eq. (8)], resulted in an unresolved pattern (see Fig. 3). The $F=5/2\rightarrow3/2$ transition was not used because its components were too weak to be accurately measured. Zeeman splittings of the remaining five hyperfine lines were observed at various values of magnetic field. The measurements used in arriving at the value of $|g_{\text{nuc}}-g_{\text{mole}}|$ are given in Table III. In every case these measurements represent the total splitting between two Zeeman components; this type of measurement eliminates the second-order effect of the off-diagonal elements since it is the same for both components, and thus discrepancies with theory are actually effects of third or higher order. Actually, as mentioned in Part II, the matrices involved in the analysis can easily be diagonalized exactly; this was done and the least square discrepancy between theory and experiment was obtained if

$$|g_{\text{nuc}}-g_{\text{mole}}|=0.449\pm0.002 \text{ nuclear unit.} \tag{13}$$

Here the error of ±0.002 is determined by the internal consistency of the measurements and does not include a possible consistent error in measuring the magnetic field. The error in magnetic field is estimated to be less than 1 percent.

Table III also gives the theoretical splittings, calculated with the value of Eq. (13), for both the exact Zeeman theory and the first-order theory only to show the magnitude of the discrepancy with experiment and the magnitude of higher order corrections. The total spread of the measured splittings for a given transition is of the order of 0.020 Mc/sec, equally contributing factors being the limitations of the frequency measuring scheme and the reproducibility of a given value of the magnetic field.

Some of the spectrograms of the π-transitions are included in the Appendix.

$g_{\text{mole}}(OCS^{32})$ was previously measured as

$$g_{\text{mole}}(OCS^{32})=-0.025\pm0.002 \text{ nuclear unit.} \tag{14}$$

Thus, as mentioned above, we can find $g_{\text{mole}}(OCS^{33})$ by multiplying by the ratio of an OCS^{33} rotational frequency to the corresponding OCS^{32} frequency. For the $J=1\rightarrow2$ transition this ratio is

$$\nu(OCS^{33})/\nu(OCS^{32})=24{,}019.59/24{,}325.92=0.9874. \tag{15}$$

Thus $g_{\text{mole}}(OCS^{33})$ should be about 1 percent lower than $g_{\text{mole}}(OCS^{32})$. It is hardly necessary to apply this correction, since it is well within the error in determining $g_{\text{mole}}(OCS^{32})$, Eq. (14).

The determination of the relative sign between g_{nuc} and g_{mole} remains. On examining the theoretical splitting of the σ-type transitions for the two possibilities,

$$g_{\text{nuc}}=-0.025+0.449=+0.424,$$

and

$$g_{\text{nuc}}=-0.025-0.449=-0.474,$$

it was found that the splitting of the $F=1/2\rightarrow1/2$ line should be most critical for deciding which was correct. The σ splitting of this line was therefore measured. Table IV (a) shows the comparison between the experimental results and the expected results calculated for the two cases. It is seen that g_{nuc} and g_{mole} must be of opposite sign, although even then the agreement is not perfect for the values of g_{nuc} and g_{mole} assumed for these calculations. It should be noted that these splittings are quite small and thus the discrepancies in percent appear large; but the absolute differences are only about 0.020 Mc/sec, which is the experimental accuracy. These differences could be introduced by the proximity of the $F=1/2\rightarrow1/2$ line to the much stronger $F=3/2\rightarrow5/2$, $5/2\rightarrow7/2$ absorption. A spectrogram of this transition is shown in Fig. 4.

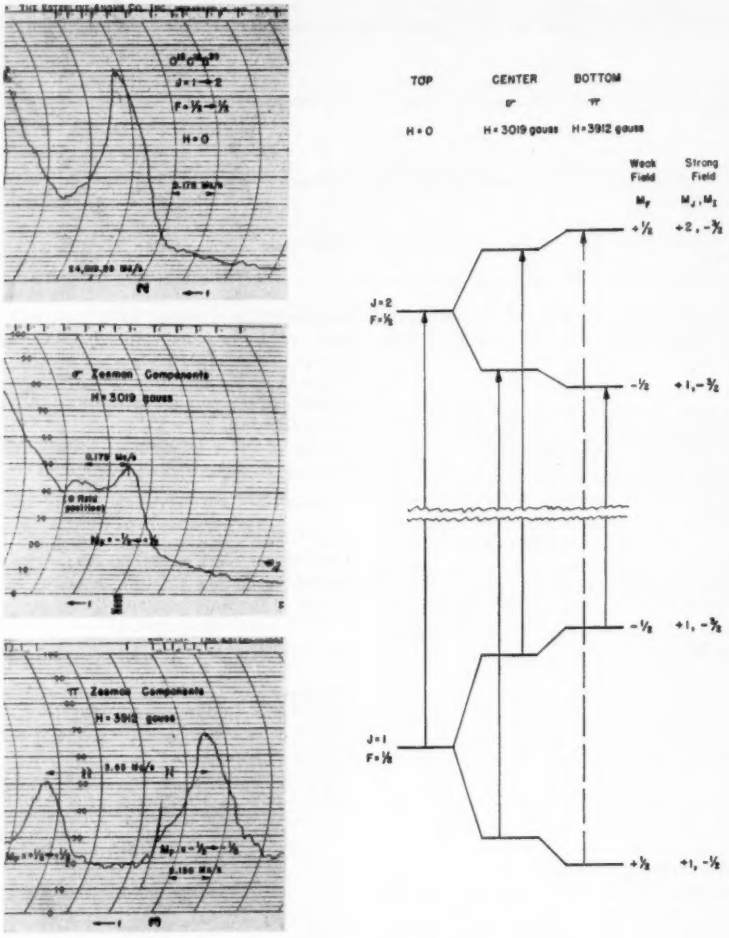

FIG. 4. σ- and π-Zeeman components of the $F=1/2\rightarrow 1/2$ line.

The σ-transition Zeeman components of the $F=3/2\rightarrow 1/2$ line were also measured and the results again compared with calculations based on the same and opposite relative signs for g_{nuc} and g_{mole}. Table IV (*b*) gives the results. Again it is definitely indicated that the g-factors have opposite signs.

As a more direct check on the absolute sign of g_{nuc} an observation was made of the $F=3/2\rightarrow 5/2$, $5/2\rightarrow 7/2$ σ components with circularly polarized radiation. This observation required careful analysis since for $\Delta M_F=+1$ (or $\Delta M_F=-1$) transitions some of the σ-components go to higher frequencies and some to lower frequencies. (The weaker hyperfine lines with fewer components could not be detected with the apparatus used for the circular polarization experiments.) This observation again indicated that g_{nuc} was positive as expected.

Finally values of g_{nuc} and g_{mole} were found which gave the best fit for all the data taken, both for π- and σ-transitions. The result becomes

$$g_{\text{nuc}}=+0.422\pm 0.004 \text{ nuclear unit}, \qquad (16)$$

where the error is that of internal consistency. Including possible consistent errors, primarily in the magnetic

field measurement, we have for the final result

$$g_{nuc} = +0.422 \pm 0.007 \text{ nuclear unit} \quad (17)$$

and according to Eq. (12) the corresponding magnetic dipole moment for the sulfur 33 nucleus is

$$\mu(S^{33}) = +0.633 \pm 0.010 \text{ nuclear magneton.} \quad (18)$$

This value is uncorrected for the partial shielding of the S^{33} nucleus from the externally applied field due to the electronic diamagnetic effects. This effect was studied theoretically for atoms by Lamb[22] and recently for molecules by Ramsey.[23] The exact theory in the molecular case is difficult to apply quantitatively, but Ramsey concludes that the shielding of a particular nucleus may be approximated by considering only its own electrons, so to speak, and by ignoring those tightly bound to other nuclei in the molecule. Thus, Lamb's theory applied to the sulfur atom may be used. This diamagnetic correction is about 0.11 percent[18] and is thus negligible to the accuracy of the present experiment.

Following the publication of the essential result of our experiment,[24] Dharmatti and Weaver have made a more accurate measurement of the S^{33} nuclear magnetic moment, using the nuclear induction method.[25] Their result is

$$\mu(S^{33}) = +0.64282 \pm 0.00014 \text{ nuclear magneton.}$$

APPENDIX. SPECTROGRAMS OF THE $O^{16}C^{12}S^{33}$ HYPERFINE PATTERN AND ZEEMAN EFFECT

In the spectrograms the absorption intensity is plotted vertically against the microwave frequency. The spectrograph receiver gain varies from one spectrogram to another, but, in general, relative gain settings may be estimated from the noise level. The frequency scale is different in the various figures and therefore a frequency scale is indicated on each spectrogram.

In Fig. 2, the lines can be compared for relative intensity and frequency splittings with the schematic pattern in Fig. 1. Note particularly the $F=1/2\rightarrow1/2$ line on the skirt of the stronger $F=3/2\rightarrow5/2$, $5/2\rightarrow7/2$ absorption. This line was especially useful for the measurement of $\mu(S^{33})$ by means of the Zeeman effect since it has only two components for either π or σ transitions.

Figure 3 shows the two π-components of the $F=1/2\rightarrow1/2$ line split out so that one of them has passed through the $F=3/2\rightarrow5/2$, $5/2\rightarrow7/2$ line and is resolved on the high frequency side. The components of the $F=3/2\rightarrow5/2$, $5/2\rightarrow7/2$ line are numerous and have low splitting factors and hence are unresolved.

In Fig. 4, the upper spectrogram is another zero field observation of the $F=1/2\rightarrow1/2$ line. The skirt of the $F=3/2\rightarrow5/2$, $5/2\rightarrow7/2$ line is again noticeable. The low splitting factor for the σ-components of this line is obvious from the center spectrogram, where at 3019 gauss one component has split only 0.179 Mc/sec from the zero field position. The high frequency component has merged with the $F=3/2\rightarrow5/2$, $5/2\rightarrow7/2$ line and the small component

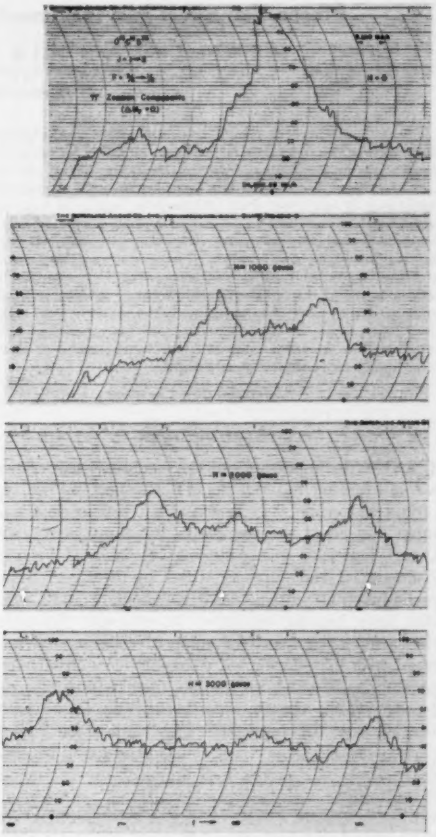

FIG. 5. π-Zeeman splitting of the $F=3/2\rightarrow1/2$ line.

at the zero field position is due to a short part of the absorption cell which extended beyond the magnetic field.

The π-components of this line had the largest splitting factor for any of the components in the entire hyperfine pattern and provided the most accurate measurements of the experiment. These components, shown in the lower spectrogram, are split out on either side of the $F=3/2\rightarrow5/2$, $5/2\rightarrow7/2$ line as in Fig. 3. Note also that the high frequency component, which is forbidden in the strong field limit, has already started to weaken in this intermediate field compared to the low freequency component which is permitted at all field strengths.

In Fig. 5, the $F=3/2\rightarrow1/2$ line is one of the weakest absorptions in the hyperfine pattern and hence the noise level appears high. However, the π-transition splitting as a function of the magnetic field is clearly visible. The four spectrograms are lined up with respect to the zero field position and a second-order shift (shift of the center of gravity of the two components) is noticeable. This shift agreed very closely with the theoretical Zeeman effect.

[22] W. E. Lamb, Jr., Phys. Rev. **60**, 817 (1941).
[23] N. F. Ramsey, Jr., Phys. Rev. **78**, 699 (1950).
[24] Eshbach, Hillger, and Jen, Phys. Rev. **80**, 1106 (1950).
[25] S. S. Dharmatti and H. E. Weaver, Phys. Rev. **83**, 845 (1951).

Meson Tail Effect and Treatment of Proton-Proton Scattering Data*†

M. C. Yovits,‡ R. L. Smith, Jr.,§ M. H. Hull, Jr., J. Bengston, and G. Breit
Yale University, New Haven, Connecticut

(Received August 13, 1951)

The fit of experimental material on proton-proton scattering by phenomenological potentials is reviewed with the inclusion of observations by Heydenburg-Little in the 300-kev region and of Cork at 30 Mev. Weighting of data by a criterion based on internal consistency is employed. Data obtained by means of Van de Graaff machines are used to determine the best fits for different shapes of potential energy curves. Other data are compared with the resultant (f, E) plots graphically. A trend towards agreement with the long-tailed Yukawa and exponential well potentials is noticeable among the supposedly more accurate measurements of Rouvina and of Cork. The meson potential $-Ce^{-r/a}/(r/a)$ with $C=(93.4\pm1.0)mc^2$, $a=(0.412\pm0.002)e^2/mc^2$ fits experiment and corresponds to a meson mass of $333\pm2m$, the limits of error being stated above somewhat arbitrarily.

The effect of the tail of the Yukawa potential on scattering is studied with particular attention to its influence on the nearly linear functions of energy used in the analysis of experiment, and on the coefficients of powers of the energy in the expansion of this function (f).

The convergence of the power series is better if the tail of the potential is chopped off. Calculation of coefficients in this series is also easier for the potential without tail. The more practical arrangements of calculations are: (a) direct calculation of f for a number of energies, the tail effect being treated by a first-order approximation; and (b) calculation of coefficients of powers of E in the series for f for potential without tail followed by first-order calculation of effect of tail on f. Results obtained in these ways are compared.

I. INTRODUCTION

SINCE the appearance of the comprehensive review of experimental and theoretical aspects of proton-proton scattering by Jackson and Blatt[1] there appeared some additional measurements by Rouvina,[2] Bruce Cork,[3] Panofsky and Fillmore,[4] Faris and Wright,[5] Zimmerman and Kreuger,[6] and by Mather.[7] Some preliminary measurements of Heydenburg and Little[8] also have become available. It appeared desirable, therefore, to compare the enlarged experimental material with expectation for different phenomenological potentials. It will be seen that there is now a slight trend towards agreement with the Yukawa or exponential type of potential. This circumstance may perhaps be significant since it has been found possible to reconcile the simple hypothesis of the symmetric Hamiltonian with neutron scattering experiments through the employment of long-tailed potentials[1] and since the exactness of the equality of n-p and p-p forces is even improved by making relativistic and magnetic effects corrections as has been found by Schwinger.[9]

In view of the usual difficulty of assigning relative weights to different sets of experimental data on a rational basis the experiment has been tried of employing general agreement with the majority of the better measurements as a criterion for establishing the relative weights. This is made possible by the employment of the f function of Breit, Condon, and Present,[10] which varies approximately linearly with energy, a circumstance successfully used by Schwinger,[11] Blatt,[12] Bethe,[13] Chew and Goldberger,[14] and others in analysis of scattering experiments. In order not to prejudice the determination of the range parameter, the criterion used disregards the manner in which the centroid of the f values falls on the f, E curve but pays attention to the way in which the slope of f, E curve is reproduced by the data of one set of observers. This criterion is manifestly unjust to data which contain an error varying systematically with energy and is present only at some energies. Such an error need not affect the position of the centroid very strongly. This is the case for the observations of Heydenburg, Hafstad, and Tuve,[15] which show other evidence of being quite accurate at their highest energy. Since a great many points are now available, such an occasional unfairness has probably an insignificant effect on the final result. The values of Heydenburg, Hafstad, and Tuve[16] obtained in the vicinity of the scattering minimum and sometimes[17] shown in surveys are not included in the analysis since the object of this work was to ascertain the existence of the minimum rather than to provide accurate phase shift values. Other questions

* Assisted by the joint program of the ONR and AEC.

† Part of a dissertation submitted by R. L. Smith for the degree of Doctor of Philosophy at Yale University.

‡ Predoctoral AEC Fellow, now at the Applied Physics Laboratory, Silver Springs, Maryland.

§ Now at Hughes Aircraft Corporation, Los Angeles, California.

[1] J. D. Jackson and J. M. Blatt, Revs. Modern Phys. **22**, 77 (1950).

[2] J. Rouvina, Phys. Rev. **81**, 593 (1951).

[3] Bruce Cork, Phys. Rev. **80**, 321 (1950).

[4] W. K. H. Panofsky and F. L. Fillmore, Phys. Rev. **79**, 57 (1950).

[5] F. Faris and B. Wright, Phys. Rev. **79**, 577 (1950).

[6] E. J. Zimmerman and P. G. Kreuger, Phys. Rev. **83**, 218 (1951).

[7] K. B. Mather, Phys. Rev. **82**, 133 (1951).

[8] N. P. Heydenburg and J. L. Little, private communication, referred to in the text as HL. The authors would like to acknowledge their indebtedness for permission to use this material.

[9] J. Schwinger, Phys. Rev. **78**, 135 (1950).

[10] Breit, Condon, and Present, Phys. Rev. **50**, 825 (1936), referred to in the text as BCP.

[11] J. Schwinger, hectographed lecture notes prepared at Harvard, unpublished.

[12] J. Blatt, Phys. Rev. **74**, 92 (1948).

[13] H. A. Bethe, Phys. Rev. **76**, 38 (1949).

[14] G. F. Chew and M. L. Goldberger, Phys. Rev. **75**, 1637 (1949).

[15] Heydenburg, Hafstad, and Tuve, Phys. Rev. **56**, 1078 (1939), referred to in the text as HHT.

[16] Heydenburg, Hafstad, and Tuve, Phys. Rev. **53**, 239 (1938).

[17] L. Rosenfeld, *Nuclear Forces* (Interscience Publishers, Inc., New York, 1948).

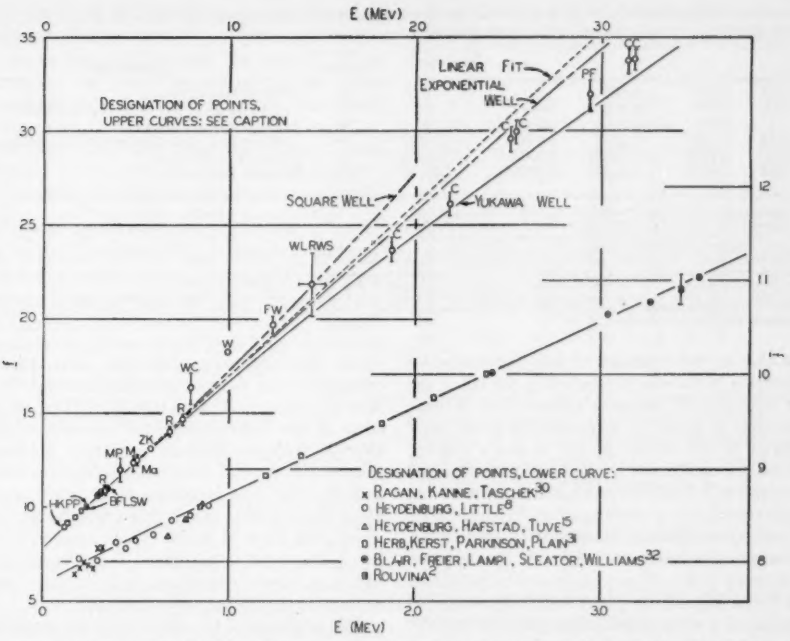

FIG. 1. *Lower curve:* Plot of f *vs* E for best fits with experimental points as designated. Use scales on right and lower margins. *Upper curves:* Plots of f *vs* E for best fits as labeled with experimental points having the following designations: HKPP—Herb, Kerst, Parkinson, and Plain (reference 31); BFLSW—Blair, Freier, Lampi, Sleator, and Williams (reference 32); R—Rouvina (reference 2); MP—May and Powell (reference 29); M—Meagher (reference 36); Ma—Mather (reference 7); ZK—Zimmerman and Kreuger (reference 6); WC—Wilson and Creutz (reference 37); W—Wilson (reference 38); FW—Faris and Wright (reference 5); WLRWS—Wilson, Lofgren, Richardson, Wright, and Shankland (reference 39); C—Cork (reference 3); PF—Panofsky and Fillmore (reference 4). Use scales on left and upper margins.

concerned with the use of data are discussed in a more detailed account contained in the body of the paper.

The differences caused by fitting data in different ways are examined as follows with special reference to the distinction between linear fits to the f, E curve and fits employing the deviations from linearity which are expected for an assumed shape of the potential energy well. These have been previously mentioned in a more limited way by Breit and Hatcher[18] in relation to the quadratic terms but are more fully covered here with a consideration of the effect of cubic and quartic terms. In addition to comparison of power series and directly computed f values mentioned below, an analytic discussion of the effects of linear fits shows that if the curvature of the (f, E) curve is produced by a quadratic term, a linear visual fit will give the same initial slope as a linear least squares fit, but will fail to reproduce the initial value $(f, E=0)$ by an amount proportional to the square of the maximum energy used in the fit. If a quadratic term is accounted for properly, but a cubic addition is fitted linearly, the addition to the slope is nearly determined, but an error in the initial value proportional to the cube of the maximum energy is left out of account.

In order not to be completely dependent on least squares analyses of the data and on semi-empirical formulas relating the potential parameters to the results of such an analysis, a further study was undertaken wherein theoretical f, E plots for various sets of parameters were compared directly with the experimental data and with an f, E plot resulting from a least squares analysis of the data. In such plots a change in the range parameter appears approximately as a rotation of the f, E plot, while a change in the depth parameter appears as change in the value of f by nearly the same amount at each energy. The comparison, therefore, allows a determination of the changes in the parameters needed to rotate and translate one of the theoretical curves into the one derived from experiment. The parameters obtained from both methods of analysis differ by much less than the estimated errors.

[18] G. Breit and R. D. Hatcher, Phys. Rev. **78**, 110 (1950), referred to in the text as BH.

TABLE I. Values of the $f^{(i)}$ in their different interpretations for the Yukawa potential with $a'=0.40$, $C'=99$.

Line	$f^{(0)}$	$f^{(1)}$	$f^{(2)}$	$f^{(3)}$	$f^{(4)}$	Tail presence	How obtained
A	7.9917	0.905	−0.005	0	0	No	HAB representations.[a]
B	7.9900	0.910	−0.006	0.00005	0	No	Least squares fit to f in Table I of HAB.[b]
C	...	0.917	−0.0063	0.000053	0	No	Least squares fit to $\partial f/\partial E$.[c]
D	7.9684	0.9295	−0.0090	0.00026	-5.3×10^{-6}	Yes	Graphical tail corrections applied to preceding entry.[d]
E	7.9900	0.9153	−0.00659	0.000051	5.4×10^{-7}	No	Integrals involving u_E.[e]
F	7.9684	0.9269	−0.00890	0.000270	-5.3×10^{-6}	Yes	Integrals involving u_E.[f]

[a] Direct substitution of $a'=0.40$, $C'=99$ into Eqs. (3) to (3.8) of HAB.
[b] Least squares fit to values of f for different values of maximum energy from 9 to 40 Mev. Value of $f^{(3)}$ proved necessary to insure energy independence of other $f^{(i)}$. Value of $f^{(0)}$ obtained agrees with that from Eq. (8.6) of BB.
[c] Calculation of $\partial f/\partial E$ by the BH extension of the Schwinger formula to arbitrary E; least squares fits at $E=0$, 1, 2.6, 6, 8, 10, 12, 14, and 16 Mev.
[d] Graphical determination of $\delta(\partial f/\partial E)$ from Fig. 2; power series fits to these values.
[e] Jackson-Blatt equations involving energy derivatives of radial functions applied to potential without tail; the value of $f^{(4)}$ was required to represent directly computed f's of HAB up to 32 Mev. It is probably not accurate since it may be including effects of $f^{(5)}$.
[f] Obtained from values given in immediately preceding entry with inclusion of tail effect corrections calculated by means of Eq. (2) employing energy differentiation of asymptotic Bessel function expansions (see reference 26) at $E=0$. A least squares fit of f up to $E=22$ Mev determined $f^{(4)}$ which is probably not accurate and may include effects of $f^{(5)}$.

The section on the treatment of data is preceded by a consideration of the effect of including the tail of the Yukawa potential at distances greater than $3e^2/mc^2$. This tail effect is found to be represented poorly by a power series in the energy E, and it has a marked influence on the coefficients $f^{(i)}$ in the power series in E which represents f. The difference between representing f by a polynomial with a small number of terms and by a power series is studied and is found to be appreciable. The power series representation of f at 32 Mev is found to require terms in E^n with $n=4$ as is seen by inspection of Table I and Fig. 1. The power series representation of the values of f without tail converges more rapidly, however, and could be used in conjunction with a directly computed tail effect obtained as in Sec. II.

The notation is the same as in Hatcher, Arfken, and Breit[10] with the following additions or changes:

r_e = interparticle separation in units e^2/mc^2.
$\mathbf{K}=\frac{1}{2}f-0.15443$ is the function introduced by Jackson and Blatt[1] in their analysis of experimental data.
$u^*=C_0\mathfrak{F}/\sin K_0$, where $\mathfrak{F}$ is the Coulomb function $F\cos K_0+G\sin K_0$.
$y=1/(C'a'^2)^{\frac{1}{2}}$.
E = energy in Mev unless otherwise stated.
δK_0 = change in K_0 caused by an addition to the potential. In the present case, the addition is taken to be the tail of the Yukawa potential from $r=3e^2/mc^2$ to $6e^2/mc^2$.

II. EFFECT OF THE TAIL OF THE YUKAWA POTENTIAL ON PHASE SHIFT

In the work reported on which follows, use is made of the fact that the effect of the tail extended from $r_e=3$ to infinity is given with an accuracy of at least 0.0003 degrees by the first-order perturbation formula

$$\delta K_0=\int_{r_e=3}^{\infty}(\delta V/E')\mathfrak{F}^2 d\rho, \qquad (1)$$

where δK_0 = change in phase shift as a result of the extension of the Yukawa potential beyond $3e^2/mc^2$ (δK_0 is to be added to K_0 of Table II of HAB to give the effect of the Yukawa potential extended to infinity), $\delta V=Ce^{-r/a}/(r/a)$ = Yukawa potential, E' = energy of relative motion, and $\mathfrak{F}$ = Coulomb function with phase shift K_0. The error is usually much less than 0.0003°. Since the tail effect is calculated here for use with the phase shift table of HAB[10] which has an accuracy of 0.01°, this error is negligible. Inaccuracies in $\mathfrak{F}$, the nature of which is explained in detail later, may give at most an additional error of 0.0002°.

The smallness of the effects of these errors in applications may be judged by observing that a one percent error in scattering at an observation angle of 45° usually introduces errors in the phase shift having absolute values between 0.01° and 0.4°. The dependence of the errors in K_0 and f on energy caused by such an error in scattering is seen in Table II. This table will be found useful for comparison with values of the tail effect arrived at later in the article.

The inherent errors introduced by the use of Eq. (1) are to be assigned to two main causes. First there is the neglect of the tail beyond $6e^2/mc^2$. The maximum effect of cutting off the Yukawa potential at $r_e=6$ was estimated by evaluating the integral of Eq. (1) from $r_e=6$ to infinity with $\mathfrak{F}=1$. Since $|\mathfrak{F}|\leqq 1$, this provides an upper limit on the error which is found to be less than $8.5\times10^{-5}/\sqrt{E}$ degrees with E in Mev. For all energies used this is less than 0.0001 degree. The inaccuracy introduced by using the square of the Coulomb function instead of the product of the Coulomb and Yukawa functions was investigated. For the higher energies, an analytical argument shows this to be less than $0.22/\sqrt{E}$ percent of δK_0, that is less than about 2×10^{-5} degree. At the low energies, numerical estimates indicate an upper limit to this type of error of about 0.0002 degree.

In order to calculate δK_0 from Eq. (1) it is necessary to obtain the wave function $\mathfrak{F}=F\cos K_0+G\sin K_0$. The phase shifts used were taken directly from Table II of HAB. Calculation of the regular and irregular

[10] Hatcher, Arfken, and Breit, Phys. Rev. **75**, 1389 (1949), referred to in the text as HAB.

Coulomb functions, F and G, proceeded in several different ways.

For energies below 2 Mev, Eqs. (13) through (21) of Yost, Wheeler, and Breit[20] were used. In this region inaccuracies in F and G present in the calculations introduced errors of less than 3×10^{-5} degree in δK_0.

For energies above and including 9 Mev, $\mathfrak{F}$ was approximated by a sine function, $A\sin[Q(b)r_e+\delta]$ where Q is defined by the Coulomb equation, $d^2\mathfrak{F}/dr_e^2+Q^2(r_e)\mathfrak{F}=0$, and b is some suitably chosen value of r_e slightly greater than 3. A and δ were found by fitting the sine function in slope and value at $r_e=3$ to $\bar{a}\sin(\varphi+K_0)$; $\bar{a}$ and φ at $r_e=3$ were obtained from previous unpublished work at this laboratory by Hatcher who used Eqs. (4(b)), (9), and (10) of Wheeler.[21] Estimates of the error introduced by this approximation for $E>9$ Mev were made by integrating

$$\int_{r_e=3}^{6}[e^{-r/a}/(r/a)][\bar{a}^2\sin^2(\varphi+K_0)-A^2\sin^2(Q(b)r_e+\delta)]d\rho,$$

taking into account first-order effects in K_0. The resultant upper limit for the error is $\sim3\times10^{-5}/E_{\text{Mev}}^3$ which is <0.0002 degree. Numerical checks on the sine approximation were made in a number of cases by comparison with accurate values of $\mathfrak{F}$. The agreement was always better than 0.0001 degree in δK_0.

For 2 Mev$<E<$9 Mev a sine function of the form $A\sin[Qr_e+\delta]$ was joined to $\mathfrak{F}$ at $r_e=3$. F and G and their derivatives at $r_e=3$ were obtained from Table I in Thaxton and Hoisington.[22] At larger values of r_e, the difference between the sine function and the desired Coulomb function was calculated by means of a Taylor's series in r_e-3, the successive derivatives of which were obtained from the Coulomb equation. The series converges rapidly requiring only two or three terms. The error in $\mathfrak{F}$ where it mattered was not more than 0.001 and the error in δK_0 was less than 0.0002 degree.

TABLE II. Errors in K_0 in degrees and f produced by a one percent error in scattering at 45° for $C=84.422mc^3$ and $a=0.4323e^2/mc^2$.

E	ΔK^0	Δf
0.25	−0.05	0.03
0.50	0.03	−0.01
0.75	0.08	−0.02
1	0.13	−0.03
2	0.23	−0.05
4	0.33	−0.09
10	0.37	−0.16
20	0.35	−0.24
30	0.33	−0.30
40	0.32	−0.35

[20] Yost, Wheeler, and Breit, Phys. Rev. **49**, 174 (1936).
[21] J. A. Wheeler, Phys. Rev. **52**, 1123 (1937).
[22] H. M. Thaxton and L. E. Hoisington, Phys. Rev. **56**, 1194 (1939), referred to in the text as TH.

TABLE III. Values of tail correction δK_0 in hundredths of degrees for meson potential. These should be added to the K_0 in Table I of HAB to allow for the effect of the potential beyond $r=3e^2/mc^2$.

a'	0.40	0.40	0.40	0.42	0.45	0.45	0.45
E (Mev) \ C'	102	99	96	89.648	84	81	78
0.8	5.8	5.3	4.8	7.5	14.9	13.6	12.2
1.4	4.3	4.3	4.2	6.1	8.7	9.4	9.6
3	0.8	1.0	1.2	1.5	2.0	2.8	3.7
5	0.1	0.2	0.1	0.2	0.5	0.3	0.3
6	0.3	0.2	0.2	0.3	0.9	0.7	0.5
7	0.5	0.4	0.3	0.6	1.5	1.2	0.9
9	0.9	0.8	0.7	1.2	2.4	2.1	1.9
16	1.0	0.9	1.0	1.4	2.3	2.3	2.2
22	0.4	0.4	0.5	···	0.9	1.0	1.0
28	0.2	0.2	0.2	0.3	0.4	0.4	0.4
32	0.2	0.2	0.2	0.3	0.5	0.5	0.4
40	0.4	0.4	0.4	0.6	1.0	1.0	0.9

Values of δK_0 for Yukawa parameters close to the best fit to experiment are listed in Table III.

Values of δf were obtained as first-order effects of δK_0 from the definition of f and are shown in Table IV.

At zero energy, it was convenient to use

$$\delta f=-2\int_0^6(\delta V/mc^2)(u^s)^2dr_e, \tag{2}$$

which follows from Eq. (1) and the relation between δf and δK_0, where at any energy

$$u^s=C_0\mathfrak{F}/\sin K_0, \tag{2.1}$$

an expression, the limit of which for $E=0$ is according to Breit and Hatcher,[18]

$$u^s=-x[K_1(x)+(\gamma-\tfrac{1}{2})I_1(x)]+(x/4)I_1(x)f, \tag{2.2}$$

where

$$x^2=8r/a_B. \tag{2.21}$$

By differentiation of Eq. (2) the energy derivatives of δf at $E=0$ can be obtained in terms of energy derivatives of u^s at zero energy which can be expressed in terms of Bessel functions. The values of δf and $\partial(\delta f)/\partial E$ at $E=0$ for various meson parameters are included in Tables IV and V. The values of δf given in Table IV are to be added to the values of f for the meson potential extended to $r_e=3$ in order to give the effect for a meson potential extending to infinity.[23]

The uncertainty in δf is roughly constant over the complete energy range and is probably not greater than about 0.0003 in most cases. At zero energy estimates indicate that the uncertainty in δf is probably not greater than 0.0005.

Tail corrections for the Yukawa parameters C'

[23] A knowledge of the phase shifts enables one to calculate f from Eq. (7.6) of BCP for various energies. For different Yukawa parameters one can calculate f up to 10 Mev to within about 0.01 from the representations given in Eqs. (3) through (3.8) of HAB. An uncertainty of 0.01 in f, for almost all energies, corresponds to an uncertainty in scattering at 45° of less than 1 percent as indicated in Table II.

TABLE IV. Values of δf caused by tail of meson potential. These should be added to f to allow for the effect of the potential beyond $r=3e^2/mc^2$.

a'	0.40	0.40	0.40	0.42	0.45	0.45	0.45
E (Mev) \ C'	102	99	96	89.648	84	81	78
0	−0.0179	−0.0216	−0.0257	−0.0299	−0.0287	−0.0366	−0.0455
0.8	−0.0110	−0.0134	−0.0166	−0.0188	−0.0169	−0.0223	−0.0286
1.4	−0.0073	−0.0093	−0.0115	−0.0128	−0.0107	−0.0147	−0.0194
3	−0.0016	−0.0024	−0.0032	−0.0035	−0.0034	−0.0057	−0.0086
5	−0.0004	−0.0006	−0.0005	−0.0005	−0.0011	−0.0009	−0.0009
6	−0.0008	−0.0006	−0.0005	−0.0009	−0.0025	−0.0021	−0.0016
7	−0.0016	−0.0014	−0.0012	−0.0020	−0.0045	−0.0039	−0.0033
9	−0.0034	−0.0033	−0.0031	−0.0047	−0.0085	−0.0080	−0.0076
16	−0.0055	−0.0058	−0.0061	−0.0083	−0.0119	−0.0126	−0.0134
22	−0.0029	−0.0032	−0.0035	···	−0.0062	−0.0069	−0.0077
28	−0.0014	−0.0014	−0.0015	−0.0022	−0.0034	−0.0035	−0.0038
32	−0.0018	−0.0017	−0.0017	−0.0026	−0.0046	−0.0045	−0.0044
40	−0.0045	−0.0044	−0.0044	−0.0064	−0.0107	−0.0106	−0.0105

$=89.648$, $a'=0.42$, can be used to determine the tail corrections for other sets of slightly different parameters within ± 0.0007 in f. The results can be summarized as follows. For $0<E\leqq 9$ Mev,

$$(\delta f-\delta f^{(0)})/(\delta f_0-\delta f_0{}^{(0)}) = 1+15(a'-0.42)[1+3.7(a'-0.42)] +0.248[1+12(a'-0.42)] \times[15.81-C'a'^2][1-0.0855E], \quad (3)$$

$$\delta f^{(0)}/\delta f_0{}^{(0)}=1+14.6(a'-0.42)[1+4.6(a'-0.42)] +0.344[1+10.5(a'-0.42)][15.81-C'a'^2]. \quad (3.1)$$

For $E\geqslant 9$ Mev,

$$\delta f/\delta f_0=1+18.3(a'-0.42)[1+5.7(a'-0.42)] +0.150[1+16.7(a'-0.42)][15.81-C'a'^2] \times\sin[0.0331E^{\frac{1}{2}}(E-12)]. \quad (3.2)$$

Here E means the energy in the laboratory system in Mev, $\delta f^{(0)}$ is the first term in a power series in energy for δf, and the subscript 0 means that δf and $\delta f^{(0)}$ for $a'=0.42$, $C'=89.648$ have been taken. Values of δf_0 and $\delta f_0{}^{(0)}$ are obtainable from Table IV, fourth column, with $\delta f_0{}^{(0)}=\delta f_0$ at $E=0$.

It may be pointed out that Eq. (3) can be used to obtain $\delta f^{(1)}$, since $[\partial(\delta f)/\partial E]_{E=0}=\delta f^{(1)}$, and $[\partial(\delta f_0)/\partial E]_{E=0}=\delta f_0{}^{(1)}$ is 0.0161 from Table V.

III. COEFFICIENTS OF E IN THE POWER SERIES OF f

The quantities $f^{(0)}, f^{(1)}, \cdots$ are defined as coefficients of powers of E in the power series representing f. In the work of HAB the primary object was to represent f as a function of the energy with an accuracy sufficient for preliminary comparison with experiment. Simplicity of representation was therefore put ahead of accuracy in the values of the $f^{(i)}$. The procedure followed by HAB was that of fitting directly computed values of f by a quadratic

$$f^{(0)}+f^{(1)}E+f^{(2)}E^2,$$

for values of E from 0.2 to 10 Mev, and while the fact that the values of $f^{(0)}$, $f^{(1)}$, and $f^{(2)}$ will be affected by the presence of $f^{(i)}$ with $i>2$ has been realized and even brought out in HAB's paper, no explicit account of them has been taken. It is clear that the effect of the omitted $f^{(i)}$ is a function of the energy range within which the fits of f are made. In the work of Jackson and Blatt,[1] on the other hand, the function f is represented by a power series in E, and the coefficients $f^{(i)}$ are used in their strict mathematical sense. The agreement between the two sets of the $f^{(i)}$ is, therefore, not as good as that between the values of f. The situation is somewhat similar to that encountered in the analysis of experimental material by means of the f function. The best that can be done without assuming a shape of the potential well is presumably to fit the experimental values of f by a polynomial using least squares with appropriate weights. The values of the $f^{(i)}$ arrived at are then functions of the assumed number of significant $f^{(i)}$. The values could be appreciably in error if the f curve contains some large enough $f^{(i)}$ with large enough i. The procedure of HAB is sufficiently close to what has to be done in treating data with respect to effects of neglected $f^{(i)}$ to make it at least comparable in usefulness with that of a mathematically rigorous representation. It sacrificed some numerical accuracy in order to cover a large range of parameters, and a direct comparison with Jackson and Blatt's work would be difficult for any one who has not carried out similar calculations. It appeared desirable, therefore, to take into account the effect of the tail of the potential energy curve on the $f^{(i)}$ both in order to make the comparison more immediate and in order to ascertain the effect of the inclusion of the tail on the $f^{(i)}$. It will be seen that the effect of the tail is not negligible and that the

TABLE V. Values of $\partial(\delta f)/\partial E$ at $E=0$. E is in Mev.

$a'=$ 0.40	0.40	0.40	0.42	0.45	0.45	0.45
$C'=$ 102	99	96	89.648	84	81	78
$\partial(\delta f)/\partial E=$ 0.0102	0.0116	0.0133	0.0161	0.0177	0.0211	0.0248

inclusion of the higher i is especially important in representing its effect. This is especially clear by inspection of Fig. 2 which shows the tail effect δf plotted against E. An expansion of this quantity in powers of E is obviously not the easiest way of representing it. The values of the $f^{(i)}$ corresponding to different conventions and purposes of employment are summarized in Table I. The fundamental constants enter the calculations for Table I in the combinations $(M/m)(e^2/\hbar c)^2 = 0.097714$ and $(mc^2/\text{Mev}) = 0.5114$. The numerical values used here are consistent with those in Breit, Thaxton, and Eisenbud,[24] Breit and Bouricius,[25] HAB, BH. The last line of Table I is in good agreement with the values of Jackson and Blatt.[1] The first four coefficients obtained from their work and adjusted with their formulas to correspond to a Yukawa well with $a' = 0.40$, $C' = 99$ and $f^{(0)} = 7.9666$, $f^{(1)} = 0.9268$, $f^{(2)} = -0.0089$, and $f^{(3)} = 0.00026$.

Table I shows that the same set of values of f can be represented in a number of ways by polynomials and that the rather tempting interpretation of data by means of the almost rectilinear plots of f against energy has its limitations. This fact has been brought out by BH in connection with the influence of quadratic terms on straight line fits to data. It is seen in Table I that cubic and quartic terms also have an appreciable influence. While the least squares fitting was made to values of f computed for a definite model rather than to values obtained from experiment, the indefiniteness in conclusions could not have been made worse by doing so. One may conclude that the mere fact that a set of experimental values of f shows no recognizable curvature in the (f, E) plot does not justify one in fitting it by a straight line if it is desired to obtain the potential well parameters.

The evaluation of f can be either made directly for a number of energies as in the work of HAB or else by the calculation of the $f^{(i)}$ as in the work of Jackson and Blatt. For a small range of energies in the immediate vicinity of $E=0$, the latter method is more efficient if one wishes to avoid the use of Coulomb functions and prefers to employ tabulations of Bessel functions (I, K) instead. For wider ranges of E the direct calculation of f or K_0 is definitely the easier approach because of the severe cancellation in the integral expressions for $f^{(i)}$ with higher i. When the meson wave function, expanded as a power series in the energy to yield coefficients which are functions of r analogous to the Bessel function coefficients of the Coulomb function,[26] is joined at $r_e = 3e^2/mc^2$ to the Coulomb function, the limits of integration for the computation of the $f^{(i)}$ are 0 and 3 on r_e, and the two terms in the integrand which are subtracted are closely equal in value over the latter part of the range of integration. The cancellation is

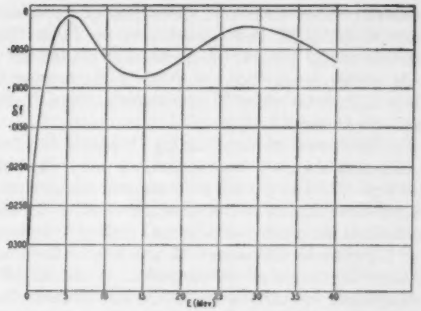

FIG. 2. A typical plot of δf vs E for the parameters $C' = 89.648mc^2$, $a' = 0.42e^2/mc^2$. Similar curves result for the other sets of parameters appearing in Table IV.

minimized, therefore, by reducing the range of integration. It appears that integration over 60 percent of the range reproduces 99 percent of $f^{(1)}$ while cancellation leaves 20 percent of $\int (u_0^e)^2 dr_e$. Integration over 85 percent of the range is necessary to give 98 percent of $f^{(2)}$ and only 2 percent of $\int u_0^e u_1^e dr_e$ is left, while in order to obtain 96 percent of $f^{(3)}$ the integration must be carried over 94 percent of the range and 0.06 percent of $\int (u_1^e)^2 dr_e$ is left. Here $u_i^e = (\partial^i u^e/\partial E^i)_{E=0}$, where u^e is the Coulomb function. This may be viewed differently by saying that if one wishes only 1 percent error in $f^{(1)}$, the integrals must be known to 0.2 percent, a 2 percent error in $f^{(2)}$ requires knowledge of the integrals to 0.04 percent, and a 4 percent error in $f^{(3)}$ is obtained if one knows the integrals to 0.0025 percent. Such numerical accuracy requirements would be too severe and could make the calculation of the $f^{(i)}$ very impractical if it were not for the fact that when the two integrals representing each $f^{(i)}$ are combined into one, the resultant integrand is a relatively smooth function of r. Numerical quadrature performed on this integrand, which changes sign within the range of integration, has not shown any special difficulties regarding the necessity of using high order quadrature formulas. Nevertheless one may have a feeling of caution regarding numerical work with this integrand, since it arises as a difference of two much larger quantities which are sufficiently complicated mathematically to make conclusions regarding the smoothness of the difference rather difficult. It may be of interest to note that computation of f by the power series method throws all of the weight on the accurate calculation of the $f^{(i)}$ while direct calculation of f distributes the accuracy requirements. In employing the power series greater care has to be taken concerning accuracy because for the larger E the errors become magnified. Direct computation has the advantage of providing a number of checks such as regularity of differences against energy and integral relations enabling one to expand logarithmic derivatives and related quantities in powers of energy differences or other

[24] Breit, Thaxton, and Eisenbud, Phys. Rev. **55**, 1018 (1939), referred to in the text as BTE.
[25] G. Breit and W. G. Bouricius, Phys. Rev. **75**, 1029 (1949), referred to in the text as BB.
[26] G. Breit and M. H. Hull, Jr., Phys. Rev. **80**, 392 (1950).

parameter value differences. Such checks have been described by BTE and related ones by HAB. The question of the number of coefficients needed for a given energy range does not enter in the method of direct calculation while it cannot be avoided if one uses a power series in E.

The direct method of calculating f is not entirely free of stringent accuracy requirements, however. In this case Eqs. (7.1) and (7.6) of BCP are used together with quantities tabulated in the appendix of BTE, in TH, or obtained some other way for the Coulomb functions, and logarithmic derivatives of the meson functions obtained by a numerical integration of the suitable Schroedinger equation or an equivalent method. The tabulated Coulomb functions are given to four decimals in the places mentioned, and an assumed uncertainty 5×10^{-5} in each quantity at, say, $E=2.6$ Mev, introduces an uncertainty in f of 0.003. If there is an error in one of the quantities, for example $\Phi_0\Theta_0$, of 1.5×10^{-4}, there is an error in f of roughly the same amount. While these uncertainties are small, they entered within the accuracy of the graphs discussed later in this paper. There is also a further mitigating circumstance in the use of the integral formulas in the fact that the tail effect contributes the major part of the coefficients $f^{(i)}$ for $i>2$, and this part may be computed directly with the aid of the first-order formula, Eq. (2), where the wave function is suitably differentiated with respect to E under the integral. Thus for the entry in Table I, line E, the error in $f^{(3)}$ without tail is estimated at ±10 percent, while in line F, the error in $f^{(3)}$ with tail is only about 3 percent, since the tail effect is known to about 0.5 percent and is four-fifths of the value. The values of $f^{(1)}$ and $f^{(2)}$ with or without tail are known to ±0.03 percent and ±0.5 percent, respectively.

It has, therefore, been found helpful in the present work to use both direct calculations of f and energy expansions with coefficients obtained by integral formulas in order that independent checking could be effected.

In deriving the values of meson well parameters from experiment, it is convenient to have available the approximate equations

$$\begin{aligned}\Delta a' &= -0.0138\Delta f^{(0)}+0.411\Delta f^{(1)}\\ \Delta[(C')^{-\frac{1}{2}}/a'] &= 0.00309\Delta f^{(0)}+0.0166\Delta f^{(1)},\end{aligned} \tag{4}$$

which follow from the representations of the $f^{(i)}$ by HAB. These formulas relate small changes in $f^{(0)}$ and $f^{(1)}$ to corresponding changes in C' and a' on the supposition that $f^{(2)}$ is varied with $f^{(0)}$ and $f^{(1)}$ in a manner required by the meson well. The effect of $f^{(i)}$ beyond $f^{(2)}$ is neglected and the variation of $f^{(2)}$ is obtainable from

$$\Delta f^{(2)}=0.000170\Delta f^{(0)}-0.0108\Delta f^{(1)}. \tag{5}$$

The tail of the meson potential beyond $r=3e^2/mc^2$ has the effect of increasing the range of nuclear force and of producing an increase in $f^{(1)}$ of approximately one percent. The change in phase shift, of course, is always positive. Since δf is proportional to $-\delta K_0$, δf is always negative, and in particular, $\delta f^{(0)}$ is negative. The curvature of the f-curve is increased in absolute value because of the tail by about 35 percent in a typical case.

The absolute value of the tail effect is greatest for $f^{(0)}$ and decreases with the order of the f-coefficients. However, in percentage, the tail has the greatest effect on the higher order coefficients. For example, the tail increases $f^{(3)}$ by about 500 percent and $f^{(4)}$ by about -1000 percent.

As would be expected, the tail has the greatest effect on the phase shift for low energies because of the Coulomb barrier. The oscillatory nature of δf arises because of the way in which the "wavelength" of the wave function decreases with energy, in combination with the exponentially decreasing factor in δV.

In the course of this work it has been found to be simpler to determine f curves by direct calculation of phase shifts rather than by determining the $f^{(i)}$ by means of integral formulas.[1,11,18,27] It is not meant, however, to deny the advantages of this latter method in showing qualitative features of the behavior of the $f^{(i)}$ with changes in potential well parameters especially for $f^{(1)}$. It is somewhat cumbersome, however, for the $f^{(i)}$ with higher i which are necessary to represent f at higher energies.

The large number of coefficients needed is illustrated by comparing results of using the values in Table I, line F at 20 Mev with a value of f computed from the HAB phase shift and corrected for tail effect. When $f^{(1)}$ was included, the series yielded a value too large by 2.11 or 9.5 percent, inclusion of $f^{(2)}$ led to an f which was too small by 5 percent, and the series with four coefficients was too large by 3.8 percent. The convergence is definitely faster, however, when the coefficients without tail of line E of Table I are used to compute values of f not corrected for the tail effect, as may be seen from the fact that at 20 Mev the series f is high by 9 percent for two terms, low by 2 percent for three terms, and low by 0.5 percent for four terms. With the same coefficients, the series disagrees with the tail-corrected f at 40 Mev by 20 percent and with the tail-uncorrected f by only 2 percent.

This comparison coupled with earlier discussions of cancellations encountered in integral formulas for the $f^{(i)}$ for $i\geq3$ leads one to the conclusion that the expansions in powers of E can most profitably be used for calculations not including the tail effect, followed by a direct calculation of the tail effect by means of Eq. (2) or interpolations in Table IV. Since the tail contributes most of the value of the coefficient from $f^{(3)}$ on, such a plan reduces the need for extreme accuracy in computing the $f^{(i)}$ without tail, and in

[27] G. Breit, Revs. Modern Phys. **23**, 238 (1951).

addition, the more rapid convergence of the series representing the tail-uncorrected f can be fully utilized.

The tail effect illustrates an extreme condition of variability with bombarding energy of sensitivity of scattering to changes in potential energy. This variability is clearly seen in Fig. 2. At energies of 30 Mev the tail effect is small, and it is small again at 5 Mev while in the region 0–1 Mev it has its largest values. The calculations by means of which the tail has been computed involve the same approximation as has been used by Hoisington, Share, and Breit[23] and BBH for the discussion of sensitivity of scattering to changes in potential in general. Figure 2 shows in conjunction with Table II that the tail effect is equivalent to a change in 45° scattering by roughly 0.7 percent at 1 Mev bombarding energy and is over 1 percent at 0.5 Mev. While small, the tail effect is seen to be not negligible from an experimental viewpoint.

It appears appropriate at this place to clear up a misunderstanding concerning statements in HSB[23] as interpreted by Jackson and Blatt. The word "shape" was used by HSB in two senses: (a) the one according to which changes in range and depth parameters do not alter the shape of the potential well (this convention has become universal since); (b) the one according to which the addition of a potential anywhere changes the shape. The latter convention was a natural one to use in a part of the discussion since the paper of HSB was written as an illustration of the method of calculating effects of such changes. A different shape in sense (b) is also a different shape in sense (a) in most cases, but in special cases it is the same shape in sense (a). By "exponential well" the well with specific values of depth and range parameters of Rarita and Present was meant throughout as is clear from references to the work on binding energies with these parameters in HSB and from the discussion of their comparison of the meson and exponential wells, which applies to what HSB considered to be the best fit to scattering data by the Yukawa potential with what appeared to be at the time the best fit to binding energies of the Rarita-Present exponential potential. The distinction in the two uses of the word "shape" should have been more clearly brought out in the HSB paper. At the time at which it was written the interest in the Rarita-Present well and the absence of binding energy calculations for the meson potential made elaborate statements unnecessary. The statement by HSB concerning the fact that the data then under consideration were in better agreement with some shapes of potential energy wells (in the currently accepted sense) than with others was correct and can be seen in Fig. 15 in Jackson and Blatt's paper and in Fig. 1 of the present paper. The points of HHT which could not have been disregarded suggested strongly a preference for the meson potential and the trend toward convexity of the (f, E) plot for the HKPP points when viewed from below is also clear. It should be stated that the comparison of the best 1939 meson potential fit with the Rarita-Present exponential well was correct. The superiority of the (f, E) plot over the (K_0, E) plot claimed by Jackson and Blatt is more esthetic than practical as may be seen from the agreement of "best fits" obtained by the two methods. It is probable that the safest method is a direct plot of experimental data such as Fig. 11 of BTE. It is more laborious than either of the other two but frees one considerably from the confusion caused by the customary and frequently rather meaningless assignment of probable errors to their results by experimenters. The inclusion of data at various angles and diagrammatic presentation of experimental rather than theoretical quantities makes judgment concerning relative goodness of different fits more concrete.

[23] Hoisington, Share, and Breit, Phys. Rev. **56**, 884 (1939), referred to in the text as HSB.

IV. COMPARISON OF THEORETICAL f WITH EXPERIMENTAL DATA

Heydenburg and Little[8] have recently performed proton-proton scattering experiments at low energies using a Van de Graaff generator. These data were analyzed using the tables in Breit, Thaxton, and Eisenbud[24] and were found, at each energy, to be consistent among themselves to within 0.04° assuming only S wave scattering. This would indicate a minimum uncertainty in f of between 0.01 and 0.04.

In order to obtain the phase shift K_0 as a function of energy two types of least squares fits were made to these data. In the first, K_0 was determined by a fit at each energy to all the observation angles. In the second, it was supposed that at each energy there is present an undetected systematic error which affects scattering yields by the same factor at all angles. The least squares calculation included an adjustment of this factor at each energy in such a way as to enforce best agreement with theory on the assumption of a pure S scattering anomaly. The value of the phase shift is not assumed but is derived from the fit to adjusted experimental values. This factor in all cases turns out to differ from unity by less than 2 percent, and for all but two energies it leaves values unchanged to within less than 1 percent. The two types of fits give results that are almost identical, differing generally by only a few hundreths of a degree. Since all of the present experimental evidence indicates the absence of any deviations from S scattering at the energy of these experiments which could have been detected, and since absolute values of scattering yields could conceivably have errors depending on energy, the second type of fit appeared preferable and is used in the following. The results are given in Table VI along with the corresponding values of f.

The experimental results are analyzed by means of the f function of Breit, Condon, and Present.[10] In terms of this function the subsequently introduced f

TABLE VI. S wave phase shifts according to experiments of Heydenburg and Little.

E(Mev)	K_0(degrees)	f
0.2	6.66	8.053
0.3	11.16	8.031
0.4	15.02	8.216
0.45	17.16	8.163
0.5	18.82	8.261
0.6	22.32	8.304
0.7	25.13	8.450
0.8	27.97	8.504
0.9	30.35	8.607

of Bethe, f_{Be}, is

$$f_{Be}=f+2-2\gamma=f+0.84557,$$

and the function used by Jackson and Blatt is

$$\mathbf{K}=\tfrac{1}{2}f+1-2\gamma=\tfrac{1}{2}f-0.15443.$$

Here γ is the Euler-Mascheroni constant. The original notation is adhered to on account of the simplicity of the relation between the logarithmic derivative of the wave function and f which is apparent in Eq. (7.5) of BCP.

The determination of $f^{(0)}, f^{(1)}, f^{(2)}$ proceeded from the more accurately measured phase shifts. In addition to the work of Heydenburg and Little, the same values as used by BH, with the exception of the value at 4.2 Mev by May and Powell,[39] were considered. The energies and the experimental f's used are shown in Table VII. The interpretation of the data is as mentioned in BH.

The proper weighting to be assigned to the work of a set of experimenters is uncertain. The use of the nominal probable error as a criterion may be of significance, but it does not necessarily correspond to the relative value of different sets of observations, since the reluctance of an experimenter to claim too much accuracy enters the nominal error in a strong but unknown manner. Nor does this criterion consider the self-consistency of a given set of data. It was desired to obtain weightings for the different observations which were free in some measure from arbitrariness. This was partially accomplished by employing a criterion based on the internal consistency of the data of a given set of observers. It is clearly impossible to devise a criterion which is completely adequate and fair, since the comparison of observations at different energies presupposes the knowledge of variation of f with energy, and this variation is one of the things which must be found. On the other hand the data of one group of observers cover a reasonably limited range of energy values, and the collection of all data with any reasonable assignment of relative weights to the observations determines df/dE with fair definiteness. It is possible, therefore, to reduce the data of a single group of observers (SGO) to one energy by correcting for the effect of df/dE and to test the quality of the data by the consistency with which the reduced values check each other. Specifically this plan was carried out as follows. A preliminary fit to data similar to that obtained by BH was used to determine approximate values $f^{(0)}=7.788$, $f^{(1)}=0.940$, $f^{(2)}=-0.0053$. The value of $f^{(2)}$ used here corresponds to that expected for the meson potential according to the representations of $f^{(0)}$, $f^{(1)}$, $f^{(2)}$ in terms of the depth parameter C' and range parameter a' of the meson potential. The corresponding fit in the BH paper gave the very similar values $f^{(1)}=0.939$, $f^{(2)}=-0.0057$, even though the weights used in the least squares calculation were very different. The fit was next corrected for tail effect employing 0.41 as the value of the range parameter. The inclusion of the tail effect is primarily responsible for the markedly different value of $f^{(2)}=-0.00935$. The values $f^{(0)}$ and $f^{(1)}$ were then adjusted so as to correspond to the best linear fit for $f-f^{(2)}E^2$ resulting in $f^{(0)}=7.780$, $f^{(1)}=0.954$. According to Appendix A, the three $f^{(i)}$ thus obtained should correspond to the best meson fit rather closely except for changes arising from the assignments of different weights to observations. Since these values were obtained by fitting what are believed to be all of the more accurate measurements, the values of $f^{(1)}$ and $f^{(2)}$ were considered to be good enough for making corrections for energy of data within the material of any SGO. A constant $f^{(0)}{}_l$ was then determined by subtracting $f^{(1)}E+f^{(2)}E^2$ from the observed f of a SGO and averaging the results. This $f^{(0)}{}_l$ is a local $f^{(0)}$ for the SGO, and the subscript l is meant for "local" in local energy. The mean deviation of the observed f from $f^{(0)}+f^{(1)}E+f^{(2)}E^2$ was calculated for the SGO, and a relative weight for any observation of the SGO proportional to the reciprocal of the square of the mean deviation was then used in a least squares adjustment of $f^{(0)}$, $f^{(1)}$, $f^{(2)}$ to the observations of all of the SGO included in the analysis.

It appears pertinent to mention that the criterion is not capable of penalizing the data on account of the presence of a systematic error which would affect all the f of an SGO by the same amount. The desirable feature of this circumstance is that all observations are on the same footing regarding the determination of the f curve as long as the quality of observations is the same in the sense tested by the criterion of internal consistency. An undesirable feature is the possibility of leaving systematic errors undetected and of occasionally permitting statistical accidents in which data with poor statistics receive a high rating because the sample happens to show small dispersion. The criterion does not in any sense provide a figure of merit for the data of a given group of observers from such viewpoints as accuracy within a certain percentage of error in the cross section. In principle poor data at an energy especially favorable for the determination of f can receive a relatively high rating. Other possibilities of unfairness to data are mentioned in the introduction.

[39] A. N. May and C. F. Powell, Proc. Roy. Soc. (London) **A190**, 170 (1947).

Since several groups of observers are involved, a degree of statistical compensation of errors committed in weight assignment may be expected. The weights per observation w, determined by this criterion, are Ragan, Kanne, and Taschek[30]: 0.00353; HL: 0.0233; HHT: 0.00843; Herb, Kerst, Parkinson, and Plain[31]: 0.08338; and Blair, Freier, Lampi, Sleator, and Williams[32]: 0.06438. This method of obtaining weights will be referred to as criterion $\mathcal{I}$ to indicate that it is primarily based on internal consistency.

In order not to depend on this criterion too heavily, a second criterion was used in which the deviation of the f values of a SGO from the f curve as determined by criterion $\mathcal{I}$ was also used to determine the quality of data. The obvious danger of relying on such considerations is apparent in the example of sampling a Gauss error distribution. Were one to omit the observations outside the probable error, perfectly valid measurements would be left out of account. The difference between the Gauss error distribution and the statistical sample for the determination of the f curve is, however, that the statistical equivalence of all observations of the Gauss error distribution can hardly be expected to apply to data obtained with different equipment in different energy regions. Observations which are removed from the f curve by several times the nominal probable error would have to be supposed to contain a systematic error with a large probability, and their weight would have to be considered as small. A partial account of this circumstance was taken by calculating a second set of relative weights w', proportional to the reciprocal square deviation from the f curve determined by criterion $\mathcal{I}$. The weights obtained were RKT: 0.00315; HL: 0.01981; HHT: 0.00441; HKPP: 0.09242; and BFLSW: 0.06113. The least squares fit was then repeated with relative weights $(w+w')/2$. The second criterion is referred to as the $\mathcal{I}\mathcal{E}$ criterion. The values obtained are

$$\begin{aligned} &f^{(0)}=7.7846, \quad f^{(1)}=0.9564, \quad f^{(2)}=-0.01041 \quad \text{(criterion } \mathcal{I}\text{)}, \\ &f^{(0)}=7.7864, \quad f^{(1)}=0.9558, \quad f^{(2)}=-0.01044 \quad \text{(criterion } \mathcal{I}\mathcal{E}\text{)}. \end{aligned} \tag{6}$$

In addition, a linear least squares fit to the data results in

$$\begin{aligned} &f^{(0)}=7.8107, \quad f^{(1)}=0.9173 \quad \text{(criterion } \mathcal{I}\text{)}, \\ &f^{(0)}=7.8132, \quad f^{(1)}=0.9165 \quad \text{(criterion } \mathcal{I}\mathcal{E}\text{)}. \end{aligned} \tag{7}$$

This procedure is admittedly arbitrary and has been tried in a somewhat experimental spirit. It is apparent, however, that the assigned weights cannot make too much difference in the least squares fit. Using their weighting, BH found by a linear least squares fit that $f^{(0)}=7.82$, $f^{(1)}=0.916$. These values are very close (with $\frac{1}{2}$ percent) to those obtained similarly by Jackson and Blatt. The present linear least squares fit gives values which differ from those of BH by about 0.1 percent for $f^{(1)}$ and less for $f^{(0)}$, as shown in Eq. (7).

TABLE VII. Values of f used in the least squares analysis. These are in addition to those for the Heydenburg-Little data.

E(Mev)	f	Source
0.25	7.984	RKT[a]
0.30	8.174	RKT
0.670	8.279	HHT[b]
0.776	8.465	HHT
0.867	8.616	HHT
0.860	8.601	HKPP[c]
1.200	8.944	HKPP
1.390	9.134	HKPP
1.830	9.478	HKPP
2.105	9.749	HKPP
2.392	10.004	HKPP
2.42	10.022	HKPP
3.04	10.637	BFLSW[d]
3.27	10.781	BFLSW
3.53	11.029	BFLSW

[a] See reference 30. [b] See reference 15. [c] See reference 31. [d] See reference 32.

The importance of considering the curvature in a fit of this type has already been discussed.[33] It is, however, not a large effect, and the fit to data offered by Eqs. (6) is perhaps just significantly better than the fit as offered by Eqs. (7). For the quadratic fit, the root mean square (rms) residual[34] is 0.0332 for the criterion $\mathcal{I}$ and 0.0309 for that using the weights of criterion $\mathcal{I}\mathcal{E}$. The rms residual for any quadratic fit to these data with $f^{(2)}$ fixed, of which the linear fit is a special case, is $0.0320(1+\Delta)$, where the average quadratic fit residual is used as the basic value. The quantity Δ will always be a positive number and is in fact $\cong 390(f^{(2)}+0.01)^2$. For a linear fit, $\Delta=0.04$. The improvement in the fit to the data which is produced by employing a quadratic rather than a linear fit is thus seen to be only 4 percent as measured by the rms residual. The rms residual apparently is sufficiently large to preclude the precise determination of three coefficients. Another condition to limit the variation of $f^{(2)}$ is needed.

Strictly speaking, one must consider the problem from the viewpoint of fitting the data by a polynomial in E such as $f^{(0)}+f^{(1)}E+f^{(2)}E^2$ with $f^{(0)}$, $f^{(1)}$, $f^{(2)}$ regarded as functions of the potential well parameters such as C' and a' for the meson well. Since $f^{(0)}$, $f^{(1)}$ can be used to determine C', a', this amounts to subjecting $f^{(2)}$ to the condition of being a definite function $f^{(2)}(f^{(0)}, f^{(1)})$ of $f^{(0)}$ and $f^{(1)}$ and regarding $f^{(0)}$, $f^{(1)}$ as independent variables. The weighted sum of squares of deviations must then be minimized with respect to $f^{(0)}$ and $f^{(1)}$. It is shown in Appendix A that in a good approximation

[30] Ragan, Kanne, and Taschek, Phys. Rev. **60**, 628 (1941), referred to in the text as RKT.

[31] Herb, Kerst, Parkinson, and Plain, Phys. Rev. **55**, 998 (1939), referred to in the text as HKPP.

[32] Blair, Freier, Lampi, Sleator, and Williams, Phys. Rev. **74**, 553 (1948), referred to in the text as BFLSW.

[33] See reference 18, Eq. (7) *et seq.*, and amplified discussions in Sec. I and Appendix A of the present paper.

[34] The residual is defined as the difference between the experimentally determined value and the value obtained from the fitted curve. The root mean square or rms residual represents an "average" deviation from the curve.

such a procedure gives nearly the same answers as are obtained by the following requirements: (A) the equations obtained by minimizing the weighted sum of squares with respect to $f^{(0)}$ and $f^{(1)}$, neglecting the entrance of $f^{(0)}$, $f^{(1)}$ into $f^{(2)}$; (B) restricting the value of $f^{(2)}$ so obtained by the requirement that $f^{(2)}=f^{(2)}(f^{(0)}, f^{(1)})$. The solution of the modified problem can be obtained in practice by an iteration procedure in which step (A) is taken with an approximate $f^{(2)}$, the resultant values of $f^{(0)}$, $f^{(1)}$ are used to compute an improved $f^{(2)}$, and the cycle repeated if necessary. The first step in this procedure is essentially what has been done in the work of Jackson and Blatt[1] and of Breit and Hatcher.[18] The question arises regarding the advisability of fitting data by least squares in preference to the simpler visual adjustment of a straight line or curve. Without trying to provide a complete answer, one may note nevertheless some pitfalls in the method of visual fits. These have been partly discussed by HAB in connection with the error involved in neglecting the curvature of the (f, E) plot. More specifically one can estimate the effect of an error of judgment in estimating the curvature of this plot. If the curvature is a result of a term in x^2 with $x=E/E_{\max}$, then the least squares representation of an error x^2 by a linear function has exactly the slope of the chord between $x=0$ and the maximum x used. A replacement of the least squares fit by a chord between end points would in this case give a reliable value of $f^{(1)}$. However, the value of $f^{(0)}$ would be seriously affected because the least squares straight line is lower than the chord by $x^2/6$, and for an error resulting in the representation of $-0.0040E^2$ by a linear fit there results a false contribution to $f^{(0)}$ of amount $0.00067E_{\max}{}^2$. For $E=3$ this contribution is 0.006 which is uncomfortably close to the desired accuracy.

Similarly, data analysis taking no account of the presence of $f^{(3)}E^3$ and assigning a correct $f^{(2)}$ will reproduce the value of the slope of the chord to within 9/10 of the true value of the omitted part and will make a false contribution to $f^{(0)}$ of $-f^{(3)}E^3/5$. For $E=10$ and $f^{(3)}=0.000270$ the error in slope is equivalent to 0.27 percent effect on range, while for $E=3$ this error is negligible. For $E=10$ the effect on $f^{(0)}$ is an objectionably large 0.05 while for $E=3.5$ it is a tolerable but nevertheless undesirable 0.002. All of the numbers quoted in connection with the cubic error are for uniform weighting of the observations. It is presumably difficult to make visual straight line fits with allowance for curvature to a degree much better than establishing the chord between end points followed by an approximate and roughly parallel displacement. The resultant errors may be appreciably greater than those arrived at in the estimates just quoted because of the confusion presented to the eye by points not following a regular line and because the cancellation of errors for the slope is accidentally small for uniform weighting.

Accordingly, therefore, the least squares equations were solved to give the best fit consistent with various types of potential wells. In order to make the solution consistent with the meson potential, for example, one can correct for the tail effect and then use values of $f^{(0)}, f^{(1)}, f^{(2)}$ consistent with the representations of these quantities in terms of depth and range parameters by formulas in HAB. For the square well, Eqs. (8.6) through (8.84) of BB were used, with Eq. (8.42) of that paper, to give an approximate value of $f^{(2)}=0.00475$ when a range was fixed. The value $f^{(2)}=-0.0015$ given by Jackson and Blatt[1] for the exponential well was used. The changes in $f^{(0)}$, $f^{(1)}$, and $f^{(2)}$ are so small that they are proportional to each other, and it is thus unnecessary to solve the least squares equations again once the solutions given by Eqs. (6) and (7) have been obtained. By the use of Eq. (5) along with Eqs. (6) and (7), one is able to find the best meson fit at once. Equations (8.6) through (8.42) of BB are used in place of Eq. (5) for the square well, while Eq. (11.3E) of Jackson and Blatt serve for the exponential well.

The results are:

(a) best meson fit,

$$\begin{aligned} &f^{(0)}=7.787\pm0.009, \quad f^{(1)}=0.953\pm0.005, \\ &\qquad f^{(2)}=-0.00949 \quad \text{(criterion } \mathcal{g}\text{)}, \\ &f^{(0)}=7.789\pm0.009, \quad f^{(1)}=0.952\pm0.005, \\ &\qquad f^{(2)}=-0.00947 \quad \text{(criterion } \mathcal{g}\mathcal{E}\text{)}. \end{aligned} \tag{8}$$

Although the values of the $f^{(i)}$ listed in Eq. (8) are referred to as "the best meson fit," the procedure followed in obtaining them contains an approximation which must now be explained. It was assumed that approximate proportionality of $f^{(2)}$ to the square of the range parameter holds for $f^{(2)}$, including tail effect, even though the proportionality of $\delta f^{(2)}$ to a a'^2 has not been investigated. Since the standard reference value of $f^{(2)}$ with tail which was used here (line F, Table I) was for $C'=99$, $a'=0.40$ a pair of parameters lying close to the values representing experiment, this approximation can be expected to be satisfactory. The values of C', a' obtained by means of it will be referred to below as "preliminary." They have been checked by two other methods which will be described presently.

(b) approximate best exponential fit,

$$f^{(0)}=7.810, \quad f^{(1)}=0.922, \quad f^{(2)}=-0.0015 \quad \text{(criterion } \mathcal{g}\mathcal{E}\text{)}; \tag{8.1}$$

(c) approximate best square well fit,

$$f^{(0)}=7.825, \quad f^{(1)}=0.899, \quad f^{(2)}=0.0048 \quad \text{(criterion } \mathcal{g}\mathcal{E}\text{)}. \tag{8.2}$$

The values of Δ are, respectively, 0.0001, 0.028, and 0.087 for the meson, exponential, and square well fits. The smallness of these values indicates that the data are not sufficiently accurate to distinguish satisfactorily among the fits. The entries preceded by $\pm$ signs such as ±0.010 for $f^{(0)}$ indicate probable errors (not standard deviations) and have been calculated from rms residuals

in the least square work. It is of interest to compare them with the error in f to be expected for one percent error in scattering which is shown for comparison in Table II. With 15 observations of equal weight and a probable error of ± 0.01 in $f^{(0)}$, the probable error of one observation can be expected to be ± 0.04, and this number is reasonable if one supposes that the scattering measurements have an accuracy of one percent and employs Table II. The approximate magnitude of the uncertainty in $f^{(1)}$ can be understood as being the uncertainty in $f^{(0)}$ at an energy distant 2 Mev from a reference energy. The distance of 2 Mev is a reasonable distance since the observations are distributed through 3.3 Mev. The uncertainty of $f^{(1)}$ is thus essentially understandable also in terms of a one percent error in scattering.

The parameters C', a' of the Yukawa potential which correspond to the f-coefficients of Eq. (8) are obtained in first approximation from Eq. (4) by the use of the values of line F, Table I for $C'=99$, $a'=0.40$ as base coefficients. Equation (4) resulted from the HAB representations, and thus does not contain the effect of the tail of the potential. The preliminary values of C' and a' resulting from Eq. (4) were used, therefore, in Eq. (3) to compute $f^{(0)}$ and $f^{(1)}$. These tail corrections were applied with opposite sign to the "experimental fit" coefficients of Eq. (8); thus a virtual chopping off of the physical tail of the potential was effected. The coefficients so obtained were used in Eq. (4) to obtain the final values of the parameters. The results are

$$\begin{aligned} &C'=93.44mc^2, \quad a'=0.412e^2/mc^2, \quad \text{(criterion } \mathcal{I}\text{)} \\ &C'=93.58mc^2, \quad a'=0.412e^2/mc^2, \quad \text{(criterion } \mathcal{I}\mathcal{S}\text{)}. \end{aligned} \tag{9}$$

Since these values differed by less than 0.5 percent from the preliminary results, the calculations of $\delta f^{(0)}$ and $\delta f^{(1)}$ were not repeated. The ranges agree within the precision with which they are written for the two weightings and correspond to a meson mass of 333 electron masses.

An independent method of arriving at the meson parameters was also used. For this purpose plots of f, E for $a'=0.410$ and 0.415 and each of three values of $1/(C'a'^2)^{\frac{1}{2}} \equiv y$ (namely, 0.2514372, 0.2511965, and 0.2509653), were compared with an f, E plot made using the coefficients of Eq. (6). The f values for the theoretical curves were computed directly from the material used to obtain the HAB phase shifts and interpolated (linearly in y, parabolically or bilinearly in a') to the desired values of a' and y. Tail corrections interpolated in Table IV were applied. In each case the quantity actually plotted was $f-(7.7941+0.9643E)$ in order that a small variation in values over the energy range 0–5 Mev would allow a very large scale to be used. Figure 3 shows the one experimental and six theoretical curves thus obtained, together with the experimental points used in the least squares analysis (Tables VI and VII). The theoretical curves show that a change in a' produces a rotation in the curves, while a change in y translates the curves up or down, and that the rotation and translation is very nearly linear in a' and y, respectively, for the small changes illustrated in the figure. It is of interest to compare Figs. 6, 7, and cogent material of BTE, where K_0, E plots with similar properties are used. The slope of chords drawn to the theoretical curves between 0 and 3.5 Mev was used as a measure of the rotation and with that of the experimental curve to determine the value of a'. With this value of a', linear interpolations at several energies for constant values of y were carried out on the graph to give several points on a curve with the experimental value of a' but with the values of y used in plotting the theoretical curves. The experimental value of y was then interpolated. The results of this analysis are:

$$C'=93.11mc^2, \quad a'=0.412e^2/mc^2. \tag{10}$$

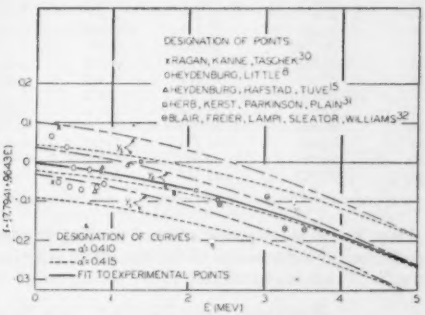

FIG. 3. Theoretical values of $f-(7.7941+0.9643E)$ for $a'=0.41$ and 0.415 with y_1, y_2, y_3 having the values 0.2514372, 0.2511965, and 0.2509653, respectively, *vs* E, together with the least squares fit to data of Eq. (6), criterion ($\mathcal{I}\mathcal{S}$), and experimental points as designated.

The close agreement between Eqs. (9) and (10) is satisfying, but is not to be taken as an indication of the precision of the present determination of the meson parameters. If one puts the probable errors of Eq. (8) into the first of Eqs. (4), an uncertainty in a' of 0.002 results. The scatter of the experimental points on Fig. 3 gives visual evidence of this uncertainty, as well as one in y. The probable errors give an uncertainty in y of 5×10^{-5}, which is actually larger than the spread in the three values of y obtained from Eq. (8) and in the graphical analysis, and is of the order of that which one might expect from the scatter (though somewhat smaller). As the most precise result of this analysis, therefore, the value of y may be stated as

$$y=0.25112\pm 0.00005.$$

Assuming this value of y and letting the uncertainty in C' be determined, therefore, by that in a', the parameters resulting from this analysis are

$$C'=93.4\pm 1mc^2, \quad a'=0.412\pm 0.002e^2/mc^2. \tag{11}$$

TABLE VIII. Values of f_0 for meson potential with parameters $C_0'=89.648$, $a_0'=0.42$, $y_0=0.2514667$, and coefficients for finding change in f with changes in a' and y.

E(Mev)	f_0	α_1	α_2	α_3
0.2	7.977	−11.350	275.5	−694
0.4	8.169	−10.889	277.4	−691
0.6	8.361	−10.436	279.2	−685
1.0	8.743	− 9.538	282.9	−673
1.4	9.122	− 8.679	286.7	−668
1.8	9.498	− 8.013	290.1	−662
2.2	9.872	− 7.033	293.7	−652
2.4	10.057	− 6.640	295.3	−647
2.6	10.242	− 6.212	297.2	−641
3.0	10.611	− 5.418	301.3	−640
4.0	11.526	− 3.467	310.3	−623
5.0	12.427	− 1.593	319.3	−610
6	13.315	0.158	327.5	−581
7	14.185	1.861	336.3	−578
8	15.056	3.523	344.6	−561
9	15.900	5.122	353.0	−547
10	16.684	6.613	359.8	−533
12	18.399	9.628	377.1	−512
14	20.012	12.457	392.6	−494
16	21.601	15.216	407.7	−470
18	23.142	17.757	422.4	−453
20	24.674	20.305	436.9	−433
22	26.181	22.778	451.0	−417
24	27.657	25.171	464.8	−399
26	29.120	27.536	478.1	−369
28	30.571	29.656	492.1	−358
30	32.000	31.909	513.0	−350
32	33.418	34.273	518.9	−312
36	36.203	38.342	544.1	−308
40	38.923	42.445	568.6	−269

From Eq. (8.1), the parameters of the best fit exponential well, if the potential of the interaction is written as $-Be^{-r/b}$, are, approximately,

$$B=214mc^2, \quad b=0.251e^2/mc^2. \tag{11.1}$$

The square well depth, D, and range, r, are determined from Eq. (8.2) to be about

$$D=12.60 \text{ Mev}, \; r=0.919e^2/mc^2, \tag{11.2}$$

$$D_c=13.50 \text{ Mev}. \tag{11.2'}$$

The square well depth, D_c, given in Eq. (11.2') includes the Coulomb potential inside the well. The correction from D of Eq. (11.2) has been made by Eq. (11) of BTE. A corresponding range correction, which is small, has not been made. These results agree well with those of BH and of Jackson and Blatt.

The series expansions of f with the coefficients of Eq. (6), (8), (8.1), and (8.2) are plotted in lower part of Fig. 1 up to 4 Mev with the experimental points included. The various sets of coefficients give essentially indistinguishable curves which fit the data equally well. It is of interest, therefore, to see how well a theoretical curve fits the higher energy data. In order to obtain the values of f needed for the meson well, an interpolation formula was obtained:

$$f=f_0+\alpha_1(a'-a_0')+\alpha_2(y-y_0)+\alpha_3(a'-a_0')(y-y_0), \tag{12}$$

where α_1, α_2, α_3 are functions of E and are given in Table VIII. Linear interpolation in E is quite accurate. The basic values of f, designated f_0 in Eq. (12), were computed for $C'=89.648$, $a'=0.420$, and corrected for tail effect from Table IV. The f_0 are also given in Table VIII. The values of a_0' and y_0 to be used are $a_0'=0.420$ and $y_0=0.2514667$. Accuracy of the order of 0.01 in f is expected if $(a'-a_0')$ and $(y-y_0)$ are $\sim$0.01 or less. Equation (12) with Table VIII may find more general application than in the present analysis. For use in converting experimental data to f values, there are also presented in Table IX values of C_0^2/η and $q_0/\eta-2ln\eta$. Equation (7.6) of BCP is then used with the experimental K_0, and this table to give f values.

For the exponential well, the value $f^{(3)}=1.2\times10^{-5}$ taken from the analysis of Jackson and Blatt was used together with the coefficients of Eq. (8.1) to plot the f curve at higher energies. The coefficients of Eq. (8.2) were used to plot the square well curve, and the plot was discontinued before the contribution from $f^{(3)}$ became significant, since $f^{(3)}>0$ for this well, and the curve had already begun diverging strongly from the experimental data at 20 Mev.

The f curves to 30 Mev corresponding to the parameters of Eqs. (11), (11.1), and (11.2) together with the linear fit of Eq. (7) and the available experimental data are shown in the upper part of Fig. 1. The data of Dearnley, Oxley, and Perry[35] have not been used because it is understood that the later work of Rouvina[2] at the same laboratory and using the same general method has a much higher accuracy. The correction to the phase shift of May and Powell,[29] the necessity of which has been noted by Jackson and Blatt,[1] has been used in preparing the graph. The other data plotted consist of work by Meagher,[36] Panofsky, and Fillmore,[4] Faris and Wright,[5] Zimmerman and Kreuger,[6] Mather,[7] Wilson and Creutz,[37] Wilson,[38] Wilson, Lofgren, Richardson, Wright, and Shankland,[39] and Cork.[3] For the value at 10 Mev by Wilson, the analysis of Peierls and Preston[40] was used. The values of f for the other two points of Wilson *et al.* were taken from Jackson and Blatt. The interpretation of Cork[41] was used for other values given by him.

Points at energies below $\sim$7 Mev do not favor any one of the potentials. Only the values of Rouvina

[35] Dearnley, Oxley, and Perry, Phys. Rev. **73**, 1290 (1949).
[36] R. E. Meagher, Phys. Rev. **78**, 667 (1950).
[37] R. R. Wilson and E. C. Creutz, Phys. Rev. **71**, 339 (1947).
[38] R. R. Wilson, Phys. Rev. **71**, 384 (1947).
[39] Wilson, Lofgren, Richardson, Wright, and Shankland, Phys. Rev. **71**, 560 (1947).
[40] R. E. Peierls and M. A. Preston, Phys. Rev. **72**, 250 (1947).
[41] The figure displaying agreement of data with theory in the paper just quoted refers to Jackson and Blatt's work for the theory used. Since the power series expansion given by Jackson and Blatt is not supposed to apply at such high energies, and since in the present work the employment of higher powers of E than the third was found necessary, there is some difficulty in understanding this statement. The curve drawn in Cork's paper differs only slightly from the f curve obtained by use of phase shifts tabulated by HAB for $a'=0.40$, $C'=99$ and could have been ascertained by substituting these phase shifts in the formula for f and applying a small correction for differences in values of potential well parameters.

indicate a slight preference for the Yukawa and exponential wells. The preference is not definite, but the value at 5.86 Mev from the measurements of Zimmerman and Kreuger[6] also appears to favor the longtailed potentials. It seems that some additional work at energies in this vicinity might be helpful in distinguishing between the phenomenologically postulated potentials. At the higher energies, the values of Cork[3] and that of Panofsky and Fillmore[4] definitely favor the longtailed potentials.

APPENDIX A

The justification for employing simple iteration in determining "best values" of potential well parameters will now be given. The complete problem with allowance for the entrance of $\partial f^{(2)}/\partial f^{(0)}$, $\partial f^{(2)}/\partial f^{(1)}$ in the answer will be considered, and it will then be shown that the effect of these quantities is insignificant. It is convenient to use the simplified notation

$$f^{(0)}=l, \quad E_{\max}f^{(1)}=m, \quad E_{\max}{}^2f^{(2)}=n, \quad E/E_{\max}=x$$
$$\partial n/\partial l=n_l, \quad \partial n/\partial m=n_m \qquad \text{(A-1)}$$
$$E_{\max}=\text{maximum energy.}$$

The least squares equations are

$$\begin{aligned}\langle(1+n_lx^2)(l+mx+nx^2-f)\rangle&=0\\ \langle(x+n_mx^2)(l+mx+nx^2-f)\rangle&=0,\end{aligned} \qquad \text{(A-2)}$$

where $\langle\ \rangle$ indicates a weighted mean. These equations are conveniently referred to the best quadratic fit (l_0, m_0, n_0) for the same relative weights. For this

$$\begin{aligned}\langle l_0+m_0x+n_0x^2-f\rangle&=0\\ \langle l_0x+m_0x^2+n_0x^3-fx\rangle&=0\\ \langle l_0x^2+m_0x^3+n_0x^4-fx^2\rangle&=0.\end{aligned} \qquad \text{(A-3)}$$

Introducing $\lambda=l-l_0$, $\mu=m-m_0$, $\nu=n-n_0$ one obtains

$$\begin{aligned}n(l_0+\lambda, m_0+\mu)-n_0-\nu&=0\\ \langle(1+n_lx^2)(\lambda+\mu x+\nu x^2)\rangle&=0\\ \langle(x+n_mx^2)(\lambda+\mu x+\nu x^2)\rangle&=0.\end{aligned} \qquad \text{(A-4)}$$

The λ, μ, ν are relatively small. The approximation corresponding to the iteration procedure described in the text is obtained by setting $n_l, n_m=0$ in Eq. (A-2). The solution of the modified equation will be called l', m', n'. To introduce $\lambda'=l'-l_0$, $\mu'=m-m_0$, $\nu'=n-n_0$, there results a way of obtaining (λ', μ', ν') as the solution of

$$\begin{aligned}n(l_0+\lambda', m_0+\mu', n_0+\nu')&=0\\ \langle\lambda'+\mu'x+\nu'x^2\rangle&=0\\ \langle\lambda'x+\mu'x^2+\nu'x^3\rangle&=0.\end{aligned} \qquad \text{(A-5)}$$

On expanding $n(l_0+\lambda, m_0+\mu)$ in Eq. (A-4) in a Taylor series and neglecting quadratic and higher order terms one obtains

$$\begin{aligned}\lambda=\{&\langle x\rangle\langle x^3\rangle-\langle x^2\rangle^2+n_l[\langle x^3\rangle^2-\langle x^2\rangle\langle x^4\rangle]\\ &+n_m[\langle x\rangle\langle x^4\rangle-\langle x^3\rangle\langle x^2\rangle]\}/D\\ \mu=\{&\langle x\rangle\langle x^2\rangle-\langle x^3\rangle+n_l\langle x\rangle\langle x^4\rangle-\langle x^2\rangle\langle x^3\rangle]\\ &+n_m[\langle x^2\rangle^2-\langle x^4\rangle]\}/D \qquad \text{(A-6)}\\ \nu=\{&\langle x^2\rangle-\langle x\rangle^2+n_l[\langle x^3\rangle^2-\langle x\rangle\langle x^3\rangle]\\ &+n_m[\langle x^3\rangle-\langle x\rangle\langle x^2\rangle]\}/D,\end{aligned}$$

with

$$\begin{aligned}[n_0-n(l_0, m_0)]D=&\langle x\rangle^2-\langle x^2\rangle+2n_l[\langle x\rangle\langle x^3\rangle-\langle x^2\rangle^2]\\ &+2n_m[\langle x\rangle\langle x^2\rangle-\langle x^3\rangle]+Q \qquad \text{(A-7)}\end{aligned}$$

$$\begin{aligned}Q=&n_l{}^2[\langle x^3\rangle^2-\langle x^3\rangle\langle x^4\rangle]+2n_ln_m[\langle x\rangle\langle x^4\rangle-\langle x^2\rangle\langle x^3\rangle]\\ &+n_m{}^2[\langle x^2\rangle^2-\langle x^4\rangle]. \qquad \text{(A-8)}\end{aligned}$$

The λ', μ', ν' are obtained by setting $n_l=n_m=0$ in these relations. If the measurements have equal weights and are distributed uniformly in the range $0<x<1$, these formulas reduce to

$$\begin{aligned}\lambda&=(1/72-n_l/240+n_m/60)/D\\ \mu&=(-1/12+n_l/60-4n_m/45)/D \qquad \text{(A-9)}\\ \nu&=(1/12-n_l/72+n_m/12)/D\end{aligned}$$

$$\begin{aligned}[n_0-n(l_0, m_0)]D=&-1/12+n_l/36-n_m/6-n_l{}^2/240\\ &+n_ln_m/30-4n_m{}^2/45. \qquad \text{(A-10)}\end{aligned}$$

For the approximate best quadratic fit to data with one of the weightings that has been tried in a preliminary way $f^{(0)}=7.789$, $f^{(1)}=0.938$, $f^{(2)}=-0.0049$, and $E_{\max}=3.5$ Mev the values are $l_0=7.79$, $m_0=3.3$, $n_0=-0.060$.

TABLE IX. Quantities for computing f from phase shifts.

E(Mev)	$C\eta^3/\eta$	$(q_0/\eta)-2ln(\eta)$
0.2	0.76448	1.50563
0.4	1.649211	2.06980
0.6	2.411586	2.42936
1.0	3.695285	2.90232
1.4	4.776889	3.22223
1.8	5.728617	3.46426
2.2	6.588139	3.65899
2.4	6.990691	3.74377
2.6	7.377889	3.82192
3.0	8.112484	3.96199
4	9.767629	4.24472
5	11.233633	4.46489
6	12.563461	4.64522
7	13.789206	4.79795
8	14.932039	4.93042
9	16.006798	5.04737
10	17.024373	5.15207
12	18.919171	5.33339
14	20.663649	5.48683
16	22.288750	5.61983
18	23.816065	5.73719
20	25.261372	5.84222
22	26.636624	5.93726
24	27.951095	6.02404
26	29.212215	6.10389
28	30.425987	6.17784
30	31.597390	6.24668
32	32.730549	6.31110
36	34.895729	6.42867
40	36.944136	6.53387

In the approximation $n=\text{const}m^2$ which takes into account the principal variations of n one has $n_l=0$, $n_m=-0.037$, and $n_m^2/45$ is quite negligible. All terms in n_m are seen to be sufficiently small to allow neglect of all but first-order effects in n_m. With this understanding and distinguishing quantities for the approximation l', m', n' by primes throughout, one obtains $D'/D=1-n_m=1.036$, $\lambda/\lambda'=0.9928$, $\mu/\mu'=0.9976$, $\nu/\nu'=1$. For the relative weights corresponding to the best quadratic fit under discussion the l', m', n' type of best meson fit to data gives $f^{(0)}=7.780$, $f^{(1)}=0.954$, $f^{(2)}=-0.00935$ which yields $\lambda'=-0.008$, $\mu'=0.056$ so that the correction factor to the l', m', n' type of solution arranged to obtain the l, m, n type is $1+\epsilon$ with $\epsilon=-0.0024(0.016/0.94)=-4\times10^{-5}$ for m', i.e., $f^{(1)}$ which amounts to a 0.004 percent correction in the range parameter. The effect on $f^{(0)}$ is a correction of the order -0.00006 in a total of 7.8 and is also of no interest. By employing the representations of the $f^{(i)}$ in HAB and taking into account n_l one estimates for the numbers under discussion that $n_m/n_l\cong-18$ so that n_m gives the main effects.

In the aforementioned estimates the effect of second- and higher order derivatives of n_0 has been neglected consistently for the complete problem corresponding to (l, m, n), and its approximation corresponding to (l', m', n'). Since these terms are small and since the difference in the two solutions, as considered, is negligible, the corrections for the second- and higher order derivatives may be considered as being practically identical and for the condition under discussion the corrections are of no practical interest.

In the more general case of arbitrary weights one has

$$\begin{aligned}\lambda/\lambda'&=1+n_l[(\langle x^3\rangle^2-\langle x^2\rangle\langle x^4\rangle)/\beta-\beta/\delta]\\&\quad+n_m(\alpha/\beta-\gamma/\delta),\\ \mu/\mu'&=1+n_l(\alpha/\gamma-\beta/\delta)\\&\quad+n_m[(\langle x^3\rangle^2-\langle x^4\rangle)/\gamma-\gamma/\delta],\end{aligned}\tag{A-11}$$

where

$$\begin{aligned}\alpha&=\langle x\rangle\langle x^4\rangle-\langle x^2\rangle\langle x^3\rangle, &\beta&=\langle x\rangle\langle x^3\rangle-\langle x^2\rangle^2\\ \gamma&=\langle x\rangle\langle x^5\rangle-\langle x^3\rangle, &\delta&=\langle x\rangle^2-\langle x^2\rangle.\end{aligned}\tag{A-12}$$

Substitution into these formulas for the fit discussed earlier in this Appendix employing values of the $\langle x^n\rangle$ which correspond to the relative weights employed in the least squares adjustment of the $f^{(i)}$, there result appreciably larger effects than in the estimates making use of uniform weighting. The values obtained by means of Eqs. (A-11), (A-12) are as follows

$$\lambda/\lambda'=0.9494,\quad \mu/\mu'=0.9802.$$

While larger than in the first estimates, the difference between the complete and approximate solutions is seen to be smaller than many other uncertainties in the determination of $f^{(0)}$, $f^{(1)}$, $f^{(2)}$.

The best linear fit corresponds to $l=l_0+\lambda''$, $m=m_0+\mu''$, $n=n_0+\nu''=0$ with

$$\lambda''+\mu''\langle x\rangle+\nu''\langle x^2\rangle=0,\quad \lambda''\langle x\rangle+\mu''\langle x^2\rangle+\nu''\langle x^3\rangle=0.$$

It follows from these relations and the result of setting n_l, n_m in Eqs. (A-6), (A-7) so as to obtain λ', μ', ν' that

$$\lambda''/\lambda'=\mu''/\mu'=-n_0/\nu'=\nu''/\nu',$$

which implies that difference between the values of l, m, n for the best quadratic and linear fits are proportional to corresponding differences between the best quadratic fit and any other fit with a preassigned $f^{(2)}$. According to the elementary relation for proportions this also implies that differences of l, m, n for two fits with arbitrarily assigned $f^{(2)}$ from the linear fit are proportional to each other. This fact follows directly from the least squares linear equations for the three fits. It gives a useful rule for avoiding repetition of similar calculations.

Neutron Scattering Lengths*

D. C. Peaslee†
Washington University, St. Louis, Missouri
(Received October 19, 1951)

The schematic treatment of nuclear reactions is applied to the case $E_n \to 0$ as a means of interpreting measurements of the scattering length a. It is found that the quantity $\Delta = (a - R)$ rather than a is significant for determining the resonance properties of the compound nucleus, where R is the phenomenological nuclear radius. In some cases this treatment can resolve ambiguity in the evaluation of a without the necessity of polarization measurements and assign the J value of a low-lying resonance or two, but it can only be used successfully for separated isotopes. For practically pure isotopes it can be used to determine rough values of level spacing D from the measured position of the levels nearest $E_n = 0$, or conversely. Values of D obtained in this way are plotted against A to yield an estimate of a parameter in the statistical formula for level density; this estimate suggests a somewhat more rapid increase in level spacing with decreasing excitation than given by the simplest statistical formula.

INTRODUCTION AND SUMMARY

A COMPLETE interpretation of the scattering length[1] for slow neutrons has been hampered by difficulty in separating the effects of near-lying resonance levels from the "potential scattering." The present note indicates how a schematic treatment of nuclear reactions[2] resolves this difficulty and allows the extraction of semi-quantitative information about the compound nuclear levels nearest $E_n = 0$.

A simple formula is presented that reduces in most cases of interest to a relation among the scattering length, nearest resonance energy, and average level spacing D in the compound nucleus (or alternatively the reduced neutron width γ^2), so that from any two quantities the third can be estimated. This relation is applied to susceptible data, and further measurements of possible interest are indicated. A very tentative order-of-magnitude curve for D (or γ^2) *vs* mass number A is extracted from presently analyzable data; this curve is then used in turn to suggest order-of-magnitude positions for unobserved levels.

I. FORMULATION

The scattering length a can be defined from the wave function of the neutron beam as $k \to 0$. Since only s-neutrons are involved, the wave function exterior to the nucleus is $\varphi = (kr)\psi = \sin k(r - a)$ and is determined by fitting its logarithmic derivative[2] at a suitable radius R:

$$R\varphi'/\varphi = kR \cot k(R - a) = f(E_n), \tag{1}$$

where the function f is determined by the nuclear forces interior to R. As $k \to 0$, this becomes

$$a - R = \Delta = -R/f(0). \tag{2}$$

All the resonance properties of the nucleus are expressed by f, so that according to (2) the significant quantity for interpretation is Δ rather than the measured scattering length. The radius R represents the point at which the incident neutrons are subject to a large, abrupt change in refractive index of the medium, which produces potential scattering. Of course this change is not perfectly sharp, and there is some uncertainty δR in the definition of R, although generally $\delta R \ll R$. As a standard value $\delta R = 1 \times 10^{-13}$ cm is assumed throughout, which implies that (2) is significant for analysis only if

$$|\Delta| > 10^{-13} \text{ cm}. \tag{3}$$

Failure to satisfy condition (3) means that there are no resonances available to s-neutrons that lie much closer than D to the position $E_n = 0$.

The function $f(E)$ has simple zeros at the resonance energies E_r, so that

$$1/f(E) = \Sigma_r [1/f'(E_r)][E - E_r], \tag{4}$$

where $f' = [\partial f/\partial E]_{E_r} = -\pi K R/D_r$ in the notation of reference 2. Here D_r is the effective level spacing at the rth resonance and may decrease rapidly with increasing E_r; K is a wave number appropriate to the motion of the neutron inside the nucleus. Thus

$$\Delta = -(1/\pi K)\Sigma_r D_r/E_r = -\Sigma_r \gamma_r^2/E_r, \tag{5}$$

where $\gamma_r^2 = \Gamma_n/2k$ is the "reduced width"[3] of the rth resonance level. The value of K is not precise and may vary considerably among the light nuclei; however, $K = 1.0 \times 10^{13}$ cm^{-1} should be in error by less than 50 percent for any particular case and will be assumed throughout.

If the level nearest $E_n = 0$ has $|D_0/E_0| \gg 1$, it is sufficient to approximate (5) by the corresponding single term, since for all other r, $|D_r/E_r| \ll 1$ unless there is an exceptional fluctuation in D_r. Thus most of the cases below are analyzed with the approximation

$$\Delta \approx -(1/\pi K)(D_0/E_0), \tag{5a}$$

although it may occasionally be necessary to include more terms of (5).

* Assisted by the joint program of the ONR and AEC.
† Now at Columbia University, New York, New York.
[1] E. Fermi and L. Marshall, Phys. Rev. **71**, 666 (1947).
[2] Feshbach, Peaslee, and Weisskopf, Phys. Rev. **71**, 145 (1947).
[3] E. P. Wigner, Am. J. Phys. **17**, 99 (1949).

Actually, E_r has an imaginary component $-\frac{1}{2}i\Gamma_a$, which has been neglected above as very small in comparison with E_r. Since $D_r/\Gamma_a \sim 10^5$ to 10^6, this is *a priori* reasonable; any exceptions would distinguish themselves as experimentally anomalous, and none is known.

For a bound resonance level the binding energy $-E_b$ does not equal E_r, for E_b is defined so that $f(-E_b) = -(2M'E_b/\hbar^2)^{\frac{1}{2}}R$, where M' is the reduced neutron mass. Assuming that a single term of (4) is sufficient in the neighborhood of a resonance, one has

$$-E_r = E_b + (M'E_b/\hbar^2)^{\frac{1}{2}}\gamma_r^2. \tag{6}$$

II. APPLICATION TO LIGHT NUCLEI

The simplest case is that of n-p scattering, for which the triplet and singlet scattering lengths are[4] $a_t = 5.3 \times 10^{-13}$ cm, $a_s = -23.8 \times 10^{-13}$ cm. The radius R should be chosen as the intrinsic range of the force, which is[5] $R_t = 1.8 \times 10^{-13}$ cm for the triplet square well. In this case $f = -KR\tan(KR - \pi/2)$, so that D_r can be computed exactly; it turns out that $D_r \approx 125$ Mev, $E_r \approx -11$ Mev before correction by (6). For the singlet system D_r and R are presumably about the same, although Δ_s is relatively insensitive to the choice of R_s. This insensitivity has been remarked in the interpretation of low-energy scattering measurements;[5] from the present point of view its cause is the great excess of resonant over "potential" scattering in the neighborhood of the low-lying resonance, which extends over a wide region $\frac{1}{2}\Gamma_n \approx 10$ Mev. Using the same R and D_r as for the triplet system, the singlet resonance is at $E_r \approx 1.9$ Mev. In comparison with the usual formulation, it must be remembered that this formulation[6] deals not with E_r but with E_v, which is defined in exact analogy to E_b, so that $f(E_v) = +(2M'E_v/\hbar^2)^{\frac{1}{2}}R$. Correction by a formula equivalent to (6) but with a reversal of sign for E_r yields $E_v \approx 0.06$ Mev, the usually quoted value. The difference between the two values of E_r represents the difference in depth of the corresponding square wells, or about 13 Mev.

The next heavier target is the deuteron, which has been studied by a number of investigators;[7-9] the most precise values[9] are

$$\left.\begin{matrix} a_{\frac{1}{2}} \\ a_{\frac{3}{2}} \end{matrix}\right\} = \begin{cases} 0.7 \pm 0.3 \\ 6.38 \pm 0.06 \end{cases} \times 10^{-13}\ \text{cm}, \tag{7a}$$

or

$$\begin{cases} 8.26 \pm 0.12 \\ 2.6 \pm 0.2 \end{cases} \times 10^{-13}\ \text{cm}, \tag{7b}$$

where polarization measurements are the only direct means to decide this characteristic ambiguity that occurs whenever the target spin is $I \neq 0$. An immediate but not surprising conclusion from these data is that an effective two-body square well interaction between neutron and deuteron[10] does not give a reasonable description of the triton. If (7b) is chosen, the two-body square well can give agreement only if there is a second bound doublet state in addition to the ground state; for (7a) this second level becomes unbound by about 1.3 Mev, which still implies an incredible doublet S level spacing of $\lesssim 10$ Mev. In both cases the well parameters are not very reasonable physically, with $R \approx 8.0 \times 10^{-13}$ cm, $V \approx 10$ Mev. One must therefore revert to somewhat less specific arguments: for the triton ground state with $E_b = -6.2$ Mev, E_r is probably on the order of -15 Mev; since the doublet S level spacing is presumably $\gg 15$ Mev, $a_{\frac{1}{2}}$ should reflect mainly the properties of the ground state. Thus $\Delta_{\frac{1}{2}}$ is positive, and the set of values (7b) is indicated. From this set, the lowest quartet S level is virtual with very uncertain position probably on the order of 10 Mev. Somewhat less uncertain is the feature that its half-width will be on the same order of magnitude as its position.

It would also be of interest to determine the singlet and triplet scattering lengths on H^3; if any indication of a resonance level in H^4 is found, the corresponding state would exist in He^4, differing only by Coulomb energy. For scattering on He^4 it is known that there are no bound S states, so that[11] $R \geq a = +(\sigma/4\pi)^{\frac{1}{2}} = 3.5 \times 10^{-13}$ cm.

The scattering length of lithium has been determined[12] for the separated isotope Li^7; because the initial spin $I \neq 0$, there is a twofold ambiguity in the assignment of $a_{I\pm\frac{1}{2}}$. If $R = 4.1 \times 10^{-13}$ cm is assumed, the two possible sets of Δ_J are $\Delta_{1,2} = (-10.8, -4.1)$ or $(-2.4, -9.1)$ in 10^{-13} cm units. Two resonances are reported[13] in neutron scattering on lithium, at 270 kev and ~ 1.15 Mev, with respective half-widths of 45 kev and ~ 2.4 Mev. If both are attributed to s-neutrons, the corresponding $\gamma_r^2/E_r = 0.7$, $\sim 4.5 \times 10^{-13}$ cm. The first of these values does not approach any of the observed Δ, so that the corresponding level is probably due[13] to neutrons with $l > 0$. The larger value of γ_r^2/E_r indicates a level spacing $D_r \approx 17$ Mev, but cannot be unambiguously associated with any particular Δ. In any case, the measured Δ indicate the presence of two such levels with dissimilar characteristics.

The respective scattering lengths on C^{12} and O^{16} targets are 6.4 and 5.8×10^{-13} cm. Comparison with the scattering of protons by these targets indicates[14] that

[4] H. A. Bethe, Phys. Rev. **76**, 38 (1949).
[5] J. M. Blatt and J. D. Jackson, Phys. Rev. **76**, 18 (1949).
[6] H. A. Bethe and R. F. Bacher, Revs. Modern Phys. **8**, 82 (1936).
[7] E. Fermi and L. Marshall, Phys. Rev. **75**, 578 (1949).
[8] Shull, Wollan, Morton, and Davidson, Phys. Rev. **73**, 842 (1948).
[9] D. G. Hurst and W. F. Alcock, Phys. Rev. **80**, 117 (1950); Can J. Research **29**, 36 (1951).
[10] M. M. Gordon, Phys. Rev. **80**, 1111 (1950).
[11] W. W. Havens, Jr., and T. I. Taylor, Nucleonics **6** (2), 66 (1950).
[12] C. G. Shull and E. O. Wollan, unpublished. All scattering data not otherwise specified are taken from this reference, and the author wishes to thank Drs. Shull and Wollan for the opportunity of seeing it.
[13] R. K. Adair, Phys. Rev. **79**, 1018 (1950).
[14] The author wishes to thank Professor H. T. Richards for this information.

the bound S levels in C^{13} have $E_b=-1.85$ Mev, $\gamma_r^2\approx 7.6\times10^{-13}$ Mev cm, and in O^{17} $E_b=-1.09$, -3.24 Mev, $\gamma_r^2\approx 0.05\times10^{-13}$, 2×10^{-13} Mev cm, respectively. Inserting these values in (6) and (5), one finds the phenomenological radius $R=4.4$, 5.2×10^{-13} cm for the two cases. If these are compared with the formula $R=r_0(A^{\frac{1}{3}}+1)$, where A is the mass number of the target nucleus, the value of the parameter is $r_0=1.41\pm0.07\times10^{-13}$ cm. This expression is used to compute R for the other light targets considered in this section, Li^7 and N^{14}.

For N^{14}, $\Delta_{\frac{1}{2},\frac{1}{2}}=(5.7, -0.3)$ or $(1.7, 7.7)$ in 10^{-13} cm, indicating at least one bound level. If the probable value of γ_r^2 suggested by neighboring light nuclei is taken as $\gamma_r^2\sim3\times10^{-13}$ Mev cm, the bound level has $E_b\sim2$ Mev.

III. APPLICATION TO HEAVIER NUCLEI

Here "heavier" nuclei are arbitrarily defined as those with $A>18$; there is less detailed knowledge of their level positions and parameters than for light nuclei. The interpretation of scattering lengths is frequently obscured by the presence of many isotopes and spins, when

$$a=\Sigma_k\rho_k a_k,\quad \sigma_{sc}/4\pi=\Sigma_k\rho_k a_k^2, \tag{8}$$

where the statistical factors are $\rho_k=\rho_I(J+\frac{1}{2})/(2I+1)$, ρ_I is the abundance of a given isotope of spin I, and $J=I\pm\frac{1}{2}$. It is clear that analysis is impossible for mixtures with two or more isotopes of comparable abundance; and even for practically single isotopes a twofold ambiguity exists in the assignment of $a_{I\pm\frac{1}{2}}$ unless $I=0$. Frequently, however, some information can be obtained in spite of the ambiguity if an independent measure of γ_r^2 or J is available for the nearest virtual states.

The cases in which known neutron resonances can be correlated with a are discussed below, referred to the compound nucleus. The one-level approximation (5a) is used throughout, and the effective R is taken from analysis of high energy neutron scattering[15] with some smoothing of fluctuations. All lengths are in units of 10^{-13} cm and γ_r^2 in units of Mev$\times10^{-13}$ cm. The effective level spacings are estimated from $D_r^J=-\pi KE_r\Delta_J$, where Δ_J is obtained from the scattering length measurements.

Na^{24}: $R=4.6$, $\Delta_{1,2}=(-6.3, +2.0)$ or $(+4.1, -4.2)$. A scattering resonance is observed[16] at $E_r=0.06$ Mev, apparently with $\Gamma_n\lesssim20$ kev; hence $\gamma_r^2/E_r\lesssim3$. This agrees best with the second set of Δ from the scattering length measurements, indicating $J=2$, $D_r^3=0.8$ Mev. A lower resonance has been found[17] at $E_r\approx3$ kev; but it does not show the characteristic dip below resonance and is therefore presumably because of neutrons with $l\neq0$.

Al^{28}: $R=4.6$, $\Delta_{2,3}=(-1.1, -1.1)$. The two lowest scattering resonances[18] are at $E_r\approx0.04$, 0.095 Mev, $\Gamma_n\lesssim6$, 15 kev, whence $\gamma_r^2/E_r\lesssim1.6$, 1.2. This is satisfactory agreement with the observed Δ, so that the two levels may be assigned $J=2$, 3 in indeterminate order; $D_r=0.1$, 0.3 Mev.

S^{33}: $R=4.5$, $\Delta_1=-1.3$. The lowest resonance[19] has $E_r=0.11$ Mev, $\Gamma_n\approx\Gamma\approx18$ kev. Thus $\gamma_r^2/E_r=1.1$, in excellent agreement with the observed Δ; $D_r^1\approx0.4$ Mev.

V^{52}: $R=5.4$, $\Delta_{3,4}(-12.6, +0.2)$ or $(1.8, -11.0)$. The lowest reported resonance[20] is at $E_r=2.7$ kev with a measured value of

$$(J+\tfrac{1}{2})/(2I+1)\gamma_r^2/E_r=5.6;$$

from this measurement $\Delta_{3,4}=(-12.7, -9.9)$. Best agreement with the observed Δ is obtained for $J=3$; $D_r^3=0.1$ Mev.

Mn^{55}: $R=5.5$, $\Delta_{2,3}=(-6.4, -10.5)$ or $(-11.2, -7.1)$, with[21] $\sigma_{sc}=1.8$ barn. Observed[19] resonances are at $E_r=0.35$, 2.4 kev; the measured values of $(J+\frac{1}{2})/(2I+1)\gamma_r^2/E_r$ lead to $\Delta_{2,3}=(-10.8, -4.2)$ or $(-5.9, -7.7)$ according as the lower level has $J=2$ or $J=3$. The agreement or disagreement with measured Δ is about the same for either choice of J for the lower level, so no assignment can be made on this basis. Independent considerations[22] indicate $J=3$ for the lower level; accordingly, $D_r^{2,3}=0.05$, 0.01 Mev.

Co^{59}: $R=5.7$, $\Delta_{3,4}=(-9.3, +2.1)$ or $(3.5, -7.9)$. The prominent resonance at $E_r=115$ ev has a peak value compatible only with[23] $J=4$. The value of $\Gamma_n\approx\Gamma$ is given[20] as 3.5 to 4.5 ev, whence $\gamma_r^2/E_r=6$ to 9, this range straddles the observed Δ only if $J=4$; $D_r^4=3$ kev.

As^{75}: $R=6.3$, $\Delta_{1,2}=(-5.3, +3.1)$ or $(5.2, -3.1)$. A resonance is reported[24] only as 115 ev$<E_r<$300 ev; combined with the ambiguity in Δ, this yields $D_r=1$ to 5 kev.

Ag^{110}: $R=6.7$, $\Delta_{0,1}=(6.9, -5.5)$ or $(-11.1, +0.7)$. The prominent resonance is reported[25] to have $E_r=5.2$ ev, $\Gamma_n\approx0.01$ ev, whence $\gamma_r^2/E_r\approx2$. This agrees with the measured Δ if $J=1$; $D_r^1=0.1$ kev. Although this assignment seems the most plausible, it should be remembered that Ag has at least two higher resonances[26] at 16 and 45 ev about which little is known.

I^{135}: $R=7.3$, $\Delta_{2,3}=(-4.3, -0.6)$ or $(+0.1, -3.7)$. In either case only one nearby virtual level is indicated, with $\Delta\approx-4$ and indeterminate spin. If Δ is associated with one of the strong resonances[27] at $E_r\approx35$ ev, $D_r=0.4$ kev.

Ta^{182}: $R=8.1$, $\Delta_{3,4}=(2.1, -3.5)$ or $(-4.3, +1.5)$. If the negative scattering length is associated with the first resonance[28] at 4.1 ev, the level spacing (indeterminate J) is $D_r\approx0.05$ kev.

Au^{198}: $R=7.8$, $\Delta_{1,2}=(-4.3, +2.5)$ or $(+4.2, -2.6)$. The scattering resonance is reported[29] to have $E_r=4.9$ ev, $\Gamma_n=0.021$ ev ($J=1$) or 0.016 ev ($J=2$). The corresponding values of γ_r^2/E_r are 8.6 and 6.6; best agreement with the measured Δ is for $J=1$, $D_r^1=0.07$ kev.

In those cases discussed above where some estimate of Γ_n is available, it is frequently possible to assign J values to low-lying resonances. These assignments generally agree with those made independently, although the present method of analysis appears to be the simplest when applicable.

The values of D_r are plotted against A of the com-

[15] H. Feshbach and V. F. Weisskopf, Phys. Rev. **76**, 1550 (1949).
[16] Adair, Barschall, Bockelman, and Sala, Phys. Rev. **75**, 1124 (1949).
[17] Hibdon, Muehlhause, Selove, and Woolf, Phys. Rev. **77**, 730 (1950).
[18] R. K. Adair, Revs. Modern Phys. **22**, 249 (1950).
[19] Adair, Bockelman, and Peterson, Phys. Rev. **76**, 308 (1949).
[20] M. Hamermesh and C. O. Muehlhause, Phys. Rev. **78**, 175 (1950).
[21] P. J. Bendt and I. W. Ruderman, Phys. Rev. **77**, 575 (1950).
[22] Harris, Hibdon, and Muehlhause, Phys. Rev. **80**, 1014 (1950).
[23] F. G. P. Seidl, Phys. Rev. **75**, 1508 (1949).
[24] C. T. Hibdon and C. O. Muehlhause, Phys. Rev. **76**, 100 (1949).
[25] W. Selove, Phys. Rev. **77**, 557 (1950).
[26] Rainwater, Havens, Wu, and Dunning, Phys. Rev. **71**, 65 (1947).
[27] Wu, Rainwater, and Havens, Phys. Rev. **71**, 174 (1947).
[28] Havens, Wu, Rainwater, and Meaker, Phys. Rev. **71**, 165 (1947).
[29] Tittman, Sheer, Rainwater, and Havens, Phys. Rev. **80**, 903 (1950).

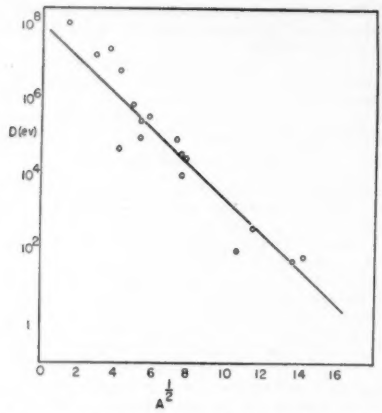

FIG. 1. Effective level spacing near $E_n=0$, regardless of J value.

pound nucleus in Fig. 1, where the straight line is drawn to fit the points without regard for the light nuclei. It must be emphasized that the curve drawn has at most order of magnitude validity; it is uncorrected for variation in J, in K, in even-odd character of A, in binding energy. Moreover, D_r is defined from the derivative $[\partial f/\partial E]_{E_r}$ and hence resembles only in order of magnitude the actual spacing between levels. The curve also yields an order of magnitude estimate for γ_r^2 and hence Γ_n for low energy neutron reactions. It provides an additional motive for associating s-neutrons with the 60-kev level in Na rather than the 3-kev level and suggests that one of the higher levels in Ag may make a major contribution to the scattering length, since this point is exceptionally far from the curve.

The form of the curve is suggested by the statistical expression[30] for the level density

$$\omega=1/D=C\exp\{(bAE)^{\frac{1}{2}}\} \tag{9}$$

where E is the excitation energy of the nucleus. Assuming that here the average $E\approx 7$ Mev, the curve of Fig. 1 corresponds to $C=0.01$ Mev^{-1}, $b=0.1$ Mev^{-1}. The inclusion of levels with all possible J values would increase C by an order of magnitude but would not be expected to alter b, which indicates a somewhat smaller level density in statistical nuclear reactions than the usual value[30] of $b'=0.2$ Mev^{-1}. Despite order of magnitude uncertainties in Fig. 1, it is unquestionable that $b<b'$. Since the excitation energy at which b' is determined generally exceeds that for b by some 5–10 Mev, this difference apparently represents a slight deviation from Eq. (8) in the sense of a relative increase of level spacing for lower excitation energies.

[30] V. F. Weisskopf and D. H. Ewing, Phys. Rev. **57**, 472 (1940).

IV. UNOBSERVED LEVELS

Figure 1 permits an estimate of the positions of unobserved levels whose presence is indicated by the scattering length. These order of magnitude values for E_r (not E_b) are presented in Table I, opposite the compound nucleus involved.

Recent velocity spectrometer studies[31] of Fe and Ni show resonances at 0.95 and 5 kev, which can be associated with Fe^{58} and Ni^{61} according to Table I. The resonance resulting from Ni^{62} will be much weaker than that resulting from Ni^{61} on account of abundance and may not be apparent in the presence of Co and Mn impurities with strong resonances in this region. This example suggests that measurement of scattering length for separated isotopes may be useful in combination with velocity spectrometer studies, where measurement of separated isotopes is precluded by the large samples required.

TABLE I. Order of magnitude E_r for levels near $E_n=0$.

Virtual			Bound		
K^{40}	14 kev		Na^{24}	−60 kev	$(J=1)$
A^{41}	20	$(J=\frac{1}{2})$	Fe^{57}	−3	$(J=\frac{1}{2})$
Ca^{45}	8	$(J=\frac{1}{2})$	Ni^{59}	−0.6	$(J=\frac{1}{2})$
Fe^{55}	7	$(J=\frac{1}{2})$	Co^{60}	−3	$(J=3)$
Fe^{58}	1		As^{76}	−0.3	
Ni^{61}	2	$(J=\frac{1}{2})$	Ag^{110}	−20 ev	
Ni^{62}	0.3	$(J=\frac{1}{2})$	Cs^{134}	−12	
As^{76}	0.3		Ta^{182}	−9	
Cs^{134}	5 ev		Au^{198}	−8	$(J=2)$

For certain isotopes the scattering length does not indicate the presence of any nearby levels for s-neutrons, namely for target nuclei He^4, Be^9, F^{19}, Ca^{40}, Cb^{93}, Bi^{209}. Isotopic mixtures of elements that are certain to include at least one nearby level are those for which $\sigma_{sc}\gg 4\pi a^2$ or a is much different from R. Such elements include Cl, Ti, Cr, Se, Rb, Sr, Zr, Mo, W. A few elements that are practically pure isotopes have unknown scattering lengths: Ne, Si, P, Sc, Y, Rh, In, La.

[31] W. W. Havens, Jr., and L. J. Rainwater, Phys. Rev. **83**, 1123 (1951).

Hyperfine Structure and Isotope Shift in the Spectrum of Tellurium*

JOHN S. ROSS† AND KIYOSHI MURAKAWA‡
Department of Physics, University of Wisconsin, Madison, Wisconsin
(Received October 19, 1951)

Using separated isotopes of tellurium, the hyperfine structure of the Te I and Te II spectra was studied. The magnetic moments of the two odd isotopes were calculated to be $\mu(Te^{125}) = -0.6 \pm 0.2$ nm, $\mu(Te^{123}) = -0.5 \pm 0.2$ nm. The ratio of the magnetic moments was determined to be $\mu^{125}/\mu^{123} = 1.186 \pm 0.007$. Anomalous shift of the even isotopes was detected in the lines λ4006 ($5s5p^4\ {}^4P_{3/2} - 5p^5({}^3P_0)6p_{3/2}$) and λ4049 ($5s5p^4\ {}^4P_{3/2} - [5p^5({}^3P_1)6p]_{3/2}$). The spacings between consecutive even isotopes in the line λ4006 were as follows: $\Delta(130-128) = 0.014$, $\Delta(128-126) = 0.011$, $\Delta(126-124) = 0.026$, $\Delta(124-122) = 0.017$, $\Delta(122-120) = 0.017$ cm^{-1}, the component due to the heaviest isotope lying on the largest frequency side. The centers of gravity of the odd isotopes in the line λ4006 were: $\Delta(124-125) = 0.002$, $\Delta(123-122) = 0.000$ cm^{-1}. λ4049 showed nearly the same isotope effect as λ4006. Regarding the μ-values, see the note §.

INTRODUCTION

THE hyperfine structure (hfs) in the spectrum of tellurium is worthy of study, since the magnetic moments of the odd isotopes have not yet been determined by the nuclear induction method and because tellurium has a large number of even isotopes (120, 122, 124, 126, 128, and 130) in addition to the two odd isotopes (123 and 125). The nuclear spins of Te^{123} and Te^{125} were determined previously[1,2] to be 1/2, and the existence of an isotope shift was also detected by Mack and Arroe.[2] A complete interpretation of the hfs and isotope shift had to wait until the spectrum of Te II was analyzed.[3]

EXPERIMENTAL DETAILS

A liquid-air cooled aluminum hollow-cathode source[4] was used. Helium or neon was used as the carrier gas. Neon enabled us to investigate the regions which were masked by the strong helium lines, and in addition several lines appeared, which were not strongly excited by helium.

In the ultraviolet region, for the study of Te I, a Bausch and Lomb medium quartz spectrograph was used. In the visible region, for the study of Te II, two different Hilger constant deviation spectrographs (flint-glass and crown-glass prisms) were used.

A Fabry-Pérot interferometer, of Invar construction, was used with quartz plates 60 mm in diameter. Invar spacers up to 40 mm were used. For use in the ultraviolet region the plates were coated with an alloy of 20 percent silver and 80 percent aluminum, and the Fabry-Pérot was mounted in front of the spectrograph, the fringes being focused on the slit with a quartz-fluorite achromat. For use in the visible region the plates were coated with silver and the interferometer was used in the usual way between the collimator and the prism of the spectrograph.

Figure 1 shows some reproductions of the interference patterns of tellurium lines.

In the study of the isotope shift, it was necessary to take spectrograms of the two isotopes on the same plate. This had to be done within a relatively short time to insure that there was no change in the interferometer. To do this, two discharge sources, each containing a different isotope, were mounted on a metal frame which could be rotated about a vertical axis.[4] It was thus possible to change from one isotope to another in a matter of a minute or so, by merely rotating the source to a predetermined position. Since the exposure times were of the order of 5 to 15 minutes, it was not necessary to maintain any pressure or temperature control over the interferometer. However, in order to be sure that there was no change, three exposures were taken on each plate: first one isotope

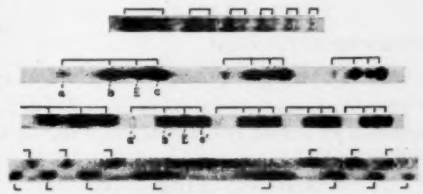

FIG. 1. (a) Te I λ2531. Isotope 125. 20-mm etalon. (b) Te II λ5449. Isotope 125. (Component E is due to even isotopes.) 6-mm etalon. (c) Te II λ5449. Isotope 123. (Component E is due to even isotopes.) 10-mm etalon. {(d) Te II λ4049. Isotope 122. (e) Te II λ4049. Isotope 130.} Taken on the same plate. 30-mm etalon.

* Supported by the ONR.

† Present address: Ansco Research Laboratory, Binghamton, New York.

‡ Present address: Institute of Science and Technology. University of Tokyo, Komaba-machi, Meguro-ku, Tokyo, Japan.

[1] G. R. Fowles, Phys. Rev. **76**, 571 (1949); **78**, 744 (1950). Fowles published a reproduction of the hfs of some Te II lines, together with the result of his measurements, but he made no mention about which component was the stronger. Since the light did not travel normally through his etalon, it is not certain whether he obtained an adequate formula for deriving the hfs. His published separations are considerably smaller than those of the present writers, who used the Fabry-Pérot etalon in the usual manner.

[2] J. E. Mack and O. H. Arroe, Phys. Rev. **76**, 1002 (1949).

[3] Mack, Murakawa, Ross, Pick, and van den Bosch, Phys. Rev. **83**, 654 (1951). In Table I of this letter, the hfs splitting[125] of the term $74_{3/2}$ was tentatively given as 0.00 cm^{-1}. This should read −0.463 cm^{-1}. This error occurred through a misinterpretation of the interference fringes of λ4049, which were largely disturbed by the presence of close lying lines Te II λ4047.2 and Hg I λ4046.6.

[4] O. H. Arroe and J. E. Mack, J. Opt. Soc. Am. **40**, 386 (1950).

TABLE I. Isotopic constitution (percent) of the samples of tellurium.

Sample label	Isotope 120	122	123	124	125	126	128	130
120	22.3	18.8	1.5	5.1	5.5	12.5	17.4	16.9
122	0.7	86.2	1.1	1.7	1.5	2.7	3.4	2.6
123		8.5	45.8	12.3	7.0	10.7	9.0	6.8
124		1.5	0.7	83.9	4.7	4.5	3.0	1.9
125		0.1	0.3	1.4	87.9	6.8	2.4	1.1
126		0.1		0.6	0.7	95.4	2.6	0.6
128					0.2	1.5	94.4	3.9
130						0.4	2.3	97.4
Natural	0.1	2.3	0.9	4.6	6.9	18.7	31.9	34.5

was photographed, then the second isotope, and then the first one again. If the first and third patterns were the same (determined by measuring the fringes), then there will have been no change in the interferometer, and the two different isotopes will have been compared under the same conditions.

Figures 1(d) and 1(e) show an example of interference patterns that were used to measure the isotope shift of 122 against 130.

Table I lists the concentration of the different samples[5] which were used.

RESULTS OF MEASUREMENTS

(A) Hfs of the Te I Spectrum

Using the enriched sample 125, two arc lines λ2530.7 ($5p^4\,{}^3P_1-5p^36s\,{}^5S_2$) and λ2385.7 ($5p^4\,{}^3P_1-5p^36s\,{}^3S_1$) were studied. The former line was found to consist of two components 0.113 cm^{-1} apart, the lower frequency component being the stronger. According to the theory of hyperfine structure splitting, the splitting factors of $5p^36s\,{}^5S_2$ and $5p^4\,{}^3P_1$ should have the same and the opposite sign as the nuclear magnetic moment, respectively, so μ^{125} must be negative. The hfs pattern of λ2530.7 taken with a 20-mm etalon is reproduced in Fig. 1. The line λ2385.7 was found to be single to an accuracy of 0.03 cm^{-1}.

The aforementioned findings can be expressed by the equations:

$$\tfrac{3}{2}A({}^3P_1)-(5/2)A({}^5S_2)=0.113\ \text{cm}^{-1}.$$
$$\tfrac{3}{2}A({}^3P_1)-\tfrac{3}{2}A({}^3S_1)=0 \qquad \text{cm}^{-1}.$$

Eliminating $A({}^3P_1)$, we get

$$(5/2)A({}^5S_2)-\tfrac{3}{2}A({}^3S_1)=-0.113\ \text{cm}^{-1}.$$

Using the hyperfine structure formulas for the configuration p^3s derived by Crawford and Wills,[6] we can easily show that

$$(5/2)A({}^5S_2)-\tfrac{3}{2}A({}^3S_1)=a(6s)$$

for both jj- and LS-coupling cases. Calculation in the intermediate coupling case is not possible, since no terms (except ${}^5S_2$ and ${}^3S_1$) of the configuration $5p^36s$ are known. However, we have assumed that the foregoing formula is a good approximation for an intermediate coupling cases, since it holds in the two extreme cases. Hence we obtain

$$a(6s)=-0.113\pm0.030\ \text{cm}^{-1}.$$

Using the Fermi-Segrè-Goudsmit formula

$$\mu=\frac{a(s)In^{*3}\cdot\frac{3}{8}\cdot1836}{R\alpha^2ZZ_0^2F(dn^*/dn)}$$

and substituting in the above value for $a(6s)$, $Z=52$, $Z_0=1$, F(relativity correction factor)$=1.34$, together with[7] n^*(effective quantum number)$=1.997$ and $dn^*/dn=1.04$, gives

$$\mu^{125}=-0.73\pm0.20\ \text{nm}.$$

(B) Hfs of the Te II Spectrum

The hfs of the isotope 125 of the Te II spectrum was examined in the visible region, and the result is summarized in Table II. The 125 sample contained 11.8 percent of even isotopes (see Table I). In no lines, except λ4049 and λ4006 (and possibly in λ5038) could any shift of the even isotopes be detected. The position of even isotopes is given in the column Te^{even}, the strongest component of Te^{125} being taken as the origin. A number in square brackets [ ] represents a relative calculated intensity, while a number in parentheses ( ) represents the calculated position of a component too weak or too near to a strong component to be measured.

Table III summarizes the hfs splitting of Te II terms for the isotope 125, which can be derived from Table II.

In the Te II spectrum, many terms of the same parity perturb each other, and it is rather difficult to find terms suitable for calculating the magnetic moment. However, the terms $5p^2({}^3P_0)6p_{1/2}$ and $5p^2({}^3P_0)6p_{3/2}$ are somewhat apart from the terms $5p^2({}^3P_1)6p$ and $5p^2({}^3P_2)6p$, so it appears reasonable to use them in the calculation of μ. From Table III, we get

$$a(6p_{1/2})=-0.053\ \text{cm}^{-1},\quad a(6p_{3/2})=-0.010\ \text{cm}^{-1}.$$
$$\delta(\text{doublet splitting of } 6p)=2166\ \text{cm}^{-1}.$$

Using the formula,

$$\mu=[a(p)Ij(j+1)(l+\tfrac{1}{2})Z_\epsilon H1836]/[\delta l(l+1)F'],$$

and putting $a(6p_{1/2})=-0.053$ cm^{-1}, $j=1$, $Z_\epsilon=52-3=49$, H(relativity correction factor)$=1.06$, F'(relativity correction factor)$=1.29$, we obtain

$$\mu^{125}=-0.51\pm0.20\ \text{nm}.$$

The error of the calculation is rather difficult to estimate owing to the difficulty in estimating the effect of the term $101_{1/2}{}^\circ$ on the term $93_{1/2}{}^\circ$ and in estimating the error of δ.

[5] The enriched isotopes were produced by the Y-12 plant, Carbide and Chemicals Division, Oak Ridge, and were obtained by allocation from the AEC.

[6] M. F. Crawford and L. A. Wills, Phys. Rev. **48**, 69 (1935).

[7] J. E. Ruedy, Phys. Rev. **41**, 588 (1932).

TABLE II. Hyperfine structure of the Te II spectrum (sample 125).

Wavelength	Combination	Hfs of Te^{125} (cm^{-1})	Te^{arcs}	Separation[125] (Fowles)
6437.1	$78_{1/2}-93_{1/2}°$	−0.227, 0, 0.053 [1] [2] [1]	−0.045	
5974.7	$85_{3/2}'-102_{3/2}°$	(−0.429), −0.173, 0, (0.258) [0.25] [3.5] [5] [0.25]	−0.073	0.169
5755.9	$82_{3/2}-100_{3/2}°$	−0.083, 0 [3] [5]		0.079
5708.1	$85_{3/2}'-103_{7/2}°$	−0.185, 0, (0.246) [7.4] [10] [0.4]	−0.075	0.176
5666.2	$83_{1/2}-101_{3/2}°$	0, 0.061, 0.140 [5] [1] [2]	0.039	0.115
5649.3	$78_{1/2}-96_{3/2}°$	−0.208, 0, (0.020) [2] [5] [1]	−0.049	0.205
5630.6	$99_{3/2}°-117_{3/2}$	(−0.064), −0.054, 0, (0.010) [1] [5] [9] [1]		
5618.5	$83_{1/2}-101_{1/2}°$	−0.078, 0, 0.082 [1] [2] [1]		
5576.4		−0.1338, 0	−0.054	0.121
5536.7	$85_{3/2}-103_{7/2}°$	0, 0.153, (0.246) [10] [7.4] [0.4]		
5487.9	$81_{3/2}-100_{3/2}°$	−0.057, 0 [3] [5]		
5479.1	$86_{3/2}-105_{3/2}°$	0, 0.031, 0.111, 0.141 [9] [1] [1] [5]	0.060	
5449.8	$85_{3/2}'-103_{3/2}°$	−0.431, −0.238, 0 [1] [9] [14]	−0.108	0.226
5366.9	$82_{3/2}-101_{1/2}°$	−0.161, −0.081, 0 [2] [1] [5]	−0.051	
5311.1	$86_{3/2}-105_{3/2}°$	0, (0.219), 0.249 [14] [1] [9]	0.115	
5300.7		0, 0.136		
5244.2	$105_{3/2}°-124_{3/2}$	(−0.222), −0.086, 0, (0.137) [0.5] [7] [10] [0.5]		
5037.9	$76_{1/2}-96_{3/2}°$	∼−0.53, 0, (0.020) [2] [5] [1]		
5000.8	$85_{3/2}'-105_{3/2}°$	(−0.429), −0.208, 0, (0.223) [0.25] [3.5] [5] [0.25]	−0.081	
4961.9	$101_{1/2}°-121_{3/2}'$	0, (0.044), 0.122 [5] [1] [2]		
4910.6	$83_{1/2}-103_{3/2}°$	0, 0.193, 0.275 [5] [1] [2]	0.088	
4895.0	$85_{3/2}-105_{3/2}°$	0, 0.221 [7] [5]	0.090	
4893.6	$81_{3/2}-102_{3/2}°$	0, 0.194, (0.256) [14] [9] [1]	0.078	
4842.9		−0.203, 0	−0.072	
4827.1	$103_{3/2}°-124_{3/2}$	−0.057, 0, 0.136 [9] [14] [1]		
4729.9	$78_{1/2}-99_{3/2}°$	−0.164, 0, 0.064 [2] [5] [1]	−0.040	
4665.4	$83_{1/2}-105_{3/2}°$	0, 0.110, 0.190 [5] [1] [2]	0.066	
4478.6	$102_{3/2}°-124_{3/2}$	(−0.256), −0.124, 0, (0.136) [0.25] [3.5] [5] [0.25]		
4364.0	$85_{3/2}-107_{3/2}°$	−0.139, (−0.093), (−0.046), 0 [5] [1] [1] [9]		
4048.9	$5s5p^4\ {}^4P_{3/2}-99_{3/2}°$	(−0.463), −0.399, 0, (0.064) [1] [5] [9] [1]	Fig. 2	
4006.5	$5s5p^4\ {}^4P_{5/2}-96_{3/2}°$	(−0.824), −0.804, 0 [1] [9] [14]	Fig. 2	

λ5410.4 ($82_{3/2}-101_{3/2}°$) has a slight broadening (observed with a 20-mm etalon), but the measurement is difficult, owing to stray light with a continuous background.
λ5709.0 ($103_{7/2}°-120_{5/2}$), λ4865.1 ($103_{7/2}°-123_{7/2}$), λ4766.0 ($101_{3/2}°-122$) and λ4686.9 ($102_{5/2}°-123_{7/2}$) were examined by a 10-mm etalon, but the hfs could not be resolved.

From $a(6p_{3/2})$ we get $\mu^{125}=-0.6$ nm, but it is generally known that the hfs of a $p_{3/2}$ term does not give a reliable value of the magnetic moment, so we can consider the aforementioned value only as confirming the order of magnitude.

Using an approximate formula,[8] the value of $a(5s)$ was calculated from the splittings of the terms $5s5p^4\ {}^4P_{5/2}$ and $5s5p^4\ {}^4P_{3/2}$, and $a(5s)=-0.36$ cm^{-1} was obtained, from which it was calculated that

$$\mu^{125}=-0.5\pm0.2 \text{ nm}.$$

Taking a weighted mean of the four values of μ^{125} obtained from the hfs of the Te I and Te II spectra

[8] P. Güttinger and W. Pauli, Z. Physik 67, 743 (1931).

TABLE III. Hfs splitting of Te II terms (isotope 125).

Configuration	Term symbol	Term value (cm^{-1})[a]	Hfs splitting (cm^{-1})[b]
$5s5p^4\ {}^4P_{5/2}$	$71_{5/2}$	71191.66	−0.824
$5s5p^4\ {}^4P_{3/2}$	$74_{3/2}$	74892.51	−0.463
$5s5p^4\ {}^4P_{1/2}$	$76_{1/2}$	76299.96	∼−0.55
$5p^36s$ and $5p^35d$	$78_{1/2}$	78447.25	−0.228
	$81_{3/2}$	81894.55	−0.057
	$82_{3/2}$	82742.49	−0.083
	$83_{1/2}$	83576.56	+0.082
	$85_{5/2}$	85048.45	−0.093
	$85_{3/2}$	85158.81	0.000
	$85_{5/2}'$	85591.02	−0.431
	$86_{3/2}$	86758.94	+0.030
$5p^37s$ and $5p^36d$	$117_{3/2}$	117338.75	−0.010
	$120_{3/2}$	120616.23	−0.25
	$121_{3/2}'$	121518.02	−0.044
	$124_{5/2}$	124645.47	−0.136
$5p^3(^3P_0)6p$	$93_{1/2}°$	93978.00	−0.053
	$96_{3/2}°$	96143.84	−0.020
	$99_{3/2}°$	99583.68	−0.064
$5p^3(^3P_1)6p$	$100_{5/2}°$	100111.18	0.000
	$101_{3/2}°$	101220.10	−0.061
	$101_{1/2}°$	101370.01	+0.078
	$102_{5/2}°$	102323.61	−0.256
	$103_{7/2}°$	103104.98	−0.246
$5p^3(^3P_2)6p$	$103_{5/2}°$	103935.04	−0.193
	$105_{3/2}°$	105005.21	−0.109
	$105_{1/2}°$	105582.14	−0.221
$5p^36p$ (or $5p^34f$)	$107_{5/2}°$	107956.82	+0.046

[a] The deepest term of Te II is taken as the origin.
[b] + and − mean that the hfs terms are normal and inverted respectively.

and assigning conservative limits of error, we obtain as our final value:

$$\mu(\mathrm{Te}^{125}) = -0.6 \pm 0.2 \text{ nm.}\S$$

If we use the value of $\mu^{125}/\mu^{123} = 1.186 \pm 0.007$ to be described, we get

$$\mu(\mathrm{Te}^{123}) = -0.5 \pm 0.2 \text{ nm.}\S$$

Besides the sample 125, the sample 123 was examined in the case of the Te II spectrum. The distances between the two strongest components in λλ5449, 5311, and 4049 were measured and the positions of the 123 components were corrected by taking the presence of the 125 components into account. The results of these measurements are given in Table IV.§

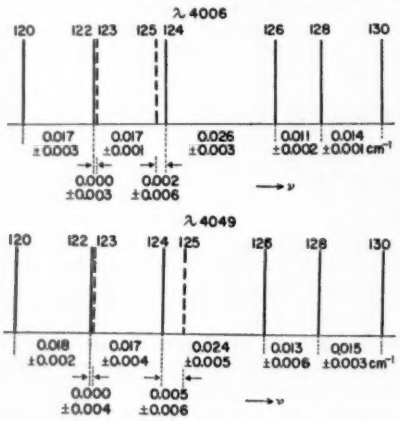

FIG. 2. Isotope shift in the Te II lines λ4006 ($5s5p^4\ {}^4P_{5/2} - 5p^3(^3P_0)6p_{5/2}$) and λ4049 ($5s5p^4\ {}^4P_{5/2} - [5p^3(^3P_1)6p]_{5/2}$). The dashed lines above the horizontal lines are centers of gravity of the odd isotopes 123 and 125.

(C) Isotope Shift in the Te II Spectrum

In two lines λ4049 ($5s5p^4\ {}^4P_{3/2} - [5p^3(^3P_1)6p]_{3/2}$) and λ4006 ($5s5p^4\ {}^4P_{5/2} - 5p^3(^3P_0)6p_{3/2}$), isotope shift of considerable magnitude was detected. This is to be expected, because the final terms of these lines contain an unpaired $5s$ electron, whereas the initial terms do not.

Since the line λ4049 was often disturbed by close lying lines Te II λ4047.2 and Hg I λ4046.6, isotope shift in the line λ4006 could be measured more accurately than in λ4049. The following seven distances were measured in λ4006.

$$\Delta(130-122) = 0.069 \pm 0.003 \text{ cm}^{-1}.$$
$$\Delta(126-122) = 0.042 \pm 0.003 \text{ cm}^{-1}.$$
$$\Delta(122-120) = 0.017 \pm 0.003 \text{ cm}^{-1}.$$
$$\Delta(128-124) = 0.039 \pm 0.002 \text{ cm}^{-1}.$$
$$\Delta(128-122) = 0.053 \pm 0.002 \text{ cm}^{-1}.$$
$$\Delta(124-122) = 0.017 \pm 0.001 \text{ cm}^{-1}.$$
$$\Delta(130-128) = 0.014 \pm 0.001 \text{ cm}^{-1}.$$

TABLE IV. Hfs of Te II of the isotopes 125 and 123.

	Hfs 125 (cm^{-1})	Hfs 123 (cm^{-1})	μ^{125}/μ^{123}
λ5449	0.2386	0.2011	1.186±0.010
λ5311	0.2486	0.2103	1.184±0.010
λ4049	0.3993	0.3367	1.186±0.007
		Mean:	1.186±0.007

The numbers following the symbol ± are approximate probable errors. From these measurements the consecutive distances of the components due to even isotopes were deduced. They are shown in Fig. 2. In Fig. 2, the centers of gravity of the 125 components and 123

§ *Note added in proof, February 8, 1952.*—Since submitting this paper we have found that, contrary to our original belief, $A(^4P_{3/2})$ is very sensitive to the coupling and introduces a large uncertainty into the calculation of μ based upon $5s5p^4\ {}^4P$. We have been able to calculate μ from $^4P_{5/2}$ alone, assuming that in Te III the distance $p^4\ {}^1D_2 - p^4\ {}^3P_2$ is sufficiently large, as it is in neighboring elements, which yields $\mu^{125} = -0.94 \pm 0.14$ nm. Substituting this for the −0.5 from $5s5p^4(^4P_{5/2}$ and $^4P_{3/2})$ which was used as one of the four data originally contributing to the final -0.6 ± 0.2 nm for μ^{125}, we now obtain as our final values

$$\mu(\mathrm{Te}^{125}) = -0.7 \pm 0.2 \text{ nm}$$

and from the ratio shown in Table IV

$$\mu(\mathrm{Te}^{123}) = -0.6 \pm 0.2 \text{ nm},$$

and whereas our values calculated before discarding $A(^4P_{3/2})$ lay just outside the much more accurate values, more recently obtained by Dharmatti and Weaver [S. S. Dharmatti and H. E. Weaver, Jr., Phys. Rev. **84**, 843 (1951)]

$$\mu(\mathrm{Te})^{125} = -0.88235 \pm 0.00004 \text{ nm}$$
$$\mu(\mathrm{Te}^{123}) = -0.73188 \pm 0.00004 \text{ nm}$$
$$\mu(\mathrm{Te}^{125})/\mu(\mathrm{Te}^{123}) = 1.20560 \pm 0.00007,$$

the final values given here leave no essential disagreement.

components are also shown. When the isotope shift investigation was begun, all the 125 sample had been sputtered in the investigation of the hyperfine structure of 125, and natural tellurium had to be used instead of 125. This explains why the center of gravity of 125 components is located with inferior accuracy in Fig. 2. In the same figure the isotope shift in λ4049 is also shown. Within experimental error, the isotope shifts in λ4006 and λ4049 are quite the same. In heavy elements, isotope shifts in the terms arising from the configuration $5s5p^4$ should be nearly the same and insensitive to the J values in one and the same element. This expectation is in agreement with the observation.

The anomalously large shift at $A=124-126$ namely at $N=72-74$ (A is the atomic weight integer and N the neutron number) is quite conspicuous, and must be connected with the structure of nuclei with $N=72$ or $N=74$.

The classification of the Te II spectrum, which is important in interpreting the hfs, was put at our disposal before publication, by Professor J. E. Mack and Dr. J. C. van den Bosch. We appreciate the deep interest of Professor Mack in our work. One of us (K.M.) would like to express his appreciation to Professor Mack for making it possible to spend this past year at the University of Wisconsin.

PHYSICAL REVIEW VOLUME 85, NUMBER 4 FEBRUARY 15, 1952

Proton Bremsstrahlung at 140 Mev*

RICHARD WILSON†
University of Rochester, Rochester, New York
(Received October 24, 1951)

The high energy gamma-rays arising from 140-Mev proton bombardment of several elements has been studied using a scintillation counter telescope to detect secondary electrons. The angular distribution is consistent with an approximately isotropic distribution in the center-of-mass system if we assume the bremsstrahlung to come from p-n collisions inside the nucleus. This is in disagreement with a phenomenological potential treatment of the p-n force or the scalar-meson theory.

The form of the spectrum is found to be consistent with the $d\nu/\nu$ shape and the dependence on Z much as would be expected from an opaque nucleus with only the neutron contributing to the bremsstrahlung.

INTRODUCTION

HIGH energy radiation has been detected from cyclotron targets bombarded with protons and deuterons.[1] The energy of the bombarding particle was, in most cases, high enough so that most of the radiation can be attributed to the decay of neutral mesons; only in the case of bombardment by 180-Mev deuterons is this explanation implausible.

It is of interest to investigate the γ-radiation directly accompanying nuclear events in the target; this will result from the deceleration of the proton in a field of force, in a similar manner to the well-known electron bremsstrahlung; but in the present case, the force is the nuclear force between the neutron and the proton rather than the Coulomb force. Thus a study of the γ-radiation should throw light on the charcater of the p-n force. The radiation is expected to arise only from p-n collisions and not from p-p collisions: calculations have neen made for p-n collisions by Ashkin and Marshak[2] and by Simon.[3] Variations might be expected in the angular distribution and spectral shape of the γ-rays according to the form of nuclear interaction.

EXPERIMENTAL

A target was set up at 43-in. radius in the Rochester cyclotron, corresponding to a maximum energy of 145 Mev, in order to be below the threshold for neutral and charged π-meson production.[4] The energy is 5 Mev above the threshold for neutral meson production in a heavy element, such as uranium, but the contribution of the γ-rays from decay of the neutral particles is expected to be less than 1 percent in this case, and for the lighter elements even a big impurity of the heavy elements could not be a cause of the radiation.

Figure 1 is a plan view of the apparatus; a collimator in the fringing field removes all charged particles, leaving only γ-rays and neutrons, to enter the counters. The γ-rays are converted on a 1.0-mm Pb sheet placed in front of 4 scintillation crystals (anthracene or stilbene) in coincidence. Absorbers may be placed in front of the collimator to analyze the primary radiation, and absorbers between counters 3 and 4 analyze the range of the secondary particles from the radiator.

The four counters are connected in pairs to two fast (10^{-8} sec) coincidence circuits, modified from a design of Garwin.[5] The outputs of the two coincidence circuits are taken to a slow (2×10^{-7} sec) coincidence circuit.

The crystals are of different sizes, as shown in Fig. 2.

* This work was assisted by the AEC.
† Now at Stanford University, Stanford, California.
[1] Bjorkland, Crandall, Moyer, and York, Phys. Rev. **77**, 213 (1950).
[2] J. Ashkin and R. E. Marshak, Phys. Rev. **76**, 58 (1949).
[3] A. Simon, Phys. Rev. **79**, 573 (1950).
[4] W. H. Barkas, Phys. Rev. **75**, 1109 (1949).
[5] R. L. Garwin, Rev. Sci. Instr. (1950).

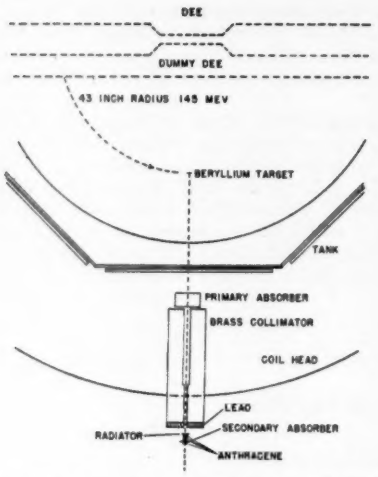

FIG. 1. Drawing of the cyclotron showing position of the collimator for observing γ-rays at 90° to the target.

The first is thin to avoid production of high energy protons or electrons from neutrons or γ-rays in the crystal, and the other crystals are thicker; the electron energy loss in the thick crystals is greater, so that the threshold bias may be increased with a reduction of background. The size of the other crystals is increased so that electrons scattered away from the forward direction by multiple Coulomb scattering will still reach the crystals. With no absorber between crystal 3 and crystal 4, they are placed close together in order to avoid scattering losses; when absorber is used, the scattering losses for the electrons which can still penetrate the absorber are less and crystal 4 is removed sufficiently far away to allow room for the absorber.

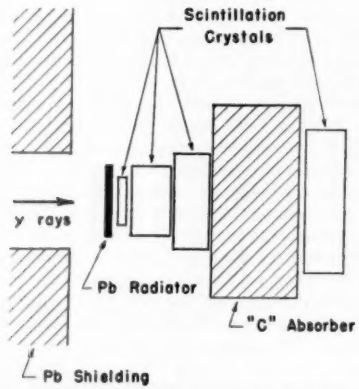

FIG. 2. The arrangement of the four scintillation crystals. The position of the fourth crystal depends on the amount of absorber used.

MONITORS

Two monitors have been used during this experiment. One, axial monitor,[6] is on the axis of the magnet and above the magnet yoke and is an anthracene scintillation counter biased at 2 Mev; it counts at approximately the same rate at whatever azimuth a target is exposed to the beam. The second, neutron monitor,[6] is a sodium iodide crystal biased at about 5–10 Mev placed in the forward direction from the target and is shielded from scattered protons by 10 cms of copper. This counts neutrons which are produced in the target and has only a 20 percent background from other parts of the cyclotron. During most of the operating runs, the neutron monitor is used to normalize the counts since if the beam conditions change so that the fraction of the beam which hits the target changes, the number of neutrons is expected to be proportional to the number of γ-rays. The neutron monitor is more stable over short periods than the axial monitor. The axial monitor is more permanent, however, and is used to give an indication of absolute beam intensities and for comparison of runs.

TABLE I. Radiator change.

Radiator	Absorber out	Absorber in
None	0.16±0.01	0.08±0.004
0.5 mm Pb	0.55±0.1	0.25±0.1
1 mm Pb	1.000	0.34±0.03
5 mm Pb	1.6±0.2	
1 cm Pb	0.8±0.2	

RESULTS

A. Proof of Photon Identity

The radiation from several targets has been examined; the absorption curves for radiation from a 1-in. beryllium target has been examined in the greatest detail. Figure 3 shows a log plot of the coincidence counting rate against primary lead absorber showing that most of the counting rate is due to a radiation heavily absorbable in lead. If we assume that the residual effect is due to fast neutrons converting in the first crystal, or the lead radiator, the radiation can be split into the two components shown; the neutron absorption cross section of lead varies little up to 100 Mev, so this separation is likely to be fairly accurate. The γ-ray energy found in this way agrees with an energy of 30–60 Mev.

The low absorption in aluminum of the primary radiation confirms the view that it is not merely an absorption of charged particles taking place.

Table I shows the variation of the counting rate for change of radiator with and without $\frac{1}{2}$ in. of lead primary absorber. The difference between these two is a

[6] The axial monitor was set up and maintained by J. Norton; the neutron by J. Perry.

measure of the contribution due to γ-rays. The interpretation of these is difficult; large thicknesses of lead radiator will scatter and absorb the low energy electrons produced, so that the increase of intensity with radiation thickness is not so great as with higher energy γ-rays.[7] However, it is not in disagreement with the calculated efficiency for the γ-ray spectra expected. A thickness of 1 mm was chosen for most experiments in order that the low energy electrons should not be attenuated by scattering. It is worth noting that the counts without the radiator in position are not heavily reduced by a primary lead absorber and are therefore mainly due to neutrons. Using a radiator equivalent to the first crystal indicates that most of this background comes from events in the first crystal, but a little may come down the collimator (presumably caused by neutrons hitting the sides). A check has been made with an anticoincidence crystal preceding the telescope to cut out any background from charged particles coming down the collimator. No difference was observed.

Chance coincidence counts are less than 1 percent of the total γ-ray count except when large thicknesses of secondary absorber are used. The main contribution to this chance coincidence rate comes from genuine events in counters 1, 2, and 3 in chance coincidence with an event in counter 4, and genuine events in counters 2, 3, and 4 in coincidence with an event in counter 1. These are assessed by inserting a delay of 5×10^{-8} sec in counter 4 and counter 1 channels in turn. The rate caused by chance coincidences between the doubles in channels 1–3 and the doubles in channels 2–4 is calculated from the observed doubles rates. The delay of 5×10^{-8} sec is the period of the cyclotron oscillator, and therefore of a beam fine structure.[8] A drop of 30 percent in chance coincidence rate is observable by using a delay which is not a multiple of the oscillator period.

Approximately 0.1 percent of the counts come from other parts of the cyclotron than the target.

In order to check that each counter was counting all the electrons, a plot was made of counting rate as a function of pulse height for the various events in the telescope. Figure 4 shows a curve of (i) the single counting rate in one crystal (ii) quadruples rate against pulse height and also for comparison a curve taken for the quadruples rate (iii) with recoil protons from fast neutrons. The counters are biased to accept virtually all the fast electrons. Some of the γ-ray events give both an electron and a positron through a crystal, which spreads the distribution out.

B. Secondary Electron System

Figure 5 shows the secondary electron spectrum obtained from Be and C targets at 90° to the proton beam, the energies being inferred from the absorption in carbon.

[7] Steinberger, Panofsky, and Steller, Phys. Rev. **78**, 802 (1950).

[8] I am indebted to Mr. H. Reynolds for communicating to me the importance of this effect in measuring chance coincidences, and for instructing me generally, in the uses of this type of equipment.

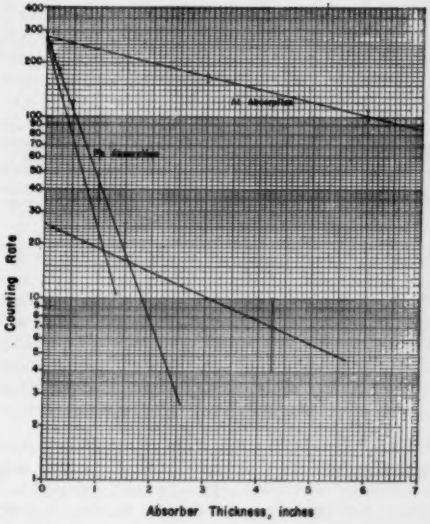

FIG. 3. Reduction of quadruple coincidences by lead and aluminum absorption of the primary γ-ray beam.

The absorption in carbon and in the hydrocarbon crystals is obtained from the calculations of Halpern

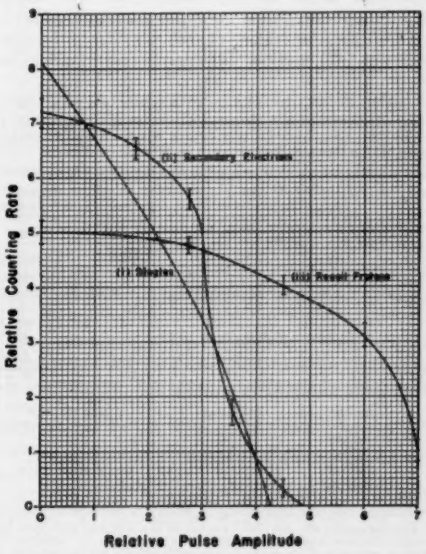

FIG. 4. Integral pulse amplitude distribution in the second crystal; (i) single pulses in the crystals, (ii) quadruple coincidences from γ rays. (iii) quadruple coincidences from recoil protons. The scale for the relative pulse amplitude should read from 2 to 9.

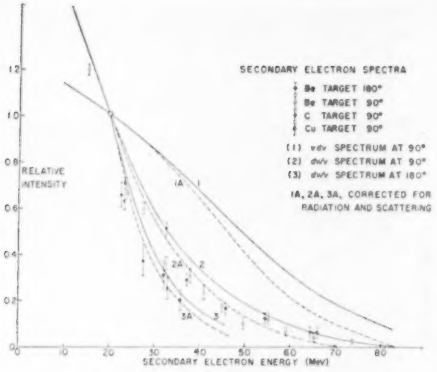
SECONDARY ELECTRON SPECTRA
Be TARGET 180°
Be TARGET 90°
C TARGET 90°
Cu TARGET 90°
(1) νdν SPECTRUM AT 90°
(2) dν/ν SPECTRUM AT 90°
(3) dν/ν SPECTRUM AT 180°
1A, 2A, 3A, CORRECTED FOR RADIATION AND SCATTERING
RELATIVE INTENSITY
SECONDARY ELECTRON ENERGY (Mev)

FIG. 5. Absorption of secondary electrons in carbon compared with theory.

and Hall.[9] The doubt which some authors have cast on the accuracy of these calculations is attributable only to confusing observable ionization with energy loss.[10] In this case the energy loss is what matters. The accuracy has been checked by experiment.[9]

These spectra are corrected for the neutron component at each point and for the background which is present in the absence of a radiator. These corrections do not alter the shape of the curve as they happen to be proportional to the electron counting rate (to within statistical error) except at the higher energies (70 Mev). Here the corrections due to chance coincidences become appreciable also, and the correction is approximately 30 percent of the observed counting rate. The statistical errors shown are standard deviations computed including allowance for the corrections.

Table II gives the angular ratio, 90° to 180°, for all electrons above 20 Mev for several target elements. An angular ratio 90° to 30° is also given for beryllium: this is not very accurate because of the large neutron count found in the forward direction.

TABLE II. (*a*) Angular ratio for all secondary electrons above 20 Mev for several target elements. (*b*) Ratio of neutron counts at different angles from Be target as a result of 80-Mev recoil protons in the forward direction.

(*a*) Angles	Target	Measured electron ratio	Corrected for aberration[a]	Corrected for Doppler shift and aberration[a]
90°/180°	Be	3.0±0.2	1.9±0.2	1.55±0.4
	C	2.9±0.3		1.5 ±0.5
	Al	2.8±0.3		1.45±0.5
	Cu	3.4±0.3		1.8 ±0.5
	Ag	3.4±0.3		1.8 ±0.5
	W	2.9±0.3		1.5 ±0.5
30°/90°	Be	2.5±1	1.5±0.8	1.0 ±0.6
45°/90°	Be	2.0±0.4	1.3±0.3	1.0 ±0.4

(*b*) Angles	Target	Ratio of neutron counts
0°/30°	Be	>2
30°/45°	Be	2.1±0.5
45°/90°	Be	50 ±20
90°/180°	Be	>2

[a] The corrections for aberration assume an *n-p* collision, and those for Doppler shift take account of the efficiency of the telescope as a function of energy. A spectrum of the shape $d\nu/\nu$ is assumed here, but there is only 5 percent difference for a $\nu d\nu$ type spectrum.

[9] O. Halpern and H. Hall, Phys. Rev. **73**, 477 (1950).
[10] H. Messel and D. M. Ritson, Phil. Mag. **41**, 129 (1950).

RADIATIVE AND SCATTERING CORRECTIONS

Corrections to these data must be applied for electrons which are lost from the telescope due to scattering and radiation. For low energy electrons, the scattering losses, in the geometry used, are less than 3 percent so long as the electron emerges from the third crystal with at least 4-Mev energy. Since a 1-Mev pulse is needed in the fourth crystal, this might introduce a spread in the energy scale of 3 Mev; a spread of 3 Mev is also introduced by radiation and absorption in the radiator, making a total of 6 Mev.

At the higher energies, large thicknesses of absorber are used and appreciable scattering can occur. This has been calculated using the method of Williams,[11] using the Born approximation for the small angle cutoff. Since we are interested only in small scattering angles, the distribution can be taken as Gaussian and the large angle cutoff chosen accordingly. Such a calculation of mean square scattering angle has been checked for electrons of 17 Mev and 115 Mev.[12] The detailed multiple scattering calculations including energy loss arise from a simple integration following a method developed by Ritson.[13] It is found that approximately 50 percent of the 70-Mev electrons can escape from the telescope when a 70-Mev absorber is in position but only 10 percent of the 80-Mev electrons. These values are considerably less at smaller absorber thicknesses and energies. Thus any electron which has sufficient energy to lose 2 Mev in the last crystal, has only a 5 percent chance of being scattered out. Radiative losses can be important even in carbon, for we have here nearly half a radiation length for absorbing 70-Mev electrons. Since the electrons are losing energy and the cross section for bremsstrahlung falls, only about 20 percent of the 70-Mev electrons are lost from this cause, and these appear as lower energy electrons. Thus the experimental curves may be corrected as shown.

The mean square angle of pair production is calculated from the formula of Stearns,[14] and it is found that the pair products are always within the angle of the telescope.

There is a possibility that an electron which radiates in the first few cm of absorber might produce γ-rays which later count in crystal 4. If the corresponding

[11] E. J. Williams, Phys. Rev. **58**, 292 (1940).
[12] L. Voyvodic and E. Pickup, Phys. Rev. **81**, 890 (1951). D. R. Corson, Phys. Rev. **80**, 303 (1950).
[13] D. M. Ritson, thesis, Oxford (1948).
[14] M. Stearns, Phys. Rev. **76**, 836 (1949).

positron was counted in crystals 1, 2, and 3, it could simulate 70-Mev γ-rays. Calculations show that this could account for at most 10 percent of the high energy electrons. A correction is made for this 10 percent in making the correction for radiation and scattering above.

SUMMARY OF CORRECTIONS

The corrections to the secondary electron spectrum are shown as corrections to the theoretically expected spectra. These corrections are unlikely to be in error by more than 25 percent. In view of the shape of the curve, this will not affect the conclusions appreciably.

PHOTON YIELDS

The total counting rate for secondary electrons above 20 Mev, from radiation at 90° to the incident proton beam, has been measured for several targets and for several maximum proton energies. The targets had approximately equal proton energy loss if recirculation is neglected. The counts were normalized to the axial monitor, which was later calibrated, as a function of target radius, at a time when the cyclotron beam was steady, by moving the targets successively into the beam with a flip coil.

We make the following assumption. (a) the circulating beam is constant with radius; (b) the recirculation of protons through a target can be calculated from the multiple scattering in the target[15] (c) the target alignment is sufficiently accurate that all protons go through all the target. Assumption (a) might be in error by a factor 2 for a beam energy change from 143 to 240 Mev, though there is no evidence for such a change. (b) is probably accurate to 10 percent at 143 Mev, where the vertical oscillation period is large. The accuracy at 240 Mev is likely to be less, and lead to an overestimate of the beam current for the lower targets. The relative accuracy between 100 and 143 Mev is likely to be higher. Assumption (c) has been studied with auxiliary measurements and it is found that 1/10° change in target alignment can be detected for a 1-in. copper target. The accuracy of alignment is about 2° and the values in the table could be 20 percent higher for the lower Z when thick targets are used.

The scattering formula used by Knox is not valid for our proton energies. We have taken the appropriate formula of the Williams theory. The discrepancy Knox finds between theory and experiment is probably due to working at a radius where the vertical oscillation period is small. Table III indicates the results. The sharp increase in yield in going from 140 to 240 Mev is presumably due to γ-rays from π^0 decay. Approximately the same dependence upon Z is found for the π^0 γ-rays as for the bremsstrahlung, although the recirculation correction is likely to be in error here.

[15] W. J. Knox, University of California Radiation Laboratory Report No. 883 (1950).

The absolute cross section has been estimated by the production of C^{11} from polyethylene foils placed on either side of a target. The total cross section for production of γ-rays above 20 Mev from 140-Mev protons on Be is 1.3×10^{-29} to within a factor of 3, or 2.5×10^{-30} cm^2/neutron in the nucleus. This is a little over $e^2/\hbar c$ times the neutron-proton scattering cross section at 140 Mev which is in agreement with the theoretical order of magnitude.

INTERPRETATIONS

A theoretical study of the radiation to be expected from high energy nucleon-nucleon collisions has been made by Ashkin and Marshak[2] using a phenomenological potential, and by Simon[3] using pseudoscalar and scalar meson field theory. The field-theoretic calculation indicates that the terms due to the interaction of the electromagnetic field with the meson are expected to be three times as large as the potential terms, so that the phenomenological treatment is expected to be in error if mesons play a part in nuclear forces.

TABLE III. Relative yield of photons (at 90°, lab sustem).[a]

Target	Max. proton energy	Recirculation correction	Yield/neutron	$A^{-\frac{1}{3}}$
Be	100		0.50±0.02	
Be	120		0.70±0.02	
Be	143	1.55	1.0	1.0
Be	240		13.5	
C	143	1.6	0.9	0.9
C	240		14	
Al	143	1.35	0.75	0.7
Al	240		11.5	
Cu	143	1.26	0.63	0.5
Cu	240		4.5	
Ag	143	1.13	0.38	0.42
Ag	240		5.8	
W	143	1.08	0.3	0.35
W	240		4.2	

[a] The statistical errors in the counts are small compared with the other errors mentioned in the text.

These authors assumed that the bremsstrahlung is due to proton-nucleon scattering with both final nucleons remaining in a free state. It appears, however, that a larger effect is to be expected from the reaction:[16] $p+n\rightarrow\gamma+d$.

The cross section for the inverse process has been calculated by Marshall and Guth[17] and by Schiff[18] with similar results. By using the principle of detailed balancing, the cross section might be expected to be 6×10^{-30} cm^2 at 140 Mev, as compared with 4×10^{-30} cm^2 for bremsstrahlung. The effect would approximately vary inversely as the energy.

A summary of these predictions is given in Table IV: the angular distribution expected is of the form

[16] I am indebted to Dr. Marshak for mentioning this possibility and to Mr. N. Francis for assistance in calculating the magnitude of the effect.

[17] J. F. Marshall and E. Guth, Phys. Rev. **78**, 738 (1950).

[18] L. Schiff, Phys. Rev. **78**, 733 (1950).

$a+b\sin^2\theta$. The energy spectrum for the bremsstrahlung theories will either be of the form $(\frac{1}{2}E_0-h\nu)^{\frac{1}{2}}d\nu/\nu$ or $(\frac{1}{2}E_0-h\nu)^{\frac{1}{2}}\nu d\nu$ in the c.m. system, where E_0 is the incident proton energy in the laboratory system. The latter form arises from the important role played by negative energy states in the pseudoscalar meson theory.

These theoretical calculations apply only to proton-neutron collisions. To apply them to proton-nucleus collisions, we regard the nucleus as composed of independent nucleons with an energy distribution given by the Fermi gas model (E^2dE up to 25 Mev). The first proton-neutron collision will give the energetic radiation; for the second collision, the nucleon energies will be reduced and the energies of the γ-rays will be correspondingly lower. The second collision has here been ignored; many of the nucleons should escape from the nucleus for low Z nuclei, so if the effect is important, it will be so only for high Z.

There are two important effects of the nuclear motion; the first is the effect on the angle of emission of the γ-ray, and the second is the change of energy in the proton-neutron system and therefore a change in cross section and γ-ray energies. So long as only the first nuclear collision need be considered, the nuclear motion cannot alter the angle of γ-emission by more than 20° for a nucleon of 140 Mev hitting a Fermi gas of nucleons. The second scattering may also occur and the angle may be as large as 90° for low energy radiation.

The effect of angle is expected to be similar, if both primary and secondary effects are included, to the effect on the angular distribution of neutrons from protons on various elements.[19] These indicate that the angular spread is greater than 20° and therefore there may be appreciable secondary scattering.

It seems probable also that the interaction between the neutron and the proton in the final state will be perturbed by the presence of other nucleons in the nucleus so that the reaction $p+n\rightarrow d+\gamma$ will not take place. One would also expect fewer collisions with emission of any γ-ray with an energy within 10 Mev of the maximum. The extra lightly bound neutron in Be^9 as compared with C^{12} might be expected to lead to a larger high energy component of the secondary electron distribution. However, there is no appreciable difference between Be^9 and C^{12} in this respect.

The effect of the nuclear motion on the energies of the gamma-rays has been calculated by J. B. French and P. B. Daitch, assuming a Fermi gas of nucleons in the nucleus. I am deeply grateful to Dr. French and Mr. Daitch for performing these calculations and allowing me to quote their results.

The calculation has been carried out for the two assumed spectra for the neutron-proton interactions, one $(\frac{1}{2}E_0-h\nu)^{\frac{1}{2}}d\nu/\nu$ and the other $(\frac{1}{2}E_0-h\nu)^{\frac{1}{2}}\nu d\nu$. With the former is assumed a dependence on energy of E_0^{-1} and with the latter a dependence on energy of E_0^2 corresponding to the predictions of Simon for scalar or phenomenological and pseudoscalar theories, respectively. The calculations were also made for two possible assumptions about the angular distribution of the reaction in the neutron-proton system; one that it is isotropic, and the other that it is $\cos^2\theta$; the results are shown in Fig. 6. Combinations of the curves can be used to predict the results for a distribution $A+B\cos^2\theta$.

If we thus compute the curves for I_{180} for the $\sin^2\theta$ case, we find that the intensity is about $I_{90}/40$ for a completely $\sin^2\theta$ distribution, compared with $I_{90}/2$ for an isotropic distribution. This confirms the contention that the angular distribution should not be markedly affected by nuclear motions.

The reduction of the intensity by the factor 2 in the 180° direction for isotropic emission in the c.m. system is the Doppler shift and aberration correction already inserted in Table II.

It is possible to compute the secondary electron spectra theoretically expected from a gamma-ray spectrum. This is plotted for comparison with the experimental curves in Fig. 5. It is clear that the spectrum $(\frac{1}{2}E_0-h\nu)^{\frac{1}{2}}\nu d\nu$ is not consistent with the data whereas the spectrum $(\frac{1}{2}E_0-h\nu)^{\frac{1}{2}}d\nu/\nu$ fits well.

There is a marked difference at the low energy end of the spectrum between the radiation from Be^9 and C^{12} or Cu. This presumably arises from a nuclear γ-ray of the order of 15 Mev. Thus the portion of the curves below 20 Mev has been disregarded for angular distribution comparisons for yield curves and for analysis of the spectrum.

TABLE IV. Summary of theoretical predictions for bremsstrahlung in p–n collisions.

Theory	Potential	I_{90}/I_0 c.m. system	Proton energy	Energy dependence	Form of spectrum
Phenomenological	$1V(r)$	7	250	E^{0-1}	$d\nu/\nu$
	$P_MV(r)$[a]	25	250		
	$\frac{1}{2}(1+P_M)V(r)$	15	250		
Scalar meson theory		230	180	E^{0-1}	$d\nu/\nu$
Pseudoscalar theory		0.8	180	E^{02}	$\nu d\nu$
$p+n\rightarrow\gamma+d$		5[b]	140	E^{0-1}	70-Mev line

[a] P_M is Majorana operator.
[b] Depends upon the nuclear forces; see reference 17.

[19] Miller, Sewell, and Wright, Phys. Rev. **81**, 374 (1951); see also the neutron background found in Table III of the present experiment.

If we assume that the rest of the spectrum is due to bremsstrahlung, a fit can best be obtained to the theory by assuming a $d\nu/\nu$ type spectrum. A $\nu d\nu$ type spectrum could only be fitted if it were true that secondary nucleon collisions are of importance. This could only be true for the heavier elements.

The angular distribution given in Table II shows that the distribution in the c.m. system is nearly isotropic—as predicted by pseudoscalar theory. If the secondary nuclear collisions are important, an intrinsic $\sin^2\theta$ distribution might simulate an isotropic distribution for the low energy gamma-rays where the angles are badly altered by collisions. The $\sin^2\theta$ distribution should still be correct for large angles. The form of the secondary electron spectrum for Be^9 at 180° agrees with the shape at 90° with appropriate Doppler shift corrections; it would appear, therefore, that this does not occur and that the phenomenological and scalar meson theories will not meet the requirement of isotropy. The reaction $p+n\rightarrow d+\gamma$ will do so under some theoretical arguments. If, however, the $p+n\rightarrow d+\gamma$ reaction were a major contribution to the radiation, the number of secondary electrons above 50 Mev would be considerably increased.

EXCITATION CURVE

If we consider now the yield of γ-rays from Be, as a function of energy, we must apply a correction for the decreased efficiency of γ-rays from lower energy protons and, taking the experimental secondary electron spectrum for this correction, it is found that the yield varies as $E^{0.3\pm0.5}$. For the low energy protons the Be nucleus in nearly opaque; every proton will therefore make a nuclear interaction. The observed energy dependence should then be the ratio of the probability of radiative to elastic proton neutron scattering. In a phenomenological theory this ratio is $e^2/\hbar c$, and in a scalar meson theory it is also independent of energy. On a pseudoscalar theory the variation will be as E^2 which is discounted by the data.

DEPENDENCE ON A AND Z

For opaque nuclei we expect the total number of nuclear interactions of the proton with the nucleus to vary as $A^{\frac{1}{3}}$; of these interactions a fraction $(A-Z)/A$ will be with a neutron and liable to give radiation. We would therefore expect a dependence on A and Z of $A^{-\frac{1}{3}}(A-Z)$ for the cross section on the nucleus as a whole, or $A^{-\frac{1}{3}}$ per neutron in the nucleus. The value of

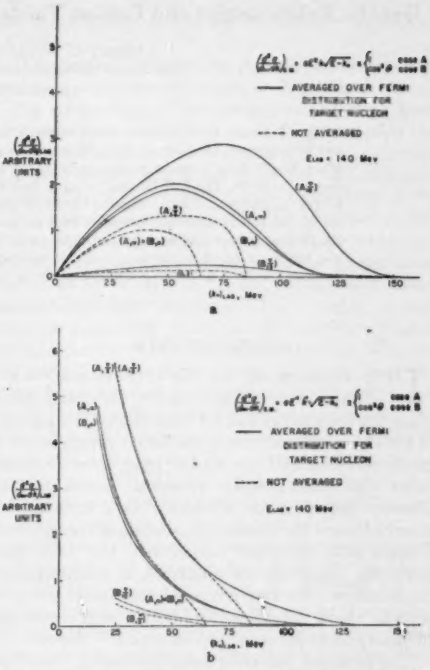

FIG. 6. Theoretical γ-ray spectra computed by French and Daitch.

$A^{-\frac{1}{3}}$ is tabulated for comparison with the yields for neutron in Table III. It is clear that the dependence on $A^{-\frac{1}{3}}$ is in general correct.

More conclusive data could be obtained from an investigation of bremsstrahlung from proton-neutron collisions. An approximation should be to use proton-deuteron collisions where the neutron is more nearly free than in most nuclei.

I am most grateful for the enthusiasm and cooperation of Dr. James Rouvina in the early stages of the experiment, and for the assistance of Mr. John Perry in taking data. I would like to thank Dr. Sidney Barnes, Mr. Hugo Logemann, Mr. R. Mortenson, and the crew of the 130-in. cyclotron for their assistance in the experiment, and Dr. R. E. Marshak, A. Simon, and J. B. French for innumerable valuable discussions on theoretical aspects of the problem.

Genetic Relationships and Fission Yields of Members of the Mass-115 Decay Chain*

ARTHUR C. WAHL† AND NORMAN A. BONNER‡
Los Alamos Scientific Laboratory, Los Alamos, New Mexico
(Received October 29, 1951)

The 21-minute Ag^{115} has been found to decay to both Cd^{115} isomers, 9 percent going to the 43-day state and 91 percent to the 53-hour state. No evidence was found for the decay of either cadmium isomer to the other. The 53-hour cadmium isomer decays to the 4.5-hour In^{115m}, but <0.02 percent of the 43-day cadmium decays to In^{115m}. The U^{235} thermal neutron fission yields of the 21-minute silver, 53-hour cadmium, and 43-day cadmium were determined to be 0.0078 percent, 0.0098 percent, and 0.00071 percent, respectively. All of the 43-day cadmium isomer formed in fission grows from the 21-minute silver, but 28 percent of the 53-hour isomer is formed by some other path. The fission yield of each of the cadmium isomers increases one hundred-fold when the energy of the neutrons is increased to 14 Mev. Evidence is presented for the formation of 3.5-year Cd^{113m} in approximately 5×10^{-6} percent yield from the thermal-neutron fission of U^{235}.

I. INTRODUCTION

THE existence of the Ag^{115} (21-minute)—Cd^{115} (53-hour and 43-day)—In^{115m} (4.5-hour) decay chain has been recognized for some time. Each member of the chain is found among the fission products and is produced by at least one nuclear reaction which establishes the mass number. However, except for the observed growth of the 4.5-hour indium from the 53-hour cadmium, the genetic relationships of the cadmium isomers with the other members of the chain were unknown. Therefore, we undertook to establish these relationships. We also measured the fission yields of several chain members for both thermal-neutron-induced and 14-Mev-neutron-induced U^{235} fission.

The principal published facts concerning this chain at the time of writing this paper are the following:

21-minute Ag^{115}

A 22-minute silver was identified among the fission products of U^{235} by Turkevich,[1] but the mass number and fission yield were not determined. Duffield and Knight[2] produced a 20-minute silver, presumably the same isotope observed by Turkevich, by the γ,p reaction on cadmium. They assigned this silver activity to mass number 115 by the use of separated cadmium isotopes. However, they were unable to observe the growth of either of the Cd^{115} isomers because of the small amount of 20-minute silver produced.

53-hour Cd^{115}

The 53-hour cadmium has been assigned to mass number 115 on the basis of a variety of nuclear reactions,[3] including the n,γ reaction on an enriched Cd^{114} sample.[4] It has been shown to be the parent of the 4.5-hour In^{115m}.[5,6]

The half-life has been variously reported to have values in the range 54 to 58 hours.[3,4]

The decay-scheme[3] involves two beta-particles, one of energy 1.10 Mev unaccompanied by gamma-rays, and one of energy 0.56 Mev in coincidence with a 0.54-Mev gamma-ray. The data of Mandeville, Scherb, and Keighton[7] indicate that about 12 percent (or slightly more) of the cadmium decays by way of the beta-gamma path, the remainder going by way of the 1.10-Mev beta-ray path.

The fission yield (thermal neutrons on U^{235}) has been reported to be 0.011 percent.[8]

43-day Cd^{115}

The 43-day cadmium has been assigned to mass number 115 principally by means of the n,γ reaction on an enriched Cd^{114} sample[4] and the n,p reaction on indium.[9] It decays almost entirely by emission of a single beta-ray, the energy of the transition being somewhere between 1.4 and 1.8 Mev.[3,4,10,11] A small fraction (~1 percent or less) decays by way of a soft beta-ray in coincidence with several gamma-rays.[10,12]

It has been reported[12] that approximately 0.007

* This Document is based on work performed at the Los Alamos Scientific Laboratory of the University of California under the auspices of the AEC during the summer of 1950, while the authors were serving as consultants to the laboratory.

† Present address: Department of Chemistry, Washington University, St. Louis, Missouri.

‡ Present address: Department of Chemistry, Cornell University, Ithaca, New York.

[1] A. Turkevich, Argonne National Laboratory Report 4010 (1947).

[2] R. B. Duffield and J. D. Knight, Phys. Rev. **75**, 1613 (1949).

[3] Way, Fano, Scott, and Thew, *Nuclear Data*, Nat. Bur. Standards Circ. 499 (1950).

[4] Cork, Rutledge, Stoddard, Branyan, and Le Blanc, Phys. Rev. **79**, 938 (1950).

[5] Goldhaber, Hill, and Szilard, Phys. Rev. **55**, 47 (1939); Nature **142**, 521 (1938).

[6] Nishina, Yasaki, Ezoe, Kimura, and Ikawa, Nature **146**, 24 (1940).

[7] Mandeville, Scherb, and Keighton, Phys. Rev. **75**, 221 (1949).

[8] R. P. Metcalf, Report CC-2310 (1945); see also *National Nuclear Energy Series* (McGraw-Hill Book Company, Inc., New York, 1951), Vol. 9, Division IV, paper 125 (p. 891) and paper 127 (p. 898).

[9] Seren, Engelkemeier, Sturm, Friedlander, and Turkel, Phys. Rev. **71**, 409 (1947); see also Paper 124, Vol. 9, Div. IV, *National Nuclear Energy Series* (McGraw-Hill Book Company, Inc., New York, 1951).

[10] Gill, Mandeville, and Shapiro, Phys. Rev. **80**, 284 (1950).

[11] G. T. Seaborg and I. Perlman, Revs. Modern Phys. **20**, 585 (1948).

[12] Argonne National Laboratory Report 4525 (1950).

percent of the 43-day cadmium decays to 4.5-hour In^{115m}.

The fission yield (thermal neutrons on U^{235}) has been reported to be 0.0008 percent.[8]

Although from nuclear shell theory it seems very probable that the 43-day cadmium is the upper isomeric state, this conclusion is not reached unambiguously from simple energy considerations.

4.5 hour In^{115m}

The 4.5-hour indium has been produced by a variety of nuclear reactions.[9] It decays principally by isomeric transition to the ground state, about 50 percent of the transitions going by internal conversion.[13] About 6 percent of the 4.5-hour indium decays to stable Sn^{115} by emission of an 0.8-Mev beta-particle.[5,14]

Martell and Libby[15] have shown that the In^{115} ground state decays to tin with the emission of a 0.6-Mev beta-particle. The half-life is nearly 10^{15} years.

II. GENERAL PROCEDURES AND CALIBRATIONS

A. Purification of Fission-Product Cadmium

Cadmium activities formed in fission were purified by a method described by Glendenin.[16] This method involves three cadmium sulfide precipitations from 0.2*M* acid, two palladium sulfide precipitations from 2*M* acid (Glendenin used 1.2*M* acid), two basic ferric acetate scavenging precipitations, one cadmium sulfide precipitation from ammonia, and one cadmium ammonium phosphate precipitation. Glendenin claims this procedure results in 43-day Cd^{115} of about 99 percent radiochemical purity as shown by decay curves. We have checked the purity of a 43-day Cd^{115} sample, obtained by the foregoing purification procedure from U^{235} which had been irradiated one week in the Los Alamos homogeneous reactor (water boiler), by carrying the purification through an additional cycle (one cadmium sulfide, one palladium sulfide, and one basic ferric acetate precipitation). The further purification did not measurably decrease the specific activity of the cadmium, so the radiochemical purity of the original sample must have been >98 percent.

B. Sample Mounting and Chemical Yields

Cadmium was mounted for counting by precipitating $CdNH_4PO_4 \cdot H_2O$ according to Glendenin's directions,[16] filtering onto tared Whatman's No. 42 filter paper, drying in a 110°C oven for 15 minutes, cooling in a desiccator for 20 minutes and in the balance case for 10 minutes, weighing to determine the chemical yield, and mounting on $\frac{1}{16}$-inch aluminum plates under Scotch Tape (9.2±0.1 mg/cm²). The weight of a precipitate was about 30 mg, and it was spread over an area of 3.5 cm².

The chemical yield for the over-all purification and mounting procedure was usually ~70 percent.

The composition of the precipitates resulting from the foregoing procedure was checked by comparing the weights of four precipitates containing tagged cadmium with the weights calculated from the radiochemical yields, which were determined from the activity of the tagged cadmium remaining in the filtrates. The activity of the cadmium recovered from the filtrates was measured on cover slips under Scotch Tape in the same manner as the activity of the original cadmium tracer solution had been measured. The weights of the cadmium ammonium phosphate precipitates averaged 2 to 3 percent lower than the calculated values. Whether this small discrepancy is real, indicating less than one molecule of water of hydration, or whether it is the result of incomplete (about 80 percent) recovery of the cadmium in the filtrates is not known. We have assumed the latter and have used the molecular weight corresponding to $CdNH_4PO_4 \cdot H_2O$ in our yield calculations.[17] If the discrepancy is real, the error introduced because of the uncertainty in the composition is <3 percent.

Indium was mounted for counting by precipitating the hydroxide with ammonia from a chloride-free nitric acid solution, igniting to the oxide at 800°C for 15 minutes, powdering the sample, suspending it in water, filtering onto tared Whatman's No. 42 filter paper, and drying, cooling, weighing, and mounting as described for cadmium ammonium phosphate. The weight of a precipitate was 15 to 20 mg and covered an area of 3.5 cm². We found that the weight of ignited indium oxide did not change when wet with water and dried by this procedure.

The uniformity of the Scotch Tape covering was checked three times during the course of this work by weighing three ~3-inch strips of 1-inch tape. All nine determinations agreed to within 0.2 mg/cm².

Carrier solutions were standardized by conventional analytical procedures. Silver was weighed as silver chloride dried at 110°C; cadmium was weighed as cadmium sulfate ignited at 500°C; indium was weighed as indium oxide ignited at 800°C.

C. Counting Efficiencies

The decay of samples mounted as described previously was followed on external beta-proportional methane-flow counters, a sample being 8 mm from a 2-inch diameter, 0.0007-inch (4.8 mg/cm²) Dural window. The counters were 2 inches inside diameter, and the window was in a side. The efficiency of this method

[13] J. L. Lawson and J. M. Cork, Phys. Rev. **57**, 982 (1940).
[14] Bell, Ketelle, and Cassidy, Phys. Rev. **76**, 574 (1949).
[15] E. A. Martell and W. F. Libby, Phys. Rev. **80**, 977 (1950).
[16] L. E. Glendenin in Report CN-1312X, p. 121 (1945); see also *National Nuclear Energy Series* (McGraw-Hill Book Company, Inc., New York, 1951), paper 265, Vol. 9, Division IV (p. 1575).

[17] Occasionally the precipitates failed to crystallize, or crystallized in some form of lower molecular weight so the specific activity of a sample was unreasonably high. In such cases the precipitate was dissolved and reprecipitated or the results were discarded.

of counting the 53-hour Cd^{115}, 43-day Cd^{115}, and 4.5-hour In^{115m} radiations was compared to the efficiency of counting these radiations from thin (<0.5 mg/cm²) samples mounted[18] on thick glass plates (a stack of microscope cover slips) on an internal beta-proportional methane-flow counter (a nucleometer). It was assumed that the efficiency of counting either the 53-hour or 43-day cadmium beta-particles in this internal geometry was the same as the radium E (Bi^{210}) counting efficiency, which we determined to be 70 percent (see following material). The approximate validity of this assumption seems reasonable because all of the beta-rays are at least fairly energetic, the decay schemes are reasonably simple, and Hudis[19] has found the efficiency of this same geometry (on a different nucleometer) for I^{131} and P^{32}, furnished by the Bureau of Standards, to be 72 and 68 percent, respectively.

Pure RaE was prepared from a RaD, RaE, RaF mixture in 25 ml of 0.1*M* HCl containing about 0.5 mg of lead carrier by depositing RaE and RaF on platinum over which hydrogen was bubbling, dissolving the RaE and RaF from the platinum in warm 6*M* HNO_3, converting them to the chlorides by several evaporations with HCl, and depositing the RaF on silver from a hot 1.5*M* HCl solution. Three cover-slip plates were prepared. The decay of the RaE was followed on the nucleometer, and the growth of RaF was followed on an alpha-proportional methane-flow counter. The efficiency of the internal beta-proportional counter for RaE radiation was calculated from the known 51 percent geometry of the alpha-counter, the half-life values of RaE and RaF, 5.0 days and 138.3 days, respectively, and the activities of the three samples. The result obtained was that 70 percent (69, 70, 72 percent) of the RaE disintegrations were counted. The purity of the RaE was demonstrated by the absence of alpha-activity in the freshly prepared samples (<0.5 percent of the alpha-activity at maximum growth) and by the decay of a RaE sample under Scotch Tape on an external proportional counter with a 5.0-day half-life over a factor of 40. A small tail indicates that ~0.3 percent of the initial RaD came through the procedure with RaE.

A second method of determining the RaE counting efficiency involved comparison of the activities of a Bureau of Standards RaD, E, F standard mounted on a silver-palladium disk with aliquots of a RaD, E, F solution mounted on glass cover slips and on silver-palladium disks. All samples were measured under a 9.5 mg/cm² aluminum absorber in the internal nucleometer. The fraction of the RaE radiation absorbed in the aluminum absorber was determined empirically with samples prepared from the pure RaE solution mentioned before. 37 percent of the radiation emitted from a sample on glass and 38 percent of the radiation emitted from a sample on palladium was absorbed. (Extrapolation of absorption curves gave an incorrect value of 26 percent absorption.) The efficiency of RaE beta-counting on glass in the nucleometer, determined by this method, was 67 percent.

4.5-hour In^{115m} is always present in 53-hour Cd^{115} samples, being essentially in transient equilibrium in all samples more than one day old. Thus it was necessary to determine what fraction of the radiation from old 53-hour Cd^{115} samples detected by the nucleometer was caused by In^{115} decay. Two runs were made in which indium was separated from cadmium samples by several cadmium sulfide precipitations from 0.3*M* acid and several indium hydroxide precipitations from ammonia. Two small aliquots of both the cadmium and indium fractions were mounted on cover slips, and the growth and/or decay followed on the nucleometer. Chemical yields were determined by weighing cadmium sulfate or indium oxide from large aliquots. Extrapolation of the indium decay curves and the sum of cadmium and indium curves, corrected for chemical yield, to separation time showed, after subtraction of the 43-day tail from the cadmium plus indium curves, that 39 percent (39.1 percent, 39.5 percent) of the total radiation detected from old 53-hour Cd^{115} samples on glass is from In^{115m}.

The final results of the calibration are that in the standard mounting under Scotch Tape on our external beta-proportional counter the 43-day Cd^{115} is counted with 43 percent efficiency, the 53-hour Cd^{115} (in equilibrium with In^{115m}) is counted with 60 percent efficiency, and the 4.5-hour In^{115m} is counted with 27 percent efficiency, assuming all of the 53-hour cadmium decays to the 4.5-hour indium, which seems probable.

The counting rates ordinarily measured were in the range of 1000 to 100,000 counts per minute. (With the counters used, the coincidence correction was about 2 percent at a counting rate of 100,000 per minute.) The initial activities of decay curves were usually in the range of 10,000 to 100,000 counts per minute, and the 43-day tail was usually reached at counting rates of about 1000 counts per minute. Background ran about 80 counts per minute.

III. EXPERIMENTS AND RESULTS

A. Mass Number Assignments

At the time this work was done the assignment of mass 115 to the 43-day cadmium seemed fairly certain, but since no direct evidence of its genetic relationship with the rest of the 115 chain was available, it seemed worthwhile to check the mass assignment. Since then, however, the mass assignment has been verified by means of the n,γ reaction on enriched Cd^{114} samples.[4]

[18] Acid solutions were evaporated to dryness on a microscope cover slip under an infrared heat lamp, the residue taken up in water, precipitated as sulfide or hydroxide, and evaporated to dryness. Cadmium was precipitated as the sulfide by blowing H_2S over the drop. Indium was precipitated as sulfide in the same manner or as the hydroxide by inverting a beaker wet with concentrated ammonia over the sample.

[19] J. Hudis (private communication from the Department of Chemistry, Washington University, St. Louis, Missouri).

We bombarded in the 20-Mev betatron beam a sandwich consisting of an ~0.002-inch cadmium foil enriched in Cd^{116} [20] inserted between two ~0.002-inch foils of normal cadmium. The whole sandwich was then wrapped in normal cadmium to stop any stray neutrons, which would confuse the issue by producing Cd^{115} by the n,γ reaction on Cd^{114}. Both the 53-hour and 43-day cadmiums were produced by the reaction $Cd^{116}(\gamma,n)Cd^{115}$. Table I gives the specific activities obtained, expressed in counts per minute per milligram of Cd^{116}, and corrected for small differences in self-absorption of the samples. No chemistry was done on the samples—the foils were merely mounted under Cellophane and counted.

The constancy of the specific activities confirms the assignment of both the 53-hour and the 43-day cadmium activities to mass 115.

From the foregoing data and the previously discussed counting efficiencies it was calculated that the ratio of γ,n cross sections for the formation of the two isomers in a 20-Mev betatron beam is about four in favor of the 53-hour isomer.

B. Nuclear Properties

21-minute Ag^{115}

We have determined the half-life of Ag^{115} by observing the growth of cadmium as a function of time (see the following section on genetic relationships). Our value, 21 minutes, is in agreement with the values of 22 minutes determined by Turkevich[1] and 20 minutes determined by Duffield and Knight.[2] We made no studies of the radiation from the silver.

53-hour Cd^{115}

On the basis of ten determinations, usually valid over about five half-lives, we obtained a best value of 53.0±1 hours for the half-life. The samples used were obtained from n,γ and γ,n reactions and from thermal and 14-Mev fission. In each case it was necessary to resolve the decay curve by subtracting the 43-day tail from the total observed activity.

Using two scintillation counters in coincidence,[21] we were able to observe beta-gamma coincidences and to measure absorption curves of the beta-ray and gamma-ray involved. The gamma-ray had a half-thickness in lead of 5.1 g/cm², corresponding to an energy of ~0.55 Mev. (A small amount of a softer component, probably x-rays and gamma-rays from the indium daughter, was also present but was not coincident with a beta-ray.) The coincident beta-ray had an end point of ~150 mg/cm² of Al, corresponding to an energy of about 0.5 Mev. This end point was difficult to determine with any degree of accuracy because of the presence of the large amount of the harder, noncoincident beta-ray.

A rough calibration of the instrument, using the known radiations of Sc^{46}, indicated that about 15 percent of the decay occurs by way of the soft beta-ray followed by the gamma-ray, the other 85 percent going by way of the 1.10-Mev beta-ray.

The measurements were made on fission-product cadmium which contained only a few percent (in terms of activity) of the 43-day cadmium. Corrections were made for the presence of this isomer and of the 4.5-hour indium daughter.

A measurement made on a sample of the indium daughter showed that none of the coincidences observed were caused by its decay.

These coincidence counting results are in agreement with the results of Mandeville, Scherb, and Keighton.[7]

43-day Cd^{115}

We have not yet determined a precise value for the half-life of this isomer, since our decay curves show a long-lived component (see Sec. IIID) and have not been resolved. The initial slopes are consistent with the previously reported 43-day and 44-day values,[3] and we have used the generally accepted value of 43 days in all calculations.

TABLE I. Specific activities[a] of cadmium foils bombarded with 20-Mev betatron x-rays.

Sample	53-hour Cd	43-day Cd
1 (normal)	830	8.8
2 (enriched)	850	8.2
3 (normal)	850	8.9

[a] Counts per minute per mg of Cd^{116} at the end of an intermittent bombardment conducted during a 7.0-hour interval.

An absorption curve indicates that if there is a gamma-component to the radiation, it is extremely weak. Using a beta-proportional counter, the beta-counting rate decreased by a factor of 4000 before the gamma-ray tail was reached. Assuming a relative counting efficiency of about 1 percent for the gamma-radiation, it appears that no more than a few percent of the beta-particles are accompanied by a gamma-ray. This result is consistent with data, published after the completion of our work, that showed that ~1 percent or less of the 43-day cadmium beta-particles are accompanied by gamma-rays.[10,12] The beta-end point is ~700 mg/cm² in Al, corresponding to an energy of ~1.5 Mev.

4.5-hour In^{115m}

Our decay curves show a half-life of 4.5 hours, in agreement with other workers.[3,11]

Since the counting efficiency of the indium is 65 percent of the efficiency of the 53-hour cadmium (in an

[20] The enriched Cd^{116} used in this investigation was supplied by Carbide and Carbon Chemicals Corporation, Y-12 Plant, Oak Ridge, Tennessee, and was obtained on allocation from the Isotopes Division of the AEC. The Cd^{116} content was 71.6 percent as compared to 7.6 percent for normal cadmium.

[21] We thank Dr. Arthur Freedman, without whose assistance and equipment these measurements could not have been made.

internal beta-proportional counter), it appears that over half of the indium decays are accompanied by either an internal conversion electron or a beta-particle. This is consistent with the reported facts that about 6 percent of the indium decays by beta-emission, and that about half of the isomeric transitions are by internal conversion.

C. Genetic Relationships

Growth of 53-hour and 43-day cadmium from 21-minute silver

A sample of about one gram of U^{235} (as uranyl nitrate) contained in a dilute nitric acid solution was irradiated in the Los Alamos homogeneous reactor (water boiler) for 20 minutes. After irradiation 20 mg of silver and 20 mg of cadmium were added and AgCl was precipitated by addition of HCl plus HNO_3. The precipitate was filtered, washed with 0.25*M* NH_4NO_3, and dissolved in ammonia. Twenty milligrams of cadmium were added to the ammonia solution, which was then acidified with HNO_3 plus HCl. The resulting AgCl precipitate was filtered and washed with NH_4NO_3. (Total time from end of bombardment to end of second filtration plus wash was 16.3 minutes, including a 10-minute wait to allow some of the short-lived fission products to decay.)

A previous tracer experiment had shown that less than 0.01 percent of the cadmium originally present was carried through this procedure. The AgCl precipitate at this stage was, therefore, free of cadmium.

The precipitate was dissolved in ammonia, and a known amount of cadmium was added. A known time after this last precipitation, AgCl was again precipitated by addition of HCl plus HNO_3. The precipitate was filtered and washed with NH_4NO_3. The time between filtrations (measured from the times at which the last drops of filtrate went through the funnel) was 20.5 minutes.

The procedure of dissolving the precipitate, adding cadmium, and reprecipitating AgCl was repeated, this time with a lapse of 136 minutes between filtrations. In 136 minutes only 1 percent of the original amount of 21-minute silver would be left.

The cadmium in the two filtrates containing the active cadmium which had grown from silver during the known time intervals was carried through the standard purification and mounting procedures. Both 53-hour and 43-day cadmium activities were present in each sample in amounts consistent with a half-life of 21 minutes for the silver parent. (The actual half-life values calculated were 20.5 minutes from the 53-hour activities in the two samples and 20.6 minutes from the 43-day activities.)

The relative amounts of 53-hour and 43-day cadmium in each sample show that 9.2 percent of the silver decays to the 43-day state and 90.8 percent decays to the 53-hour state.

TABLE II. Thermal neutron fission yields of the Cd^{115} isomers.

Aliquot	Fission yield, percent 53-hour	43-day	Ratio 53-hour/43-day
1	9.8×10^{-3}	7.1×10^{-4}	
2	9.8×10^{-3}	7.2×10^{-4}	
Av	9.8×10^{-3}	7.1×10^{-4}	13.8

Growth of 4.5-hour In^{115m} *from 53-hour cadmium*

The 4.5-hour indium is known to be the product of at least some of the 53-hour cadmium disintegrations.[5,6] The energies[7,13] involved in the two known decay paths of 53-hour Cd^{115} indicate that both of these principal paths lead to the same state of In^{115}. That this state is the 4.5-hour excited isomeric state is shown by the comparable counting efficiency of this isomer and its 53-hour cadmium parent.

Growth of In^{115m} *from 43-day* Cd^{115}

The growth of 4.5-hour indium from the 43-day cadmium had not been reported at the time the following work was done. Since then it has been reported[12] that approximately 0.007 percent of the 43-day cadmium decays to In^{115m}.

By means of a chemical separation involving three precipitations of cadmium sulfide from 0.3*M* HCl, alternating with three precipitations of indium hydroxide from ammoniacal solution, cadmium holdback carrier being added after each cadmium sulfide step, it was possible to separate indium from large amounts ($\sim10^6$ disintegrations per minute) of 43-day cadmium. The final indium fraction was essentially inactive ($\sim$10 c/m above a background of 80) and contained 79 percent of the original indium carrier added. The indium carrier had been added to an acid solution of cadmium tracer the day before the separation was carried out in order to prevent the loss of carrier-free indium by adsorption on the walls of the vessel, radiocolloid formation, etc. The cadmium used had been produced by fission of U^{235} and carefully purified.

Calculations involving the counting data and counting efficiencies show that less than 0.02 percent of the 43-day cadmium decays to the excited state of indium, either directly by beta-particle emission or indirectly by isomeric transition to the 53-hour cadmium. Considering all the evidence, it appears that the decay of the 43-day cadmium involves principally a single beta-ray, the product being the ground state of In^{115}.

D. Total Fission Yields; Thermal Neutrons

The thermal neutron fission yields of the Cd^{115} isomers were determined by purifying two aliquots of a U^{235} solution that had been irradiated in the water boiler for two hours and following the decay of the samples on an external beta-proportional counter. The number of fissions that occurred in the solution was

calculated from the Mo^{99} activity determined[22] in an aliquot of the solution, the relationship between the Mo^{99} activity and the number of fissions having been previously determined by irradiation of U^{235} samples in a double fission chamber in the thermal columns of the water boiler and fast reactor.[23] Results are summarized in Table II.

The decay of a sample of 43-day cadmium formed by thermal-neutron fission of U^{235} has been followed for eleven months. The decay curve shows definite curvature. A year after the irradiation, about 35 percent of the activity of the sample was caused by a component of half-life greater than 43 days. This estimate was made by drawing a line of 43-day half-time through the early points of the curve. The long-lived component was shown to be an isotope of cadmium by repurifying the sample by the Glendenin procedure[16] and finding the specific activity had not changed. It seems probable that this long-lived cadmium isotope is the 3.5-year Cd^{113m}.[24,25] If it is, its yield in U^{235} thermal-neutron fission is approximately 5×10^{-5} percent. Formation by neutron capture in cadmium impurity would have required about 75 mg of cadmium in the uranium (~2 percent impurity) calculated from Cassidy's[24] activation cross section of 0.02 barn. This amount of cadmium would have shown up in a chemical yield greater than 100 percent, whereas a normal 80 percent yield was obtained based on 20 mg of added cadmium carrier.

E. Independent Fission Yields; Thermal Neutrons

The fission yield of the 21-minute Ag^{115} and the independent fission yields of the Cd^{115} isomers were determined in duplicate runs performed as follows. Crystals of U^{235} nitrate were irradiated 10.1 minutes (timed from half-power) in the thermal column of the fast reactor and quickly dissolved in 10 ml of 0.7*M* HNO_3 containing 40 mg each of silver, cadmium, and indium[26] carriers as nitrates. The solution was split approximately in half. One-half was added to 7 ml of hot 1.7*M* HNO_3 and allowed to stand in hot water for 30 seconds, 1 ml of 6*M* HCl was added, and the silver chloride filtered onto a fine fritted funnel and washed with 5 ml of 0.25*M* ammonium nitrate. The total time required for the precipitation, filtration, and wash was one minute; the separation time was taken as the end of the filtration, which was about midway between the start of the precipitation and the end of the wash. The time interval between the end of the irradiation and the silver-cadmium separation was 5.1 minutes in run I and 6.2 minutes in run II. The efficiency of this silver-cadmium separation procedure had been tested previously with cadmium tracer, and it was found that only ~0.2 percent of the cadmium remained with the silver chloride. Later, the filtrate was worked up for cadmium, the activities of the cadmium isomers in the resulting sample, corrected for growth from the 21-minute silver before the separation, being a measure of their independent fission yields.

Table III. Thermal neutron fission yield of 21-minute Ag^{115} and the "independent" fission yields of the Cd^{115} isomers.

Run	Total fission yield (percent) of 21-minute Ag^{115}	"Independent" fission yields (percent) 53-hr Cd^{115}	43-day Cd^{115}
I	7.7×10^{-4}	2.8×10^{-4}	$<2\times10^{-5}$
II	7.8×10^{-4}	2.6×10^{-4}	$<2\times10^{-5}$
Av	7.8×10^{-4}	2.7×10^{-4}	

The silver chloride precipitate was dissolved in 6*M* ammonia containing 20 mg of cadmium carrier. This solution was allowed to stand three hours to allow all the 21-minute Ag^{115} to decay, then silver chloride was reprecipitated, dried, and weighed for the chemical yield determination, and the cadmium in the filtrate was purified by the standard cadmium purification procedure. The activity of the 53-hour cadmium in the resulting sample was a measure of the fission yield of the 21-minute silver. The ratio of the 53-hour and 43-day activities gave a 9.0 percent value for the fraction of the 21-minute silver decaying to the 43-day cadmium, in good agreement with the 9.2 percent value we had determined previously.

The other half of the irradiated U^{235} solution was treated with cold, saturated H_2S solution, and the silver and cadmium sulfides filtered onto a fine fritted funnel containing Celite filter aid. (This step was taken to separate cadmium and silver from indium.[26]) The sulfides were dissolved in concentrated HCl, and the solution allowed to stand three hours to allow silver to decay. Then the solution was evaporated to dryness, and the residue leached with 0.2*M* HCl to remove the cadmium from the silver chloride. The cadmium was purified by the usual procedure. The 53-hour activity, corrected for chemical yield, was used to calculate the number of fissions that had occurred in the sample, the 53-hour cadmium total fission yield having been previously determined (see preceding section).

Use of the counting and chemical yield data, the irradiation and separation times, and the decay constants of the 21-minute Ag^{115}, 53-hour Cd^{115}, and 43-day Cd^{115} in the standard growth and decay equations along with the branching ratio of the Ag^{115} and the total fission yield of the 53-hour Cd^{115} enabled us to calculate the fission yield of 21-minute Ag^{115} and the independent fission yields of both cadmium isomers. The results of the calculations are summarized in Table III.

[22] We thank C. O. Minkkinen for determining the Mo^{99} activity for us.

[23] We thank R. W. Spence and members of his group for making this information available to us.

[24] J. M. Cassidy, Phys. Rev. **83**, 483 (1951).

[25] Carss, Gum, and Pool, Phys. Rev. **80**, 1028 (1950).

[26] It was originally intended to determine the independent fission yield of In^{115m}. However, the 4.5-hour period was masked in the purified samples by the 117-minute In^{117} and other fission products not removed in the purification.

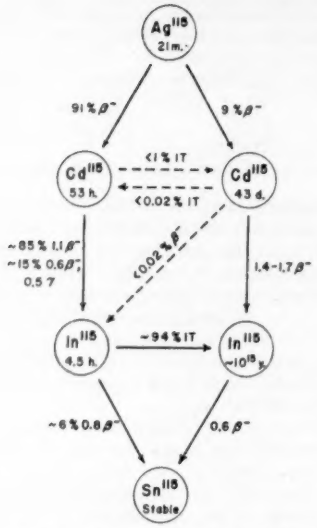

FIG. 1. Genetic relationships of the mass-115 decay chain.

It should be pointed out that the difference between the 53-hour cadmium total fission yield and the 21-minute silver total fission yield (corrected for branching) is 2.8×10^{-3} percent, in agreement with the directly determined value for the independent fission yield of 53-day cadmium listed in Table III. A similar calculation for the 43-day cadmium indicates that the independent fission yield is essentially zero, in agreement with the value in Table III.

F. Total Fission Yields; 14-Mev Neutrons

The yields of the cadmium isomers from U^{235} fission induced by 14-Mev neutrons were determined by purifying and counting cadmium samples from two aliquots of a solution made by dissolving a U^{238} button that had been irradiated directly behind the tritium target of the Cockroft-Walton machine. The number of fissions that occurred was calculated from the Mo^{99} activity determined[22] in an aliquot of the solution. It was assumed that the 14-Mev neutron fission yield of Mo^{99} is 90 percent of the thermal neutron fission yield. This assumption was made in order to compensate for rise of the valleys of the fission-yield curve with the increase in neutron energy.[23] Results are summarized in Table IV.

TABLE IV. 14-Mev neutron fission yields of the Cd^{115} isomers.

Aliquot	Fission yields (percent) 53-hour Cd^{115}	43-day Cd^{115}	Ratio 53-hr/43-day
1	0.99	0.070	—
2	0.97	0.068	—
Av	0.98	0.069	14.3

G. Relative (n,γ) Yields

A cadmium nitrate solution was irradiated in the water boiler and the decay of a sample followed.

From the relative activities observed, combined with the measured counting efficiencies, it was calculated that the relative cross sections for the formation of 53-hour and 43-day cadmium were in the ratio of 7.5/1 in favor of the 53-hour isomer.

IV. DISCUSSION

Present knowledge of the genetic relationships within the mass-115 decay chain, including contributions presented in this paper, are summarized in Fig. 1. The results of our determinations of the fission yields for members of this chain are summarized in Table V.

Since it is not entirely certain which of the two cadmium isomers is the upper state, it is necessary to consider each of the two isomeric transition possibilities. The fact that the 4.5-hour In^{115m} grows from the 53-hour but not the 43-day isomer clearly shows that the 43-day state does not decay to the 53-hour state. The evidence against the occurrence of the reverse transition is less direct and has to do with the independent fission formation of 28 percent of the 53-hour cadmium. If some of the 53-hour cadmium decayed to the 43-day isomer, some of the independent fission yield of the former would be reflected as an apparent independent yield of the latter. Since the ratio of the experimentally determined independent fission yields of the two cadmium isomers is >100, <1 percent of the 53-hour decays to the 43-day state.

It seems unlikely that the relatively large independent fission yield of the 53-hour Cd^{115} is caused by its formation as a primary fission product. It seems more reasonable to postulate the existence of an earlier member of the chain, such as a short-lived Ag^{115} isomer, which decays to 53-hour cadmium. From the constancy of the ratio of the 53-hour to 43-day cadmium activities in the two fractions milked from the 21-minute Ag^{115}

TABLE V. U^{238} fission yields of members of the mass-115 decay chain.

Nuclide	Thermal neutron fission yield, percent[a] total	independent	14-Mev neutron fission yield, percent[a] (total)	Ratio 14-Mev to thermal yield
21-min Ag^{115}	7.8×10^{-3}	—	—	—
53-hr Cd^{115}	9.8×10^{-3}	2.7×10^{-3}	0.98	100
43-day Cd^{115}	7.1×10^{-4}	$<2\times10^{-4}$	0.069	97

[a] The estimated error because of inaccuracies in sample mounting and counting and chemical yield determinations is about 3 percent. This is the error in the relative values of the thermal neutron fission yields of the 21-minute Ag^{115} and the 53-hour Cd^{115}, both total and independent, since all three values were obtained from activity measurements of the 53-hour Cd^{115}. The error in the absolute values of the fission yields is larger, perhaps about 10 percent, because the absolute beta-counting calibration is involved.

for the branching ratio determination, an upper limit of 3 minutes can be placed on the half-life of this postulated short-lived Ag^{115} isomer.

The fact that the 14-Mev neutron fission yield of each of the cadmium isomers is one hundred times the yield from thermal neutrons indicates that both isomers have a common ancestor whose yield increases the hundred-fold. This common ancestor could be the short-lived Ag^{115} isomer (postulated in the previous paragraph), which branches, 75 percent undergoing isomeric transition to the 21-minute silver and 25 percent decaying by beta-emission directly to the 53-hour cadmium isomer. The common ancestor could also be a short-lived palladium isotope which branch decays to the Ag^{115} isomers.

V. ACKNOWLEDGMENTS

It is a pleasure to thank Dr. R. W. Spence and the members of his group for their hospitality and assistance during the summer of 1950 when this work was carried out. We also wish to express our appreciation to the groups responsible for the operation of the water boiler, fast reactor, Cockroft-Walton, and betatron for making their facilities available to us.

PHYSICAL REVIEW VOLUME 85, NUMBER 4 FEBRUARY 15, 1952

Neutron Yield from the Nuclear Photoeffect

J. S. LEVINGER
Louisiana State University, Baton Rouge, Louisiana

AND

H. A. BETHE
Cornell University, Ithaca, New York

(Received October 30, 1951)

The yields of neutrons produced in photonuclear reactions by a bremsstrahlung-photon-spectrum are analyzed in terms of the multiplicity of neutron production. Approximating the neutron multiplicity as proportional to the photon energy, we derive the integrated photonuclear cross section from the experimental neutron yields. The integrated cross section from copper to bismuth is $\int_0^\infty \sigma dW = 0.14NZ/A$. (Uranium has a neutron yield 35 percent higher than given by this relation, probably due to photofission.) This relation has the correct form, but a somewhat higher absolute value than the theoretical relation $\int_0^\infty \sigma dW = 0.060(NZ/A)(1+0.8x)$, where x is the fraction of exchange force.

I. INTRODUCTION

IN a previous paper,[1] we calculated the integrated photonuclear cross section, and found satisfactory agreement between our theoretical result and preliminary experiments.[2-5] Since that time very many new experimental results have appeared, some of which are in apparent contradiction with theory.

First, let us summarize the theoretical results of our previous paper,[1] and the assumptions behind them. The summed oscillator strength $\sum_n f_{0n}$ for electric dipole transitions by a nucleus containing N neutrons and Z protons is

$$\sum_n f_{0n} = (NZ/A)(1+0.8x). \quad (1)$$

Here x is the fraction of the neutron-proton force that has an exchange character. High energy neutron-proton scattering experiments[6] indicate the value $x=\frac{1}{2}$. The cross section σ for photon absorption is proportional to the oscillator strength f. The cross section for photon absorption integrated over all photon energies W is given by

$$\begin{aligned}\int_0^\infty \sigma dW &= (2\pi^2 e^2 \hbar/Mc)\sum_n f_{0n} \\ &= 0.060(NZ/A)(1+0.8x) \\ &= 0.015A(1+0.8x) \text{ Mev-barns}. \quad (2)\end{aligned}$$

The last numerical result is for the case $N=Z=A/2$.

The sum rule $\sum_n f_{0n} = NZ/A$ is completely independent of any nuclear model. The modification shown by the $0.8x$ term in Eq. (1) occurs for any potential that does not commute with the position, such as an exchange potential or a velocity dependent potential. This modification was first found by Feenberg.[7] Recently Austern and Sachs[8] have considered the general problem of modifications for all multipole transitions due to potentials that do not commute with position. The coefficient 0.8 in Eq. (1) is based on the

[1] J. S. Levinger and H. A. Bethe, Phys. Rev. **78**, 115 (1950).
[2] J. L. Lawson and M. L. Perlman, Phys. Rev. **74**, 1190 (1948).
[3] G. C. Baldwin and G. S. Klaiber, Phys. Rev. **73**, 1156 (1948).
[4] M. L. Perlman and G. Friedlander, Phys. Rev. **74**, 442 (1948); and Phys. Rev. **75**, 988 (1949).
[5] E. R. Gaerttner and M. L. Yeater, Phys. Rev. **77**, 714 (1950).
[6] Hadley, Kelly, Leith, Segrè, Wiegand, and York, Phys. Rev. **75**, 351 (1949); R. S. Christian and E. W. Hart, Phys. Rev. **77**, 441 (1950); Kelly, Leith, Segrè, and Wiegand, Phys. Rev. **79**, 96 (1950).
[7] E. Feenberg, Phys. Rev. **49**, 328 (1936).
[8] N. Austern and R. G. Sachs, Phys. Rev. **81**, 710 (1951).

nuclear model of a degenerate Fermi gas with parameters specified in our previous paper.

Equation (2) predicts that the integrated photonuclear cross section should be a smooth function of atomic number. In our previous paper we explained the lack of smoothness in the experimental results[4] as due to Perlman and Friedlander's use of the method of measuring induced radioactivity. This method measures only partial cross sections which are always less than the cross section for photon absorption by an unknown and fluctuating factor. Further the less endothermic nuclear reactions—those leading to stable isotopes—are not measured by this technique. Also the disintegration schemes of the induced activities may not be accurately known.

Measurements of particle yields—neutrons or protons—avoid the above difficulties but have the problem of multiplicity of particle production, which is discussed below. Measurements on neutron yields from photonuclear reaction induced by bremsstrahlung radiation have recently been made by Baldwin and Elder[9] at G.E., by Price and Kerst[10,11] at the University of Illinois and by Terwilliger, Jones, and Jarmie[12] at Berkeley, while Halpern and Mann[13] at the University of Pennsylvania have studied proton yields from photonuclear reactions. Gaerttner and Yeater[5,14] have observed photonuclear reactions induced in gas in a cloud chamber. This method has the advantage that photon absorption leads to one and only one observable event. It has the disadvantages of limited applicability and of poor statistics. Their data for He, C, N, and O agree with our Eq. (2) within the rather large experimental uncertainties. The measurements[9–12] of neutron yield *vs* atomic number disagree with our Eq. (2) in two respects: First, the yield is not a smooth function of atomic number for elements up to copper; second, while for heavier nuclei the yield is a fairly smooth function of Z, it increases more rapidly with Z than predicted by Eq. (2), i.e., about as Z^2 rather than as NZ/A or $Z^{1.2}$.

The first discrepancy has been removed by the proton yield measurements of Halpern and Mann.[13] They found that the proton yield was also not a smooth function of Z, but that the sum of their proton yield and the neutron yield of Price and Kerst[10] was a smooth function of Z within experimental error. (The measurements of Halpern and Mann, and Price and Kerst are made for similar conditions: the former for protons from bremsstrahlung from 25-Mev electrons, the latter for neutrons from bremsstrahlung from 22-Mev electrons.) For 8 elements from $_{12}$Mg to $_{30}$Zn the combined neutron plus proton yield is proportional to NZ/A, with the sole exception of $_{22}$Ti, which has a low particle yield.

The competition between proton emission and neutron emission following photon absorption is significant up to $_{30}$Zn. For higher Z the proton yield is greatly decreased due to the increased Coulomb barrier. The experimental values of the proton/neutron yield ratio are in reasonable agreement with the calculation of Heidmann and Bethe.[15] They calculated the proton/neutron yield ratio for 17.5-Mev excitation using the compound nucleus model. The fluctuations in this ratio are due to fluctuations from element to element of the relative values of the proton and neutron binding energies.

While competition between proton and neutron emission was the source of the discrepancy for low Z mentioned previously, it cannot be significant for high Z as according to both experiment and theory, the proton yield is very small for this case. The explanation for the high Z discrepancy is suggested by Heidmann and Bethe who calculate that the average number of neutrons emitted at 17.5-Mev excitation is 0.83 for $_{29}$Cu, 1.22 for $_{53}$I, and 1.98 for $_{73}$Ta, the increase with Z being principally due to the decrease of neutron binding energy. The possible importance of multiple neutron production is also suggested by the measurements of Sugarman and Peters,[16] who measured induced activities produced in bismuth by 86-Mev bremsstrahlung. They found activities due to the emission of from 3 up to perhaps 10 neutrons. (Tl^{199} could be produced by $\gamma-10n$ or $\gamma-9n$, p followed by electron capture or by $\gamma-8n$, $2p$.) As the counting efficiencies for many of the induced activities are not known well, and as the $\gamma-n$ and $\gamma-2n$ reactions could not be measured by this method due to the very long half-lives of the produced activities, we cannot at present interpret these measurements quantitatively.

The experimental results indicate that emission of one neutron is the predominant photonuclear process only for elements in the neighborhood of copper. For lower atomic number, proton emission is generally favored, while for higher atomic number, multiple particle emission appears to be the predominant process. Even for the case of copper, the cross sections for processes other than the $\gamma-n$ are by no means negligible, amounting to about one third of the absorption cross section.[17] Ge^{76} appears to be the isotope for which emission of a single neutron is most strongly favored.[1] For elements either much lighter or much heavier than copper, study of the reactions by the method of induced activity[18,19] may well not provide reliable information as to the shape of the curve of absorption cross section

[9] G. C. Baldwin and F. R. Elder, Phys. Rev. **78**, 76 (1950).
[10] G. A. Price and D. W. Kerst, Phys. Rev. **77**, 806 (1950).
[11] D. W. Kerst and G. A. Price, Phys. Rev. **79**, 725 (1950).
[12] Terwilliger, Jones, and Jarmie, Phys. Rev. **82**, 820 (1951).
[13] J. Halpern and A. K. Mann, Phys. Rev. **82**, 733 (1951).
[14] E. R. Gaerttner and M. L. Yeater, Phys. Rev **82**, 461 (1951); and Phys. Rev. **83**, 145 (1951).
[15] J. Heidmann and H. A. Bethe, Phys. Rev. **84**, 274 (1951).
[16] N. Sugarman and R. Peters, Phys. Rev. **81**, 951 (1951).
[17] P. R. Byerly, Jr., and W. E. Stephens, Phys. Rev. **83**, 54 (1951).
[18] Katz *et al.*, Phys. Rev. **80**, 1062 (1950); Phys. Rev. **81**, 815 (1951); Phys. Rev. **82**, 270 (1951); Phys. Rev. **82**, 271 (1951).
[19] R. Sagane, Phys. Rev. **83**, 174 (1951).

against photon energy, or as to the area under this curve.

The purpose of this paper is to interpret the measurements of neutron yield *vs* Z for large Z ($Z \geq 29$) in terms of multiple neutron production. We shall show that Eq. (2) is in accord with experimental results on the neutron yield. We wish to make clear that establishing the validity of Eq. (2) does not verify any particular nuclear model or any specific mechanism for photonuclear reactions. Equation (2), or a rather similar equation, must hold for any theory of electric dipole transitions. The comparison with experiment does indicate that electric dipole transitions are indeed the predominant effect, as we would expect from theory.[1]

II. NEUTRON YIELD

Let $\sigma(W)$ be the cross section for absorption of a photon of energy W; let $\gamma(W)$ be the differential energy spectrum of the photon beam; and let $\nu(W)$ be the neutron multiplicity for the nucleus subsequent to photon absorption. (Note that $\nu(W)$ can be less than unity, due to proton competition.) The measured neutron yield Y is then

$$Y = \int \sigma(W)\gamma(W)\nu(W). \tag{3}$$

To relate Eq. (3) for the measured yield to the theoretical result given in Eq. (2) we make the following two approximations. For the photon spectrum $\gamma(W)$ we take

$$\gamma(W) \cong \begin{cases} n dW/W, & W \leq W_m \\ 0, & W > W_m. \end{cases} \tag{4}$$

The neutron yields are given[11,12] as neutrons/mole per erg/cm^2 of bremsstrahlung striking the sample. For the low energy end of the bremsstrahlung spectrum the number of photons in an erg is[20] $(1.3/W_m)dW/W$, where the maximum energy W_m is expressed in ergs. Then $n = 1.3/W_m$. Second, the neutron multiplicity $\nu(W)$ is approximated as

$$\nu(W) \cong W/E_n. \tag{5}$$

Here E_n represents the average energy spent in producing a neutron, and varies from isotope to isotope but generally decreases with increasing atomic number.

Substituting in Eq. (3) we have the neutron yield

$$Y = (n/E_n)\int_0^{W_m} \sigma dW. \tag{6}$$

If the maximum bremsstrahlung energy is very high, such as 325-Mev, we make a third approximation by replacing W_m by infinity, and find the integrated cross section in terms of the neutron yield

$$\int_0^\infty \sigma dW = E_n Y/0.602n = E_n Y/1500 \text{ Mev-barns}. \tag{7}$$

We have taken $W_m = 325$-Mev. The factor 0.602 is to convert from cm^2/mole to barns per nucleus.

TABLE I. Neutron multiplicity.

Element	Neutron binding energies (Mev) L_1	L_2	L_3	L_4	Level density parameter a (Mev^{-1})	Average energy E_n (Mev)
$_{29}$Cu	10.5	18.7	29.7	38.4	1.9	21
$_{53}$I	9.3	16.8	26.6	34.6	7.3	13
$_{73}$Ta	7.7	14.0	22.2	28.6	9.4	11
$_{83}$Bi	7.4	13.5	21.4	28.0	10.2	10
$_{92}$U	5.6	10.0	16.1	21.0	11.5	8

The average energy expended per neutron emitted, E_n, has been evaluated by means of the statistical compound nucleus model[21,22] for the 5 elements, $_{29}$Cu, $_{53}$I, $_{73}$Ta, $_{83}$Bi, and $_{92}$U. In each case we calculate and plot the multiplicity as a function of excitation energy of the compound nucleus—i.e., the function $\nu(W)$—and approximate it by a straight line through the origin.

The nuclear parameters used, and the results obtained, are summarized in Table I. The neutron binding energies L_1, L_2 (L_i for removal of i neutrons) are taken from Heidmann and Bethe.[15] L_1 for removal of the first neutron is based on thresholds for $\gamma - n$ reactions; the higher L's are based on the semi-empirical Weizsäcker mass equation. The level density parameter a occurs in determining the nuclear temperature, $T = (E/a)^{\frac{1}{2}}$, where E is the nuclear excitation energy. The values for a are found by interpolation from Blatt and Weisskopf.[21] The values for E_n are found by approximating the functions $\nu(W)$ by a straight line. Figure 1 shows the curve $\nu(W)$ up to $W = 30$-Mev, together with the straight line approximation for Ta. The maximum deviation from the approximation is 30 percent. For the case of copper we calculated $\nu(W)$ and $E_n = 15$-Mev for neutron emission, neglecting the proton competition; and subsequently corrected for proton competition using the experimental result[17] neutron yield/particle yield = 0.7. Proton competition is negligible for the heavier nuclei.

We note that to a good approximation $E_n = \frac{1}{2}(L_1 + L_2)$, which is evident from Fig. 1.

We can now compare the relation between experimental values of the integrated cross section derived from the yield by Eq. (7) with the quantity NZ/A, to find if Eq. (2) holds. We shall use the experimental data of Kerst and Price[11] and Terwilliger, Jones, and Jarmie[13] for neutrons/mole erg/cm^2 of bremsstrahlung. (The lower energy measurements of Baldwin and Elder[9] and Price and Kerst[10] agree with the general features of

[20] B. Rossi and K. I. Greisen, Revs. Modern Phys. **13**, 240 (1941).

[21] J. M. Blatt and V. F. Weisskopf, Massachusetts Institute of Technology Laboratory Nuclear Science and Engineering Technical Report 42 (1950), Chapter 6.

[22] Orear, Rosenfeld, and Schluter, *Nuclear Physics* (University Press, Chicago, 1950), p. 162.

the measurements referred to above. We have selected the high energy measurements since we are making the approximation $W_m=\infty$. The former measured neutrons produced by 320-Mev bremsstrahlung, the latter by 330-Mev bremsstrahlung. The energy in the photon beam was measured calorimetrically by the former group, and using the method of Panofsky *et al.*[23] by the latter group. The neutrons were detected at 90° in each case, and additional measurements showed that they were emitted isotopically. The former group used rhodium foils in paraffin as neutron detectors, while the latter group used a large BF_3 counter in paraffin. The efficiency of detection of the second method should be less sensitive to the neutron energy. The two sets of data are in fairly good agreement: the ratio of the Berkeley to Illinois neutron yields vary between 1.44 and 1.17 for the 5 elements considered here. We shall average the two sets of data, since there is no clear basis for preference of one against the other.

The product

$$VE_n/1500=\int_0^\infty \sigma dW$$

is plotted against NZ/A in Fig. 2. We find that the linear relationship between them predicted by theory holds quite well for the four elements $_{29}$Cu, $_{53}$I, $_{73}$Ta, and $_{83}$Bi. The agreement is almost within the experimental errors of measuring Y, and well within the approximations we have made. However, $_{92}$U falls 35 percent above the straight line predicted from theory.

As Kerst and Price[10] have pointed out, it is most likely that this excess neutron emission by U is due to the possibility of photofission. Koch, McElhinney, and Gasteiger[24] and Anderson and Duffield[25] have measured the threshold for photofission. Both groups found it to be 5.1 Mev, close to the neutron binding energy of 5.6 Mev, in conformity with the prediction of the theory of Bohr and Wheeler.[26] Charbonnier, Scherrer, and Wäffler[27] have measured the photofission cross section at 17-Mev photon energy and found it to be 9 percent of the cross section for neutron emission at the same energy. Goward, Jones, Watson, and Lees[28] find a value of 14 percent for this ratio, for 23-Mev bremsstrahlung. Let us assume that generally fission may be substituted for neutron emission with a probability y. Then, e.g., at a γ-ray energy at which normally 3 neutrons are emitted, fission may occur instead of the emission of the first neutron with a probability y. With a probability $1-y$, a neutron is emitted first; but in this case, there is again a probability that fission occurs as the second step, and similarly for the third step. The total probability of fission is then

$$y+y(1-y)+y(1-y)^2=1-(1-y)^3=3y(1-y+\tfrac{1}{3}y^2).$$

If y is small, as in fact it is, this is close to $3y$, or ny if normally n neutrons are emitted. If fission occurs, the remaining $n-1$ neutrons can still be emitted because the necessary energy is still available; they may be emitted either before or after the fission. In the fission of U^{235} by slow neutrons, $\nu_F=2.5$ neutrons are emitted, so that if fission occurs after γ-ray absorption, the total number of neutrons emitted is $n+\nu_F-1=n+1.5$, or 1.5 more than without fission. The probability of obtaining these 1.5 additional neutrons was found above to be about ny, so that on the average the number of neutrons is increased by $1.5ny$, or by a factor

$$F=1+(\nu_F-1)y. \tag{8}$$

To get agreement with the 35 percent increase which we deduced above from the observations, we would have to assume that $y=0.23$. Although this is considerably higher than the values of y observed,[27,28] it is in good agreement with the branching ratio for the fission of U^{238} by fast neutrons.

The straight line drawn in Fig. 2 gives the experimental result

$$\int_0^\infty \sigma dW=0.14NZ/A. \tag{9}$$

In Eq. (2) the value of the right-hand side is $0.060\times(1+0.8x)(NZ/A)$. Thus the experimental value of the coefficient is 30 percent larger than the theoretical value 0.108 for the case of complete exchange force ($x=1$), or 65 percent larger if we use the value $x=\frac{1}{2}$. This disagreement seems within the errors of the absolute measurement of neutron yield, combined with the approximations of our analysis. Gaerttner and Yeater[5,14] also found some integrated cross sections higher than

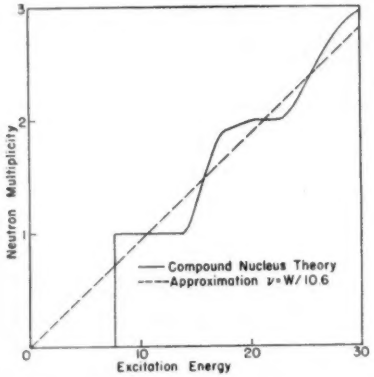

FIG. 1. Neutron multiplicity from Ta^{181} *vs* excitation energy in Mev.

[23] Blocker, Kenney, and Panofsky, Phys. Rev. **79**, 419 (1950).
[24] Koch, McElhinney, and Gasteiger, Phys. Rev. **77**, 329 (1950).
[25] R. E. Anderson and R. B. Duffield, Phys. Rev. **85**, 728(A) (1952).
[26] N. Bohr and J. A. Wheeler, Phys. Rev. **56**, 426 (1939).
[27] Charbonnier, Scherrer, and Wäffler, Helv. Phys. Acta **22**, 385 (1949).
[28] Goward, Jones, Watson, and Lees, Proc. Phys. Soc. (London) **A64**, 95 (1951).

the maximum theoretical value, while Halpern and Mann[13] found

$$\int_0^{25} \sigma dW = 0.090 NZ/A.$$

We can suggest two corrections to make in comparing the absolute cross sections given by theory and experiment. First, the measured neutron yield includes neutrons produced in high energy nuclear stars, which appear to be in large part caused by photomeson production, and subsequent reabsorption of the meson in the same nucleus, producing a star. The calculations which led to Eqs. (1) and (2) did not include interaction of mesons with photons, so the experimental neutron yield could be larger than that calculated in Eq. (2). The integrated cross sections for photomesonic effects can be estimated from the measurements of Miller,[29] and Kikuchi.[30] Miller found that the cross section of the silver nucleus for production of stars of 3 or more prongs was about 7 mb for photons from 160 to 240-Mev, and 8 mb for photons from 240 to 320-Mev. A large part of this cross section—say 5 mb—is probably due to the process of meson production and reabsorption. Using the mesonic cross section $\sigma_m = 5$ mb from 160 to 320-Mev, and using Eq. (2) with $x=1$ for the denominator we have as an order of magnitude estimate for this correction C_1

$$C_1 = \int_0^{325} \sigma_m dW \Big/ \int_0^{\infty} \sigma dW = 0.3. \qquad (10)$$

Second, the nonmesonic part of the photonuclear cross section is not negligible above $W_m = 325$-Mev, so that the experimental measurement is expected to be somewhat smaller than the theoretical result. A theoretical estimate of the high energy nuclear photoeffect[31] gives us a correction for this effect

$$C_2 = \int_{325}^{\infty} \sigma dW \Big/ \int_0^{\infty} \sigma dW = 0.1. \qquad (11)$$

The ratio between experimental and theoretical yields should be $1+C_1-C_2$ or roughly 1.2, but the corrections can only be made very approximately at the present.

Note added in proof.—Eyges has recently discussed the contribution of high energy mesonic processes to the neutron yield; his estimate is somewhat higher than ours. The significance of mesonic processes in the high energy deuteron photoeffect has been shown by the high cross sections found recently at Berkeley (Kikuchi, and also Gilbert and Rose) and at Cornell (Benedict and Woodward, and also Keck and Littauer).

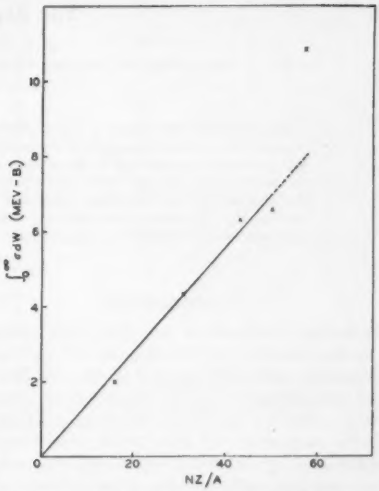

FIG. 2. Integrated photonuclear cross sections. The five points shown are for the elements. $_{29}$Cu, $_{53}$I, $_{73}$Ta, $_{83}$Bi, and $_{92}$U. $N=A-Z$ is the number of neutrons in the nucleus.

We conclude that there is no clear discrepancy between theoretical and experimental results for the absolute value of the neutron yield from photonuclear reactions. There is quite good agreement between theory and experiment on the relative values of the particle yield (neutrons plus protons) for the various nuclei, uranium being high probably due to photofission. This confirms that the photonuclear process is predominantly electric dipole in character, and that the integrated cross section is increased due to exchange forces between neutron and proton. Much more experimental and theoretical work must be done to confirm, or refute, any given nuclear model for the dipole transitions.

One of us (J.S.L.) did much of this work while employed as a research associate at Cornell University under an ONR contract. We are grateful to G. C. Baldwin, D. W. Kerst, and N. Sugarman for discussions of their experiments.

[29] R. D. Miller, Phys. Rev. **82**, 260 (1951).
[30] S. Kikuchi, Phys. Rev. **81**, 1060 (1951).
[31] J. S. Levinger, Phys. Rev. **84**, 523 (1951).

The Reaction $Be^9(p,a\gamma)Li^6$

R. B. DAY AND R. L. WALKER
Kellogg Radiation Laboratory, California Institute of Technology, Pasadena 4, California
(Received November 5, 1951)

The energy of the gamma-radiation produced when Be^9 is bombarded by 2.6-Mev protons has been measured with a scintillation spectrometer and found to be 3.58±0.04 Mev. A suggestion of Hushley that this gamma-ray is produced in the reaction $Be^9(p,a\gamma)Li^6$ was verified by observing coincidences between the gamma-rays and low energy alpha-particles. The excited state of Li^6 which emits the gamma-rays probably has spin zero and even parity and is presumably the analog of the ground state of the isobaric nucleus, He^6. The thick target yield and cross section at resonance were found to be 4.8×10^{-6} gamma-rays per proton and 0.11×10^{-24} cm², respectively.

I. INTRODUCTION

IN the bombardment of beryllium with protons, a strong resonance for production of both gamma-rays and neutrons was observed at 2.56 Mev by Hushley.[1] From measurements of the absorption of secondary electrons, Hushley found that the energy of the gamma-radiation was about 3.0 Mev, which is less than half the 8.8 Mev available for simple capture radiation. From this fact and from the great intensity of the gamma-radiation, Hushley concluded that the gamma-rays were probably emitted by a residual nucleus left after particle decay of the compound nucleus, B^{10}. After considering various possibilities, he concluded that the reaction was probably $Be^9+p\rightarrow B^{10*}\rightarrow Li^{6*}+\alpha$, $Li^{6*}\rightarrow Li^6+h\nu$.

We have used a scintillation counter to obtain a more accurate value for the energy of the gamma-ray.

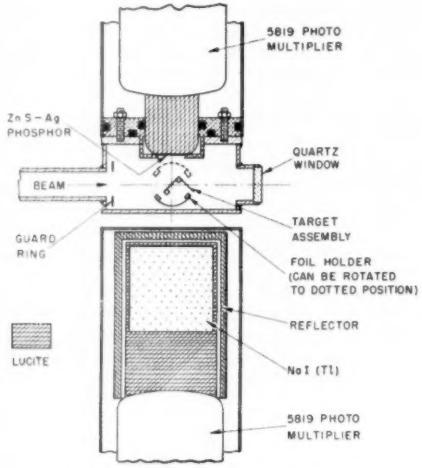

FIG. 1. Arrangement for measuring alpha-gamma coincidences. A 0.00015-inch aluminum foil is mounted on a rotatable holder so that it may be inserted between the target and the particle counter to cut out low energy alpha-particles.

[1] W. J. Hushley, Phys. Rev. **67**, 34 (1945).

and have confirmed Hushley's conclusion about the origin of the gamma-radiation by measuring coincidences between the gamma-rays and low energy alpha-particles.

II. THE GAMMA-RAY ENERGY

The energy of the gamma-radiation produced by bombarding a thin beryllium target with 2.6-Mev protons was measured by the scintillation counter technique now in widespread use.[2] The scintillation counter consisted of a cylindrical NaI(Tl) crystal 1½ inches long and 1½ inches in diameter mounted on a selected 5819 photomultiplier tube (the bottom counter of Fig. 1). Pulses from the photomultiplier were amplified and then analyzed by a single-channel differential discriminator designed by M. Sands. The observed pulse-height spectrum is shown in Fig. 2, where the usual three peaks corresponding to a single gamma-ray may be seen. The lowest energy peak, the pair peak, results from pairs produced in the NaI crystal if both the subsequent annihilation quanta escape from the crystal. The highest energy peak corresponds to the full gamma-ray energy, while the central peak results from Compton scattering and from pair production with escape of one of the annihilation quanta. Figure 2 shows also the pulse-height spectrum from the 2.62-Mev gamma-ray of ThC″. This was used for the energy calibration. To minimize the effects of small drifts in the apparatus, the lowest energy Be^9 peak and the highest energy ThC″ peak were measured several times alternately. A value 3.58±0.04 Mev was obtained for the Be^9+proton gamma-ray. The gamma-ray energy was also measured at a proton bombarding energy of 2.3 Mev. The result obtained here was $E_\gamma=3.56\pm0.04$ Mev.

The pulse-height spectrum was examined carefully in the region 1.2–2.6 Mev with the aid of the differential discriminator and also by photographing the pulses on an oscilloscope. Neither method disclosed any further peaks. From the fluctuations in the pulse-height curve

[2] S. A. E. Johanssen, Arkiv Fysik **2**, 171 (1950); R. Hofstadter and J. A. McIntyre, Phys. Rev. **80**, 631 (1950); W. H. Jordan and P. R. Bell, Nucleonics **5**, 30 (1949).

we estimate that the intensity of any lower energy gamma-ray is less than two percent of the 3.58-Mev gamma-ray. This is of particular interest in view of the fact that a level in Li^6 has recently been found at 2.187 Mev by Browne, *et al.*,[3] by means of the reaction $Be^9(p,\alpha)Li^{6*}$. Above 3.6 Mev we find no gamma-rays with relative intensity greater than one-half percent.

The fact that only one gamma-ray of appreciable intensity is observed and that it does not change energy as the proton energy is varied indicates that the radiation comes from a residual nucleus, thus supporting Hushley's suggestion that the gamma-radiation is produced in the reaction $Be^9(p,\alpha\gamma)Li^6$. To obtain further evidence on this origin we looked for coincidences between the gamma-rays and the low energy alpha-particles expected to precede them.

III. ALPHA-GAMMA COINCIDENCES

Coincidences between the gamma-rays and low energy alpha-particles were observed with the detector and target arrangement shown in Fig. 1. The alpha-particle scintillation counter employed a layer of activated ZnS phosphor sufficiently thin that protons scattered from the Be target lost only part of their energy in traversing it. Thus the pulses from scattered protons and other reaction products, which were about 15 times as numerous as the low energy alpha-particle pulses, were reduced to a size comparable with that of the latter. The target was a thin beryllium foil, nominally 22 micro-inches thick, mounted over a hole in a brass support. Behind it was a piece of tantalum, arranged to collect the protons passing through the target but not to scatter protons into the particle counter.

Figure 3 shows the excitation curve near the resonance for both gamma-rays and alpha-gamma coincidences. The latter curve has been corrected for accidental coincidences and is plotted on such a scale that the two curves would coincide if every gamma-ray followed a low energy alpha-particle and if the efficiency of the alpha-particle counter were 100 percent. Because of the large background of scattered protons it was not possible to measure the efficiency for low energy alpha-particles. However we feel that the value of 60 percent indicated by Fig. 3 is quite reasonable.

In order to see whether the observed coincidences were actually produced by low energy alpha-particles, counts were taken with a thin aluminum foil between the target and the particle counter. For this purpose a 0.00015-inch aluminum foil was mounted on a rotatable holder in the target chamber as shown in Fig. 1. This thickness is sufficient to stop alpha-particles of about 850 kev (those expected from the $Be^9(p,\alpha\gamma)Li^6$ reaction have an energy of about 400 kev at 90°), but will allow more energetic alpha-particles and scattered protons to pass through. Since most of the individual counts in the particle counter were produced by higher energy

[3] Browne, Williamson, Craig, and Donahue, Phys. Rev. **83**, 179 (1951).

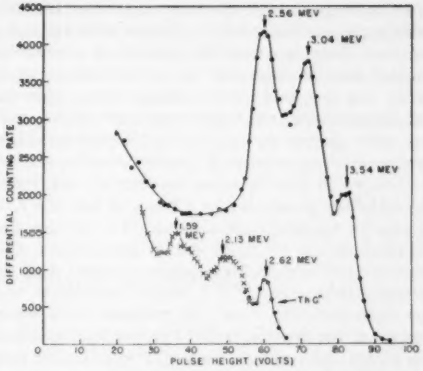

FIG. 2. Differential pulse-height distributions for gamma-rays from $Be^9(p,\alpha\gamma)Li^6$, and for the 2.62-Mev gamma-rays from ThC'' used as an energy calibration. The channel width of the differential discriminator was 1 volt.

particles, the aluminum foil did not change appreciably either the "singles" rate of the particle counter or the accidental coincidence rate. It did, however, reduce the coincidence counting rate to about 16 percent of the rate without the aluminum filter. The remaining 16 percent are presumably accidental coincidences since the insertion of a 1.5 μsec delay line in one arm of the coincidence circuit produced no further reduction in coincidence rate. Furthermore, the coincidence counts with aluminum filter dropped to 6 percent when the proton beam intensity was decreased by about a factor of three. During the coincidence measurements the proton beam current was kept at about 2×10^{-9} amp in order to reduce the accidental coincidences to an acceptable rate. The resolving time of the coincidence circuit was approximately 0.1 μsec.

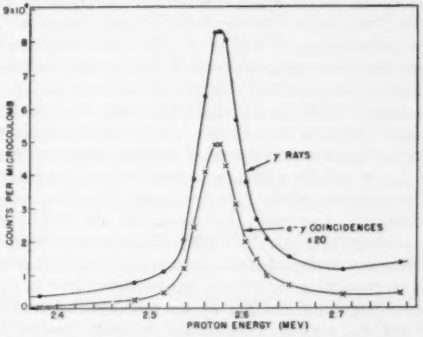

FIG. 3. Excitation curves for the reaction $Be^9(p,\alpha\gamma)Li^6$ for gamma-rays and for alpha-gamma coincidences. A background of accidental coincidences (about 16 percent) has been subtracted from the coincidence curve.

As a further check to show that the 3.58-Mev gamma-ray was the one in coincidence with the alpha-particles, the pulses from the gamma-ray scintillation counter were photographed on an oscilloscope whose sweep was triggered by the output pulses from the coincidence circuit. Although it seemed unlikely that any other gamma-ray could be sufficiently intense to produce the large number of observed coincidences, this method would have increased its intensity relative to the 3.58-Mev gamma-ray by a factor of five (the ratio of true to accidental coincidences). The picture thus obtained showed no pulses due to gamma-rays other than the one at 3.58 Mev, which appeared with the intensity to be expected if it were in coincidence with the alpha-particles. Thus, the evidence is in strong support of the hypothesis that the reaction produces a low energy alpha-particle, leaving Li^6 in an excited state at 3.58 Mev which decays by emitting a gamma-ray.

IV. THE CROSS SECTION

Several gamma-ray excitation curves were run in order to determine the cross section, energy, and width of this resonance. The protons from the electrostatic generator were analyzed in energy by a 90° electrostatic analyzer, operated with a resolution of about 0.1 percent. The proton charge striking the target was measured with a current integrator having an accuracy of better than one percent, while the detector was the NaI scintillation counter used previously. The curves thus obtained showed an asymmetry which was at first thought to be due to the superposition of the resonance on a rising background. However, when the data were corrected for the energy dependence of Γ_α, the width for alpha-particle emission, the excitation curves exhibited the characteristic symmetrical shape of the Breit-Wigner formula.

In order to determine the true resonance width and energy it was necessary to measure the target thickness. This was done by measuring the shift in the 1754 kev resonance[4] of $C^{13}(p,\gamma)N^{14}$, which has a width of less than 2 kev, when the beryllium foil was interposed in the proton beam. A shift of 16.6 kev was found, corresponding to a target thickness of 12.7 kev at 2.58 Mev. Since in the beryllium reaction the foil was placed at an angle of 45° to the beam, the value used for the target thickness was 18 kev. Applying this value to the excitation curves corrected for the energy variation of Γ_α we find the resonance energy to be 2.565 ± 0.005 Mev and the width Γ to be 39 ± 2 kev. The energy calibration was made by means of the 873.5 kev resonance in $F^{19}(p,\alpha\gamma)O^{16}$ using the mass-three beam.

The absolute yield of the gamma-rays was determined by extrapolating the integral pulse-height curve to zero pulse height and dividing by the calculated absorption of the NaI crystal. This method has been checked by measuring in the same way the gamma-ray yield in the reaction $F^{19}(p,\alpha\gamma)O^{16}$ produced by bombarding a CaF_2 crystal with 1.00-Mev protons. A value 7.14×10^{-7} gamma-ray per proton was obtained for the fluorine reaction, to be compared with the best value 6.68×10^{-7}.[5] The agreement is better than the estimated accuracy of our method, which is 10–15 percent.

The thick target yield of the 3.58-Mev gamma-ray was measured with a thick beryllium target and checked by integrating the thin target curve, the two methods giving very good agreement. In this reaction the thick target curve does not have the usual shape, but continues to rise at high energies because of the rapid decrease in the barrier factor for the low energy alpha-particles. Above 2.68 Mev the rise is approximately linear and at 2.72 Mev the thick target yield is 4.76×10^{-6} gamma-ray per proton. From the maximum yield in the thin target curve we have calculated the cross section at resonance, obtaining $\sigma_r=0.11\times10^{-24}$ cm^2. Both the cross section and yield values were calculated under the assumption that the gamma-rays are emitted isotropically. It will be shown in the next section that this assumption is quite reasonable.

V. DISCUSSION

For some time there was a question as to whether the gamma-ray observed by Hushley could actually occur in the decay of an excited state of Li^6. The difficulty is that disintegration into an alpha-particle and a deuteron is possible for energies above 1.53 Mev and in general this mode of disintegration would proceed so quickly that gamma-decay could not compete with it. A possible explanation was suggested by W. A. Fowler and others at this laboratory, who pointed out that if an excited state in Li^6 has spin zero and even parity then the particle disintegration is forbidden by the conservation of angular momentum and parity. Thus it is reasonably certain that any strong gamma-ray of energy greater than 1.53 Mev that occurs in the de-excitation of a Li^6 state must be from a state with spin zero and even parity.

On the basis of both the alpha-particle and independent particle models the ground state of He^6 would be expected to have spin zero and even parity. The *ft* value of 590 for its β-decay to the ground state of Li^6 is consistent with this, providing Gamow-Teller selection rules apply. Using the estimated Coulomb energy and the $n-H^1$ difference, Lauritsen[6] has calculated that the analogous state in Li^6 should lie at about 3.7 Mev. Thus it seems quite reasonable that the level at 3.58 Mev is indeed this level. From the spin zero property one would expect both the gamma-ray angular distribution and the α-γ angular correlation to be isotropic. We intend to measure the first of these to test this hypothesis. In addition, an experiment to measure the

[4] Seagrave, Day, and Perry, Phys. Rev. **81**, 661 (1951).

[5] This is actually $4\pi Y(90°)$. The value was obtained by Perry and Day (unpublished) by comparison with a calibrated Co^{60} source and is also in excellent agreement with the alpha-particle yield.

[6] T. Lauritsen, *Energy Levels of Light Nuclei—1950*, Annual Review of Nuclear Science for 1950, to be published.

coefficient for internal pair conversion is being carried out at this laboratory by Mr. R. J. Mackin and Mr. C. Wong. This should provide information on the character of the gamma-ray and hence on the change of spin and parity occurring in the transition. Preliminary results indicate that the gamma-ray is magnetic dipole as is to be expected from the above considerations.

We should like to express our thanks to Professors T. Lauritsen and R. F. Christy for suggesting this problem and for several enlightening discussions on it. We are also indebted to Mr. Torben Huus for assistance in operating the electrostatic generator.

This work was supported by the joint program of the AEC and ONR.

PHYSICAL REVIEW VOLUME 85, NUMBER 4 FEBRUARY 15, 1952

The (p, n) Reaction on Separated Isotopes of Chromium*

J. A. Lovington,† J. J. G. McCue, and W. M. Preston
Laboratory for Nuclear Science and Engineering, Massachusetts Institute of Technology, Cambridge, Massachusetts
(Received November 7, 1951)

Several hundred resonances have been observed in the neutron yield from proton bombardment of the enriched isotopes Cr^{50} and Cr^{54}. No characteristic groups of resonances are observed. Upper limits to the level spacing in the compound nuclei Mn^{54} and Mn^{55} are 4 and 5 kev, respectively. The thresholds are found to be 1406±8 kev for $Cr^{50}(p,n)$ and 2202±5 kev for $Cr^{54}(p,n)$.

A. INTRODUCTION

RESONANCES in the neutron yield of the reaction $Mn^{55}(p,n)Fe^{55}$ have been studied by McCue and Preston.[1] In continuation of a program at this laboratory of investigating a number of light-intermediate weight elements with the best energy resolution practical with our equipment, we have measured the relative yield as a function of energy from the reactions $Cr^{53}+p\rightarrow Mn^{54}\rightarrow Mn^{53}+n$ and $Cr^{54}+p\rightarrow Mn^{55}\rightarrow Mn^{54}+n$. Chromium was chosen because its two heaviest stable isotopes, Cr^{53} and Cr^{54}, could be obtained from Oak Ridge enriched to a high degree and had (p,n) thresholds estimated to be conveniently low. Neutron yield resonances in these reactions correspond to excited states in the compound nuclei Mn^{54} and Mn^{55}. We wished to measure the reaction threshold energies, to search for possible regularities in the level spectra, and to compare the level spacing in two neighboring nuclei with the same number of protons, but containing, respectively, an odd and an even number of neutrons.

B. EXPERIMENTAL METHODS

The proton source was the Rockefeller electrostatic generator[2] at M.I.T. The absolute energy calibration of the machine is based on the $Li^7(p,n)Be^7$ threshold, taken as 1882.2 kev, ±0.1 percent.[3] Relative to this standard, we believe our energy measurements of sharp resonances in the present work should be accurate to ±0.1 percent, allowance being made for long-term drifts in the calibration constant, target contamination, and other sources of error. Resetting accuracy and short-term stability, as in measuring the profiles or separation of neighboring resonances, is close to 0.01 percent. Tests indicate that the effective beam energy resolution width is not over 0.08 percent when the defining slits of the magnetic analyzer are opened to 1 mm, and half as great with 0.5-mm slit openings.

Neutrons were detected by a counter consisting of a 1-inch diameter tube, filled with enriched BF_3 at a pressure of 55 cm of mercury, and embedded in an 8-inch diameter, cadmium-covered cylinder of paraffin. The counter was operated in the proportional region and the pulse-height discriminator, which followed the linear amplifier, was set at a sufficiently high level so that gamma-rays were not counted. The counter assembly was mounted with its axis perpendicular to the proton beam and its side a few centimeters from the target, at which it therefore subtended a rather large angle in the forward direction. The counter was operated in this position in order to get satisfactory counting rates despite the low reaction yields; we cannot assume that the neutron detection efficiency was inde-

TABLE I. Isotopic analysis of target materials.

Isotope	Natural abundance	Enriched Cr^{50}	Enriched Cr^{54}
Cr^{50}	4.4%	0.193%	0.2%
Cr^{52}	83.5	9.28	7.0
Cr^{53}	9.5	90.06	3.9
Cr^{54}	2.6	0.465	89.0

* This work was supported by the Bureau of Ships and the ONR.
† Lt. Commander, U.S.N. This work was done in partial fulfillment of the requirements for the degree of Master of Science in Physics at M.I.T.
[1] J. J. G. McCue and W. M. Preston, Phys. Rev. 84, 1150 (1951).
[2] W. M. Preston and C. Goodman, Phys. Rev. 82, 316 (A) (1951). See reference 1 for additional details.
[3] Herb, Snowdon, and Sala, Phys. Rev. 75, 246 (1949).

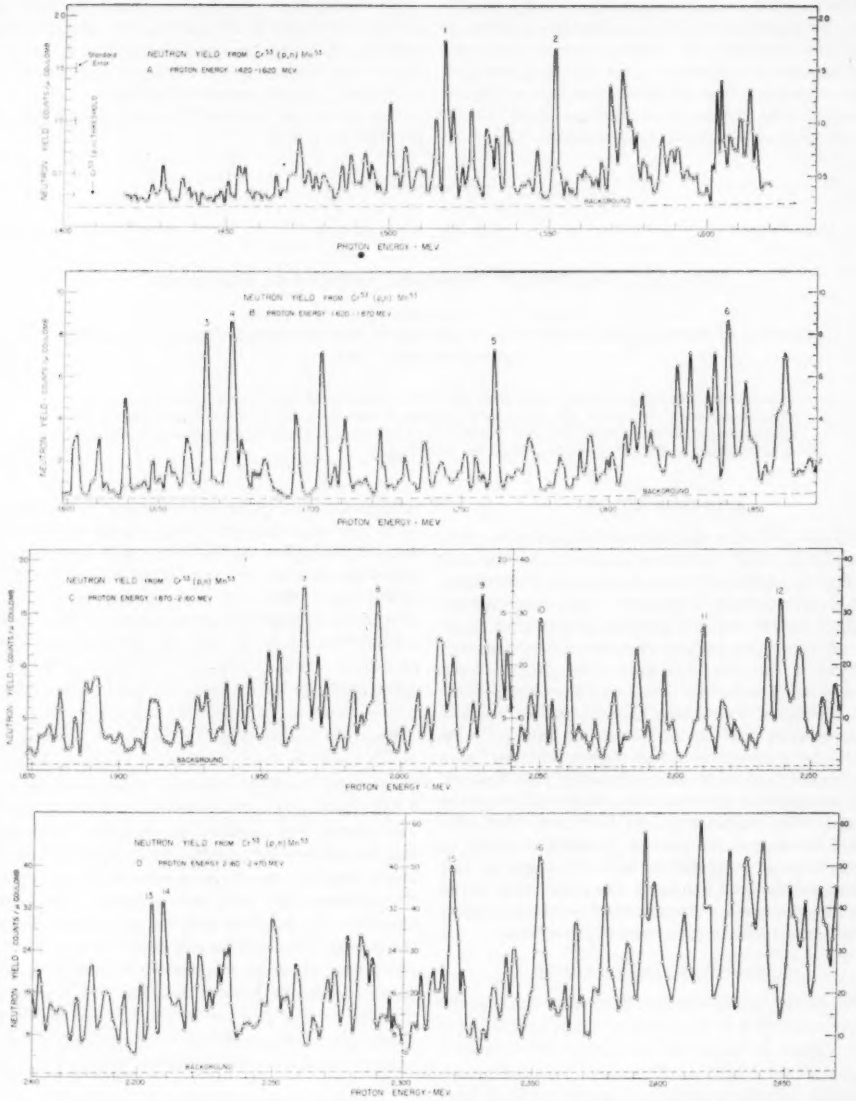
NEUTRON YIELD FROM $Cr^{53}(p,n)Mn^{53}$
A PROTON ENERGY 1420-1620 MEV
B PROTON ENERGY 1620-1870 MEV
C PROTON ENERGY 1870-2160 MEV
D PROTON ENERGY 2160-2470 MEV
Standard Error
BACKGROUND
NEUTRON YIELD - COUNTS/μ COULOMB
PROTON ENERGY - MEV

FIG. 1. Relative neutron yield from the reaction $Cr^{53}(p,n)Mn^{53}$. Note the several changes in the ordinate scale. The resolution is about 2 kev.

pendent of energy, as in the case of Hanson and McKibben's "long counter."[4]

The enriched chromium isotopes were obtained in the form of Cr_2O_3 from the Oak Ridge National Laboratory, through the courtesy of the Atomic Energy Commission. Spectroscopic analysis showed the presence of no significant chemical impurities. Table I shows the isotopic analysis furnished by Oak Ridge.

[4] A. O. Hanson and J. L. McKibben, Phys. Rev. 72, 673 (1947).

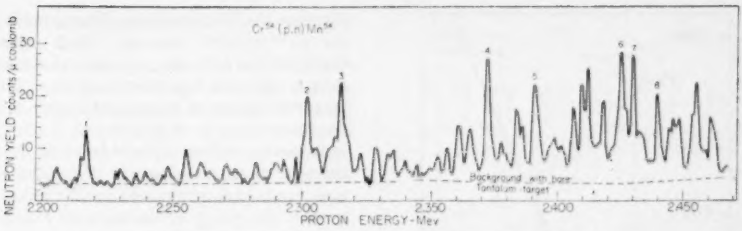

FIG. 2. Relative neutron yield from $Cr^{54}(p,n)Mn^{54}$, resolution about 2 kev.

The Cr_2O_3 was evaporated onto 10-mil tantalum target disks by Baird Associates of Cambridge, Massachusetts. The oxide decomposed on heating and thin metallic films were obtained readily. Targets of 1- to 3-kev stopping power for 2000-kev protons proved to be exceptionally stable. Using a conventional rotating target assembly, little deterioration occurred after 12 hours of operation with beam currents of 6–8 microamperes.

C. EXPERIMENTAL RESULTS

Yield Spectra

Figure 1 shows the yield spectrum of Cr^{52} up to a bombarding energy of 2470 kev. The ordinates are counts per microcoulomb proton current to the target; note that the ordinate scale changes by a factor of 25 from the low energy end to the high. Except on the first strip [Fig. 1(A)] where its magnitude is indicated near the ordinate scale, the statistical probable error is smaller in most cases than the diameter of the circles which designate experimental points. The energy scale is not linear; the kilovolts/unit length increase as $E^{\frac{1}{2}}$. The dashed curve, representing the background, was taken with a clean, bare tantalum target. This small residual yield probably comes from deuteron reactions within the analyzing chamber, as a result of the normal 0.015 percent of deuterium present in the hydrogen gas supplied to the ion source. Figure 2 shows the spectrum of enriched Cr^{54} from 2200 to 2470 kev. The background, as shown, was somewhat higher in this case.

From Table I, the Cr^{54} contamination in the enriched Cr^{52} is negligible, but there is 4 percent of Cr^{53} in the enriched Cr^{54} material. However, a careful comparison of the data of Figs. 1(D) and 2 indicates that none of the clearly defined peaks in the latter come from Cr^{53}.

Table II gives the resonance energy of a number of the stronger peaks in the spectra of $Cr^{53}(p,n)$ and $Cr^{54}(p,n)$. The peaks are identified by numbers in Figs. 1 and 2.

Resolution

In the $Cr^{53}(p,n)$ spectrum of Fig. 1, we have measured the experimental width at half-maximum of a number of the stronger peaks which, from their symmetry, appear to be single resonances. The average width of the three narrowest peaks on each of the four strips, *A*, *B*, *C*, and *D* of Fig. 1, is 1.5, 1.7, 2.0, and 2.4 kev, respectively. These numbers represent upper limits to the effective resolution width in the corresponding energy ranges, due to spread in energy of the incident beam and to energy loss in the target. The broadest symmetrical peaks have observed widths of less than 3 kev. Since the average level spacing is less than 5 kev, there is a good chance that the broader peaks have unresolved components. We conclude that the natural resonance widths are not over 2 kev and that they may actually be much less. Similar remarks apply to the case of $Cr^{54}(p,n)$, Fig. 2, for which an upper limit to the resolution width is 2.2 kev.

Level Spacing

From the data of Figs. 1 and 2, there is no experimental indication that the number of resonances in a given energy range is finite. The observed widths do not differ greatly, since they are determined mainly by the experimental resolution. Under these conditions, two

TABLE II. Resonance energies from the reaction $Cr(p,n)$.

$Cr^{52}(p,n)$ Ref. No. (Fig. 1)	E_R(kev)	$Cr^{53}(p,n)$ Ref. No. (Fig. 1)	E_R(kev)	$Cr^{54}(p,n)$ Ref. No. (Fig. 2)	E_R(kev)
1	1516	9	2027	1	2215
2	1552	10	2050	2	2300
3	1665	11	2108	3	2313
4	1674	12	2136	4	2370
5	1759	13	2202	5	2389
6	1838	14	2206	6	2423
7	1963	15	2316	7	2430
8	1989	16	2350	8	2437

TABLE III. Estimated level spacing in Mn^{54} and Mn^{55}.

Target nucleus	Compound nucleus	Energy range	No. of peaks	Average spacing, kev	
Cr^{52}	Mn^{54}	1420–1620	70	2.9	
Cr^{53}	Mn^{54}	1620–1870	64	3.9	Average
Cr^{53}	Mn^{54}	1870–2160	64	4.5	3.9
Cr^{52}	Mn^{54}	2160–2470	73	4.3	
Cr^{54}	Mn^{55}	2200–2470	56	4.8	

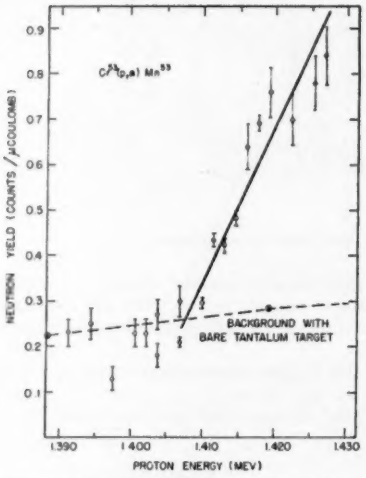

FIG. 3. Threshold measurement for $Cr^{53}(p,n)Mn^{53}$, 20-kev target.

neighboring resonances will be resolved if their separation is equal to, or greater than, their width, provided they are of comparable intensity. If their intensity ratio is as great as ten to one, their separation must be somewhat greater in order to be resolved. Below a certain minimum intensity, peaks will be lost in the background.

Table III shows the number of observed resonances in several energy intervals. The range of intensity covered is about twenty to one; that is, few peaks could be distinguished whose intensity was less than five percent of the strongest peaks in the interval. Note that the ratio of average level spacing to observed width is about two.

Thresholds

The threshold for the reaction $Cr^{53}(p,n)Mn^{53}$ was determined, using a thick target. The data are plotted in Fig. 3, which also shows the background counting rate for a pure tantalum target. The threshold is at 1406 ± 8 kev; a large error is assigned because of the poor statistical accuracy.

Figure 4 shows a similar threshold-curve for $Cr^{54}(p,n)Mn^{54}$. The threshold in this case is at 2203 ± 5 kev. The high neutron background comes from Cr^{53}, which is present to 4 percent in the enriched Cr^{54} sample (see Table I). This is further illustrated in Fig. 5, which shows the thin target data for the two isotopic samples in the region of the Cr^{54} threshold. The weak peaks in the enriched Cr^{54} curve, below 2200 kev, check well with those in the Cr^{53} curve. Their relative intensities are approximately as expected from the isotopic ratios. The peak marked (b) in the Cr^{54} curve does not coincide with that maked (a) in the Cr^{53} plot; it is therefore the first resonance of measurable intensity in the $Cr^{54}(p,n)Mn^{54}$ reaction. From these data, the threshold is at 2202 kev, with somewhat better accuracy than in the thick target determination. While the true threshold cannot be appreciably higher, it is clear that the uncertainty in its position on the low energy side is necessarily at least of the order of the average spacing between strong resonances in this region. An unequivocal threshold determination would require the measurement of the energy of the neutrons emitted.

D. DISCUSSION

The yield spectra of Cr^{53} and Cr^{54} show many resonances, but these do not fall into any obvious, repeated groups. As in the work on $Mn^{55}(p,n)$,[1] the small average level separation makes it extremely difficult to measure natural resonance widths.

Under our experimental conditions (proton energies well below the Coulomb barrier, poor resolution) the peak yield at a resonance for the p,n reaction is almost proportional to $(2J+1)\Gamma_p^l$, where J is the total angular momentum of a resonance formed by protons of angular momentum l, and Γ_p^l is the width for proton emission.[6] The barrier penetration factors for chromium, for protons of 2.4 Mev, are roughly 21×10^{-5}, 9×10^{-3}, 2×10^{-3}, and 0.2×10^{-3} for protons of $l=0$, 1, 2, and 3, respectively. Hence the observed resonances are limited by intensity considerations to those states of the compound nucleus which can be formed by protons of $l=0$, 1, and 2, and, of these, a larger fraction of the weaker resonances will be missed because of the limited resolution. This is about as far as one can go

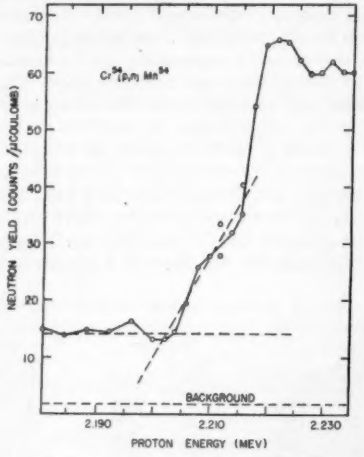

FIG. 4. Threshold measurement for $Cr^{54}(p,n)Mn^{54}$, 20-kev target. The yield below 2202 kev comes from a 4-percent impurity of Cr^{53} in this target.

[6] This is true because the proton width for $l=0$ is still considerably less than the neutron width for $l=2$, and so $\Gamma\approx\Gamma_n$.

in defining the significance of the measured level spacings listed in Table III.

From Q-values of nuclear reactions we have sufficient information to plot on an energy scale the relative positions of the ground states of the nuclei Cr^{53}, Cr^{54}, Mn^{53}, Mn^{54}, Mn^{55}, Fe^{55}, and Fe^{56}, as shown in Fig. 6. We have also indicated the excitation ranges in the compound nuclei Mn^{54}, Mn^{55}, and Fe^{56} in which the level spacing has been estimated, in the present work and in reference 1.

Nuclear theories predict a general decrease in level spacing with increase in excitation energy. One might expect that the level density in two neighboring nuclei would be approximately the same at equal excitation energies, E_x, measured from the ground state. Hurwitz and Bethe[6] suggest instead that E_x should be measured from a reference level, R, which depends in a smooth way upon the number of protons and neutrons in the nucleus as does, for example, the semi-empirical formula for the nuclear binding energy with the omission of the "odd-even" term. This is equivalent to assuming that, although the ground state is raised above the average smooth curve in odd-Z, odd-N nuclei and depressed in even-Z, even-N nuclei, the influence of the odd-even factors is negligible at high excitation energies.

In Figure 6, the reference marks A are drawn 10.3 Mev above the ground states of Mn^{55}, Fe^{56}, and Mn^{54}, while the marks B are 10.3 Mev above the reference levels R. Since Mn^{55} is odd-Z, even-N, the odd-even term δ in the mass formula is zero; R coincides with the ground state and A and B are identical. Fe^{56} is an even-Z, even-N nucleus and its ground state is below R by an amount $\delta = 1.6$ Mev ($\delta = 33^{-1}$ Mev). Similarly, the ground state of Mn^{54} is above R. If the level spacing is determined by the excitation energy measured from the ground state (reference arrows A in Fig. 6), we see that it should be approximately the same, in the ranges investigated, for Mn^{54} and Mn^{55}, but smaller for Fe^{56}.

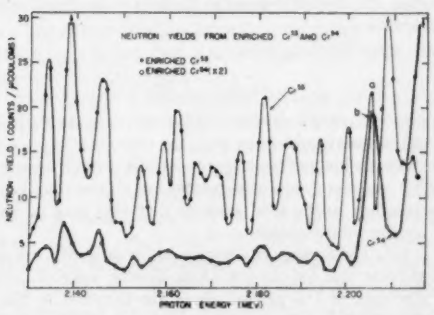

FIG. 5. Comparison of the Cr^{53} spectrum and that of Cr^{54} with a trace (4 percent) of Cr^{53}, near the threshold for the reaction $Cr^{54}(p,n)$. The peak (b), which does not coincide with (a), is the first observed Cr^{54} resonance above the threshold.

[6] H. Hurwtiz, Jr., and H. A. Bethe, Phys. Rev. **81**, 898 (1951).

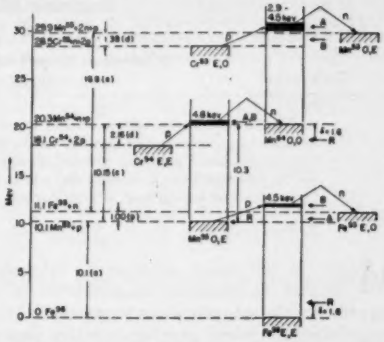

FIG. 6. Excitation energy diagram. The diagram shows the energies, relative to Fe^{56}, of the ground states of the nuclei involved in three p,n reactions: $Mn^{55}+p \rightarrow Fe^{56*} \rightarrow Fe^{56}+n$; $Cr^{54}+p$ $Mn^{55*} \rightarrow Mn^{54}+n$; and $Cr^{53}+p \rightarrow Mn^{54*} \rightarrow Mn^{53}+n$. The black bands in the high excitation regions of the compound nuclei Fe^{56}, Mn^{55}, and Mn^{54}, indicate the regions for which the average level spacing was measured in the present work, and in reference 1. The relative ground-state energies were computed from the following references:

a.	$Mn^{55}(n,\gamma)Mn^{56}$	$E_\gamma = 7.25$ Mev	Kinsey, Bartholomew, and Walker, Phys. Rev. **78**, 481 (1950).
	$Mn^{56} \rightarrow Fe^{56}+\beta+\gamma$	$E_\beta + E_\gamma = 3.63$ Mev	A. C. G. Mitchell, Revs. Modern Phys. **22**, 42 (1950).
b.	$Mn^{55}(p,n)Fe^{55}$	$Q = -1.00$ Mev	Reference 1.
c.	$Mn^{55}(\gamma,n)Mn^{54}$	$E_t = 10.15$ Mev	A. O. Hanson, *et al.*, Phys. Rev. **76**, 578 (1949).
d.	$Cr^{54}(p,n)Mn^{54}$	$Q = -2.16$ Mev	Present paper.
	$Cr^{53}(p,n)Mn^{53}$	$Q = -1.38$ Mev	Present paper.
e.	$Fe^{56}(\gamma,n)Fe^{55}$	$E = 13.8$ Mev	J. McElhinney, *et al.*, Phys. Rev. **75**, 542 (1949).
	$Fe^{56} \rightarrow Mn^{56}+\beta^+$	$E_\beta = 2.5$ Mev	F. I. Boley and L. J. Laslett, Phys. Rev. **83**, 215 (1951).
	$Fe^{56}(n,\gamma)Fe^{57}$	$E_\gamma = 9.28$ Mev	Kinsey, Bartholomew, and Walker, Phys. Rev. **78**, 481 (1950).

If the comparison ought to be made at the reference marks B, as suggested by the theory of Hurwitz and Bethe, Mn^{55} and Fe^{56} should have similar spacing, Mn^{54} smaller.

The experimental results show a slightly smaller average level spacing for the compound nucleus Mn^{54} than for the two others, but it cannot be stated with confidence that this difference is experimentally significant. The fraction of unresolved, and therefore undetected, resonances will increase with the ratio of average level width to level spacing. This may be the cause for the observed increase in level spacing with energy in Mn^{54}; however, some statistical fluctuation in the level density is to be expected. We must conclude that the results given in Table III represent no more than upper limits to the true average level spacing, in a region where virtually no information has been available heretofore.

We wish to express our sincere appreciation to the Rockefeller generator operating and maintenance group: Mr. Donald Thompson, Mr. I. E. Slawson, and Mr. John Adams.

Intrinsic Magnetization in Alloys

W. J. Carr, Jr.
Westinghouse Research Laboratories, East Pittsburgh, Pennsylvania
(Received November 12, 1951)

The intrinsic magnetization of alloys among the iron transition group of metals has been explained using a Heitler-London model for the 3*d* electrons. The magnetic moment associated with each atom is determined by the principle of maximum spin and the sign of the interaction between neighboring pairs from the overlap of the wave functions. It is found that a large number of alloys derive their spontaneous magnetization from an antiparallel arrangement of atomic spins.

MOST of the recent attempts to calculate the intrinsic or saturation magnetization of ferromagnetic metals and their alloys (especially in the iron group) have been based upon the collective electron or band concept. This approach was used successfully by Stoner[1] in calculating the magnetization of nickel-base alloys, mainly those containing elements, such as copper with filled 3*d* shells. The further work of Stoner and Wohlfarth has been adequately summarized.[2,3] Although this work is still in progress, it seems apparent that the alloys such as Ni—Cu were deceptively simple and correct results for some of the other alloys are not readily forthcoming. In particular, the large effect of order on the intrinsic magnetization does not seem to fit naturally into a collective electron picture.

More qualitative calculations have been given by Slater[4] and Pauling.[5] As used by Shockley[6] and Smoluchowski,[7] the Pauling treatment consists in splitting the 3*d* band, somewhat arbitrarily, into two unequal parts in a way to give agreement with experiment for the points in Fig. 1[8] which fall approximately on two straight lines intersecting between Fe and Co. The remaining points appear to be ignored. Other recent treatments are partly empirical.[9,10]

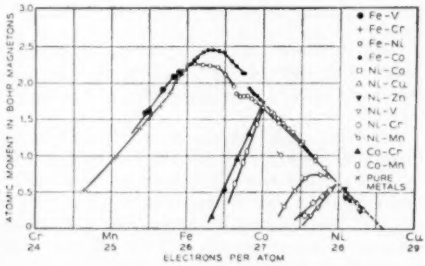

FIG. 1. The average atomic moment in Bohr magnetons as measured by various investigators, plotted against the average number of electrons per atom. The upper point of Ni—Mn is for an ordered alloy (see reference 8).

In this paper we avoid the band approximation and take the point of view that for the 3*d* electrons a Heitler-London approximation is closer to reality, and thus the electrons are to be associated with the individual atoms. This viewpoint is in many respects similar to that of Néel.[11] The atomic spins may be aligned parallel or antiparallel and it is proposed that "antiferromagnetism" is more common in the iron transition group of metals than is "ferromagnetism" itself. All the curves in Fig. 1 can be explained in a simple and straightforward manner on the basis of the three following considerations:

(I) The total spin of each ion is determined by using Zener's hypothesis[12] (analogous to Hund's rule for the gaseous state) that the 3*d* shell has the largest spin possible consistent with the exclusion principle. Hund's rule comes from the fact that electrons on the same atom with parallel spins have a negative exchange energy. For the solid state Zener's hypothesis is tantamount to assuming that the spin coupling between electrons on the same atom is large compared with that between electrons on different atoms and is almost implied by the original assumption that a Heitler-London model is applicable.

Since the *d* shell has room for 10 electrons, five of each spin, the magnetic moment in Bohr magnetons on an atom A is

$$\mu_A = 10 - n_{dA}, \quad n_{dA} \geqslant 5 \tag{1a}$$

$$\mu_A = n_{dA}, \quad n_{dA} \leqslant 5, \tag{1b}$$

where n_{dA} is the number of 3*d* electrons in A. We have the occasion to consider only the case (1a).

As one knows from experiment, the orbital moments (for the iron group of elements) are almost completely quenched in the solid state so that (1a) may be used for the total moment.

(II) The number of electrons in the 3*d* shell is not the same as that for the free atom. Firstly, some of the 4*s* electrons of the gaseous state are demoted to the *d*

[1] E. C. Stoner, Phil. Mag. **15**, 1018 (1933).
[2] E. C. Stoner, Phys. Soc., Rep. Progr. Phys. **11**, 43 (1946–47).
[3] E. C. Stoner, J. phys. et radium **12**, 372 (1951).
[4] J. C. Slater, J. Appl. Phys. **8**, 385 (1937).
[5] L. Pauling, Phys. Rev. **54**, 899 (1938).
[6] W. Shockley, Bell System. Tech. J. **18**, 645 (1939).
[7] R. Smoluchowski, J. phys. et radium **12**, 389 (1951).
[8] After R. M. Bozorth, *Ferromagnetism* (D. Van Nostrand Company, Inc., New York, 1951.)
[9] R. Forrer, J. phys. et radium **12**, 402 (1951).
[10] T. G. Owe Berg, J. phys. et radium **12**, 418 (1951).
[11] L. Néel, *Le Magnétisme, II Ferromagnétisme* (Strasbourg 1939), p. 65.
[12] C. Zener, Phys. Rev. **81**, 440 (1951).

shell, as one knows from the number of conduction electrons found in the solids. (For nickel the number of conduction electrons, n_e, is approximately 0.6, for cobalt $n_e \simeq 0.7$. The extrapolated value for iron would be about 0.8.) Secondly, there is the possibility suggested by Zener (see the preceding paper) that a lowering of the energy can be obtained by the transfer of some of the d electrons of atom A to atom B. Such a process would take place in a manner which maximizes the number of pairs of parallel spins and in our examples would result in a tendency for half-filled and completely filled shells.

For example, consider a Mn atom dissolved in the Ni lattice. After the proper contribution to the conduction band, the Mn d shell is somewhat more than half-filled, whereas the Ni shell is almost complete. Such a situation is the most favorable for the Mn atom achieving a half-filled shell of five parallel spins, with the Ni atoms accepting the remainder. Whether phenomena of this type occur generally in alloys need not be discussed here, since in most cases this knowledge is not needed for an approximate calculation of the magnetic moment.

(III) Of the interactions of an atom A in a lattice of B atoms, the combinations Ni−Ni, Ni−Co, Co−Co, Ni−Fe, Co−Fe, and Ni−Mn among the iron group of elements tend to give a parallel alignment of atomic spins for all the cases in Fig. 1. All other interactions in this transition group tend towards an antiparallel alignment in our examples, the principal reason being that for a fixed interatomic distance the $3d$ shells of the above atoms overlap the least, and thus either on Zener's or Heisenberg's theory of ferromagnetism would be most likely to tend towards a parallel orientation.

For qualitative purposes we have listed in Table I the sum of the radii of various $3d$ shells as given by Slater.[13] These "radii" will give an indication of the overlap, assuming the interatomic distance to be about the same for all the alloys to be considered. Going from nickel to the left on the periodic chart one finds that the $3d$ radii of the transition elements get bigger as the nuclear charge decreases since this decrease, as a result of incomplete screening, is not fully compensated by the decrease in $3d$ electrons.

Thus taking the demarcation between positive and negative interaction, on the basis of experiment, to be just below Ni−Mn, one has a ready interpretation from Table I why the interactions listed above should be positive. This listing, of course, has neglected such things as variations in interatomic distance, number of d electrons as mentioned in II, and in Zener's theory, differences in the interaction of conduction electrons with the d shells, all of which are probably important in some cases. It evidently is possible to overlook them among the alloys of Fig. 1.

[13] J. C. Slater, *Introduction to Chemical Physics* (McGraw-Hill Book Company, Inc., New York, 1939), p. 349.

TABLE I. Qualitative estimate of the overlap of $3d$ shells for various pairs of nearest neighbors from the sum of the $3d$ "radii." Those pairs above the line are assumed to tend toward parallel alignment of spins, those below toward antiparallel alignment.

Interaction	Sum of $3d$ radii
Ni−Ni	0.68
Ni−Co	0.70
Co−Co	0.72
Ni−Fe	0.73
Co−Fe	0.75
Ni−Mn	0.76
Fe−Fe	0.78
Co−Mn	0.78
...	...

1. The Case of Parallel Spins

For simplicity only binary alloys will be considered, although for this particular case the result would be the same for any number of components. If f_A and f_B are the atomic fractions of atoms A and B, then the average number of Bohr magnetons per atom is

$$\mu = f_A\mu_A + f_B\mu_B = 10 - f_A n_{dA} - f_B n_{dB}. \quad (2)$$

One can write (2) in terms of the average number of electrons per atom, N, which is given for elements in the iron group by $N = 18 + f_A n_{dA} + f_B n_{dB} + n_e$, where n_e is the average number of conduction electrons per atom. Thus (2) becomes

$$\mu = 28 + n_e - N \quad (3)$$

and

$$d\mu/dN \simeq -1, \quad (4)$$

where it is assumed that the number of conduction electrons remains practically constant, independent of composition for a given alloy system.

According to the sign of the interactions given in III, one would definitely expect points for Ni−Co alloys to fall along a line with slope of minus unity since all three types of interactions involved (Ni−Ni, Co−Co, and Ni−Co) tend toward a parallel alignment. Also copper and zinc with complete d shells, when alloyed with cobalt or nickel, should fall on this curve since in these cases only Ni−Ni or Co−Co interactions are involved and the outer electrons of the copper or zinc would go into the conduction band and into filling up the d shells of the cobalt or nickel.

Other alloys which fit this curve over a limited range of composition will be discussed separately.

2. Antiparallel Spins

When the atomic spins of A are aligned antiparallel to those of B, the expression for the average magnetic moment is not as simple as (3). Assuming the B atoms contribute the greater part to the magnetization, one has

$$\mu = f_B(10 - n_{dB}) - f_A(10 - n_{dA}). \quad (5)$$

We shall fix our attention on the case where n_{dA} is independent of composition in a given alloy system, but we shall not overlook the possibility mentioned previously that, in the solid, some of the electrons of atom A will go into the $3d$ shell of atom B. The average

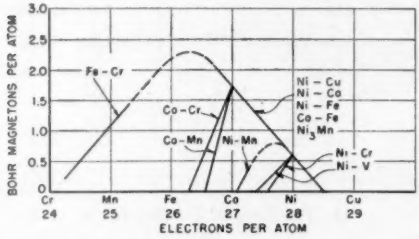

FIG. 2. Calculated atomic moment *versus* electron concentration.

number of electrons in the d shell of atom B can be obtained from

$$n_{dB}=(N-18-n_e-f_An_{dA})/f_B. \quad (6)$$

Since the number of electrons per atom can be written in terms of the atomic numbers as $N=f_BZ_B+f_AZ_A$ and since $f_A+f_B=1$, one can express (5) as

$$\mu=28-Z_B+n_e+[(N-Z_B)/(Z_B-Z_A)] \times[Z_A-Z_B+2(10-n_{dA})]. \quad (7)$$

Again assuming the variation of n_e with composition to be small, one has

$$d\mu/dN\simeq[2(10-n_{dA})/(Z_B-Z_A)]-1, \quad (8)$$

where B is the dominant element.

Thus when the spins of A are antiparallel to those of B, the points for various compositions in a given alloy AB can fall upon a straight line of positive slope, but not necessarily the same line for each alloy system.

As an example, we cite the case of Cr($Z_A=24$) alloyed in Co($Z_B=27$). The Co—Co interaction is positive whereas Co—Cr and Cr—Cr are negative. The measured points in Fig. 1 are in the region where f_{Cr} is small. Thus the Cr—Cr interactions make only a small contribution to the energy and the other two interactions, which predominate, will insure that the cobalt atoms point in the plus direction and the chromium in the minus. Since a free chromium atom has six electrons outside of closed shells, it will very likely exhibit five $3d$ electrons in the solid. Equation (8) gives $d\mu/dN=2.3$ as compared with the observed value of 2.28.

The Co—Mn, Ni—Cr, and Ni—V alloys in Fig. 1 fit this same pattern. The agreement with experiment for the nickel alloys is not as exact, but nevertheless reasonably correct. The calculated curves are shown in Fig. 2.

The results are really not based on the assumption of five electrons in the $3d$ shell of the A atoms (Mn, Cr, V), but rather, only on the assumption of five or less, since for this case of atomic spins oppositely directed, if $n_{dB}\geqslant 5$ and $n_{dA}\leqslant 5$, the average moment by (1a) and (1b) is easily shown to be

$$\mu=18+n_e-[10Z_A/(Z_B-Z_A)] +[N(Z_A-Z_B+10)/(Z_B-Z_A)]. \quad (7a)$$

3. Nickel-Manganese

The Ni—Mn alloys come under a case in which two types of interaction (Ni—Ni and Ni—Mn) are positive, whereas one Mn—Mn is negative. Thus one would expect the following behavior: For a small percentage of manganese the Mn—Mn interactions can be neglected, so to this approximation all spins should be parallel and the points should fall upon the curve with slope minus one. As the manganese composition increases, there are still no Mn—Mn nearest neighbors if the alloy is ordered, such as Ni_3Mn, and consequently, the points should continue to fall on the same line (assuming the number of conduction electrons to be approximately constant). This behavior is qualitatively observed in Fig. 1.

For a disordered alloy with an appreciable percentage of manganese atoms, the Mn—Mn interaction begins to outweigh the weaker Ni—Mn interactions, and one eventually finds the manganese spins start to cancel one another. This behavior becomes clearer in the energy calculations which follow and which indicate that the bending over of the curve as observed in Fig. 1 should occur for a relatively small fraction of manganese. Beyond this point, the magnetic moment is derived principally from the nickel ions and diminishes with increasing manganese content because of the replacement of nickel and to the filling up of the nickel d shell. Assuming the manganese ions to have five electrons in the $3d$ shell, one finds from (6) that the nickel shells become completely filled at about 30 percent manganese. The moment thus goes to zero at this composition in approximate agreement with experiment.

4. Cobalt-Iron and Nickel-Iron

As far as the interactions are concerned, these alloys are of the same type as nickel-manganese. Iron alloys, in the iron-rich region, however, are somewhat of a special case, for the apparent reason as postulated by Zener that the arrangement in the pure metal is an antiparallel one (in agreement with the scheme of Table I) between ions with different magnitudes of spin. Thus for the body centered cubic lattice in the iron rich region one has two types of iron ions as well as the solute ions, a somewhat more difficult case to treat. Since this case is discussed in reference 12, we shall not consider iron base alloys in the region near the pure metal.

In the cobalt-rich or nickel-rich regions the negative Fe—Fe interactions are overpowered by the Fe—Co or Fe—Ni so the magnetization falls on the line with

negative slope, all spins being parallel. At some composition, however, the Fe—Fe interactions should become sufficiently numerous to be predominant and the curves should bend over as the nickel-manganese curve does. In the Ni—Fe alloy a tendency to bend over occurs just before the phase change from f.c.c. to b.c.c. Likewise, the slope of the Co—Fe curve eventually changes sign.[14]

5. Iron-Chromium and Iron-Vanadium

For these alloys all interactions are negative. For appreciable fractions of Cr or V, however, the Cr—Cr or V—V will dominate since they are the largest interactions individually. Thus the Cr or V will largely cancel itself, consistent with the energy calculations in the next section.

The six electrons of the chromium atoms will supply five to the d shell in addition approximately to their correct share for the conduction band, leaving the moment of the iron unchanged. Thus chromium to a first approximation will act only as a diluent, and the magnetic moment of the alloys will approach zero as the fraction as iron approaches zero.

The points for the Fe—V alloys in Fig. 1 are mostly well within the iron-rich region and so will not be discussed here in detail. However, in a qualitative way Fe-V should behave as Fe—Cr, although V with only five electrons will not act as well as a diluent since it would be expected to change the moment of the iron ions somewhat.

6. Energy Considerations

In order to determine whether (a) all spins will align parallel, (b) all A spins antiparallel to B spins, or (c) some intermediate situation, one must determine which arrangement in the particular alloy makes the energy a minimum. It is assumed the dipoles point only to the right or to the left (Ising approximation).

In the Heisenberg theory of ferromagnetism, one would write the average energy per atom as

$$E=\frac{1}{2n}\sum\sum_{i\neq j}\alpha_{ij}S_{di}S_{dj}, \tag{9}$$

for n atoms in the solid with S_{dj} the spin in Bohr magnetons of the ith ion and a_{ij} the exchange interaction between the ith and jth ions. We shall assume the summation to be over nearest neighbors.

In the framework of Zener's theory[12] the energy is

$$E=\frac{1}{2n}\sum\sum_{i\neq j}\alpha_{ij}S_{di}S_{dj}-\frac{1}{n}\sum\beta_jS_{dj}S_e+\frac{\gamma}{2}S_e^2, \tag{10}$$

where S_e is the excess number of positive over negative spins per atom of the conduction electrons, and α_{ij}, β_j, and γ positive coupling constants giving, respectively, the direct exchange coupling between ions, the exchange coupling between ions and conduction electrons, and the coupling between conduction electrons.

In the Appendix I it is shown that (10) can be put into the same form as (9), and the average energy per atom for a random distribution of ions in an alloy of two components A, B is

$$E=-\tfrac{1}{2}\{(2f_{A+}-f_A)^2W_{AA}S_{dA}^2+(2f_{B+}-f_B)^2W_{BB}S_{dB}^2 +2(2f_{A+}-f_A)(2f_{B+}-f_B)W_{AB}|S_{dA}S_{dB}|\}. \tag{11}$$

Here, W is a constant which determines the sign of the interaction, f_A is the atomic fraction of A, and f_{A+} the atomic fraction of positive A spins ($f_{A+}+f_{A-}=f_A$). The W's are given by $W_{AA}=(\beta_A\beta_A/\gamma)-\alpha_{AA}z$, with z the number of nearest neighbors for the particular type lattice. For different atoms the principal change in the expression for W is in α, which depends upon the overlap of nearest neighbor wave functions (see Table I).

For a fixed composition f_A, f_B, one must find what fraction of the atoms A and B must possess positive spins to minimize the energy. By using the average energy (11) one neglects the effect of statistical fluctuations in the environment of the various atoms. Consider the following cases:

(a) W_{AA}, W_{BB}, W_{AB} positive

If W_{AA} and W_{BB} have the same sign, W_{AB} will probably have that sign too. When the sign is positive, it is obvious that $f_{A+}=f_A$ and $f_{B+}=f_B$ for minimum energy, i.e., all the spins are parallel and the average magnetic moment per atom is given by (2).

(b) W_{AA}, W_{BB}, and W_{AB} negative

If $W_{AA}W_{BB}>W_{AB}^2$, then $f_{A+}=\frac{1}{2}f_A$ and $f_{B+}=\frac{1}{2}f_B$ or, in other words, each of the components has a net moment of zero. This classification should contain a group of alloys, but our attention at the present is focused on the other cases which exhibit a net magnetization.

If $W_{AA}W_{BB}<W_{AB}^2$, from Appendix II

$$\mu=|f_BS_{dB}[1-(W_{AB}/W_{AA})]|$$

for

$$|S_{dB}W_{AB}/S_{dA}W_{AA}|\leq f_A/f_B. \tag{12}$$

This equation gives only one end of the curve between A and B but suffices for our purpose. Iron-chromium apparently fits this case in the chromium rich region, if one lets f_A be the fraction of chromium. Since one might expect $|W_{AB}/W_{AA}|\ll 1$ for this case, Eq. (12) shows that the moment should result almost entirely from the iron atoms.

(c) W_{AA} negative and W_{BB} positive

$$\mu=|f_BS_{dB}[1-(W_{AB}/W_{AA})]|$$

for

$$|S_{dB}W_{AB}/S_{dA}W_{AA}|\leq f_A/f_B \tag{13}$$

[14] This does not occur until after the lattice has become b.c.c. and an alternative explanation is given by C. Zener, Phys. Rev. 85, 324 (1951).

and for $|S_{dB}W_{AB}/S_{dA}W_{AA}| \geq f_A/f_B$,

$$\mu = f_B|S_{dB}| + f_A|S_{dA}| \tag{14}$$

if W_{AB} is positive and

$$\mu = |f_B|S_{dB}| - f_A|S_{dA}|| \tag{15}$$

for W_{AB} negative. These results come from Appendix II.

Equation (14) is the same as (2), and (15) the same as (5). The equations confirm the qualitative statements made previously. If A represents the solute atoms, then for small fractions of A the $A-A$ interactions can be neglected, and one has either parallel or antiparallel spins between A and B depending upon the sign of W_{AB}.

For larger fractions of A (13) applies and if $|W_{AB}/W_{AA}| \ll 1$, the magnetization is caused almost entirely by the B ions, i.e., the A cancel. For the Ni–Mn alloys (13) should apply down to a relatively small fraction of manganese since S_{dB}/S_{dA} is small (less than 0.12).

7. Discussion

According to the ideas presented here, it will be observed that there are more metals which derive a spontaneous magnetization from an antiparallel arrangement of unequal spins than from a parallel arrangement of spins. Nickel and cobalt are the prototypes of the parallel spins.

Although the calculations made are generally in good agreement with experiment (compare Fig. 2 with Fig. 1), several corrections could be applied in the interest of exactness. For example, the small contribution of the orbital moment could be subtracted from the measured moment to give the spin-only values. Also in Zener's ferromagnetic theory one must subtract out the small contribution of the conduction electrons. In addition, statistical fluctuations in atomic enviroment could be taken into account.[7] Most of these corrections appear futile, however, since there is an uncertainty in the number of conduction electrons.

The present calculations have been confined to metals of the iron transition group, since these have seemed to be the most puzzling. The intrinsic magnetization of nonmetals such as ferrites has been considered rather extensively by Néel and others.

APPENDIX I

The value of S_c which makes (10) a minimum is $(1/\gamma n)\Sigma\beta_j S_{dj}$, so the last two terms on the right in (10) become $-(1/2\gamma n^2)\Sigma\beta_j S_{dj}\Sigma\beta_i S_{di}$.

Let there be several types of ions in the solid, designated by A, B, C, etc. Each of these can exist at absolute zero with plus or minus spin which we designate by A^+, A^-, B^+, B^-, etc. The sum $(1/n)\Sigma\beta_j S_{dj}$ may be replaced by $\Sigma' f_\alpha \beta_\alpha S_{d\alpha}$, where the prime indicates a summation over all the types A^+, A^-, B^+, B^-, and f_α is the atomic fraction of that type. Likewise, we assume only nearest neighbors to be important in the first summation in (10) and write

$$(1/2n)\Sigma S_{di}\Sigma\alpha_{ij}S_{dj} = \tfrac{1}{2}\Sigma' f_a S_{da}\Sigma' \bar{n}_{ab}\alpha_{ab}S_{db}, \tag{16}$$

where $\bar{n}_{ab}$ is the average number of nearest neighbors an atom of type a has of type b. Thus the energy becomes

$$\begin{aligned} E &= \tfrac{1}{2}\Sigma'\Sigma'(f_a\bar{n}_{ab}\alpha_{ab} - \gamma^{-1}f_a f_b\beta_a\beta_b)S_{da}S_{db} \\ &= -\tfrac{1}{2}\Sigma'\Sigma'\xi_{ab}S_{da}S_{db}. \end{aligned} \tag{17}$$

For qualitative purposes we consider a distribution for which $\bar{n}_{ab} = f_b z$ with z being the number of nearest neighbors. Thus $\xi_{ab} = f_a f_b W_{ab}$, where $W_{ab} = (\beta_a\beta_b/\gamma) - \alpha_{ab}z$ and is independent of the sign on the spins.

In a binary alloy with components A, B there will be four types of spins in (17) to sum over, i.e., S_{dA}, $-S_{dA}$, S_{dB}, $-S_{dB}$. Therefore,

$$\begin{aligned} E = -\tfrac{1}{2}\{&(f_{A+}-f_{A-})^2 S_{dA}{}^2 W_{AA} + (f_{B+}-f_{B-})^2 S_{dB}{}^2 W_{BB} \\ &+ 2(f_{A+}-f_{A-})(f_{B+}-f_{B-})|S_{dB}S_{dA}|W_{AB}\}. \end{aligned} \tag{18}$$

Making use of $f_{A+}+f_{A-}=f_A$ and $f_{B+}+f_{B-}=f_B$, one obtains (11).

APPENDIX II

One can transform (11) to the following form

$$\epsilon = Y^2 + CX^2, \tag{19}$$

where

$$\epsilon = \frac{-2E}{f_A{}^2 S_{dA}{}^2 W_{AA}}, \quad C = \frac{f_B{}^2 S_{dB}{}^2}{f_A{}^2 S_{dA}{}^2}\left(\frac{W_{BB}}{W_{AA}} - \frac{W_{AB}{}^2}{W_{AA}{}^2}\right),$$

$$Y = Y' + \frac{f_B|S_{dB}|}{f_A|S_{dA}|}\frac{W_{AB}}{W_{AA}}X, \quad X = \frac{2f_{B+}}{f_B} - 1, \quad Y' = \frac{2f_{A+}}{f_A} - 1,$$

and $1 \geq X \geq -1$, $1 \geq Y' \geq -1$. We shall always consider W_{AA} to be negative so ϵ must be a minimum.

It is immediately apparent that for C positive ϵ is a minimum when $X = Y = 0$,i .e., $f_{A+} = \frac{1}{2}f_A$ and $f_{B+} = \frac{1}{2}f_B$. This includes the case where all three interactions are negative and $W_{AA}W_{BB} > W_{AB}{}^2$.

The constant C can be negative if W_{BB} is positive and W_{AA} negative, or if both W_{AA} and W_{BB} are negative and the additional condition $W_{AA}W_{BB} < W_{AB}{}^2$ applies. It is obvious that for $|(f_B S_{dB}/f_A S_{dA})(W_{AB}/W_{AA})| \leq 1$, ϵ is minimum when $Y = 0$, and $X^2 = 1$. The average magnetic moment is $|f_A Y'|S_{dA}| + f_B X|S_{dB}||$ so

$$\mu = |f_B S_{dB}[1 - (W_{AB}/W_{AA})]|. \tag{20}$$

If for a given value of X, $|(f_B S_{dB}W_{AB}/f_A S_{dA}W_{AA})X| > 1$, then Y will wish to be as small as possible, having the magnitude $|(f_B S_{dB}W_{AB}/f_A S_{dA}W_{AA})X| - 1$. (For positive X, $Y' = 1$ if W_{AB} is positive and -1 if W_{AB} is negative.) Putting this magnitude into (19) and solving for the minimum ϵ, one finds that for the case W_{BB} positive and W_{AA} negative $|X| = 1$.

These results are collected in Eqs. (12) to (15).

Neutron Transmission Cross Sections in the Kilovolt Region

CARL T. HIBDON, ALEXANDER LANGSDORF, JR., AND ROBERT E. HOLLAND
Argonne National Laboratory, Chicago, Illinois

(Received November 12, 1951)

Neutron transmission cross sections have been measured with about 2 kev resolution in the energy range from 2 kev to 25 kev, and to higher energies in some case. The neutrons, produced by the $Li^7(p,n)Be^7$ reaction with a van de Graaff generator, were detected by a highly efficient (~15 percent) bank of boron trifluoride filled proportional counters placed to detect neutrons emitted at an angle of 120° from the proton beam direction. Measurements at the lower energies were made possible by a collimator and shield around the counters, which reduced background, and by the high efficiency obtained by many counters embedded in an array in a paraffin moderator. Resonances were observed in Na, Ti, V, Mn, Fe, Co, and Ni.

INTRODUCTION

HITHERTO, a gap has existed in the data on neutron cross sections between the lowest energies that could be satisfactorily measured with the electrostatic generator (about 15 kev) and the highest energies for which velocity spectrometers have adequate resolution (about 3 kev). Several groups[1–4] have been developing methods of increasing the upper energy limit of time of flight spectrometers and undoubtedly in the near future improved resolution will be obtained.

The lower energy limit to the electrostatic generator technique as developed by Barschall *et al.*[5] has been determined by the rapid fall in neutron yield of very low energy neutrons and the large background counting rate (for the $Li^7(p,n)Be^7$ reaction; no other reaction has been used so successfully, as yet, for this low energy neutron work). In this work to be reported, a new detection scheme has been employed in which a massive shield reduces the background counting rate and the large group of boron trifluoride proportional counters embedded in paraffin increases the counting efficiency to overcome the decline in yield of low energy neutrons. This equipment has been briefly described[6] and will be more fully described in a later publication elsewhere. Figure 1 shows the essence of the device.

PROCEDURE

The collimator and shield, Fig. 1, was set up with its axis at 119.6° to the proton beam direction, as determined by triangulation with a transit. Transmission samples were placed immediately in front of the collimator hole entrance. No corrections for scattering-in by the transmission sample are necessary in this arrangement. Monitoring of the neutron flux was achieved by a standard boron trifluoride "long counter"[7] placed in the neutron flux along a line extended from the proton beam direction. Presence or absence of a transmission sample does not appreciably disturb this monitor since scattering by the face of the shield is already complete and the sample scarcely perturbs the scattering equilibrium. Measurements were made with and without the transmission samples and with and without a paraffin plug 2 inches in diameter by 5½ inches long placed at the scattering sample position inside the counter assembly in the collimated beam. Measurements without the paraffin plug are the background measurements. This technique of background measurement differs from the prior method involving use of a paraffin cone[8,9] and is probably more reliable and less likely to be disturbed by systematic errors. The paraffin plug when in position was located at a point at which the counting rate was a maximum (except in some of the earlier exploratory data.)

The lithium targets were evaporated onto the tantalum end cap of the rotating target, and the thickness was controlled by observing the neutron yield during evaporation and then measured by the rise curve, as described by Taschek.[9] A typical rise curve is shown at the left side of Fig. 2. The rise curve was usually re-run before and after each day's work and a new target prepared if the old one was found to be too thick. Proton energies were measured relative to the $Li(p,n)$ threshold

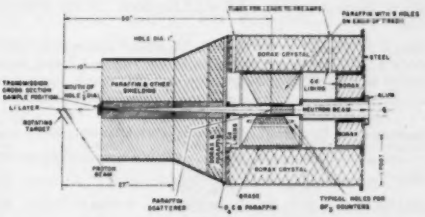

FIG. 1. Collimator and shield with neutron counter assembly inside the shield. In this work the collimator was placed at 119.6° to the proton beam direction. The solid angle subtended by the collimator at the neutron source is 0.001 steradian.

[1] Nuclear Sci. Abst. **5**, 636 (1951) (refers to CUD-65, Sec. 1; DR-1578).
[2] W. Selove, Phys. Rev. **76**, 187 (1949).
[3] Hibdon, Muehlhause, Selove, and Woolf, Phys. Rev. **77**, 730 (1950).
[4] A. W. Merrison and E. R. Wiblin, Nature **167**, 346 (1951).
[5] Barschall, Bockelman, and Seagondollar, Phys. Rev. **73**, 659 (1948).
[6] A. Langsdorf, Jr., Phys. Rev. **80**, 132 (1950).
[7] A. O. Hanson and J. L. McKibben, Phys. Rev. **72**, 673 (1947).
[8] J. M. Blair and J. R. Wallace, Phys. Rev. **79**, 28 (1950).
[9] R. F. Taschek and A. Hemmendinger, Phys. Rev. **74**, 373 (1948).

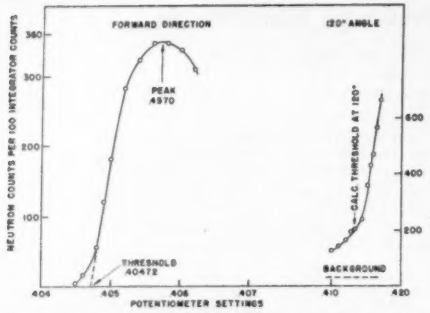

FIG. 2. At left: typical target thickness and threshold determination data. At right: neutron counting rate at 120° to proton beam using collimator-detector, in the region from just below to just above the threshold for appearance of neutrons at this angle. The point marked "threshold at 120°" is calculated from the threshold point determined by the graph at the left. The tail of the counting rate curve below threshold at 120° was higher here than it should have been because a small air blower accidentally was in the flux of neutrons at 60° to the proton beam and in the line of sight of the collimator so neutrons were back-scattered into the detector.

at 1.882-Mev and neutron energies calculated as described by Hanson *et al.*[10] Neutron counting rates near the 120° threshold are shown at the right side of Fig. 2. A typical measurement and calculation is shown in Table I.

ENERGY RESOLUTION

The best measure of the over-all energy resolution is attained by observation of the measured widths of the sharpest observed resonances, which are about 1.5 to 2-kev full width at half-maximum. Part of the energy spread is due to the finite angular spread of neutrons accepted by the detector, namely, $\pm 1°$ from the mean angle of 119.6°. This introduces[10] a spread of about ± 500 ev which is a small error compared to the over-all resolution observed.

Three remaining sources of energy spread are those which relate to the actual energy of a proton at the instant when it reacts with a Li nucleus. In the energy region of interest in this work, the spread in energy of protons at the instant of reaction is about double the spread in energy of neutrons emitted near 120°; the exact relation depends upon the energy itself.[10] The three sources of energy spread referred to are: target thickness, spread in proton energy within the ion beam, and fluctuations in this energy due to imperfect constancy of the generator voltage. Since the Li targets have a known thickness of about 2-kev stopping power, one may conclude that the latter two sources of fluctuation correspond to not over 2.5 to 3.5 kev, which is the best available measure of the true energy resolution of the proton beam in this electrostatic generator.

SOURCES OF ERROR

In addition to the usual random statistical errors, two known sources of systematic error should be mentioned. One of these is a defect in the energy control system of this electrostatic generator, which is observable as a shift in the electrostatic analyzer voltage setting for the Li(p,n) reaction threshold when the focus of the proton beam is modified. It is believed that the shift, which has a maximum observed value of about 2 kev at the Li(p,n) threshold of 1.882 Mev, is a result of the design of the electrostatic analyzer. This analyzer focuses a parallel incident beam at the pick-up electrodes for the emergent beam. Hence, if the direction of the incident beam is changed, the position of the focused emergent beam is changed for constant analyzer deflection voltage. Presumably changes in beam focusing change the effective direction of the incident beam. Knowing of this effect, an effort was made to keep the focusing conditions constant during each series of measurements. It is believed that the actual errors in resonance positions observed in the data were much less than 2 kev.

The other known source of systematic error chiefly perturbs transmission measurements and hence causes errors in transmission cross sections so determined, without, however, causing a large systematic shift in the energy at which a resonance is found. This source of error was observed during some work just subsequent

TABLE I. Typical data. Neutron threshold observed at potentiometer setting 0.40420 v. Potentiometer setting for these data 0.41574 v. Lithium target thickness by rise curve, 1.4 kev. Peak neutron energy at 119.6° calculated 2 kev; mean energy 1.7 kev. Time for each 40,000 monitor counts about 320 seconds. Beam current approximately 10μa.

Transmission sample	Detector scatterer	Monitor counts	Detector counts	Reduced[a] detector counts	Net counts, I	I_0/I	Atoms/cm^2 $\times 10^{-24}$	σ_t calc. barns
None	In	40,003	2897	2897	$2595(I_0)$			
	Out	40,360	305	302	...	...	...	...
Na	In	39,670	2483	2504	2212	1.173	0.0165	9.5±2
	Out	39,968	292	292				
Mn	In	40,984	1301	1270	978	2.65	0.0510	19±1
	Out	...	...	292[b]				

[a] Corrected to 40,000 monitor counts.
[b] Background assumed same as measured for Na, error in this assumption is negligible.

[10] Hanson, Taschek, and Williams, Revs. Modern Phys. **21**, 635 (1949).

to the work reported in this article. It has been noticed that the yield of neutrons for a given amount of integrated beam current varies systematically as a function of slight shifts in the position and shape of the proton beam spot on the lithium target. Furthermore, the variation is not the same at different angles of neutron emission, relative to the proton beam direction. Hence, flux monitoring by the long counter at 0° is inaccurate, and monitoring by a beam integrator is also inaccurate. Deviations of yield at 120° might occasionally be as large as 10 percent, by extrapolation from similar data at higher proton energy. No direct information is available to evaluate this source of error properly, in the data reported here. It is clear that, in the future, such errors in this type of measurement can be minimized most surely by using a neutron flux monitor which consists of an auxiliary collimator and counter, oriented at the same angle to the proton-beam direction as the main apparatus. The reasons for this type of error are known to reside in non-uniformity in thickness of the lithium-layer and in variations in the thickness of the layers of oxide and carbon which build up upon the lithium layer during operation. It seems to be very difficult to hold errors, because of these effects, to as low as one percent, even when great care is taken to keep them minimized.

RESULTS

Iron

The iron sample used was "Puron" brand of specially pure iron made by Westinghouse Electric Company.

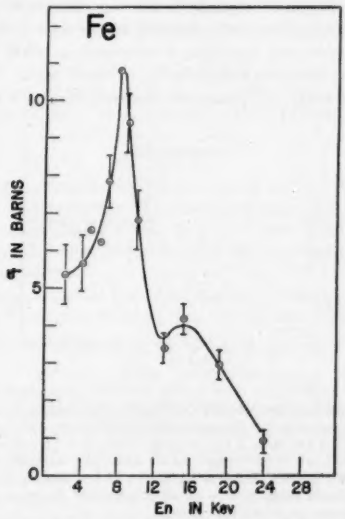

FIG. 3. Transmission cross section of iron. Thickness 0.1613×10^{24} atoms/cm². Li target thickness 2.9 kev.

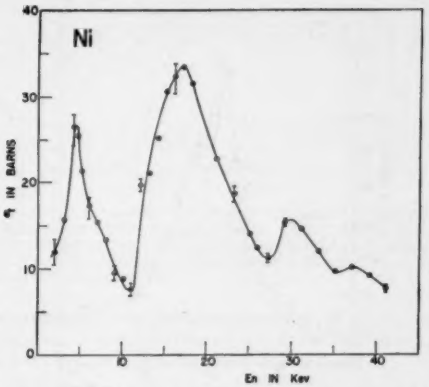

FIG. 4. Transmission cross section of nickel. Thickness 0.0698×10^{24} atoms/cm². Li target thickness: 3.0 kev to 6 kev neutron energy; 3.5 kev, 7 to 24 kev neutron energy; 2.4 kev, 26 to 41 kev neutron energy. Probable errors of all points similar to those of nearby points for which it is shown.

Spectrographic analysis showed no impurity sufficient to interfere in these measurements. Figure 3 presents the results. The resonance observed at 8.5 kev was expected to be present, as prior unpublished resonance overlap data obtained by the annular chamber technique using a pile beam and a vanadium detector had shown overlapping resonances. The resonance overlap method has been described by Hibdon and Muehlhause.[11] The results on V presented in Fig. 6 confirm the overlap of resonances at about 8 kev. There may be a weak resonance in Fe at 16 kev but the data are insufficient to establish it. The 8.5-kev resonance is certainly in one of the iron isotopes of minor abundance.

Nickel

The nickel sample contained somewhat under one percent cobalt impurity, and less of other known impurities. Resonance peaks are evident in the data (Fig. 4) at 4.5 and 17 kev and possibly a weaker resonance at 30 kev. The 17-kev resonance is undoubtedly the one reported by Barschall *et al.*[5] at 15 kev. The lower resonance may be the one observed in the 4-kev region by the Columbia University group.[12] At this laboratory, strong resonance overlapping has been observed between nickel and sodium and also nickel and vanadium (not published). One may conclude that the nickel 4.5-kev resonance shows some overlapping with the 2.8-kev resonance in Na and the 7-kev resonance in V.

[11] C. T. Hibdon and C. O. Muelhause, Phys. Rev. **76**, 100 (1949); C. T. Hibdon, Phys. Rev. **79**, 747 (1950).
[12] W. W. Havens, Jr., and L. J. Rainwater, Phys. Rev. **75**, 1296 (1949).

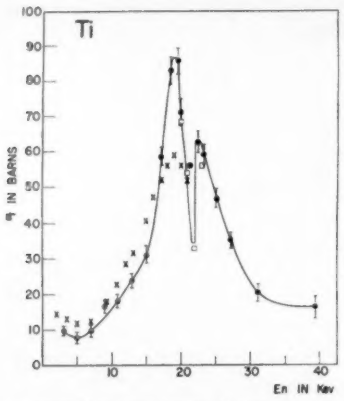

FIG. 5. Transmission cross section of titanium. Open circles: titanium thickness 0.1037×10^{24} atoms/cm², lithium target 3.7 kev. Solid circles titanium thickness 0.011×10^{24} atoms/cm², lithium target thickness 3.7 kev. Crosses: titanium sample 0.0343×10^{24} atoms/cm², lithium target thickness 3.1 kev. Squares: titanium sample 0.011×10^{24} atoms/cm², lithium thickness 3.1 kev. Probable errors of all points about the same as for those indicated.

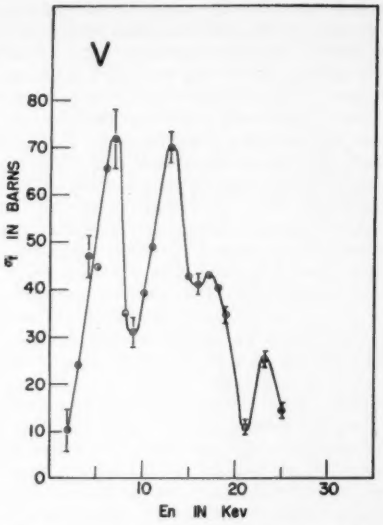

FIG. 6. Transmission cross section of vanadium. Thickness 0.0228×10^{24} atoms/cm², lithium target thickness 1.6 kev to 11-kev neutron energy, 2.6 kev above.

Titanium

Figure 5 presents the results for several separate runs on this element. Resonances are indicated at 19 and 23 kev with a narrow minimum near 22 kev which was best resolved with a thin sample. The largest known impurity in the titanium is 0.1 percent of manganese. The fall in cross section from 2 to 6 kev suggests there may be a resonance below 2 kev. Results from annular chamber measurements, using a vanadium detector, indicated resonance overlapping with titanium, which, comparing Fig. 5 and 6, may be due to overlap of the 17-kev resonance in V with the 19-kev resonance in Ti.

Cobalt

In Fig. 7 results of three runs on cobalt are presented. Resonances are indicted at 5.5 and 29.5 kev and a poorly resolved resonance at 8 kev is probably present. Insufficient data were obtained to determine higher energy resonances which may lie in the vicinity of 53, 78, and 88 kev. The cobalt samples contained major impurities of Cr 0.5 percent, Fe 1 percent, Ni 0.5 percent. Prior unpublished resonance overlap observations with Na and V detectors are explained by the overlap of the 5.5-kev Co resonance with the 2.8-kev Na resonance (Fig. 8) and the 7-kev V resonance (Fig. 6). Data obtained with time of flight spectrometers at Columbia University[1] and Argonne National Laboratory (unpublished) had indicated a resonance in the 3 to 10 kev region which is undoubtedly the doublet observed here at 5.5 and 8 kev.

Vanadium

The resonance overlapping of vanadium and cobalt which had been observed previously led us to measure both V and Co by this new technique. The results for V are shown in Fig. 6. Strong resonances are apparent at 7 kev and 13 kev, and a partially resolved resonance at 17 kev. There is probably a smaller resonance near 23 kev. The major impurity in the vanadium sample is 0.5 percent carbon. Data obtained with a time-of-flight spectrometer had indicated a resonance at 3300 ev[13] which has been recalculated to lie at about 6 kev. This is undoubtedly the resonance observed here at 7 kev.

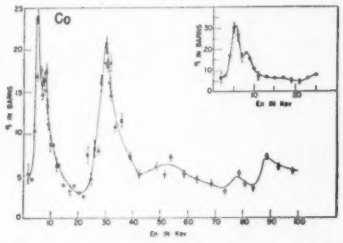

FIG. 7. Transmission cross section of cobalt. Large graph, open circles: cobalt thickness 0.0822×10^{24} atoms/cm², lithium thickness 4.4 kev. Crosses: cobalt thickness 0.0419×10^{24} atoms/cm²; lithium thickness 1.4 kev to 17.5 kev neutron energy and 4.6 above kev. Inset graph at upper right: cobalt thickness $\sim0.02097\times10^{24}$ atoms/cm²; lithium thickness 1.6 kev to 11 kev neutron energy, 2.6 kev above. Probable error of all points about the same as for nearby points for which it is shown.

[13] S. P. Harris, Phys. Rev. **83**, 235 (1951).

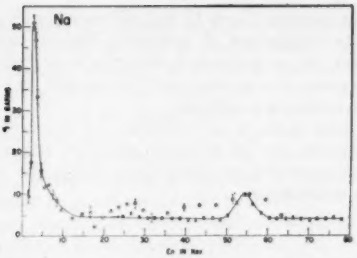

FIG. 8. Transmission cross section of sodium. Circles: sodium thickness 0.0165×10^{24} atoms/cm², lithium target thickness 1.4 kev to 17.5 kev neutron energy, 4.6 kev above. Crosses: sodium thickness 0.0666×10^{24} atoms/cm², lithium thickness 7.1 kev. Probable error of all circled points similar to those for which indicated, for crosses about the size of the cross.

Sodium

The existence of a resonance in sodium was first discovered[9,11] by the unexpected resonance overlap effect found with a manganese detector using the annular scattering chamber. The fact that this overlap was related to resonances near 3 kev was determined by measurements made with a neutron time-of-flight spectrometer. The present work confirms this earlier work, and has better resolution, especially on the high energy side of the resonances. The sodium data are shown in Fig. 8. The first sodium sample used to obtain clearer results near 2.8 kev was too thin at higher energies. Better data above 25 kev were later obtained using a thicker sample. Another resonance occurs at 55 kev; it is undoubtedly the same one observed by Adair *et al.*[14] at 60 kev.

The sodium used was ordinary commercial metal sealed in a cylinder with one-mil thick steel diaphragm covers on the ends. It was not analyzed chemically.

Manganese

The results for manganese are shown in Fig. 9. In addition to the resonance mentioned above, at 2.8 kev, others are clearly shown at 8, 23, and 38 kev. Less pronounced ones probably occur in the vicinity of 60, 67, and 78 kev.

The manganese contained about 1 percent iron; all other impurities were less than 0.01 percent by spectrographic analysis.

CORRELATION OF THE RESULTS

Some of the data discussed above were obtained by grouped measurements on several elements in sequence while holding the energy setting of the electrostatic generator fixed. Also, several elements were measured on more than one run. Thus a check upon consistency of the data is obtained which indicates that the sources

[14] Adair, Barschall, Bockelman, and Sala, Phys. Rev. **75**, 1124 (1949).

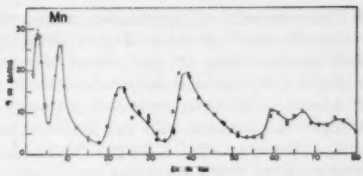

FIG. 9. Transmission cross section of manganese. Manganese thickness 0.051×10^{24} atoms/cm². Open circles: lithium target thickness 1.4 kev; solid circles: lithium thickness 4.6 kev; crosses: lithium thickness 7.1 kev. Probable errors of all points about the same as for those indicated.

of systematic error previously discussed did not in fact cause errors as large as they might have. The following are the groups of data obtained simultaneously:

Group I. Na data, all points shown as circles; Mn data, all points shown as open and solid circles; Co data, all points shown as crosses.

Group II. All data on V; all Co data in inset graph at upper right of Fig. 6.

Group III. Na data, points shown as crosses; Mn data, points shown as crosses.

DISCUSSION

The most important feature of the work reported is the presentation of a method for extending the electrostatic generator techniques downward to neutron energies of 2 kev or even lower. The new method of detecting neutrons with a highly efficient shielded detector is responsible for this extension in range. It is a fortunate feature of the technique of measurement at "back-angles" (e.g., at 120° to the proton beam direction as here employed) that the neutron energy resolution is about twice the resolution in energy of the proton beam and lithium target thickness. This circumstance leads us to believe that with the use of a new 40-inch radius electrostatic analyzer, now under construction, similar to the one at the University of Wisconsin,[15] sufficient resolution will be attained to permit measurements with about 1-kev resolution down to as low as 1-kev neutron energy before difficulties become insuperable.

It will also be possible to apply resonance self-detection and resonance overlap techniques to neutron cross section measurements with this equipment. If a scattering sample made of some element under investigation is placed inside the paraffin and counter tube assembly instead of the paraffin plug used in the measurements reported here, additional data concerning resonance widths and peak cross sections can be obtained by transmission measurements. This technique will permit determination of resonance properties with resolution better than that allowed by the actual spread of energies in the neutron beam.

It may also be pointed out that this equipment

[15] Warren, Powell, and Herb, Rev. Sci. Instr. **18**, 559 (1947).

permits measurements of transmission cross sections with relatively small samples of rare elements or separated isotopes. Since the spot source of neutrons can be held to a region about $\frac{1}{16}$-inch diameter and the angular spread of the detector is only 2°, many materials might be measured with fair accuracy in the region of a resonance with a sample (about $\frac{5}{16}$-inch diameter) weighing about one gram.

The closing of the gap in knowledge of neutron cross sections between 2 and 15 kev will now permit more accurate calculations of interesting thermal neutron properties of many elements, including such properties as the phase of scattering and the coherent and incoherent scattering amplitudes.

We wish to thank J. R. Wallace for extensive help in operating the electrostatic generator and aid in measurements and trouble-shooting during the course of the experiments.

PHYSICAL REVIEW VOLUME 85, NUMBER 4 FEBRUARY 15, 1952

Fission Neutron Spectrum of U^{235}*

NORRIS NERESON
University of California, Los Alamos Scientific Laboratory, Los Alamos, New Mexico
(Received November 12, 1951)

The energy distribution of neutrons (prompt and delayed) arising from thermal fission of U^{235} has been studied with nuclear plates. The spectrum obtained shows a maximum in the region of 0.7–0.8 Mev and an exponential slope of 3.9±0.2 Mev per decade of intensity in the energy region above 2 Mev. The data extend over the energy range from 0.4 to 7 Mev.

I. INTRODUCTION

A NUCLEAR plate measurement of the spectrum of neutrons from the fission of U^{235} was first made by Richards[1] using Ilford half-tone plates. These measurements agreed with the original ionization chamber measurements of Staub and Nicodemus[2] above an energy of 1.8 Mev but at lower energies uncertainty existed as to the shape of the spectrum curve. The ionization chamber data showed a maximum height around 1 Mev and indicated more low energy neutrons than the plate data which gave a broad maximum centering in the vicinity of 1.8 Mev. In the light of present knowledge, this discrepancy was most likely caused by the unreliability of the half-tone emulsions for tracks corresponding to energies less than 1.5 Mev. A measurement by Hill[3] using a coincidence-anticoincidence counter arrangement (the Argonne "ranger") gave an energy distribution with a maximum around 0.8 Mev and an exponential shape in the 2–7 Mev region.

The present experiment (performed in 1948–1949) was planned to furnish additional data concerning the uncertain region of the spectrum in the vicinity of the maximum as well as to contribute more information over the energy region from 0.5 to 6 Mev. The experiment was improved over Richards' preliminary work by (1) using the newer Ilford C2 plates which are reliable down to an energy of 0.5 Mev and (2) measuring more tracks so as to improve the statistics. Other contemporary experiments on the fission spectrum have provided detailed data over certain limited energy regions of the spectrum, *viz.*, Bonner's[4] cloud-chamber work covering the low energy region from 0.075 to 0.6 Mev and Watt's[5] coincidence counter arrangement emphasizing the high energy region from 3 to 16 Mev.

II. EXPERIMENTAL ARRANGEMENT

The experimental arrangement is illustrated in Fig. 1. A 10-mil thickness of U_3O_8 was coated on a $\frac{1}{32}$-inch thick aluminum strip measuring 1×4 inches. The thermal column of the Los Alamos water boiler was arranged to provide a thermal neutron beam of cross section 4×4 inches. The uranium foil was placed approximately perpendicular to this beam with the aluminum side facing the beam. Ilford type C2 nuclear plates, 100 microns thick, were placed outside of the

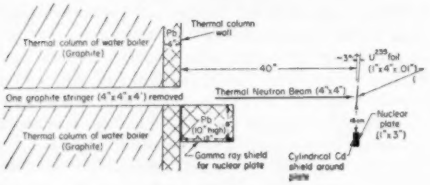

FIG. 1. Experimental arrangement.

* This work was performed under the auspices of the AEC.
[1] H. Richards, private communications (1944–1945).
[2] H. Staub and D. Nicodemus, private communication (1944). (To be published.)
[3] D. Hill, private communication (1947).
[4] T. Bonner, private communication (1948).
[5] B. Watt, private communication (1948). Using the results of the previous two references and those of his own experiment, Watt has obtained a semi-empirical formula which fits the U^{235} fission spectrum over the energy region from 0.075 to 16 Mev. (In process of publication.)

neutron beam at a distance of 16 cm from the nearest edge of the foil. In order to prevent fission neutrons from traveling through the aluminum backing of the foil, the foil was slightly tilted so that it made an angle of about 3° with the center line of the nuclear plates. A cylindrical cadmium enclosure, $\frac{1}{32}$-inch thick, was placed around the plates in order to shield them from thermal neutrons present in the room. This precaution was taken to guard against the possibility of thermal neutrons entering the emulsion and producing 0.6-Mev protons by means of the $N^{14}(n,p)C^{14}$ reaction.

Both the plates and the U^{235} foil were 40 inches from the wall of the thermal column and 52 inches above the floor. The above dimensions were made large compared to the distance of the plates from the foil; this insured a minimum degradation of the neutron spectrum by back-scattering of fission neutrons from the wall and floor into the plates. The thermal neutrons emerging from the water boiler had a cadmium ratio of about 500 and, at a power of 5.5 kilowatts, the flux at the position of the foil was 6×10^5 neutrons per cm^2 per sec. This flux produced a source of approximately 4×10^7 neutrons per sec coming from the U^{235} foil. A 15-hour run at a power of 5.5 kilowatts gave an appropriate proton recoil track density on the nuclear plates.

In order to increase the shielding of the plates against gamma-rays, a lead shield $8\times12\times10$ inches was erected at one side of the thermal port so it was positioned between the plates and the thermal column wall. This shield primarily acted to screen the plate from gamma-rays coming from the vicinity of the open port of the thermal column. Subsequent experiments showed that this shield aided in reducing plate fogging but was not essential in obtaining readable plates.

A background experiment was performed by removing the U^{235} foil and substituting a piece of aluminum which was identical to that on which the uranium was coated. A similar irradiation was given with a nuclear plate in place.

III. NUCLEAR PLATE ANALYSIS

The nuclear plates were analyzed by the method of measuring proton recoils about a small angle of the forward neutron direction. This technique has been discussed previously[6,7] and only the necessary facts relating to the method for this particular experiment will be presented here.

The area analyzed on the 1×3-inch plates was restricted to an area $\frac{3}{4}$ inch wide$\times1$ inch long located at the end of the plate nearest to the foil. The proton recoils measured in the processed emulsion were those which made less than a 10° angle with the center line of the nuclear plate. The above criteria were simplified in practice to the following procedure: from any point in the processed emulsion, all recoils contained within the emulsion surfaces were measured which lay within a rectangular pyramid having half-angles of 10° in the horizontal and vertical planes. Since these angular criteria were applied to the processed emulsion and since the emulsion thickness shrinks vertically by a factor 2.5 upon processing, acceptable proton recoils in the unprocessed emulsion lay within a rectangular pyramid of half-angle 10° in the horizontal plane and half-angle 25° in the vertical plane. In an analysis, the above angular limits represent average values since the actual limits fluctuate about the chosen values on account of (1) microscopist error in the determination of the dip angle,[7] and (2) the fact that the forward neutron direction is not always parallel to the center line of the plate. In the present geometry, the maximum angles which a fission neutron entering the analysis area could make with the plate center line were 3.4° in the horizontal plane and 4.5° in the vertical plane. However, the average entrance angles were 1.2° and 1.6° in the horizontal and vertical planes, respectively; these angles are quite small compared to the average track angular limits of 10° and 25° in the unprocessed emulsion.

The energy resolution resulting from these angular critieria is 12 percent at 0.5 Mev and 6 percent at 2 Mev.[7] Energy resolution is defined as the energy half-width of the proton recoil distribution obtained from neutrons of energy E_n divided by E_n. Thus a neutron peak possessing a half-width (at half-maximum) of 60 kev could be resolved at 0.5 Mev and 120 kev at 2 Mev. This is ample resolution for the spectral curve obtained in the present experiment.

The track data were accumulated by taking successive swaths in the analysis area along the 3-inch dimension of the plate; these swaths were 1 inch long and about 0.2 mm apart. Consecutive fields were examined along each swath; using this method, every acceptable track originating in a swath would be measured. This horizontal projection of each track was measured to an accuracy of ±1 microscope scale division$\cong\pm1$ micron. The track data was tabulated in microscope scale division intervals corresponding to proton recoil energy intervals of approximately 0.1 Mev. After observing the curve shape, the 0.1-Mev intervals were kept if the curve necessitated this resolution, but if not, the data were grouped into larger intervals (about 0.5 Mev) and averaged. The procedure of first grouping the tracks into scale division intervals and then converting to proton energy seemed to be the most accurate method of treating the data. In the method of first sorting the tracks into even energy intervals, the scale division corresponding to the energy interval end points usually come out in fractions of a division; since the track lengths are only measured to ±1 division, the question often arises as to the proper energy interval for a measured track length. This uncertainty does not occur with the present method.

In order to obtain the true number of proton recoil tracks, the number of measured tracks must be cor-

[6] H. Richards, Phys. Rev. **59**, 796 (1941).
[7] N. Nereson and F. Reines, Rev. Sci. Instr. **21**, 534 (1950).

rected for those tracks leaving the emulsion surfaces. Since 100-micron thick emulsions[8] were used in the experiment, the usual method of analyzing the entire emulsion thickness was slightly modified so as to reduce the percentage of long tracks leaving the emulsion surfaces. The method consisted of analyzing a restricted central portion of emulsion thickness t and ignoring a small thickness t_s adjacent to each emulsion surface. In the present case, the processed emulsion thickness measured 35 microns and the values of t and t_s chosen were 25 and 5 microns, respectively. The probability of a track leaving the emulsion surface from a particular point in the thickness t is A_0/A_T where A_T is the total area traced out by the end of the track as it moves within its prescribed angular limits and A_0 is the area formed by the end of the track moving outside of the emulsion surfaces. The average probability P of a track leaving the emulsion surfaces from any point in the thickness t is

$$P=\int_0^{t/2} A_0/A_T dt.$$

This derivation assumes that the proton recoil tracks were uniformly distributed within the angular limits about the forward neutron direction. This assumption results in only a 3 percent error in the correction if the average angle of the proton recoils is 15° in the unprocessed emulsion.

The above integral was evaluated graphically by summing A_0/A_T over six points in the thickness t. A column in Table I shows the correction factor $C=1/(1-P)$ by which the number of measured tracks are to be multiplied to obtain the actual number of tracks.

The number of corrected proton recoil tracks is proportional to the collision cross section of hydrogen σ_p and to the neutron flux $N(E)$. The neutron spectrum or $N(E)$ can then be obtained after correcting the measured tracks for recoils leaving the emulsion surface and for $\sigma_p(E)$.[9] Since it is desirable to plot the spectral curve in terms of neutron energy E rather than proton recoil energy E_p, it is necessary to convert the track data from E_p to E. This conversion can be obtained by either calculating the energy correction of $\theta^2/2$[10] or by using experimental values.[7] In either case the correction is approximately 6 percent or $E=1.06E_p$. Table I shows the values of E_p and E.

IV. RESULTS

The data obtained from the experiment are tabulated in Table I. The column listing microscope scale divisions per 0.1 Mev was obtained from a smoothed curve of the above quantity plotted *vs* E_p; the points for this curve were calculated from range-energy values.[11] The data represent a measurement of about 4700 proton recoil tracks and were obtained by two microscopists working independently. The separate results of the two microscopists showed good agreement. The lowest energy point at 0.39 Mev is uncertain by more than

TABLE I. Data and calculations on fission neutron spectrum of U^{235}.

Microscope scale division interval[a]	Number of measured tracks	Scale divisions per 0.1 Mev	Proton recoil energy $=E_p$[b]	Correction factor $=C$	Neutron energy $=E$	$\sigma_p(E)$ (barns)	Neutron flux $=N(E)\propto N_C(E)^c/\sigma_p\times10^{24}$
3– 4	263	1.33	0.37 Mev	1.00	0.39 Mev	7.15	58.6 ±3.6[d]
4– 5	221	1.40	0.45	1.00	0.48	6.25	49.5 ±3.3
5– 6	228	1.46	0.53	1.00	0.56	5.85	57.0 ±3.8
6– 8	432	1.53	0.64	1.00	0.68	5.35	61.8 ±3.0
8– 10	377	1.65	0.76	1.00	0.80	4.90	63.5 ±3.3
10– 14	523	1.85	0.94	1.00	0.98	4.45	54.4 ±2.4
14– 18	446	2.00	1.13	1.00	1.20	4.00	55.7 ±2.6
18– 24	471	2.22	1.36	1.00	1.44	3.60	48.5 ±2.2
24– 32	437	2.47	1.65	1.00	1.75	3.20	42.2 ±2.0
32– 46	521	2.80	2.06	1.02	2.18	2.80	37.9 ±1.7
46– 62	348	3.18	2.56	1.06	2.71	2.45	30.0 ±1.6
62– 82	173	3.68	3.06	1.12	3.24	2.18	16.3 ±1.3
82–105	106	4.10	3.57	1.20	3.78	1.98	11.5 ±1.1
105–130	79	4.45	4.14	1.34	4.39	1.78	10.6 ±1.2
130–155	33	4.83	4.68	1.54	4.95	1.63	6.0 ±1.1
155–180	29	5.20	5.17	1.79	5.48	1.52	7.1 ±1.3
180–210	18	5.60	5.69	2.09	6.03	1.42	4.9 ±1.2
210–240	7	6.00	6.17	2.40	6.55	1.33	2.5 ±0.9
240–270	1	6.30	6.63	2.72	7.02	1.28	0.45±0.5

[a] Microscope scale calibration: 1 scale division = 1.06 micron.
[b] Since the horizontal projections of the tracks were measured, a 3-percent correction was added to the midpoint of the microscope scale division interval to obtain the average true track length; this length was used to determine E_p.
[c] $N_C(E)$ = Number of corrected tracks per 0.1 Mev = number of measured tracks per scale division × number of scale divisions per 0.1 Mev × C.
[d] This result at E = 0.39 Mev has been increased by 20 percent to adjust for emulsion inefficiency at low energies (see reference 7).

[8] The actual measured thickness of the unprocessed emulsions ranged from 85 to 90 microns. Emulsions of 200-micron thickness would have been more appropriate for this experiment but, at the time, none were available.
[9] The values of $\sigma_p(E)$ were obtained from Goldsmith, Ibser, and Feld, Revs. Modern Phys. **19**, 259 (1947).
[10] M. Livingston and H. Bethe, Revs. Modern Phys. **9**, 290 (1937). The angle θ in this expression is the half-angle (in radians) for a cone in which proton recoils are measured. From proton recoil energy considerations, a rectangular pyramid having half-angles of 10° and 25° is approximately equivalent to a cone of half-angle 19°.
[11] Lattes, Fowler, and Cuer, Proc. Phys. Soc. (London) **A59**, 883 (1947).

the statistical error shows but the remaining points above this energy should be reliable to the extent that the statistical error indicates. Beyond the 5- to 6-Mev region the statistical errors are large since few tracks were measured in this energy region due to these long tracks leaving the emulsion and also on account of the shape of the spectral curve.

A graph of the results on the fission neutron spectrum is shown in Fig. 2. The spectral curve shows a maximum in the 0.7–0.8 Mev energy region and at energies greater than about 2 Mev the curve diminishes exponentially with a "relaxation energy" of 1.7±0.1 Mev. This result is very similar to that of Hill[3] who obtained a maximum in the same energy region and a relaxation energy of 1.55 Mev. The semi-empirical relation, $e^{-E}\sinh\sqrt{(2E)}$, where E is in Mev, obtained by Watt[3] fits the data of this experiment quite well; the above equation was matched to the experimental data in the vicinity of 1 to 2 Mev which is considered the most accurate region of the data. An experimental curve drawn through the data points would be only slightly higher in the region of the maximum and at energies above 5 Mev.

Tracks on the background plate were less than 5 percent of the number of measured tracks on the regular data plate. Therefore, the background was neglected in the analysis of the data.

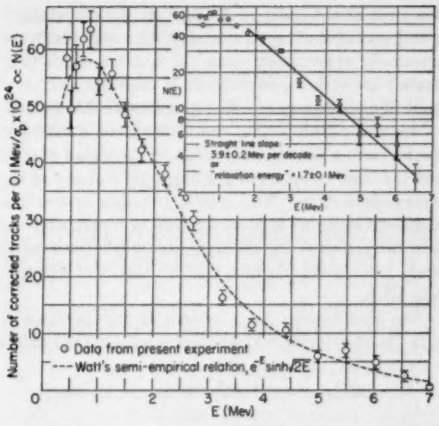

FIG. 2. Fission neutron spectrum of U^{235}. Inset: Spectrum plotted on semi-log paper.

The author wishes to thank Esther Allison and Dorothy Squires of the nuclear plate laboratory for their services in reading the plates used in this experiment.

PHYSICAL REVIEW VOLUME 85, NUMBER 4 FEBRUARY 15, 1952

Spin-Spin Relaxation in a Simple System*

JULIAN EISENSTEIN
University of Wisconsin, Madison, Wisconsin
(Received October 17, 1951)

A system of two particles of spin ½ coupled by their dipolar interaction and in an arbitrary magnetic field is considered. It is shown that exact expressions for the energy levels of the system can be obtained. The density matrix is calculated exactly for the cases where a magnetic field is suddenly applied, parallel or perpendicular, to the line joining the dipoles. It is used in the evaluation of the magnetic moment of the system. Instead of there being a gradual approach to an equilibrium situation the magnetic moment varies harmonically in time. A partially successful attempt is made to calculate the density matrix when the functional dependence of the magnetic field on the time is more complicated than a step function. The exact calculations for this simple system are compared with the approximate calculations of Waller for a system of N spins. It is pointed out that there may be no gradual approach to equilibrium in the N-spin system, either.

THE problem of calculating the time required for the establishment of statistical equilibrium in a system of interacting spins, when the external magnetic field is varied, was first considered by Waller[1] in 1932. Although it has been known for some years that Waller's results are of limited validity when applied to an actual paramagnetic crystal, his basic conclusion that there is a spin-spin relaxation process seems to have gone unchallenged. Qualitative discussions of spin-spin relaxation are frequently based on his calculations. According to Waller, for temperatures not too low and for external magnetic fields small in comparison with the internal field, statistical equilibrium is established in the spin system about 10^{-11} sec after the external field is varied.

Broer[2] applied a different, but none the less approximate, method to the problem. He calculated a relaxa-

* This work was supported in part by the AEC.
[1] L. Waller, Z. Physik **79**, 370 (1932).
[2] L. J. F. Broer, Physica **10**, 801 (1943).

tion time of the order of 5×10^{-9} sec for a system of spin $\frac{1}{2}$ particles. The results of Waller and Broer are necessarily approximate since the systems which they treated are rather complicated. If there are only two spins in an arbitrary external magnetic field the eigenvalues and eigenfunctions can be obtained exactly; in special cases a density matrix can be calculated exactly and the time variation of the magnetic moment of the system determined. This simple two-spin system can hardly be regarded as a good model of a paramagnetic salt. Nevertheless, as will be shown, it is interesting to study it in connection with Waller's theory of spin-spin relaxation.

The Hamiltonian for a system of two particles of spin $\frac{1}{2}$ in an external field which is parallel to the z-axis is

$$\mathcal{H}=g\beta H(\sigma_{1z}+\sigma_{2z})+g^2\beta^2r^{-5}(r^2\boldsymbol{\sigma}_1\cdot\boldsymbol{\sigma}_2-3\boldsymbol{\sigma}_1\cdot\mathbf{r}\boldsymbol{\sigma}_2\cdot\mathbf{r}).$$

$\mathbf{r}$ is the vector from particle 1 to particle 2; $\boldsymbol{\sigma}_1$ and $\boldsymbol{\sigma}_2$ are the spin matrices of the two particles in units of $\hbar$.

These matrices are

$$\boldsymbol{\sigma}_1=\tfrac{1}{2}\begin{pmatrix}\mathbf{k} & \mathbf{i}-i\mathbf{j} & 0 & 0\\ \mathbf{i}+i\mathbf{j} & -\mathbf{k} & 0 & 0\\ 0 & 0 & \mathbf{k} & \mathbf{i}-i\mathbf{j}\\ 0 & 0 & \mathbf{i}+i\mathbf{j} & -\mathbf{k}\end{pmatrix},$$

$$\boldsymbol{\sigma}_2=\tfrac{1}{2}\begin{pmatrix}\mathbf{k} & 0 & \mathbf{i}-i\mathbf{j} & 0\\ 0 & \mathbf{k} & 0 & \mathbf{i}-i\mathbf{j}\\ \mathbf{i}+i\mathbf{j} & 0 & -\mathbf{k} & 0\\ 0 & \mathbf{i}+i\mathbf{j} & 0 & -\mathbf{k}\end{pmatrix}.$$

The rows and columns are labeled by $\sigma_{1z}=1$, $\sigma_{2z}=1$; $\sigma_{1z}=-1$, $\sigma_{2z}=1$; $\sigma_{1z}=1$, $\sigma_{2z}=-1$; and $\sigma_{1z}=-1$, $\sigma_{2z}=-1$, respectively.

The total spin and the z-component of the total spin can be diagonalized by the canonical transformation

$$S_1=\begin{pmatrix}1 & 0 & 0 & 0\\ 0 & 2^{-\frac{1}{2}} & 0 & 2^{-\frac{1}{2}}\\ 0 & 2^{-\frac{1}{2}} & 0 & -2^{-\frac{1}{2}}\\ 0 & 0 & 1 & 0\end{pmatrix}.$$

When the transformation S_1 is applied to the spin-spin part of the Hamiltonian the result[3] is

$$S_1^{-1}\mathcal{H}_{SS}S_1=\tfrac{1}{4}g^2\beta^2r^{-5}\begin{pmatrix}r^2-3z^2 & -3\sqrt{2}z(x-iy) & -3(x-iy)^2 & 0\\ -3\sqrt{2}z(x+iy) & 2(3z^2-r^2) & 3\sqrt{2}z(x-iy) & 0\\ -3(x+iy)^2 & 3\sqrt{2}z(x+iy) & r^2-3z^2 & 0\\ 0 & 0 & 0 & 0\end{pmatrix}.$$

The matrix of the spin-spin interaction can be diagonalized by applying a second canonical transformation S_2, where

$$S_2=\begin{pmatrix}2^{-\frac{1}{2}} & -2^{-\frac{1}{2}}\sin\theta & -2^{-\frac{1}{2}}\cos\theta & 0\\ 0 & e^{i\varphi}\cos\theta & -e^{i\varphi}\sin\theta & 0\\ 2^{-\frac{1}{2}}e^{2i\varphi} & 2^{-\frac{1}{2}}e^{2i\varphi}\sin\theta & 2^{-\frac{1}{2}}e^{2i\varphi}\cos\theta & 0\\ 0 & 0 & 0 & 1\end{pmatrix}.$$

The result is

$$S_2^{-1}S_1^{-1}\mathcal{H}_{SS}S_1S_2=\begin{pmatrix}-2A & 0 & 0 & 0\\ 0 & 4A & 0 & 0\\ 0 & 0 & -2A & 0\\ 0 & 0 & 0 & 0\end{pmatrix},$$

where $A=\frac{1}{4}g^2\beta^2r^{-3}$.

In zero external field the possible energies of the two-spin system are, therefore, $-2A$ (doubly degenerate), $4A$, and 0. The first three eigenvalues are for the parallel alignment of the two spins (triplet state) and the last is for the antiparallel alignment (singlet state).

The Zeeman part of the Hamiltonian,

$$\mathcal{H}_Z=g\beta H(\sigma_{1z}+\sigma_{2z}),$$

is diagonal in the original representation and remains diagonal when the transformation S_1 is applied to it. When S_2 is applied one obtains

$$S_2^{-1}S_1^{-1}\mathcal{H}_ZS_1S_2=\begin{pmatrix}0 & -g\beta H\sin\theta & -g\beta H\cos\theta & 0\\ -g\beta H\sin\theta & 0 & 0 & 0\\ -g\beta H\cos\theta & 0 & 0 & 0\\ 0 & 0 & 0 & 0\end{pmatrix}.$$

The secular equation corresponding to the complete Hamiltonian is

$$E\{E^3-12A^2E-16A^3-E(g\beta H)^2 +2A(g\beta H)^2(3\cos^2\theta-1)\}=0.$$

The energy of the singlet state is zero, independent of the applied field. Since the remaining equation is of third degree in E the exact eigenvalues for the triplet state can be determined. The expressions for these eigenvalues are, in general, rather complicated. In the special case $\theta=0$ (line joining the dipoles parallel to H) they are $-2A\pm g\beta H$ and $4A$. In case $\theta=\pi/2$ the triplet state eigenvalues are $-2A$ and $A\pm(9A^2+(g\beta H)^2)^{\frac{1}{2}}$.

[3] My attention has been called to papers by Pake [J. Chem. Phys. **16**, 333 (1948)], and by Andrew and Bersohn [J. Chem. Phys. **18**, 159 (1949)]. Pake gives the diagonal elements of the spin-spin interaction of a two-spin system in a representation which diagonalizes the total spin and its z-component. His results agree with those given here. Andrew and Bersohn calculated the interaction matrix for a three-spin system and the eigenvalues of the dipole-dipole energy. Neither Pake nor Andrew and Bersohn

The mean value of the z-component of the magnetic moment of the system can be calculated by means of the following formula if the density matrix is known.

$$\bar{M}_z = \mathrm{Tr}(\rho M_z) = \sum_{mn} \rho_{mn} M_{znm}. \tag{1}$$

When the external field is time-varying one cannot use the density matrix corresponding to a canonical distribution because even if this distribution is initially established it is not necessarily preserved. Instead ρ must be calculated from the general equation

$$i\hbar\dot{\rho} = \mathcal{H}\rho - \rho\mathcal{H}.$$

To compute ρ it is convenient to choose the representation which diagonalizes the spin-spin interaction since one then has

$$i\hbar\dot{\rho} = \mathcal{H}_Z\rho - \rho\mathcal{H}_Z.$$

It may appear simpler to choose the representation which diagonalizes the complete Hamiltonian. However, the complicated expressions for the eigenvalues of $\mathcal{H}$ make computations tedious. In addition, when H is a function of time the representation is always changing.

In the representation which diagonalizes $\mathcal{H}_{SS}$ one obtains the nine simultaneous equations

$$\begin{aligned}
i\hbar\dot{\rho}_{11} &= (\rho_{12}-\rho_{21})R\sin\theta + (\rho_{13}-\rho_{31})R\cos\theta \\
i\hbar\dot{\rho}_{12} &= -\alpha\rho_{12} - \rho_{32}R\cos\theta + (\rho_{11}-\rho_{22})R\sin\theta \\
i\hbar\dot{\rho}_{13} &= (\rho_{11}-\rho_{33})R\cos\theta - \rho_{23}R\sin\theta \\
i\hbar\dot{\rho}_{21} &= \alpha\rho_{21} + (\rho_{22}-\rho_{11})R\sin\theta + \rho_{23}R\cos\theta \\
i\hbar\dot{\rho}_{22} &= -(\rho_{12}-\rho_{21})R\sin\theta \\
i\hbar\dot{\rho}_{23} &= \alpha\rho_{2s} + \rho_{21}R\cos\theta - \rho_{13}R\sin\theta \\
i\hbar\dot{\rho}_{31} &= -(\rho_{11}-\rho_{33})R\cos\theta + \rho_{32}R\sin\theta \\
i\hbar\dot{\rho}_{32} &= -\alpha\rho_{32} + \rho_{31}R\sin\theta - \rho_{12}R\cos\theta \\
i\hbar\dot{\rho}_{33} &= -(\rho_{13}-\rho_{31})R\cos\theta.
\end{aligned}$$

In these equations we have put $\alpha = 6A$ and $R = g\beta H$. One also obtains the equations

$$\begin{aligned}
i\hbar\dot{\rho}_{14} &= -2A\rho_{14} - \rho_{24}R\sin\theta - \rho_{34}R\cos\theta \\
i\hbar\dot{\rho}_{24} &= -\rho_{14}R\sin\theta + 4A\rho_{24} \\
i\hbar\dot{\rho}_{34} &= -\rho_{14}R\cos\theta - 2A\rho_{34} \\
i\hbar\dot{\rho}_{44} &= 0.
\end{aligned}$$

There is also a set of equations similar to the last group except that the indices are interchanged and the signs on the right-hand side reversed. The last equation above states that the occupation of the singlet state does not change when the field is changed. Inasmuch as no terms involving ρ_{4i} or ρ_{i4} appear in the formula for the mean value of M_z (since $M_{zi4} = M_{z i4} = 0$) these quantities will not be evaluated.

A closed solution of the above equations can be obtained only in special cases. One of these cases is that in which H is taken to be a step function

$$\begin{aligned}
H &= 0 \quad t < 0 \\
H &= H_0 \quad t \geq 0.
\end{aligned}$$

In this case the equations for the ρ_{mn} can be solved by a Laplace transform method. If one puts

$$\bar{\rho}_{mn}(\lambda) = \int_0^\infty e^{-\lambda t}\rho_{mn}(t)dt,$$

one obtains a set of nine simultaneous linear equations for the transforms $\bar{\rho}_{mn}(\lambda)$. These equations can be solved for arbitrary θ. Although the denominator of $\bar{\rho}_{mn}$ is of ninth order in λ, it factors into λ^3 and an expression of third order in λ^3. Consequently, the inverse Laplace transformation can always be performed. The results are particularly simple when $\theta = 0$ or $\theta = \frac{1}{2}\pi$ and are given below. The components of the density matrix have been required to satisfy the initial conditions $\rho_{mn} = 0$ for $m \neq n$ and $t = 0$ and $\rho_{mm} = \rho_m(0)$ at $t = 0$. One finds, for $\theta = 0$,

$$\begin{aligned}
&\rho_{12} = \rho_{21} = \rho_{23} = \rho_{32} = 0 \\
&\rho_{13} = -\rho_{31} = \tfrac{1}{2}i[\rho_2(0) - \rho_1(0)]\sin(2Rt/\hbar) \\
&\rho_{11} = \rho_1(0)\cos(2Rt/\hbar) + \tfrac{1}{2}[\rho_1(0) + \rho_2(0)][1 - \cos(2Rt/\hbar)] \\
&\rho_{22} = \rho_2(0) \\
&\rho_{33} = \rho_3(0)\cos(2Rt/\hbar) + \tfrac{1}{2}[\rho_1(0) + \rho_2(0)][1 - \cos(2Rt/\hbar)].
\end{aligned}$$

We shall put $S = (4R^2 + \alpha^2)^{\frac{1}{2}}$. Then for $\theta = \frac{1}{2}\pi$ we have

$$\begin{aligned}
&\rho_{13} = \rho_{31} = \rho_{23} = \rho_{32} = 0 \\
&\rho_{12} = \rho_{21}^* = -iRS^{-1}[\rho_1(0) - \rho_2(0)]\sin(St/\hbar) \\
&\qquad + \alpha RS^{-2}[\rho_1(0) - \rho_2(0)][1 - \cos(St/\hbar)] \\
&\rho_{11} = \rho_1(0) - 2R^2S^{-2}[\rho_1(0) - \rho_2(0)][1 - \cos(St/\hbar)] \\
&\rho_{22} = \rho_2(0) + 2R^2S^{-2}[\rho_1(0) - \rho_2(0)][1 - \cos(St/\hbar)] \\
&\rho_{33} = \rho_3(0).
\end{aligned}$$

The mean value of the z-component of the magnetic moment as calculated from (1) is 0 for $\theta = 0$; for $\theta = \pi/2$ it is

$$-2\alpha g\beta RS^{-2}[\rho_1(0) - \rho_2(0)][1 - \cos(St/\hbar)].$$

One can easily show that in the latter case M_z is an oscillatory function regardless of the special choice of the initial conditions. It follows that no spin-spin relaxation takes place.

It is of interest to compare these results with those obtained by Waller for a system of N spins. Waller also calculated the value of the magnetic moment by first evaluating (approximately) the density matrix. The values of ρ_{mn} for $m \neq n$ obtained here agree with Waller's values if we retain only terms of first order in H_0 and if $g\beta H_0 \ll 3A$. If the trigonometric functions appearing in the expressions for ρ_{mn} are expanded one sees that the ρ_{mm} contain no terms linear in H_0. This result also agrees with Waller's calculations.

For the situation where the magnetic field is suddenly turned on, Waller calculated a root-mean-square value for the oscillatory part of the magnetic moment of the system of N spins. He showed that this average value

considered the case where the spin-spin energy is comparable with the Zeeman energy. Dr. J. Luttinger has informed me that he has also obtained the secular equation given below for the determination of the eigenvalues of the two-spin system in arbitrary external field.

is small in comparison with the equilibrium value of the moment. This procedure is misleading since it minimizes the importance of the oscillatory terms. Although the time average value for the square of the oscillatory part of the moment is small, the amplitude of the oscillatory part is comparable with the equilibrium value of the moment.

Waller's expression for the oscillatory part of M is

$$M'=(g\beta)^2H_0(kT)^{-1}2^{-N}\sum_{nn'}|S_{nn'}|^2\cos\nu_{nn'}t,$$

where S_z is the z-component of the total spin measured in units of $\hbar$ and $h\nu_{nn}$ is the energy separation of the levels n and n' of the spin system in zero external field. When $t=0$ one has $M'=M_0$, the equilibrium value of the moment in a field H_0. For some sufficiently large t, M' must approach M_0 arbitrarily closely. The condition that $\cos\nu_{nn'}t=1$ for some t and every $\nu_{nn'}$ is just that $\nu_{nn'}t=2\pi n$ where n is integral. Consider the two equations

$$\nu_{nn'}T=2\pi n, \quad \nu_{mm'}T=2\pi m.$$

If the first equation is satisfied for some T than for the second equation to hold it is necessary that

$$\nu_{mm'}/\nu_{nn'}=m/n.$$

This equation can obviously be satisfied to any desired degree of approximation by taking m and n sufficiently large. It follows that all the equations $\nu_{nn'}t=2\pi n$ can be satisfied for some t, to any degree of exactness, if the n are chosen sufficiently large.

Waller considered two other functional relations between H and t. They are

case I	$H=0$	$t<0$
	$H=H_0t/T$	$0\leqslant t<T$
	$H=H_0$	$T\leqslant t$

and

case III	$H=0$	$t<0$
	$H=H_0\cos(\omega t+\varphi)$	$0\leqslant t$.

In these two cases it appears from Waller's results that relaxation actually occurs. Consequently, it is worthwhile to compute the density matrix for the two-spin system.

If H is along the z-axis ($\theta=0$) the components of the density matrix for the two-spin system can be determined exactly. The results in case I for $0<t\leqslant T$ are

$$\rho_{11}(t)=\tfrac{1}{2}\{\rho_3(0)+\rho_1(0)-[\rho_3(0)-\rho_1(0)]\cos(g\beta H_0t^2/\hbar T)\}$$
$$\rho_{22}(t)=\rho_2(0)$$
$$\rho_{33}(t)=\tfrac{1}{2}\{\rho_3(0)+\rho_1(0)+[\rho_3(0)-\rho_1(0)]\cos(g\beta H_0t^2/\hbar T)\}$$
$$\rho_{13}(t)=-\rho_{31}(t)=\tfrac{1}{2}i[\rho_3(0)-\rho_1(0)]\sin(g\beta H_0t^2/\hbar T).$$

In case III one has, for $t>0$

$$\rho_{11}(t)=\tfrac{1}{2}\{\rho_3(0)+\rho_1(0)+[\rho_3(0)-\rho_1(0)]\times\cos\{2g\beta H_0\hbar^{-1}\omega^{-1}[\sin(\omega t+\phi)-\sin\phi]\}\}$$
$$\rho_{22}(t)=\rho_2(0)$$
$$\rho_{33}(t)=\tfrac{1}{2}\{\rho_3(0)+\rho_1(0)-[\rho_3(0)-\rho_1(0)]\times\cos\{2g\beta H_0\hbar^{-1}\omega^{-1}[\sin(\omega t+\phi)-\sin\phi]\}\}$$
$$\rho_{13}(t)=-\rho_{31}(t)=\tfrac{1}{2}i[\rho_3(0)-\rho_1(0)]\times\sin\{2g\beta H_0\hbar^{-1}\omega^{-1}[\sin(\omega t+\phi)-\sin\phi]\}.$$

In both cases the values of the other ρ's are zero. The results, of course, agree with Waller's, if only terms up to those in H_0^2 are retained. However, these exact solutions differ from Waller's in one very important respect. According to Waller, the oscillatory part of ρ_{mn} can be made very small in case I by choosing T sufficiently large and in case III by choosing $\theta=0$. According to the above formulas for ρ_{13} the oscillatory part can never be neglected. This difference is due to the zero field degeneracy of states 1 and 3.

It is probably not possible to obtain closed solutions for the components of the density matrix in either case I or case III when $\theta=\frac{1}{2}\pi$. The equations which one has to solve for this value of θ can be written as

$$i\hbar(\dot\rho_{12}-\dot\rho_{21})=2R(\rho_{11}-\rho_{22})-\alpha(\rho_{12}+\rho_{21})$$
$$i\hbar(\dot\rho_{12}+\dot\rho_{21})=-\alpha(\rho_{12}-\rho_{21})$$
$$i\hbar(\dot\rho_{11}-\dot\rho_{22})=2R(\rho_{12}-\rho_{21})$$
$$i\hbar(\dot\rho_{11}+\dot\rho_{22})=0.$$

In case I, one can obtain a power series solution. Put

$$\rho_{12}-\rho_{21}=\sum_{n=0}^{\infty}a_nt^n.$$

Then $a_0=0$, $a_2=\frac{1}{2}[\rho_1(0)-\rho_2(0)]$, $a_{2n+1}=0$, and the recursion relation for the a's is

$$a_{n+4}=-\alpha^2a_{n+2}/\hbar^2(n+4)(n+3)-(2g\beta H_0/\hbar T)^2a_n/(n+4)(n+2).$$

If the condition

$$(2g\beta H_0)^2/\hbar^2T^2\ll\alpha^4/\hbar^4$$

is imposed, Waller's solution is obtained. If the inequality signs are reversed, one finds that

$$\rho_{12}(t)=\tfrac{1}{2}i[\rho_2(0)-\rho_1(0)]\sin(g\beta H_0t^2/\hbar T),$$

which is again an oscillatory function of t.

The conclusions to be drawn from a comparison of the explicit calculations on the two-spin system with Waller's approximate formulas are as follows: (1) If the external magnetic field is suddenly turned on, the magnetic moment of a system of interacting spins will never reach an equilibrium value. (2) The high degree of degeneracy in such a system makes the application of Waller's formulas somewhat uncertain. (3) In large fields no spin-spin relaxation can take place in a rigid lattice. This fact was first pointed out by Waller.

The Absorption Curve of the Cosmic Radiation in the Stratosphere*

MARCEL SCHEIN AND VICTOR H. YNGVE
Department of Physics, University of Chicago, Chicago, Illinois
(Received August 30, 1951)

The absorption in lead of cosmic-ray particles has been measured at an altitude of 5.7 cm Hg with hitherto unattained accuracy. The absorption at this altitude is compared with the absorption at sea level. It is found that the soft component shows an increase by about a factor of 90. The hard component shows an absorption length of about 220 grams per cm² of Pb, very different from the sea level absorption of μ-mesons. It is concluded that most of the penetrating particles at 5.7 cm Hg are nucleons.

BALLOON flights have been made to measure the absorption in lead and in air of the cosmic radiation. Absorption in lead was measured by a technique which gives the penetration through a number of thicknesses simultaneously with one apparatus on one flight. This technique has a number of advantages over the other one of sending up many flights each with a simple telescope. In the first place, errors in measurement of the pressure cannot affect the shape of the absorption curve in lead at any one altitude. Secondly, time variations and atmospheric temperature effects can have no effect on the absorption curve in lead at any one altitude. Finally, internal checks are possible on the proper operation of the apparatus by observing the number of counts recorded simultaneously in the different telescopes.

The geometry is shown in Fig. 1. Altogether 17 counters were used in eight fourfold coincidences. Six of these coincidences form telescopes giving the counting rate through lead thicknesses of 0, 2, 4, 8, 12, and 18 cm. All of these telescopes subtend the same solid angle for single particles passing through along straight lines.[1] Five of the six have the solid angle defined by the two extreme counters, which are 28 cm apart. However, in the case of the telescope with 18-cm Pb, the counters defininin the solid angle for straight line particles are not the extreme counters, because it was not possible to put this much lead between counters *H* and *M*. In order to make an 18-cm telescope, the three counters *G*, in parallel, were placed above the lead and they more than cover the solid angle. The solid angle of this telescope thus becomes larger than the others for particles which interact in the lead to produce secondaries which can trip the lower counters. Corrections can be made for this effect because the 18-cm telescope shares part of its solid angle with other telescopes with lesser amounts of lead. These corrections were obtained by counting the events in which a count was registered simultaneously in the 18-cm telescope and in various other telescopes.

The circuits which were developed in this laboratory use cathode follower input circuits followed by germanium diode coincidence circuits, multivibrators, and a photographic recorder using neon bulbs. The telescopes *ABCF* and *BCDH* also included a scale of two with two neon bulbs which flashed alternately. The resolving time of the coincidence circuits was 20 μsec, and hence, accidentals were negligible. The diode coincidence circuits make possible a considerable saving in

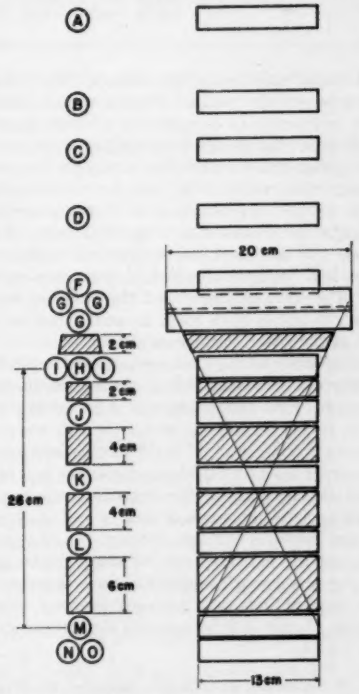

FIG. 1. The counter geometry. The counters are one inch in diameter. The active lengths shown are the lengths of the center wires. Coincidences are:

Cm Pb	0	2	4	8	12	18
Counters	*ABCF*	*BCDH*	*CDFJ*	*DFJK*	*FJKL*	*GHLM* *BDHI* *HMNO*

* Assisted by the joint program of ONR and AEC. The data contained in this paper was presented by one of the authors (Marcel Schein) at the Cosmic-Ray Conference in Pasadena in 1948.

[1] The other two registered multiple events below 2 and 18 cm of lead and had counting rates of 4.2 and 1.9 counts per minute, respectively.

vacuum tubes. In this apparatus the saving amounted to 10 tubes.

The apparatus was launched from Chicago and was carried by a cluster of 20 rubber J2000 balloons to the stratosphere. After reaching a maximum altitude, the balloons leveled off at a pressure of 5.7 cm Hg for 6½ hours while each telescope gave several thousand counts. The total length of the flight was 10 hours. It landed in the hills of West Virginia, about 450 miles from Chicago.

Corrections for the dead time of the counters and for the dead time of the recorder have been applied to the actual counting rate. The corrected counting rate at 5.7 cm Hg is shown in Table I, and gives the absorption

TABLE I. Counting rate at an altitude of 5.7 cm Hg through various thicknesses of lead absorber.

Cm Pb	0	2	4	8	12	18
Counts per minute	19.96	15.22	11.20	8.42	6.78	4.93
Total uncertainty	±0.23	±0.20	$+0.26$ -0.22	$+0.21$ -0.19	$+0.18$ -0.15	±0.35

of the cosmic radiation at this altitude. The indicated errors represent the total uncertainty of each point.

It is instructive to compare the absorption at this altitude with that at sea level. Rather good sea level counting rate data was obtained during pre-flight tests. However, since most of the tests were made indoors, they do not give a true indication of the absorption in the smaller thicknesses of lead. So, for purposes of comparison, the sea level curve obtained outdoors by Nielsen and Morgan[2] is shown in the lower curve in Fig. 2. The curve of Nielsen and Morgan is represented by the line and is made to fit accurately our sea level points at the larger thicknesses of lead.

A comparison of the two curves shows very clearly the difference in the composition of the cosmic radiation between sea level and an altitude of 5.7 cm Hg, which is close to the altitude at which the soft component exhibits a maximum at 52° north geomagnetic latitude. Both curves show a steep absorption in the first few cm of lead characteristic of the electronic component. If one extrapolates the curve of greater lead thickness to zero and measures the area between the extrapolated curve and the measured one for small thicknesses of lead, one gets a rough measure of the soft component. From this one finds that the soft component increases by about a factor of 90 between sea level and an altitude of 5.7 cm Hg.

[2] W. M. Nielsen and K. Z. Morgan, Phys. Rev. **54**, 245 (1938).

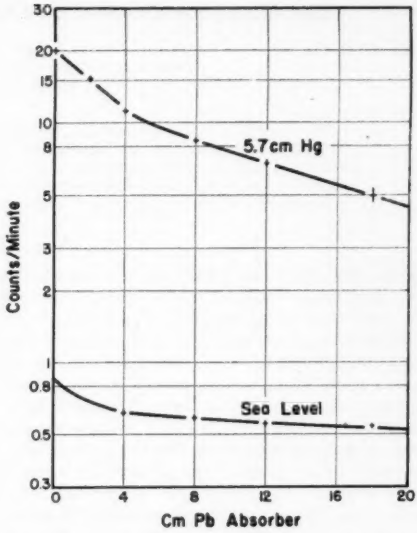

FIG. 2. The upper curve gives the counting rate through several thicknesses of lead obtained at an altitude corresponding to 5.7 cm Hg pressure. The lower curve gives the sea level data of Nielsen and Morgan normalized to our sea level data, which is shown by the points.

With larger thicknesses of lead, the absorption curve at 5.7 cm Hg shows a further significant drop with lead thickness, which is practically missing from the sea level curve. At sea level the remarkable flatness of the curve is known to be due to the fact that the particles penetrating more than a few cm Pb predominantly consist of μ-mesons.[3] In contrast to this flatness at sea level, it is interesting to note that the absorption curve for more than a few cm Pb at an altitude corresponding to 5.7 cm Hg pressure is nearly exponential with an absorption mean free path of about 220 grams per cm^2 similar to that of high energy nucleons.[4]

It is then concluded that most of the particles of the penetrating type consist of nucleons rather than μ-mesons at high elevations. This conclusion is further supported by the fact that the comparison of the absorption in lead and in air does not show an anomalous absorption in air between 4 cm Pb and 12 cm Pb. Due to the low density of the air at this high elevation, a very considerable anomalous absorption would be expected if the particles discharging the telescope were μ-mesons.

[3] M. G. Mylroi and J. G. Wilson, Proc. Phys. Soc. (London) **A64**, 404 (1951).
[4] T. G. Stinchcomb, Phys. Rev. **83**, 422 (1951).

Semiconductivity and Diamagnetism of Polycrystalline Graphite and Condensed Ring Systems

S. MROZOWSKI
Department of Physics, University of Buffalo, Buffalo, New York
(Received July 20, 1951)

The analysis of results obtained from studies of electric resistivity as a function of temperature, and sample preparation, and of other available evidence, leads to a clarification of the electronic processes in the class of substances extending from condensed ring molecular solids to polycrystalline graphite. In all these solids, the electric current flows preferentially along the benzene-ring planes. Scattering of electrons is due to thermal lattice vibrations and to the boundaries of molecular planes, where electrons pass through potential barriers into the neighboring crystallites. These barriers are quite transparent in polycrystalline graphite and baked carbons, since the flow occurs along the carbon-carbon bonds, but are quite opaque in molecular solids where the barriers are due to the presence of foreign atoms attached at the periphery of the molecules.

In contrast with the infinite graphite crystal, systems of benzene-rings of finite dimensions possess a finite energy gap between the filled and the conduction bands, the energy gap steadily decreasing with increase of molecular size—from about 1 ev for molecules several benzene rings wide, to 0.2–0.3 ev for systems 30–40A in diameter and to 0.05 ev for graphite crystallites with diameters of the order of 1000A. When in the process of carbonization, foreign atoms are removed from peripheries, the carbon atoms left with free, unattached valencies play a role of donors, that is, become a source of conduction (excess) electrons. The concentration of such excess electrons increases as long as gases are driven out from the carbons, but starts decreasing as a result of growth of crystallite size for samples treated to higher temperatures. The complete interpretation of the dependence of resistivity on temperature is based on a combination of these three factors: scattering, concentration of the excess electrons, and concentration of holes and electrons activated from the lower band (over the energy gap).

The anisotropic component of the diamagnetism of condensed ring systems has a twofold origin: (1) diamagnetism of the filled band (closed shell) of resonance (π) electrons, which is proportional to the number of benzene rings in a molecule; and (2) the Landau diamagnetism of the free electrons and holes. The contribution of the Landau diamagnetism is by far the larger of the two for graphite, but decreases fast with the crystallite size and becomes negligible for molecules with diameters of 30A or below, due to an increase in the effective mass of carriers.

INTRODUCTION

THIS paper originated in an attempt to find a consistent picture of electronic processes in a large class of solids, which until recently has attracted comparatively little attention of physicists.[1] These solids are all made by heat-treating organic materials in a neutral or reducing atmosphere. They range from the so-called raw cokes obtained at the lower temperatures through materials, graphitic in structure, produced at the highest temperatures of treatment. No matter what the original organic substance is, if it remains fluid up to a relatively high temperature (~450°C), large condensed ring molecules are created in the heating process. At the setting temperature, some kind of polymer is formed in which the molecules are stacked parallel in groups like pennies in a bag full of money.[2] Higher heat treatment produces continuing growth of these molecules; at temperatures above 700°–800°C, these substances, having lost most of the atoms or groups attached at the periphery of the molecules, become the so-called calcined or baked carbons. These are essentially solids built of very small (20–30A diam) turbostratic crystallites of graphite: packs of parallel graphite planes having no directional relationship to each other. Only at considerably higher temperatures, when the molecular planes reach a diameter of about 150A[3] a rotation starts to bring the planes into a regular directional arrangement and into a consecutive order corresponding to the large crystals of graphite.

Some of the organic substances solidify at a much lower temperature—for instance, the so-called hardening resins.[4] The early stabilization by crisscross bonding, impairs the growth of molecular planes in the heating process; the carbons thus obtained show a glassy structure and do not graphitize so easily. Several years ago, the author had introduced the name "hard carbons" in order to distinguish such materials from the highly crystallized carbon obtained from petroleum or coal tar pitches.[5] It must be realized, however, that there is a continuous transition from hard carbons to the soft, easily graphitizing materials, and that the term hard carbon covers quite a broad variety of structures.

I. GENERAL CONSIDERATIONS

As checked by a number of investigators, the resistance of graphite crystals in the direction parallel to the graphite planes is about $5\times10^{-5}\Omega$cm at room temperature. This value might be a little too high since it is possible that not all graphite layers are effective in carrying the current if a direct contact with each of them is not established in the experiment. The parallel resistivity varies probably linearly with temperature

[1] See the preliminary note S. Mrozowski, Phys. Rev. **77**, 838 (1950).

[2] A wealth of information is contained in papers by Riley and his collaborators: Blayden, Gibson, and Riley, Proc. of the Conference on the Ultrafine Structure of Coals and Cokes, B C U R A London, 1943, and a number of other publications.

[3] R. E. Franklin, Acta Cryst. **4**, 253 (1951).

[4] See for instance R. Houwink, *Elasticity, Plasticity, and Structure of Matter* (Cambridge University Press, London, 1937), p. 152.

[5] Recently Franklin (reference 3) suggested the name of "non-graphitizing carbons." Such a name does not seem appropriate, since these carbons do graphitize after all, although at correspondingly higher temperatures.

over a wide range. This has been found to hold for low temperatures,[6,7] and it seems almost certain from the study of polycrystalline graphites that the approximate linear relationship should hold up to the highest temperatures, the slope being about $1.7\times10^{-7}\Omega$cm/°C or somewhat less.

Calculations made by Coulson,[8] and Wallace,[9] for an infinite lattice show that graphite along the plane is an intrinsic semiconductor with a zero activation energy and with a density of electronic levels decreasing to zero as one approaches the boundary between the filled and empty energy bands. However, the results of the more detailed calculations of Wallace cannot be considered as satisfying. For instance, no explanation of the temperature dependence of the anomalous diamagnetic susceptibility and of the linear temperature dependence of the electric resistivity is given. Furthermore, the ratio of the resistivity in two directions is calculated to be of the order of 100. The resistivity in the transverse direction is large and very difficult to determine. Only a lower limit can be obtained with the best crystals available. Krishnan and Ganguli[10] found for the two directions a ratio of resistivities equal to about 10^5. The transverse resistivity of graphite is therefore of the order of 3Ωcm or larger. Thus Wallace's estimate fails by a factor of 10^3. The general picture undoubtedly is correct, but the theory seems to require considerable refinements.

As a result of the great anisotropy of the graphite crystallites, the electric current flows in polycrystalline materials preferentially along the graphitic planes. Consequently, in the rest of this paper only this kind of flow will be considered. In comparing the resistivity of polycrystalline materials with each other or with graphite crystals, a number of corrections should be kept in mind:

(1) The increase in length of current path through the crystallites. Passing N planes of diameter d the zigzag path has a length Nd, but the direct distance is only $Nd\langle\cos\theta\rangle_{Av}$, where θ is the angle between the given direction and the graphitic plane, so that $f_1=1/\langle\cos\theta\rangle_{Av}$. For an isotropic material with a perfectly random distribution of the crystallite planes, the average increase is by a factor $f_1=4/\pi=1.28$. If the crystallites show any kind of alignment relative to a certain axis, for instance, if the planes of crystallites align parallel to the direction of extrusion, the factor along the axis becomes smaller and larger across (for a perfectly random distribution in the normal plane $f_1=\pi/2=1.57$). On the other hand, if the sample is made by compressing graphite powder, the crystallites align with planes normal to the direction of pressure and the factor becomes large for the axial direction and small (nearly 1) for a crosswise direction.

(2) Due to a disordered crisscross bonding between crystallites, some planes might happen not to carry any current, that is, might happen to be ineffective. It seems very improbable that in such a polymer any graphitic plane could remain completely unattached and ineffective, so that the assumption of every fourth plane being totally ineffective would probably exaggerate the situation. Thus, the correction factor f_2 will be somewhere between 1 and 1.33.

(3) The "real density" correction. It is known that the smaller crystallites of graphite have larger interplanar distances. Consequently, there are fewer graphitic planes per unit volume, and the so-called real density d of the material is lower than that of a graphite single crystal; the resistivity is consequently higher by a factor $f_3=(2.26/d)^4$. This is a small correction relative to the others and will not be considered further.

(4) The microporosity correction. In a crisscross arrangement, some spaces are left unfilled between crystallites. The voids are mainly formed as a result of a differential shrinkage in the process of cooling.[11] Since these voids represent less than 10 percent of the total volume, this correction $f_4=(2.26/d)^4$ is again quite small and in the following will be neglected $(1<f_4<1.03)$.

(5) The macroporosity, which is due to the method of preparation of carbons, consisting of empty spaces between particles of coke and pores left in larger particles of coke. The corresponding correction is not a simple function of the bulk density. For a reasonable evaluation, the original mix formula must be known. For average commercial products (coke flour mixes) the correction factor f_5 is around 1.5. Great caution is necessary since some of the materials prepared with small amounts of binder might require considerably larger corrections.

(6) Microcracks are created in cokes and especially in the binder coke during the baking process. These microcracks form a network all through the material[12] and probably are only partly sealed in the process of graphitization. The number of microcracks varies with the kind of treatment and, as found by us, the resistivity of the polycrystalline graphite is increased in the more unfavorable cases by as much as 25 percent.

Applying these corrections to an actual case of a commercial well-graphitized rod for the direction along the axis of extrusion: $f_1\leqslant1.28$, $f_2\leqslant1.33$, $f_5\cong1.5$, and $f_6\leqslant1.25$, it is found that the total correction factor is $f\leqslant3.25$. At a temperature of 900°K the resistivity of graphite is $\leqslant15\times10^{-5}\Omega$cm, and the corresponding resistivity of the polycrystalline rod should consequently be $\rho\leqslant48\times10^{-5}\Omega$cm. The temperature of 900°K is selected

[6] W. J. de Haas and P. M. van Alphen, Proc. Roy. Acad. Amsterdam **34**, 70 (1931).
[7] H. Kammerlingh Onnes and K. Hoff, Proc. Roy. Acad. Amsterdam **17**, 520 (1915).
[8] C. A. Coulson, Nature **159**, 265 (1947).
[9] R. P. Wallace, Phys. Rev. **71**, 622 (1947).
[10] K. S. Krishnan and N. Ganguli, Nature **144**, 667 (1939).
[11] The existence and formation of these voids, as well as the influence of the differential shrinkage on the mechanical properties of carbons will be discussed elsewhere.
[12] As shown on electron micrographs obtained by E. Kmetko at our laboratory.

so as to fall into the linear range. The measured value for good rods without defects is about $70\times10^{-6}\Omega$cm, as may be seen in Fig. 2. Thus a considerable part of the total resistivity of the polycrystalline graphite is accounted for by the temperature lattice scattering in the graphite crystallites. The estimate given above shows, however, that at least one-third of the measured resistivity of the polycrystalline graphite at 900°K is due to other scattering processes.

This extra scattering must be due to the finite dimensions of crystallites and to intercrystalline contacts. The flow of carriers from one crystallite to another probably occurs at places of their nearest approach where the graphite planes belonging to the two crystallites are held together by peripheral C−C bonds, and where the carriers pass through low potential barriers. Some carriers are reflected by these barriers, however; furthermore, almost all carriers are scattered by the remaining parts of the crystalline boundaries (high barriers). Thus, this extra scattering is a process not easily amenable to calculations. A complicating factor is that the electric field is probably not uniform throughout the crystals, but is more concentrated in the neighborhood of the intercrystalline contacts (barriers). In the following sections, a simplified treatment of this extra scattering will be used in which the scattering by the crystal boundaries and the contact resistance will be regarded as two different processes. The splitting of the scattering, however, will be done only in order to separate in a purely formal way the part of the scattering which is variable (with temperature) from that part which is constant, and not too much meaning should be attached to each of these quantities separately.

Since carbons can be made with different microcrystallinic structures, that is with crystallites held together by variable numbers and distribution of C−C bonds, it could be expected that the real (corrected) resistivity is not simply a function of crystallite size, but might vary within large limits with the type of carbon structure. It is remarkable therefore that the crystallite size is found actually to be the greatly preponderant factor which determines resistivity of a solid carbon sample. According to the experience of the author, gained during his several years of association with the Research Laboratory of the Great Lakes Carbon Corporation and later at the University of Buffalo with a great number of laboratory prepared samples, the resistivities after being corrected for the effects 1, 5, and 6, correlate well with the widths of the assymetric x-ray diffraction line 110 (from which the size of the graphitic planes is estimated). In other words, the corrected resistivity can be quite accurately predicted from the microcrystal size and vice versa. There is even a better correlation of the shapes of the resistivity-temperature curves with the x-ray diffraction patterns. A definite evidence of individual differences among samples is available showing that other effects do have an influence, but the differences are relatively small and in the broad discussion of the problem of resistivity of polycrystalline carbons they will not be considered. However, they have to be brought into discussion when one desires to explain the nature of these individual differences. Some examples of such differences will be mentioned later.

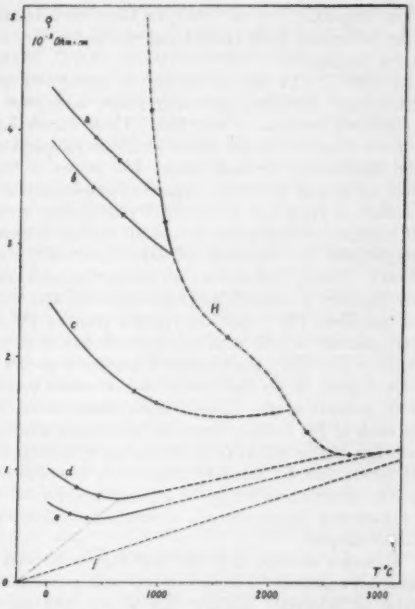

FIG. 1. Electric resistivity as function of temperature for a carbon rod treated to temperatures: (a) 1000°, (b) 1100°, (c) 2200°, (d) 2600°, and (e) 3000°C. Full lines mark the region in which the actual measurements were performed; broken lines represent the expected trend outside of this region. Line *f* is the limit to which the curves probably tend with increasing degree of graphitization. Curve *H* gives the variation of the resistivity during the heat treatment of the carbon (irreversible).

If a carbon is made from a mixture of coke, with addition of a carbon black, for instance, or if it is made using a binder which graphitizes differently from the coke—the correlation between temperature of treatment, the resistivity, and the type of x-ray diffraction pattern may be obscured or even may, in special limiting cases, become completely obliterated. The lack of knowledge of the composition of carbons and the mix formula according to which they were prepared can probably be blamed in many cases for the divergent opinions one finds in the literature on the subject of resistivity of carbons.

II. POLYCRYSTALLINE GRAPHITE

A system of resistance-temperature curves as they are found for solid carbon is presented in Fig. 1. All five curves were obtained by actual measurements from

room temperature up to 1100°C for the same petroleum coke laboratory rods treated successively to five different temperatures—1000°C, 1100°C, 2200°C, 2600°C, and 3000°C. The two lowest curves correspond to a graphitized material, and their shape is typical of graphitized carbons of any kind. These curves have definite mimima beyond which at higher temperatures the relationship becomes linear. The slopes of these lines are steeper for higher degrees of graphitization. A number of years ago Nishiyama[13] published a system of resistance-temperature curves for carbon filaments graphitized to temperatures 2000°C, 2500°C, and 3000°C. Though his curves are similar to mine, they are incorrect in a number of important respects. It can be seen from Fig. 1 that the crossing point of the line extrapolated to 0°K with the ordinate axis is always positive (in Nishiyama's curves it becomes negative for high degrees of graphitization) and decreases steadily with increase of the graphitization temperature. The increase of the holding time t (for $t \gtrsim 10$ min) in graphitization has an influence in decreasing resistivity, less, however, than was found by Nishiyama. The resistivity at the minimum seems to be a linear function of the temperature (dotted curve), at least for highly graphitized samples.

It seems obvious that the first step is to look at electron scattering processes for an explanation of this type of behavior. Wallace[9] has shown that for the model of a two-dimensional intrinsic semiconductor with zero energy gap, the resistivity in graphitic planes is $\rho = A/kT\tau$, where $A = h^2c/16\pi e^2 k \ln 2$ with $c = 6.75$A (double distance of graphite planes). Wallace's formula shows that $(N/m)_{eff} = kT/Ae^2$, the proportionality with temperature being a quite general result independent of the character ot the change of the density of electronic states with energy near the Brillouin zone corners. The scattering probability by thermal vibrations of the lattice $1/\tau_e$ must vary as T^2 in order to give a linear relationship $\rho = aT$ found experimentally for large graphite crystals. Wallace did not investigate the temperature dependence of the mean free path and left this question unsolved. It so happens that the case of graphite is quite unique, since the scattering probability by the lattice vibrations $1/\tau_e$ is proportional to TE and the velocities of all electrons being the same, the mean free path depends on the energy E of the scattered electron $l \cong 1/TE$. This is a simple consequence of the linear relationship between the energy and the momentum vector at the Brillouin zone corners, the number of states per unit energy and unit surface in k-space being independent of energy.[14] Since $\bar{E} \cong kT$, we find $1/\tau_e \cong T^2$ as required.[15]

If the crystal has a finite dimension L (or has lattice defects), the probability of scattering at the boundaries $1/\tau_b$ will be, for the same reason as above, proportional to E. This time, however, no additional proportionality, with temperature, will be present, since the scattering is caused, not by thermal vibrations, but by the permanent boundary of the crystal. In order to get the total resistivity of the polycrystalline graphite, a member representing the resistance of all intercrystalline contacts also should be included. The scattering at the contacts is not uniform in all directions so that the arguments used above are inapplicable,[14] and all that can be said is that this contribution is probably a decreasing function of temperature and that its importance should rapidly increase as the crystallite sizes decrease. Thus, the resistivity should be $\rho = (A/kT)(1/\tau_e + 1/\tau_b) + c(T) = aT + b + c(T)$, where the constant contribution of the boundary scattering is inversely proportional to the dimensions of crystallites.

The system of curves (Fig. 1), however, cannot be represented by such a formula for two reasons: (a) the contribution $c(T)$ increases with decrease of the size of the crystallites; therefore, for a definite temperature T the slope of the curves ρ *vs* T should increase as we go to less graphitized samples. This is not found to be true in Fig. 1. The slope at room temperature, for instance, is found to be about independent of the degree of graphitization for samples graphitized up to 3200°C. (b) The experimental curves join the linear relationship at higher temperatures so quickly without the curvature extending over a wide temperature range, that this immediately suggests the presence of some kind of exponential factor.[16]

An exponential relationship cannot be due to scattering processes. Such a relationship will be obtained, however, if the graphite crystals should happen to possess a finite energy gap ΔE between the filled and empty energy bands. Thus, we are led to the conclusion that the Coulson-Wallace result is true only for infinitely large crystals of graphite. For small crystals of graphite, consequently, $\rho = [aT + b + c(T)]e^{\Delta E/2kT}$ with ΔE decreasing to zero with increase of the size of the graphite crystals. Such a relationship will remove the objection (b); it will, however, still be subject to objection (a). However, if it is assumed that there are excess electrons in the upper energy band, the objection (a) can also be satisfied, as will be shown below, and a good explanation of the curve ρ *vs* T obtained.

[13] Z. Nishiyama, Z. Physik **71**, 600 (1931).

[14] W. Shockley, *Electrons and Holes in Semi-Conductors* (D. Van Nostrand and Company, Inc., New York, 1950). See the discussion of the conditions under which the mean free path is independent on energy (p. 493) and the formula (29).

[15] In a rigorous calculation of the resistivity, τ should not be taken out from under the integral, as was done by Wallace (see reference 9) (his Eqs. (3.11) and (3.12)). The temperature dependence, however, turns out to be the same for both procedures, so that the simplified treatment is given here.

[16] Two attempts were made recently to interpret the shape of the resistivity curves purely by scattering processes, both leading to identical formula $\rho = aT + (b/T)$. D. Bowen [Phys. Rev. **76**, 1878 (1949)] has overlooked, in derivation of the formula, the energy dependence of the scattering probability, and the existence of intercrystalline barriers, furthermore, he was unaware of objections (a) and (b). S. Mizushima and J. Okada [Phys. Rev. **82**, 94 (1951)] obtained the relationship from an analysis of Nishiyama's incorrect curves.

Figure 2 gives a resistivity curve for well-graphitized commercial graphite. This curve is a combination of results obtained by Goetz and Holser,[17,18] (temperature range 12°K–300°K) and by Powell and Schofield[19] (1400°C–2500°C), with a central part (0°–1000°C) fitted from the author's own data. It is unfortunate that no studies of resistivity have been made which would cover the whole range using the same sample of graphite. The author believes, however, that the general relations are brought out sufficiently well by such fitting of data. The whole curve from 150°K to highest temperatures can be represented by an empirical formula

$$\rho=(aT+b)/(r+e^{-\Delta E/kT}) \qquad (1)$$

with $a=3.5\times10^{-7}\Omega$cm/°C, $b=1.7\times10^{-4}\Omega$cm, $r=\frac{1}{3}$, and $\Delta E=600k=0.05$ ev.

This relationship can be interpreted in the following way: two scattering processes contributing to the resistivity at temperatures above 150°K are the thermal lattice scattering and the boundary scattering, the latter being approximately independent of temperature. The number of carriers consists of a constant number of excess electrons, n_e, and a variable number of electrons, n, activated from the lower band over the energy gap ΔE and a corresponding number of holes; therefore, the expression $re^{\Delta E/kT}$ represents roughly the ratio of the number of excess electrons to the number of activated electrons and holes.

The linear (high temperature) part of the curve corresponds to temperatures for which $kT>\Delta E$, where the number of activated electrons and holes is so large that the presence of a few excess electrons and of the energy gap is immaterial and the type of the curve becomes essentially similar to the one for a single graphite crystal. To the left of the resistivity minimum as we proceed towards lower temperatures, the number of activated electrons decreases due to the finite width of the gap. Here the resistivity would increase very strongly (exponentially), were it not for the excess electrons whose presence comes to be more and more felt in cutting down the rate of increase. Finally, below 150°K a stage is reached where there are so few activated electrons and holes that the current is conducted exclusively by the excess electrons. From there on down, either the number of carriers remains constant or decreases due to immobilization of the excess electrons on the surface sites. The immobilization of the excess electrons takes place, however, at considerably lower temperatures (~5°K, see Sec. V). The existence of the finite energy gap might lead to a rounding off of the Brillouin zone energy peaks (see Sec. VI) and change the linear into a parabolic relationship just near the corners of the zone. It seems that this cannot be the cause of the observed increase of resistivity at low temperatures and that the deviation of the expression (1) from the experimental curve below 150°K is mainly due to the contact resistances $c(T)$. Goetz and Holser[17] and Buerschaper[18] found that the ratio of the resistivities in a direction transverse to and parallel to the extrusion axis is a function of temperature. Goetz and Holser found that this ratio increased from 1.87 at room temperature to a value 2.03 at the lowest observed temperature (12°K). Extruded rods have a preferential arrangement of crystallites parallel to the axis. The higher resistivity in the transverse direction is partly because of this arrangement. In the transverse direction, the actual path length is larger (more zigzagging); consequently, the variation of the resistivity ratio with temperature shows that the resistance due to intercrystalline barriers (contacts) increases more for slow electrons if the change in direction of the flow of the current at the barriers is larger. Thus, the existence and a temperature dependence of the contribution $c(T)$ at low temperatures seems to be demonstrated by their experiments.

A slow decrease of the combined resistivity contributions b and $c(T)$ with increase of temperature in the range above 500°C could, in conjunction with the exponential factor, explain the changes in the linear slope with degree of graphitization (Fig. 1). On the other hand, the type of thermal vibrations of small crystallites might be sufficiently different from the larger ones to give such a variation.

As calculated by Wallace,[9] the number of activated electrons per atom at room temperature is of the order 2×10^{-4} or 2×10^{-3} (the lower value obtained for the

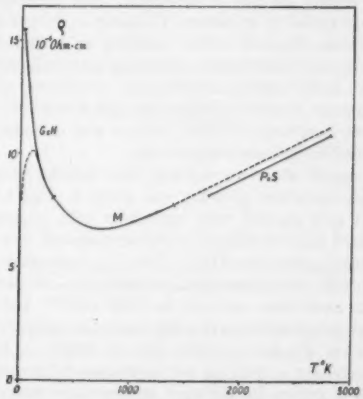

FIG. 2. Electric resistivity of polycrystalline graphite (carbon heat-treated to about 2900°C) as function of temperature. Experimental results due to: G&H—Goetz and Holser (see reference 14), *M*—the author, P&S—Powell and Schofield (see reference 16). Broken curve is calculated from Eq. (1) of the text.

[17] A Goetz and A. Holser, Trans. Am. Electrochem. Soc. **82**, 391 (1942).

[18] R. A. Buerschaper, J. Appl. Phys. **15**, 452 (1944). Buerschaper's results are believed to be either erroneous or obtained for a different type of carbon. His curve for baked carbons cannot be fitted with ours.

[19] R. W. Powell and F. H. Schofield, Proc. Phys. Soc. (London) **51**, 153 (1939).

plane model is probably the more reliable of the two, since the tridimensional model leads to an inacceptable ratio $\rho_{11}/\rho_{\perp}$). Due to the existence of a gap, the number of activated electrons and holes will be reduced for the polycrystalline graphite by the factor $e^{-\Delta E/kT}$ (Fermi level near the bottom of the conduction band). Multiplying this by the ratio of the number of excess electrons to the number of activated electrons and holes $re^{\Delta E/kT}$ (see above), we find the number of excess electrons roughly to be of the order 8×10^{-6} or 8×10^{-4} per atom (lower value preferred).

Formula (1) can be derived under very simplified assumptions for the region where $n_e \gg n$; that is, where the Fermi level is located close to the bottom of the conduction band. Strictly speaking, it is not applicable to the rest of the curve. It does, however, give a linear dependence for $kT > \Delta E$ as required and it is believed that the rigorous solution which should be obtained by using the Fermi-Dirac statistics and considering the variation in the position of the Fermi level and of the quantity $(N/m)_{\text{eff}}$ with temperature would yield a curve similar in shape to the one given by (1). Therefore, it is hoped that ΔE as determined from fitting (1) with the experimental curve should differ not too much from the real width of the gap.

III. BAKED CARBONS

The dependence of resistivity on temperature for baked carbon rods has been measured by many investigators. As in the case of graphitized rods there is, however, only one instance known to the author where a system of curves relating to the same sample treated to different temperatures was obtained. This was done by Powell and Schofield,[19] who measured the resistivity of baked rods to temperatures over 2000°C. However, their results are not in agreement with expectations and are probably erroneous. Crossings of curves occur only when there is either cracking or oxidation of samples, and their results show many such irregularities which, under correct experimental conditions, should not appear. It seems possible that the admixture of 20 percent lampblack in their carbons was in some way responsible for these irregularities.

A system of curves starting from baked carbon up to polycrystalline graphite was given in Fig. 1. The baked rods studied were petroleum coke laboratory-prepared samples with no component treated to a temperature higher than 1000°C. This is an important point to consider since commercial products contain particles which have been calcined to 1200–1300°C and consequently are mixtures of cokes treated to different temperatures (binder is baked only to 1000°C!). Unfortunately, the author has not investigated the complete series of curves for different intermediate treatments, and the measurements were performed only from room temperature up to 1100°C. For the latter reason, the remaining parts of the curves (*c*), (*d*), and (*e*) in Fig. 1 represent the probable trend of curves as can be expected on the basis of Powell's and Schofield's[19] curve for graphitized material and from the known temperatures at which the curves end (temperatures of heat treatment determine the general trend of curve *H*). We are in the process of preparing more extensive studies of such systems of curves for carbon rods and also for cokes at our laboratory. The upper part of Fig. 1 is given here only because these preliminary results for baked carbons deviate essentially from those of Powell and Schofield.

If the interpretation of the resistivity curves for graphitized materials suggested above is accepted, the character and shape of the system of curves in Fig. 1 can be easily understood. When the curve for a baked carbon is extrapolated beyond the line of treatment, it becomes evident that a minimum in resistivity would not be reached below 2000°C. Thus, from the position of the minimum, the estimated energy gap between the occupied and conduction bands is of the order of 0.2 ev or more. Studies of thermoelectric power performed recently at our laboratory by E. Loebner[20] show that the power at room temperature is negative and about equal for both baked and graphitized states.[21] Assuming the effective mass of carriers in the baked state to be $m \leq m_{\text{eff}} \leq m/6$ (see Sec. VII) a concentration of electrons 2×10^{-2} to 10^{-3} per atom is calculated from Loebner's results. On the other hand, at room temperature, the number of activated electrons for a gap 0.2 ev wide is about 1×10^{-7} and at 1000°C about 2.6×10^{-5}. It means that the conduction of baked carbons is due almost entirely to a constant number of excess electrons throughout the whole range for the curves (*a*) and (*b*) (Fig. 1).

It is seen then, that the decrease of the resistivity in curves (*a*) and (*b*) Fig. 1 is caused primarily by a decrease in scattering. These curves are essentially analogous to the low temperature part of the curve for polycrystalline graphite (below 150°K, Fig. 2). The dimensions of crystallites being smaller by a factor of more than 20, almost the whole resistance of the baked carbons is due to boundary scattering and contact resistances. Since the relative contributions of b and $c(T)$ are not known, the exact form of the function $c(T)$ cannot be estimated from the experimental data.

As mentioned before, different types of baked carbons show about the same resistivities when observed values are multiplied by the correction factors f_1, f_b, and f_θ. The individual differences are real, however, as can be seen from the slopes of the curves resistivity *vs* temperature. Hard carbons in the baked state show a steeper slope—the relative decrease becomes, for very hard carbons, as much as 25 percent (for soft carbons 22 percent, see Fig. 1).

Figure 3 gives the variation of the room temperature

[20] E. E. Loebner, Phys. Rev. **84**, 153 (1951).

[21] That it is negative for both states was found some time before by E. Man in our laboratory by rough experiments on the Hall effect.

resistivity of a carbon as a function of temperature of treatment. The part below 1100°C was obtained using raw cokes, and the part above 1000°C using commercial and laboratory carbon rods. The curves were fitted to overlap in the range 1000–1100°C. Three distinct regions are easily recognizable. The first is the region of the extremely rapid decrease from the raw state to a baked state. This occurs parallel to a strong evolution of gases and a considerable shrinkage of the material and is due to the transformation of the molecular solid, which is an intrinsic semiconductor with a large gap (see Sec. IV), into the baked carbon, which is an excess semiconductor with a high concentration of free electrons. The fast increase of the number of carriers is demonstrated by the strong drop of the thermoelectric power for samples treated from 700°C to 1000°C.[20] This transition occurs for all carbons (soft and hard) in the same temperature region; it will be further discussed in Sec. IV.

The second region is the flat plateau from about 1000°C to 2000°C. A very small change in resistivity is observed, although the size of crystallites (diameter) grows from about 25A up to almost 150A.[3] The expected decrease of the resistivity (scattering) due to growth of crystallites is compensated, however, by a decrease in concentration of the excess electrons. In fact, Loebner[20] found an increase of thermoelectric power in this range. The plateau is remarkable, since it occurs for most types of carbons. It extends to somewhat higher temperatures (by several hundred degrees) for hard carbons, which are more difficult to graphitize. The existence of the plateau is quite a general feature; in his experience the author has found only one type of carbon which showed a steady decrease of resistivity with increase of degree of graphitization. Also, once the author prepared a special carbon type which showed an increase of resistivity with increase of degree of graphitization (slightly rising plateau). These anomalous cases can be easily explained by variations in the mutual relation between the growth of crystallites and the concentration of excess electrons. The fact, however, that in most cases a good compensation of the two effects results in the formation of a plateau is remarkable in itself, and it seems compelling to look for a deeper meaning of this relationship. This question will be taken up again when the origin of the excess electrons is discussed.

The third region shown in Fig. 3 corresponds to the graphitization of samples. Here the microcrystalline size increases strongly with temperature of treatment. The drop in resistivity above 2000°C is due to a further decrease in boundary and contact scattering, and to the overbalancing of the continuing decrease in number of excess electrons (from about 2×10^{-2} or 1×10^{-3} in the baked state to $\sim8\times10^{-5}$ for 2900°C graphite samples) by the increase in activation of electrons from the lower band, since the energy gap decreases steadily with increase of crystallite size and for samples treated above

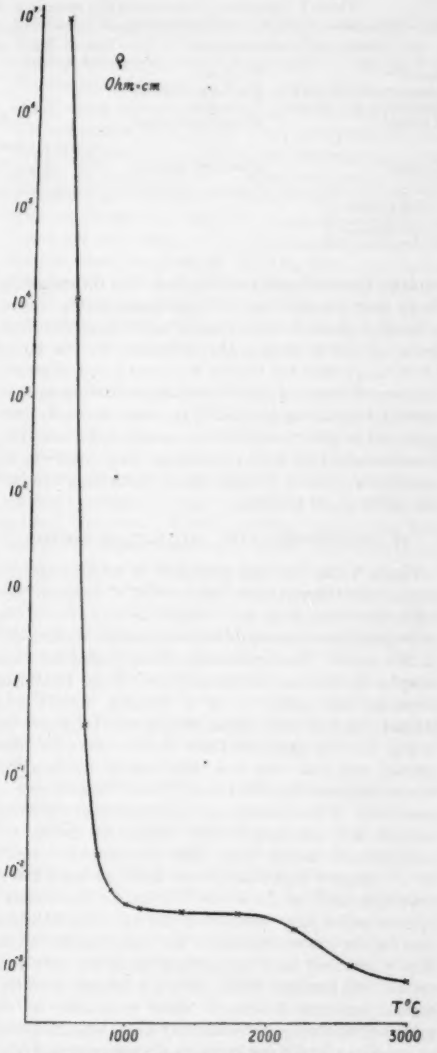

FIG. 3. Electric resistivity of a carbon at room temperature as function of the heat-treatment.

2000°C the width of the gap becomes so small that considerable activation occurs at room temperature. The total concentration of carriers in polycrystalline graphite ($\sim1.5\times10^{-4}$ for 2900°C sample) is smaller than in the baked state, but the effective masses of carriers are also smaller. The factor $(N/m)_{eff}$ comes out to be about 2–4 times smaller than for the baked state. This

TABLE I. Energy gap in condensed ring systems as obtained from temperature variation of resistivity in ev.

Temperature of treatment °C		300	350	425	500	520	450	630	690	700	715	800
Sandor[a]	Coal coke								0.144			0.042
Akamatu and Inokuchi[b]	8–9 rings 1.06–0.75											
Mizushima and Okada[c]	Pitch coke					0.2					0.06	
Kmetko[d]	Pyrolysed cellulose			0.80	0.62		0.41	0.22		0.09		0.03
		Energy gap from infrared absorption										
Kmetko[d]	Pyrolysed cellulose	1.2	0.9	0.7	0.5		0.35	0.25		0.2		

[a] See reference 22.
[b] See reference 23.
[c] See reference 16.
[d] See reference 24.

explains the previously puzzling fact, that the resistivity drops from the baked to the graphitized state, only by a factor of about 6, when the crystallite sizes differ by a factor of 20 or more. The difference in the factor $(N/m)_{eff}$ clarifies the matter and shows that, after all, the contribution of the boundary scattering and of contact resistances $[b+c(T)]$ is about inversely proportional to the crystallite size, as expected. Correcting the resistivities for lattice scattering $(a-\frac{1}{3}\cdot f)/(e-f)=7$ and multiplying by the ratio of $(N/m)_{eff}$ we get in fact the factor 21, as required.

IV. CONDENSED RING MOLECULAR SOLIDS

Figure 1 has not been extended to samples of coke treated to temperatures below 1000°C because raw cokes have very high resistivities (see Fig. 3) and the corresponding curves could not be conveniently included in this graph. The interesting characteristic of these samples is that as the temperature of the treatment decreases the curves ρ *vs* T become steeper and steeper; (in fact, many times steeper than the curve (*a*) in Fig. 1). The great steepness of the curves for compressed raw coal coke has been noticed by Sandor.[22] Sandor believed the effect to be due to the existence of some kind of nontransparent intermolecular potential barriers and calculated their height by fitting the experimental curves with the exponential formula $e^{\Delta E'/kT}$. Sandor found $\Delta E'$ to be 0.072 ev for a 690°C coke and 0.021 ev for a 800°C coke. In the author's opinion such a large variation on the $\Delta E'$ value indicates that Sandor's interpretation of the exponential relationship is incorrect since $\Delta E'$ cannot be in any way connected with barriers, which, after all, consist of contact regions between molecules. Some molecules, in the solidified substance, are bound by C−C valence bonds to neighbors and these contacts do not represent high barriers. In the rest of the contacts the carbon ring systems are separated by peripheral foreign atoms (H, N, O) and these are the opaque barriers partly responsible for the high resistance of this substance. The high resistance barriers are high, but narrow (~10A), and therefore have some transparency for the conduction electrons. The transparency of such barriers is proportional to the energy of the electrons, and its temperature dependence is overshadowed by the exponential variation. Furthermore, these barriers decrease in numbers but not in quality as the size of the condensed ring systems increases and therefore cannot be the cause of the variation of $\Delta E'$. If, however, it is assumed that condensed ring systems are intrinsic semiconductors with an energy gap $\Delta E(\Delta E=2\Delta E')$, then the experimental temperature variation can be understood as a variation in the number of activated carriers and represented by the factor $e^{\Delta E/2kT}$. Akamatu and Inokuchi[23] reached independently the same conclusion in interpreting their results on resistivities of violanthrone and pyranthrone powders under pressure. Their work is remarkable since the experiments were performed with substances of uniform molecular structure. The resistivity of condensed ring systems has been investigated recently also by Mizushima and Okada[16] and in our laboratory by Kmetko.[24] In all cases, the variation of the resistivity with temperature is approximately exponential and the ΔE values found by these authors are collected in Table I.*

Our interpretation has been directly confirmed by the work of Kmetko,[24] who has shown the existence of a close agreement between the ΔE values obtained from curves of the resistivity and from the position of the edge of a continuous absorption band in the infrared. Kmetko's infrared values are included for comparison in Table I.

As can be seen, the size of the energy gap decreases as the condensation process progresses. The interesting feature is the general agreement between different authors who worked with different original starting substances—and also the individual differences, which directly correlate with the degree to which these substances resist graphitization (hardness).

The ΔE values in Table I decrease as we go from raw cokes towards baked carbons. For samples treated above 600°C, however, the slope of the resistivity curves does not yield the real value of the energy gap, the slope

[22] J. Sandor, Proc. Conf. Ultrafine Structure of Coals and Cokes, London, 1944, p. 342.

[23] H. Akamatu and H. Inokuchi, J. Chem. Phys. **18**, 810 (1950).
[24] E. A. Kmetko, Phys. Rev. **82**, 456 (1951).

* *Note added in proof.*—Shortly H. Inokuchi investigated the resistivities of a number of aromatic substances, from 6 up to 10 ring systems, and found gaps ranging from 1.7 to 0.75 ev. [Bull. Chem. Soc. Japan **24**, 222 (1951)].

becoming smaller due to the presence of the increasing numbers of excess electrons. In fact, as mentioned before, Loebner[20] has shown that for samples treated to 700°C and higher the thermoelectric power becomes measurable and decreases strongly in absolute value as one proceeds toward the baked state. For samples treated 700°C or above, Kmetko[24] found an increasing continuous absorption all through the infrared which must be due also to the presence of increasing numbers of free electrons. For samples treated below 600°C, no excess electrons are present; the resistivity and infrared values vary in a parallel manner, the infrared values being lower since the absorption edge gives information about the smallest gaps and the resistivity about the largest ones in a mixture of molecules of different sizes.

The great drop in room temperature resistivity by a factor 2×10^9 (Fig. 3) from $10^7\Omega$ cm for raw cokes (500°C samples) to around $5\times10^{-2}\Omega$ cm for baked carbons (1000°C samples or higher) is to a great extent due to the increase in number of carriers. Raw cokes (treated below 600°C) are essentially intrinsic semiconductors with a very large energy gap; consequently, the number of activated electrons is very small; for instance, for a 0.6 ev gap, the number is of the order 10^{-9} per carbon atom at room temperature. Baked carbons, on the other hand, have, as calculated before, about 10^{-3} excess electron per carbon atom or more; thus, a change in resistivity by a factor 10^6 is explained by the variation in number of carriers. The rest of the variation in resistivity is undoubtedly due to a process of a gradual replacement of the high opaque intermolecular barriers by low resistance C—C contacts, which occurs at the time when the peripheral gases are driven out in baking.

V. THE ORIGIN OF EXCESS ELECTRONS

The great regularity with which the resistivity of organic substances drops over the range of coking from 500°C where they are practically insulators to about a 0.005Ω cm for baked carbons (1000°C) requires explanation. No matter what the impurities in the parent organic substance are, the drop occurs always at the same temperatures and leads to approximately the same resistivity (corrected for f_1, f_b, and f_s). This regularity forces us to look not to the impurities for a source of the free conduction electrons (excess electrons), but to the carbon itself. A clue to the origin of excess electrons is furnished by the results previously mentioned, which show that the excess electrons appear in great numbers at the time when most of the peripheral gases are driven out of the carbon. The molecular condensation process is not fast enough to take care of all the newly formed free valence bonds on the peripheries; furthermore, many molecules are not in favorable positions relative to their neighbors, so that a great number of free peripheral valence bonds are left without having anything to be attached to. Consequently, a strong valence adsorption and also a chemical activity would be expected for carbons and polycrystalline graphite. But this is not what is observed in experiments. The adsorption of carbons is mainly of molecular Van der Waals type. For instance, baked (calcined) carbon blacks show in adsorption a very small percentage of chemical bonds.[25] The adsorption of radon on graphite crystals is about uniform around the crystal; in catalysis the whole surface of microcrystals is equally effective without preference for the edges.[26] Calcined cokes and graphite resist oxidation very well. They are also remarkable in that there is no formation on their surface of any oxide films at room temperature. The free peripheral carbon valences do not seem to be present where they are expected; consequently the peripheral carbon atoms have changed their state into a different hybridized state which does not show the activity of an unsaturated valence.

Some information about the process of transformation into this new hybridized state is obtained from experiments of Savage and Brown.[27] They showed that graphite, ground up mechanically, has the power of attaching hydrogen and other gases by a chemical bond at the freshly created peripheries along the broken surface. The power is lost after the carbon has been heated to temperatures above 800°C. The author had similar experiences with the oxidation of ground carbons. Evidently there is some activation energy necessary to induce the transition from the regular state with three valence bonds in a plane into this new hybridized state, which seems to be the more stable of the two. When gases are driven out in the baking (calcining) process, the temperature is sufficient to form this more stable state right from the start, and therefore no chemical activity in the calcined or graphitized carbon is detectable at room temperature.

It is suggested here that the carbon atoms in this new state are the source of the excess electrons. The formation of the excess electrons can be pictured as follows: when the atom attached to the peripheral carbon is removed, the energy of the electron taking part in the bond is raised. When tied in a bond the electron belongs to the energy band of the planar valence electrons of graphite; when, however, the valence becomes free, the electron is lifted above the filled band of the resonance electrons to a level higher in energy than the bottom of the conduction band. From this state the electron jumps into the conduction band, if the activation energy necessary to change the state of the atom happens to be supplied by the heat vibrations. In the bottom of the conduction band, the electron is almost free; a very small amount ϵ of kinetic energy will suffice to tear it away from the positive ion left behind. Consequently, this electron will, at very low temperature, be bound in

[25] Beebe, Biscoe, Smith, and Wendell, J. Am. Chem. Soc. **69**, 95 (1947) and **72**, 40 (1950).
[26] U. Hofmann and W. Hoper, Naturwiss. **32**, 225 (1944).
[27] R. H. Savage and C. Brown, J. Am. Chem. Soc. **70**, 2362 (1948).

some sort of a surface state with a very low energy of activation ϵ. It seems possible, then, that the existence of this activation energy ϵ is responsible for the strong variation of conductivity of carbons observed at very low temperatures.[28]

Thermoelectric studies of carbons[20] have shown that the concentration of excess electrons decreases for cokes treated above 1400° with increasing temperature. This decrease could well be the result of a gradual driving out of impurities by heating; these impurities might be supplying some excess electrons present in addition to the carbon's own sources. If this decrease in the number of excess electrons should be caused by a foreign matter, it would be difficult to understand why the formation of the plateau, Fig. 3, for most of the reasonably pure carbons (not too impure), is such a regular occurrence. It seems very improbable that in all these varieties of carbons investigated a definite concentration of a certain impurity was present. Furthermore, it was estimated from the thermoelectric power of carbon that the concentration of the excess electrons is about $10^{-2}-10^{-3}$ per atom. If there are that many excess electrons due to the peripheral carbon atoms, large amounts of impurities would be necessary to change definitely the general trend of correlations. (On the other hand, the properties of polycrystalline graphite should be much more sensitive to impurities, since this substance possesses a much lower concentration of excess electrons.) It seems attractive to the author to ascribe the existence of the resistivity plateau to processes occurring in the carbon itself, and to blame impurities for smaller deviations from the general relationship and for the few anomalous cases observed.

As discussed above, the excess electrons present in pure carbons are due to those peripheral atoms which happen not to be bonded to neighboring crystallites. The proportion of the nonbonded peripheral atoms to the total number of atoms in a crystallite will certainly decrease with the growth of crystallites. Let it be assumed that the nonbonded ones constitute a certain constant proportion of all peripheral atoms. The concentration of excess electrons will then be inversely proportional to the linear dimensions of crystallites. On the other hand, the contribution of the contact resistances between crystallites to the total scattering will also be about inversely proportional to the dimension of crystallites—thus there will be a cancellation of the two factors and a resistivity independent of size of crystallites will be obtained. On the other hand, if the proportion of nonbonded to bonded peripheral atoms increases with the size of crystallites, then the concentration of excess electrons will decrease less with increase of crystallite size, but the contribution of the contact resistances will also be larger for large sizes (less intercrystalline bondings), so that, again, a resistivity plateau will be obtained. Thus, the general occurrence of the plateau can be understood irrespective of the variations in the polycrystalline structure of carbons.

The quantitative agreement is not unreasonable. Loebner's data give about 1.35 for relative change in number of excess electrons for samples heated to 1400°C and 2200°C. Pinnick's x-ray crystallite size determination[29] for the same carbons gives an increase by a factor 2.6 for the diameter in the direction of the graphite plane. When one considers the presence of activated electrons from the lower band in the 2200°C carbon, the disagreement of the two numbers does not seem to be serious, especially if one notices that 2200°C is located already beyond the end of the resistivity plateau and that in the evaluation of thermoelectric data, the variation of the effective mass of carriers has been neglected.

VI. THE NATURE OF THE ENERGY GAP

Wallace[9] has expressed the opinion that the existence of the zero energy gap between the filled and empty bands is presumably a consequence of the symmetry of the graphite lattice and is independent of the approximations considered. If so, the energy gap should not be different from zero for crystals of finite dimensions unless a deviation from hexagonal symmetry is introduced into the system of benzene-rings by peripheral tensions, or some other reasons. Since the electronic energy rises linearly at the corners of the hexagonal Brillouin zone, there will be a tendency for a crystal of finite dimensions to change its shape so as to round off the sharp energy peaks in the Brillouin zone corners, the decrease in the electron energy being used up to distort the benzene-rings system. Thus a finite energy gap would be formed as observed experimentally in polycrystalline graphite.[30]

It is hard to understand how the molecular planes can be sufficiently distorted as to acquire such large energy gaps as observed. It seems that these gaps are real energy gaps at the Brillouin zone boundaries and not merely manifestations of the discontinuity in molecular electronic energy levels. The calculated distances of levels, assuming a free electron plane box model, are at least by one order of magnitude too small for that. Moreover, in polymerized substances like carbons the electronic levels are broadened by bonding of molecules to their neighbors and coupling of their vibrations to such an extent that the discrete structure inside the bands becomes wiped out. Thus the continuous appearance of the infrared and visible absorption is probably real and not simulated by a dispersion in molecular sizes. Bonding of molecules to the neighbors brings distortions in the system. The differential shrinkage in cooling[11] leads to existence of large strains inside of polycrystalline graphite. It seems probable that these strains affect the size of the gap and are responsible for

[28] Giauque, Stout, and Clark, J. Am. Chem. Soc. **60**, 1053 (1938).

[29] H. T. Pinnick, unpublished results.

[30] The author is indebted to Dr. G. H. Wannier of the Bell Telephone Laboratories for pointing out to him this possible explanation.

the slow decrease in the size of the gap from the baked to the graphitized state. Single crystallites of graphite, or crystallites less strained, as, for instance, in graphitized carbon blacks, might have considerably smaller energy gaps.

In studying the ultraviolet spectra of unsaturated hydrocarbon chains, Kuhn[31] reached the conclusion that the lowest electronic absorption frequency in the spectrum can be represented by an empirical relation which definitely points toward the existence of an energy gap at the Brillouin zone boundary of an order 2 ev for molecules 15 carbon atoms long. Kuhn has proposed an explanation based on the assumption that the presence of the free ends of the molecule stabilizes preferentially one of the resonating structures, thus introducing a double periodicity into the lattice and breaking the series of electronic levels into distinct groups (or bands). It seems doubtful that a variation in bond length, large enough to give an energy gap of the size 1–2 ev, is really present in such molecules.[32] Kuhn's explanation, however, is very interesting, to say the least, especially in light of the recently detected deviations of the graphite lattice from hexagonal symmetry, deviations which according to Hoerni and Weigle[33] possess a double periodicity along the carbon chains (direction of motion for zero energy gap in graphite). These deviations might be in some way related to the finite size of the energy gap in polycrystalline graphites; it is felt, however, that the whole problem at the present stage requires a thorough theoretical clarification.

VII. DIAMAGNETIC ANISOTROPY[34]

The existence of the energy gap and the presence of excess electrons are factors which have to be taken into consideration when an explanation of the diamagnetic properties of large aromatic systems is attempted. Pauling[35] was the first to realize that in order to reconcile the values of the anisotropic component found for susceptibilities of benzene and other small aromatic molecules on the one hand and for graphite on the other, some new assumptions have to be made about the motion of resonance electrons. He proposed a semiclassical theory of induced currents in the benzene-ring network which leads to a very rapid increase in the anisotropic component with the size of the molecule. The value corresponding to graphite is reached according to Pauling for molecular diameters of about 40A. The increase is definitely too rapid: already for pyrene (4 benzene rings) Pauling's theory gives a value larger than experimental by 60 percent. The susceptibility found in experiments for baked carbons with molecular diameters about 40A represents only a small fraction of the susceptibility of the large graphite crystals. Grinding the graphite crystals to a size below 1 micron decreases measurably the susceptibility.[36] In a study of carbons of different origin Miwa[37] has shown that, very roughly, the susceptibility increases linearly with the molecular size and rises to about 30 percent of the graphite value for crystallite planes of about 200A diameter (70A thickness). Even for polycrystalline graphite, the susceptibility is still considerably below the limiting value.

The large graphite susceptibility does not seem to be due to an effect present in smaller aromatic systems. Examination of experimental data obtained for small aromatic molecules[38] shows that the molar anisotropic component of susceptibility is proportional to the number of rings in the systems. Quantum-mechanical calculations of London[39] and Brooks[40] performed for a few of the simplest molecules are in rough agreement with the experimental data.[41] The molar anisotropic component for benzene is $\Delta\chi_B = -54\times10^{-6}$ and for the other molecules roughly a multiple of this, with small deviations probably due to the specific molecular ring arrangement. Extrapolating this to larger aromatic molecules, it is expected therefore that aromatic molecules have, in general, molar susceptibilities $\Delta\chi \cong n\cdot\Delta\chi_B$ where n is the number of benzene-rings. This result seems to be a natural consequence of the fact that the resonance electrons form closed shells in aromatic molecules and fill exactly a Brillouin zone. For a full Brillouin zone the diamagnetism should be proportional to the molecular volume, that is, to the number of benzene-rings.†

This closed shell diamagnetism of London type is not the main cause of the large diamagnetism of graphite. The anisotropic component of susceptibility for a graphite crystal is -30×10^{-6} per gram, that is -720×10^{-6} per benzene-ring mole; this is about 13.5 times larger than the diamagnetism of the closed shell of resonance electrons. Per gram atom the susceptibility of graphite (-360×10^{-6}) is even superior to the susceptibility of bismuth (-315×10^{-6}). Ganguli and Krishnan[42] have studied the temperature dependence of the susceptibility of graphite and attempted to explain it by assuming that the resonance electrons form a free two-dimensional electronic gas. The general theoretical formulas for the Landau diamagnetism of free electrons, as developed by Stoner, have been adapted by

[31] H. Kuhn, J. Chem. Phys. **17**, 1198 (1949). See also, J. R. Platt, J. Chem. Phys. **17**, 484 (1949).
[32] C. A. Coulson, Proc. Roy. Soc. (London) **A169**, 413 (1939).
[33] J. Hoerni and J. Weigle, Nature **164**, 1088 (1949). See also J. S. Lukesh, Phys. Rev. **80**, 226 (1950).
[34] See the preliminary note: S. Mrozowski, Phys. Rev. **80**, 123 (1950).
[35] L. Pauling, J. Chem. Phys. **4**, 673 (1935).
[36] C. H. Gregory, thesis, California Institute of Technology (1935); J. R. Rao, Indian J. Phys. **6**, 241 (1931).
[37] M. Miwa, Science Report, Tohoku University **23**, 242 (1934).
[38] K. Lonsdale, Proc. Roy. Soc. (London) **159**, 149 (1937).
[39] F. London, J. phys. et radium **8**, 397 (1937).
[40] H. Brooks, J. Chem. Phys. **8**, 939 (1940) and **9**, 463 (1941).
[41] See also R. McWeeny, Proc. Phys. Soc. (London) **64**, 261 (1951).
† *Note added in proof:*—Recently ovalene (10 compact rings) has been found to have a magnetic anisotropy of -616×10^{-6} by Akamatu, Inokuchi, and Handa [Nature **168**, 520 (1951)].
[42] W. Ganguli and K. S. Krishnan, Proc. Roy. Soc. (London) **117**, 168 (1941).

them to the case of an existence of a crystalline field with the energy surfaces $E=(h^2/2m)(\alpha_1 k_x^2+\alpha_2 k_y^2+\alpha_3 k_z^2)$. The formulas lead to a perfect agreement with experiments, when it is assumed that $N_{eff}\alpha_1\alpha_2=1$; furthermore, by fitting the theoretical curve to the experimental results a very low degeneracy temperature of 520°K is obtained. The remarkably good agreement between the experimental and the theoretical curves makes it difficult to believe the agreement to be fortuitous. On the other hand, Ganguli and Krishnan's theory is unacceptable since, for instance, it leads to a large electronic specific heat of the order of 2 kcal/mole! Ganguli and Krishnan were not aware of the decrease in the density of electronic levels to zero at the Brillouin zone boundary between the occupied and empty bands; they treated the electronic gas as in a metal and assumed all resonance electrons to be effective.

It appears, however, that by a reinterpretation of the constants in the Ganguli-Krishnan theory, a reasonable picture of the diamagnetism of graphite can be obtained. This diamagnetism is due to the Landau diamagnetism of holes in the lower band and electrons in the conduction band. The effective number of electrons and holes is small ($N_{eff}\sim 10^{-2}$) and their effective mass for the motion in the direction of the graphite plane also small. From the Ganguli-Krishnan relation $N_{eff}\alpha_1\alpha_2=1$ obtained by fitting their high temperature data with theoretical formula, the effective mass is $m_{11}=m/\alpha_1=m/\alpha_2=m/30$ of the order required by Wallace's[9] calculations. The degeneracy temperature is low since the electrons and holes have approximately Maxwellian velocity distributions. From the second Ganguli-Krishnan relation $\alpha_3 N_{eff}=\alpha_1\alpha_2\alpha_3 N_{eff}^2=(1/190)^2$ obtained by fitting their low temperature data with theoretical formula, taking for low temperatures $N_{eff}\sim 10^{-4}$, it is found $1/\alpha_3\cong 700$, that is, a mass about 25 times larger for the motion across the graphite planes than obtained by Wallace, but this is just what is expected, since Wallace's calculations yield a too high conductivity across the planes. The remaining other difficulties of the Ganguli-Krishnan theory are also removed; in the modified model the electronic specific heat is small (about 100 times smaller) and the free electron paramagnetism is also negligible in comparison to the diamagnetism ($3/\alpha_1\alpha_2\cong 1/300$).

In this modified Ganguli-Krishnan theory the numbers N_{eff} and α_1, α_2 are functions of temperature; it so happens, however, that the relation $N_{eff}\alpha_1\alpha_2=1$ is independent of temperature since $N_{eff}\sim(kT)^2$ and $1/m_{11}\sim\alpha_1=\alpha_2\sim(kT)$. (See Wallace[9]). The cancellation of the temperature dependence is the direct reason for the excellent agreement of the Ganguli-Krishnan theoretical curve with experimental data over the whole range of temperatures. The theory as given by Ganguli and Krishnan and modified here is certainly not sufficiently refined to give anything but a rough description of the effects, especially in view of the use of the ellipsoidal expression for the energy surfaces.

In order to explain the decrease of the diamagnetism with crystallite size, it is necessary to assume that the effective masses of carriers increase as the size of the crystallites decreases. This might be caused by the increase in the concentration of excess electrons (shift of the Fermi level) or the rounding off of Brillouin zone corners, or both. For crystals of finite size formation of the finite energy gap and rounding off of the Brillouin zone energy peaks (corners) will bring about a decrease in the curvature of the energy surfaces (decrease in α_1 and α_2) near the zone corners. Similarly, the presence of an excess of electrons or holes will shift the position of the Fermi level into regions of smaller curvature of the energy surfaces. The Landau diamagnetism being proportional to $N_{eff}\alpha_1\alpha_2$, we see by substituting $N_{eff}=10^{-2}$ for the baked state, that a decrease of the susceptibility by a factor 10 to 20 in comparison to graphite (as required by Miwa's[37] results) leads to effective masses $m_{eff}\cong m/2$ to $m/3$ in crystallites of about 30A diameter. On top of the Landau diamagnetism, there is the diamagnetism of the full band (shell) of resonance electrons present, which is a function of the molecular size: 2.2×10^{-6} for graphite, decreasing to 0.245×10^{-6} per gram for a pure disordered benzene ring polymer.

It is felt that at this time it is more important to gather some additional data on susceptibilities of carbons under different conditions than to try to develop the theory further. We are now in our laboratory preparing to investigate some well-defined carbon and graphite samples.

CONCLUSION

In the process of developing a consistent picture of electronic processes in carbonized substances up to graphite it was shown above that the experiments lead us to assume (1) the existence of a finite energy gap between the occupied and empty bands, and (2) the presence of excess electrons due to peripheral carbon atoms with free, unattached valencies. Both these assumptions, as well as the proposed theory of the diamagnetic susceptibility of carbons and graphite require a thorough, theoretical study. Further experimental verifications beyond those reported in this paper are in process of preparation at our laboratory.

It should be pointed out here that considerations presented in this paper can be further extended and applied to carbon systems which have undergone deformations or atomic displacements. The transformation of a free valence electron into an excess conducting electron being connected with an energy of activation and with a dissipation of the energy difference might be a factor which should be taken into consideration in thermochemical studies when properties of carbons with strongly differing crystallite sizes are compared.

The author is greatly indebted to Professors C. A. Coulson (London) and W. Opechowski (Vancouver) for illuminating correspondence.

Multiple Scattering of Waves. II. The Effective Field in Dense Systems*

MELVIN LAX
Physics Department, Syracuse University, Syracuse, New York
(Received October 30, 1951)

The multiple scattering of waves interacting with a system of particles is treated by a self-consistent approach. Scattering processes are described by operators that permit anisotropy, absorption, and creation. The scattering system may be randomly, partially, or completely ordered.

The propagation constant k' of the coherent wave in the scatterer medium differs from the vacuum constant k by $(k')^2=k^2+4\pi nc f(\mathbf{k}',\mathbf{k}')$, where n is the scatterer density and f is an operator whose matrix elements $f(\mathbf{b},\mathbf{a})$ represent the scattering amplitude in direction $\mathbf{b}$ for a wave incident in direction $\mathbf{a}$ on a single scatterer bound by the forces of its neighbors. The parameter c, defined by $cf(\mathbf{k}',\mathbf{k}')=\int \exp(-i\mathbf{k}'\cdot\mathbf{r})f\times\psi_s(\mathbf{r})d\mathbf{r}$, is a measure of the ratio of the effective field $\psi_s(\mathbf{r})$ to the average field.

An integral equation is found for $\psi_s(\mathbf{r})$ with the help of a "quasi-crystalline" approximation. A variational expression is then found for c that becomes exact for point scatterers.

A comparison is made of finite and infinite scattering systems. The extinction theorem is proven. The macroscopic viewpoint is found to be applicable to small systems whose size is large compared to the scatterer potential range, and the range of scatterer position correlations.

I. INTRODUCTION

EWALD[1] in 1916 developed a fairly complete theory of optical dispersion in crystals based on the multiple scattering of light by atoms acting as induced dipoles. Foldy[2] has applied a similar self-consistent scattering calculation to obtain the index of refraction for scalar waves travelling in a medium of randomly distributed, isotropic scatterers. The author[3] in 1949 generalized the self-consistent procedure to include (1) anisotropic scattering in addition to the monopole and dipole cases, (2) inelastic scattering, including the creation and absorption of particles, and (3) scattering systems that are randomly, partially, or completely ordered.

The results obtained by the self-consistent procedure were an equation for the total (coherent) wave in terms of the effective field with one particle held fixed, an equation for the effective field with one particle fixed in terms of the field with two particles fixed, etc. A solution of these equations by an iteration procedure using the incident wave as starting function would lead to an expansion in waves that were singly scattered, doubly scattered, triply scattered, etc. Such a procedure is poorly converging because it assumes that the effective field is similar to the incident wave, whereas it has the propagation constant of the total wave.

The author therefore suggested a procedure similar to that of Lorentz—assuming that the effective field (with one scatterer fixed) bears a simple relation to the total field—for point scatterers a proportionality constant is sufficient. In this way, the first of the set of equations described can be used to obtain an equation for the index of refraction. The succeeding equations must then be used to obtain the relationship between the effective and the coherent fields.

The equation obtained by the author for the index of refraction, containing as it does, the unknown relation between the effective and coherent fields has been criticized[4] as an "approximation." This is by no means the case. The determination of the effective field was merely considered to be a problem of sufficient intricacy to warrant separate discussion.

We intend to show in this paper that a good approximation can be obtained for the effective field by using the second in the set of equations mentioned. Additional accuracy can, of course, be obtained by using the third equation, and then higher order equations. We have decided to publish results at this point, using only two equations, because the accuracy involved is equivalent to the use of the Lorentz-Lorenz formula for nonpolar liquids. A detailed treatment of the electrostatic problem using a self-consistent procedure by Brown[5] indicates (in addition to the experimental evidence), that the corrections to the Lorentz-Lorenz formula in nonpolar liquids are small.

II. FORMULATION

In previous work[3] (see I-3.7 and I-3.8) it was shown that a self-consistent description of the total field $\psi(\mathbf{r};\mathbf{1},\mathbf{2},\cdots\mathbf{N})$ and the i effective field $\psi^i(\mathbf{r};\mathbf{1}\cdots\mathbf{N})$ could be given by the equations

$$\psi(\mathbf{r})=\phi(\mathbf{r})+\textstyle\sum_s(E-H)^{-1}T(\mathbf{s})\psi^s(\mathbf{r}), \qquad (2.1)$$

$$\psi^i(\mathbf{r})=\phi(\mathbf{r})+\textstyle\sum_{s\neq i}(E-H)^{-1}T(\mathbf{s})\psi^s(r), \qquad (2.2)$$

where the symbols $\mathbf{1},\mathbf{2},\cdots\mathbf{i},\mathbf{j},\mathbf{s}\cdots\mathbf{N}$ refer to the positions of the scatterers (which are omitted for simplicity in ψ and ψ^i). The energy and Hamiltonian of the wave are E and H. The transition operator[6] $T(\mathbf{s})$

* This work supported in part by the ONR.
[1] P. P. Ewald, Ann. Physik **49**, 1, 117 (1916).
[2] L. L. Foldy, Phys. Rev. **67**, 107 (1945).
[3] M. Lax, Phys. Rev. **77**, 756 (1950). For a detailed account see Revs. Modern Phys. **23**, October (1951) hereafter referred to as I.
[4] H. Ekstein, *Multiple Elastic Scattering and Radiation Damping II*, ONR report, Armour Research Foundation, Chicago; see also Phys. Rev. **83**, 721 (1951).
[5] W. F. Brown, J. Chem. Phys. **18**, 1193, 1206 (1950).
[6] For properties of the transition operator T see I or M. Lax, Phys. Rev. **78**, 306 (1950). A detailed discussion is given by B. A. Lippmann and J. Schwinger, Phys. Rev. **79**, 469 (1951).

describes the scattering produced when the wave interacts with a single scatterer at **s**. (Strictly speaking, the scatterer is not fixed at **s** but merely bound by the forces exerted by other particles in the system. This point will be established in paper III of this series.)

In principle, one should solve Eqs. (2.1) and (2.2) for a fixed set of scatterer positions and then average $\psi(\mathbf{r};\mathbf{1},\cdots\mathbf{N})$ against the quantum-mechanical distribution of scatterer positions. The resulting average $\langle\psi(\mathbf{r})\rangle$ will be the coherent wave. Such a procedure is analogous to the Born-Oppenheimer calculation of electron wave functions in molecules: the wave functions are calculated for fixed nuclear configurations; then the nuclei are allowed to move.

The solution of Eqs. (1) and (2) for an arbitrary, fixed set of scatterer positions is quite difficult unless one is willing to resort to iteration methods. Instead, we can follow Foldy's[2] procedure of averaging first and then solving. Using the methods of I-Secs. IV and V, the averages of (1) and (2) are:

$$\langle\psi(\mathbf{r})\rangle=(E-H)^{-1}\int n(\mathbf{s})d\mathbf{s}T(\mathbf{s})\langle\psi^s(\mathbf{r})\rangle_s, \tag{2.3}$$

$$\langle\psi^j(\mathbf{r})\rangle_j=(E-H)^{-1}\int n(\mathbf{j}|\mathbf{s})d\mathbf{s}T(\mathbf{s})\langle\psi^s(\mathbf{r})\rangle_{sj}, \tag{2.4}$$

$$\langle\psi^{ij}(\mathbf{r})\rangle_{ji}=(E-H)^{-1}\int n(\mathbf{ji}|\mathbf{s})d\mathbf{s}T(\mathbf{s})\langle\psi^s(\mathbf{r})\rangle_{sji}. \tag{2.5}$$

Subscripts denote variables held fixed in a given averaging process. Particle variables have been suppressed when their presence is obvious. For example, $\langle\psi^s(\mathbf{r})\rangle_s$, the effective field holding particle s fixed, clearly depends on the position of that particle and should be written in full $\langle\psi^s(\mathbf{r};\mathbf{s})\rangle_s$.

The incident wave $\phi(\mathbf{r})$ has been omitted from Eqs. (3)–(5). This is permissible for infinite systems. A discussion of this point and of finite systems will be presented in Sec. VI. The density of scatterers at s is given by $n(\mathbf{s})$ if no information is available, by $n(\mathbf{j}|\mathbf{s})$ if a scatterer is known to be at **j**, and by $n(\mathbf{ji}|\mathbf{s})$ if scatterers are known to be at **j** and **i**. For a set of fixed scatterers, e.g., a crystal, these density functions are given by

$$n(\mathbf{s})=\sum\delta(\mathbf{s}-\mathbf{s}^0), \tag{2.6}$$

$$n(\mathbf{j}|\mathbf{s})=-\delta(\mathbf{s}-\mathbf{j})+\sum\delta(\mathbf{s}-\mathbf{s}^0), \tag{2.7}$$

and for a liquid they are averages of thes eexpressions with symbols to the left of the vertical bar held fixed. For a liquid $n(\mathbf{s})=n=a$ constant and

$$w(\mathbf{s})=n(0|\mathbf{s})/n \tag{2.8}$$

is the usual pair correlation function normalized to unity at large distances.

In the crystalline case, Eqs. (3) and (4) constitute a complete description of the problem since no additional information can be gained by holding additional particles fixed. Thus for any fixed set of scatterers, $\langle\psi^s\rangle_s$ does not differ from $\langle\psi^s\rangle_s$ so that (4) involves only effective fields of a single type. Thus no approximations are required to treat the crystalline case.

In the case of a liquid or gas, the field on the right-hand side (RHS) of any equation has one more particle held fixed than the left-hand side (LHS). A suitable approximate procedure is then to take one such equation and modify the RHS by dropping an index on one field variable. The solution of this equation, with the help of the preceding equations in the series, can be used to determine the index of refraction. The accuracy of such a procedure will depend on the equation chosen. If the Nth equation were used, where all particles are held fixed, then no approximation is involved whatever.

III. THE INDEX OF REFRACTION

In this section, an equation for the index of refraction will be developed starting from (2.3) without the use of any approximations. Instead, we shall make use of the general properties of the transition operator and the various fields under displacements.

The operator $T(\mathbf{s})$ differs from the corresponding operator $T(0)$ for a scatterer at the origin by a displacement transformation of the usual form:

$$T(\mathbf{s})=\exp(-i\mathbf{p}\cdot\mathbf{s})T(0)\exp(i\mathbf{p}\cdot\mathbf{s}), \tag{3.1}$$

where $\mathbf{p}=-i\nabla$ is the momentum operator in units $\hbar=1$. The corresponding statement in matrix rotation

$$T_{ba}(\mathbf{s})=\exp[i(\mathbf{a}-\mathbf{b})\cdot\mathbf{s}]T_{ba}(0) \tag{3.2}$$

was established in Eq. I-(3.4), where **a** and **b** are the initial and final propagation constants previously written $\mathbf{k}_a$ and $\mathbf{k}_b$.

In a manner similar to that used in deriving the properties of Bloch waves in crystals, it can be shown that $\psi(\mathbf{r};\mathbf{1},\cdots\mathbf{N})$ and $\psi^s(\mathbf{r};\mathbf{1},\cdots\mathbf{N})$ are multiplied by a factor $\exp(i\mathbf{k}'\cdot\mathbf{d})$ if all the variables **r**, **1**, $\cdots$**N** are subject to the same displacement **d**. For a liquid, **d** is an arbitrary displacement; for an ideal crystal, **d** is a lattice displacement. It follows from these general considerations that

$$\begin{aligned}\exp(i\mathbf{p}\cdot\mathbf{s})\langle\psi^s(\mathbf{r};\mathbf{s})\rangle_s&=\langle\psi^s(\mathbf{r}+\mathbf{s};\mathbf{s})\rangle_s\\&=\exp(i\mathbf{k}'\cdot\mathbf{s})\langle\psi^s(\mathbf{r};0)\rangle_s.\end{aligned} \tag{3.3}$$

The propagation constant k' is, as yet, unknown. The use of these translational properties, however, permits (2.3) to be rewritten in the simpler form:

$$\begin{aligned}\langle\psi(\mathbf{r})\rangle&=[E-H(\mathbf{p})]^{-1}DT(0)\psi_s(\mathbf{r}),\\D&=\int n(\mathbf{s})d\mathbf{s}\exp[i(\mathbf{k}'-\mathbf{p})\cdot\mathbf{s}],\end{aligned} \tag{3.4}$$

where we abbreviated the effective field $\langle\psi^s(\mathbf{r};0)\rangle_s$ by $\psi_s(\mathbf{r})$.

The matrix elements of D in the liquid case are then given by

$$D_{ba}=n\delta(\mathbf{b},\mathbf{a})\delta(\mathbf{k}',\mathbf{a}), \tag{3.7}$$

where $\delta(\mathbf{b}, \mathbf{a})$ is a Kronecker delta that equals unity when $\mathbf{b}=\mathbf{a}$, and zero otherwise. In the crystalline, use must be made of the periodic density (2.6) and

$$D_{\mathbf{bc}}=n\delta(\mathbf{b}, \mathbf{a})\sum_K \delta(\mathbf{k}'+\mathbf{K}, \mathbf{a})F(\mathbf{K})/Z, \quad (3.8)$$

where the $\mathbf{K}$ are the reciprocal lattice vectors, Z is the number of particles per unit cell, and $F(\mathbf{K})$ is the cell structure factor:

$$F(\mathbf{K})=\sum_{i \text{ in cell}} \exp[i\mathbf{K}\cdot(\mathbf{j}-\mathbf{i})] \quad (3.9)$$

taken relative to a particular atom i in the cell. The average of $F(\mathbf{K})$ over the positions i in the cell is given by

$$\langle F(\mathbf{K})\rangle=|F(\mathbf{K})|^2/Z. \quad (3.10)$$

The total or coherent wave is given by

$$\psi(\mathbf{r})=\sum_b \phi_b(\mathbf{r})(\phi_b(\mathbf{r}), \psi(\mathbf{r})), \quad (3.11)$$

where the $\phi_b(r)=\exp(i\mathbf{b}\cdot\mathbf{r})$ constitute a set of plane waves normalized in a box of unit volume. For the liquid and crystalline cases, respectively, we obtain:

$$\langle\psi(\mathbf{r})\rangle=[E-H(\mathbf{k}')]^{-1}U(\mathbf{k}', \mathbf{k}')\exp(i\mathbf{k}'\cdot\mathbf{r}), \quad (3.12)$$

$$\psi(\mathbf{r})=\sum_K \frac{U(\mathbf{k}'+\mathbf{K}, \mathbf{k}')}{E-H(\mathbf{k}'+\mathbf{K})}\left|\frac{F(\mathbf{K})}{Z}\right|^2 e^{i(\mathbf{k}'+\mathbf{K})\cdot\mathbf{r}}, \quad (3.13)$$

where

$$U(\mathbf{b}, \mathbf{k}')=n(\phi_b(\mathbf{r}), T(0)\psi_e(\mathbf{r})). \quad (3.14)$$

In the crystalline case, no averaging symbol should be used since no average has been taken.

Thus we have established that for the liquid, the coherent wave is a plane wave, and in the crystal a plane wave plus plane waves in all the possible Bragg reflection directions. In fact, (3.13) has the Bloch form of a plane wave $\exp(i\mathbf{k}'\cdot\mathbf{r})$ times a function with the crystal periodicity. If the periodic factor is replaced by its space average, i.e., $\mathbf{K}=0$ part, we obtain the macroscopically observable part of the solution. Since $F(0)=Z$, the macroscopic average of (3.13) is identical in form to (3.12). Therefore, the macroscopic average coherent field can for both the crystalline and liquid cases be denoted, without ambiguity, by the same symbol $\langle\psi(\mathbf{r})\rangle$. In both cases, then, $\langle\psi(\mathbf{r})\rangle$ is obtained by replacing $n(\mathbf{s})$ by a constant in (3.4).

Since Eqs. (2.3)–(2.6) are homogeneous, the normalization of $\langle\psi(\mathbf{r})\rangle$ can be chosen at our convenience to be:

$$\langle\psi(\mathbf{r})\rangle=\exp(i\mathbf{k}'\cdot\mathbf{r}) \quad (3.15)$$

for both liquid and crystalline cases. With this choice of normalization the index of refraction in both cases is given by

$$H(\mathbf{k}')=E-U(\mathbf{k}', \mathbf{k}'). \quad (3.16)$$

If in (3.14) the effective field $\psi_e(\mathbf{r})$ is replaced by the plane wave $\langle\psi(\mathbf{r})\rangle$, then we obtain $U(\mathbf{k}', \mathbf{k}')=nT_{k'k'}$ and the elementary result that the index of refraction is determined by the forward scattered amplitude. Deviations from this result depend on the extent to which the effective field differs from the macroscopic average field and can be referred to as effective field corrections. The author has previously suggested[3] that these corrections be taken into account by using the formula:

$$H(\mathbf{k}')=E-ncT_{k'k'}, \quad (3.17)$$

where c is a measure of the ratio of the effective field $\psi_e(\mathbf{r})$ to the average field $\langle\psi(\mathbf{r})\rangle$.

For point isotropic scatterers, the matrix element $U(k', k')$ depends only on the value of $\psi_e(\mathbf{r})$ at the origin, so that c can be interpreted as $\psi_e(0)/\langle\psi(0)\rangle$. For point dipole scatterers $c=\nabla\psi_e(0)/\nabla\langle\psi(0)\rangle$. For non-point scatterers, the matrix (3.14) depends on the properties of $\psi_e(\mathbf{r})$ over a region. The correctly weighted ratio of effective to average fields is in all cases $c=U(\mathbf{k}', \mathbf{k}')/(nT_{k'k'})$ or:

$$c=(\phi_{k'}, T\psi_e)/(\phi_{k'}, T\langle\psi\rangle). \quad (3.18)$$

For Schrödinger type waves, $E=(\hbar k)^2/(2m)$ and $H(k')=(\hbar k')^2/(2m)$, so that (3.17) can be rewritten in the form:

$$(k')^2=k^2+4\pi ncf(\mathbf{k}', \mathbf{k}'), \quad (3.19)$$

where $f(\mathbf{b}, \mathbf{a})$ is the scattering amplitude in direction $\mathbf{b}$ for a wave $\mathbf{a}$ incident on a bound single scatterer. The scattering amplitude operator is proportional to the transition operator and may be defined by:[3]

$$f=-2\pi mT/h^2. \quad (3.20)$$

IV. THE QUASI-CRYSTALLINE APPROXIMATION

In the preceding section, the calculation of the index of refraction was reduced to a determination of the effective field, using only (2.3) and the translation properties of the fields. With the help of the translational requirement

$$\langle\psi^s(\mathbf{r}+\mathbf{s}; \mathbf{s}, \mathbf{j})\rangle_{js}=\exp(i\mathbf{k}'\cdot\mathbf{s})\langle\psi^s(\mathbf{r}; 0, \mathbf{j}-\mathbf{s})\rangle_{sj} \quad (4.1)$$

the effective field according to (2.4) is given by:

$$\psi_e(\mathbf{r})=\int n(\mathbf{j}|\mathbf{s})\exp[i(\mathbf{k}'-\mathbf{p})\cdot(\mathbf{s}-\mathbf{j})]$$
$$\times(E-H)^{-1}T(0)\langle\psi^s(\mathbf{r}; 0, \mathbf{j}-\mathbf{s})\rangle_{js}d\mathbf{s}. \quad (4.2)$$

This result has again been obtained without making approximations. And $\langle\psi^s\rangle_{sj}$ should be investigated with the help of (2.5). In this way, each effective field can be expressed in terms of an effective field with one more particle held fixed. The accuracy of the result depends on how many of the Eqs. (2.3), (2.4), (2.5), etc. are used.

An iteration procedure, applied to (2.2), is equivalent to choosing for $\psi_e(\mathbf{r})$ a plane wave $\exp(i\mathbf{k}\cdot\mathbf{r})$ with the vacuum propagation constant k, and then inserting this result into the formula (3.14) for the index of refraction. A double iteration procedure is approximately equivalent to replacing $\langle\psi^s\rangle_{sj}$ by $\exp(i\mathbf{k}\cdot\mathbf{r})$, inserting this result into (4.2) and then inserting the

resulting $\psi_e(\mathbf{r})$ into (3.14). Such a procedure is essentially an expansion in powers of the scattering amplitude.

Instead, we shall suggest an approximation:

$$\langle\psi^s(\mathbf{r};\mathbf{s},\mathbf{j})\rangle_{s,j}\simeq\langle\psi^s(\mathbf{r};\mathbf{s})\rangle_s, \tag{4.3}$$

that is (1) at least as good as the double iteration procedure, (2) is not strictly an expansion in powers of the scattering amplitude, and (3) is most accurate for dense systems where multiple scattering corrections are most important.

Equation (4.3) may be referred to as the quasi-crystalline approximation since it is strictly valid in the crystalline case. This approximation is tacitly made in many treatments of homogeneous media,[7,8] since the notation used does not distinguish between various types of effective fields. The quasi-crystalline assumption is equivalent to the neglect of the fluctuation of the effective field as $\mathbf{s}$ due to a deviation of particle j from its average position. The success of this assumption is based on the approximate validity of the cellular model for liquids. Certainly further investigation of this assumption is necessary. Because of their usefulness, however, we shall present here the results obtained by a multiple scattering treatment using the quasi-crystalline approximation.

The assumption (4.3) is equivalent to neglecting the difference between $\langle\psi^s(\mathbf{r};0,\mathbf{j}-\mathbf{s})\rangle_{s,j}$ and the effective field $\psi_e(\mathbf{r})$. If $n(\mathbf{j}|\mathbf{s})$ is written in the form:

$$n(\mathbf{j}|\mathbf{s})=n+n(0|\mathbf{s}-\mathbf{j})-n, \tag{4.4}$$

the effective field is found to obey the integral equation:

$$\psi_e(\mathbf{r})=\langle\psi(\mathbf{r})\rangle+(E-H)^{-1}GT(0)\psi_e(\mathbf{r}), \tag{4.5}$$

where

$$G(\mathbf{p}-\mathbf{k}')=\int[n(0|\mathbf{r})-n]\exp[i(\mathbf{k}'-\mathbf{p})\cdot\mathbf{r}]d\mathbf{r}. \tag{4.6}$$

Equations (4.5) and (4.6) are strictly valid for crystals providing the pair correlation function is interpreted in agreement with (2.7).

For a crystal, (4.5) and (2.7) can readily be combined to verify that the effective field $\psi_e(\mathbf{r})$ is equal to the total field (3.13) minus the field emitted by the scatterer at the origin. For a liquid (4.5) may be interpreted as saying that the effective field differs from the total field by the scattering produced by the hole $n-n(0|\mathbf{r})$ left by the scatterer whose center is at $\mathbf{r}=0$.

In the limiting case of point scatterers in a liquid, the hole $n-n(0|\mathbf{r})$ approaches zero and it is very tempting to say that G approaches zero so that according to (4.5) the effective field can be represented accurately by the average field $\exp(i\mathbf{k}'\cdot\mathbf{r})$. That this is not generally the case follows from a consideration of the case of scattering of electromagnetic waves by induced dipoles. There, the effective field correction factor $(\epsilon+2)/3$ arises precisely because the field within a hole, no matter how small, differs from the field in the external medium.

It is therefore necessary to investigate the solution of (4.5) for each particular problem and make approximations, if necessary, in the solution but not in the kernel of the integral equation. For present purposes, we are not interested in a complete evaluation of the effective field but merely in the matrix element

$$U(\mathbf{k}',\mathbf{k}')=n(\varphi,T\psi_e).$$

In order to obtain a variation expression for $U(\mathbf{k}',\mathbf{k}')$, methods were developed for integral equations in which neither the kernel $L=(E-H)^{-1}G$ nor the perturbing operator $V=T(0)$ were Hermitian.[6] With an appropriate transcription of notation, the variational expression for U_{ba} is given by:

$$U_{ba}=\frac{n({}^1\psi_e{}^b,T(0)\phi_a)(\phi_b,T(0)\psi_e{}^a)}{({}^1\psi_e{}^b,[T(0)-T(0)(E-H)^{-1}GT(0)]\psi_e{}^a)}, \tag{4.7}$$

where $\psi_e{}^a$ is the effective field when the average field is $\exp(i\mathbf{a}\cdot\mathbf{r})$. The fields ${}^1\psi_e(\mathbf{r})$ are solutions[6] of an equation adjoint to (4.5). If the guess

$${}^1\psi_e{}^{k'}(\mathbf{r})\simeq\psi_e{}^{k'}(\mathbf{r})\simeq c\exp(i\mathbf{k}'\cdot\mathbf{r}) \tag{4.8}$$

is inserted into (4.7), the diagonal matrix element of U is given by:

$$U(\mathbf{k}',\mathbf{k}')\simeq nT_{k'k'}(1-J)^{-1},$$
$$J=(T_{k'k'})^{-1}\sum_b T_{k'b}(E-E_b)^{-1}G(\mathbf{b}-\mathbf{k}')T_{bk'}. \tag{4.9}$$

One of the advantages of the variational method (4.7) is that U is insensitive to the choice of c. For point scatterers, therefore, (4.9) is exact. The integral Eq. (4.5), in fact, reduces for point scatterers to a linear equation for the constant c. For scatterers that are small but not point scatterers, (4.9) should be quite accurate.

The ratio of the effective field to the average field (3.18), can be written according to (4.9) and (3.20) in terms of scattering amplitudes:

$$c=(1-J)^{-1}, \tag{4.10}$$

$$J=\int\frac{f(k',b)f(b,k')}{f(k',k')}\frac{G(\mathbf{b}-\mathbf{k}')}{b^2-k^2}\frac{d\mathbf{b}}{2\pi^2}.$$

V. BOUNDARY CONDITIONS AT INFINITY

In scattering problems it is customary to introduce a boundary condition that describes radiation travelling outward at infinity. This boundary condition is included in our formalism provided we understand the operator $(E-H)^{-1}$ everywhere to mean[9]

$$(E-H)^{-1}=P(E-H)^{-1}-i\pi\delta(E-H) \tag{5.1}$$

[7] M. Born, *Optik* (Julius Springer, Berlin, 1933), p. 313 ff.
[8] L. Rosenfeld, *Theory of Electrons* (North-Holland Publishing Company, Amsterdam, 1951), Chapter VI.
[9] P. A. M. Dirac, *Principles of Quantum Mechanics* (Oxford University Press, London, 1947), third edition, Section 50; see also reference 6.

where P stands for the principle valued reciprocal. The transition operator T for a single scatterer with potential V is in fact the solution of the equation

$$T=V+V(E-H)^{-1}T, \tag{5.2}$$

with the above boundary condition. Because of this condition the operator T is nonhermitian and $T_{k'k'}$ is complex. Thus, if we would neglect the correction factor c, the index of refraction would have an imaginary part determined by the imaginary part of the forward scattered amplitude—i.e., by the total cross section, scattering plus absorption.[6]

Ekstein[4] has recently suggested that for an infinite system, the radiation condition should be replaced by a standing wave condition, i.e., that $(E-H)^{-1}$ be interpreted as the principal valued reciprocal. This is equivalent to replacing T of (5.2) by a new operator K satisfying

$$K=V+VP(E-H)^{-1}K. \tag{5.3}$$

If no true absorption is present, V is Hermitian, and because of (5.3) K is Hermitian.

Since no explicit use has been made in our paper of the radiation condition (5.1), all of our equations can be applied with either boundary condition. An examination of (4.7) and (4.9), assuming T is Hermitian (i.e., replaced by K) and using principal-valued reciprocals, demonstrates that under these circumstances the diagonal matrix elements of U are real. Thus Ekstein's boundary condition is equivalent to asserting that when no true absorption is present, the index of refraction for an infinite system is real.

Let us now examine the consequences of the usual radiation condition (5.1). For this purpose we need to evaluate the diagonal matrix element of U. A slight generalization of the cross-section theorem[6] to Eq. (4.5) leads to the relation:

$$\begin{aligned}\mathrm{Im}U_{aa}=&\mathrm{Im}(\psi_a^a, T\psi_a^a)\\ &-\pi\textstyle\sum_b G_{ba}|(\phi_b, T\psi_a^a)|^2\delta(E_b-E_a).\end{aligned} \tag{5.4}$$

To understand this result, introduce the approximation (4.8) valid for point scatterers and rearrange terms:

$$\begin{aligned}\mathrm{Im}U_{aa}=&|c|^2[\mathrm{Im}T_{aa}+\pi\textstyle\sum_b|T_{ba}|^2\delta(E_b-E_a)]\\ &-\pi|c|^2\textstyle\sum_b[1+G(\mathbf{b}-\mathbf{a})]|T_{ba}|^2\delta(E_b-E_a).\end{aligned}$$

Multiplication of (5.5) by $-2/\hbar$ converts each term into a transition probability. The term in $\mathrm{Im}T_{aa}$ is the total transition probability for the single scattering problem (aside from the factor $|c|^2$). The second terms in $|T_{ab}|^2$ is the negative of the transition probability for scattering. The sum of these two terms is then the absorption probability. The term in $(1+G_{ba})$ is the transition probability for scattering modified by the position correlation between a given atom and its neighbors. In short, the second line is what is usually referred to as the fluctuation scattering. Both lines are corrected by a factor $|c|^2$ signifying the enhancement of the scattering power due to the effective field correction.

If the transition probability is divided by the incident flux $\mathrm{Re}(\hbar k')/m$ to obtain cross sections, (5.5) can be written in the form:

$$4\pi\,\mathrm{Im}(fc)/\mathrm{Re}(k')=|c|^2(\sigma_{\mathrm{abs}}+\sigma_{\mathrm{fl}}), \tag{5.6}$$

where σ_{abs} in the total cross section for true absorption, and σ_{fl} is the total scattering cross section due to density fluctuations:

$$\sigma_{\mathrm{fl}}=\int d\sigma_{ae}(1+G_{ba}). \tag{5.7}$$

Here f is an abbreviation for the forward scattered amplitude $f(\mathbf{k}', \mathbf{k}')$. The imaginary part of the index of refraction determined by (3.19) and (5.6) is found to produce an attenuation in agreement with that predicted by a direct calculation of the fluctuation scattering[3] I-(6.20).

Thus the use of the radiation boundary condition has led to the physically reasonable result that even in the absence of true absorption the coherent beam will attenuate at a rate determined by scattering due to density fluctuations in the medium. For a gas, these fluctuations are large, $G_{ba}\simeq 0$, and the fluctuation cross section is essentially equal to the scattering cross section. Thus the attenuation for a gas is determined by the total cross section corrected by the factor $|c|^2$. For the liquid and solid states, fluctuations are greatly reduced, since the density fluctuation is proportional to the compressibility I-(1.14). Thus G is negative, the fluctuation cross section is small, and the attenuation will be more nearly determined by the absorption cross section. In any case, to a good approximation, the attenuation constant is given by

$$\tau=n|c|^2(\sigma_{\mathrm{abs}}+\sigma_{\mathrm{fl}}). \tag{5.8}$$

VI. FINITE SCATTERING SYSTEMS

Some question has been raised by Ekstein[3] as to the proper manner of treating infinite scattering systems. In this paper, the questionable procedure has been adopted of omitting the incident wave in setting up the self-consistent Eqs. (2.3)–(2.5) for an infinite system. It seems necessary, therefore, to investigate the index of refraction for a finite scattering system and compare the result with the previous calculation for an infinite system. An important by-product of this investigation will be an answer to the question: how small can a system be and still obey the "macroscopic" coherent wave equation for an infinite system. This question is of some interest in view of the recent application of a macroscopic viewpoint to describe diffraction of high energy neutrons by nuclei.[10]

Equation (2.3) can be modified to describe finite systems by adding the incident wave $\phi(\mathbf{r})$ and limiting the integration over $\mathbf{s}$ to a region bounded by the surface S. Rewriting these results in the space representation

[10] Fernbach, Serber, and Taylor, Phys. Rev. **75**, 1352 (1949).

with the help of (3.1) and (3.20), (2.3) takes the form:

$$\langle\psi(\mathbf{r})\rangle=\phi(\mathbf{r})+\int d\mathbf{r}'\int_S n(\mathbf{s})G(\mathbf{s})\chi(\mathbf{s})d\mathbf{s}, \tag{6.1}$$

$$\chi(\mathbf{s})=f(\langle\psi^s(\mathbf{r}'+\mathbf{s};\mathbf{s})\rangle_s;$$
$$G(\mathbf{s})=[\exp(ik|\mathbf{r}-\mathbf{r}'-\mathbf{s}|)/|\mathbf{r}-\mathbf{r}'-\mathbf{s}|]. \tag{6.2}$$

Equation (6.1) describes the macroscopic average field in the crystalline as well as liquid cases provided $n(\mathbf{s})$ is regarded as a constant in both cases. Outside the surface S, $\langle\psi(\mathbf{r})\rangle$, like $\phi(\mathbf{r})$, is a solution of the homogeneous unperturbed wave equation since all the "sources" are within S. (More precisely, these sources are within S plus a thin boundary layer whose thickness depends on the spatial extent of the operator f. For point scatterers, this layer vanishes.)

Inside the surface S, the field $\langle\psi(\mathbf{r})\rangle$ will not be a plane wave because of diffraction effects. If the concept of a medium is to be at all applicable, the average field must be representable as a sum of plane waves of various orientations and propagation constant k':

$$\langle\psi(\mathbf{r})\rangle=\sum M(\mathbf{k}')\exp(i\mathbf{k}'\cdot\mathbf{r}). \tag{6.3}$$

The translational consideration (3.3) must now be replaced by the more general condition

$$\langle\psi^s(\mathbf{r}'+\mathbf{s};\mathbf{s})\rangle_s=\sum M(\mathbf{k}')\exp(i\mathbf{k}'\cdot\mathbf{s})\psi_s(\mathbf{k}',\mathbf{r}), \tag{6.4}$$

where $\psi_s(\mathbf{k}',\mathbf{r})$ is the effective field for an average field in direction $\mathbf{k}'$. Since the operator f does not act on s, $\chi(\mathbf{s})$ is a solution of the medium wave equation. With the help of the replacement

$$\chi(\mathbf{s})=-(k')^{-2}\nabla_s^2\chi(\mathbf{s}), \tag{6.5}$$

and Green's second identity, the volume integral in (6.1) can be written as the usual integral over all space plus a correction term in the form of a surface integral:

$$\int G(\mathbf{s})\chi(\mathbf{s})d\mathbf{s}=4\pi[(k')^2-k^2]^{-1}[\chi(\mathbf{r}-\mathbf{r}')-I],$$
$$I=\int[\chi(\mathbf{s})(\partial G/\partial n)-G(\partial\chi/\partial n)]dS, \tag{6.6}$$

where the derivatives are outward normal to the surface S.

With the help of (6.3) and (6.4) we may verify that

$$\int\chi(\mathbf{r}-\mathbf{r}')d\mathbf{r}'=\langle\psi(\mathbf{r})\rangle g, \tag{6.7}$$

$$g=\int\exp(-i\mathbf{k}'\cdot\mathbf{r}')f\psi_s(\mathbf{k}',\mathbf{r}')d\mathbf{r}'. \tag{6.8}$$

Finally the average field can be written in the form:

$$\langle\psi(\mathbf{r})\rangle=4\pi ng[(k')^2-k^2]^{-1}\langle\psi(\mathbf{r})\rangle+\phi(\mathbf{r})$$
$$-n\int dS[(\partial G(\mathbf{s})/\partial n)\int d\mathbf{r}'f\langle\psi^s(\mathbf{r}'+\mathbf{s};\mathbf{s})\rangle_s$$
$$-G(\mathbf{s})\int d\mathbf{r}'(\partial/\partial n)f\langle\psi^s(\mathbf{r}'+\mathbf{s};\mathbf{s})\rangle_s]. \tag{6.9}$$

The surface integral may be interpreted as the field due to a set of sources on the surface (or in a thin layer) whose field within the region is like $\phi(\mathbf{r})$ a solution of the unperturbed wave equation. The only way (6.9) can be satisfied inside the system is for the surface term to cancel the incident wave and for

$$(k')^2=k^2+4\pi ng. \tag{6.10}$$

The first statement constitutes the "extinction" theorem: the unperturbed incident wave is extinguished within the medium by waves induced at the boundary of the system. This theorem justifies the procedure adopted earlier in the paper of omitting the incident wave and neglecting boundary effects.

The second statement is equivalent to the validity of the previous index of refraction formula (3.19), since g is formally equivalent to $cf(\mathbf{k}',\mathbf{k}')$. The only question to be investigated is whether the effective field entering into the definition of g is the same as the one previously used for an infinite system.

Applying to (2.4), for the effective field, a procedure similar to the above calculation of the average field, we obtain:

$$\langle\psi^j(\mathbf{r};\mathbf{j})\rangle_j=\phi(\mathbf{r})+\int d\mathbf{r}'\int_S n(\mathbf{j}|\mathbf{s})G(\mathbf{s})\chi(\mathbf{s})d\mathbf{s}, \tag{6.11}$$

where we have made of the quasi-crystalline approximation (4.3). Writing $n(\mathbf{j}|\mathbf{s})=n+n(\mathbf{j}|\mathbf{s})-n$ and using (6.1) the effective field obeys the equation

$$\langle\psi^j(\mathbf{r};\mathbf{j})\rangle_j=\langle\psi(\mathbf{r})\rangle+\int d\mathbf{r}'\int_S[n(\mathbf{j}|\mathbf{s})-n]G(\mathbf{s})\chi(\mathbf{s})d\mathbf{s}. \tag{6.12}$$

This equation would reduce to the previous Eq. (4.5) for the effective field provided the integral over $\mathbf{s}$ could be extended over all space. However $n(\mathbf{j}|\mathbf{s})-n$ vanishes quite rapidly for large $|\mathbf{s}-\mathbf{j}|$. Thus if the region of integration is large compared to the region of importance of the correlation density $n(\mathbf{j}|\mathbf{s})-n$, the "macroscopic" index of refraction will be valid. For liquid type systems, this condition is easily satisfied, since it merely requires that the system be large in size compared to the interparticle separation. Nonideal, vibrating lattices obey a similar restriction. Ideal lattices require further investigation of the convergence involved in the sum implied by (6.12). Convergence can certainly be secured in the ideal case by using a system large compared to the wavelength as well as the interparticle separation. This

wavelength condition is sufficient, but probably not necessary.

Another restriction on the use of a macroscopic viewpoint is that the region should be large compared to the boundary layer associated with the surface S because of the finite range of the scatterer potentials.

A third restriction on the above discussion has been the use of a constant density. This restriction can be removed by introducing an index of refraction that varies with position because of density changes. Such a procedure can be useful, for example, in treating a nucleus as a system, since for this case the density is not completely uniform.

When the restrictions mentioned above are met, the continuity of $\langle\psi(\mathbf{r})\rangle$ and its gradient in (6.1) across the surface S justifies the usual procedure of finding an external solution and an internal solution, and matching them at the boundary.

VII. NEUTRON SCATTERING IN LIQUIDS AND CRYSTALS

The results of the preceding sections can be applied to neutron scattering in the low energy range by replacing the operator f_{op} by $f\delta(\mathbf{q})$ where f is the bound scattered amplitude for scattering of neutrons by the nucleus in question [see Eq. (3.20)]. This is equivalent to replacing the matrix $f(\mathbf{b}, \mathbf{a})$ by the constant amplitude f. Thus the usual index of refraction formula (3.19) is applicable with $c=(1-J)^{-1}$ where J according to (4.10) can be written as:

$$J=f\int(b^2-k^2)^{-1}G(\mathbf{b}-\mathbf{k}')d\mathbf{b}/(2\pi^2), \tag{7.1}$$

with $G(\mathbf{p}-\mathbf{k}')$ given by (4.6). Utilizing the radiation condition

$$(k^2-b^2)^{-1}=P(k'-b^2)^{-1}-i\pi\delta(k^2-b^2), \tag{7.2}$$

we have

$$J=-f[A+ik(1-E)], \tag{7.3}$$

where

$$A=P\int(k^2-b^2)^{-1}G(\mathbf{b}-\mathbf{k}')d\mathbf{b}/(2\pi^2) \tag{7.4}$$

$$=n\int r^{-1}\cos kr[1-w(\mathbf{r})]\cos(\mathbf{k}'\cdot\mathbf{r})d\mathbf{r}, \tag{7.5}$$

and

$$E=1+\int G(\mathbf{b}-\mathbf{k}')d\Omega_b/4\pi \tag{7.6}$$

$$=\int d\Omega_b/4\pi\left\{1+n\int e^{i(\mathbf{k}'-\mathbf{k})\cdot\mathbf{r}}[w(\mathbf{r})-1]d\mathbf{r}\right\}. \tag{7.7}$$

The index of refraction Eq. (3.19) can now be written in the form:

$$(k')^2=k^2+4\pi n|c|^2[f-ik|f|^2+A^*|f|^2+ik|f|^2E^*]. \tag{7.8}$$

If we neglect the fact that k' may have a small imaginary part, A and E will be real. E can be recognized as the ratio by which the effective scattering cross section is modified by interference due to correlation of scatterer pairs. In the long wavelength limit, E can be interpreted as proportional to the mean square fluctuation in number of particles [I-(6.23) and I-(1H4)]:

$$E(0)=\langle(\Delta N)^2\rangle/\langle N\rangle=-n(kT)(\partial\ln V/\partial P)_T. \tag{7.9}$$

Thus E is equal to the relative compressibility of the liquid or solid to a perfect gas at the same pressure and temperature. In other words, the fluctuation scattering is small in a liquid or solid (vanishing in an ideal nonvibrating crystal) and the imaginary part of $(k')^2$ is determined by $\mathrm{Im}(f-ik|f|^2)$, which vanishes unless true absorption is present.[4]

The long wavelength approximation for A is:

$$A(0)=n\int[1-w(\mathbf{r})]d\mathbf{r}/r. \tag{7.10}$$

The rigid sphere model (valid at low densities) indicates that $A(0)=2\pi na^2$. In other words, $A(0)$ is of order a^{-1} and its effect as a correction is of order f/a, the ratio of scattering amplitude to size of scatterer. For neutron scattering, where only the nucleus is effective but a is of atomic size, $f/a\sim10^{-4}$.

A detailed evaluation of E in the short wavelength limit has been given by Placzek, Nijboer, and van Hove,[11] in the approximation $\mathbf{k}'\simeq\mathbf{k}$. The average of E over all orientations of $\mathbf{k}$ has been denoted in their paper by σ_{tot} and $1+G(\mathbf{k}-\mathbf{b})$ is designated $\sigma(\mathbf{h})$ where $\mathbf{h}=(\mathbf{k}-\mathbf{b})/2\pi$. Their results may be summarized by:

$$\int Ed\Omega_h/4\pi=\sigma_{tot}=1-(\lambda^2/8\pi)n^{\frac{1}{2}}I, \tag{7.11}$$

where I is a pure number defined by

$$I=n^{-\frac{1}{2}}\int[1-\sigma(\mathbf{h})]d\mathbf{h}/h, \tag{7.12}$$

when the integration is extended over a sphere in h space of radius $2/\lambda$. They approximate (8.12) by extending the integration over all $\mathbf{h}$ space, and then revert to ordinary space:

$$I\simeq n^{\frac{1}{2}}\int[1-w(\mathbf{r})]d\mathbf{r}/\pi r^2. \tag{7.13}$$

They can establish (*a*) $I<3$, (*b*) for close-packing $I\simeq2.88$, (*c*) for rigid spheres of radius a, $I=4an^{\frac{1}{2}}K$, and $K=1-0.6488\gamma$ for $\gamma\ll1$, and $K\simeq0.64\gamma^{-\frac{1}{2}}$ for $\gamma\sim1$, where $\gamma=na^3/\sqrt{2}$ is a measure of the closeness of packing such that γ cannot exceed unity. Placzek *et al.*[11] give numerical results for I for ideal lattices and for vibrating lattices.

[11] Placzek, Nijboer, and van Hove, Phys. Rev. **82**, 392 (1951).

For ideal lattices and arbitrary wavelength, A can be written in the form of a poorly converging series in reciprocal space:

$$-A=\lim_{r\to 0}\left[4\pi n\sum_{\mathbf{K}\neq 0}\frac{\cos(\mathbf{k}'-\mathbf{K})\cdot\mathbf{r}}{(\mathbf{k}'-\mathbf{K})^2-k^2}\left|\frac{F(\mathbf{K})}{Z}\right|^2-\frac{\cos kr}{r}\right]. \tag{7.14}$$

This may be converted into a sum of two rapidly converging series, one in ordinary space and one in reciprocal space with the help of the device originally introduced by Ewald:[1]

$$[(\mathbf{k}'-\mathbf{K})^2-k^2]^{-1}=\int_0^\eta+\int_\eta^\infty \exp\{[k^2-(\mathbf{k}'-\mathbf{K})^2]t\}dt. \tag{7.15}$$

The resulting series are:

$$\begin{aligned}-A=4\pi n\sum_{\mathbf{K}\neq 0}&\frac{\exp\{[k^2-(\mathbf{k}'-\mathbf{K})^2]\eta\}}{(\mathbf{k}'-\mathbf{K})^2-k^2}\left|\frac{F(\mathbf{K})}{Z}\right|^2\\&-4\pi n[(k')^2-k^2]^{-1}[1-\exp\eta(k^2-k'^2)]\\&+\textstyle\sum_{j\neq 0}\cos(\mathbf{k}'\cdot\mathbf{j})G(k,\mathbf{j})\\&+\lim_{r\to 0}[G(k,\mathbf{r})-r^{-1}],\end{aligned} \tag{7.16}$$

where

$$G(k,\mathbf{r})=\tfrac{1}{2}\pi^{-\frac{1}{2}}\int_0^\eta \exp[k^2t-r^2/(4t)]dt/t^{\frac{3}{2}}. \tag{7.17}$$

The sum over $\mathbf{j}$ is taken over all lattice points, except $\mathbf{j}=0$. For $j^2/\eta\gg 1$, $G(k,\mathbf{j})$ can be approximated by:

$$\begin{aligned}G(k,\mathbf{j})\simeq 2(\eta/\pi)^{\frac{1}{2}}\{1-[2\eta+(2k\eta)^2]/j^2\}\\\times\exp[k^2\eta-j^2/(4\eta)].\end{aligned} \tag{7.18}$$

The $\mathbf{j}=0$ term requires special consideration:

$$\lim_{r\to 0}[G(k,r)-r^{-1}]=-(\pi\eta)^{-\frac{1}{2}}+\tfrac{1}{2}\pi^{-\frac{1}{2}}\int_0^\eta[\exp(k^2t)-1]dt/t^{\frac{3}{2}}. \tag{7.19}$$

In the limiting case of long wavelengths, A reduces to the more familiar form:

$$\begin{aligned}-A(0)\simeq 4\pi n\sum_{\mathbf{K}\neq 0}&|F(\mathbf{h})/Z|^2[\exp(-K^2\eta)/K^2]\\&+\sum_{j\neq 0}G(0,\mathbf{j})-4\pi n\eta-(\pi\eta)^{-\frac{1}{2}},\end{aligned} \tag{7.20}$$

$$rG(0,r)=(2/\sqrt{\pi})\int_x^\infty \exp(-u^2)du;\quad x=\tfrac{1}{2}r\eta^{-\frac{1}{2}}. \tag{7.21}$$

Rapidity of convergence can be secured for the two series by choosing, for example, $\eta=a^2/(4\pi)$, where a is a typical lattice constant. In any case A will have the order of magnitude of $(1/a)$ except in the immediate neighborhood of a Bragg reflection.

It should be emphasized that the scattering amplitude operator f has been defined in terms of the transition operator T by (3.20). And the transition operator is to be obtained by solving a one-body interaction problem: namely, a scattering problem in which the wave interacts with a single scatterer while the latter is subject to the forces of its neighbors—i.e., a scatterer that is neither completely bound nor completely free.

The one-body interaction problem was first considered by Fermi[12] in treating the scattering of neutrons by protons bound in a molecule. A more accurate treatment by Breit[13] using integral equation methods led to corrections of the order of 0.3 percent. A variational approach to the same problem by Lippmann and Schwinger[14] led to results in agreement with Breit. Fermi's result for elastic scattering can be written in the form [reference 14, Eq. (2.21)]:

$$T_{\text{bo}}=\int T_{\text{bo}}(\mathbf{s})p(\mathbf{s})d\mathbf{s}, \tag{7.22}$$

where $p(\mathbf{s})$ is the probability of finding the scatterer at position $\mathbf{s}$ in the molecule and $T_{\text{bo}}(\mathbf{s})$ is the transition operator for a free scatterer at $\mathbf{s}$. Of course f is still related to T by (3.20), but the free scattering length a obeys a similar relation with the neutron mass m replaced by the corresponding reduced mass μ relative to the scattering nucleus, so that $f=(am/\mu)$. Aside from this change in scattering amplitudes that does not affect T, the primary effect of the binding is taken into account by calculating the appropriate interference sum over the distribution of scatterer positions. This interference sum is automatically included in our original formulation (2.3)–(2.5).

The results of this section on the neutron index of refraction can therefore be understood to be correct in Fermi approximation if for f we use the scattering amplitude appropriate to bound scatterers. The small corrections obtained by Breit can be included if the scattering amplitude is modified to include the small effect of tightness of binding. The modified scattering amplitude $f(\mathbf{b},\mathbf{a})$ will, however, be slightly anisotropic, and a rigorous calculation, even for the neutron case, can be made only by returning to the general anisotropic formulas (3.19) and (4.10).

VIII. SUMMARY

In previous work[3] the author has treated the multiple scattering of waves by a system of particles using a self-consistent approach. In this treatment, the use of transition operators permitted the individual scattering

[12] E. Fermi, Ricerca sci. **7**, Part 2, 13 (1936).
[13] G. Breit, Phys. Rev. **71**, 215 (1947); G. Breit and P. R. Zilsel, Phys. Rev. **71**, 232 (1947); Breit, Zilsel, and Darling, Phys. Rev. **72**, 576 (1947).
[14] B. H. Lippmann and J. Schwinger, Phys. Rev. **79**, 469 (1950).

processes to possess anisotropy and includes the possibility of absorption or creation of waves in a generalized scattering act. The scattering system was described by a quantum-mechanical distribution function in configuration space. The final results depended largely on the density of scatterers and the pair correlation density of scatterers. The treatment was sufficiently general to handle scattering systems that are randomly, partially, or completely ordered, i.e., gases, liquids, imperfect and ideal crystals.

One of the principal results of the self-consistent approach was an adequate definition of the coherent wave and a proof that the latter obeys a suitable wave equation, i.e., a proof that a distribution of scatterers can, for this purpose, be represented by a medium. Most calculations[7,8] proceed by assuming the existence of such a "medium" equation.

The propagation constant k' associated with the medium equation was found to differ from the corresponding vacuum constant k by

$$(k')^2=k^2+4\pi nc f(\mathbf{k}', \mathbf{k}'), \tag{8.1}$$

where n is the scatterer density and f is an operator whose matrix elements $f(\mathbf{b}, \mathbf{a})$ represent the scattering amplitude with propagation vector $\mathbf{b}$ for a wave incident in direction $\mathbf{a}$ on a bound scatterer.

The parameter c is a measure of the ratio of the effective field $\psi_e(\mathbf{r})$ to the macroscopic average field $\langle\psi(\mathbf{r})\rangle$. For point isotropic scatters $c=\psi_s(0)/\langle\psi(0)\rangle$ and for point dipole scatterers, c is simply the ratio of gradients at the origin. In this paper, we have demonstrated that a valid general formula for c including finite scatterers is

$$c=\int \exp(-i\mathbf{k}'\cdot\mathbf{r})f\psi_s(\mathbf{r})d\mathbf{r}\Big/\int \exp(-i\mathbf{k}'\cdot\mathbf{r})f\langle\psi(\mathbf{r})\rangle d\mathbf{r}. \tag{8.2}$$

Following the procedure described in *I*, a set of equations [(2.3)–(2.5)] were developed expressing the coherent field $\langle\psi(\mathbf{r})\rangle$ in terms of the effective field $\langle\psi^s(\mathbf{r})\rangle_s$ with one particle fixed, and the latter in terms of the effective field $\langle\psi^s(\mathbf{r})\rangle_{sj}$ with two particles fixed, etc. This infinite sequence of equations was broken by the quasi-crystalline approximation:

$$\langle\psi^s(\mathbf{r})\rangle_{sj}\simeq\langle\psi^s(\mathbf{r})\rangle_s. \tag{8.3}$$

An integral Eq. (4.5) was thus obtained for the effective field. This integral equation reduces to a linear equation for point scatterers. Using (4.5), a variational expression (4.10) [see also (8.2)] was developed for c, valid for finite scatterers and exact for point scatterers.

The preceding results were obtained using an infinite scattering system with the radiation boundary condition (5.1). The imaginary part of the index of refraction was found to lead to an attenuation constant (5.8) produced by the cross section for true absorption plus the cross section for fluctuation scattering, each enhanced by a factor $|c|^2$. This result is in exact agreement with a direct calculation of the attenuation I-(6.20).

In Sec. VI, a comparison was made between finite and infinite scattering systems. A general proof was given for the extinction theorem: the unperturbed incident wave is extinguished within the medium by waves induced at the boundary of the system.

An investigation was made of the validity of applying the macroscopic medium viewpoint to small scattering systems. This procedure was found applicable for systems whose size is large (1) compared to the range of the potential presented by a single scatterer to the wave and (2) compared to the distance over which correlations in scatterer positions are significant. (For ideal crystals, the last condition is too stringent.) These conditions can be relaxed somewhat by making direct use of (6.9) and (6.12).

In Sec. VII, applications are made to neutron scattering. It is emphasized that the scattering amplitudes to be used must be those of a scatterer bound by interaction with its neighbors. It is demonstrated (7.22) that the corrections used by Fermi are automatically included in this paper if $T(\mathbf{s})$ is the transition operator for a free scatterer. However, additional small corrections[12-14] must be included by making a small change in the operator $T(\mathbf{s})$. This point will be considered in more detail in a subsequent paper.

Masses of Lead and Bismuth*

P. I. RICHARDS, E. E. HAYS,† AND S. A. GOUDSMIT
Brookhaven National Laboratory, Upton, Long Island, New York

(Received November 8, 1951)

The masses of Pb^{208} and Bi^{209} have been determined by measuring the time of flight of their ions in a magnetic field. The mass values are: $Pb^{208}=208.0416\pm0.0015$, $Bi^{209}=209.0466\pm0.0015$, $Bi^{209}-Pb^{208}=1.0050\pm0.0015$.

THE helical-orbit time-of-flight mass-spectrometer previously described[1] has been used to measure the masses of Pb^{208} and Bi^{209}. A magnetic field regulator has been added which holds the field constant to about one part in 10^5 during a run. This feature has greatly improved the consistency of the runs and has enabled us to see small disturbances previously masked by scatter in the data. The resulting precision at mass 200 is thus very close to the theoretical value of ±1 mMU.

In all measurements reported here, ion fragments of cyclo-$C_6F_{11}-CF_3$ were used as standards. All values reported below are based on[2] $C=12.003895$ and $F=19.00445$, the latter being obtained from the $F^{19}(p,\alpha)O^{16}$ reaction data.[3] Lead and/or bismuth vapor obtained from a bead of metal fused on a heated molybdenum wire was fed directly to the electron impact ion source into which C_7F_{14} vapor was also flowing.

The energy of these heavy ions is quite low in our apparatus, namely between 10 and 15 ev. They are therefore easily affected by disturbing fields. In this case interpolation using three standards, instead of the usual two, was required to yield results which were consistent within the accuracy aimed at. This means essentially that not only a small quadratic correction but also a small cubic term was used in the relation between mass and time of flight. The standards used were the fragments $C_3F_5^+$ (mass approximately 131), $C_4F_7^+$(181), and $C_5F_9^+$(231). Although the total correction in the case of Pb arranged from 2 to 20 mMU (presumably depending on surface potentials within the vacuum can) the largest deviation from the mean of 13 separate runs (each involving about eight consecutive readings of each of the time intervals) was only -2.6 to $+2.3$ mMU; the probable error of the mean was ±0.4 mMU. From this series of measurements the mass $Pb^{208}=208.0410\pm0.0015$ was derived. The more conservative value given for the limits of error allows for possible systematic effects and is a better representation both of the design precision of the instrument and of the actual accuracy of individual readings.

For the measurements of Bi^{209} the total correction in nine runs varied from 15 to 31 mMU, but the cubic term turned out to be zero within our experimental error. Nevertheless, using the three standards, the largest deviations from the mean value for the mass were -2.6 to $+3.1$ mMU; the probable error was again ±0.4 mMU and the derived mass $Bi^{209}=209.0472\pm0.0015$.

An independent check was made by measuring Bi^{209} with respect to Pb^{208} and one standard C_4F_7(181). Because of the proximity of Bi and Pb, knowing the mass of Pb to ±10 mMU was sufficient to evaluate the quadratic correction (only 3 mMU at most) from the time of flight of C_4F_7 and Pb; the mass difference $Bi^{209}-Pb^{208}$ was then derived. The largest deviations from the mean of twelve runs were ±4 mMU; the probable error was 0.4 mMU. The value obtained for the difference was $Bi^{209}-Pb^{208}=1.0050\pm0.0015$. It will be seen that this is in agreement with the individual values given previously.

Since these three measurements are independent, they may be combined to produce presumably more accurate values of Pb and Bi individually. This has been done in the final values displayed in Table I.

If the masses of the standards change, the mass (M) of lead or bismuth must be changed by amount δM given by

$$\frac{\delta M}{M}=\frac{\delta A}{A}\left(\frac{M-B}{A-B}\right)\left(\frac{M-C}{A-C}\right)+\frac{\delta B}{B}\left(\frac{M-A}{B-A}\right)\left(\frac{M-C}{B-C}\right)+\frac{\delta C}{C}\left[\left(\frac{M-A}{B-A}\right)\left(\frac{M-B}{C-B}\right)+\left(\frac{M-B}{A-B}\right)\left(\frac{M-A}{C-A}\right)\right],$$

where A, B, C represent the masses of C_3F_5, C_4F_7, and C_5F_9, respectively, and δA, δB, δC represent possible future changes in their total masses.

The mass of Pb^{208} agrees with the one given by Duckworth and Preston,[4] namely $Pb^{208}=208.0422\pm0.0015$.

TABLE I. Masses[a] of Pb and Bi.

$Pb^{208}=208.0416\pm0.0015$
$Bi^{209}=209.0466\pm0.0015$
$Bi^{209}-Pb^{208}=1.0050\pm0.0015$

[a] Based on $C=12.003895$, $F=19.00445$ (see text).

* Research carried out at Brookhaven National Laboratory, under the auspices of the AEC.

† Now at the University of Toledo, Toledo, Ohio.

[1] S. A. Goudsmit, Phys. Rev. **74**, 622 (1948); Hays, Richards, and Goudsmit, Phys. Rev. **84**, 824 (1951).

[2] K. T. Bainbridge, Phys. Rev. **81**, 146 (1951).

[3] Strait, Van Patter, Buechner, and Sperduto, Phys. Rev. **81**, 747 (1951).

[4] H. E. Duckworth and R. S. Preston, Phys. Rev. **82**, 468 (1951).

The indicated limit of error in this latter value is the standard deviation derived from seven measurements.

The fact that the difference $_{84}Bi^{209}-{}_{82}Pb^{208}$ is 5 mMU larger than unity indicates a sharp increase in the slope of the packing fraction curve. This agrees with the expectation since Bi^{209} has one proton more than the magic number 82. The addition of this single proton adds, in this case, only 3 Mev to the binding energy of the nucleus. This result is in reasonable agreement with the difference of 1.004 mass units derived from the disintegration data of Harvey.[5]

[5] J. A. Harvey, Phys. Rev. **81**, 353 (1951).

PHYSICAL REVIEW VOLUME 85, NUMBER 4 FEBRUARY 15, 1952

Divergence of Perturbation Theory in Quantum Electrodynamics

F. J. Dyson
Laboratory of Nuclear Studies, Cornell University, Ithaca, New York
(Received November 5, 1951)

An argument is presented which leads tentatively to the conclusion that all the power-series expansions currently in use in quantum electrodynamics are divergent after the renormalization of mass and charge. The divergence in no way restricts the accuracy of practical calculations that can be made with the theory, but raises important questions of principle concerning the nature of the physical concepts upon which the theory is built.

ALL existing methods of handling problems in quantum electrodynamics give results in the form of power-series in e^2. The individual coefficients in these series are finite after mass and charge renormalization. The technique of renormalization can at present be applied only to the separate coefficients, and not to the series as a whole. If the series converges, its sum is a calculable physical quantity. But if the series diverges, we have no method of calculating or even of defining the quantity which is supposed to be represented by the series.

Several authors have remarked[1] that the series after renormalization will be divergent in a trivial way, if the series represents a scattering amplitude of a free particle, in circumstances where the particle has a possibility of being captured into a permanently bound system. In this situation a perturbation expansion of the scattering amplitude will diverge, even in nonrelativistic quantum mechanics,[2] and in the relativistic theory the series will diverge for the same reason. It is to be expected that such trivial divergences will not impose any fundamental limitations on the use of the renormalization method. In fact, a new method of carrying through the renormalization program has been developed,[3] a method which is applicable to problems involving bound systems and in which divergences of this elementary nature cannot occur. In the new method the series expansion arises from a formal integration of the equations of motion over a finite interval of time, and in an elementary nonrelativistic theory such a perturbation expansion would necessarily be convergent. For this reason it was claimed as probable[4] that the power series arising from the application of the new method in quantum electrodynamics would always converge. If the claim had been accompanied by a proof of convergence, then the theoretical framework of quantum electrodynamics could have been considered closed, being within its limits a complete and consistent theory.

The purpose of this note is to present a simple argument which indicates that the power-series expansions obtained by integrating the equations of motion in quantum electrodynamics will be divergent after renormalization. The divergence is of a basic character, different from the trivial divergences mentioned above, and is present equally in the results obtained from the new and the older methods of calculation. The argument here presented is lacking in mathematical rigor and in physical precision. It is intended only to be suggestive, to serve as a basis for further discussions. To me it seems convincing enough to merit publication in its present incomplete form; also I am glad to have this opportunity to withdraw the erroneous argument previously put forward[5] to support the claim that the power series should converge.

The argument for divergence is as follows. According to Feynman,[6] quantum electrodynamics is equivalent to a theory of the motion of charges acting on each other by a direct action at a distance, the interaction between two like charges being given by the formula

$$e^2\delta_+(s_{12}^2), \tag{1}$$

where e is the electron charge. The action-at-a-distance formulation is precisely equivalent to the usual formulation of the theory, in circumstances where all emitted radiation is ultimately absorbed. We shall suppose that

[1] B. Ferretti, Nuovo cimento **8**, 108 (1951); K. Nishijima, Prog. Theor. Phys. **6**, 37 (1951).
[2] R. Jost and A. Pais, Phys. Rev. **82**, 840 (1951).
[3] F. J. Dyson, Proc. Roy. Soc. (London) **A207**, 395 (1951). Phys. Rev. **83**, 608, 1207 (1951).
[4] Phys. Rev. **83**, 608 (1951), Section XII.
[5] See reference 4. The error in the argument lay in using the concept "the number of times that an interaction operates" in an intuitive and imprecise way.
[6] R. P. Feynman, Phys. Rev. **76**, 769 (1949), Eq. (4); Phys. Rev. **80**, 440 (1950), Appendix B.

conditions are such as to justify the use of the Feynman formulation of the theory. Then let

$$F(e^2)=a_0+a_2e^2+a_4e^4+\cdots \tag{2}$$

be a physical quantity which is calculated as a formal power series in e^2 by integrating the equations of motion of the theory over a finite or an infinite time. Suppose, if possible, that the series (2) converges for some positive value of e^2; this implies that $F(e^2)$ is an analytic function of e at $e=0$. Then for sufficiently small values of e, $F(-e^2)$ will also be a well-behaved analytic function with a convergent power-series expansion.

But for $F(-e^2)$ we can also make a physical interpretation. Namely, $F(-e^2)$ is the value that would be obtained for F in a fictitious world where the interaction between like charges is $[-e^2\delta_+(s_{12}^2)]$ instead of (1). In the fictitious world, like charges attract each other. The potential between static charges, in the classical limit of large distances and large numbers of elementary charges, will be just the classical Coulomb potential with the sign reversed. But it is clear that in the fictitious world the vacuum state as ordinarily defined is not the state of lowest energy. By creating a large number N of electron-positron pairs, bringing the electrons together in one region of space and the positrons in another separate region, it is easy to construct a "pathological" state in which the negative potential energy of the Coulomb forces is much greater than the total rest energy and kinetic energy of the particles. This can be done without using particularly small regions or high charge densities, so that the validity of the classical Coulomb potential is not in doubt. Suppose that in the fictitious world the state of a system is known at a certain time to be an ordinary physical state with only a few particles present. There is a high potential barrier separating the physical state from the pathological states of equal energy; to overcome the barrier it is necessary to supply the rest-energy for the creation of many particles. Nevertheless, because of the quantum-mechanical tunnel effect, there will always be a finite probability that in any finite time-interval the system will find itself in a pathological state. Thus every physical state is unstable against the spontaneous creation of large numbers of particles. Further, a system once in a pathological state will not remain steady; there will be a rapid creation of more and more particles, an explosive disintegration of the vacuum by spontaneous polarization. In these circumstances it is impossible that the integration of the equations of motion of the theory over any finite or infinite time interval, starting from a given state of the fictitious world, should lead to well-defined analytic functions. Therefore $F(-e^2)$ cannot be analytic and the the series (2) cannot be convergent.

The divergence of the series in the real world is associated with virtual processes in which large numbers of particles are involved. Therefore the divergence will only become noticeable when terms of very high order in the expansion (2) are considered. A crude quantitative estimate indicates that the terms of (2) will decrease to a minimum and then increase again without limit, the index of the minimum term being roughly of the order of magnitude 137. This estimate assumes the system to be such that the trivial kind of divergence discussed earlier does not occur. The nontrivial and unavoidable divergence will not prevent practical calculations being made with the series (2), to an accuracy far beyond anything at present required or contemplated. Only if similar arguments should be found to be applicable to meson theory, the divergence might impose a severe limitation on the possible accuracy of practical calculations in that field.[7]

If the conclusion of the foregoing argument is accepted, then there are two alternative possibilities for the future development of quantum electrodynamics. Alternative A: There may be discovered a new method of carrying through the renormalization program, not making use of power series expansions. In this case every physical quantity $F(e^2)$ will be well-defined and calculable, and the series (2) will be an asymptotic expansion for it in the limit of small e. Since $F(e^2)$ is not analytic at $e=0$, the asymptotic expansion will not be sufficient to determine the function uniquely. The additional information necessary to determine $F(e^2)$ will be obtained from the existing formalism, using no new physical hypotheses but only some improved mathematical methods. Alternative B: All the information that can in principle be obtained from the formalism of quantum electrodynamics is contained in the coefficients $a_0, a_2, a_4, \cdots$ of series such as (2). In this case the quantity $F(e^2)$ is neither physically well-defined nor mathematically calculable, except in so far as the asymptotic expansion (2) gives some workable approximation to it. In order to define $F(e^2)$ precisely, not merely new mathematical methods but a new physical theory is needed.

I wish to call attention to the attractive features of alternative B in the present state of physics. If B were true, it would imply that quantum electrodynamics is in its mathematical nature not a closed theory, but only a half-theory giving insufficient information for the exact prediction of events. Experimentally we know that the world contains one group of phenomena which is accurately in agreement with the results of quantum electrodynamics, and another group of phenomena which is not understood at all. We need to develop new physical ideas to understand the second group, and still we cannot abandon the theory which successfully accounts for the first. If quantum electrodynamics were a closed theory, this would be a difficult dilemma. But if the theory itself leaves room for new ideas, no such dilemma arises. In conclusion, I wish to thank Professors Pauli, Bethe, Pais, and Oppenheimer for valuable discussions of these problems.

[7] C. A. Hurst in a private communication informs me that he has discovered by direct calculation the fact that the S-matrix diverges in the way here described, in the case of a simple scalar meson theory, assuming that certain terms which are not yet calculated do not decisively change the behavior of the series.

Geometrical Optics and the Theory of Multiple Small Angle Scattering

GEORGE H. VINEYARD
Department of Physics, University of Missouri, Columbia, Missouri
(Received July 2, 1951)

The theory of the small angle scattering of x-rays or thermal neutrons by particles of matter, in the case of particles large enough to produce large phase shifts, is re-examined. A theory based entirely on geometrical optics has been frequently employed in the past, and it is pointed out that, in the case of a single particle, this treatment gives an incomplete account of the scattering. A Huygen's principle approximational method (which is known to duplicate the results of wave theory in the single particle case), is applied to the many particle case, and it is shown that, here, the theory based entirely on geometrical optics is justified.

INTRODUCTION

SEVERAL theoretical treatments have been given of small angle scattering of x-rays or thermal neutrons by finely divided matter.[1] The earlier treatments fell essentially into two categories, diffraction theories, and refraction-reflection (ray) theories. The diffraction theories are wave theories, but have used the basic assumption of single scattering within each particle. This has been done mainly out of mathematical necessity; in some cases it has been feasible to take account of repeated *inter-particle* scattering. The refraction-reflection theories, on the other hand, are theories of ray optics, treating the individual scattering acts as geometrical refraction and reflection at each interface within the sample. From a wave point of view, each refraction event is essentially a process of highly multiple scattering, but the ray calculation can take no account of phase coherence in the various rays which arrive at the detector. The original treatment in this vein was given by von Nardroff.[2]

A comprehensive treatment of the scattering of electromagnetic waves by a single homogeneous sphere, starting from Maxwell's equations, has more recently been given by van de Hulst.[3] For the small-angle problem, the index of refraction of the sphere is always close to unity, and in this case van de Hulst shows that the rigorous formula reduces to two different limiting forms, depending upon whether $R|\delta|/\lambda$ is small or large compared with unity. Here R is the radius of the sphere, δ is one minus the refractive index, and λ is the wavelength. When $R|\delta|/\lambda$ is small, the scattering pattern is accurately described by the single scattering diffraction theory. When $R|\delta|/\lambda$ is large, the scattered radiation consists of two parts, one part as described by the ray theory (as, e.g., derived by von Nardroff), interpretable as radiation which has passed through the particle, and a second part interpretable as radiation diffracted around the particle, exactly as if it were an opaque obstacle. The total scattered energy in each portion is the same, but the diffracted part is confined to smaller angles, of the order λ/R, while the refracted beam extends to angles of the order of $|\delta|$. Discussions of the van de Hulst results and extensions thereof may be found in recent papers by Weiss[4] and by Hart and Montroll.[5]

Most measurements of small angle scattering are made with samples containing many particles, so that account of repeated inter-particle scattering must be taken before theory can be compared with experiment. Von Nardroff[2] treats the multiple scattering as a (two-dimensional) random flight process, and finds a resulting scattered intensity which is a Gaussian function of scattering angle with a width[6]

$$w_{VN}=p^{\frac{1}{2}}2|\delta|[\tfrac{1}{2}+\ln 2-\ln|\delta|]^{\frac{1}{2}}. \qquad (1)$$

Here w_{VN} is the angle at which the scattered intensity is reduced to $1/e$ of the forward scattered intensity, and p is the mean number of scatterers pierced by a ray. A more accurate treatment of the multiple scattering from the ray point of view may be based upon the calculations of Snyder and Scott.[6,7] These show that the distribution is not quite Gaussian, but give only modest quantitative differences from the von Nardroff result.

Von Nardroff's own x-ray experiments and also those of Dragsdorf[8] give, in the case of many large particles ($R|\delta|/\lambda>1$), fair confirmation of this formula. The more recent experiments of Weiss with neutron scattering confirm it even more closely. In view of the fact that the single particle scattering, as shown by the work of van de Hulst, contains an important component which is very different from the ray theory result, the confirmation of a purely ray theory calculation seems

[1] J. D. H. Donnay and C. G. Shull, *X-Ray Small Angle Scattering Annotated Bibliography* (Am. Soc. X-Ray and Electron Diffraction, March 1, 1946).

[2] R. von Nardroff, Phys. Rev. **28**, 240 (1926).

[3] H. C. van de Hulst, Recherches Astronomiques de l'Observatoire d'Utrecht **11** (1946). The portion of van de Hulst's results which we employ is equally applicable to the scattering of scalar, vector, and spinor waves, since it involves only scattering at small angles.

[4] R. J. Weiss, Phys. Rev. **83**, 379 (1951).

[5] R. W. Hart and E. W. Montroll, J. Appl. Phys. **22**, 376 (1951).

[6] As given in von Nardroff's paper, the first term in brackets is 1 instead of $\frac{1}{2}$. This can be seen to be erroneous. I am indebted to R. D. Dragsdorf for pointing this out. Also it should be noted that the final formulas in von Nardroff's paper refer to the case of illumination through narrow slits, and allow for a Gaussian spread in angle of the incident radiation. For simplicity we suppose throughout this paper that the incident radiation is perfectly collimated and of small cross-sectional dimensions.

[7] H. S. Snyder and W. T. Scott, Phys. Rev. **76**, 220 (1949).

[8] R. D. Dragsdorf, Dissertation, M.I.T., Cambridge, Massachusetts, 1949.

somewhat surprising. The fact that the additional (diffraction) scattering is confined to smaller angles than the ray theory scattering was considered by Weiss to be sufficient reason for ignoring it. Several objections may be brought against this: (a) Both components of the scattering must be broadened by the action of an assemblage of scatterers, and it is conceivable that the neglected part would be broadened more than the part which has been considered. (b) For values of $R|\delta|/\lambda$ not too much greater than one, the diffracted part (in the single particle case) is not clearly separated in angle from the ray part. Finally, because of the generally approximate nature of ray optics and its neglect of the effects of coherence, its use in such problems must always be questioned.

On the other hand, we may argue that, since the diffracted part arises because there is radiation passing around the particle, in the many particle case all the radiation passes through some particles, and the part which is simply diffracted around particles should cease to exist.

To clarify this situation and to provide a more firmly based theory of large-particle, multiple, small-angle scattering, we have carried through the calculations presented below.

MULTIPLE SCATTERING CALCULATION

Any straightforward wave equation approach to the many body scattering problem in our case seems hopelessly complicated. However, a hybrid approximation[9] method based on Huygen's principle can be devised. First we consider an intermediate plane just beyond the scatterers and perpendicular to the incident beam. The field is calculated on this intermediate plane under the assumptions that the phase at any point is determined by the optical path length on a line straight through the scatterers and reaching that point, and that the amplitude is unaffected by the scatterers. The scattered field reaching the detector is then found from the field on this intermediate plane by use of Kirchoff's form of Huygen's principle. Van de Hulst has shown that this method, with precisely these assumptions, is justified in the case of a single spherical scatterer with $R\gg\lambda$ and $|\delta|\ll 1$, because it reproduces the results of the wave equation calculation.

We consider an assemblage of N spherical particles, each of radius R and refractive index $1-\delta$, where $|\delta|\ll 1$ and $R|\delta|/\lambda\gg 1$.[10] Let the particles be illuminated by a collimated, monochromatic beam of radiation. Let P be a plane immediately beyond the assemblage and perpendicular to the incident beam. Take the perpendicular projection onto P of the center of the nth particle. Assign this point the (vector) coordinate $\mathbf{x}_n$. Because of the smallness of δ, a ray arriving at the point $\mathbf{x}$ of P will have come very nearly in an undeviated straight line. Its phase will be altered by the presence of the scattering particles, but its amplitude will be virtually unchanged, unless it chanced to strike a particle at about the critical angle. This will happen to only a minute fraction of all the rays, again because of the smallness of δ. The phase shift engendered in the ray by the nth particle may be denoted $f(\mathbf{x}, \mathbf{x}_n)$, and, to our approximation

$$f(\mathbf{x}, \mathbf{x}_n)=(4\pi\delta/\lambda)[R^2-(\mathbf{x}-\mathbf{x}_n)^2]^{\frac{1}{2}}, \text{ if } |\mathbf{x}-\mathbf{x}_n|\leq R',$$
$$f(\mathbf{x}, \mathbf{x}_n)=0 \text{ if } |\mathbf{x}-\mathbf{x}_n|>R'. \tag{2}$$

R' is a distance very slightly smaller than R at which we cut off the phase shift function in order to best allow for the rays which are strongly reflected near the limb of the particle. Its value will be assigned subsequently. The total phase shift of a ray reaching P at $\mathbf{x}$ is then $\sum_n f(\mathbf{x}, \mathbf{x}_n)$, and our approximation consists in using for $\varphi(\mathbf{x})$, the electric field at $\mathbf{x}$, the formula

$$\varphi(\mathbf{x})=\varphi_0 \exp\{i\sum_{n=1}^{N} f(\mathbf{x}, \mathbf{x}_n)\}, \tag{3}$$

where φ_0 is the (constant) amplitude of the incident field.

We consider scattering at an angle θ with the direction of incidence. Letting the component of $\mathbf{x}$ along the intersection of P and the plane of scattering be called y, the further relative phase shift between $\mathbf{x}$ of P and the detector is $g(\mathbf{x})=(2\pi/\lambda)y\sin\theta$. The Kirchoff formula then states that the intensity (per unit solid angle) of radiation reaching the detector is

$$I=\lambda^{-2}\left|\int_P \varphi(\mathbf{x}) \exp\{ig(\mathbf{x})\}dP\right|^2, \tag{4}$$

where dP is an element of surface in P, and the integral extends over so much of P as is illuminated by the incident beam. Equation (4) may be rewritten, by using Eq. (3) and re-expressing the square,

$$I=(1/\lambda)^2\int_P\int_P \exp\{ig(\mathbf{x})-ig(\mathbf{x}')\}$$
$$\times\exp\{i\sum_{n=1}^{N}[f(\mathbf{x}, \mathbf{x}_n)-f(\mathbf{x}', \mathbf{x}_n)\}dPdP'. \tag{5}$$

Here we have assumed unit-incident intensity. We next average this expression for all values of $\mathbf{x}_1, \mathbf{x}_2, \cdots\mathbf{x}_N$, assuming that all N particles are located with independent randomness within the illuminated region of P. This will correspond closely to the actual situation in

[9] Work along lines suggested by M. Lax (*Multiple Scattering of Waves*, Technical Report of the Institute of Industrial Research, Syracuse University, 1950) may ultimately be of use in this connection.

[10] Although in the single particle case this method proves to be valid for all values of $R\gg\lambda$, we must here tighten the restrictions. This is necessary because of the approximations by which we calculate the field on the intermediate plane, and also for mathematical convenience later. Actually, our results appear to have approximate validity even near the point where $R|\delta|/\lambda=1$. For the many particle case with $R|\delta|/\lambda\ll 1$, the multiple scattering theory has been worked out on another basis by D. L. Dexter and W. W. Beeman, Phys. Rev. **76**, 1782 (1949).

most experiments. The average is

$$\langle I\rangle = |P|^{-N}\int_P\cdots\int_P I dP_1 dP_2\cdots dP_N,$$

where dP_n is the element of surface associated with $\mathbf{x}_n$ and $|P|$ stands for the area of the illuminated portion of P. Inserting Eq. (5) into this formula, only the second exponential factor is affected by the new integrations, and the N-fold integral splits into N identical single (surface) integrals. Thus

$$\langle I\rangle = \lambda^{-2}\int_P\int_P \exp\{ig(\mathbf{x})-ig(\mathbf{x}')\}X^N dP dP',$$

where

$$X = |P|^{-1}\int_P \exp\{if(\mathbf{x},\mathbf{x}_n)-if(\mathbf{x}',\mathbf{x}_n)\}dP_n.$$

Since the integrand in X is unity over most of P, it is convenient to write

$$X = |P|^{-1}\left\{\int_P dP_n - \int_S dP_n + \int_S \exp\{if(\mathbf{x},\mathbf{x}_n) - if(\mathbf{x}',\mathbf{x}_n)\}dP_n\right\},$$

where S is that portion of P for which either $|\mathbf{x}-\mathbf{x}_n|$ or $|\mathbf{x}'-\mathbf{x}_n|$, or both is not greater than R'. Let the area of S be $|S|$. Let $N\pi R^2|P|^{-1}=p$, so that p is the mean number of particles pierced by a geometrical ray through the sample. Then

$$X = 1-pN^{-1}G(r),$$

where

$$G(r) = (\pi R^2)^{-1}\left[|S| - \int_S \exp\{if(\mathbf{x},\mathbf{x}_n) - if(\mathbf{x}',\mathbf{x}_n)\}dP_n\right] \quad (6)$$

and $r=|\mathbf{x}-\mathbf{x}'|$. Then since $N\gg 1$,

$$X^N = [1-pN^{-1}G(r)]^N \cong \exp\{-pG(r)\},$$

and the exponential form will be valid so long as $N\gg pG(r)$. Thus

$$\langle I\rangle = \lambda^{-2}\int_P\int_P \exp\{ig(\mathbf{x})-ig(\mathbf{x}')-pG(r)\}dP dP'.$$

Further reduction depends upon the function $G(r)$, which is defined by very intractable integrals. $G(r)$ is zero at $r=0$, and, for small r, varies quadratically with r. For sufficiently large p (and we subsequently assume $p\gg 1$), $\langle I\rangle$ is affected only by the value of G at small r, and thus only the quadratic term in its power series expansion need be used. Simultaneously, the first integration over the illuminated portion of P may be replaced by an integral over the infinite plane. Let $\mathbf{x}$ be described by the polar coordinates r, ψ, relative to $\mathbf{x}'$, so that $y-y'=r\sin\psi$. Then $g(\mathbf{x})-g(\mathbf{x}')=2\pi\lambda^{-1}r\sin\psi\times\sin\theta$, and $dP=rdrd\psi$. Setting $G(r)=ar^2$, where a is a coefficient yet to be computed, we have

$$\langle I\rangle = \lambda^{-2}\int_P dP'\int_0^\infty\int_0^{2\pi} \times\exp\{2\pi i\lambda^{-1}r\sin\psi\sin\theta - par^2\}rdrd\psi.$$

The integration with respect to ψ yields a Bessel function of zero order,[11] after which the integral with respect to r is Weber's first exponential integral and may be evaluated in terms of an exponential function.[12] The integration with respect to P' then multiplies the result by $|P|$, so one finally has

$$\langle I\rangle = \pi|P|\lambda^{-2}p^{-1}a^{-1}\exp\{-(\pi^2\sin^2\theta)/(\lambda^2 pa)\}.$$

Replacing $\sin\theta$ by θ, the width of the scattering pattern, w, as previously defined, becomes

$$w = \lambda\pi^{-1}(pa)^{\frac{1}{2}}. \quad (7)$$

With this replacement of $\sin\theta$ by θ, the total power scattered may be written $\int_0^\infty\langle I\rangle 2\pi\theta d\theta$, which works out to be $|P|$. This is the same as the total power incident on the sample, since we have assumed unit incident intensity.

It has not been found possible to evaluate the function $G(r)$ explicitly. However, successive coefficients of a Taylor series representation may be worked out by evaluating derivatives of G with respect to r at $r=0$. This involves differentiating the two-dimensional integral which defines G [Eq. (6)] and recognizing that both the integrand and the limits of integration depend on r. The zero- and first-order coefficients of the Taylor series are seen to vanish, and after a tedious calculation, which will not be reproduced, the second-order coefficient is found to be

$$a = 4\pi^2\delta^2\lambda^{-2}[1-\ln\{1-(R'/R)^2\}]. \quad (8)$$

The singularity of this expression for $R'=R$ arises from the fact that our assumptions concerning the phase shift and intensity of the radiation on P are quite inaccurate when extended into the region of total external reflection very near the edge of a particle. Without removing these assumptions, a step which would greatly complicate the calculation, a reasonably accurate answer would seem to be achievable by simply taking the cut-off radius, R', equal to the radius at which total external reflection sets in.[13] This limiting radius is found to be $R(1-|\delta|)$. Inserting this value of R' into Eq. (8), we have (treating $|\delta|$ as much less than 1) $a=4\pi^2\delta^2\lambda^{-2}[1-\ln 2|\delta|]$, and the width of scattering is

$$w = p^{\frac{1}{2}}|\delta|[1-\ln 2-\ln|\delta|]^{\frac{1}{2}}. \quad (9)$$

[11] G. N. Watson, *Treatise on the Theory of Bessel Functions* (The Macmillan Company, New York, 1945), p. 20.

[12] See reference 11, p. 393.

[13] If δ is negative, the reflection will not be total, but still will become very large at about $R(1-|\delta|)$.

The ray theory of von Nardroff gives very nearly the same answer, Eq. (1).

The discrepancy between the two formulas apparently arises from the difference in treatment of intensity of rays near the edge of a particle. The von Nardroff calculation also errs in this respect, since it assumes perfect transmission of all rays except those suffering total external reflection. The difference in the formulas is actually very minor: for $\delta=10^{-6}$, the von Nardroff value of w is only about 3 percent larger than the width calculated here.

Confirmation of the supposition that "edge" effects are responsible for the above discrepancies is afforded rather easily by considering an artificial case in which such effects would be absent, namely, the scattering from right circular cones. We suppose the cones to have altitude h, radius of base R, and to be oriented always with their axes parallel to the incident beam. Every ray striking a cone will then be deviated, according to geometrical optics, by an angle $h|\delta|/R$ (to first order in δ). The root mean square deviation of rays will then also be $h|\delta|/R$, and von Nardroff's considerations of multiple scattering by an average of p scatterers per ray would lead to a Gaussian distribution of scattered rays with a width $w_{VN}'=p^{\frac{1}{2}}h|\delta|/R$. If, instead, the Huygen's principle calculation be applied to this case, the phase shift function $f(\mathbf{x}, \mathbf{x}_n)$ of Eq. (2) is replaced by $f'(\mathbf{x}, \mathbf{x}_n)$, where

$$f'(\mathbf{x}, \mathbf{x}_n)=(2\pi\delta/\lambda)(h/R)(R-|\mathbf{x}-\mathbf{x}_n|), \quad |\mathbf{x}-\mathbf{x}_n|\leq R,$$
$$f'(\mathbf{x}, \mathbf{x}_n)=0, \quad |\mathbf{x}-\mathbf{x}_n|>R.$$

All of the previous calculation for spheres now applies, and it is only necessary to work out the new value for the coefficient a, say a', corresponding to the phase shift f'. This proves to be $a'=(\pi^2h^2\delta^2)/(\lambda^2R^2)$. Inserting this in Eq. (7), the width becomes $w'=\lambda\pi^{-1}(pa')^{\frac{1}{2}}=p^{\frac{1}{2}}h|\delta|/R$. This width agrees precisely with the ray theory width given above, and, of course the distribution of scattered intensity is also Gaussian.

We conclude that the von Nardroff formulation is indeed justified for the case where (*a*), the scattering is highly multiple and, (*b*), the particles are sufficiently large that $R|\delta|/\lambda\gg 1$, but that it is not justified for scattering by one, or only a few isolated particles. It is not clear whether formula (9) or formula (1) is the better approximation, but for δ as ordinarily encountered, the discrepancy between them is not important.

PHYSICAL REVIEW VOLUME 85, NUMBER 4 FEBRUARY 15, 1952

The Impulse Approximation*

GEOFFREY F. CHEW
Brookhaven National Laboratory, Upton, New York, and University of Illinois, Urbana, Illinois

AND

GIAN CARLO WICK
Carnegie Institute of Technology, Pittsburgh, Pennsylvania

(Received November 8, 1951)

An analysis is made of the assumption that the scattering of an elementary particle by a complex nucleus is well approximated by the superposition of outgoing waves generated by the individual nucleons acting independently. The special case of nucleon-nucleon scattering is discussed in detail and an estimate given of the order of magnitude of the error in the approximation. Application of the method to meson problems is also discussed.

INTRODUCTION

IN an earlier paper[1] one of us proposed an "impulse approximation" for the study of collisions between fast nucleons and deuterons. This method, which can also be applied to other collision problems,[2] was advanced on the basis of plausibility arguments, while a more careful analysis of its validity by the present authors was promised. Some crude estimates of the errors involved in the method were quickly obtained for a typical case; further efforts led to some formal improvements, but in trying to explore the validity of the approximations under much more general conditions, we encountered serious difficulties. In view of the improbability of further rapid progress and because of the appearance of new applications,[3] we have decided to publish our present crude and incomplete results as a partial answer to the need for a better justification of the method.

Owing to the well-known inadequacy of the Born approximation in the case of nuclear forces,[3] one has no really good and simple method for the study of nuclear

* Work partially supported by the AEC.

[1] G. F. Chew, Phys. Rev. **80**, 196 (1950).

[2] Fernbach, Green, and Watson, Phys. Rev. **82**, 980 (1951); B. Segall, Phys. Rev. **83**, 1247 (1951); W. Cheston, Phys. Rev. (to be published); Y. Fujimoto and Y. Yamaguchi, Prog. Theor. Phys. **6**, 166 (1951); G. F. Chew and H. W. Lewis, Phys. Rev. **84**, 779 (1951).

[3] R. Jost and A. Pais, Phys. Rev. **82**, 840 (1951).

collisions involving more than two nucleons. There are many circumstances, however, under which the many-body character of a problem is only a secondary feature, and the collision may be decomposed, as it were, into a superposition of simple two-body collisions. This is a familiar thought, which finds expression in a variety of approximations, ranging from the crude additivity rule for cross sections, which is seldom applicable, to more sophisticated procedures, such as the Fermi theory of the effect of the chemical bond on slow neutron scattering.[4] The impulse approximation is another expression of the same thought.

Mention should be made of a modification of the Born approximation[5] which leads to expressions essentially equivalent to those obtained with the impulse approximation. The difference between the two methods is then mainly one of emphasis and physical picture. The assumption on which the modified Born method is based can perhaps be expressed as follows. One calculates in the first approximation the scattering amplitudes for (a) the nucleon-nucleon and (b) the nucleon-deuteron collision problem, for example; one then assumes that the relationship that one obtains between the two, via the elimination of the Fourier components of the nucleon-nucleon interaction, is valid even though the Born approximation is not.

The assumptions underlying the impulse approximation are somewhat different and perhaps a little more physically plausible. Consider as a typical case a simple particle (say a nucleon) striking a complex system (deuteron, light nucleus). The assumptions are then the following: (I) The incident particle never interacts strongly with two constituents of the system at the same time; (II) the amplitude of the incident wave falling on each constituent (nucleon) is nearly the same as if that constituent were alone; and (III) the binding forces between the constituents of the system are negligible during the decisive phase of the collision, when the incident particle interacts strongly with the system.

Of these assumptions, I and III are seen to be vital, if one wants to avoid essential n-body features in the problem; II, which may be called the transparency requirements, is less vital, but simplifies matters considerably. Condition I is the one that perhaps needs least justification in most applications, for instance in the case of a loose structure like the deuteron, in which the average distance between the constituents is noticeably larger than the range of the interaction. I and II will be discussed in the third section of the paper.

The main part of the paper is thus devoted to a study of the consequences and validity of condition III, which is in fact the most interesting one. It is from this condition that the name of the approximation is derived, in analogy with those problems in classical dynamics in which one considers the effect on a system of a force acting for a time so short, that all other forces may be neglected during that time.[6] In a quantum-mechanical problem, of course, such an assumption involves some well-known paradoxical features. For example, the binding forces determine the energy levels of the struck system before and after the collision, so that in the case of discrete energy levels it is obvious that the change in energy suffered by the incident particle in the collision is directly affected by the binding forces, in a manner which at first sight is incompatible with our assumption. A proper formulation of the "impulse" assumption in quantum mechanics is possible, however, as soon as due attention is paid to some perfectly familiar points. Thus the energy paradox is removed when one remembers that the very concept of a collision of short duration τ implies the description of the incident particle by means of a short train of waves, whereby any attempt to control the energy E of the system to better than $\Delta E \sim \hbar/\tau$ becomes impossible. Clearly, the process under study must not be too strongly energy dependent, or the whole method is meaningless.

The basic assumption is then that τ can be chosen so small that the change of the many-body wave function during the collision is not noticeably affected by the binding forces. The role of the binding forces is then merely to determine the eigenstates in terms of which the wave function is expanded before and after the collision.

Now to put these ideas into formulas.[7] Let K be the total kinetic energy operator, V the interaction between the incident particle and the system, and U the potential of the binding forces, so that the total Hamiltonian is

$$H = K + V + U, \tag{1}$$

while

$$H_0 = K + U \tag{2}$$

is the "unperturbed" Hamiltonian.

Let Φ_a be the wave function for some initial state, say the product of the eigenfunction of some definite state of the struck system by a wave packet for the motion of the incident particle relative to the system. We write the time dependence of the wave function explicitly as a factor multiplying Φ_a (for simplicity in the rest of this discussion we set $\hbar = 1$). This will hold until some time t_1 when the collision begins. At that time, therefore, the wave function is

$$\exp(-iH_0 t_1)\Phi_a. \tag{3}$$

From then on the wave function evolves according to the complete Hamiltonian, so that at the end of the collision, at a time

$$t_2 = t_1 + \tau,$$

[4] E. Fermi, Ricerca Sci. **VII-II**, 13 (1936).
[5] R. L. Gluckstern and H. A. Bethe, Phys. Rev. **81**, 761 (1951).
[6] The further assumption, often made, that the displacement of the struck system can be neglected during the collision, will not be made here.
[7] See Ashkin and Wick, this issue of *The Physical Review*, for a formulation much improved over the one presented here.

the wave function is

$$e^{-iH\tau}e^{-iH_0t_1}\Phi_a. \tag{4}$$

To find the probability of transition to some final state Φ_b, defined analogously to Φ_a, and which is, therefore, given at the time t_2 by

$$\exp(-iH_0t_2)\Phi_b, \tag{5}$$

one must take the scalar product of (4) and (5), which is equal to the matrix element $(\Phi_b, S\Phi_a)$, where

$$S=e^{iH_0t_2}e^{-iH\tau}e^{-iH_0t_1}. \tag{6}$$

It is easy to see that (6) is the transformation function which Schwinger, Dyson, and others[8] use to define the Heisenberg S-matrix. The exact S-matrix is obtained in the limit $t_1\rightarrow-\infty$, $t_2\rightarrow+\infty$, in which case the energy of the wave packets Φ_a and Φ_b can be defined with arbitrary accuracy. We here use (6) as an approximate expression for S, applicable only to suitably chosen wave packets, such that $t_2-t_1=\tau$ can be assumed very small.

Our basic assumption is now that in the middle exponential in (6) one can neglect U, i.e., that

$$|U|\tau\ll 1 \tag{7}$$

(in ordinary units: $|U|\tau\ll\hbar$). For the same reason one can neglect U in the lateral exponentials; to see this most simply consider that, for the wave packets to which it is to be applied, S is obviously independent of how we choose the origin of time. Let then $t_1+t_2=0$, so that $t_1=-\tau/2$, $t_2=+\tau/2$. Neglecting then $\pm U\tau/2$ in the side exponentials, one has approximately $S\approx s$ where

$$s=e^{iKt_2}e^{-i(K+V)(t_2-t_1)}e^{-iKt_1}. \tag{8}$$

Now s is just the transformation which in the limit $t_1\rightarrow-\infty$, $t_2\rightarrow+\infty$ defines the S-matrix for the collision between the incident particle and a system of unbound particles. In order to arrive at the simple expression of the impulse approximation one has still to argue that owing to the high velocity of the incident particle and short range of the force, the expression (8) is already practically equal to the limit, $t_1=-\infty$, $t_2=+\infty$, when the collision time, $\tau=t_2-t_1$ satisfies (7); furthermore, one has to use assumptions (I) and (II) (we have only used III so far) to reduce s to an expression involving only two particles at a time. These assumptions clearly imply that the initial spatial distribution of the scattering particles is such that, once these particles are treated as free, the scatterings of the incident particle by particles number 1, 2, $\cdots$ are independent.

Thus the transition operator for the complex system, when our three assumptions are valid, will be simply a linear superposition of the two particle transition operators which describe the scattering of the incident particle by the individual target particles. This result is given its most useful expression in terms of that form of the T matrix[8] which does not contain as a factor the energy delta-function

$$T\approx t=t_1+t_2+\cdots, \tag{9}$$

where t_i is the t-matrix for the scattering of the incident particle by particle i. The probability amplitude for the transition from state a to state b is finally,

$$(\Phi_b, [t_1+t_2+\cdots t_n]\Phi_a). \tag{10}$$

This is the basic formula that has been used so far under the name of impulse approximation. The ambiguities about treatment of energy conservation which may trouble the reader at this point will be completely removed in the next section, where a systematic study is to be made of the error arising from assumption III. For that purpose we shall consider a simplified problem in which only that assumption is involved, namely, the case in which the incident particle interacts with a single target particle bound to a fixed field of force.

THE IMPULSE ASSUMPTION

Using the formalism of Lippmann and Schwinger,[8] the exact solution of the simplified problem is a wave function Ψ_a, which satisfies the integral equation,

$$\Psi_a=\Phi_a+\frac{1}{E_a+i\eta-K-U}V\Psi_a. \tag{11}$$

The quantity η is a real positive number which is to be allowed to go to zero after one has performed the sum over states required to give meaning to the operator $(E_a+i\eta-K-U)^{-1}$. The function Φ_a is a product of an incident plane wave in the first particle's coordinates and a bound state function in the coordinates of the second. That is to say, Φ_a is an eigenfunction of the operator, $K+U$, with the eigenvalue, E_a.

If we know Ψ_a, then the exact T-matrix is given by

$$T_{ba}=(\Phi_b, V\Psi_a). \tag{12}$$

The impulse approximation (10) amounts in this simple case of a single scatterer to the statement that $T\approx t$ or

$$T_{ba}\approx(\Phi_b, t\Phi_a), \tag{13}$$

where t is the operator which describes the free, two particle scattering. We can define t in terms of the wave function, ψ_n, which describes the free scattering of the pair of particles, starting from an eigenstate χ_n of the kinetic energy operator, K. That is, the function ψ_n satisfies the integral equation

$$\psi_n=\chi_n+\frac{1}{E_n+i\eta-K}V\psi_n, \tag{14}$$

if E_n is the eigenvalue of K belonging to χ_n. In the χ_n representation, the matrix elements of t are defined by

$$t_{mn}=(\chi_m, V\psi_n). \tag{15}$$

[8] See, for instance, B. A. Lippmann and J. S. Schwinger, Phys. Rev. 79, 469 (1950).

The function $t\Phi_a$ is, therefore, to be understood in terms of the expansion of Φ_a in the set χ_n,

$$t\Phi_a=\sum_{m,n}\chi_m t_{mn}(\chi_n,\Phi_a)=V\sum_n\psi_n(\chi_n,\Phi_a). \quad (16)$$

Comparing (16) with (13) and (12) we see that an alternative way of expressing the impulse approximation is to say that where V is important (has large matrix elements), one assumes the correct wave function, Ψ_a, to be well represented by the function,

$$\Psi_a^0=\sum_n\psi_n(\chi_n,\Phi_a). \quad (17)$$

As already discussed by Chew,[1] this function represents the scattering of the incident particle by a wave packet of the free target particle, a packet which contains the same momentum distribution as the actual bound state.

Since there is a one to one correspondence between the two particle scattering functions ψ_n and the basis functions χ_n, one may define a matrix,

$$\Omega_{mn}=(\chi_m,\psi_n), \quad (18)$$

and write (17) in the shorthand form[9]

$$\Psi_a^0=\sum_{m,n}\chi_m\Omega_{mn}(\chi_n,\Phi_a)=\Omega\Phi_a. \quad (19)$$

It is now proposed to investigate the accuracy of the impulse approximation (13) by employing Ψ_a^0 as the trial function in a variational expression for T_{ba}. Such an expression has been given by Lippmann and Schwinger,[8]

$$\mathcal{T}_{ba}=(\Phi_b, V\Psi_a^+)+\left(\Psi_b^-, V\left[\Phi_a+\frac{1}{E_a+i\eta-K-U}V\Psi_a^+-\Psi_a^+\right]\right). \quad (20)$$

This expression is stationary with respect to independent variations of the functions Ψ_a^+ and Ψ_b^- about the solutions of the following equations:

$$\Psi_a^+=\Phi_a+\frac{1}{E_a+i\eta-K-U}V\Psi_a^+, \quad (21)$$

$$\Psi_b^-=\Phi_b+\frac{1}{E_b-i\eta-K-U}V\Psi_b^-. \quad (21')$$

Thus $\mathcal{T}_{ba}$ is stationary about $\Psi_a^+=\Psi_a$, since Eq. (11) is identical with (21). The stationary value of $\mathcal{T}_{ba}$ is T_{ba}, the matrix element we are seeking.

We argue now that to replace Ψ_a^+ in (20) by Ψ_a^0 will give a better value for T_{ba} than simply substituting into (12), the latter procedure being the one which leads to the impulse approximation. The reason, of course, is that (20) is stationary, whereas (12) is not. Thus we can expect to find a correction to the impulse approximation by employing (20).

[9] We are indebted to M. Gell Mann for calling to our attention the appropriate nature of the matrix notation in this problem. Ω is essentially the matrix wave function of C. Møller, Kgl. Danske Videnskab. Selskab, Mat.-fys. Medd. **23**, No. 1 (1945).

Using Ψ_a^0 as a trial function in this way, one finds

$$T_{ba}=(\Phi_b, V\Psi_a^0)+(\Psi_b^-, V\Psi_a'), \quad (22)$$

where

$$\Psi_a'=\Phi_a+\frac{1}{E_a+i\eta-K-U}V\Psi_a^0-\Psi_a^0. \quad (23)$$

Equation (22) is an identity so long as Ψ_b^- is exact. It is clear even from (23) that the smallness of Ψ_a' is somehow a measure of the accuracy of the function Ψ_a^0, for if the latter were exact, then Ψ_a' would vanish identically.

Using the fact that from (14) and (17),

$$\Psi_a^0=\Phi_a+\sum_n\frac{1}{E_n+i\eta-K}V\psi_n(\chi_n,\Phi_a), \quad (24)$$

one finds

$$\Psi_a'=\sum_n\left[\frac{1}{E_a+i\eta-K-U}-\frac{1}{E_n+i\eta-K}\right]V\psi_n(\chi_n,\Phi_a), \quad (25)$$

which may be contracted by using the operator relation,

$$A^{-1}-B^{-1}=A^{-1}(B-A)B^{-1}. \quad (26)$$

In our case, $B-A=(E_n-E_a)+U$, so that a useful further relation is

$$(E_a-E_n)(\chi_n,\Phi_a)=(\chi_n,U\Phi_a). \quad (27)$$

This last equality is simply the Schrödinger equation for the state Φ_a, expressed in the χ_n representation. Putting together (26) and (27) and once again making use of (14), one finds

$$\Psi_a'=\frac{1}{E_a+i\eta-K-U}\sum_n\{U\psi_n(\chi_n,\Phi_a)-\psi_n(\chi_n,U\Phi_a)\}. \quad (28)$$

Using the shorthand notation as in (19), this may be rewritten as

$$\Psi_a'=\frac{1}{E_a+i\eta-K-U}[U,\Omega]\Phi_a. \quad (28')$$

Returning to (22) one may consistently replace the function Ψ_b^- by

$$\sum_n\psi_n^-(\chi_n,\Phi_b), \quad (29)$$

where ψ_n^- satisfies the integral equation

$$\psi_n^-=\chi_n+\frac{1}{E_n-i\eta-K}V\psi_n^-. \quad (30)$$

This is analogous to the replacement of Ψ_a^+ by Ψ_a^0 and has exactly the same justification. Corresponding to the matrix t, one can define a matrix t^- with elements

$$t_{mn}^-=(\psi_m^-, V\chi_n), \quad (31)$$

and it can be shown[8] that for $E_m=E_n$, $t_{mn}^-=t_{mn}$. In

fact, since T_{ba} can just as well be written $(\Psi_b^-, V\Phi_a)$ as $(\Phi_b, V\Psi_a^+)$, one may expect t^- to be equally as accurate as t as an approximation to T. Evidently the validity of the impulse approximation implies that the relevant matrix elements of t^- are not much different from those of t.

Making the approximation (29) for Ψ_b^- as it appears in (22), one finds for the second term of (22)

$$\sum_n (\Phi_b, \chi_n)(\psi_n^-, V\Psi_a'),$$

which by virtue of (31) can be expressed as

$$(\Phi_b, t^-\Psi_a'). \tag{32}$$

Now we have argued that if the second term of (22) is small compared to the first, then the difference between t^- and t cannot be important. Thus it is consistent to replace t^- by t in (32), so long as we regard the latter as only a correction term and rewrite (22) in the form

$$\begin{aligned} T_{ba} &\approx (\Phi_b, t\Phi_a)+(\Phi_b, t\Psi_a') \\ &= (\Phi_b, t\{1+(E_a+i\eta-K-U)^{-1}[U, \Omega]\}\Phi_a). \end{aligned} \tag{22'}$$

There exists a strong suspicion that the derivation of (22′) presented here is unnecessarily complicated. Evidently an expansion of the T matrix in powers of U is the desired goal, and we have here obtained the zeroth- and first-order terms, *viz.*,

$$T=t\left\{1-i\int_{-\infty}^{0} dx e^{\eta x} e^{iKx}[U, \Omega]e^{-iKx}+0(U^2)\right\} \tag{33}$$

using a manner of expression recommended by Snyder.[10] Since the corresponding exact integral equation for T is

$$T=V\left\{1-i\int_{-\infty}^{0} dx e^{\eta x} e^{i(K+U)x} T e^{-i(K+U)x}\right\}, \tag{34}$$

while that for t is

$$t=V\left\{1-i\int_{-\infty}^{0} dx e^{\eta x} e^{iKx} t e^{-iKx}\right\}, \tag{35}$$

the suggestion is unavoidable that (33) can be obtained directly by expanding (34) with reference to (35) in powers of U. The technique of carrying out this expansion has eluded us so far, however, and we have resorted to the variational approach as a temporary "crutch."

The form (22′) shows that what was meant in the introduction, when speaking of the "collision time" τ, was $1/\langle \Delta E\rangle_{Av}$, where $\langle \Delta E\rangle_{Av}$ is some kind of average of the extent to which energy conservation is "violated" during the collision. This average is represented formally by the denominator in (28′). On the other hand, the assumption (7) was unnecessarily strong. We have found that (7) should be replaced by

$$\langle |\tau[U, \Omega]| \rangle_{Av} \ll 1, \tag{7'}$$

so that strong binding potentials, if they depend "weakly" on the nucleon variables, may be tractable with the impulse approximation. Actually, nuclear forces are strongly spin dependent, so the difference between (7) and (7′) is not important when the target is a nucleus. The difference would be important if the binding were molecular.

ASSUMPTIONS I AND II

A quantitative criterion has been achieved for the validity of assumption III, the impulse assumption, which can be used for any type of scattering problem. We have not yet succeeded in formulating so generally the criterion for the validity of assumption II, the transparency assumption.† One can, however, make two qualitative statements.

(1) When the target system contains many particles, the "mean free path" for the incident particle in the scattering material must certainly be large compared to the over-all dimensions of the scatterer. Otherwise the target particles on the "far" side of the scattering region will be shielded and will not contribute as much as if they were free and alone. It is well known that for special cases a correction for this attenuation of the incident beam can be made without difficulty, and it seems not impossible that a general formulation of the correction procedure may yet be achieved. However, for the time being, applications of the impulse approximation must be restricted to light nuclei. The exact value of the maximum permissible radius will depend on the value of the single particle scattering cross section. If we assume constant nuclear density, so that the nuclear radius is given by $r_0A^{\frac{1}{3}}$ ($r_0=1.4\times10^{-13}$ cm), then the mean free path within the nucleus is $(4\pi/3)r_0^3/\sigma$ (σ is the single nucleon cross section), and the transparency requirement becomes

$$(3/4\pi)\sigma A^{\frac{1}{3}}/r_0^2 \ll 1. \tag{36}$$

(2) For target systems with only a few particles, the transparency requirement has a more subtle aspect. The amplitude of the scattered wave sent out by a particular nucleon must, by the time it reaches another nucleon have become negligible in comparison to the amplitude of the incident wave. Otherwise "multiple scattering" effects will be significant. Naively, one would expect the multiple scattering error to be of the order of the amplitude of the scattered wave from a single nucleon evaluated, for unit incident amplitude, at a distance $\bar{R}$, if $\bar{R}$ is the average internucleon distance. In terms of the cross section, σ, this becomes

$$(\sigma/4\pi)^{\frac{1}{2}}/\bar{R} \ll 1. \tag{37}$$

Actually, it will be shown that when the wavelength of the scattered particle is small compared to the average nucleon separation distance R, interference reduces the average amplitude of the scattered wave by a factor

[10] H. Snyder, private communication.

† This formulation will be presented in a forthcoming paper by G. F. Chew and M. L. Goldberger.

$\sim\lambda/\bar{R}$, so that (37) is replaced by

$$(\lambda/\bar{R})(\sigma/4\pi)^{\frac{1}{2}}/\bar{R}\ll 1. \tag{37'}$$

It is plausible that (36) and (37) or (37′) together form the general criteria for the validity of assumption II. However, no systematic quantum-mechanical treatment comparable to that of the last section for assumption III has yet been achieved.† The situation with regard to assumption I is even worse. One might say that the "range" of the interaction of the incident particle with a target nucleon must be much less than $\bar{R}$; but in some cases the range of the interaction may be difficult to define. Each problem requires individual study. The next section will discuss in some detail the special case of nucleon-nucleon scattering. The following one will treat, in a more qualitative way, meson-nucleon scattering. These two examples will fairly well illustrate the meaning of requirement I with respect to that of II and III.

THE SCATTERING OF HIGH ENERGY NUCLEONS BY COMPLEX NUCLEI

With the usual assumption that the interaction between two nucleons is describable in terms of a velocity independent potential, the "range" of the fundamental interaction would seem to have a fairly definite meaning. Nevertheless this "range" decreases with increasing particle energy as the wavelength becomes shorter, and it would be incorrect to use the effective range as defined by low energy scattering experiments to estimate the validity of assumption I in the hundred million-volt region. Probably a more reasonable way to make the estimate at high energies is to say the total cross section is "geometrical," that is define the range, ρ, by $\pi\rho^2=\sigma^{\text{total}}$. Using $\sigma^{\text{total}}=4\times10^{-26}$ cm^2 as an average value, this estimate leads to $\rho\approx1.1\times10^{-13}$ cm. Assumption I is thus marginal for an average nucleus where $\bar{R}=2.2\times10^{-13}$ cm but valid for the deuteron. For the deuteron, where $\bar{R}=3.2\times10^{-13}$ cm, one can make a simple geometrical estimate of the probability that a particle which is less than 1.1×10^{-13} cm from the proton should at the same time be less than 1.1×10^{-13} cm from the neutron. The result is about 10 percent. Note that it does not necessarily follow that the error in the impulse approximation due to this source is as much as 10 percent. (For example, if the Born approximation were valid, there would be no error at all!)

The analysis of the transparency requirement (II) can be carried out quite simply if the target nucleons are replaced by fixed scattering centers of zero range force whose individual total cross sections are equal to those of the actual nucleons. It is evident that the essence of the transparency question is unaltered by this simplification. Consider, then, two fixed centers, separated by a displacement $\mathbf{R}$, which would individually have scattering lengths a_1 and a_2 (e.g., for unit incident amplitude, the scattered wave from the first center alone would have amplitude $(a_1/r_1)\exp(ir_1/\lambda)$, where r_1 is the distance from the center). A short calculation shows that in the presence of the second center the effective scattering length of the first is altered to

$$a_1'=a_1\frac{1+\exp(i\mathbf{k}_a\cdot\mathbf{R})(a_2/R)\exp(ik_aR)}{1-(a_1/R)\exp(ik_aR)(a_2/R)\exp(ik_aR)}, \tag{38}$$

where $\mathbf{k}_a$ is the wave number of the incident particle ($k_a=1/\lambda$). The modification in the numerator is obviously due to the initial outgoing wave from the second center which impinges upon the first. The denominator represents waves which bounce back and forth many times. Keeping only linear and quadratic terms in the scattering lengths, the denominator of (38) may be neglected; and if one averages the displacement vector R over a spherical distribution, one finds for $k_a\bar{R}\gg1$,

$$a_1'\approx a_1(1+ia_2/2k_a\bar{R}^2), \tag{39}$$

so that the error involved in approximating a_1' by a_1 is $\sim(a_2/\bar{R})(\lambda/\bar{R})$. This is just the result (37′) with $\sigma=4\pi a_2^2$. For 200-Mev nucleon-deuteron scattering, $\lambda/\bar{R}\approx\frac{1}{8}$ and $a/\bar{R}\approx\frac{1}{6}$. This makes the multiple scattering error ~3 percent. The wavelength varies inversely with the square root of the energy, and below 100 Mev the nucleon-nucleon cross sections increase sharply. Thus at 50 Mev, $\lambda/\bar{R}\approx\frac{1}{2}$ and $a/\bar{R}\approx\frac{1}{3}$, pushing the multiple scattering error to 16 percent.

It is doubtful that one can or ought to talk of "attenuation" in a structure as simple as the deuteron. In a nucleus heavier than the alpha-particle, however, an estimate should be made of the requirement (36). We find, with $\sigma=4\times10^{-26}$ cm^2, that

$$(3/4\pi)\sigma A^{\frac{1}{3}}/r_0^2\approx\tfrac{1}{2}A^{\frac{1}{3}}. \tag{40}$$

Thus the attenuation error can be very serious in complex nuclei.

We come finally to assumption III, the impulse assumption. The problem is to estimate the importance of the second term in (22′) with respect to the first. As stated above, the order of magnitude is $\tau[U,\Omega]$, where $1/\tau$ is the "average" violation of energy conservation "during" the collision. The value of this ratio depends considerably on the model adopted to describe the nucleon-nucleon interaction, i.e., on Ω. For a zero range force with strong spin dependence, for example, one finds, upon evaluation of (22′) in the limit $\lambda\ll\bar{R}$,

$$\tau[U,\Omega]\sim(\langle\Delta U\rangle_{\text{Av}}/E_a)(a/\lambda), \tag{41}$$

where $\langle\Delta U\rangle_{\text{Av}}$ is the average change of potential energy of the target nucleon in its ground state when its spin is flipped, and a is the scattering length for spin flip. E_a is the kinetic energy of the incident nucleon. One may interpret this result by saying that a zero range force is intrinsically capable of an arbitrarily large "violation" of energy conservation. The average value of $1/\tau$ then is determined by the incident energy itself.

A simpler interpretation is that the collision time is the time required for one wavelength of the incident particle to pass a fixed point. This is $\sim 1/E_a$.

The occurrence of the factor a/λ in (41) is surprising until one remembers that when the first Born approximation is valid there is no error in the impulse approximation. The error in the Born approximation decreases as the scattering becomes weaker. Therefore, so must the error in the impulse approximation.

The situation is quite different when field theory is used to describe the scattering as occurring through the exchange of a meson. Here the scattering cannot proceed in first Born approximation, so the impulse error is not proportional to the scattering length. On the other hand the average violation of energy conservation is greater, being of the order of the total energy of the exchanged meson. Thus (41) is replaced by

$$\langle \Delta U \rangle_{\text{Av}} / (\mu^2 c^4 + c^2 k_a^2)^{\frac{1}{2}}, \tag{42}$$

if μ is the meson mass and $\langle \Delta U \rangle_{\text{Av}}$ is now the change in potential energy which occurs when a meson is emitted by the target nucleon. This may be due to a flip of either the spin or the isotopic spin or both.

Taking $\langle \Delta U \rangle_{\text{Av}} \approx 10$ Mev, one finds for $E_a = 200$ Mev and $a = 0.6 \times 10^{-13}$ cm that (41) gives about 5 percent for the impulse error. Formula (42) gives an error of 2 percent, so there is no significant difference between (41) and (42) at high energies. However, below 100 Mev (41) becomes very much larger with decreasing energy, whereas (42) approaches a constant value of only a few percent. At the lower energies, however, the probability of exchanging more than one meson in a collision becomes large and (42) cannot be expected to hold. That is to say, account must be taken of important higher order intermediate states in which no mesons are present and which violate energy conservation by much less than μc^2.

Neither of the models upon which (41) and (42) are based can be taken literally. The fact that both predict only a small error in the impulse assumption at high energies, however, is certainly significant. It would be very surprising if the correct model of the nuclear force, when and if it is discovered, should lead to a large error.

We see in retrospect that the most serious limitations of the "impulse" approximation, as applied to the collisions of nucleons with nuclei, are not associated with the impulse assumption itself but rather with the "secondary" assumptions I and II. All three assumptions are valid to within a few percent for high energy nucleon-deuteron scattering. In more tightly packed nuclei, however, assumption I becomes questionable. Assumption II definitely will lead to a large error for any target heavier than the alpha-particle.

THE SCATTERING OF MESONS BY COMPLEX NUCLEI

The scattering of mesons by nucleons is even less understood theoretically, if that is possible, than the scattering of nucleons by nucleons. Nevertheless, the validity of the impulse approximation is highly probable. In the hundred million-volt region, the meson-nucleon cross section is of about the same size[11] as the nucleon-nucleon cross section. All statements made in the previous section about assumptions I and II, therefore, apply equally well to the scattering of high energy mesons by complex nuclei. The meson cross section decreases sharply with decreasing meson momentum, however, so the transparency assumption (II) gets better instead of worse at low energies, and the method can be applied there to correspondingly heavier target nuclei.

With respect to the impulse assumption one can argue that formula (42) should give the order of magnitude of the error, if $\mathbf{k}_a$ is now the incident meson momentum. That is, if the scattering process takes place via an intermediate state in which there are either no mesons or two mesons present, the violation of energy conservation is simply the energy of the one meson which has been created or destroyed. Segall[2] demonstrates this result in detail for meson-deuteron scattering, showing that the impulse error, even for slow mesons, is unlikely to be more than about 10 percent.

One may worry that, as in the case of nucleon-nucleon scattering, formula (42) is completely untrustworthy at low energies. Empirically, however, there does not seem to be a strong resonance in meson-nucleon scattering comparable to that which occurs at low energies in nucleon-nucleon scattering.‡ Therefore, while the weak coupling theory is certainly quantitatively inadequate, one may hope that the estimate of the collision time which it yields is not wrong by an order of magnitude.

The above considerations apply almost word for word to the problem of photomeson production and its inverse, meson capture with gamma-ray emission. The application to processes involving gamma-rays alone is trivial because the Born approximation is genuinely applicable there. An application has also been made to the production of mesons in nucleonic collisions.[12] The criterion of validity is here obscured by the great loss of energy suffered by the incident nucleon in creating the meson. It thus interacts much more strongly with the nucleus after emitting the meson than it did before. This case merits independent study.

Note added in proof.—The formal deficiencies of this paper have been remedied, partly by Ashkin and Wick (this issue of the Phys. Rev., p. 686), who use a time dependent formalism to make a systematic expansion of T in powers of U, and partly by Chew and Goldberger (forthcoming publication in the Phys. Rev.) who use a stationary state formalism. The latter authors have placed assumptions I and II and the corrections thereto on a basis comparable to that for assumption III.

[11] Chedester, Isaacs, Sachs, and Steinberger, Phys. Rev. **82**, 958 (1951). H. L. Anderson, Phys. Rev. this issue, p. 729.

‡ There may be a P-state resonance, but the width is so large ($\sim$100 Mev) that the collision time is still short compared to nuclear periods.

[12] H. P. Noyes, Phys. Rev. **81**, 924 (1951).

Classification of Energy Levels in Al^{25}*

LOUIS J. KOESTER, JR.†
University of Wisconsin, Madison, Wisconsin
(Received October 1, 1951)

The differential cross section for the elastic scattering of protons by Mg^{24} has been measured by Mooring, Koester, Goldberg, Saxon, and Kaufmann in the range of bombarding energies between 0.4 Mev and 3.95 Mev. In the present work, the energy dependence of this cross section is interpreted in terms of the combination of Coulomb and nuclear potential scattering with resonant scattering. This resonant scattering arises from the excitation of energy levels of the compound nucleus Al^{25}. The general trend of the observed cross section between 0.4 Mev and 3.4 Mev, including the three broadest resonances, is well fitted theoretically.

A method is developed to calculate the effects of imperfect energy resolution on the shapes of resonances, and the results are used to rule out certain assignments.

The excited states corresponding to the three broadest resonances have been classified as follows: 3.11 Mev, $P_{3/2}$; 3.88 Mev, $P_{1/2}$; 5.34 Mev, $P_{3/2}$. These energies are the dissociation energy, which is 2.32 Mev, plus the resonant energy in the center-of-mass system. A twofold ambiguity remains in the angular momentum values assigned to the narrow resonances because the experimental resolution was not sufficient to determine their true maximum cross sections. The assignments are as follows: 3.75 Mev, *F*; 3.91 Mev, *D*; 4.25 Mev, *D*; 4.63 Mev, *D*; 5.83 Mev, *D*. The last assignment is somewhat doubtful because the phase shifts due to higher, unobserved resonances are not known.

The odd parity levels have reduced widths between 10 percent and 30 percent of the value corresponding to single particle excitation, while the even parity levels have reduced widths only a few tenths of one percent of this value. An explanation of the level structure is offered in terms of a nuclear shell model. The spin-orbit splitting of the 3.11 Mev and 3.88 Mev *P* states is small compared with doublet splitting observed in closed-shell plus-one nuclei.

I. INTRODUCTION

A PHASE shift analysis of the elastic scattering of protons by a light, spinless nucleus yields the energy, angular momentum, and relative parity quantum numbers of the excited states formed in the compound nucleus. By analyzing the energy dependence of the differential cross section for the elastic scattering of protons by O^{16}, Laubenstein and Laubenstein[1] classified the excited states observed in F^{17}; and Jackson and Galonsky[2] similarly classified levels in N^{13}. The considerations which permit this type of identification of the excited states observed as scattering resonances can be stated briefly. Since the spin of the target nucleus is zero, the angular momentum value j of a state formed in the compound nucleus is given by the relation,

$$j=l\pm 1/2,$$

where l is the orbital angular momentum value of the incident proton and 1/2 is its spin value. In addition the parity P of this state is related to the parity p of the ground state of the target nucleus by the expression,

$$P=(-1)^l p.$$

Only one value of l satisfies both equations; hence a unique combination of spin and orbital angular momentum of the incident proton is specified. Because the resonant scattering interferes with Coulomb and nuclear potential scattering, the qualitative shape of a resonance depends strongly upon the particular values of j and l; thus the angular momentum and parity of the level are determined.

An important consideration in the choice of a target nucleus for these experiments is that the binding energy of the added proton be low. When this requirement is met, a study of the low-lying excited states of the compound nucleus is permitted, and the spectrum is relatively simple. The binding energy of an additional proton to Mg^{24} is only 2.32 Mev,[3] and the angular momentum of the ground state of Mg^{24} is zero.[4] Using the separated Mg^{24} isotope, Mooring, Koester, Goldberg, Saxon, and Kaufmann[5] measured the differential scattering cross section in the region of proton bombarding energies between 0.4 Mev and 3.95 Mev. The present work concerns the interpretation of their results—the classification of levels observed in the compound nucleus Al^{25} and a brief consideration of the theoretical implications of this level structure, especially in connection with the nuclear shell model proposed by Mayer.[6]

The expression used for the differential scattering cross section is presented and discussed in references 1 and 2. The terminology of these papers is followed here, and the same method of analysis is employed.

II. ANALYSIS OF YIELD CURVE

A. The 0.825-Mev Resonance

Figure 1 shows the yield curve obtained by Mooring *et al.*[5] At energies below 0.8 Mev, this curve is well fitted by Rutherford scattering, and thus the absolute

* Supported by the Wisconsin Alumni Research Foundation and the AEC.
† AEC Predoctoral Fellow. Now at University of Illinois, Urbana, Illinois.
[1] R. A. Laubenstein and M. J. W. Laubenstein, Phys. Rev. **84**, 18 (1951).
[2] H. L. Jackson and A. I. Galonsky, Phys. Rev. **84**, 401 (1951).
[3] Computed from mass values listed in H. A. Bethe, *Elementary Nuclear Theory* (John Wiley and Sons, Inc., New York, 1947).
[4] J. E. Mack, Revs. Modern Phys. **22**, 64 (1950).
[5] Mooring, Koester, Goldberg, Saxon, and Kaufmann, Phys. Rev. **84**, 703 (1951).
[6] M. G. Mayer, Phys. Rev. **78**, 16 (1950).

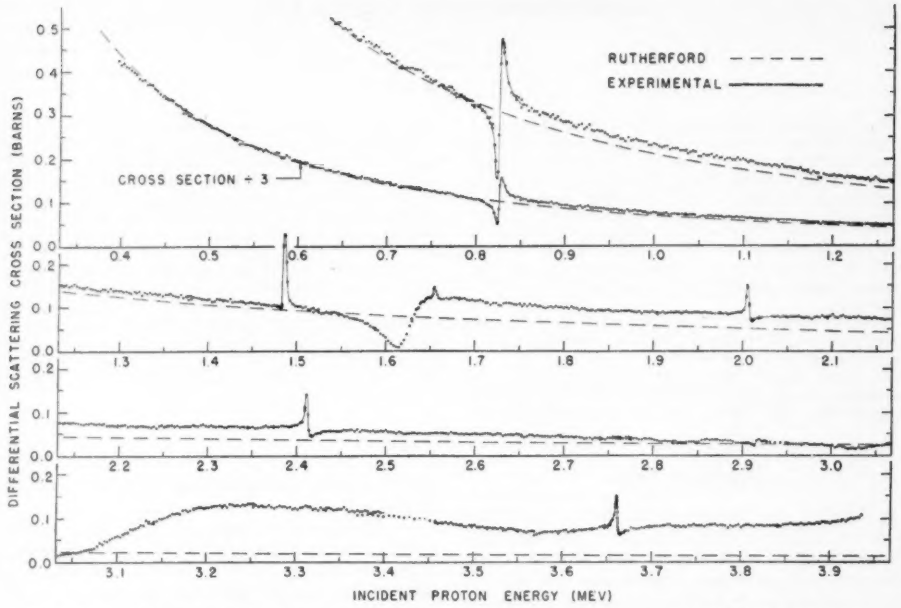

FIG. 1. Differential cross section for the elastic scattering of protons by Mg^{24} at a laboratory angle of $164° \pm 5°$ (in barns per steradian). From the work of Mooring *et al.* [Phys. Rev. **84**, 703 (1951)].

cross section is determined. The resonance at 0.825 Mev provides a good starting point for the analysis because the nuclear potential phase shifts are all negligible, and in first approximation the scattering formula (see references 1 and 2) reduces to the Rutherford term plus a resonance term. All but two possible assignments of angular momentum and parity can immediately be ruled out on grounds of qualitative shape. Wigner's sum rule on reduced widths[7] is used throughout this analysis to limit the number of l values considered for each resonance according to its observed width. For this first resonance, values of l greater than two need not be considered.

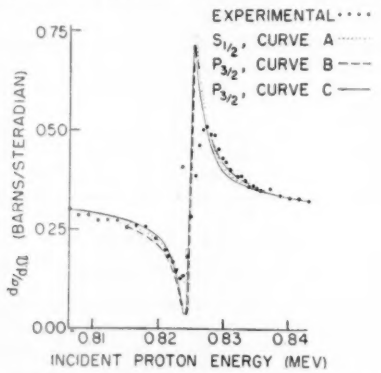

FIG. 2. Theoretical fits of the 0.825-Mev resonance: curve A, approximate calculation for $S_{1/2}$ resonance, in which the incoherent term is neglected and only the resonant phase shift is allowed to vary with energy; curve B, similar approximate calculation for $P_{3/2}$ resonance; curve C, calculation for $P_{3/2}$ resonance without any approximations.

The shape of a $P_{1/2}$ resonance at this energy is qualitatively similar to that of the resonance near 1.6 Mev, with a dip but only a very small maximum, unlike the observed cross section; hence the $P_{1/2}$ assignment is ruled out. The $D_{3/2}$, $D_{5/2}$, $F_{5/2}$, and $F_{7/2}$ assignments are all ruled out because they predict the maximum before the minimum cross section as the energy increases.

Curves A and B of Fig. 2 show, respectively, the approximate calculations for $S_{1/2}$ and $P_{3/2}$ resonances, in which the incoherent term is neglected and only the resonant phase shift is allowed to vary with energy. This approximation is good for an S resonance because the incoherent term is zero. The $P_{3/2}$ assignment is favored here because the averaging effect of imperfect energy resolution in the experiment tends to increase the minimum cross section as well as to decrease the maximum. Better approximations support the con-

[7] E. P. Wigner and L. Eisenbud, Phys. Rev. **72**, 29 (1947); T. Teichmann, Ph.D. Thesis, Princeton University (1949).

TABLE I. Energy levels of Al^{25}, interaction radius: $a_s = 5.05 \times 10^{-13}$ cm.

Bombarding energy in lab system	Resonant energy in center-of-mass system	Resonant energy relative to ground state	Characteristic energy in center-of-mass system	Observed resonance width	Reduced width	Ratio of γ^2 to $A^2/\mu a_s$	Classification
E(Mev)	E_r(Mev)	E_r(Mev)	E_λ(Mev)	Γ(kev)	γ^2(Mev cm)	Percent	
0.825	0.792	3.11	0.405	1.5	2.2×10^{-13}	27.	$P_{3/2}$
1.49	1.43	3.75	1.26	0.3	2.7×10^{-13}	33.	F
1.62	1.56	3.88	1.38	36.	1.7×10^{-13}	21.	$P_{1/2}$
1.66	1.59	3.91	1.59	0.1	$2. \times10^{-15}$	0.2	D
2.01	1.93	4.25	1.93	0.15	$2. \times10^{-15}$	0.2	D
2.40	2.31	4.63	2.31	0.3	$2. \times10^{-15}$	0.2	D
3.14	3.02	5.34	3.03	200.	1.0×10^{-13}	12.	$P_{3/2}$
3.66	3.52	5.83	...	...	...	...	D?

clusion that the 0.825 Mev resonance is a $P_{3/2}$ resonance. Curve C of Fig. 2 shows the fit to the observed cross section that is obtained after the incoherent term, effects of higher resonances, and variation of all the quantities with energy are taken into account. Observation of the scattering at 90° would distinguish conclusively between the $S_{1/2}$ and $P_{3/2}$ possibilities because a P resonance would have no minimum.[1]

The resonant energy is defined herein as the energy, E, in the center-of-mass system, at which the resonance denominator $E_\lambda + \Delta_\lambda - E$ is zero. The characteristic energy E_λ is constant, but the level shift Δ_λ varies with the energy. The value of the observed resonance width Γ is given by the expression

$$\tfrac{1}{2}\Gamma = k\gamma^2/A_l^2,$$

evaluated at the resonant energy; k is the wave number of the incident proton, $1/A_l^2$ is the barrier penetrability, and γ^2 is the reduced width of the level. According to this terminology, the energies and widths of the various levels are given in Table I.

B. The 1.6-Mev Resonance

Because the observed resonance width increases with the wave number and barrier penetrability of the incident proton, the resonant phase shift due to the 0.825-Mev resonance never exceeds 176° in the energy range considered. Similarly, the broad resonances at 1.6 Mev and 3.1 Mev contribute to the phase shifts over most of this energy range. In the analysis of the yield curve, therefore, one must first identify these broad resonances and then piece them together to fit the general trend of the curve. The narrow resonances can then be superimposed without disturbing this fit.

The next resonance to be analyzed is the one that consists of the broad minimum near 1.6 Mev and the broad, flat maximum at higher energies. The small peak near 1.65 Mev is a separate resonance, so narrow that its influence is limited to a region of a few kilovolts; hence it is omitted in the first approximation. The only resonance assignment that does not predict a high maximum cross section at this energy is $P_{1/2}$. The qualitative agreement of the approximate calculation for a $P_{1/2}$ resonance with the experimental results is shown in Fig. 3.

The value of the incoherent term at the minimum cross section is 0.01 barn, which is just the value needed to account for the experimental cross section. Curve B of Fig. 3 shows the result of including the incoherent term and of letting the proton wavelength, the resonant energy, the observed resonance width, and the Rutherford and nuclear potential vectors vary with energy in the calculation. This calculation does not include the effects of other resonances.

C. The Cross Section above 2.8 Mev

The cross section between 2.8 Mev and 3.4 Mev can be interpreted in terms of a single broad resonance, although the shallow minimum near 3.6 Mev suggests another broad resonance at higher energies. The assignment for the resonance between 2.8 Mev and 3.4 Mev can be restricted to $S_{1/2}$ or $P_{3/2}$ on the basis of qualitative shape. The maximum cross section predicted by a $P_{1/2}$ resonance is about half the observed maximum, and the maximum of any of the D or F resonances is much too large.

Figure 4 shows the results of the approximate calculations for $P_{3/2}$ and $S_{1/2}$ resonances. The maximum cross section is too great in either case, although it is worse for the $S_{1/2}$ resonance. More accurate calculations do not improve these fits.

As Jackson and Galonsky[2] state, a value for the interaction radius must be chosen at the beginning of

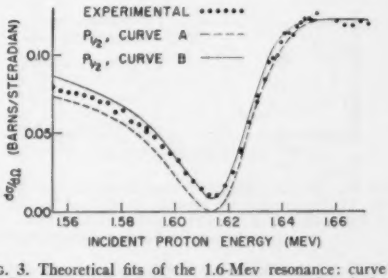

FIG. 3. Theoretical fits of the 1.6-Mev resonance: curve A, approximate calculation for $P_{1/2}$ resonance; curve B, calculation for $P_{1/2}$ resonance without approximations, except that effects of other resonances are omitted.

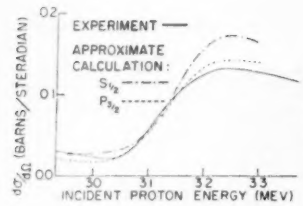

FIG. 4. Approximate calculations for $S_{1/2}$ and $P_{3/2}$ resonances near 3.1 Mev for the interaction radius value 5.83×10^{-13} cm.

the analysis. The first value chosen in this work was

$$a_0=1.5\times10^{-13}(A^{1/3}+1^{1/3})=5.83\times10^{-13}\text{ cm},$$

where A is the mass number of Mg^{24}. If all existing resonances are properly taken into account, a fit to the cross section can, in principle, be obtained with any value of the interaction radius in the approximate range from $1.5\times10^{-13}A^{1/3}$ cm to $1.5\times10^{-13}(A^{1/3}+1)$ cm. This statement is verified for the fits of the lower resonances in this experiment.

In the analysis of the cross section between 2.8 Mev and 3.4 Mev, however, a little experimenting shows that the $P_{3/2}$ resonance can be brought into reasonable agreement with observation by changing the value of the interaction radius to 5.05×10^{-13} cm, which lies midway between the above limits. Figure 5(a) shows the result. This calculation includes all the terms of the formula and allows all of the quantities to vary with energy. Phase shifts due to lower resonances are also included. The sharp resonance at 3.65 Mev is omitted because it is not expected to influence the rest of the curve.

The fit of the $S_{1/2}$ resonance is not good for any reasonable value of the interaction radius. The result of the exact calculation for an $S_{1/2}$ resonance with the new value of the interaction radius is shown in Fig. 5(b).

For simplicity, the interaction radius was assumed to be constant for all energies and for all l values of the incident proton. After the value was changed to 5.05×10^{-13} cm, the lower resonances were recalculated. The only changes involved were in the values of the characteristic energies and reduced widths. The classifications and the fits were not affected.

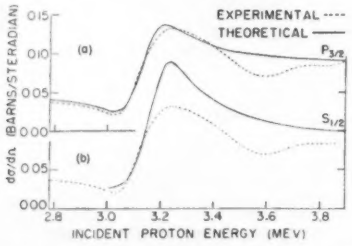

FIG. 5. (a) Calculation for a $P_{3/2}$ resonance near 3.1 Mev (without approximations) if the interaction radius has the value 5.05×10^{-13} cm. (b) Calculation for an $S_{1/2}$ resonance (without approximations) for this value of the interaction radius.

As Fig. 5(a) shows, the observed minimum in the cross section near 3.6 Mev is not reproduced by the calculation for a $P_{3/2}$ resonance alone. It is also highly unlikely that this broad dip is associated with the narrow resonance at 3.65 Mev. Since the introduction of a resonance broad enough to produce this dip destroys the existing fit below 3.4 Mev, the cross section must be refitted in the whole interval between 2.8 and 3.9 Mev. Attempts were made to fit the cross section in this interval with various combinations of two resonances. No combinations of three resonances were considered.

Pairs of resonances of the same angular momentum and parity, such as $S_{1/2}-S_{1/2}$, can immediately be ruled out on the same grounds as for the case of a single resonance of the same angular momentum and parity. The expression for the resonant phase shift is

$$\beta=\tan^{-1}\left[\frac{\frac{1}{2}\Gamma_1}{E_1+\Delta_1-E}+\frac{\frac{1}{2}\Gamma_2}{E_2+\Delta_2-E}\right],$$

where the subscripts 1 and 2 refer to the two resonances. Thus, the vector diagram still involves only one circle, and the cross section must pass through essentially the same maximum and minimum as if there were only a single resonance. The end point of the resonance vector traverses the circle more rapidly with energy than in the case of a single resonance, and goes twice around the circle. A pair of $P_{3/2}$ resonances is the only combination of this type that might appear possible, and the second minimum cross section predicted by this combination is much too small.

A slight modification of the vector diagram permits a study of the cross section predicted by a pair of resonances with a minimum of numerical calculation. One of the resonance vectors can be added to the end of the Rutherford vector as usual, while the other is added to the beginning of the potential vectors. The locus of starting points of this second resonance vector is the usual circle reflected in the point $\delta=0$, and the beginning of the vector traverses this circle in a counterclockwise direction as the phase shift δ increases. Figure 6 shows a diagram of this type in which a $P_{1/2}$ resonance vector is added to the beginning of the potential vectors and an $S_{1/2}$ resonance vector to the end of the Rutherford vector. In the first approximation, the cross section is proportional to the square of the distance $|A|$ measured between points on the two circles. Since the values of $|A|$ corresponding to the cross sections at the first minimum (3.0 Mev), the maximum (3.2 Mev), and the second minimum (3.6 Mev) are about 0.5, 1.4, and 1.0 unit, respectively (see scale at bottom of Fig. 6), inspection of this diagram rules out the $S_{1/2}-P_{1/2}$ combination.

All other pairs of resonances are ruled out in a similar manner except $P_{3/2}-S_{1/2}$ and $P_{3/2}-P_{1/2}$. The

best fits obtained with these combinations, by means of the complete formula, are shown in Fig. 7.

The conclusion drawn from these results is that the cross section between 2.8 and 3.4 Mev can be interpreted most simply in terms of the $P_{3/2}$ resonance shown in Fig. 5(a), but that the cross section above 3.4 Mev can probably not be explained without additional data. Extension of the elastic scattering data to higher energies and other angles, and further study of the inelastic scattering cross sections would probably be helpful.

D. General Trend of the Cross Section

The three broad resonances discussed above must now be joined together to fit the general trend of the cross section over the entire energy range of observation. In the scattering formula, the phase shift δ_{l+} is always given by the expression

$$\delta_{l+}=\beta_{l+}-\phi_l,$$

where ϕ_l is the potential phase shift and β_{l+} is the resonant phase shift. In this calculation, the $P_{3/2}$ resonant phase shift is

$$\beta_1{}^{+}=\tan^{-1}\left[\frac{\frac{1}{2}\Gamma_1}{E_1+\Delta_1-E}+\frac{\frac{1}{2}\Gamma_2}{E_2+\Delta_2-E}\right],$$

where the subscripts 1 and 2 refer to the $P_{3/2}$ resonances near 0.825 Mev and 3.1 Mev, respectively. If more $P_{3/2}$ resonances were known, they would be included in this sum. Similarly,

$$\beta_{1^-}=\tan^{-1}[\tfrac{1}{2}\Gamma_3/(E_3+\Delta_3-E)],$$

where the subscript 3 refers to the $P_{1/2}$ resonance near 1.6 Mev, the only one known. All other resonant phase shifts are neglected.

Computed values of the cross section are shown as solid circles in Fig. 8, and the solid curve is traced through the experimental points of Fig. 1. Calculations show that none of the narrow resonances contribute phase shifts that could appreciably change this fit between resonances. The general excellence of this fit below 3.4 Mev is taken as evidence that the interpretation presented thus far is correct and that it is safe to proceed to the identification of the narrow resonances.

E. Effects of Imperfect Energy Resolution

The observed half widths of the narrow peaks in the cross section near 1.5, 1.65, 2.0, 2.4, and 3.65 Mev (see Fig. 6 of reference 5) are all approximately equal to the energy spread of the proton beam combined with that introduced by energy loss in the target. The actual peaks may be much narrower and higher than the observed peaks. In each of these cases, the only theoretical resonances possessing the right qualitative shape predict a maximum cross section much higher than that observed. To discover how narrow the resonance must be in order that its maximum be degraded by the effects

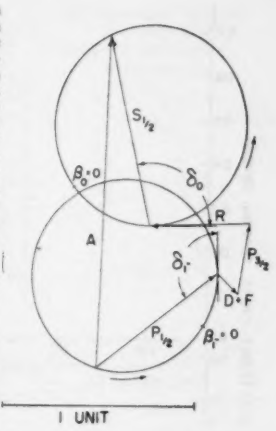

FIG. 6. Vector diagram for a combination of an $S_{1/2}$ and a $P_{1/2}$ resonance above 3 Mev. The beginning of the $P_{1/2}$ vector starts at the point marked $\beta_{1^-}=0$ and traverses the circle in a counterclockwise direction as energy increases. This point does not coincide with the point $\delta_{1^-}=0$ because the potential phase shift is about 9°. Similarly, the end of the $S_{1/2}$ vector starts at the point marked $\beta_0=0$ and traverses its circle in a counterclockwise direction. In first approximation, the cross section is proportional to the square of the length of the resultant A. The scale gives the length corresponding to unit amplitude (dimensionless).

of imperfect energy resolution to the value observed, a method is developed to compute the observed cross section from the theoretical curve.[8] This method cannot be used to prove that a given assignment is correct, but it can be used in conjunction with the sum rule on reduced widths[7] to rule out certain assignments.

When the cross section is measured at an energy E, which is determined by the voltage of the electrostatic generator, the number of incident protons with energies between E' and $E'+dE'$ is $Qg(E-E')dE'$, where Q is the total number of protons incident, and $g(E-E')$ is the energy distribution of protons in the beam. This function is triangular[9] in shape and is normalized. After a proton of energy E has penetrated a distance x into the target, its energy has decreased to the value $E-ax$, where a is the stopping power of the target material. The energy distribution of protons at the depth x in the

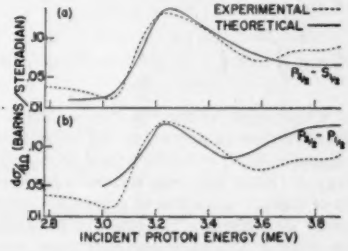

FIG. 7. (a) Calculation for a combination of a $P_{3/2}$ and an $S_{1/2}$ resonance above 3 Mev (without approximations). (b) Calculation for a combination of a $P_{3/2}$ and a $P_{1/2}$ resonance above 3 Mev (without approximations).

[8] J. L. Powell has developed a similar method to apply to reaction cross sections (symmetric resonance peaks) (private communication).

[9] Herb, Snowden, and Sala, Phys. Rev. 75, 246 (1949).

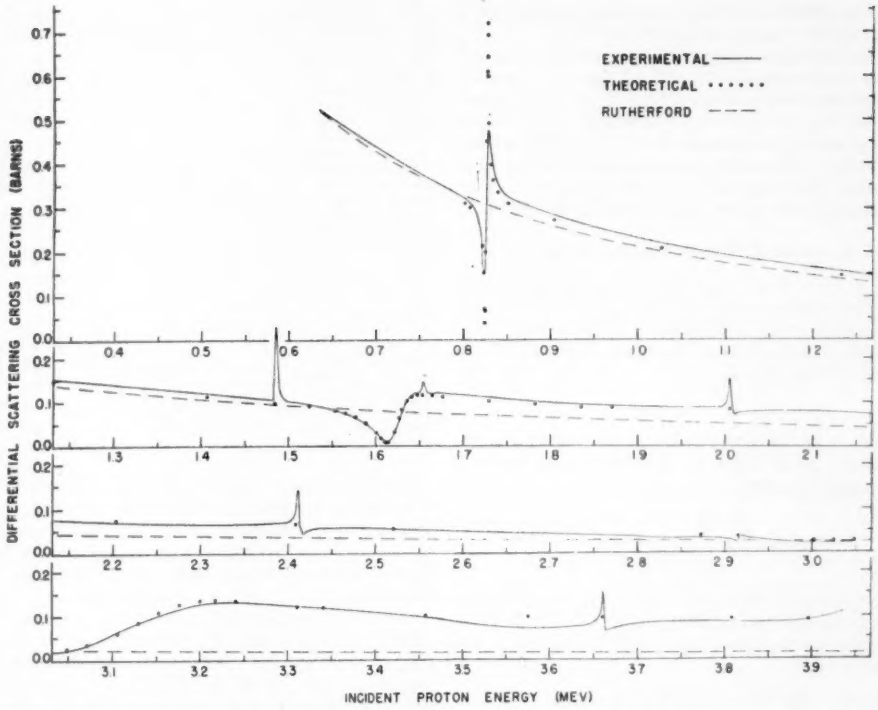

FIG. 8. Theoretical cross sections (solid circles) compared with the experimental curve (traced through the points of Fig. 1). Effects of narrow resonances were omitted in these calculations. The interaction radius value 5.05×10^{-13} cm is used throughout.

target is thus $g(E-v-E')$, where $v=ax$. The effect of thermal motion in the target is neglected, although it contributes an energy spread of the order of 100 ev.

The measured differential cross section at the nominal energy E and angle θ is

$$\sigma_0(E,\theta)=\frac{1}{at}\int_0^{at}dv\int_{E-v-\delta}^{E-v+\delta}g(E-v-E')\sigma(E',\theta)dE',$$

where at is the target thickness in energy units, δ is the maximum deviation of protons in the beam from the energy E, and $\sigma(E',\theta)$ is the theoretical cross section at the energy E'. Since this cross section is not a simple function of energy, numerical or graphical integration over energy is necessary. The order of integration is therefore changed. The integration over target thickness is elementary and results in an expression of the form,

$$\sigma_0(E,\theta)=\frac{1}{at}\int_{E-\delta-at}^{E+\delta}\sigma(E',\theta)F(E'-E)dE',$$

where the function $F(E'-E)$ (see Fig. 9) gives the distribution of energies available for collisions in the target. The integrand for any value of E' is obtained by reading the corresponding values of $F(E'-E)$ and $\sigma(E',\theta)$ from their graphs and multiplying them together. The result of the integration is the cross section $\sigma_0(E,\theta)$ that would be observed at the nominal energy E if the proposed cross section curve were correct. By repeating the integration for a series of energies E similar to those used in the experiment, one obtains a cross section curve to be compared with the one actually observed. If this comparison is good, the proposed cross section curve is plausible, although it may not be unique. The result of this treatment is that the qualitative shape of a resonance is preserved even though the energy distribution function is several times wider than the resonance, but that peaks are spread out and flattened. It follows from the normalization of the function $F(E'-E)$ that the area between the energy axis and the cross section curve of a resonance is conserved.

F. The 1.485-Mev Resonance

The F and G resonances are the only ones that predict the qualitative shape of the peak in the cross section observed at this energy. The G resonances are

ruled out because, even if the width be chosen equal to the upper limit, the area under the calculated curve is much less than that under the experimental curve. Figure 10 shows an $F_{5/2}$ resonance compared with the experimental data. The area under the theoretical curve was made equal to that under the experimental curve by setting the width Γ equal to 300 ev, which corresponds to a reduced width of about a third or fourth of the upper limit. In this and all the other calculations for the narrow resonances, the incoherent term is included, but only the resonant phase shift is allowed to vary with energy.

In view of the above arguments, there appears to be good evidence that this resonance has odd parity relative to Mg^{24}, and that its angular momentum value is either 5/2 or 7/2. The only distinction between these two values would be in the height of the peak.

G. The 1.655-Mev Resonance

This resonance is extremely narrow, and its maximum appears at a lower energy than its minimum. On the basis of this qualitative shape, circle diagrams immediately rule out all possibilities except D and H resonances. The upper limit computed for the observed width of an H resonance is 10 ev. It seemed doubtful that a resonance this narrow could be observed at all, and for this reason the study of resolution effects described in Sec. E was undertaken.

Figure 11(a) shows that an $H_{11/2}$ resonance has a shape qualitatively similar to the observed shape, except that the maximum is 3 barns instead of 0.19 barn. The observed cross section to be expected on the basis of the instrumental resolution is calculated point by point, with the result shown in Fig. 11(b). It would be necessary to double or triple the width in order to make this curve coincide with the experimental curve, and this seems to be a sufficient argument to rule out an H resonance.

The same procedure was carried out for a $D_{5/2}$ resonance with a width of 100 ev. The theoretical cross section and the observed cross section to be expected are shown in Fig. 12. The result indicates that the resonant energy and width chosen were both too large, but with small adjustments the curve might be brought into agreement with experiment. The reduced width of this resonance is only a few tenths of one percent of the upper limit. This resonance appears to have even parity and either 3/2 or 5/2 units of angular momentum.

H. The Resonances Near 2.01 Mev and 2.41 Mev

These resonances are similar to the one just considered in that each is narrow and each has a maximum at lower energies than the minimum. At these energies, however, the H circle is reoriented so that only the D resonances have the proper qualitative shape. Figure 13 compares $D_{5/2}$ and $D_{3/2}$ resonances with the cross section near 2.01 Mev, and Fig. 14 shows a $D_{3/2}$ reso-

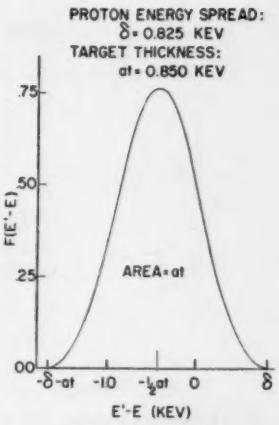

FIG. 9. The distribution of energies available for collisions in the target, for a bombarding energy, E, of 1.655 Mev. This calculation neglects the effects of thermal motion.

nance near 2.41 Mev. In each case, the reduced width is only a few tenths of one percent of the upper limit.

At 2.41 Mev a peak in the inelastic scattering was observed.[5] The fact that the elastic scattering width is less than the total width may partially explain why the maximum cross section observed is less than that predicted by the formula. These two levels are assigned even parity and angular momentum quantum numbers of either 3/2 or 5/2.

I. The Cross Section near 2.91 Mev

The small variation in the cross section near 2.91 Mev was studied only with the survey target,[5] and the shape is not well determined. No definite assignment of quantum numbers can be made, but a brief investigation was carried out to determine the possibilities. Cal-

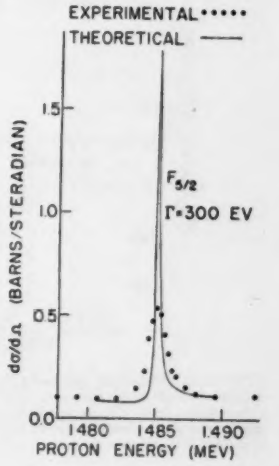

FIG. 10. Comparison of an $F_{5/2}$ resonance with the observed resonance at 1.485 Mev. The width is chosen to make the areas under the two curves equal.

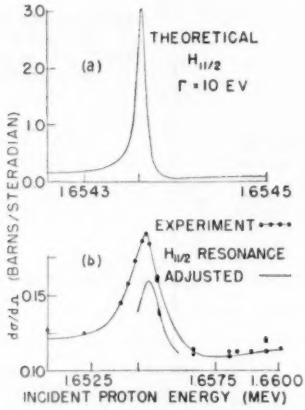

FIG. 11. (a) Theoretical shape of an $H_{11/2}$ resonance near 1.655 Mev. (b) Comparison of experimental data with this $H_{11/2}$ resonance adjusted for effects of finite energy resolution. Note the difference in scales of graphs. Energy scales coincide at the marks under the peaks.

culations show large fluctuations in the cross section associated with any resonance up to $l=6$. Circle diagrams indicate that an S resonance has the best qualitative shape, but the maximum would be about 0.13 barn and the reduced width extremely small. That this resonance can be attributed to an impurity in the target is rather unlikely because it exhibits a minimum, and impurities scatter incoherently.

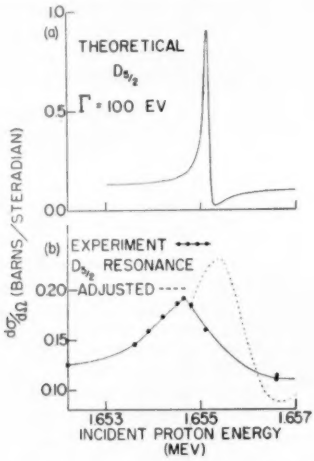

FIG. 12. (a) Theoretical shape of a $D_{5/2}$ resonance at 1.655 Mev; (b) Comparison of experimental data with this $D_{5/2}$ resonance adjusted for effects of finite resolution, showing that the resonant energy and width chosen were too large. Note difference in scale of ordinates.

J. The 3.65-Mev Resonance

This resonance also was studied only with the survey target, but its qualitative shape is clearly similar to those at 2.01 and 2.41 Mev. The principal difficulty in identifying this resonance is that the other phase shifts in the vicinity are not well understood. The background fit (Fig. 8) deviates markedly from experiment here. It is likely, however, that the phase shifts which form the potential background are not grossly in error, and that future changes will be small. Circle diagrams indicate that very large changes in the potential phase shifts would be necessary to make anything but a D resonance look reasonable, if resonances up to $l=6$ are considered.

The S wave phase shift at this energy is about $-29°$. If it were zero or a few degrees positive, a D resonance would fit the data very well. The background cross section under this condition would also agree with observation. Unfortunately, however, it seems impossible to choose parameters for an $S_{1/2}$ resonance such that the cross section agrees with experiment over the entire interval of observation. Under the circumstances, it appears that a definite classification of the 3.65 Mev resonance is not justified.

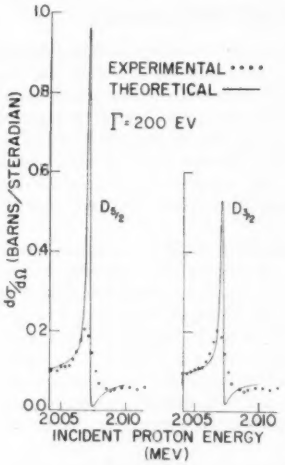

FIG. 13. Comparison of $D_{5/2}$ and $D_{3/2}$ resonances with experimental cross sections near 2.01 Mev.

K. Summary of Analysis

The interpretation of the three broad resonances near 0.825, 1.6, and 3.1 Mev is simple and unambiguous. They all have odd parity relative to Mg^{24}, and they have reduced widths of the order of 10–30 percent of the single particle limit $\hbar^2/\mu a_s$, where μ is the reduced mass and a_s is the interaction radius.[10] The analysis of the 1.49-Mev resonance leaves a twofold ambiguity in the angular momentum value, but the evidence for odd

[10] R. K. Adair, Phys. Rev. 82, 750 (1951).

parity is fairly strong. The reduced width of this resonance seems to be of the same order of magnitude as those of the first three mentioned.

All of the other resonances observed seem to have very small reduced widths. With the exception of the one near 2.91 Mev, about which little is known, they all appear to have even parity and 3/2 or 5/2 units of angular momentum. The high energy cross section seems to indicate a combination of two or more broad resonances above 3 Mev, but the yield curve could not be fitted simultaneously at all energies with any combination of two resonances in this region.

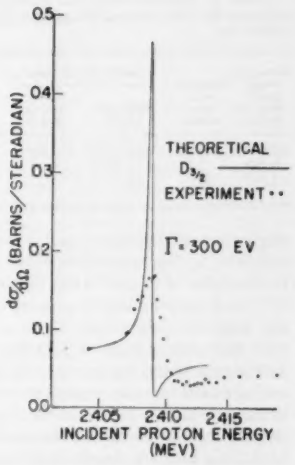

FIG. 14. Comparison of a $D_{3/2}$ resonance with experimental cross sections near 2.41 Mev.

III. CONCLUSION

A. Energy Level Diagram and Mirror Nucleus

Figure 15 shows the energy levels of the mirror nuclei Mg^{25} and Al^{25} placed so that the ground states coincide. The excitation energy of each level plotted in Al^{25} is the dissociation energy, which is 2.32 Mev, plus the resonant energy E_r, in the center-of-mass system. This energy is used in preference to the characteristic energy E_λ, because although E_λ is associated with the internal wave functions of the compound nucleus, its value depends on the choice of interaction radius. The two lowest excited states shown in Al^{25} were observed by Grotdal *et al.*[11] but not by Mooring *et al.*[5]

The Mg^{25} levels are taken from the results of Schelberg, Sampson, and Cochran.[12] These are all bound levels in that their energies are less than the dissociation energy of a proton or neutron, and none of them is classified. For the present, therefore, the comparison shows only that the level densities are about the same in the two nuclei.

B. Characteristic Energies, Reduced Widths, and Interaction Radii

In principle, the exact value of the interaction radius is not important to the analysis. The values of the characteristic energies and reduced widths of resonances do, however, depend on the value chosen for the interaction radius. Table II compares the values of these parameters of the broad resonances near 0.825 Mev and 1.6 Mev for two different values of the radius. Although these results should not be generalized, they are in qualitative agreement with theoretical predictions by Wigner and Eisenbud and by Teichmann.[7]

C. Comparison with the Shell Model of the Nucleus

According to the shell model proposed by Mayer,[6] the levels that are filled by protons (and by neutrons) in Mg^{24} are given by the expression

$$(1s_{1/2})^2(1p_{3/2})^4(1p_{1/2})^2(1d_{5/2})^4,$$

where the superscript indicates the number of protons (or of neutrons) occupying the state. Since only four of the six available $d_{5/2}$ states are filled, the additional proton is assumed to occupy a $d_{5/2}$ state for the ground state of Al^{25}. This assumption is verified experimentally[4] for the additional neutron in Mg^{25}.

If the single particle picture were valid, the sequence of excited states in Al^{25} should be the same as that following $1d_{5/2}$ in Table II of reference 6, with the provision that spin-orbit splitting might cause pairs of levels like $2p_{3/2}$ and $1f_{5/2}$ to cross. The degree of validity of the

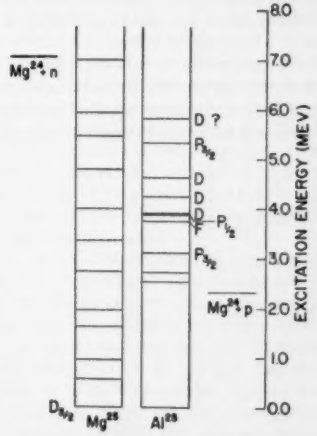

FIG. 15. Energy level diagrams of Mg^{25} (from the data of Schelberg, Sampson, and Cochran [Phys. Rev. **80**, 574 (1950)]) and Al^{25}. Excitation energies in Al^{25} are the dissociation energy (2.32 Mev) plus the resonant energy in the center-of-mass system. The two lowest excited states in Al^{25} were observed by Grotdal *et al.* (reference 11).

[11] Grotdal, Lönsjö, Tangen, and Bergström, Phys. Rev. **77**, 296 (1950).
[12] Schelberg, Sampson, and Cochran, Phys. Rev. **80**, 574 (1950).

TABLE II. Reduced width and characteristic energy for two values of the interaction radius a_s: $a_s = 5.83 \times 10^{-13}$ cm., $a_s = 5.05 \times 10^{-13}$ cm.

Resonant energy center-of-mass system	Observed resonance width	$a_s = 5.83 \times 10^{-13}$ cm		$a_s = 5.05 \times 10^{-13}$ cm	
		Reduced width	Characteristic energy	Reduced width	Characteristic energy
E(Mev)	Γ(kev)	γ^2(Mev cm)	E_λ(Mev)	γ^2(Mev cm)	E_λ(Mev)
0.792	1.5	1.2×10^{-13}	0.61	2.2×10^{-13}	0.41
1.557	36.	1.0×10^{-13}	1.47	1.7×10^{-13}	1.38

single particle approximation for a certain state may be estimated by the ratio of the value of its reduced width to the value of $\hbar^2/\mu a$.[10] Four of the levels classified in Al^{25} have reduced widths greater than ten percent of the single particle value. These are the $P_{3/2}$ level at 3.11 Mev, the F level at 3.75 Mev, the $P_{1/2}$ level at 3.88 Mev, and the $P_{3/2}$ level at 5.34 Mev. These energies are measured from the ground state as in Fig. 15. If the angular momentum value of the F level is 5/2, the first three of these levels fit into the predicted sequence. The $1d_{3/2}$, $2s_{1/2}$, and $1f_{7/2}$ levels might then lie in the region below the classified levels.

None of the other resonances observed is considered to represent a single particle level because the values of their reduced widths are only a few tenths of one percent of the limit. The abundance of narrow levels of even parity is striking and deserves some consideration. If some of the core nucleons are excited in the bombardment of Mg^{24}, the mean life of the state of the compound nucleus is greater than it would be if only the added proton were excited, because time is required for the energy to be concentrated on the emitted proton. By the uncertainty principle, therefore, the width of a level involving multiple particle excitation is smaller than that of a single particle level.

Of the core nucleons, those in the unfilled $1d_{5/2}$ shell should be most easily excited. In the region of excitation above 3.88 Mev, the energy required to excite two or more of these nucleons into the next lowest unoccupied states (e.g., $1d_{3/2}$, $2s_{1/2}$, $\cdots$) might be less than that required to excite a single proton into the $1g_{9/2}$ state. Since these two lowest unoccupied states are of even parity, as are the $1d_{5/2}$ states, one might expect a fairly large number of multiple particle states of even parity.

A subject of current interest is the spin-orbit splitting of nuclear energy levels. In the present experiment, a $P_{3/2}-P_{1/2}$ doublet is observed (the 3.11-Mev and 3.88-Mev levels of Fig. 15). The separation is approximately 0.77 Mev. This splitting is rather small compared with the 5-Mev splitting of the $P_{3/2}-P_{1/2}$ doublets[10] in He^5 and Li^5, and compared with the 4.4-Mev splitting of the $D_{5/2}$ and $D_{3/2}$ levels[1] in F^{17}. Correlation of recent evidence obtained by Bockelman *et al.*[13] with the assignments of Jackson and Galonsky[2] indicates that the $D_{5/2}-D_{3/2}$ splitting in C^{13} and N^{13} is of the order of 3 Mev. The above levels in He^5 and Li^5, however, have very large reduced widths, corresponding to single particle excitation, and the same is true to a lesser extent of the D levels in C^{13}, N^{13}, and F^{17}, while these two P levels in Al^{25} are only approximately "twenty-percent-single-particle" levels. Also, He^5, Li^5, C^{13}, N^{13}, and F^{17} are closed-shell-plus-one nuclei; and the energies of the lowest excited states of the core nuclei, He^4, C^{12}, and O^{16}, are greater than 4 Mev.

The foregoing discussion is rather speculative in nature, but the simplicity of this level structure for a nucleus like Al^{25} is fascinating. Although these suggestions may be incorrect, simplifying assumptions seem to be indicated, and the gradual accumulation of systems of classified excited states of nuclei may result in similarities of structure that will lead to a better picture of the nucleus.

The author wishes to express his gratitude to Professor R. G. Herb for inspiration and guidance. Valuable discussions with Professor H. T. Richards and Dr. R. K. Adair and Dr. F. P. Mooring are also gratefully acknowledged.

[13] Bockelman, Miller, Adair, and Barschall, Phys. Rev. **84**, 69 (1951).

PHYSICAL REVIEW VOLUME 85, NUMBER 4 FEBRUARY 15, 1952

Point Transformations in Quantum Mechanics

BRYCE SELIGMAN DEWITT*
Ecole d'Eté de Physique Théorique de l'Université de Grenoble, Les Houches, Haute Savoie, France
(Received September 14, 1951)

An isomorphism is shown to exist between the group of point transformations in classical mechanics and a certain subgroup of the group of all unitary transformations in quantum mechanics. This isomorphism is used to indicate that the quantum analogs of physically significant classical expressions can be constructed uniquely in any coordinate system. There is no ambiguity in the ordering of noncommuting quantum operators, and the method of constructing the quantum analogs is covariant under general coordinate transformations. The method is actually only applicable to systems having Lagrangians which are at most quadratic in the velocities, but this includes all systems which are presently of interest in physics. The method is applied to two intrinsically nonlinear examples, one of which is the gravitational field. The correct Hamiltonian operator for a quantized version of Einstein's gravitational theory is constructed.

1. INTRODUCTION

PRESENT day methods of formulating quantum mechanics are based more or less completely on analogy with classical mechanics. There are certain well-known rules for passing from the classical theory to the quantum theory. One replaces ordinary numbers by operators and Poisson brackets by commutator brackets. In principle, however, an ambiguity always presents itself when one is faced with the task of constructing the quantum analog of a classical expression which involves the product of two factors whose poisson bracket does not vanish. One does not know, *a priori*, how the corresponding quantum factors should be ordered.

Fortunately, the systems occurring in nature are for the most part simple enough in their mathematical description so that one has no trouble in deciding what the correct order should be. Nevertheless the aforementioned ambiguity represents a real deficiency in the present theory, because (1) the simplicity of natural systems is only apparent and is due to the fact that for such systems there usually exist what may be called "natural" coordinates in which the dynamical equations take particularly simple forms, and (2) the transformation theory of dynamics, which plays such an important role in the quantum theory, owes its validity to the invariance of classical Hamiltonian systems under a much wider group of transformations than one has heretofore been able to incorporate sensibly into the quantum scheme, owing to said ambiguity.

It is known that a true correspondence between the classical and quantum theories exists with respect to a certain subgroup of the group of all canonical transformations, namely the subgroup of all linear inhomogeneous canonical transformations. If one restricts oneself to this subgroup, then an isomorphism can be set up between classical quantities and their quantum analogs, when these quantities are at most quadratic in the canonical variables. A similar isomorphism does not exist, however, for other classical quantities, even under this restricted subgroup.[1] The question therefore arises: Is it possible, for a given dynamical system, to choose the canonical variables in such a way that the important physical quantities, energy, momentum, etc., become quadratic in these variables? Unfortunately, the answer to this question is no in many cases of importance, e.g., interacting fields.

Even in the case of interacting systems, however, no ambiguity in formulating the quantum theory has arisen in practice, because one has always supposed that a clear distinction could be made between the various systems in interaction, and one has usually imagined that it makes sense to talk about "free systems" and to treat the interactions as perturbations. For the "free systems" the answer to the above question is in the affirmative and a set of "natural" dynamical variables does exist. But, as we have already remarked, the existence of "natural" variables is more apparent than real, and may be more a reflection of the way our minds work than of the way nature works.

More pertinent to the present discussion is the fact that the linear inhomogeneous subgroup of canonical transformations is never used, as such, in practice. Indeed, the restriction to this subgroup is highly artificial. A type of canonical transformation which has much more physical content and which is much more frequently used in solving actual problems is a general transformation of the coordinate variables, i.e., a so-called point transformation.

In using point transformations in quantum theory, one usually first "quantizes" a given system in a set of "natural" coordinates (e.g., rectilinear coordinates) and then carries out the coordinate changes afterwards. However, if we adopt seriously the philosophy of general relativity, then we should say that one coordinate system is as good as another, and we need not have felt obliged to carry out the quantization in a "natural" coordinate system. Our rules of quantization, as well as our quantum-mechanical equations, should be

* Now a Fulbright grantee at the Tata Institute of Fundamental Research, Bombay, India.

[1] For a full discussion of this point, see L. Van Hove, "Sur le problème des Relations entre les Transformations Unitaires de la Mécanique Quantique et les Transformations Canoniques de la Mécanique Classique." (To be published.)

covariant under general point transformations. These requirements become all the more necessary when it is pointed out that there do exist systems in nature for which there are no "natural" coordinates; e.g., a particle constrained to move on a curved surface; the gravitational field in the general theory of relativity (see Sec. 6 below); any intrinsically nonlinear system.

It is the purpose of this paper to show (1) that it is possible to formulate a set of well-defined rules for passing from the classical to the quantum theory in a variety of cases which appears to be wide enough to include all systems occuring in nature, (2) that these rules are covariant under the canonical subgroup of all point transformations of a certain very general type, (3) that there exists an isomorphism between this subgroup and a corresponding subgroup of the group of all unitary transformations in Hilbert space, and, finally, (4) that there exists a unique correspondence between the classical expressions for the important physically observable quantities, and their quantum analogs, which persists under these subgroups of transformations. In connection with this last assertion it must be pointed out that the quantum analog of a classical expression may contain, in addition to a term which has the same appearance as the classical expression, also a term which vanishes as $\hbar \to 0$. All that one must require is that the form of this nonclassical term as well as that of the classical term, remain invariant under point transformations.

2. REPRESENTATION THEORY IN GENERAL COORDINATES

We begin by considering an arbitrary set of general coordinates x^i $(i=1\cdots n)$ and conjugate momenta p_i which may be used to describe the dynamical behavior of some system. In the quantum theory these coordinates and momenta are Hermitian operators. We shall work in the Schrödinger representation in which the algebra generated by the x's and p's refers to a fixed instant of time, while the actual temporal behavior of the system is described by a time dependent state vector $|\ \rangle_t$. We shall suppose that each of the operators x^i possesses a continuum of eigenvalues ranging from $-\infty$ to ∞. We shall further suppose that the x's are coordinates in an n-dimensional Riemannian manifold possessing a metric tensor g_{ij}. We shall see later that the metric tensor, which is a function of the x's alone, is determined in each case by the dynamical system itself.

The state vector $|\ \rangle_t$ may be expanded in terms of the eigenvectors $|x'\rangle$ of the x's in the following fashion,

$$|\ \rangle_t = \int |x'\rangle\langle x'|\ \rangle_t d\omega'. \tag{2.1}$$

$d\omega'$ denotes the volume element of the manifold, and the integration is to be carried out over the entire range of coordinate values. The quantity $\langle x'|\ \rangle_t$ is the wave function of the system, and may be denoted in more customary form by

$$\psi(x', t) \equiv \langle x'|\ \rangle_t. \tag{2.2}$$

$|\psi(x', t)|^2 d\omega'$ is the probability that the coordinates of the system will be found in the volume $d\omega'$ in the neighborhood of the point x' at the time t. This interpretation of $\psi(x', t)$ as a "probability amplitude" depends upon a normalization condition for the eigenvectors $|x'\rangle$ which may be expressed in the form

$$\langle x'|x''\rangle = \delta(x', x''). \tag{2.3}$$

$\delta(x', x'')$ is the "generalized delta-function" for the manifold and is defined by the conditions

$$\delta(x', x'') = 0 \text{ for } x' \neq x'', \tag{2.4}$$

and

$$\int f(x')\delta(x', x'')d\omega' = f(x'') \tag{2.5}$$

for all "reasonably well-behaved" functions $f(x')$.

The representation of the invariant volume element $d\omega'$ in the form $d\omega' = g^{\frac{1}{2}}(x')dx'$, where $g(x')$ is the determinant of the metric tensor at the point x', enables one to put the generalized delta-function into the following analytic form involving the ordinary delta-function

$$\delta(x', x'') = g^{-\frac{1}{2}}(x')\delta(x'-x'') = g^{-\frac{1}{2}}(x'')\delta(x'-x''). \tag{2.6}$$

Using this form, one may readily derive the following two important identities

$$(x'^i - x''^i)\frac{\partial}{\partial x'^j}\delta(x', x'') = -\delta_j{}^i\delta(x', x''), \tag{2.7}$$

$$\frac{\partial}{\partial x'^i}\delta(x', x'') = -\frac{\partial}{\partial x''^i}\delta(x', x'') - \left\{ \begin{matrix} j \\ j\ i \end{matrix} \right\}\delta(x', x''). \tag{2.8}$$

The contracted Christoffel symbol appearing in (2.8) may be evaluated at either x' or x''.

The adoption of the above so-called "coordinate representation," in which the eigenvectors of the x's are chosen as basis vectors, depends on the existence of the commutation relations

$$[x^i, x^j] = 0 \quad \text{for all } i, j. \tag{2.9}$$

The matrix elements of the operators x^i in the coordinate representation are given by

$$\langle x'|x^i|x''\rangle = x'^i\delta(x', x'') = x''^i\delta(x', x''). \tag{2.10}$$

The corresponding matrix elements of the operators p_i are obtained from the commutation relations

$$[x^i, p_j] = i\hbar\delta_j{}^i, \tag{2.11}$$

$$[p_i, p_j] = 0. \tag{2.12}$$

In matrix form, (2.11) becomes

$$\begin{aligned} i\hbar\delta_j{}^i\delta(x', x'') = \int \{&\langle x'|x^i|x'''\rangle\langle x'''|p_j|x''\rangle \\ &- \langle x'|p_j|x'''\rangle\langle x'''|x^i|x''\rangle\} d\omega''' \\ = (x'^i - x''^i)&\langle x'|p_j|x''\rangle, \end{aligned} \tag{2.13}$$

of which the most general solution is (see (2.7))

$$\langle x'|p_j|x''\rangle=-i\hbar\frac{\partial}{\partial x'^j}\delta(x',x'')+F_j\delta(x',x''), \quad (2.14)$$

where F_j is an arbitrary function of the coordinates which may be evaluated at either x' or x''.

The solution (2.14) must also satisfy relations (2.12). This imposes certain conditions on the functions F_j. Introducing the functions

$$\bar{F}_i=F_i+i\hbar\left\{\begin{matrix}j\\ji\end{matrix}\right\},$$

we have

$$\begin{aligned}0=\int\{&\langle x'|p_i|x'''\rangle\langle x'''|p_j|x''\rangle\\&-\langle x'|p_j|x'''\rangle\langle x'''|p_i|x''\rangle\}d\omega'''\\=g^{-\frac{1}{4}}(x')\int\Big\{&\Big[-i\hbar\frac{\partial}{\partial x'^i}\delta(x'-x''')+\bar{F}_i(x')\delta(x'-x''')\Big]\\&\times\Big[-i\hbar\frac{\partial}{\partial x'''^j}\delta(x'''-x'')+\bar{F}_j(x'')\delta(x'''-x')\Big]\\&-\Big[-i\hbar\frac{\partial}{\partial x'^j}\delta(x'-x''')+\bar{F}_j(x')\delta(x'-x''')\Big]\\&\times\Big[-i\hbar\frac{\partial}{\partial x'''^i}\delta(x'''-x'')+\bar{F}_i(x'')\delta(x'''-x')\Big]\Big\}dx'''\\=i\hbar&\Big[\frac{\partial}{\partial x'^i}\bar{F}_i(x')-\frac{\partial}{\partial x'^i}\bar{F}_j(x')\Big]\delta(x',x''), \quad (2.15)\end{aligned}$$

which implies that the $\bar{F}_i$ are of the form

$$\bar{F}_i(x')\equiv\frac{\partial}{\partial x'^i}\bar{F}(x') \quad (2.16)$$

where $\bar{F}(x')$ is some function independent of the index i. Since the Christoffel symbol $\left\{\begin{matrix}j\\ji\end{matrix}\right\}$ is also of this form, being in fact equal to $\frac{1}{2}\partial(\log g)/\partial x'^i$, we may write

$$\langle x'|p_i|x''\rangle=-i\hbar\frac{\partial}{\partial x'^i}\delta(x',x'')+\frac{\partial F(x')}{\partial x'^i}\delta(x',x'') \quad (2.17)$$

where $F=\bar{F}-i\hbar\log g^{\frac{1}{4}}$.

Owing to the fact that the p's are Hermitian operators, the function F is not entirely arbitrary. The Hermitian condition may be expressed in the form

$$\langle x'|p_i|x''\rangle=\langle x''|p_i|x'\rangle^*, \quad (2.18)$$

which leads, in virtue of the identity (2.8), to the condition

$$F^*=F+i\hbar\log g^{\frac{1}{4}}. \quad (2.19)$$

F must therefore have the form

$$F=R-\tfrac{1}{2}i\hbar\log g^{\frac{1}{4}}, \quad (2.20)$$

where R is a real function of the coordinates.

The function R may always be removed from the scene by a trivial unitary transformation. One introduces a new set of basic eigenvectors $|x'\rangle^\dagger$, which are connected with the old eigenvectors by the relation

$$|x'\rangle^\dagger=\exp[-iR(x')/\hbar]|x'\rangle. \quad (2.21)$$

That is, the two bases differ only by a phase transformation. We shall suppose this transformation already to have been carried out. The matrix elements of the p_i then reduce to

$$\langle x'|p_i|x''\rangle=-i\hbar\frac{\partial}{\partial x'^i}\delta(x',x'')-\tfrac{1}{2}i\hbar\left\{\begin{matrix}j\\ji\end{matrix}\right\}\delta(x',x''). \quad (2.22)$$

If we confine ourselves to coordinate space representations, the operators x^i, p_i may be regarded as being able to act directly on the wave function $\psi(x',t)$ itself, by means of the definitions

$$\langle x'|x^i|\ \rangle_t=x^i\psi(x',t), \quad \langle x'|p_i|\ \rangle_t=p_i\psi(x',t). \quad (2.23)$$

The x's and p's then have the following coordinate space representations,[2]

$$x^i=x'^i, \quad p_i=-i\hbar\frac{\partial}{\partial x'^i}-\tfrac{1}{2}i\hbar\left\{\begin{matrix}j\\ji\end{matrix}\right\}(x'). \quad (2.24)$$

In subsequent sections we shall drop the primes used to designate particular eigenvalues of the coordinate operators. The use of primes will be reserved to designate general point transformations.

3. POINT TRANSFORMATIONS

In classical mechanics, for every transformation of the generalized coordinates of the form[3]

$$x'^i=x'^i(x), \quad i=1,\cdots n, \quad (3.1)$$

there exists a corresponding transformation of the conjugate momenta, of the form

$$p_i'=(\partial x^j/\partial x'^i)p_j, \quad (3.2)$$

which preserves the canonical nature of the x's and p's. Equations (3.1) and (3.2) together define what is called a point transformation of the x's and p's.

Point transformations may also be defined in quantum mechanics, in an unambiguous manner. Since the coordinates x^i all commute with one another there is clearly no ambiguity in writing down the quantum analog of Eq. (3.1). There is likewise actually no ambiguity in

[2] The fact that the representation of the momentum operators in curvilinear coordinates differs from that in rectilinear coordinates in flat space, by the presence of the contracted Christoffel symbol, has already been noted. See, for example, W. Pauli, *Wellenmechanik*, Handbuch der Physik, Band 24, I, p. 120 (1933).

[3] The Jacobian of the transformation is assumed to be nonvanishing.

formulating the quantum analog of Eq. (3.2). For the only problem here is that of correctly symmetrizing the right-hand side of (3.2) so as to make it Hermitian. One may easily convince oneself that all methods of symmetrization lead to the same result, namely,[4]

$$p_i' = \tfrac{1}{2}[\partial x^j/\partial x'^i,\ p_j]_+. \tag{3.3}$$

That Eq. (3.3) gives the correct quantum transformation law for the momentum operators may be shown by making explicit use of expressions (2.24). We have

$$p_i' = \frac{\partial x^j}{\partial x'^i} p_j + \frac{1}{2}\left[p_j, \frac{\partial x^j}{\partial x'^i}\right] = -ih\frac{\partial}{\partial x'^i} - \frac{1}{2}ih\begin{Bmatrix} j \\ j\ i \end{Bmatrix}', \tag{3.4}$$

where

$$\begin{Bmatrix} i \\ j\ i \end{Bmatrix}' = \frac{\partial x^i}{\partial x'^i}\begin{Bmatrix} k \\ k\ j \end{Bmatrix} + \frac{\partial}{\partial x^j}\frac{\partial x^j}{\partial x'^i}. \tag{3.5}$$

Equation (3.5) is, however, just the usual transformation law for the contracted Christoffel symbol. Expressions (2.24) are therefore covariant under point transformations.

That there exists an isomorphism between the group of point transformations in classical mechanics and a corresponding subgroup of the group of all unitary transformations in quantum mechanics is thus quite evident. The group property ensures that each point transformation has an inverse. It is instructive to display explicitly the inverse of Eq. (3.3). We write

$$\begin{aligned}
&\tfrac{1}{2}[\partial x'^i/\partial x^i,\ p_j']_+ \\
&= \tfrac{1}{4}[\partial x'^i/\partial x^i,\ [\partial x^k/\partial x'^j,\ p_k]_+]_+ \\
&= \tfrac{1}{4}[[\partial x'^i/\partial x^i,\ \partial x^k/\partial x'^j]_+,\ p_k]_+ \\
&\qquad + \tfrac{1}{4}[\partial x^k/\partial x'^j,\ [p_k,\ \partial x'^i/\partial x^i]] \\
&= \tfrac{1}{2}[\delta_i^{\,k},\ p_k]_+ - \tfrac{1}{4}ih[\partial x^k/\partial x'^j,\ \partial^2 x'^i/\partial x^k \partial x^i] = p_i,
\end{aligned} \tag{3.6}$$

which shows that the inverse transformation has the same form as (3.3).

The unitary representations of the point-transformation group may be obtained by determining the infinitesimal generators of the group. An infinitesimal point transformation may be expressed in the form

$$x'^i = x^i + \epsilon\Lambda^i(x), \tag{3.7}$$

$$p_i' = p_i - \tfrac{1}{2}\epsilon[(\partial/\partial x^i)\Lambda^j(x),\ p_j]_+, \tag{3.8}$$

where ϵ is an infinitesimal constant and Λ^i is a function of the x's. More generally, every function f of the x's and p's transforms under (3.7, 8) according to

$$f' = f + (\epsilon/ih)[f, S] \tag{3.9}$$

where

$$S = \tfrac{1}{2}[\Lambda^i(x),\ p_i]_+. \tag{3.10}$$

S is the generator of the infinitesimal point transformation.

The subgroup of unitary transformations in quantum mechanics which corresponds isomorphically to the group of all point transformations in classical mechanics is given by the set of all unitary operators $\exp(\tau S/ih)$, where S has the form (3.10) and where τ is an arbitrary parameter. Each set of functions Λ^i defines a one-parameter subgroup of the point-transformation group.

4. DYNAMICAL SYSTEMS IN GENERAL COORDINATES

In this section we shall consider the set of all dynamical systems which, in the classical theory, have a Lagrangian function of the form

$$L = \tfrac{1}{2}G_{ij}\dot{x}^i\dot{x}^j + A_i\dot{x}^i - V, \tag{4.1}$$

where G_{ij}, A_i, and V are functions of the x's and where the matrix $\|G_{ij}\|$ is symmetric and nonsingular. We assert that this set includes all systems in nature which satisfy Bose-Einstein statistics, i.e., for which Poisson brackets, involving coordinates and momenta singly as well as multiply, correspond to commutator brackets in the quantum theory. The case of Fermi-Dirac systems will be discussed briefly in Sec. 7.

There exist, to be sure, Bose-Einstein systems which have Lagrangians of the form (4.1) but for which the matrix $\|G_{ij}\|$ is singular. The singularity of the matrix, however, simply implies that the momenta are not all independent, and the lagrangian for such a system can always be replaced by a Lagrangian for which $\|G_{ij}\|$ is nonsingular, together with a set of supplementary conditions expressing the relations between the momenta. The existence of such supplementary conditions does not alter the discussion which follows.

Under general coordinate transformations the quantities V, A_i, and G_{ij} transform like a scalar, a covariant vector, and a covariant tensor respectively. V and A_i have respectively the nature of a scalar and a vector potential. G_{ij} can likewise be regarded as a tensor potential. However, it is a true potential only if it cannot be "transformed away," i.e., if there exists no coordinate system in which it is everywhere constant. We shall tentatively identify G_{ij} with the metric tensor of the manifold of the x's—or rather with some constant multiple of it,

$$G_{ij} = \mu g_{ij}. \tag{4.2}$$

We shall subsequently discuss in fuller detail the reasons for this identification.

The Hamiltonian function corresponding to the Lagrangian (4.1) has the form

$$H = (1/2\mu)g^{ij}(p_i - A_i)(p_j - A_j) + V, \tag{4.3}$$

where g^{ij} is the contravariant inverse of the metric tensor and the momenta are given by

$$p_i = \mu g_{ij}\dot{x}^j + A_i. \tag{4.4}$$

[4] For example, one might expand $\partial x^j/\partial x'^i$ in a power series in the x's. The operator p could then be inserted between the x's in any symmetrical fashion in each term of the series. The result of commuting p symmetrically to the left and to the right through the x's is to produce two terms of order h which cancel each other, leaving simply the expression (3.3).

The question we now have to answer is how to put expression (4.3) into quantum form in a covariant and unambiguous manner. Actually there is no ambiguity in the symmetrization of the terms linear in the p's, so the question reduces simply to that of finding the quantum analog of $g^{ij}p_ip_j$.

Let us first investigate the transformation law of the wave function $\psi(x, t)$, because, when all is said and done, it is the Schrödinger equation

$$i\hbar\partial\psi/\partial t = H\psi, \tag{4.5}$$

which must transform covariantly. If the quantized system has no nonclassical degrees of freedom, such as spin, then the interpretation of $|\psi|^2$ as a probability per unit volume of the x-manifold implies that ψ is a simple scalar quantity. If, however, ψ is composed of a multiplet of components describing spin angular momentum, then the spin transformations of ψ are not independent of coordinate transformations and ψ is no longer a scalar.[5] We shall here consider only the scalar case, as the generalization to the other cases will be obvious at the end of the discussion.[6]

The quantum analog of the expression $g^{ij}p_ip_j$ is now readily determined by considering the well-known special case in which the x-manifold is flat and the coordinates are rectilinear and normalized. The expression then takes the form p_ip_i and the corresponding quantum operator is simply $-\hbar^2\partial^2/\partial x^i\partial x^i$. Using the convenient shorthand notation in which indices following a comma indicate ordinary differentiation with respect to the corresponding coordinates, we may write

$$p_ip_i\psi \equiv -\hbar^2\psi_{,ii}. \tag{4.6}$$

The generalization of expression (4.6) to the case of curvilinear coordinates is

$$-\hbar^2 g^{ij}\psi_{\cdot ij}, \tag{4.7}$$

where the dot $\cdot$ denotes covariant differentiation.

The simplest method of symmetrizing the expression $g^{ij}p_ip_j$ in the quantum theory is to write it in the form $p_ig^{ij}p_j$. We are thus led to investigate the quantity $p_ig^{ij}p_j\psi + \hbar^2 g^{ij}\psi_{\cdot ij}$. Using the explicit expression (2.24) for the momentum operators, and remembering that ψ is a scalar in calculating its covariant derivatives, we find

$$-\hbar^2 g^{ij}\psi_{\cdot ij} - p_ig^{ij}p_j\psi = 2\mu\hbar^2 Q\psi \tag{4.8}$$

where

$$Q = \frac{1}{4\mu}g^{ij}\left[\left\{\begin{matrix} k \\ k\,i \end{matrix}\right\}_{,j} - \left\{\begin{matrix} k \\ i\,j \end{matrix}\right\}\left\{\begin{matrix} l \\ l\,k \end{matrix}\right\} - \frac{1}{2}\left\{\begin{matrix} k \\ k\,i \end{matrix}\right\}\left\{\begin{matrix} l \\ l\,j \end{matrix}\right\}\right]. \tag{4.9}$$

[5] In the case of isotopic spin, on the other hand, the components of ψ are each scalar quantities, for isotopic spin rotations bear no connection with coordinate transformations.

[6] The extension to the nonzero integral-spin cases is well known in the theory of tensors. For the theory of spinors in general coordinates see W. Pauli, Ann. Physik (to be published).

If we now write the quantum analog of the Hamiltonian function in the form

$$H = (1/2\mu)(p_i - A_i)g^{ij}(p_j - A_j) + \hbar^2 Q + V \tag{4.10}$$

the Schrödinger equation takes the covariant form

$$\begin{aligned} i\hbar\partial\psi/\partial t = H\psi \\ = -(\hbar^2/2\mu)g^{ij}\psi_{\cdot ij} + (i\hbar/\mu)(A^i\psi_{\cdot i} + \tfrac{1}{2}A^i{}_{\cdot i}\psi) \\ + [(1/2\mu)A^iA_i + V]\psi. \end{aligned} \tag{4.11}$$

The quantity $\hbar^2 Q$ may be regarded as a kind of quantum-mechanical potential which goes to zero as $\hbar \to 0$. It is the quantity which must be added to the covariant classical Hamiltonian in order to produce the covariant quantum Hamiltonian. From the covariance of Eq. (4.11) it is evident that the form of expression (4.10) remains invariant under all point transformations (3.1). Furthermore, we have been led to this quantum expression in an unambiguous manner.[7]

5. THE HEISENBERG REPRESENTATION AND THE EQUATIONS OF MOTION

The passage to the time-independent state vector of the Heisenberg representation is effected by the unitary transformation

$$|\ \rangle_0 = \exp(iHt/\hbar)|\ \rangle_t, \tag{5.1}$$

together with a corresponding transformation of all operators. The new Hamiltonian operator will have the same form as (4.10), except that all operators will be written in bold face type to indicate that we are working in the Heisenberg representation. The time dependence of the Heisenberg operators is given by the canonical equation

$$d\mathbf{f}/dt = (1/i\hbar)[\mathbf{f}, \mathbf{H}]. \tag{5.2}$$

In particular we have

$$d\mathbf{x}^i/dt = (1/2\mu)[\mathbf{g}^{ij}, \mathbf{p}_j]_+ - (1/\mu)\mathbf{A}^i, \tag{5.3}$$

which may be solved for the $\mathbf{p}$'s to give

$$\mathbf{p}_i = \tfrac{1}{2}\mu[\mathbf{g}_{ij}, d\mathbf{x}^j/dt]_+ + \mathbf{A}_i. \tag{5.4}$$

If $\mathbf{f}$ is a function of the $\mathbf{x}$'s alone, then Eq. (5.3) tells us that

$$[\mathbf{f}, d\mathbf{x}^i/dt] = (i\hbar/\mu)\mathbf{g}^{ij}\mathbf{f}_{,j}. \tag{5.5}$$

Using Eqs. (5.2), (5.4), and (5.5) one may readily show that the time derivative of $\mathbf{f}$ is given by

$$d\mathbf{f}/dt = \tfrac{1}{2}[\mathbf{f}_{,i}, d\mathbf{x}^i/dt]_+. \tag{5.6}$$

[7] There does remain a slight ambiguity in the fact that we could add to expression (4.10) a term of the form $\alpha(\hbar^2/\mu)R$, where R is the contracted curvature tensor of the x-manifold and α is an arbitrary number. However, α would then be an extra dimensionless "constant of nature" for which there seems to be no present need. More interesting, perhaps, is the possibility of introducing constants having the dimensions of length by adding invariant terms proportional to R^2, $R^{ij}R_{ij}$, etc.

The time dependence of the momentum operators is a little more complicated. One finds

$$dp_i/dt=\tfrac{1}{2}\mu(dx^j/dt)\mathbf{g}_{jk,i}dx^k/dt+\tfrac{1}{2}[\mathbf{A}_{j,i},dx^j/dt]_+ -(\hbar^2\mathbf{Q}+\mathbf{V})_{,i}+\hbar^2\mathbf{W}_i \quad (5.7)$$

where

$$\mathbf{W}_i=(1/4\mu)[\mathbf{g}^{km}(\mathbf{g}^{jl}{}_{,i}\mathbf{g}_{jk,l})_{,m}+\tfrac{1}{2}\mathbf{g}^{jl}{}_{,i}\mathbf{g}^{km}{}_{,m}\mathbf{g}_{jk,l}]. \quad (5.8)$$

Finally, taking the time derivative of Eq. (5.3), using Eqs. (5.6) and (5.7), and juggling factors a bit, one obtains the following equations of motion for the $\mathbf{x}$'s:

$$\frac{d^2\mathbf{x}^i}{dt^2}+\frac{dx^j}{dt}\left\{\begin{matrix}\mathbf{i}\\ \mathbf{j}\ \mathbf{k}\end{matrix}\right\}\frac{dx^k}{dt}-\frac{1}{2\mu}\left[\mathbf{F}^i{}_j,\frac{dx^j}{dt}\right]_+ +\frac{1}{\mu}\mathbf{g}^{ij}(\hbar^2\mathbf{Q}+\mathbf{V})_{,j}-\frac{\hbar^2}{\mu}\mathbf{Z}^i=0, \quad (5.9)$$

where

$$\mathbf{F}_{ij}=\mathbf{A}_{j,i}-\mathbf{A}_{i,j} \quad (5.10)$$

and

$$\mathbf{Z}^i=\mathbf{g}^{ij}\mathbf{W}_j-(1/4\mu)\mathbf{g}^{ln}[(\mathbf{g}^{km}\mathbf{g}^{ij}{}_{,k}\mathbf{g}_{jl})_{,n} +\mathbf{g}^{ij}{}_{,l}(\mathbf{g}^{km}\mathbf{g}_{jk,m})_{,n}+(\mathbf{g}^{km}\mathbf{g}^{ij}{}_{,m}\mathbf{g}_{kl,j})_{,n}]. \quad (5.11)$$

6. EXAMPLES OF INTRINSICALLY NONLINEAR SYSTEMS

Perhaps the simplest example of a system for which there exist no "natural" coordinates and for which the methods of the preceding sections are therefore mandatory if a quantum theory of the system is desired, is that of a particle which is constrained to move on the surface of a sphere but which is otherwise free.

It will immediately be objected that this system does not satisfy one of the conditions which we imposed at the outset, namely that it be describable in terms of coordinates whose values range from $-\infty$ to ∞. However, we may suppose that the particle, instead of being constrained to move on the surface of a sphere, is constrained to move on a surface which has the topological properties of an infinite plane but which, in a certain region, is shaped like a portion of a sphere. It is this portion that we will be interested in. (Alternatively, we may say that the particle is indeed constrained to move on the spherical surface, but that it is forbidden to approach a certain point on that surface.) This means that if we construct a wave packet to represent the particle, the theory of the preceding sections—in particular, the equations of motion (5.9)—will describe the behavior of the wave packet only so long as its dimensions remain small compared to those of the sphere. When its dimensions are no longer small, the Schrödinger equation (4.11) will still remain valid, but it will then be necessary to impose cyclic conditions on the wave function ψ.

We shall use customary spherical coordinates, in which the element of length is given by $r^2(d\theta^2+\sin^2\theta d\varphi^2)$, r being the radius of the sphere. The momentum operators conjugate to the coordinates θ and φ have the forms

$$p_\theta=-i\hbar(\partial/\partial\theta+\tfrac{1}{2}\cot\theta), \quad (6.1)$$

$$p_\varphi=-i\hbar\partial/\partial\varphi. \quad (6.2)$$

The "quantum-mechanical potential" Q is given by

$$Q=-(8\mu r^2)^{-1}(\csc^2\theta+1), \quad (6.3)$$

where μ may now be identified with the mass of the particle. The operator equations of motion become

$$\frac{d^2\theta}{dt^2}-\frac{1}{2}\frac{d\phi}{dt}(\sin 2\theta)\frac{d\phi}{dt}+\frac{\hbar^2}{4\mu^2r^4}\cot\theta\csc\theta=0, \quad (6.4)$$

$$\frac{d^2\phi}{dt^2}+\frac{d\phi}{dt}(\cot\theta)\frac{d\theta}{dt}+\frac{d\theta}{dt}(\cot\theta)\frac{d\phi}{dt}+\frac{3\hbar^2}{\mu^2r^4}\cot\theta\csc^2\theta=0. \quad (6.5)$$

As $\hbar\to 0$, or as $\mu\to\infty$, these equations are seen to reduce to the classical forms.

Another system of interest for which there exist no "natural" coordinates is the gravitational field. In this case, the "coordinates" are the gravitational potentials, which are customarily chosen to be the components $g_{\mu\nu}$ of the metric tensor of space-time. To say that there exist no "natural" coordinates for the gravitational field is to say that there exists no representation in which the gravitational field equations become linear. For example, we might use the contravariant density $(-g)^{\frac{1}{2}}g^{\mu\nu}$ instead of $g_{\mu\nu}$. This would be a "coordinate" or "point" transformation, but in terms of the new "coordinates" the field equations would still be nonlinear.

Recently Pirani and Schild,[8] using some methods developed by Dirac,[9] have constructed an explicit Hamiltonian for the gravitational field. Their ultimate purpose in doing this was to obtain an eventual quantization of the gravitational field. However, one of the terms in their Hamiltonian is quadratic in the momenta conjugate to the $g_{\mu\nu}$, and thus they are faced with the factor-ordering ambiguity. One could attempt to obtain a quantum Hamiltonian from their classical Hamiltonian by using the simplest possible symmetrization procedure, but then one would not know whether or not an equivalent quantum theory would have been obtained if another set of gravitational "coordinates," such as $(-g)^{\frac{1}{2}}g^{\mu\nu}$, had been used instead, with a similar symmetrization procedure. What is necessary, in order to remove this uncertainty, is to calculate and include the "quantum-mechanical potential" $\hbar^2Q$ for the problem.

We shall need for this purpose only the quadratic term of the Pirani-Schild Hamiltonian. This has the

[8] F. A. E. Pirani and A. Schild, Phys. Rev. **79**, 986 (1950).

[9] P. A. Dirac, Can. J. Math. **2**, 129 (1950); see also Mimeographed Notes, Canadian Mathematical Congress, Vancouver, B. C., (Summer, 1949).

form

$$H_{\text{quad}}=\frac{1}{2}\int \dot{x}^\sigma l_\sigma l^{-2}(-g)^{-\frac{1}{2}}(g_{\alpha\gamma}g_{\beta\delta}+g_{\alpha\delta}g_{\beta\gamma} -g_{\alpha\beta}g_{\gamma\delta})\pi^{\alpha\beta}\pi^{\gamma\delta}du. \quad (6.6)$$

The integral on the right is a triple integral, with respect to three parameters u^1, u^2, u^3. Without entering into too much detail, we may say that the points x of space-time are labeled by these parameters, together with a fourth parameter t, which plays the same role as the time in conventional Hamiltonian theory. A dot denotes differentiation with respect to t. l_σ is a vector normal to the space-like surface $t=$constant, and is defined by $l_\sigma\equiv l_{,\sigma}\partial(x)/\partial(u,t)$. Also, $l^2=g^{\alpha\beta}l_\alpha l_\beta$. The coordinates x^σ on any space-like surface are regarded, in the present scheme, as dynamical variables on an equal footing with the $g_{\mu\nu}$. Since the parameters u^i, t are completely arbitrary, the "velocities" $\dot{x}^\sigma$ are arbitrary. For each such arbitrary "velocity variable" there exists what Dirac[3] calls a "first class ϕ." Only a part of one of the first class ϕ's occuring in gravitational theory appears in expression (6.6).

In the quantized theory the momenta $\pi^{\alpha\beta}$ will satisfy the commutation relation

$$[g_{\alpha\beta}(u),\ \pi^{\gamma\delta}(u')]=\tfrac{1}{2}ih(\delta_\alpha{}^\gamma\delta_\beta{}^\delta+\delta_\alpha{}^\delta\delta_\beta{}^\gamma)\delta(u-u'). \quad (6.7)$$

The π's do not correspond to the momenta of systems of a finite number of degrees of freedom. We must replace them by p's given by $p^{\alpha\beta}=[\delta(0)]^{-1}\pi^{\alpha\beta}$ in order that we have commutation relations of the form

$$[g_{\alpha\beta}(u),\ p^{\gamma\delta}(u)]=\tfrac{1}{2}ih(\delta_\alpha{}^\gamma\delta_\beta{}^\delta+\delta_\alpha{}^\delta\delta_\beta{}^\gamma) \quad (6.8)$$

for each u. The Hamiltonian (6.6) then appears as the Hamiltonian of a nondenumerably infinite set of identical systems, each having 10-degrees of freedom and a Hamiltonian of the form

$$\mathcal{H}_{\text{quad}}=\tfrac{1}{2}\dot{x}^\sigma l_\sigma[\delta(0)]^2(du)l^{-2}(-g)^{-\frac{1}{2}} \times(g_{\alpha\gamma}g_{\beta\delta}+g_{\alpha\delta}g_{\beta\gamma}-g_{\alpha\beta}g_{\gamma\delta})p^{\alpha\beta}p^{\gamma\delta}. \quad (6.9)$$

If the "mass constant" μ of each system is taken to be

$$1/\mu=2\dot{x}^\sigma l_\sigma[\delta(0)]^2du, \quad (6.10)$$

then the "contravariant" metric tensor of the $g_{\mu\nu}$-manifold is

$$G^{(\alpha\beta)(\gamma\delta)}=\tfrac{1}{2}l^{-2}(-g)^{-\frac{1}{2}}(g_{\alpha\gamma}g_{\beta\delta}+g_{\alpha\delta}g_{\beta\gamma}-g_{\alpha\beta}g_{\gamma\delta}). \quad (6.11)$$

The "covariant" metric tensor is

$$G_{(\alpha\beta)(\gamma\delta)}=\tfrac{1}{2}l^2(-g)^{\frac{1}{2}}(g^{\alpha\gamma}g^{\beta\delta}+g^{\alpha\delta}g^{\beta\gamma}-g^{\alpha\beta}g^{\gamma\delta}), \quad (6.12)$$

satisfying

$$G_{(\alpha\beta)(\epsilon\zeta)}G^{(\epsilon\zeta)(\gamma\delta)}=\tfrac{1}{2}(\delta_\gamma{}^\alpha\delta_\delta{}^\beta+\delta_\delta{}^\alpha\delta_\gamma{}^\beta). \quad (6.13)$$

Using the relations

$$(\partial/\partial g_{\mu\nu})(-g)^{\frac{1}{2}}=\tfrac{1}{2}(-g)^{\frac{1}{2}}g^{\mu\nu}, \quad (6.14)$$

$$(\partial/\partial g_{\mu\nu})g^{\alpha\beta}=-\tfrac{1}{2}(g^{\alpha\mu}g^{\beta\nu}+g^{\alpha\nu}g^{\beta\mu}), \quad (6.15)$$

$$(\partial/\partial g_{\mu\nu})l^2=-l^\mu l^\nu, \quad (6.16)$$

we may readily construct the Christoffel symbols for the 10-dimensional $g_{\mu\nu}$-manifold. We have

$$\begin{aligned}
&[(\alpha\beta)(\gamma\delta),\ (\epsilon\zeta)]\\
&=\tfrac{1}{2}[G_{(\alpha\beta)(\epsilon\zeta),\,(\gamma\delta)}+G_{(\gamma\delta)(\epsilon\zeta),\,(\alpha\beta)}-G_{(\alpha\beta)(\gamma\delta),\,(\epsilon\zeta)}]\\
&=\tfrac{1}{2}l^{-2}[-l_\gamma l^\delta G_{(\alpha\beta)(\epsilon\zeta)}-l^\alpha l^\beta G_{(\gamma\delta)(\epsilon\zeta)}+l^\gamma l^\delta G_{(\alpha\beta)(\gamma\delta)}]\\
&\quad+\tfrac{1}{4}l^2(-g)^{\frac{1}{2}}[g^{\gamma\delta}(g^{\alpha\epsilon}g^{\beta\zeta}+g^{\alpha\zeta}g^{\beta\epsilon}-g^{\alpha\beta}g^{\epsilon\zeta})\\
&\quad-g^{\delta\zeta}(g^{\alpha\gamma}g^{\epsilon\delta}+g^{\alpha\delta}g^{\epsilon\gamma})-g^{\alpha\epsilon}(g^{\beta\gamma}g^{\zeta\delta}+g^{\beta\delta}g^{\zeta\gamma})\\
&\quad-(g^{\alpha\gamma}g^{\zeta\delta}+g^{\alpha\delta}g^{\zeta\gamma})g^{\beta\epsilon}-g^{\alpha\zeta}(g^{\beta\gamma}g^{\epsilon\delta}+g^{\beta\delta}g^{\epsilon\gamma})\\
&\quad+(g^{\alpha\gamma}g^{\beta\delta}+g^{\alpha\delta}g^{\beta\gamma})g^{\epsilon\zeta}+g^{\alpha\beta}(g^{\epsilon\gamma}g^{\zeta\delta}+g^{\epsilon\delta}g^{\zeta\gamma})] \quad (6.17)
\end{aligned}$$

which gives

$$\left\{\begin{matrix}(\alpha\beta)\\(\alpha\beta)(\gamma\delta)\end{matrix}\right\}=G^{(\alpha\beta)(\epsilon\zeta)}[(\alpha\beta)(\gamma\delta),\ (\epsilon\zeta)] =-5l^{-2}l_\gamma l^\delta, \quad (6.18)$$

$$G^{(\alpha\beta)(\gamma\delta)}\left\{\begin{matrix}(\epsilon\zeta)\\(\alpha\beta)(\gamma\delta)\end{matrix}\right\}=2l^{-2}(-g)^{-\frac{1}{2}}(2l^{-2}l_\epsilon l_\zeta-g_{\epsilon\zeta}), \quad (6.19)$$

$$G^{(\gamma\delta)(\epsilon\zeta)}\left\{\begin{matrix}(\alpha\beta)\\(\alpha\beta)(\gamma\delta)\end{matrix}\right\}_{,(\epsilon\zeta)}=(35/2)l^{-2}(-g)^{-\frac{1}{2}}, \quad (6.20)$$

and finally, the "quantum-mechanical potential" for each system,

$$\hbar^2Q=\hbar^2(85/8)\dot{x}^\sigma l_\sigma l^{-2}(-g)^{-\frac{1}{2}}[\delta(0)]^2du. \quad (6.21)$$

The correct quantum-mechanical Hamiltonian is therefore written in the form

$$H_{\text{quad}}=\int \dot{x}^\sigma l_\sigma[\pi^{\alpha\beta}G^{(\alpha\beta)(\gamma\delta)}\pi^{\gamma\delta} +\hbar^2(85/8)l^{-2}(-g)^{-\frac{1}{2}}[\delta(0)]^2]du. \quad (6.22)$$

The "quantum-mechanical potential" is seen to be a strongly divergent quantity in the present case. It must nevertheless be retained in all quantum expressions in order that the Hamiltonian operator be invariant under changes in the variables used to describe the gravitational field.

Those terms in the total Hamiltonian which do not appear in (6.22) are (at most) linear in the π's, and their symmetrization does not give us any trouble.

7. CONCLUSION

The formalism of the preceding sections is unsymmetrical in the coordinates and momenta. Such an

asymmetry does not exist in the transformation theory of classical mechanics, where one deals only with Poisson brackets in which coordinates and momenta are on a completely equal and complementary footing.

Actually, a kind of symmetry can be retained in the formalism of Sec. 2. In any given coordinate system there do exist eigenvectors $|p'\rangle$ of the momentum operators, satisfying

$$p_i|p'\rangle = p_i'|p'\rangle. \tag{7.1}$$

The coordinate-space representation of these eigenvectors may be taken in the form

$$\langle x'|p'\rangle = (2\pi\hbar)^{-\frac{1}{2}n} f^{-\frac{1}{2}}(p') g^{-\frac{1}{2}}(x') \exp(ip_i'x'^i/\hbar), \tag{7.2}$$

and any coordinate-space wave function can then be transformed into a momentum-space wave function by the transformation

$$\langle p'| \ \rangle = \int \langle p'|x'\rangle\langle x'| \ \rangle d\omega'$$

$$= (2\pi\hbar)^{-\frac{1}{2}n} f^{-\frac{1}{2}}(p') \int g^{\frac{1}{2}}(x') \times \exp(-ip_i'x'^i/\hbar)\langle x'| \ \rangle dx'. \tag{7.3}$$

The normalization condition

$$\langle p'|p''\rangle = \int \langle p'|x'\rangle\langle x'|p''\rangle d\omega' = f^{-\frac{1}{2}}(p')\delta(p'-p''), \tag{7.4}$$

and the representation of the operators x^i in momentum-space in the form

$$\langle p'|x^i|p''\rangle = \int \langle p'|x'\rangle x'^i \langle x'|p''\rangle d\omega'$$

$$= i\hbar \frac{\partial}{\partial p_i'}[f^{-\frac{1}{2}}(p')\delta(p'-p'')] + \frac{i\hbar}{4}\frac{\partial}{\partial p_i'}[\log f(p')] f^{-\frac{1}{2}}(p')\delta(p'-p''), \tag{7.5}$$

allow one to identify $f^{\frac{1}{2}}(p')dp'$ as the volume element of momentum-space. The function $f(p')$ is completely arbitrary.

The symmetry between coordinates and momenta which is obtained via Eq. (7.2) is, however, quite artificial, for the concept of "plane wave," as expressed by this equation is not a covariant one. If a state vector is an eigenvector of the momentum operator in one coordinate system, it will not, in general, be a momentum eigenvector in another coordinate system.

When the formalism is applied to actual physical systems then, of course, the symmetry between coordinates and momenta disappears completely, for the Hamiltonian will, in general, be quite unsymmetric in the two sets of conjugate variables. This type of asymmetry exists in both the classical and quantum theories. For this reason, it is quite natural in both theories to speak of a state in which the position (i.e., configuration) of a system has a fixed definite value regardless of what momentum it may have, while it may be quite unnatural to speak of a state in which the momentum of the system has a fixed numerical value which is the same regardless of what its configuration is.

Only for certain special systems is it possible to bring about a complete symmetry between coordinate and momentum operators, namely systems having Hamiltonians which are at most quadratic in all the canonical variables taken together. These systems we have called "free" systems in this paper, following the nomenclature of quantum field theory, in which, for example, an unperturbed harmonic oscillator is regarded as a "free" system.

For "free" systems, the subgroup of linear inhomogeneous canonical transformations have some meaning. Coordinates and momenta can be mixed together or interchanged, sometimes to advantage. A consideration of these systems alone, however, provides a very inadequate description of nature, for the really important aspect of nature is change, and change involves interactions which destroy linearity and nullify the existence of "natural" coordinates.

We have asserted that all Bose-Einstein systems in nature, even those in interaction, may nevertheless still be characterized by the fact that their Hamiltonians are at most quadratic in the momenta. This is not true of Fermi-Dirac systems, whose Hamiltonians may involve the momenta to powers higher than the second. Fermi-Dirac Hamiltonians, however, are always characterized as being expressible as functions of the n^2 products p_ix^j:

$$H = H(p_ix^j, f_\alpha). \tag{7.6}$$

The f_α may be functions of the dynamical variables of other systems which are in interaction with the Fermi-Dirac system in question, but they are independent of the p's and x's of the system itself. The p's and x's satisfy anticommutation relations among themselves,

$$[x^i, x^j]_+ = 0, \tag{7.7}$$

$$[p_i, p_j]_+ = 0, \tag{7.8}$$

$$[x^i, p_j]_+ = i\hbar\delta_j^{\ i}, \tag{7.9}$$

but they commute with the dynamical variables of the other interacting systems. In constructing the quantum Hamiltonian (or operators corresponding to other physical observables) for such systems, the p's must always be placed to the left of the x's. The anticommutation relation (7.9) requires that the x's and p's must be non-Hermitian, or complex quantities.[10]

[10] In practice, the Hermitian adjoints of the coordinates will be related to the momenta by means of supplementary conditions of the form $p_i = A_{ij}x^{j*}$, where the A_{ij} are coefficients which may involve the dynamical variables of other interacting systems.

There is nothing analogous to point transformations for Fermi-Dirac systems, and, in fact, the dynamical variables are themselves not physically observable. Only products of p's and x's correspond to physical quantities. Fermi-Dirac systems depend for their existence on the fact that there are for them what amounts to "natural" coordinates, because their Hamiltonians must always be functions of the bilinear forms $p_i x^j$. The existence of these "natural" coordinates is, in this case, independent of interactions with other systems.

As we have already remarked, point transformations can be introduced in a very natural way into the quantum theory of systems having Hamiltonians quadratic in the momenta, and there is no ambiguity in the proper ordering of noncommuting factors. If there were systems in nature having Hamiltonians of a more complicated type, then the situation would be quite different. To be sure, in the classical theory, one can make a canonical transformation of a completely arbitrary type, thus destroying the simplicity of a given Hamiltonian. The question that imposes itself is therefore the following: Given a Hamiltonian function, What conditions must it satisfy in order that it be transformable by a canonical transformation into a Hamiltonian which is quadratic in one of the sets of canonical variables?

The answer to the preceding question is not easy. However, supposing we do arrive at a Hamiltonian of the prescribed type, we must then decide what the metric tensor of its coordinate manifold is. The choice of a metric tensor is intimately related with the process of measurement. In simple cases, such as that of a particle constrained to move on a surface, the choice is obvious. In more complicated examples, such as the gravitational Hamiltonian discussed above, there may appear to be some uncertainty.

Suppose we have arbitrarily chosen the metric tensor, and that it corresponds to a flat manifold. In order that there be no factor-ordering ambiguity, the tensor G_{ij} of (4.1) must, in a set of rectilinear coordinates, satisfy the equation

$$G_{ij,k}=0. \tag{7.10}$$

The generalization of this condition to curved manifolds is

$$g^{jk}G_{ij\cdot k}=0. \tag{7.11}$$

For a given metric there are an infinity of tensor G_{ij} satisfying (7.11). Conversely, for a given tensor G_{ij}, there are an infinity of metrics which will cause (7.11) to be satisfied. Even if we impose the stronger condition

$$G_{ij\cdot k}=0 \tag{7.12}$$

the metric will still be undetermined. It is only by adopting the point of view that everything about a given system should be described by its Hamiltonian, that we are led to the identification (4.2).[11] It is to be noted that the choice of the "mass constant" μ does not affect the "quantum-mechanical potential" $\hbar^2 Q$.

The author is indebted to Professor Pauli for reading the manuscript and making helpful suggestions prior to publication.

[11] A very special uncertainty exists in the case of Hamiltonians reducible to the form

$$H=(\tfrac{1}{2}A^{ij}p_ip_j+B^ip_i+C)(\tfrac{1}{2}D_{kl}x^kx^l+E_kx^k+F),$$

where $\|A^{ij}\|$ and $\|D_{kl}\|$ are nonsingular matrices and the expressions inside the parentheses are positive-definite inhomogeneous quadratic forms. In this case the Hamiltonian is quadratic in both the coordinates and the momenta taken separately, and there is no way of deciding, *a priori*, whether the coordinates, or the momenta, are the variables which should be allowed to suffer general point transformations. Once the decision is made, however, such point transformations will quickly destroy the special symmetry which the Hamiltonian above possesses. The quantum Hamiltonian operator will be different depending on which transformation group is selected. The "quantum-mechanical potential" for x-transformations has the form

$$\hbar^2Q=\tfrac{1}{12}\hbar^2n^2(\tfrac{1}{2}D_{mn}x^mx^n+E_mx^m+F)^{-1}A^{ij}(D_{ik}x^k+E_i)\times(D_{jl}x^l+E_j)-\tfrac{1}{8}nA^{ij}D_{ij},$$

where n is the number of degrees of freedom of the system. The quantum-mechanical potential for p-transformations is given by a similar expression involving the p's.

Further Calculations of X-Ray Diffusion in an Infinite Medium*

L. V. Spencer and Fannie Stinson
National Bureau of Standards, Washington, D. C.
(Received October 17, 1951)

The problem of x-ray diffusion in an infinite homogeneous medium can be solved numerically by a method of expansion into suitable polynomial systems. This method has already been applied to determine the spectrum of scattered radiation as a function of distance from the radiation source for several cases of interest. This note presents further numerical applications of the polynomial method.

I. PLANE MONODIRECTIONAL 1.33-MEV SOURCE IN WATER

THIS calculation extends to include scattered photons with energies as low as 214 kev. These low energy photons are present at and behind the source plane. Thus, expansions into Laguerre polynomials, which are only defined between the source plane and $+\infty$, could not be used. Instead, an expansion was made into the U_n, V_n polynomial systems.[1] The spectrum as a function of distance from the source plane can be written in the following way in terms of these polynomials:

$$I_0(E,\mu_0 z)=e^{-|\mu_0 z|}\left\{\sum_{n=0}^{\infty} I_{0n}{}^{a}(E)U_n(|\mu_0 z|)+\mu_0 z\sum_{n=0}^{\infty} I_{0n}{}^{as}(E)V_n(|\mu_0 z|)\right\}. \quad (1)$$

Here $I_0(E,\mu_0 z)$ is the energy density of the radiation component with photon energy E, at a distance z from the source plane. μ_0 refers to the total attenuation coefficient of the unscattered radiation. The superscripts a and as indicate that the first term in the curly brackets is a symmetric function of the penetration variable z while the second term is antisymmetric in z. Our calculation determined the first three terms in both sums. This seemed sufficient to show some of the main features of $I_0(E,\mu_0 z)$ both qualitatively and quantitatively. (Inclusion of more terms would, of course, improve the accuracy of the solution, particularly where I_0 is very small.)

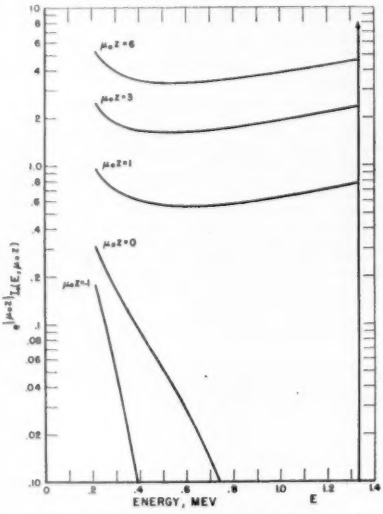

FIG. 1. Differential spectra $I_0(E,\mu_0 z)$ of the x-ray intensity (energy flux/Mev) at various distances z from a plane monodirectional source of 1.33-Mev photons in water. (Note that the ordinate is actually $\exp(|\mu_0 z|)I_0$.) The scale of ordinates is normalized to correspond to a source of unit energy flux. The narrow beam attenuation coefficient of the source radiation is $\mu_0=0.0612$ cm^{-1}.

In Fig. 1 the spectrum of the scattered radiation is given at several distances from the source plane. (The exponential controlling the attenuation has been divided out.) Behind the source plane the high energy photons are attenuated more strongly than those with lower energies. This reflects the fact that high energy photons which do penetrate behind the source plane are in general traveling nearly parallel to it. All photons at $\mu_0 z=0$, -1 with energies greater than 369 kev must have been scattered at least twice, while all above 527 kev must have been scattered at least three times.

II. POINT ISOTROPIC Co^{60} SOURCE IN WATER: DIRECTIONAL DISTRIBUTION

For calculation purposes, the photon distribution is expressed as a sum of spherical harmonics:

$$I(E,\theta_r,r)=\frac{1}{4\pi r^2}e^{-\mu_0 r}\sum_{l=0}^{\infty}\frac{2l+1}{4\pi}I_l(E,\mu_0 r)P_l(\cos\theta_r), \quad (2)$$

where $I(E,\theta_r,r)$ is the energy density of the scattered component with photon energy E, at a radial distance r from the source, and traveling at an angle θ_r with the line from the source to the photon.

* The calculations reported here, which were supported by the ONR, are of an exploratory nature and were accomplished with a desk computer. A large program of calculations of this type is in progress, supported by the AEC. This program relies upon the Bureau of Standards Eastern Automatic Computer to accomplish the heavy numerical work involved in finding x-ray distributions in some 206 cases, involving various source energies and geometries in a number of different materials. This program will be the subject of a later report.

[1] L. V. Spencer and U. Fano, Phys. Rev. **81**, 464 (1951); J. Research Natl. Bur. Standards **46**, 446 (1951).

In this problem the interlinkages between integral equations permit the calculation of the moments

$$\int_0^\infty (\mu_0 r)^n I_l(E, \mu_0 r) r^2 dr$$

only for $n \geqslant l$, but the moments with $n < l$ do not vanish. Because of this circumstance, the calculation of the I_l's requires expansions into sets of polynomials more general than the U_n's and V_n's.[5] These sets have been mentioned in a footnote of reference 1 and are solutions of a third-order differential equation. The sets consist of non-self-adjoint polynomials of degree n with the weight function $(\mu_0 r)^l \exp(-\mu_0 r)$. They will be called $U_n^l(\mu_0 r)$, so that $U_n^0 = U_n$ and $U_n^1 = V_n$.

We now write

$$I_l(E, \mu_0 r) = \sum_{n=0}^{\infty} I_{ln}(E) U_n^l(\mu_0 r), \tag{3}$$

where the $I_{ln}(E)$ are determined by solving a matrix of integral equations.

In our calculation we computed the first four I_{0n}, the first four I_{1n}, and the first three I_{2n}. In order to obtain swift convergence in the summation (2) the first scattered beam was subtracted out of the I_l and calculated independently.

Figure 2 gives the resulting directional distribution of various spectral components at several distances from the photon source. Several features of these curves deserve comment: (1) The integrable infinity at $\theta_r = 0$ is caused by those photons which are scattered only once, very near the source where the photon density diverges quadratically. (2) The two close-together discontinuities in each curve are also a feature of the first scattered beam and correspond to the two Co^{60} source energies. (At the point of scattering, θ_r is given by the Compton relationship. This defines the position of the discontinuities.) (3) Finally, the directional distributions for a given photon energy seem to approach an equilibrium angular distribution as $\mu_0 r$ increases, i.e., the shape of the curves tends to become independent of the penetration. [The tails of the curves have been dashed in to indicate that they are not accurately given by only three terms of the expansion (2).]

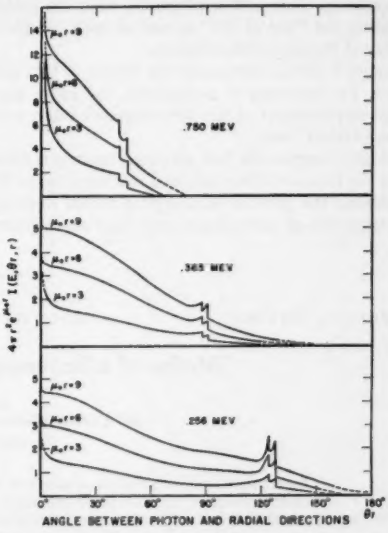

FIG. 2. Directional distribution $I(E, \theta_r, r)$ of the x-ray intensity for several spectral components at a distance r from a point isotropic source of Co^{60} in water. The quantity $4\pi r^2 \exp(\mu_0 r) \times I(E, \theta_r, r)$ given above is a function of $\mu_0 r$, and is measured in (Mev/sec)/Mev/steradian. The ordinate is normalized to correspond to a source producing one photon of each type per second. μ_0 relates to the 1.33-Mev component.

III. POINT MONODIRECTIONAL 1.33-MEV SOURCE IN WATER

A "gun" source is the elementary one in that any other source geometry, no matter how complicated, may be obtained from it by integration. Because problems involving this type of source have five independent variables instead of three, as in the two previously mentioned problems, the number of integral equations which must be solved per problem is vastly larger. In order to reduce the amount of work to reasonable proportions, the calculation was limited as follows: (1) Only scattered components above 730 kev in photon energy were considered. (2) The calculations were for two equal point monodirectional sources "back to back," i.e., we considered only the spatially symmetric part of the point monodirectional source. This is a reasonable thing to do in view of the restriction to high energy photons. (3) Instead of calculating the spectrum as a function of the radial distance ρ from the original "line of fire," we calculated only the mean square radial displacement $\langle \rho^2 \rangle_{Av}$ of the various scattered

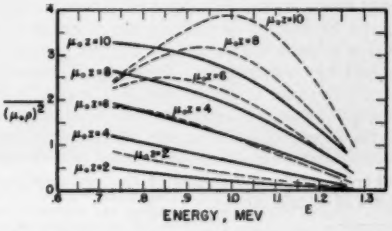

FIG. 3. Mean square sideways displacement of the scattered radiation produced by a point monodirectional 1.33-Mev source in water. The dashed lines correspond to the radiation scattered once only.

components. This varies, of course, with the position (z) along the "line of fire" as well as with the photon energy of the scattered radiation.

Figure 3 gives a picture of the results of this calculation. For purposes of comparison, the mean square radial displacement of the first scattered beam is also given (dashed lines).

At high energies the first scattered beam gets farther from the line $\rho=0$ than the total scattered beam. This is because the photons of energy E which have been scattered two or more times have done much more of their penetrating while they had an energy still greater than E. At these higher energies, the photons tended to stay close to the original "line of fire."

On the other hand, at low E and high z the total scattered beam tends to be farther from $\rho=0$. This is because the low energy photons do not travel far. If they appear very far from the original line they must have accomplished most of their radial displacement at an energy or energies greater than E but less than the source energy. This requires more than one scattering.

PHYSICAL REVIEW VOLUME 85, NUMBER 4 FEBRUARY 15, 1952

Motion of a Ferromagnetic Domain Wall in Fe_3O_4

JOHN K. GALT
Bell Telephone Laboratories, Murray Hill, New Jersey
(Received October 25, 1951)

Experiments have been made on a sample of Fe_3O_4 cut from a single crystal in such a way that its ferromagnetic domain pattern includes an individual domain wall whose motion can be studied. This sample has a permeability which is high (about 5000) at low frequencies and drops off rapidly above 1000 cycles. A hysteresis loop and data on wall velocity *vs* applied field were also taken. The data are discussed in terms of recent developments in the theory of the ferromagnetic domain wall. It appears that this theory explains our data satisfactorily, and that in using it to explain our data we determine some of the fundamental magnetic constants of Fe_3O_4. We are also able to gain some insight into domain wall motion in ferrites generally in this way.

I. INTRODUCTION

LANDAU and Lifshitz[1] first discussed the relation between the velocity of a ferromagnetic domain wall and the field which causes it to move. They neglected eddy current effects. Williams and Shockley[2] have produced in silicon iron a domain boundary whose motion can be detected and studied. Eddy current effects are overwhelmingly important in determining the motion of a wall in this alloy, as they and Kittel[3] have shown, but these authors[3] have suggested that even in silicon iron the relaxation behavior of the spin system as discussed by Landau and Lifshitz may have an effect. The object of the present paper is to study the motion of a domain wall in Fe_3O_4 where the eddy current effects are small enough so that the spin relaxation can be studied in a fairly direct manner. Our results will be shown to contain internal checks, and they will be compared with ferromagnetic resonance data. Furthermore it will be seen that our results are explainable in terms of recent theoretical developments and the Landau-Lifshitz results, and they therefore provide confirmation for these theories. It is therefore possible to produce a theory of the permeability of samples of certain shapes.

The sample used has a shape analogous to that of the rectangles used by Williams and Shockley,[2] being a polygonal ring with each leg along a direction of easy magnetization. Since the [111] direction is the direction of easy magnetization in Fe_3O_4, the ring was diamond-shaped with its face in the (110) plane, as shown schematically by the solid lines in Fig. 1. Each leg is 0.051 cm across and 0.102 cm thick as shown in Fig. 1.

The first samples studied were cut from natural crystals of Fe_3O_4, and they were unsuccessful. They required fields of the order of 30 oersteds to saturate, presumably because of such impediments to wall motion as cracks, imperfections, and impurities. It is in fact doubtful that they had the appropriate domain pattern at all. The successful final experiment was made possible by the growth of synthetic Fe_3O_4 crystals[4] of high purity and mechanical perfection in the Laboratory for Insulation Research at the Massachusetts Institute of Technology. One such crystal was made available for these experiments by Professor von Hippel of that Laboratory.

II. EXPERIMENTAL RESULTS

A hysteresis loop, data on wall velocity *vs* applied field, and data on permeability *vs* frequency were ob-

[1] L. Landau and E. Lifshitz, Physik. Z. Sowjetunion **8**, 153 (1935).
[2] H. J. Williams and W. Shockley, Phys. Rev. **75**, 178 (1949).
[3] Williams, Shockley, and Kittel, Phys. Rev. **80**, 1090 (1950).

[4] These crystals were grown under a contract sponsored jointly by the ONR, the Army Signal Corps, and the Air Force. See Progress Report V, Laboratory for Insulation Research, Massachusetts Institute of Technology, 1949, p. 58.

tained first, and observations were made on the domain pattern in the sample later. We will start the description of results with our observations of the domain pattern, however. The complete pattern has not been observed, as the sample was broken in the process of preparing it for these observations. Observations of the pattern on the sample, fitted back together after the break, however, show the essential features expected from the experience of Williams and Shockley.[3] This pattern, which consists of a movable wall all around the ring parallel to the (110) face of the sample and four stationary walls across the corners, is shown by the dotted lines in Fig. 1. A picture showing the intersection of the movable wall with the surface of the sample along one leg is shown in Fig. 2. The extra walls visible in Fig. 2 we attribute to the presence of the break in the sample. We have also observed some of the stationary walls across the corners of the sample. This picture was taken using the technique of Williams and Shockley.[3] The other data will be interpreted on the assumption that this pattern is correct, although the fracture of the sample has made it impossible to observe all its details.

In view of the incompleteness of the observations of the domain pattern, it seems desirable to comment on two alternative patterns which may seem plausible. First, if several parallel movable walls had been present, the hysteresis loop (see below) would have been somewhat different from that observed. Second, it may seem possible that the movable wall was in the $(11\bar{2})$ plane, which is perpendicular to the (110) plane indicated above. This would produce a pattern more closely analogous geometrically to that observed by Williams and Shockley,[3] but aside from the fact that observations definitely indicate that this is not the pattern, the wall has twice the area and therefore approximately twice the energy if it is in the $(11\bar{2})$ plane. The difference in our results which would be produced by changing the assumed pattern from one of these to another is not large and would not change any of our qualitative conclusions in any case.

Some experimentation with surface treatments was necessary before it was possible to observe the domain patterns of Fig. 2 on these artificially prepared surfaces. It was found quite easy to observe the pattern when the surface was clean and free down to the undisturbed material. The best procedure found for achieving this condition was to rub the ground surfaces of the original sample smooth with the finest emery cloth obtainable, and then to etch the sample by boiling it in 30 percent H_2SO_4 for $\frac{1}{2}$ to 1 hour under a reflux condenser.

The hysteresis loop of the sample, observed on the Cioffi recording fluxmeter,[5] is shown by the solid line in Fig. 3. It will be seen from Fig. 3 that the loop deviates from the square shape achieved in the silicon iron sample of Williams and Shockley.[3] It is felt that this is due to the fact that there were chips out of the sample so that the wall could not remain plane as it approached the sample faces, and a much larger field was therefore required to make it move in this region. By manipulating the field in the course of taking a loop such as that in Fig. 3, one finds that the actual loop has a bulge where the straight vertical portion begins and then contracts as shown by the dotted lines, so that the coercive force is actually only approximately 0.1 oersted. This effect has also been observed by Williams[6] in silicon iron rectangles. Maximum permeabilities read off the loop of Fig. 3 are approximately 25,000.

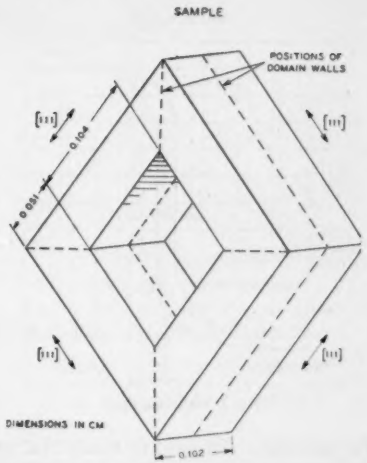

FIG. 1. Sample.

FIG. 2. Domain pattern on $11\bar{2}$ plane which was outer face of a leg of the sample. The movable wall is indicated by white arrows. The other walls did not extend as far along the leg, and are therefore identified with the break in the sample. The edge of the sample runs from the top of the picture toward the left.

[5] P. P. Cioffi, Phys. Rev. 67, 200 (1945).

[6] Private communication.

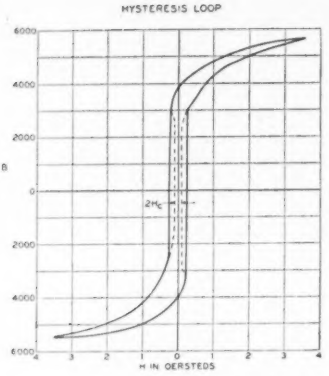

FIG. 3. Hysteresis loop.

Pulse techniques were used to obtain data on the relation between domain wall velocity and applied field. The sample was wound with a primary and a secondary winding, and the experiment was conducted as follows. A square pulse of positive voltage was applied to the primary winding in series with a resistor so that the rise time of this primary pulse was short compared to its length. This pulse was long enough so that the steady field it produced lasted for longer than the time required for the wall to move from one side of the sample to the other. The signal induced in the secondary winding was observed during this pulse on an oscilloscope whose sweep was synchronized with the pulser. A second pulse of negative voltage was applied to the primary during each duty cycle in order to bring the wall back to its original position. At low fields, a short high spike was introduced just at the start of the pulse in order to get the wall over the hump in the hysteresis loop shown by the dotted lines in Fig. 3. This initial spike had no effect on the subsequent motion.

The applied field due to the primary pulse H_{app} is deduced from the current in the primary winding and the solenoid formula $H_{app}=4\pi NI$. To obtain the relation between wall velocity and induced voltage per secondary turn we have

$$\text{Volts/turn}=(d\Phi/dt)\times 10^{-8}$$
$$=8\pi M_s(\Delta z/\Delta t)w_{wall}\times 10^{-8}, \quad (1)$$

where $\Delta z/\Delta t$ is equal to domain wall velocity v, and w_{wall} is the width of the wall between the boundaries of the sample in the direction perpendicular to the magnetization. The wall is at right angles to the direction of the velocity of course.

The calculation of wall velocity from the observed signal and Eq. (1) is of course based on the domain pattern. The results are shown in Fig. 4, where wall velocity is plotted *vs* applied magnetic field. It will be seen that we may write $v=1900(H_{app}-H_c)$ where H_c is approximately equal to the coercive force of 0.1 oersted as read from the hysteresis loop. It is clear that $(H_{app}-H_c)$ is the field which is effective in producing wall motion. From the oscilloscope trace of wall velocity *vs* time it is clear that H_c varies as the wall moves, so that the value of H_c read from Fig. 4 is an average. The variations are essentially independent of applied field, however, as one would expect if they are caused in this way. Figure 5 is an example of one of the traces with the average velocity indicated by a straight line. One notices a fairly gradual decrease in velocity to zero, as one would expect from the hysteresis loop.

The data on initial permeability $\mu(=\mu'-j\mu'')$ *vs* frequency at room temperature is given in Fig. 6. This data was obtained from bridge measurements[7] of the inductance of a coil wound on the sample. The data shows simple relaxation behavior as the frequency increases from low values where the wall follows the applied field to high values where it no longer can do so. The relaxation frequency is about 3000 cycles. The value of μ' at low frequencies is comparable with the value read from the hysteresis loop at $H=0$, as we should expect. The instability of the wall, however, makes the value difficult to read from the hysteresis loop, so that this comparison cannot be made accurately.

The relaxation shown in Fig. 6 must be a domain wall relaxation since the permeabilities involved cannot be accounted for without invoking wall motion.

III. THEORY

We will now correlate our data with recent theories of domain wall motion which start from the equation of motion of a unit area of the domain wall. We may use our data in this way to determine the constants of motion (mass, viscous resistance, and stiffness) of a

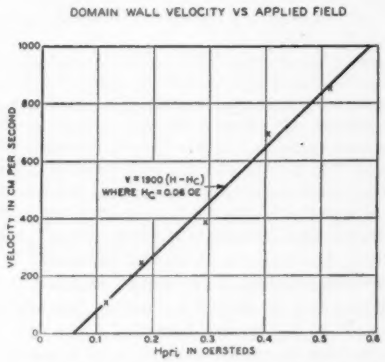

FIG. 4. Domain wall velocity *versus* applied field.

[7] W. D. Voelker, Bell Labs. Record **20**, 133 (1942).

unit area of wall. This point of view has been developed recently by Kittel,[8] Becker,[9] Rado,[10] and Döring.[11]

We consider unit area of a 180° domain wall between two regions of saturated magnetic material. Such a system has an equation of motion for small amplitudes of the applied magnetic field H which may be written

$$m\ddot{z}+\beta\dot{z}+\alpha z=2M_sH, \tag{2}$$

where z is the displacement of the domain wall along its normal, m is its mass per unit area, β is a parameter measuring viscous resistance, and α is a stiffness parameter measuring viscous resistance, and α is a stiffness parameter, which has meaning only for small fields such as those used in initial permeability measurements. When fields larger than the coercive force are applied as in the experiment on wall velocity *vs* applied field, this term disappears and the effective field inside the material is less than the applied field by an amount equal to the coercive force; this is shown by Fig. 4. These results are quite reasonable when one remembers the spikes which pull back on the wall in the experiments of Williams and Shockley[2] for small wall motions and snap off entirely if the wall moves a large distance.

Let us consider the initial permeability data. We have for the relation between z and μ,

$$\mu=\Delta B/\Delta H=\Delta\Phi/A_{\text{coil}}\Delta H=8\pi M_szw_{\text{wall}}/A_{\text{coil}}H, \tag{3}$$

where w_{wall} is the width of the domain wall between the boundaries of the sample in a direction perpendicular to the magnetization and A_{coil} is the cross-sectional area of the coil around the sample. The general solutions of Eq. (2) for a sinusoidal applied field are too familiar to be reproduced here, but we note that Eq. (2) can be further simplified since we observe a relaxation mechanism (see Fig. 6). The values of α, β, and m will be calculated later; suffice it to say here that the order of magnitude of m is such that the first term on the left in Eq. (2) is negligible, and we may write

$$\beta\dot{z}+\alpha z=2M_sH, \tag{4}$$

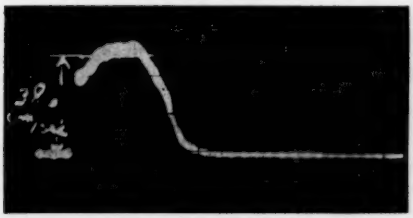

FIG. 5. Oscilloscope trace of secondary signal voltage *versus* time. The average velocity is shown by the horizontal straight line.

[8] C. Kittel, Phys. Rev. **79**, 214 (1950); Proceedings of Grenoble Conference (1950).
[9] R. Becker, Proceedings of Grenoble Conference (1950).
[10] Rado, Wright, and Emerson, Phys. Rev. **80**, 273 (1950).
[11] W. Döring, Z. Naturforsch. **3a**, 374 (1948).

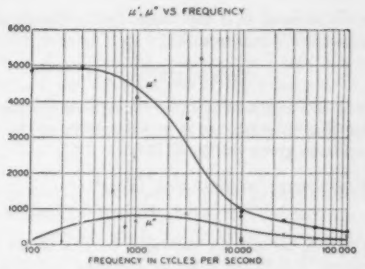

FIG. 6. μ' and μ'' *versus* frequency.

which we may solve to give, if $H=H_0e^{j\omega t}$;

$$z=\frac{2M_sH_0}{\alpha}\left[\frac{1}{1+\omega^2\beta^2/\alpha^2}-\frac{j\omega\beta/\alpha}{1+\omega^2\beta^2/\alpha^2}\right]e^{j\omega t}. \tag{5}$$

As the remarks above indicate, under the conditions of the experiment in wall velocity, Eq. (2) takes the form

$$\beta\dot{z}=2M_s(H_{\text{app}}-H_c). \tag{6}$$

This relation obviously fits the data of Fig. 4.

We shall use Eqs. (5) and (6) later to derive values for α and β.

We next carry the *theoretical* analysis one step further. The constants m, β, and α characterize a ferromagnetic domain wall. We now use the analysis originated by Landau and Lifshitz[1] for uniaxial crystals, and later developed by Kittel,[12] to derive β and m in terms of the constants which characterize the ferromagnetic material in general.

In order to derive β in this way, we calculate the power dissipated by a unit area of wall moving with velocity v in an applied field H_0 from the equation of motion of the magnetization in a small volume. We then set this expression equal to $2H_0M_sv$ in order to find a relation between v and H_0, and β is derived by comparing this relation with (6). The equation of motion is

$$d\mathbf{M}/dt=\gamma[\mathbf{M}\times\mathbf{H}]-(\lambda/M^2)(\mathbf{M}\times[\mathbf{M}\times\mathbf{H}]). \tag{7}$$

The power dissipated per unit volume is $\mathbf{H}\cdot d\mathbf{M}/dt$, which is

$$\mathbf{H}\cdot d\mathbf{M}/dt\cong\lambda H_e^2, \tag{8}$$

where $\mathbf{H}=\mathbf{H}_0+\mathbf{H}_e$, $\mathbf{H}_0$ is the applied field and $\mathbf{H}_e$ is a field associated with the motion of the wall as Becker[9] has shown. It exists only in the wall and is perpendicular to the wall. The value of this field is determined from the precessional angular velocity of the spins in the moving wall by means of the Larmor relation. It is

$$\mathbf{H}_e=-(\mathbf{v}/\gamma)(\partial\theta/\partial z), \tag{9}$$

where γ is the gyromagnetic ratio and θ is the rotational

[12] C. Kittel, Phys. Rev. **80**, 918 (1950).

angle of the spins in a 180° wall. In the theory of the domain wall[13] it is shown that

$$\partial\theta/\partial z=[g(\theta)/A]^{\frac{1}{2}}, \tag{10}$$

where A is a measure of the exchange energy per unit volume due to gradients in the direction of the magnetization as given by Eq. (11).

$$\text{Exchange energy/unit vol.}=A[(\nabla\alpha_1)^2+(\nabla\alpha_2)^2+(\nabla\alpha_3)^2]. \tag{11}$$

Here α_1, α_2, α_3 are the direction cosines of the magnetization. $g(\theta)$ is the anisotropy energy density

$$g(\theta)=K_1(\alpha_1^2\alpha_2^2+\alpha_2^2\alpha_3^2+\alpha_3^2\alpha_1^2), \tag{12}$$

expressed in terms of θ. K_1 is the first-order anistropy constant.

If we use Eqs. (9) and (10) in Eq. (8) and integrate over z to get the power dissipated for unit area of wall, we have

$$\int_{-\infty}^{\infty}\mathbf{H}\cdot\frac{d\mathbf{M}}{dt}dz=2H_0M_s v=(\lambda v^2/\gamma^2A^{\frac{1}{2}})\int_0^{\pi}[g(\theta)]^{\frac{1}{2}}d\theta, \tag{13}$$

where we have used Eq. (10) to transform from integration over z to integration over θ as well as to evaluate Eq. (9). We may now write

$$v=\frac{2M_s\gamma^2A^{\frac{1}{2}}}{\lambda\int_0^{\pi}[g(\theta)]^{\frac{1}{2}}d\theta}H_0. \tag{14}$$

This is the desired relation between v and H_0 which is to be compared with Eq. (6). In this way we find

$$\beta=(\lambda/\gamma^2A^{\frac{1}{2}})\int_0^{\pi}[g(\theta)]^{\frac{1}{2}}d\theta. \tag{15}$$

We derive m from the energy of motion of the wall, which we equate to $\frac{1}{2}mv^2$. This was first done by Becker.[9] He pointed out that this energy was equal to $(1/8\pi)\int H_s^2dV$, and by means of Eq. (9) he was able to write

$$m=(1/4\pi\gamma^2)\int_{-\infty}^{\infty}\left(\frac{\partial\theta}{\partial z}\right)^2dz. \tag{16}$$

If we use Eqs. (10), (11), and (12) this becomes

$$m=(1/4\pi\gamma^2A^{\frac{1}{2}})\int_0^{\pi}[g(\theta)]^{\frac{1}{2}}d\theta. \tag{17}$$

It will be noted that the above analyses neglect the effect of eddy currents. As Williams, Shockley, and Kittel[3] have shown, these will contribute part of the measured value of the ratio of v to H_0 and of the damping constant β which also affects the data of Fig. 6. The equations of Williams, Shockley, and Kittel will be used in the next section to correct the data for eddy current effects.

[13] C. Kittel, Revs. Modern Phys. **21**, 541 (1950); see Eq. (3.3.9).

IV. DISCUSSION

If we evaluate the various factors in Eq. (15), we can use it to evaluate λ from the data given in Fig. 4. Since the wall is in a (110) plane, we have

$$g(\theta)=\tfrac{1}{4}K_1[\cos^4(\theta+35°16')+\sin^2(\theta+35°16')], \tag{18}$$

where $\theta=0$ on one side of the wall and π on the other. Then,

$$\int_0^{\pi}[g(\theta)]^{\frac{1}{2}}d\theta=1.38|K_1|^{\frac{1}{2}}. \tag{19}$$

In performing this integration, care must be taken to use the positive value of the square root over the whole interval. The evaluation of A requires some discussion. It may be done from the Curie constant and the Curie temperature as described by Néel.[14] This method gives $A=5.62\times10^{-7}$ if we use the data of Kopp[15] to evaluate the Curie constant. This evaluation of the Curie constant is unsatisfactory, however, since (as Néel[16] has later shown it should) the reciprocal of the susceptibility above the Curie temperature follows a curved line. A more satisfactory evaluation can be made from a fundamental relation recently derived by Herring and Kittel[17] between A and the Bloch constant:

$$A=[S_0/\Omega]^{\frac{1}{3}}[k/13.3C^{\frac{1}{3}}], \tag{20}$$

where k is Boltzmann's constant, C is Bloch's constant as used in the relation $M_s=M_0(1-CT^{\frac{1}{2}})$, S_0 is the atomic spin, and Ω is the atomic volume. (S_0/Ω) is equal to the saturation magnetization at 0°K divided by the Bohr magneton. From (20) we find $A=1.53\times10^{-6}$, and this is the value we shall use. The Bloch constant used in this evaluation ($C=4\times10^{-6}$) was obtained by fitting the Bloch $T^{\frac{3}{2}}$ law to the saturation magnetization measurements of Weiss and Forrer.[18] Because of the square root in (13), the value of λ we obtain will not depend critically on the value used for A. Using $M_s=460$ cgs units at room temperature, $\gamma=1.76\times10^7$ and $K_1=-1.1\times10^5$ ergs/cc as given by Bickford,[19] we find for Fe_3O_4 from Eq. (14),

$$v/H_0=7.7\times10^{11}/\lambda. \tag{21}$$

The data in Fig. 4 give $v/H_0=1900$. Before using this in (21) to calculate λ, however, we must correct for eddy current losses. Equation (6) may be written in the form

$$\beta\dot{z}=(\beta_s+\beta_r)\dot{z}=2M_s(H_{\text{app}}-H_c), \tag{22}$$

[14] L. Néel, Cahiers Physique **25a**, 1 (1944).
[15] W. Kopp, thesis, Zurich (1919).
[16] L. Néel, Ann. phys. **3**, 137 (1948).
[17] C. Herring and C. Kittel, Phys. Rev. **81**, 869 (1951); see Eq. (5).
[18] P. Weiss and R. Forrer, Ann. phys., series 10, **12**, 279 (1929).
[19] L. R. Bickford, Jr., Phys. Rev. **78**, 449 (1950).

where β_e measures the contribution due to eddy currents and β_r measures the effect described by Eq. (21). From Fig. 4 we now have $\beta_e+\beta_r=2M_s/1900=0.484$. From the low field approximation for eddy current effects given by Williams, Shockley, and Kittel (see reference 3, Eq. (11)) we find $\beta_e=0.078$. Hence, experimentally,

$$\beta=0.484, \quad \beta_r=0.406, \tag{23}$$

for Fe_3O_4. From Eqs. (21) and (22) $7.7\times10^{11}/\lambda=2M_s/\beta_r$, and we find

$$\lambda=3.5\times10^8. \tag{24}$$

It is appropriate to compare this with the value determined from the ferromagnetic resonance line width observed by Bickford.[19] His line width at half-power points for magnetic absorption is approximately 1500 oersted. The relation between line width and λ has been given elsewhere.[20] Sample shape enters into this relation, but not in a critical way, and we therefore ignore it except as it affects H_{res}. The relation is

$$2\Delta H\gamma M_s/H_{res}=\lambda, \tag{25}$$

where the line width is $2\Delta H$. From Bickford's data and Eq. (25) we find $\lambda=1.9\times10^9$. Thus our value predicts a line about $\frac{1}{5}$ as wide as Bickford's.

The difference between our value for λ and Bickford's may be due at least partly to field inhomogeneities in the samples used by Bickford. Such inhomogeneities have been observed to affect ferromagnetic resonance line widths in ferrite samples,[20,21] and Bickford's samples were large enough to indicate that such effects are expected.

All the factors in Eq. (17) have now been evaluated, and when we make the numerical calculation we find $m=9.5\times10^{-11}$ g/cm^2. This value is so small that the first term in Eq. (2) does not affect our experiments significantly.

From $\beta=\beta_e+\beta_r$ as given by Eq. (23), and from Fig. 6 using Eqs. (3) and (5) we can determine α for our sample. We note that μ' has dropped to $\frac{1}{2}$ its value at low frequency when $\omega\beta/\alpha=1$. Figure 6 shows that this occurs at 3000 cycles. In this way we find

$$\alpha=9100. \tag{26}$$

We can also check our value of β by determining it from the data of Fig. 6. If we make a reasonable estimate of A_{coil} from the cross-sectional area of a leg of the sample and the thickness of the windings, we may use Eqs. (3) and (5) to find α. We may then derive β from the fact that $\omega\beta/\alpha=1$ at $\omega=2\pi\times3000$. This leads to $\beta=0.5$, which checks the value given in Eq. (23) satisfactorily. The accuracy of the check is not as good as we should like, however, as it was impossible actually to measure A_{coil}. It is hoped that this can be done when larger samples are available for these experiments.

It should be emphasized that β is a fundamental property of the material whereas α is a constant characteristic only of a particular sample. As Eq. (2) shows, α measures the rate at which magnetostatic energy is built up as the position of the wall changes, and in our sample it has a uniquely low value. If it were increased, as it would be if the sample shape were such that the wall could not move so easily without building up a magnetic field, the permeability at low frequency would drop, the relaxation frequency for μ would increase, and the wall motion might begin to show resonant behavior. Bickford[19] has given a permeability for Fe_3O_4 at room temperature of about 45 in a sample where the domain pattern is not controlled, but in which we may think of the effective α as being enough higher than ours to reduce μ' from our value (4900) to his.

It may be noted here that single crystal samples of the shape and orientation used in these experiments may be of use in devices involving saturable reactors such as memory devices and magnetic amplifiers.

V. ACKNOWLEDGMENTS

The author wishes to express his gratitude to several friends and colleagues for assistance with various aspects of this research. The crystal from which the sample was cut was provided by Professor von Hippel of the Laboratory for Insulation Research at MIT.[4] H. J. Williams has been of considerable help in observing the domain patterns. W. L. Bond and J. Andrus cut the samples from bulk crystal. The author has had useful conversations with C. Kittel, R. M. Bozorth, C. L. Luke, and W. Yocum. H. G. Hopper has given technical assistance with all the work, and technical assistance on specific points was given by P. P. Cioffi, C. D. Owens and R. G. Conway, R. D. Heidenreich, H. R. Moore, and N. R. Pape.

[20] Yager, Galt, Merritt, and Wood, Phys. Rev. **80**, 744 (1950); see Eq. (A-6). The λ of the present paper is euqal to $\gamma\alpha M_s$ in the notation of this reference.

[21] Yager, Merritt, and Guillaud, Phys. Rev. **81**, 477 (1950).

Ion Clustering*

STANLEY BLOOM AND HENRY MARGENAU
Sloane Physics Laboratory, Yale University, New Haven, Connecticut
(Received November 2, 1951)

Kinetic theory is employed in investigating the extent to which polarizable molecules attach themselves to slowly moving ions in a gas, the underlying picture being that commonly used in deriving the barometric equation, i.e., the aggregation of molecules in a constant field of force. A potential energy of the form $-\kappa r^{-4}$ for $r \geqslant r_0$ but ∞ for $r \leqslant r_0$, leads to a large cluster formation. This hard-sphere potential, however, packs most of the clustered molecules into the sharp crevasse near r_0 and therefore falsifies the result. When the cusp is removed by the more adequate potential $\lambda r^{-12} - \kappa r^{-4}$, the tendency to cluster is reduced nearly 100-fold. Results are obtained in general agreement with experiment, except for $Li^+ - Kr$, where theory predicts a much smaller cluster than that inferred from mobility measurements.

I. INTRODUCTION

A SIMPLE approach to the problem of ion clustering is given by Loeb.[1] As this author himself has recognized, and as is emphasized in his forthcoming book, this schematic treatment makes no allowance for the statistical weights of different states of motion of the ion-molecule system. More elaborate calculations,[2] on the other hand, introduce complications which the problem hardly possesses, for they fashion it after the theories of molecular dissociation and take explicit account of quantization.

Whether or not this is necessary depends primarily on the spacing of the energy levels in the potential trough describing the interaction between ion and molecule. If it is narrow and the number of levels is small, quantum effects are certainly important. Otherwise classical statistics may be applied. Computations made with simplified potentials show the latter alternative to prevail. The number of vibrational levels is of the order of 50 in all interesting instances, though for the case of H_2 interacting with Li^+ it is but 10 (because of the small mass of these systems). We are therefore entitled to attack the clustering problem in the spirit of classical kinetic theory. The work will be limited to simple nonpolar gases. The underlying picture is that commonly used in deriving the barometric equation, i.e., the aggregation of molecules in a constant field of force.

II. THEORY

A. Hard-Sphere Repulsion

Let $V(r)$ be the potential energy of a neutral molecule at a distance r from the center of the ion. The number of molecules with velocity near v and contained in a spherical shell of radius r is

$$d^2N = Ar^2 dr v^2 dv \exp[-(V+\tfrac{1}{2}mv^2)/kT]. \quad (1)$$

The number within the spherical shell having any velocity, obtained by integrating d^2N over v, is

$$dN = (\pi^{\frac{1}{2}}/4\beta^3) A r^2 dr \exp(-V/kT)$$

where $\beta^2 \equiv m/2kT$. Now consider a spherical container of volume $\tau = (4\pi/3)(R^3 - r_0^3)$ containing N_0 molecules. Then

$$N_0 = (\pi^{\frac{1}{2}}/4\beta^3) A \int_{r_0}^{R} dr r^2 \exp(-V/kT), \quad (2)$$

r_0 being the distance of closest approach of ion and molecule. This relation determines the constant A. We wish to find the number N_B of bound molecules, i.e., those whose total energy is negative:

$$V(r) + \tfrac{1}{2}mv^2 \leqslant 0. \quad (3)$$

In this first part of the analysis, the ion and molecule will be considered as exhibiting a "hard-sphere" repulsion. The attraction considered here is that arising between the ion and the ion-induced dipole moment on the molecule; other effects will first be neglected. The potential energy is then given by

$$\begin{aligned} V(r) &= -\kappa r^{-4}, \quad r \geqslant r_0 \\ &= \infty, \qquad r \leqslant r_0 \quad \text{(see Fig. 1).} \end{aligned} \quad (4)$$

The clustering criterion (3) is therefore

$$v \leqslant (2\kappa/m)^{\frac{1}{2}} r^{-2} = \alpha^{\frac{1}{2}}/\beta r^2, \quad (5)$$

where $\alpha \equiv \kappa/kT$. From Eq. (1) we obtain

$$N_B = 4N_0\beta^3\pi^{-\frac{1}{2}} \times \frac{\int_{r_0}^{R} r^2 \exp(\alpha/r^4) dr \int_0^{\alpha^{\frac{1}{2}}/\beta r^2} v^2 \exp(-\beta^2 v^2) dv}{\int_{r_0}^{R} r^2 \exp(\alpha/r^4) dr}. \quad (6)$$

* Assisted by the ONR.

[1] L. B. Loeb, *Fundamental Processes of Electrical Discharge in Gases* (John Wiley and Sons, Inc., New York, 1939). Taking all molecules to have the mean thermal velocity, Loeb describes clustering in terms of a region of stability about the ion. His criterion for clustering is $-V(r) \geqslant \frac{1}{2}m\langle v^2 \rangle_{Av}$, which gives a radius r_{max}, beyond which a molecule remains free. The number of clustered molecules is then taken to be that which can be close-packed into a sphere of radius r_{max}.

[2] Eyring, Hirschfelder, and Taylor, J. Chem. Phys. **4**, 479 (1936). For a discussion of the influence of clustering on ion mobilities in mixed gases, see A. W. Overhauser, Phys. Rev. **76**, 250 (1949).

The numerator of this expression is

$$2N_0\pi^{-\frac{1}{2}}\int_{r_0}^{R} r^2 \exp(\alpha/r^4)\Gamma(\tfrac{3}{4}, \alpha/r^4)dr$$

provided we introduce the incomplete Γ-function

$$\Gamma(\tfrac{3}{4}, y)=\int_0^y dx e^{-x}x^{\frac{1}{4}}.$$

If we write the denominator in the form

$$\tfrac{1}{3}(R^3-r_0^3)+\int_{r_0}^{R} dr r^2[\exp(\alpha/r^4)-1]$$

we see that both r_0^3 and the integral are negligible against R^3 as $R\to\infty$. The number density $n_0=N_0/\tau$, hence in the limit as $R\to\infty$

$$N_B=8n_0\pi^{\frac{1}{2}}\int_{r_0}^{\infty} dr r^2 \exp(\alpha/r^4)\Gamma(\tfrac{3}{4}, \alpha/r^4)$$

$$=2n_0\pi^{\frac{1}{2}}\alpha^{\frac{1}{4}}\int_0^b dx e^x x^{-7/4}\Gamma(\tfrac{3}{4}, x), \qquad (7)$$

where $b\equiv\alpha/r_0^4$. For convenience we write this in the form

$$N_B/2n_0r_0^3\pi^{\frac{1}{2}}=b^{\frac{1}{4}}\int_0^b dx e^x x^{-7/4}\Gamma(\tfrac{3}{4}, x)\equiv Q(b). \qquad (8)$$

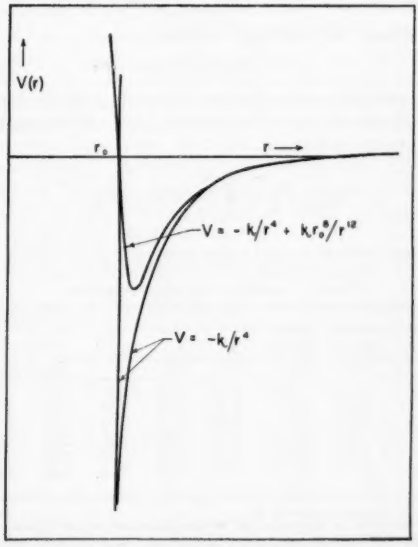

FIG. 1. Potential energy $V(r)$ *vs* r (schematic).

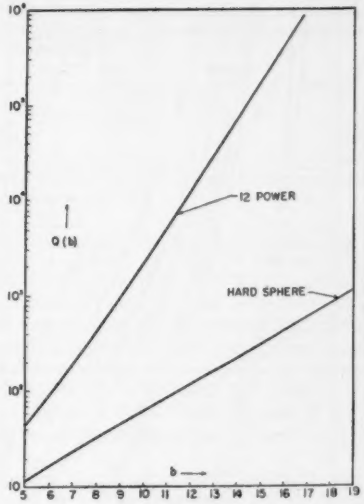

FIG. 2. $Q(b)$ *vs* b. [See Eqs. (8) and (17).]

Because of the divergence of the integrand at $x=0$, the integration is split into two parts:

$$Q(b)/b^{\frac{1}{4}}=\int_0^{\epsilon}+\int_{\epsilon}^{b}\equiv K''+K'. \qquad (9)$$

ϵ was chosen to be $0.6\sqrt{\frac{3}{4}}$, which is a convenient value. K'' is found by series expansion of the integrand; it is

$$K''=0.807. \qquad (10)$$

The integral

$$K'=\int_{0.6(\frac{3}{4})^{\frac{1}{2}}}^{b} dx e^x x^{-7/4}\Gamma(\tfrac{3}{4}, x)$$

is computed by numerical quadrature. Figure 2 represents $Q(b)$ *vs* b.

It is to be noted that our analysis treats the ion as stationary and the molecule as having the velocity v. If the calculation is made in terms of relative velocities, as it should be, the only effect on the preceding formulas is the replacement of the molecular mass by the reduced mass. This appears in $\beta=(m/2kT)^{\frac{1}{2}}$, which drops out from our equations, indicating that they will not change when the ion is allowed to have its own temperature motion.

To obtain N_B for specific systems we must know κ, the force law constant, and r_0, the distance of closest approach of ion and molecule. Neither is known accurately, and indeed r_0 is not a well-defined concept. For κ we shall use the dielectric law of attraction,

$$\kappa=(D-1)e^2/8\pi L \qquad (11)$$

where L is the Loschmidt number and D is the dielectric

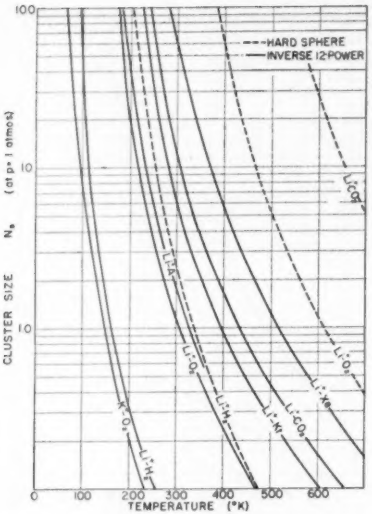

FIG. 3. Cluster size N_B *vs* temperature, at 1 atmosphere.

constant of the molecule. This, of course, is an approximation since Eq. (11) is derived for low uniform fields. As Loeb[1] points out, experimental values for the dielectric constant lead to values of κ which are probably 10 to 20 percent too high. However, in view of our neglect of Van der Waals attractions, which would give higher effective values of κ, there seems little point in attempting to improve upon Eq. (11).[3] A more serious difficulty arises in connection with r_0, since it enters in a more sensitive way into the formulas. We have taken Margenau's[2] values which are the sum of the radii of ion and molecule.

Figure 3 gives the resulting values of N_B at various temperatures for some representative ion-molecule systems. The numerical constants used are given in Table I. Since N_B is proportional to the number density, we have arbitrarily kept n_0 fixed at $2.687(10^{19})$ per cm^3, the value for 0°C and 1 atmosphere.

Figure 3 shows that at room temperature and a pressure of one atmosphere, the present model leads to appreciable clustering in all cases considered. This is due, as we shall now show, to the presence of the deep crevasse in the hard-sphere model. (See Fig. 1.)

B. Inverse 12-Power Repulsion

We shall now take as the potential energy

$$V(r)=\lambda r^{-12}-\kappa r^{-4}. \tag{12}$$

The analysis proceeds as before, the criterion for clustering being $v\leqslant(-2V/m)^{\frac{1}{2}}\equiv v_m$, for $V\leqslant 0$. This gives

$$N_B=16n_0\beta^3\pi^{\frac{1}{2}}\int_{r_1}^{\infty}drr^2e^{-V/kT}\int_0^{v_m}dvv^2\exp(-\beta^2v^2). \tag{13}$$

Here r_1 is defined by the relation

$$V(r_1)=0, \quad \text{or} \quad r_1=(\lambda/\kappa)^{1/8}. \tag{14}$$

Integration over v results in

$$N_B=8n_0\pi^{\frac{1}{2}}\int_{r_1}^{\infty}drr^2\exp(\alpha r^{-4}-\gamma r^{-12})$$
$$\times\Gamma(\tfrac{3}{2},\ \alpha/r^4-\gamma/r^{12}) \tag{15}$$

provided we write $\alpha=\kappa/kT$, $\gamma=\lambda/kT$. Since the force-law constant γ is not known, we shall replace r_1 by the hard-sphere value r_0 previously used. Then $\gamma=\alpha r_0^8$ and

$$N_B=8n_0\pi^{\frac{1}{2}}\int_r^{\infty}drr^2\exp[(1-r_0^8/r^8)\alpha/r^4]$$
$$\times\Gamma[\tfrac{3}{2},\ (1-r_0^8/r^8)\alpha/r^4]. \tag{16}$$

This integral can be put into a more convenient form by the substitution $y=r_0^4/r^4$. Then

$$N_B=2n_0r_0^3\pi^{\frac{1}{2}}\int_0^1dyy^{-7/4}\exp[by(1-y^2)]$$
$$\times\Gamma[\tfrac{3}{2},\ by(1-y^2)] \tag{17}$$

where, as before, $b\equiv\alpha r_0^{-4}$. The integral

$$N_B/2n_0r_0^3\pi^{\frac{1}{2}}\equiv Q(b) \tag{18}$$

is evaluated numerically for various values of b. Because of the divergence of the integrand as $y\to 0$, it is again necessary to take

$$Q(b)=\int_0^{\epsilon}+\int_{\epsilon}^{1.0}\equiv P(b)+M(b).$$

(Here $\epsilon=0.01$ is used.) The integral $P(b)$ is obtained

TABLE I. Constants of ion-molecule systems.

	Dielectric constant $(D-1)$ $\times 10^5$	Force constant $\kappa\times 10^{44}$ erg-cm^4	r_0(A)[a] Li$^+$	Na$^+$	K$^+$	Rb$^+$	Cs$^+$
H_2	2.64[b,c]	9.014	2.16	2.36	2.71	2.87	3.03
O_2	5.43[c]	18.54	2.23	2.43	2.78	2.94	3.10
CO_2	9.85[b]	33.62	2.39	2.59	2.94	3.10	3.26
A	5.68[c]	19.39	2.21	2.41	2.76	2.92	3.08
Kr	8.50[c]	29.02	2.35	2.55	2.90	3.06	3.22
Xe	13.78[c]	47.05	2.49	2.69	3.04	3.20	3.36

[2] H. Margenau, Philosophy of Science **8**, 603 (1941). In this paper values are given of the interaction energy between various ions and foreign molecules at the distance of closest approach, with and without Van der Waals' forces.

[a] H. Margenau, reference 3.
[b] *Handbook of Chemistry and Physics* (Chemical Rubber Publishing Company).
[c] J. Jeans, *The Dynamical Theory of Gases* (Cambridge University Press, London, 1925).

by series expansion and $M(b)$ by numerical quadrature. Figure 2 gives the values of $Q(b)$ for the case of the 12-power law. Extrapolation was used to extend the plot of $Q(b)$ to the larger values of b. It is seen that $Q(b)$ is nearly an exponential function of b on both models. With these values of $Q(b)$ we obtain the results for N_B shown in Fig. 3.

It is seen that the inclusion of the "soft" repulsion reduces the number of clustered molecules by a factor greater than 100. At 273°K and a pressure of one atmosphere the highly polarizable CO_2 molecules form a cluster about a Li^+ ion of about 28 molecules. Oxygen, with intermediate polarizability, "clusters" to the extent of only 2 molecules, and H_2, with very low polarizability, has an N_B of about 0.08—i.e., no clustering. The alkali ions in order of increasing radii are Li^+, Na^+, K^+, Rb^+, and Cs^+, so that Li^+ is the strongest clustering agent. Figure 3 shows N_B for K^+-O_2; at normal temperature and pressure, N_B has the negligible value of about 0.05.

The present calculations are incomplete inasmuch as they neglect interactions between clustering molecules, which are treated as points. In other words, no account has been taken of steric exclusion. This could be introduced in qualitatively satisfactory fashion by supposing that, whenever the present theory gives a number of clustered molecules greater than can be packed into the surrounding space considered by Loeb, it must be reduced to that number. At any rate, it is clear that steric effects reduce the clusters here computed. Since we have shown that clustering is a rare phenomenon even on the present basis, the steric refinement seems unimportant.

A rough idea of the spatial distribution of those few molecules that might cluster can be had from the fact that in Eq. (17) the contribution to the integral from $y=0$ to $y=0.01$ is, for the important values of b, approximately 1 percent or less of that coming from the remaining range. But this small interval in y corresponds to the large interval in r between $(10)^{\frac{1}{6}}r_0$ and ∞. In other words, roughly 99 percent of the molecules that do cluster congregate within a distance of about $3.2r_0$ from the ion.

III. COMPARISON WITH EXPERIMENT

Munson and Hoselitz,[4] in their measurements of the mobilities of alkali ions in inert gases, present some data on clustering. They find that only Li^+ can serve as a clustering agent and that the greater the atomic weight of the rare gas atom (and, therefore, the greater its polarizability) the higher the temperature at which it may form a cluster with the lithium ion. An attempt was made to observe a cluster with K^+ in argon. This was unsuccessful even at the relatively low temperature of 126°K. On the other hand, Li^+ in argon readily formed clusters at 195°K. Table II gives Munson and Hoselitz's experimentally deduced values for the cluster sizes.

TABLE II. Experimental and theoretical values of N_B.

System	Temp. (°K)	N_B Experiment[a]	N_B Theory (at $p=19$ mm of Hg)
Li^+-A	195	2	1.7
Li^+-Xe	290	2	2.3
Li^+-Kr	290	2	0.2
Li^+-Kr	225	...	~2

[a] See reference 4.

Unfortunately, Munson and Hoselitz do not give values for the pressures they used. The last column in Table II gives our calculated N_B for the pressure $p=19$ mm Hg, which is of the order of magnitude of the pressures usually employed in mobility experiments of this kind.

It is seen that for the cases of Li^+ in argon and xenon, our N_B is comparable to the experimentally deduced values. However, in the case of krypton, we obtain $N_B \simeq 0.2$, i.e., negligible clustering, whereas experiment seems to yield the value of 2 at the temperature $T=290$°K. In order for our analysis to give $N_B=2$ at $p=19$ mm Hg, we would have to lower the temperature to 225°K; or keeping $T=290$°K, the pressure would have to be raised to as much as 190 mm Hg. Lacking information as to the experimental pressures, it is difficult to understand this apparently discrepant result for Li^+-Kr. Munson and Hoselitz's indication of two clustered atoms for both Xe and Kr on Li^+ at the same temperature does seem strange, however. Xenon has a force constant (proportional to the polarizability) of $\kappa=47\times10^{-44}$ erg cm^4, and with Li^+, $r_0=2.49$A. Now, even though the distance of closest approach r_0 for Li^+-Kr is less than that for Li^+-Xe, the fact that κ for Xe is 1.6 times as large as that for Kr far outweighs the difference in the r_0 values. Hence Xe should be more clusterable than Kr.

[4] J. R. Munson and K. Hoselitz, Proc. Roy. Soc. (London) A17 2, 43 (1939).

Letters to the Editor

PUBLICATION of brief reports of important discoveries in physics may be secured by addressing them to this department. The closing date for this department is five weeks prior to the date of issue. No proof will be sent to the authors. The Board of Editors does not hold itself responsible for the opinions expressed by the correspondents. Communications should not exceed 600 words in length and should be submitted in duplicate.

Atmospheric Absorption of Solar Infrared Radiation

ROMUALD ANTHONY
U. S. Naval Ordnance Test Station, Inyokern, China Lake, California
(Received December 17, 1951)

AS a result of some measurements of solar radiation taken with a KBr double monochromator in the infrared region 1.5 to 20 microns, the data collected were assessed and values of absorption coefficients for the continuous absorption spectrum in the region 8–20 microns were evaluated. The coefficients were obtained from the slopes of the lines shown in Fig. 1, which indicate adherence to the well-known Lambert's law. The resulting coefficients were compared with those of Adel[1] and Elsasser[2] in Fig. 2. The computed values indicated by Elsasser's curve were based on line width of 0.25 cm^{-1} and should be reduced in accordance with the more recent value of the line width in the water vapor rotation spectrum measured by Adel[3] to be 0.11 cm^{-1}. In the 8–13 microns region of the solar spectrum the absorption coefficient can be taken to be proportional to line width. When thus reduced, these values come to closer agreement with the smaller values of the coefficients.

In a recent paper presented at an American Physical Society meeting[4] it was pointed out that there appears approximately a factor of 2 difference in the experimental determination of the absorption coefficients by Adel and the author. Actually, in terms of percent transmission, there is agreement within 8 percent in the values obtained for this region of low absorption for, say, 1 cm of precipitable water in the optical path. Furthermore, we have found that the window in the region 17–20 microns recorded by Adel[5] has shown up quite well with a slit width four times that used in the region 8–14 microns. This region is highly sensitive to water vapor content.[6]

The observations were made from the top of Table Mountain, California, with the cooperation of the Smithsonian Institution group stationed there.

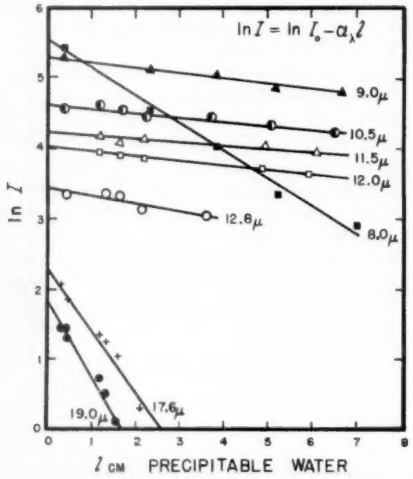

FIG. 1. Experimental curves for the logarithm of the solar intensity *versus* precipitable water with wavelength as parameter. Water vapor content determined spectroscopically using Fowles method (reference 6).

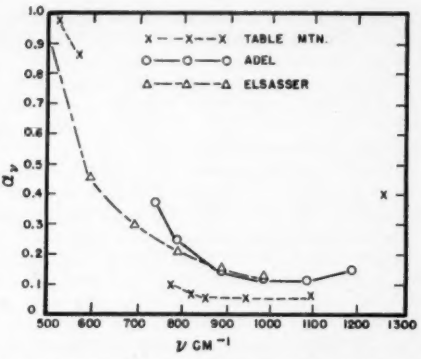

FIG. 2. Comparison of computed values with experimental values of absorption coefficient α_ν, as a function of ν cm^{-1}.

[1] Arthur Adel, Astrophys. J. **89**, 1 (1939).
[2] W. M. Elsasser, Phys. Rev. **53**, 768 (1938).
[3] Arthur Adel, Phys. Rev. **71**, 806 (1947).
[4] Romuald Anthony, American Physical Society Meeting, June 25, 1951, Vancouver, B. C. [Phys. Rev. **83**, 888 (1951)].
[5] Arthur Adel, Astrophys. J. **96**, 239 (1942).
[6] F. E. Fowle, Astrophys. J. **42**, 394 (1915).

Diurnal Variations in High Energy Cosmic-Ray Intensities*

PAUL H. BARRETT AND Y. EISENBERG
Cornell University, Ithaca, New York
(Received December 26, 1951)

EXPERIMENTS were performed in a salt mine near Ithaca, New York, at a depth of 1600-meters water equivalent to investigate the properties of high energy cosmic rays. The apparatus consisted of five counter telescopes, each containing two trays of Geiger counters (30 in.×36 in.) separated by 4 in. of Pb and ½ in. Fe, and shielded above and below by 2 in. of Pb. From July 15, 1951 to October 9, 1951, 90,702 coincidences were recorded with an average rate per telescope of 10.46 hr^{-1}. The accidental coincidence rate was about 5 percent. The number of coincidences in each telescope was recorded every hour.

Other experiments, to be reported later, indicate that the particles observed are mu-mesons. In order to penetrate to this depth the meson must have an energy of at least 5×10^{11} ev. On the average, the mesons are created with 10^{13} electron volts by pi-mesons of 1.3×10^{12} ev energy, and these pi-mesons are created by nuclear interactions of primary nucleons having an average energy on the order of 5×10^{13} ev. Because of the zenith angle distribution of the mesons the angular resolution of the telescope is about 60 degrees, and therefore, only variations in the coincidence rate lasting for four hours or more should be considered significant.

The variation of intensity with solar time is shown in Fig. 1. The errors are standard errors. The mean square deviation of the observed coincidence rates from the average agrees with that expected from a normal distribution. These data indicate that

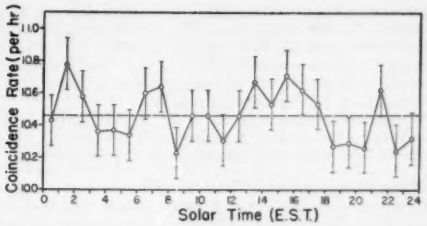

FIG. 1. Solar-time variation of cosmic rays at 1600-m water equivalent depth. Errors shown are standard errors. The horizontal line indicates the average coincidence rate per telescope.

within two standard errors the root-mean-square value of a solar diurnal effect is less than one percent for the particles observed.

In Fig. 2 the data are grouped in sidereal time intervals and plotted against local sidereal time. The local sidereal time at 0000 hours Eastern Standard Time on July 22, 1951, was taken as 19 hr 50 min. On the basis of these data the existence of a sidereal diurnal variation greater than two percent would seem highly improbable. However, the deviations of the hourly rates from the average are slightly larger than expected from a normal distribution, and the results are indecisive as to the probable existence of a sidereal diurnal effect of about one percent.

A sidereal diurnal effect of about ten percent has been reported by Sekido and collaborators[1] based on a total number of 1720 particles observed at a depth of 1400 meters H_2O equivalent. They show a peak in intensity coming at five hours and 20 minutes local sidereal time. Our data reveal no peak in intensity near this hour, and as our standard error is much smaller and our angular resolution is similar to theirs, such an effect should have been readily detectable.

Any observed anisotropy of cosmic rays depends not only on the anisotropy in the distribution of sources, but also on the deflections of the rays while crossing the space between the sources and the earth. Considerations of the energy density in cosmic rays[2] lead to the belief that they come from sources within our galaxy and are confined to the galaxy by magnetic fields. These magnetic fields would cause large and irregular changes in direction of the cosmic rays, resulting in a high degree of isotropy in the incident radiation, even if the sources are highly localized. In spite of this smearing, there should be a broad maximum in the intensity coming from the direction of any strong source. The width of the peak should be so great that the poor angular resolution of our apparatus would have little effect on it. But if curling due to magnetic fields is sufficiently strong, the departure from complete isotropy may not be observable. This has been discussed quantitatively by Cocconi,[3] who concluded from the observed isotropy of the cosmic rays of 10^{12}–10^{14} ev that the galactic fields must have a strength of at least 10^{-9} gauss. Our data confirm his order of magnitude.

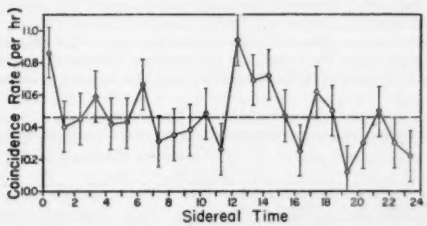

FIG. 2. Sidereal-time variation of cosmic rays at 1600-m water equivalent depth. Errors shown are standard errors. The horizontal line indicates the average coincidence rate per telescope.

We are grateful to Professors G. Cocconi and K. I. Greisen for their helpful criticism and suggestions.

* This work has been supported by the Air Force Cambridge Laboratories.

[1] Sekido, Masuda, Yoshida, and Wada, Phys. Rev. **83**, 658 (1951).
[2] R. D. Richtmeyer and E. Teller, Phys. Rev. **75**, 1729 (1949).
[3] G. Cocconi, Phys. Rev. **83**, 1193 (1951). In a private communication from Dr. Cocconi he states that his accuracy of measurement should give $a \lesssim 6\times10^{-2}$ instead of $a \lesssim 3\times10^{-2}$, as stated in his article. Our results give $a \lesssim 4\times10^{-2}$.

The Scattering of 0.5-Mev Circularly Polarized Photons in Magnetized Iron*

FORREST P. CLAYT AND FRANK L. HEREFORD
University of Virginia, Charlottesville, Virginia
(Received December 31, 1951)

THE possibility of detecting circularly polarized photons by Compton scattering in magnetized ferromagnets has been both implied[1,2] and explicitly suggested[3] in several recent theoretical treatments. The dependence of the scattering cross section of circularly polarized (c.p.) photons upon both the sense of polarization and the polarization state of the scattering electrons is perhaps most clearly seen in the formalism adopted by Fano.[4] He describes the intensity and polarization state of an incident photon by means of a four-vector constructed from the Stoke's parameters and the scattering of this photon into another state

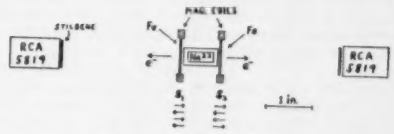

FIG. 1. Experimental arrangement.

by a 4×4 matrix which relates the Stoke's parameters of the incident and scattered radiation. In the case of unpolarized incident radiation this matrix transformation reduces to the well-known Klein-Nishina formula.

However, the intensity of c.p. incident radiation scattered at an angle θ by an electron with initial spin of direction $\mathbf{S}$ is of the form

$$\Phi(\theta)=C[A(\theta)\pm(1-\cos\theta)(\mathbf{k}_0\cos\theta+\mathbf{k})\cdot\mathbf{S}], \quad (1)$$

$$\Phi(\theta)=C[A\mp B\mathbf{n}_0\cdot\mathbf{S}], \quad \text{for} \quad \theta=\pi, \quad (2)$$

where $\mathbf{k}_0$ and $\mathbf{k}$ represent, respectively, the incident and scattered photon momenta in electron rest mass units, $\mathbf{k}_0=k_0\mathbf{n}_0$, and the upper or lower signs refer to right or left c.p. photons, respectively.

We have investigated this dependence of intensity upon $\mathbf{S}$ by observing in coincidence the forward direction Compton electrons ($\theta=\pi$) produced in magnetized Fe foils by annihilation quanta. Wheeler[4] was the first to point out that two-photon annihilation of positronium can proceed only from the singlet state (zero angular momentum). Hence, an experiment detecting coincidentally the polarization states of the annihilation photon pair must verify plane polarized photons with crossed planes or c.p. photons of opposite senses. The first possibility has been confirmed experimentally by several workers;[5,6] the second provides the c.p. photons employed in the experiment described here.

The experimental arrangement is depicted in Fig. 1. Forward direction Compton electrons from two magnetized Fe foils (0.1 g/cm²) were detected by two thin (0.5 mm) stilbene crystals covered by 0.004 g/cm² Al foil. Scintillations were recorded by a fast coincidence circuit[7] (2×10^{-8} sec resolving time), and rates

were measured for each of the four possible configurations of the magnetic fields shown in Fig. 1. The photomultipliers were magnetically shielded to reduce effects incurred upon reversing the magnetic fields. After each change in the fields the single rates were carefully adjusted to the unique values employed throughout the experiment.

The thin stilbene crystals were less than 0.4 percent efficient for detection of photons but were very nearly 100 percent efficient for forward direction Compton electrons. Thus far we have not made an accurate measurement of the fraction of the singles rates which was caused by photons or by Compton electrons produced in the magnetizing coils rather than the Fe foils. However, geometrical considerations indicate that Compton electrons from the coils correspond to photons scattered at $\theta \gtrsim 135°$ and, hence, for these electrons $E \gtrsim 0.06$ Mev. The efficiency for their coincidence detection by the circuit employed was small relative to that for the forward direction electrons ($E \approx 0.34$ Mev). Hence, the coincidence circuit was biased strongly against detection of electrons other than those in the forward direction produced in the Fe foils.

Another possible contribution to the coincidence rate was the result of the 1.3-Mev gamma-ray following the beta-transition of Na^{22}. However, the possibility of observing these gammas in coincidence with an annihilation quantum was small since the 1.3-Mev gammas are of spherical directional symmetry while the relative direction of an annihilation pair is π-radians. This argument is supported experimentally by previous work.[6]

TABLE I.[a] Observed coincidence rates.

Mag. fields S_1	Mag. fields S_2	Coinc. counts	Time (min)	Coinc./min	Average
←	←	12,850	425	30.23	
←	←	19,270	637	30.24	
→	→	10,866	350	30.98	
→	→	19,730	683	28.90[b]	
→	→	5227	174	30.06	
→	→	9437	316	29.90	
→	→	18,807	622	30.26	
		76,457	2524		30.29 ± 0.11
→	←	6313	220	28.70	
→	←	9472	327	28.97	
→	←	18,432	625	29.51	
←	→	20,480	694	29.60	
←	→	8877	310	28.65	
		63,574	2176		29.22 ± 0.12

[a] Difference $= 1.07 \pm 0.23$; percent difference $= 3.5 \pm 0.75$ percent.
[b] At the end of this run the single counting rate of one counter failed to repeat. Hence, this low rate is not included in the computation of the average coincidence rate for the first field configuration. Subsequent data confirmed previous coincidence rates for this configuration. If one includes this run, the observed difference is 2.6 ± 0.07 percent.

The collected data from 12 independent runs and the difference in coincidence rates for the indicated field configurations are presented in Table I. From Eq. (2) and the knowledge that a coincident photon pair are left and right or right and left circularly polarized, one deduces for the expected coincidence rates for $\theta_1 = \theta_2 = \pi$

$$\Phi_1\Phi_2 = C^2(A^2 + B^2), \quad \text{for} \quad \begin{cases} \rightarrow \ \rightarrow \\ \leftarrow \ \leftarrow \end{cases},$$

$$\Phi_1\Phi_2 = C^2(A^2 - B^2), \quad \text{for} \quad \begin{cases} \rightarrow \ \leftarrow \\ \leftarrow \ \rightarrow \end{cases}.$$

After substituting appropriate values for k_0, k, etc., and taking into account that only 2.2 of the 26 orbital electrons in Fe are polarized, one finds for the expected difference 0.9 percent. The expected difference has also been computed for $k_0 \gtrsim 1.5$ by Halpern,[3] whose result predicts a 2 percent difference in a coincidence experiment of this kind.

The somewhat greater observed difference, 3.5 ± 0.8 percent, may be a discrimination by the coincidence circuit against the detection of K and L shell (unpolarized) Compton electrons. It is known[8] that orbital binding changes the intensity of the scattered radiation and gives rise to a coherent (unshifted) scattering in addition to Compton scattering. We have been unable to find a computation of this effect for high energy photons scattered in Fe. This possibility is being investigated further.

The authors are much indebted to Mr. Stephan Berko of this laboratory for his assistance in computations and to Dr. U. Fano of the National Bureau of Standards for his helpful comments.

* Supported by U. S. Navy Bureau of Ordnance.
† DuPont Company Fellow.
[1] A. Wightman, Phys. Rev. **74**, 1813 (1948).
[2] U. Fano, J. Opt. Soc. Am. **39**, 859 (1949).
[3] O. Halpern, Nature **168**, 782 (1951). We wish to thank Dr. Halpern for communicating his results prior to publication.
[4] J. A. Wheeler, Ann. N. Y. Acad. Sci. **48**, 219 (1946).
[5] E. Bleuler and H. L. Bradt, Phys. Rev. **73**, 1398 (1948); R. C. Hanna, Nature **162**, 332 (1948); C. S. Wu and I. Shaknov, Phys. Rev. **77**, 136 (1950).
[6] F. L. Hereford, Phys. Rev. **81**, 482 (1951).
[7] R. L. Garwin, Rev. Sci. Instr. **21**, 569 (1950).
[8] G. Wentzel, Z. Physik **43**, I and 779 (1927); F. Bloch, Phys. Rev. **46**, 674 (1934).

Phenomena Associated with Negative μ-Mesons Stopped in Photographic Emulsions*

W. F. FRY†
Department of Physics, University of Chicago, Chicago, Illinois
(Received December 28, 1951)

ELECTRON sensitive Ilford G-5 plates of 400-micron thickness were exposed behind absorbers in the 145-Mev negative π-meson beam from the University of Chicago cyclotron. The geometry of the exposures is shown in Fig. 1. A fraction of the π-mesons decay in flight before entering the Cu absorbers. The μ-mesons from the decay of the π-mesons in the forward direction have an additional range of about one inch in Cu compared to the range of the π-mesons. The additional range of the μ-mesons makes it possible to separate the μ-mesons from the π-mesons.

Meson tracks were studied which entered the emulsions within 45° of the direction of the π-meson beam and which stopped in the emulsion further than 30 microns from the surfaces. A total of 1008 meson endings was studied. In 8 cases it is difficult to determine the phenomena associated with the mesons. In 6 cases a track of an electron of a few hundred kev is associated with each meson. The electron tracks are due either to decay electrons or to electrons which were ejected in the process of capture of the mesons. In 2 cases the mesons either produced one-prong stars or were scattered through a large angle near the end of the tracks. In 32 cases the mesons produced stars of one or more prongs of length greater than 10 microns. The prong distribution of these stars and the prong distribution of negative π-meson stars[1] are given in Table I. The prong distribution of the 32-meson stars indicate that nearly all of these stars are due to negative μ-mesons rather than negative π-mesons. No protons of energy greater than 30 Mev were observed from any of the stars. One of the stopped mesons ejected a single proton of 20 Mev. It seems probable that the event is due to a negative π-meson. It is possible that a portion of the 2- and 3-prong stars were produced by negative π-mesons. However, the various energies of the charged particles from the 2- and 3-prong stars are considerably lower than the energies of the charged particles from negative π-meson

TABLE I. Prong distribution of μ^- and π^- meson stars.

	Number of prongs of the star 1	2	3	4	5
No. of μ^- meson stars of N prongs	27	4	1	···	···
Percentage of μ^- mesons which produced N-prong stars	2.6	0.5	0.1	···	···
Percentage of π^- mesons which produced N-prong stars	21	27	15	7.8	1.8

stars. For this reason it is assumed that all of the 2- and 3-prong stars were produced by negative μ-mesons. The percentage of stopped negative μ-mesons which produce stars in emulsions is then 3.1 ± 0.6 percent. This percentage of stars produced by negative μ-mesons appears to be somewhat lower than the percentages reported by George and Evans[2] and Fry[3] who found that 8.7 ± 1.7 and about 8 percent of the μ-mesons which were captured produced stars. Since 61 percent of the negative μ-mesons are captured in the emulsion, the percentage of captured negative μ-mesons which produce stars is then $(3.1/0.61)=5.2\pm1$, which is to be compared with 8.7 ± 1.7 found by George and Evans. The low percentage of stars produced by negative μ-mesons indicate that the nuclear capture of negative μ-mesons results in very little excitation of the nucleus.

A search was made for decay electron tracks associated with the end of 500 of the 1000 meson endings. In 196 cases a decay electron

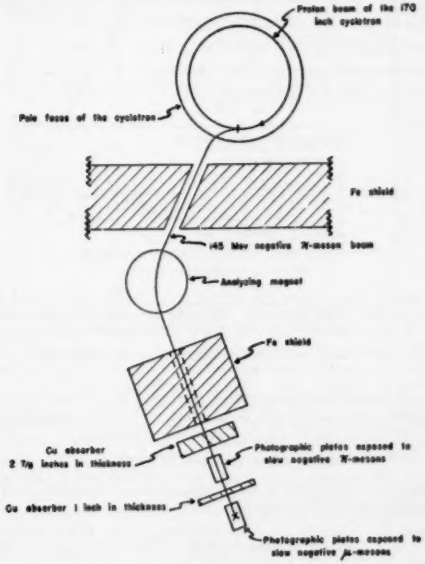
Proton beam of the 170 inch cyclotron
Pole faces of the cyclotron
Fe shield
145 Mev negative N-meson beam
Analyzing magnet
Fe shield
Cu absorber 2 7/8 inches in thickness
Photographic plates exposed to slow negative N-mesons
Cu absorber 1 inch in thickness
Photographic plates exposed to slow negative μ-mesons

FIG. 1. The geometry of the exposure of photographic plates to slow negative μ-mesons.

track was observed from the end of the meson track. In 288 cases the meson tracks stopped without associated tracks other than low energy electron tracks[4] ($15<E_e<100$ kev). The percentage of negative μ-mesons which decay in photographic emulsions is then $(196/500)(100)=39\pm3$. In order to estimate the efficiency of detecting the decay electrons from μ-mesons, 88 positive π-μ decays were studied in plates from the same batch of emulsion. The decay electron tracks were observed from the end of the μ-meson tracks in all but two cases. It is known that mesons which stop in a material of $Z=11$ have about equal probabilities of capture and decay.[5] If it is assumed[6] that the capture probability is proportional to Z^4, then nearly all of the negative μ-mesons which stop in gelatin should decay, while essentially all of the μ-mesons which stop in silver bromide crystals should be captured. Since the emulsions consist of crystals of Ag and Br imbedded in gelatin, the relative numbers of mesons which stop in the crystals and in the gelatin would seem to be proportional to the stopping power of the two materials for very low energy mesons. Using the percentage of negative μ-mesons which decay and the composition of the emulsions, the ratio of the stopping power per atom of Ag or Br to the average stopping power per atom in the gelatin, for low energy mesons, is found to be 4.8. If the stopping power per atom is incorrectly assumed to be proportional to Z, the ratio of the two stopping powers is about 12.

The author is greatly indebted to Professor H. L. Anderson and the cyclotron group for the meson exposures and to Professor Marcel Schein for the use of the facilities of the Cosmic-Ray Laboratory.

* Assisted by the joint program of the ONR and AEC.
† AEC Postdoctoral Fellow.
[1] F. L. Adelman and S. B. Jones, Phys. Rev. **75**, 1468 (1949).
[2] E. P. George and J. Evans, Proc. Phys. Soc. (London) **64**, 193 (1951).
[3] W. F. Fry, Phys. Rev. **82**, 747 (1951).
[4] Cosyns, Dilworth, Occhialini, and Schoenberg, Proc. Am. Phil. Soc. **A62**, 801 (1949); W. F. Fry, Phys. Rev. **83**, 594 (1951); Groeyzinger, Leder, and Ribe, Phys. Rev. **81**, 626 (1951); A. Bonetti and G. Tomasini, Nuovo cimento **8**, 603 (1951).
[5] H. K. Tichio, Phys. Rev. **74**, 1337 (1948).
[6] J. Wheeler, Phys. Rev. **71**, 462(A) (1947).

Striations in the Hydrogen Glow Discharge

W. A. GAMBLING
Department of Electrical Engineering, The University of Liverpool, Liverpool, England
(Received December 4, 1951)

IN a recent letter, Fowler[1] states that the striations obtained in a low pressure hydrogen glow discharge do not form opposite the entrance to a side arm of the main tube. He suggests that striations can only exist when completely bounded on their periphery by solid matter. This condition does not hold for pressures $\sim$760 mm Hg, as can be seen from the enclosed photographs (Fig. 1) and those of Fan,[2] showing the striations in a high pressure glow discharge in hydrogen.

For low pressure discharges, Druyvesteyn and Penning[3] state that for striations to appear in hydrogen the product of pressure (p mm Hg) and tube radius (R cm) must satisfy the empirical relation

$$pR=m,$$

where $m\sim2$ but depends on the current.

(a) (b) (c)

FIG. 1. Striations in a high pressure glow discharge in hydrogen, at 1 atmos pressure. Length = 3 mm. (a) Current = 0.1 amp, (b) current = 0.25 amp, (c) current = 0.5 amp.

The side arm in Fowler's apparatus increases the effective radius of the main tube at the junction of the side arm with the main tube, and it may be that at this point the product $p\times$effective radius has a value greater than that necessary to cause striations. On the other hand, Lau and Reichenheim[4] have concluded that the recombination of H atoms to H_2 molecules at the walls is important for the appearance of striations.

A satisfactory theory of striations has not yet been put forward, and it appears indeed that the complete interpretation of striation phenomena will not be easy.

[1] R. G. Fowler, Phys. Rev. **84**, 145 (1951).
[2] H. Y. Fan, Phys. Rev. **55**, 769 (1939).
[3] M. J. Druyvesteyn and F. M. Penning, Revs. Modern Phys. **12**, 87 (1940), Fig. 78.
[4] E. Lau and O. Reichenheim, Ann. Physik **3**, 840 (1929); **5**, 296 (1930).

Properties of Thermally Produced Acceptors in Germanium

C. S. FULLER, H. C. THEUERER, AND W. VAN ROOSBROECK
Bell Telephone Laboratories, Murray Hill, New Jersey
(Received December 26, 1951)

IT was discovered by Scaff and Theuerer that when n-type germanium is heated to 800°C and rapidly cooled, it is converted to p-type; that this conversion may be reversed by prolonged heating at 500°C; and that n-type germanium of very low resistivity cannot be converted.[1]

Recent studies have indicated that (1) the process is characterized by the diffusion of a $p-n$ boundary from the surface of the germanium into the interior and that (2) the concentration of acceptor centers approaches an equilibrium value dependent on temperature in a conversion range of about 550°C to the melting point.

Measurements were made at various temperatures of the locations for given heating times of $p-n$ junctions in samples of different resistivities and also of the equilibrium n- or p-type resistivities in partially or completely converted samples. Assuming that all donor and acceptor centers are ionized, the concentration of added acceptors equals the decrease in electron concentration in partially converted material, equals the initial electron concentration at a $p-n$ junction, and equals this plus the final hole concentration if the conversion is complete. These electron and hole concentrations are[2] $1/(e\mu_n\rho_n)=1.73\times10^{15}/\rho_n$ and $1/(e\mu_p\rho_p)=3.7\times10^{15}/\rho_p$, where ρ_n and ρ_p are the respective resistivities in ohm-cm, with e the electronic charge and μ_n and μ_p the mobilities.[3]

In experiments of the first author, $p-n$ junction locations were determined to within 0.002 cm by probing electrically, employing n-type samples of known uniform initial resistivity, as well as a sample possessing a unidirectional resistivity gradient. These were heated in helium for various times at temperatures in the conversion range (with the conversions reversed by heating at 500°C for 24 hours) and rapidly cooled. Assuming the surface concentration A_0 of acceptors to be constant at a given temperature, the concentration A at a $p-n$ boundary is given by

$$A=A_0\,\mathrm{erfc}(x/2D^{\frac{1}{2}}t^{\frac{1}{2}})=1.73\times10^{15}/\rho_n, \tag{1}$$

where x is the depth of the boundary below the surface, t is heating time, D is the diffusion constant, and

$$\mathrm{erfc}u=1-\frac{2}{\sqrt{\pi}}\int_0^u e^{-\beta^2}d\beta. \tag{2}$$

Measurements on two samples of differing ρ_n heated at the same temperature determine D and A_0. Values so determined are given in Table I. The first column applies to different samples,[4] the others to different locations on the variable resistivity sample.[5] The initial resistivities along this sample, computed from D and A_0 (and the values of x and t) are in fairly good agreement with the observed values, as Fig. 1 indicates. The values of D, among the largest observed for diffusion in solids,[6] are given by

$$D=0.02\exp(-12{,}000/RT), \tag{3}$$

where R equals 1.98 calories and T is absolute temperature, corresponding to an activation energy of about 0.5 ev.

The equilibrium concentrations were determined both from $p-n$ junction locations, and, by the second author, from resistivity data. The junctions were observed in two variable resistivity samples[7] subjected to prolonged heatings at temperatures from 560° to 760°C. The resistivity data were obtained for the center, bottom, and top of an ingot from a bar[8] cut from along its axis, and heated for 24 hours at various temperatures both before and after treatment at the highest temperature, 900°C.

Figure 2 shows the dependence of the concentrations so deter-

TABLE I. The diffusion constant D and the surface concentration A_0 of acceptors, at several temperatures.

Temperature, °C	760	670	770	850
$(\rho_n)_1$, ohm-cm	5.0	3.2	3.0	1.5
$(\rho_n)_2$, ohm-cm	18.5	6.3	6.0	6.0
D, cm² sec⁻¹	5.9×10^{-9}	3.2×10^{-9}	5.5×10^{-9}	9.5×10^{-9}
A_0, cm⁻³	21×10^{14}	8.0×10^{14}	7.8×10^{14}	13.7×10^{14}

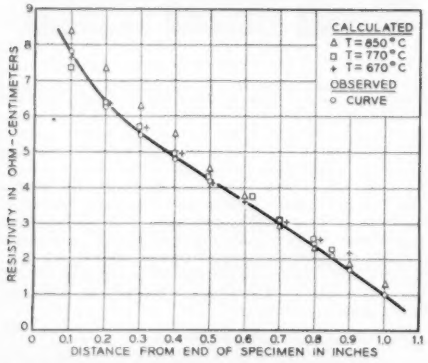

FIG. 1. Agreement between the calculated and observed values of resistivity.

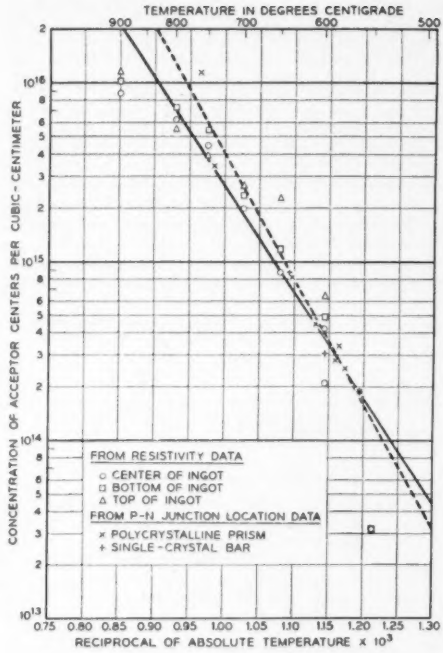
TEMPERATURE IN DEGREES CENTIGRADE
CONCENTRATION OF ACCEPTOR CENTERS PER CUBIC-CENTIMETER
FROM RESISTIVITY DATA
○ CENTER OF INGOT
□ BOTTOM OF INGOT
△ TOP OF INGOT
FROM P-N JUNCTION LOCATION DATA
× POLYCRYSTALLINE PRISM
+ SINGLE-CRYSTAL BAR
RECIPROCAL OF ABSOLUTE TEMPERATURE × 10³

FIG. 2. Variation of acceptor concentration with temperature.

mined on temperature of heat treatment; all the data are in substantial agreement. These equilibrium concentrations are, however, some 10 times larger than the values found for A_0. The solid line gives an activation energy of 27,000 cal or 1.2 ev and an extrapolated concentration for infinite temperature of 2.4×10^{21} cm^{-3}. The dashed line gives 32,000 cal or 1.4 ev and 4.55×10^{22} cm^{-3}, the concentration of germanium atoms which, Shockley has pointed out, the extrapolated concentration should approximately equal, whatever be the nature of the acceptors. This line fits the data fairly well, particularly in view of a comparatively slow quench of the ingot bar.

[1] H. C. Torrey and C. A. Whitmer, *Crystal Rectifiers* (McGraw-Hill Book Company, Inc., New York, 1948), pp. 365ff.; J. H. Scaff and H. C. Theuerer, Trans. Am. Inst. Mining. Met. Engrs. **189**, 59, J. Metals, TP2996E (1951).
[2] It is an unnecessary refinement, since the actual resistivity is in general appreciably less than the intrinsic resistivity, to deal with the exact expressions for the carrier concentrations in terms of these two resistivities.
[3] The electron and the hole mobilities are taken as 3600 and 1700 cm^2 volt^{-1} sec^{-1}; J. R. Haynes and W. Shockley, Phys. Rev. **81**, 835 (1951).
[4] The 5.0-ohm-cm sample was 1.8 cm in diameter, 0.4 cm thick, and polycrystalline, while the 18.5-ohm-cm one was a single-crystal bar 0.5 $\times$1.0 $\times$2.0 cm.
[5] This sample was a polycrystalline prism about 3 cm long cut from an ingot.
[6] W. Jost, *Diffusion und chemische Reaktion in festen Stoffen* (T. Steinkopff, Leipzig, 1937).
[7] One sample was the polycrystalline prism used in the junction measurements, the other, a single-crystal bar.
[8] This polycrystalline bar was about 3 mm in cross section and 2 cm long.

The Lateral Spread of Cosmic-Ray Showers in Air and Lead

H. S. Green and H. Messel
University of Adelaide, Adelaide, South Australia
(Received November 26, 1951)

PREVIOUS theoretical work[1-3] on the lateral spread of extensive air showers has been devoted almost exclusively to the electron-photon component. This has been partly the result of an early misconception of the nature of the primary component, but mainly to ignorance of the differential cross sections for nuclear collisions at ultrarelativistic energies. We recently tried to remedy this situation by deriving semiempirical cross sections suggested by analysis of data on the energy spectrum of nucleons in cosmic radiation. We found in this way[4] that the mean square angle of scatter of particles with energy U resulting from a nucleon-nucleon collision at ultrarelativistic energies should be $(U+U')/UU'$, where U' is the energy of the primary measured in proton-mass units. By tracing the development of a nucleon cascade within the nucleus, we have also obtained[5] the mean square angle of scatter in a nucleon-nucleus collision.

We have now applied these results to investigate the lateral development of the nucleon cascade in air. If $f(\mathbf{p},\mathbf{r})dp_1dp_2dp_3dr_1dr_2$ is the differential probability of finding a particle with momentum $\mathbf{p}$ at depth r_3 in the atmosphere and at a displacement (r_1, r_2) from the shower axis, one has

$$\frac{1}{k\delta(r_3)}\frac{\mathbf{p}}{p}\cdot\frac{\partial f(\mathbf{p})}{\partial \mathbf{r}}+f(\mathbf{p})=\int f(\mathbf{p}')n(\mathbf{p}',\mathbf{p})d\mathbf{p}', \qquad (1)$$

where $n(\mathbf{p}',\mathbf{p})d\mathbf{p}$ is the differential probability of finding a particle with momentum $\mathbf{p}(d\mathbf{p})$ as a result of the collision of a nucleon of momentum $\mathbf{p}'$ with an air nucleus; $\delta(r_3)$ is the density of air, which in this application we have supposed to vary vertically as in an isothermal atmosphere; and $k=(1/75)$ cm^2/g.

We have solved Eq. (1) as far as required to compute the mean square lateral displacement $\langle r^2\rangle$, as a function of depth

$$\langle r^2\rangle=\frac{\int\int\int\int\int(r_1^2+r_2^2)fdp_1dp_2dp_3dr_1dr_2}{\int\int\int\int\int fdp_1dp_2dp_3dr_1dr_2} \qquad (2)$$

for nucleons with energy exceeding any given value U. The only approximation which we found necessary was to neglect the mean fourth power of the angular deviation of the particles from the shower axis. The validity of this approximation we confirmed by calculating the mean square angular deviation. For particles with energies greater than U (which is assumed to exceed the geomagnetic cutoff) and assuming an integral power law with exponent 1.1 for the primary spectrum, the mean square angle is

$$\langle\chi^2\rangle=1.34U^{-1}(1-e^{-0.2\theta})(\text{radians})^2 \qquad (3)$$

where θ is the depth measured in cascade units of 75 g/cm^2. This is obviously small for the ultrarelativistic energies which we consider.

The mean square distance from the shower axis was found to be

$$\langle r^2\rangle=162U^{-1}e^{-0.2\theta}\left\{\frac{0.2\theta}{1^2\cdot1!}+\frac{(0.2\theta)^2}{2^2\cdot2!}+\cdots\right\}\text{km}^2. \qquad (4)$$

This result is exhibited in Fig. 1. It will be noticed that the lateral spread of particles with energy above a given value is very rapid at great heights; this is because of the long mean free path, which allows particles to travel freely in a lateral direction. At 6500 meters the lateral spread attains its maximum value, and below this level there is a gradual decrease, owing to the increasing degradation of the energies of the nucleons concerned. The mean radius of the shower is inversely proportional to the square root of the minimum energy of the particles observed, and proportional to the mean absolute temperature, assumed to be 273°K in (4). The shape of the curve depends rather sensitively on the power law of the primary spectrum at the very high energies which are almost exclusively responsible for the result.

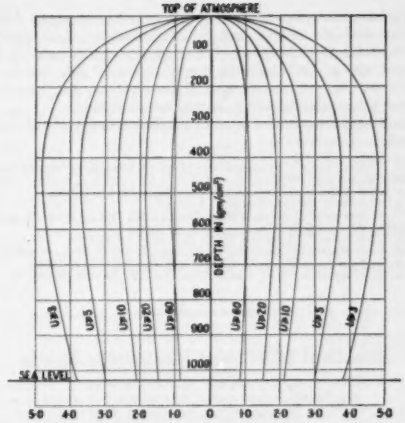

FIG. 1. A plot of the root-mean-square lateral spread of nucleons with energies greater than U, against atmospheric depth measured in g/cm^2. The middle line corresponds to the axis of the shower. The horizontal scale is in kilometers, and U is measured in proton mass units. The curves are for an incident integral primary power law spectrum with exponent 1.1.

The root-mean-square distance at sea level of a particle with energy greater than 10 Bev from the axis of the shower is 2.1 km; this value is in qualitative agreement with recent experimental indications[6-8] and supports the evidence for an integral power law of 0.1.

It is now widely accepted that the electron-photon component arises from the decay of neutral mesons produced in nuclear collisions; it is therefore heavily dependent on the lateral spread of the nucleon component for its own lateral development. High energy electrons and gamma-rays produced early in the cascade may be expected to multiply and form a density populated core to the shower. However, any account of the development of the soft component outside this core, which left out of account the nucleon component, would be meaningless.

We have made similar calculations for the lateral spread of high energy nucleons in lead and find, for example, that under a block of 56-cm thickness the root-mean-square distance from the shower axis of particles with energy above 10 Bev is 6.4 cm. Owing to the constant density of the medium, the maximum spread is not attained within several meters of lead.

It is hoped to present a more detailed account of this work shortly.

[1] G. Molière, *Cosmic Radiation*, edited by W. Heisenberg (Dover Publications, New York, 1946).
[2] J. Roberg and L. W. Nordheim, Phys. Rev. **75**, 444 (1949).
[3] A. Borsellino, Nuovo cimento **7**, 4 (1950).
[4] H. S. Green and H. Messel, Phys. Rev. **83**, 842 (1951); Proc. Phys. Soc. (London) (to be published).
[5] H. Messel and H. S. Green, Phys. Rev. **83**, 1279 (1951).
[6] D. V. Skobeltsyn *et al.*, Dokl. Akad. Nauk. S.S.S.R. **73**, 1157 (1950).
[7] G. T. Zatsepin *et al.*, Dokl. Akad. Nauk. S.S.S.R. **74**, 29 (1950).
[8] L. K. Eidus *et al.*, Dokl. Akad. Nauk. S.S.S.R. **75**, 669 (1950).

The Drift Mobility of Electrons in Silicon

J. R. Haynes and W. C. Westphal
Bell Telephone Laboratories, Murray Hill, New Jersey
(Received December 26, 1951)

THE mobility of electrons injected into p-type silicon has been determined by measuring transit times between the emitter and collector points with single crystal rods.

The techniques used to measure the drift mobility of injected carriers in germanium[1] were altered in these measurements not only because the shape of the advancing wave front of injected carriers in silicon is affected by a temporary trapping but also because of the much higher impedance of voltage probe points.

A schematic diagram of the circuit used successfully with silicon is shown in Fig. 1. Electrons are injected at the time of the current pulse and flow down the crystal under the influence of the electric field. When the pulse of electrons arrives at the collector point, a signal is produced.[2] A sketch of the oscilloscope pattern obtained is shown in Fig. 2. The dots represent 10-μsec marker intervals. The current pulse used to inject the electrons produces a corresponding voltage pulse at the start of the oscilloscope trace as a result of the resistance of the silicon rod between the collector point and ground. After this initial pulse the voltage remains constant for some 40 microseconds. During this time the injected electrons are moving down the silicon crystal from the emitter point which was placed a centimeter away from the collector. When the electron pulse arrives at the collector, the voltage pulse shown is observed. The transit time, t, for the injected electrons is the time represented by the distance from the center of the voltage pulse to the maximum signal produced by the arrival of the electron pulse.

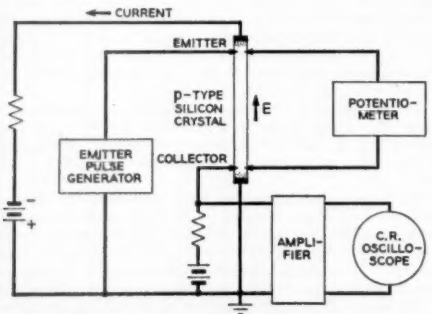

FIG. 1. Schematic of circuit used to measure the drift mobility of injected electrons in silicon.

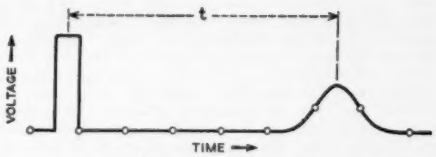

FIG. 2. Drawing of oscilloscope trace showing time of injection pulse and subsequent electron arrival.

It is found that the transit time measured in this way is a function of the amplitude of the current pulse as a result of conductivity modulation of the silicon rod. As the amplitude of the current pulse is continuously decreased, the signal arrival time becomes earlier, at first rapidly and then more slowly. The transit time corrected for conductivity modulation could therefore easily be obtained visually by extrapolating the locus of arrival time points to zero signal.

The drift mobility μ_D of electrons in silicon was calculated from the relation $\mu_D = L^2/Vt$, where t is the transit time, L is the distance from emitter to collector, and V is the voltage difference in silicon between emitter and collector.

Representative values of L and V used are shown in Table I together with the resultant measured transit time. The corresponding value of μ_D has been corrected for nonuniformity of electric field and temperature rise produced by the dc current.[1] The average value of mobility obtained for all data is 1210 cm^2/volt sec.

TABLE I. Representative values of electron drift mobility data.

Sample No.	L(cm)	V(volts)	t(μ sec)	μ_D(cm^2/volt sec)
I	0.537	5.70	43.9	1204
I	1.10	12.3	84.0	1248
I	1.12	29.5	41.8	1194
II	0.64	5.56	63.3	1190
II	0.64	11.8	32.6	1162
II	0.64	4.49	73.8	1283

This value is more than four times as large as the mobility of electrons in silicon reported by Pearson and Bardeen[3] (300 cm^2/volt sec for electrons, 100 cm^2/volt sec for holes). Their values, however, were obtained from Hall effect data in multicrystalline samples, and their extremely low values were most probably caused by inhomogeneities produced by crystal grain boundaries.

In view of the experience with germanium, it is felt that even though only two samples have been examined, the drift mobility of electrons in silicon is within 10 percent of 1200 cm^2/volt sec. Preliminary measurements with injected holes in n-type silicon indicate a drift mobility for holes in the neighborhood of 250 cm^2/volt sec giving a ratio of electron to hole mobility of 4.8.

The authors are indebted to W. Shockley for advice and to G. K. Teal and E. Buehler who provided the silicon ingot.

[1] J. R. Haynes and W. Shockley, Phys. Rev. **81**, 835 (1951).
[2] See reference 1 for a more complete description of the main features of the circuit.
[3] G. L. Pearson and J. Bardeen, Phys. Rev. **75**, 865 (1949).

Photomeson Production in Carbon and Hydrogen*

B. T. Feld, D. H. Frisch, I. L. Lebow, L. S. Osborne, and J. S. Clark
Physics Department and Laboratory for Nuclear Science and Engineering, Massachusetts Institute of Technology, Cambridge 39, Massachusetts
(Received January 4, 1952)

CYLINDRICAL targets of paraffin, heavy paraffin, and graphite were exposed simultaneously to the x-ray spectrum produced by 330-Mev electrons in the M.I.T. synchrotron. The

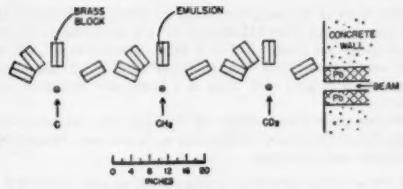

FIG. 1. Schematic diagram of the experiment for the observation of the spectra of photomesons from hydrogen, deuterium, and carbon.

energy distributions of photomesons from carbon and hydrogen have been obtained at angles of 90° and 26° to the photon beam. The mesons were slowed down in 2½-in. wide×4-in. high×5-in. long brass blocks, and the ends of their tracks were observed in 200-μ unbacked Ilford C-3 photographic emulsions embedded radially in blocks, as shown in Fig. 1. The location of each meson track ending was recorded as a function of its depth in the block.

Positive π-mesons are identified by their μ-decay. Negative π-mesons are identified as those which produce nuclear disintegrations (stars), plus a predetermined fraction of those mesons ending without any visible disintegration products.[1] The distribution of mesons in energy is obtained by dividing the emulsions into intervals of equal meson energy, assuming the meson energy to be given by the range in brass corresponding to the distance from the face of the block to the meson ending. (A slight correction of ~10 Mev is applied for the thickness of the target.) The hydrogen distributions were obtained by subtracting the carbon distributions from those of the paraffin.

The number of positive mesons per proton in carbon as compared to hydrogen, averaged over the above energy ranges, is 0.32±0.05 (standard deviation) at 90° and 0.07±0.01 at 26°. This large decrease in production efficiency for carbon at forward angles is qualitatively as expected on the basis of the Pauli exclusion principle, since the recoil momentum of the product neutron is small when the meson is emitted forward. Due to the smallness of the carbon production at small angles, the subtraction procedure, to obtain the H cross section, introduces only small uncertainties at 26°.

The negative-positive ratio from carbon shows no strong dependence on meson energy and has the average value of 1.43±0.13 at 90° and 1.03±0.25 at 26°. Peterson, Gilbert, and White[2] found a value of 1.30±0.12 at 90°. The energy spectra at 90° are in good agreement with previous experiments[3,4] and with theory.[5]

From energy and momentum conservation and assuming a photon spectrum,[6] the hydrogen distributions are converted into cross sections in the center-of-mass system. In Fig. 2, we plot the experimental cross sections *vs* photon energy for hydrogen together with the predictions of pseudoscalar theory,[7] the Berkeley data[8] at 107°, and our data at 107°. Averaging our cross sections over the approximate range $h\nu=210$ to $h\nu=305$ Mev, we find $\bar{\sigma}(34°)/\bar{\sigma}(107°)=0.80\pm0.18$. This result is not strictly comparable with the observed[8] $h\nu=250$ Mev angular distribution, but together they indicate that the average cross section over this energy range does not drop off extremely rapidly at small angles.[9]

We wish to thank Mmes. T. Kallmes, D. Calhoun, and M. Goode who performed most of the arduous work of scanning the plates.

* This work was supported in part by the joint program of the ONR and AEC.

[1] Our determination of the fraction of negative π-mesons which give rise to zero-pronged (neutron) stars is 35±4 percent in a total of 585 stars, which agrees well with the 32.6±2.1 percent found by W. B. Cheston and L. J. B. Goldfarb, Phys. Rev. **78**, 683 (1950).

[2] Bernardini, Booth, and Lederman, Phys. Rev. **83**, 1075 (1951).
[3] Peterson, Gilbert, and White, Phys. Rev. **81**, 1003 (1951).
[4] J. Steinberger and A. S. Bishop, Phys. Rev. **78**, 494 (1950).
[5] M. Lax and H. Feshbach, Phys. Rev. **81**, 189 (1951).
[6] Powell, Hartsough, and Hill, Phys. Rev. **81**, 213 (1951).
[7] H. Feshbach and M. Lax, Phys. Rev. **76**, 134 (1949).
[8] Bishop, Steinberger, and Cook, Phys. Rev. **80**, 291 (1950); J. Steinberger and A. S. Bishop, private communication. Their value for the ratio of cross sections at 58° to 107° (45° and 90° in the laboratory system) for 250-Mev photons is 0.70 (assuming the correction for nuclear absorption suggested by reference 2).
[9] K. A. Brueckner, Phys. Rev. **79**, 641 (1950).

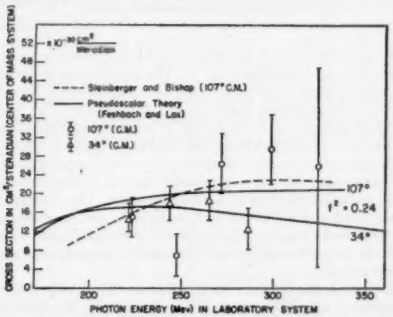

FIG. 2. Comparison of experiment with theory for the differential cross section for photomeson production in hydrogen *vs* photon energy, for mesons emitted at 34° and 107° in the C.M. system. The experimental points have been corrected for nuclear interactions in the brass moderator. The broken curve summarizes the results of Steinberger and Bishop (see reference 8) at 107°. Our cross sections agree within the factor of two in uncertainty about our absolute intensity at the time of exposure. The points as plotted here are normalized to the experimental curve of Steinberger and Bishop. The solid curves are computed from the theory of Feshbach and Lax (see reference 7), for a (pseudoscalar meson with pseudovector-) coupling constant $f^2=0.24$.

Photomeson Production from Deuterium*

I. L. LEBOW, B. T. FIELD, D. H. FRISCH, AND L. S. OSBORNE
Physics Department and Laboratory for Nuclear Science and Engineering, Massachusetts Institute of Technology, Cambridge 39, Massachusetts

(Received January 4, 1952)

WE have measured the energy distributions of the positive and negative π-mesons from deuterium at 90° and 26° to the photon beam. A heavy paraffin target was exposed to the 330-Mev bremsstrahlung spectrum from the M.I.T. synchrotron simultaneously with the exposures of carbon and parafin targets described in the preceding communication. The methods of detection and analysis of data are also as previously described. The observations are displayed in Figs. 1(a) and 1(b).

Special interest is attached to the investigation of photomeson production from deuterium, mainly for two reasons: (1) The deuteron is the simplest nucleus that can be used to study the production of mesons from neutrons since the ratio of negative to positive production gives a comparison of production from neutrons and protons. We find experimentally that the average π^-/π^+ yield ratio from the deuteron is 0.5±0.5 at 90° and 0.90±0.23 at 26°. Our present statistics and uncertain knowledge of the absorption in brass do not permit us to conclude that the apparent decrease of the negative to positive ratio with increasing meson energy and angle is real. White[1] has found a ratio of 0.96±0.10 over the spectrum at 45° and a value of 0.98±0.14 for the ratio at 90° for 70-Mev mesons. Littauer and Walker[2] obtained a ratio of 1.19±0.12 for 50-Mev mesons at 135°.

(2) The photoproduction of a charged meson from a deuteron results in a pair of identical nucleons, whose possible quantum states are limited by the Pauli exclusion principle. Since the initial deuteron state is predominantly $^3S_1$, the possibility of leaving the final two-nucleon system in an S-state depends on the occurrence of "spin-flip" in the charged photomeson production reaction. Thus, there should be a greater reduction of π^+ production in deuterium, relative to hydrogen, for a spin-independent interaction than for a spin-dependent interaction. This is a marked effect

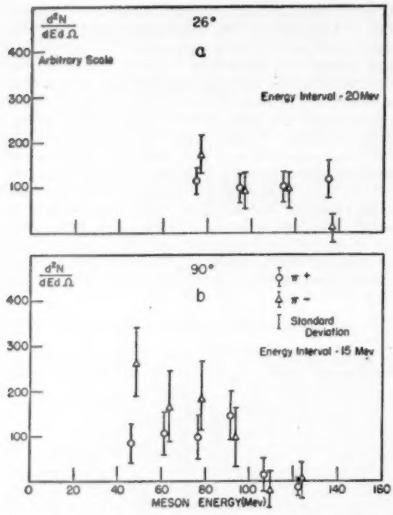

FIG. 1. Negative and positive photomeson yields (per unit solid angle and unit meson energy) from deuterium at 26° (a) and at 90° (b) in the laboratory system.

only at small meson angles, where the two product nucleons come off with a low relative speed.

Chew and Lewis[3] and Feshbach and Lax[4] have developed a phenomenological theory of meson production from deuterons. The solid curves sketched in Fig. 2 give the predicted ratio of yield of positive mesons from deuterons, relative to that from free protons, as a function of angle. The yields are averaged over a broad meson energy interval suitable for comparison with the experimental data at each angle. The different curves are for various values of the parameter K^3/L^3 formed from the Hamiltonian $H=\sigma\cdot\mathbf{K}+L$. For $K^3/L^3=0$ there is no spin-dependent interaction. For $K^3/L^3=\infty$ there is only spin-dependent interaction. In evaluating these curves it has been assumed that there is no interaction between the product neutrons.

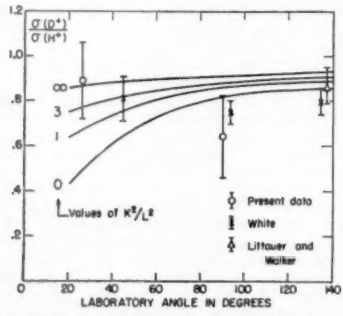

FIG. 2. Ratio of photoproduction of positive π-mesons from deuterium and hydrogen *vs* laboratory angle of meson emission. The solid curves are from the phenomenological theory of Feshbach and Lax (see reference 4), assuming various ratios K^3/L^3 of spin-dependent and spin-independent meson interactions. The experimental points represent our data, the data of White (see reference 1) and of Littauer and Walker (see reference 2).

Our ratios of the total number of π^+ mesons from D and H in the energy range 65 to 145 Mev at 26° and in the 40- to 105-Mev range at 90° are plotted in Fig. 2. White's[1] ratios at 45°, 90°, and 135° and Littauer and Walker's ratios[2] at 145° are also plotted. These data suggest that there is a large spin-dependent interaction.

We are grateful to Professor H. Feshbach for making available unpublished theoretical calculations on photomeson production in hydrogen and deuterium.

* This work was supported in part by the joint program of the ONR and AEC.

[1] R. S. White, University of California Radiation Laboratory Report No. 1319 (1951).
[2] R. M. Littauer and D. Walker, Phys. Rev. **82**, 746 (1951).
[3] G. F. Chew and H. W. Lewis, Phys. Rev. **84**, 779 (1951).
[4] H. Feshbach and M. Lax (to be published).

Hyperfine Structure in the Paramagnetic Resonance of the Ion $(SO_3)_2NO^{--}$*

G. E. PAKE, J. TOWNSEND, AND S. I. WEISSMAN
Washington University, St. Louis, Missouri
(Received December 31, 1951)

WE have investigated the paramagnetic resonance absorption of the free radical ion $(SO_3)_2NO^{--}$ (peroxylamine disulfonate ion). In dilute solution, the absorption was first observed at a frequency of about 9000 Mc/sec in fields near

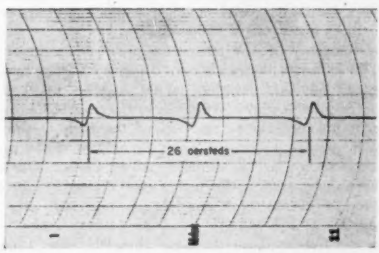

FIG. 1. Paramagnetic resonance derivatives for peroxylamine disulfonate ion at a frequency near 9000 Mc/sec.

3200 oersteds and was found to consist of three evenly spaced peaks of equal intensities (Fig. 1). The g-value corresponding to the central peak is 2.0054 ± 0.0004, based upon comparison with that of polycrystalline diphenyl picryl hydrazyl.[1] The interval between adjacent peaks is about 13 oersteds, corresponding to 36 Mc/sec. The breadth of the individual peaks is dependent upon concentration, increasing with increasing concentration.

The simple microwave apparatus used is a klystron-excited wave guide terminating in a crystal rectifier. The crystal signal is amplified and fed into a lock-in detector and recording milliammeter which registers the amplitude of the component coherent with the 60-cycle modulation of the external magnetic field applied to the sample.

Typical is the behavior of solutions in chloroform of the salt tetraphenyl stibonium peroxylamine disulfonate. A solution $0.5M$ in the odd ion, although exhibiting the color of this ion, apparently possesses an absorption too broad for measurement in our apparatus. At $0.25M$, the three peaks appear, each about 4 oersteds wide. At $0.02M$, the width between points of extreme slope for each peak is about 0.8 oersted. Several salts, in a variety of solvents, including dioxane, pyridine, alcohol, ether, dimethyl formamide, and water, have yielded apparently identical spectra at low concentrations.

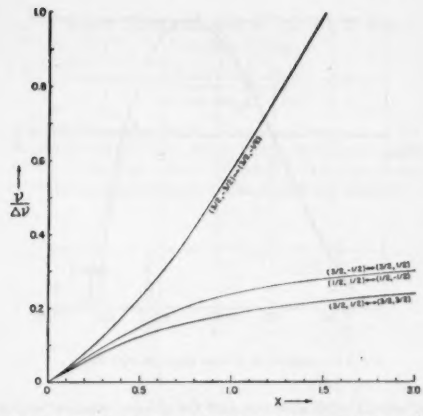

FIG. 2. Frequencies for those π-transitions of reference 4 which approach zero frequency with decreasing values of the magnetic field parameter $x=(g_J-g_I)\mu_0 H/h\Delta\nu$.

It is likely that the structure is hyperfine, arising from an interaction between the magnetic moments of the odd electron and the N^{14} nucleus. Nitrogen is the only atom of the ion with an abundant isotope which possesses a magnetic nucleus, and the three components correspond to its spin of one.

Since the g-value of the central peak is close to that of a free electron spin (no orbital contribution to the splitting), we have attempted to apply the Breit-Rabi formulas[2] for the Zeeman effect of a system consisting of an s electron and a nucleus of spin 1 to this admittedly more complicated system. These formulas are consistent with the observed line separation in fields near 3200 oersteds if the zero field hyperfine splitting $\Delta\nu$ is 54 ± 1 Mc/sec. The assumption of Paschen-Back effect in these fields is supported by the work of Holmes,[3] who studied the isotope shifts for the low lying states of N^{14} and N^{15}; no hyperfine splittings were found, and an upper limit of 900 Mc/sec was set for them.

The paramagnetic resonance absorption of this ion in magnetic fields near 10 oersteds affords a simple test for the proposed model. The Breit-Rabi energy level scheme[4] predicts transitions in such low fields at ratios of frequency to field which differ markedly from that for a free electron spin because of the coupling between J and I. Figure 2 plots frequency *versus* the parameter[5] $x=(g_J-g_I)\mu_0 H/h\Delta\nu$ for those π-transitions which should be observable with a recording rf spectrometer such as that designed and constructed in this laboratory by Schuster.[5] The two lowest frequency lines of Fig. 2 are observable by a magnetic field modulation technique only in the low field region where the slope of the ν *versus* x curve differs appreciably from zero. In addition to those transitions graphed in Fig. 2, there are of course π-transitions which approach $\Delta\nu$ itself with decreasing field; if $\Delta\nu$ is 54 Mc/sec, these frequencies are inaccessibly high for our spectrometer in its present form.

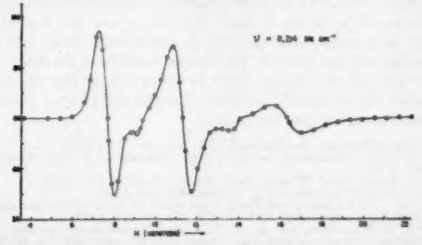

FIG. 3. Absorption derivatives for the paramagnetic resonance of peroxylamine disulfonate ion at 9.214 Mc/sec. The ordinates are in arbitrary units.

With the spectrometer operating at a fixed frequency of 9.214 Mc/sec, we have observed the three transitions of Fig. 2 at resonant fields of 7.73 ± 0.10, 11.32 ± 0.10, and 16.34 ± 0.10 oersteds (Fig. 3). The Helmholtz coils were calibrated by means of an organic free radical whose g-value had been compared in low fields with that of the proton.[6] The three resonant field values of Fig. 3 yield from the Breit-Rabi formulas $\Delta\nu$-values of 58 ± 4, 54 ± 2, and 55.7 ± 1.0 Mc/sec, respectively. The relatively large errors are attributable to denominators, in the expressions for $\Delta\nu$, which involve subtraction of comparable terms. However, the values listed above are in sufficiently good agreement with the microwave measurement to lend support to the proposed model.

Experiments to improve the accuracy of the $\Delta\nu$-measurement by studying transitions which approach $\Delta\nu$ in zero field are now in progress.

Part of the equipment used was provided through a grant-in-aid from the Research Corporation.

* Assisted by the joint program of the ONR and AEC.

[1] C. A. Hutchison and R. C. Pastor, Phys. Rev. **81**, 282 (1951).
[2] G. Breit and I. I. Rabi, Phys. Rev. **38**, 2082 (1931). The formulas for transition frequencies of the system $J=\frac{1}{2}$, $I=1$ are conveniently tabulated by J. E. Nafe and E. B. Nelson, Phys. Rev. **73**, 718 (1948).
[3] J. R. Holmes, Phys. Rev. **63**, 41 (1943).
[4] J. E. Nafe and E. B. Nelson, Phys. Rev. **73**, 718 (1948), Fig. 1 (b).
[5] N. A. Schuster, thesis, Washington University (1951).

Hyperfine Structure in the Spectrum of Erbium

KIYOSHI MURAKAWA AND SHIGEKI SUWA
Institute of Science and Technology, Komaba-machi, Meguro-ku, Tokyo, Japan
(Received December 26, 1951)

SOME time ago Ross and one of the authors[1] published a diagram in which the isotope shift per one $6s$ electron in the neutral atom, per addition of two neutrons, was plotted for many heavy elements *versus* the neutron number. In order to complete the diagram in which erbium data were lacking, the hyperfine structure of the erbium spectrum was studied and the work of Wilets and Bradley[2] was extended.

A water-cooled hollow-cathode discharge tube containing some erbium oxalate was used as the light source, and a Fabry-Perot etalon was used in order to examine the hyperfine structure.

More than twenty lines were found to possess a measurable isotope shift. Since natural erbium[3] is known to have the abundance Er^{170} 14.2, Er^{168} 26.9, Er^{167} 24.4, Er^{166} 32.9, Er^{164} 1.5, and Er^{162} 0.1 percent, the correlation of the components to respective isotopes could be done easily. However, the Er^{162}-component was not observed owing to its small abundance. The isotope Er^{167} which is known[4] to have a spin of 7/2, was found in many lines to have components distributed between the Er^{168}- and the Er^{166}-components. Table I lists the isotope shift in some typical lines of

TABLE I. Isotope shift in the erbium spectrum.

Line (A)	170−168 (cm^{-1})	168−166 (cm^{-1})	166−164 (cm^{-1})	(170−168) : (168−166) : (166−164)
5172.8[a]	0.0381	0.0341	···	1 : 0.90 : ···
4944.4[a]	0.0482	0.0447	0.043	1 : 0.93 : 0.89
4722.7[b]	0.0527	0.0480	0.046	1 : 0.91 : 0.87
4606.6[b]	0.0482	0.0445	0.042	1 : 0.92 : 0.87
4086.7[b]	0.040	0.037	0.035	1 : 0.92 : 0.88

[a] The Er^{170}-component lies on the lowest frequency side.
[b] The Er^{170}-component lies on the highest frequency side.

erbium. The weighted mean of the last column gives (170−168):(168−166):(166−164) = 1:0.92±0.05:0.88±0.07, where the disturbance of the Er^{167}-components is roughly taken into account in considering the limits of error.

Classification of the erbium lines into arc and spark lines was also tried, and it was found that λ5173 belongs to the Er I spectrum. It seems probable that the isotope shift in λ5173 represents approximately the contribution of one 6s electron to the isotope shift in the neutral erbium atom, because it fits reasonably well in the diagram referred to at the beginning of this letter.

The present work was started in the Department of Physics of the University of Wisconsin by Mr. J. S. Ross and one of us (K.M.), and resumed in Tokyo by us. One of us (K.M.) would like to express his appreciation for the kind cooperation of Mr. Ross in the work.

[1] K. Murakawa and J. S. Ross, Phys. Rev. **83**, 1272 (1951).
[2] L. Wilets and L. C. Bradley, Phys. Rev. **84**, 1055 (1951). We thank Mr. Wilets for showing us their manuscript before publication.
[3] For example, H. A. Bethe, *Elementary Nuclear Theory* (J. Wiley and Sons, Inc., New York, 1947).
[4] B. Bleaney and H. E. D. Scovil, Proc. Phys. Soc. (London) **64**, 204 (1951).

Is There a Neutral μ-Meson?

G. E. Uhlenbeck and C. S. Wang Chang
H. M. Randall Laboratory of Physics, University of Michigan, Ann Arbor, Michigan
(Received January 7, 1952)

THE recent experiments of Sagane, Gardner, and Hubbard[1] on the continuous beta-spectrum in the μ^- decay seem to indicate that the spectrum goes to zero at the upper limit. The same authors put the value of the upper limit at 53±2 Mev, which is in agreement with the accepted view that the μ^- meson decays into an electron and two neutrinos. However, it seems to us that such a conclusion is perhaps premature, and that one should consider again the possibility of a neutral μ-meson of finite mass.

The reason is the following. If the μ^- decay is similar to the ordinary beta-decay as is suggested by the value of the lifetime of the μ-meson, then one would expect that the shape of the spectrum would not differ in a qualitative way from the so-called statistical factor which arises from the available phase space. Now, it is well known[2] that for the decay into electron and two neutrinos the statistical factor gives a finite value at the upper limit, which is $\frac{1}{2}\mu c^2$. This is because of the fact that at the upper limit the electron and the neutrinos go off in opposite directions, and since the momentum of the electron can be balanced by the momenta of the two neutrinos in an infinite number of ways, there is still phase space available at the upper limit. The simplest way to obtain a zero value at the upper limit is, therefore, to assume that the μ^- meson decays into a neutral meson of finite mass μ_0 and an electron and a neutrino. The statistical factor then goes to zero, since the μ_0 momentum will then balance the electron momentum at the upper limit. The value of the upper limit will be reduced by $(\mu_0/2\mu)\mu_0c^2$, so that an experimental uncertainty of 2 Mev would still allow a mass μ_0 of the order of $40m$.

These simple considerations were, of course, well recognized in the theoretical discussions of the μ-decay by Tiomno and Wheeler[3] and by Michel.[4] However, since at that time only the Wilson chamber data of Leighton, Anderson, and Seriff[5] on the μ-decay spectrum were available, which were more compatible with a finite value at the upper limit, the reaction $\mu^\pm \to e^\pm + 2\nu$ seemed to be the most natural assumption to make. It is, of course, not impossible to obtain a zero value at the upper limit with the same assumption, but it requires a special form of the beta-interaction between the four spinor fields. This possibility has recently been investigated in an interesting report by MacCallum and Wightman[6] especially in connection with the question whether there is a universal beta-interaction, which would account both for the μ-decay and for all the known facts of beta-radioactivity. It may well be that this is the correct point of view and there is no doubt that the data of Sagane and co-workers can be represented in this fashion. However, we think that one should not forget the possibility of a finite mass for the μ_0 meson. The choice of the beta-interaction becomes then much more flexible and much less can be concluded from the μ-decay spectrum.

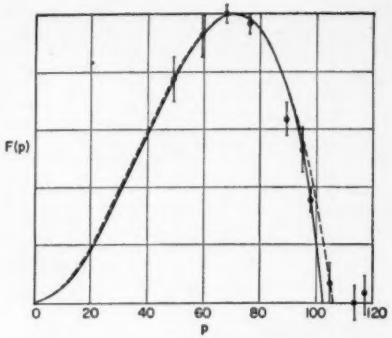

FIG. 1. Comparison of μ-decay spectrum with theory.

The situation is perhaps best summarized by Fig. 1, where the experimental data are compared with two theoretical curves. The dotted curve represents the equation[7]

$$F(p)dp \sim (\mu - 2p)p^2dp,$$

and results from the scalar interaction with so-called charge retention (which means that the spinors of μ-meson and electron, and the spinors of the two neutral particles are paired together) and with zero mass for the μ_0 meson. This is one of the few interactions which fit the data. The full curve represents the equation

$$F(p) \sim p^2\left\{5\mu(\mu-2p)\left(\mu-\frac{28}{15}p\right)+\mu_0^2(\mu-\tfrac{2}{3}p)\right\}\frac{(\mu^2-\mu_0^2-2\mu p)^2}{(\mu-2p)^3}$$

and results from the tensor interaction with the usual pairing $(\mu^-, \mu_0)(\sigma^-, \nu)$ of the spinor fields and with the mass $40m$ for the μ_0 meson. We have not investigated whether this is the best choice; there are no doubt many other possibilities.

In conclusion we may perhaps point out, that if there is a triad of μ-mesons, one would expect that they are connected with the triad of π-mesons in a similar way. This means that the reaction $\pi_0 \to \mu_0 + \nu$ should occur with the same coupling constant as the reactions $\pi^\pm \to \mu^\pm + \nu$. It could presumably, therefore, not compete with the decay of the π_0 meson into two γ-rays, but it would have as a consequence that the μ_0 meson could decay into a neutrino and two photons. The lifetime would be of the order of 10^{-9} sec, and the photons would be rather soft, so that the detection will be difficult. However, it would make the μ_0 meson much less elusive than the neutrino.

[1] Sagane, Gardner, and Hubbard, Phys. Rev. **82**, 557 (1951).
[2] E. Fermi, *Elementary Particles* (Yale University Press, New Haven, 1951), p. 44.
[3] J. Tiomno and J. Wheeler, Revs. Modern Phys. **21**, 144 (1949).
[4] L. Michel, Proc. Phys. Soc. (London) **A63**, 514 (1950).
[5] Leighton, Anderson, and Seriff, Phys. Rev. **75**, 1432 (1949); see also A. Lagarrigue and C. Peyrou, J. phys. et radium **12**, 848 (1951).
[6] C. J. MacCallum and A. S. Wightman, Technical Report No. 7, Princeton University Cosmic-Ray Group, June 15, 1951. See also E. R. Caianiello, Nuovo cimento **8**, 749 (1951).
[7] Rational units are used: $\hbar = c = \hbar = 1$; rest-mass of the electron is neglected.

Auger Enhancement of the $M\alpha$ X-Ray Satellite Lines

F. R. Hirsh, Jr.
Pasadena, California
(Received January 4, 1952)

IN 1931 the writer published visual measurements[1] on the $M\alpha$- and $M\beta$-satellite lines. Much later, in 1950, the writer plotted up[2] the sharp maxima noted on the $M\beta$-density plots[3] and discovered that there were six distinct satellites on these plates.[1] In the hope of finding similar sharp maxima for the $M\alpha$-satellites, these plates of my 1931 thesis[1] were very kindly photometered by Professor Jesse Greenstein of the California Institute of Technology at the suggestion of Dr. Robert F. Bacher. The results are shown in Fig. 1. Each $M\alpha$-envelope line is the arithmetical average of three runs made on the top, middle, and bottom of each $M\alpha$-spectral line. The fact to be noted is the complete absence of sharp satellite maxima; this is caused by Auger broadening of the satellites, while in the case of the $M\beta$-satellites the Auger effect has been shown to be impossible.[3]

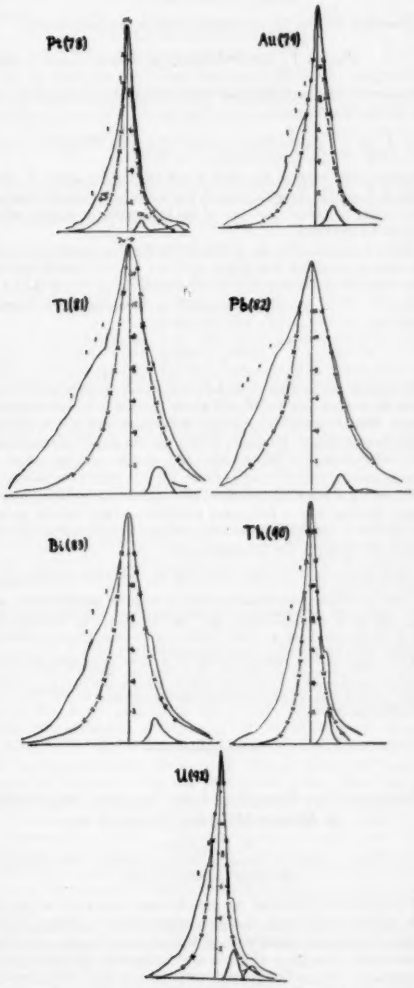

FIG. 1. Microphotometric records of plates of reference 1 fitted with "classical" $M\alpha_1$-lines, delineating satellite area S and the $M\alpha_2$-line which is subtracted off. Original ordinate and abscissa scale: one unit = $\frac{1}{2}$ inch. Vertical dashes on short wavelength side of lines (left) are visual measurements of reference 1.

TABLE I. The pertinent line data.

Plate No.	El. Z	a_2b_2/a_1b_1	$S/\pi a_1b_1$	$\sigma_\nu(\Delta\nu/K)\sigma_{\alpha_1}$	Crystal
55	Pt(78)	0.04	0.17	0.4″	calcite
53	Au(79)	0.05	0.14	0.5	calcite
35	Tl(81)	0.05	0.28	0.8	calcite
27	Pb(82)	0.03	0.12	0.9	calcite
37	Bi(83)	0.04	0.21	0.8	calcite
41	Th(90)	0.05	0.33	0.5	quartz
47	U(92)	0.06	0.21	0.55	quartz

Each $M\alpha$-line envelope was fitted with a classical $M\alpha_1$-line so that $M\alpha_2$, subtracted off, had very closely the relative intensity $\alpha_2/\alpha_1=0.05$ (see Table I). The area at the left (short wavelength) side of each $M\alpha$-line has been assigned to energy of double ionization-satellites (denoted as S in the Pt $M\alpha$-envelope). The classical line formula is $y=a/[1+(x/b)^2]$, where a is the maximum ordinate and b the half-width at half maximum. The area under the curve is πab, and hence the relative intensity of two such lines is a_1b_1/a_2b_2. The relative energy of multiple to single ionization is $S/\pi a_1b_1$. In Table I are given the pertinent line data: plate No., element, atomic No., Z, a_2b_2/a_1b_1, $S/\pi a_1b_1$. In Fig. 2 is plotted $S/\pi a_1b_1$ *vs* Z; it will be noted there are two maxima of relative energy at $Z=81$ and near $Z=90$. The Auger crossovers I found[4] at $Z=88$ and 91 for the energy of the radiationless transition $M_{\text{III}}\rightarrow M_{\text{V}}$ and the ionization energy plots for the $N_{\text{IV, V}}$ shells ($M_{\text{V}}N_{\text{IV, V}}\rightarrow N_{\text{VII}}N_{\text{IV, V}}$). Coster and Bril[5] find the upper crossover for ν/R, N_{V} with ν/R, $M_{\text{III}}\rightarrow M_{\text{V}}$ at $Z=93$ or 94. Thus quite confidently, one may assign the two intensity maxima in Fig. 2 to the crossovers of the ν/R values for $M_{\text{III}}\rightarrow M_{\text{V}}$ and the values of ν/R for the ionization energy of N_{IV} and N_{V}. (The intensity maximum should occur at 4 or 5 atomic numbers below the particular crossover.[6,7]) This is another bit of evidence in favor of the theory of Coster and Kronig.[6]

The use of microphotometer records to represent intensity may seem questionable, but it would seem to be not so naive. The function $y=a/[1+(x/b)^2]$ accurately represents the intensity plots of simple x-ray spectral lines. In this work, this function closely fits these average microphotometer curves (see Fig. 1). Moreover, the plot of Fig. 2 has exactly the same range of ordinate

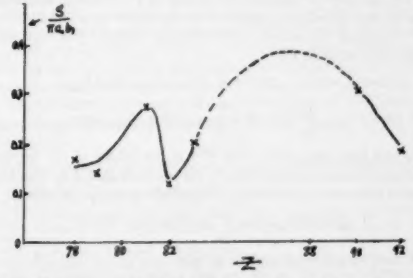

FIG. 2. Relative energy of double to single ionization plotted against atomic number, showing two maxima for the double Auger crossover.

values as shown in the plot of p. 194, reference 4, secured from density plots. These microphotometer plots are thus essentially lines in absorption.

[1] F. R. Hirsh, Jr., Phys. Rev. **38**, 914 (1931).
[2] F. R. Hirsh, Jr., Physica **XVI**, 377 (1950).
[3] F. R. Hirsh, Jr., Phys. Rev. **62**, 137 (1942).
[4] F. R. Hirsh, Jr., Phys. Rev. **50**, 191 (1936).
[5] D. Coster and A. Bril, Physica **9**, 84 (1942).
[6] D. Coster and R. DeL. Kronig, Physica **2**, 13 (1935).
[7] A similar curve for the Auger effect has been presented by J. N. Cooper, Phys. Rev. **61**, 284 (1942).

Comment on the "Impulse Approximation"

J. ASHKIN AND G. C. WICK
Carnegie Institute of Technology, Pittsburgh, Pennsylvania
(Received December 26, 1951)

THE expansion in powers of U' mentioned just above Eq. (33) of the paper "Impulse Approximation"[1] by Chew and Wick can be achieved by the following, perhaps not very rigorous, procedure.

First define a generalized Møller operator Ψ by the equation,

$$\Psi\phi_a=\psi_a. \tag{1}$$

Because of the fact that the states ϕ_a form a complete system, Eq. (1) defines Ψ completely. One can then write Eq. (12) of I.A. in the more symmetrical form,

$$T_{ba}=(\phi_b, V\Psi\phi_a) \tag{2}$$

or

$$T=V\Psi. \tag{3}$$

We now intend to expand the operator T in powers of U. Needless to say, the matrix elements T_{ba} of T cannot be so expanded, since the wave functions ϕ_a and ϕ_b contain as a factor quantized states of the bound system with the potential U. It turns out, however, that Eq. (2) separates out successfully the features in T_{ba} which prevent the expansion.

A simple expression for the operator Ψ is obtained from the remark that ψ_a is the wave function that evolves, under the action of the full Hamiltonian $H=K+U+V$, from an initial state $e^{-iH_0t_1}\phi_a$ at a remote time t_1 in the past. That is

$$\psi_a(t)=\lim_{t_1\to-\infty} e^{-iH(t-t_1)}e^{-iH_0t_1}\phi_a, \tag{4}$$

where $H_0=K+U$. It will be understood that if (4) has to be applied to a state ϕ_a of exactly defined energy, the following sequence has to be observed: first apply (4) to a wave packet state ϕ_a and take the limit to $t_1\to-\infty$, then let ϕ_a tend to the desired state. In the following the "lim" sign will often be omitted.

In Eq. (1) ψ_a was written for the space part of the wave function, i.e., $\psi_a(t)=e^{-iHt}\psi_a$. Hence ψ_a is obtained from (4) simply by setting $t=0$. Hence the operator Ψ of Eq. (1) is

$$\Psi=e^{iHt_1}e^{-iH_0t_1} \tag{5}$$

(in the limit $t_1\to-\infty$).

This can now be expanded in powers of U (although this may seem at first questionable since U is multiplied by a large t_1!) by the customary formulas of perturbation theory.[2] For instance, to the first order in U;

$$\Psi=e^{i(K+V)t_1}e^{-iKt_1}+ie^{i(K+V)t_1}\int_{t_1}^{0}e^{-iKt}Ue^{iK(t-t_1)}dt$$
$$-i\int_{t_1}^{0}e^{i(K+V)t}Ue^{-i(K+V)(t-t_1)}dte^{-iKt_1}+\cdots. \tag{6}$$

Now the first term $e^{i(K+V)t_1}e^{-iKt_1}$ is the analog of (5) for the problem without binding, that is the operator Ω of I.A. The last term is also seen to contain Ω. The middle term can be written

$$ie^{i(K+V)t_1}e^{-iKt_1}\int_{t_1}^{0}dte^{iK(t_1-t)}Ue^{\ K(t-t_1)}, \tag{7}$$

and then transformed by $t_1-t=s$ into

$$ie^{i(K+V)t_1}e^{-iKt}\int_{t_1}^{0}e^{+iKs}Ue^{-iKs}ds. \tag{8}$$

Here again one recognizes to the left, the operator which tends to Ω when $t_1\to-\infty$. Although the operator is here applied after the integral term, which also depends on t_1, it may be shown that the limit can be taken on the two factors independently.[3] Then,

$$\Psi=\Omega+i\Omega\int_{-\infty}^{0}e^{iKt}Ue^{-iKt}dt$$
$$-i\int_{-\infty}^{0}e^{i(K+V)t}Ue^{-i(K+V)t}\Omega dt+\cdots.$$

With $f(K+V)\Omega=\Omega f(K)$, this transforms easily to

$$\Psi=\Omega+i\int_{-\infty}^{0}e^{i(K+V)t}[\Omega, U]e^{-iKt}dt+\cdots. \tag{9}$$

By inserting (9) into (3) and writing $V\Omega=\mathbf{t}$, we have finally,

$$T=\mathbf{t}+i\int_{-\infty}^{0}Ve^{i(K+V)t}[\Omega, U]e^{-iKt}dt+\cdots. \tag{10}$$

The second-order term has also been evaluated and simplified. It can be written, for instance,

$$V\int_{-\infty}^{0}dt\int_{-\infty}^{0}dse^{i(K+V)s}[U, e^{i(K+V)t}[\Omega, U]e^{-iKt}]e^{-iKs}. \tag{11}$$

The first-order term in Eq. (10) is not exactly the same as that given in I.A. but the structure of the terms is extremely similar, and it does not seem that any of the estimates previously made have to be modified.

These formulas also allow one to clarify the connection with the time-symmetrical treatment, see I.A., Eq. (31) and following lines. One can of course define an operator Ψ^- such that $\Psi^-\phi_a=\psi_a^-$ and a $T^-=\Omega^{-\dagger}V$ which is equivalent to T on the $K+U$ energy shell, i.e., $T_{ba}^-=T_{ba}$ if $E_r=E_b$. One finds

$$T^-=\mathbf{t}^--i\int_0^{+\infty}dte^{iKt}[\Omega^{-\dagger}, U]e^{-i(K+V)t}V+\cdots. \tag{10'}$$

The equivalence between T and T^- can then be verified as follows. First show that $\mathbf{t}-\mathbf{t}^-=[\Omega^0, K]$ where $\Omega^0=\Omega+\Omega^{-\dagger}$. This identity shows that Ω^0, unlike Ω and Ω^-, is finite on the kinetic-energy shell (because $\mathbf{t}=\mathbf{t}^-$ thereon). Hence on the $K+U$ energy shell, $\mathbf{t}-\mathbf{t}^-=[\Omega^0, K+U]-[\Omega^0, U]=[U, \Omega^0]$, which vanishes when U goes to zero because Ω^0 remains finite. Thus in taking the difference between the expansions (10) and (10'), the zero-order terms nearly cancel leaving only a first-order residuum, which may be shown to be nearly canceled after some simple manipulations by the first-order terms in the expansions, etc.

[1] G. F. Chew and G. C. Wick, Phys. Rev. **85**, 636 (1952), quoted as I.A. in the following.
[2] The advantage of the time-dependent formulation lies just in the ease with which such expansions can be made (Schwinger, Feynman, etc.). See especially R. P. Feynman, Phys. Rev. **84**, 108 (1951). G. F. Chew and M. L. Goldberger, however, have kindly communicated to us a stationary method which gives results essentially equivalent to ours.
[3] The effect of the integral operator on a given finite wave packet is easily examined in the momentum representation, where it can be seen that the transformed wave function is again (even in the limit $t_1\to-\infty$) an essentially finite wave packet for which the identification of $e^{i(K+V)t_1}e^{-iKt_1}$ with Ω is legitimate.

Nonlinearities Resulting from Vacuum Polarization in Meson-Nucleon Interactions

B. J. MALENKA
Department of Physics, Harvard University, Cambridge, Massachusetts
(Received December 26, 1951)

INVESTIGATIONS of the pseudoscalar interaction of pseudoscalar mesons with nucleons show that in addition to the usual divergences associated with mass and charge, there is a distinct ϕ^4 divergence which is associated with the scattering of mesons by mesons.[1,2] We wish to point out that to understand the origin of this effect, it is sufficient to consider a simple vacuum polarization calculation which takes account of the creation of virtual nucleon-antinucleon pairs by a prescribed slowly varying pseudoscalar meson field.

We employ the notation and follow the proper time technique introduced in a recent paper by Schwinger.[3] The field equations for a nucleon-antinucleon Dirac field in pseudoscalar interaction with a prescribed neutral pseudoscalar meson field, in units where $\hbar=c=1$, are

$$(-i\gamma_\mu\partial_\mu+g\gamma_5\phi+M)\psi(x)=0, \quad (1)$$

$$-i\partial_\mu\bar{\psi}(x)\gamma_\mu-g\phi\bar{\psi}(x)\gamma_5-M\bar{\psi}(x)=0, \quad (2)$$

$$(-\Box^2+\mu_0{}^2)\phi=\langle j(x)\rangle+J(x), \quad (3)$$

where $J(x)$ is some real prescribed meson source and $\langle j(x)\rangle$ is the source in the vacuum of the Dirac field. We have[4]

$$\langle j(x)\rangle=ig\,\mathrm{Tr}\gamma_5 G(x,x')]_{x'\to x}, \quad (4)$$

where

$$G(x,x')=i\langle(\psi(x)\bar{\psi}(x'))_+\rangle_0(x-x') \quad (5)$$

is the Green's function for the nucleon field.

We assume that the meson field varies slowly for distances of the order of a nucleon Compton wavelength. Then, in operator notation, $[p_\mu,\phi]=0$ and we can write

$$G=1/(\gamma p-g\gamma_5\phi+M)$$
$$=[-(\gamma p-g\gamma_5\phi)+M]/(p^2+g^2\phi^2+M^2). \quad (6)$$

The procedure for determining $G(x,x')$ is quite analogous to that used in Schwinger's paper,[5] where here $M^2+g^2\phi^2$ plays the role of the mass and $A_\mu=0$. We obtain

$$G(x,x')=[i\gamma_\mu\partial_\mu+g\gamma_5\phi+M](4\pi)^{-2}\int_0^\infty ds\,s^{-2}$$
$$\times\exp[-i(M^2+g^2\phi^2)s]\exp[i\tfrac{1}{4}(x-x')^2/s]. \quad (7)$$

Then from (4), since $\mathrm{Tr}\gamma_5=\mathrm{Tr}\gamma_5\gamma_\mu=0$,

$$\langle j(x)\rangle=-ig^3\phi(2\pi)^{-2}\int_{is_0}^\infty ds s^{-2}\exp[-i(M^2+g^2\phi^2)s], \quad (8)$$

where we have replaced the zero lower limit of integration by the relativistically invariant term is_0 in order to exhibit the divergent terms explicitly. We note that $\langle j(x)\rangle$ can also be considered as the derivative with respect to ϕ of a term $\mathfrak{L}^{(1)}$ corresponding to the interaction of the meson field with the vacuum in the Lagrangian density. From (8), it then follows that

$$\mathfrak{L}^{(1)}=\tfrac{1}{2}(2\pi)^{-2}\int_{is_0}^\infty ds s^{-3}\exp[-i(M^2+g^2\phi^2)s] \quad (9)$$

to within an additive constant. It is readily seen by inspection that all terms in $\mathfrak{L}^{(1)}$ of higher than fourth order in ϕ are finite. If we expand the exponential in (9) in terms of $g\phi/M$, which is essentially of the order of the ratio of the nuclear well depth to the nucleon rest energy and therefore quite small, we get upon integrating (omitting constant terms and restoring $\hbar$ and c)

$$\mathfrak{L}^{(1)}=\frac{-\kappa^2}{8\pi^2}\frac{g^2}{\hbar c}\left[\frac{1}{\kappa^2 s_0}+\ln\frac{1}{\gamma\kappa^2 s_0}+1\right]\phi^2-\frac{1}{16\pi^2}\frac{g^4}{(\hbar c)^3}\left[\ln\frac{1}{\gamma\kappa^2 s_0}\right]\phi^4, \quad (10)$$

where $\gamma=1.780$ and κ is the inverse nucleon Compton wavelength. We have neglected terms of sixth order and higher in $g\phi/M$. The divergent ϕ^3 term can be viewed as a self energy addition to the mass term $-\frac{1}{2}\mu_0{}^2\phi^2$ in the free meson Lagrangian, but the logarithmically divergent ϕ^4 term is distinct in that it cannot be associated with any free meson term. There are no other divergent terms.

If we consider an extremely strong meson field, we would want to integrate (9) directly. This can readily be carried out and essentially adds a term $[1+(g\phi/M)^2]\ln[1+(g\phi/M)^2]$ to (10), but since the logarithmic term now varies very slowly as compared to the other terms, $\mathfrak{L}^{(1)}$ still behaves like a function linear in ϕ^2 and ϕ^4.

By taking the variational derivative with respect to ϕ of the total Lagrangian, we obtain the meson-wave equation as modified by vacuum polarization.

$$-\Box^2\phi+\mu^2\phi+g^4(\hbar c)^{-3}\lambda\phi^3=J(x), \quad (11)$$

where μ is the observed weak field inverse meson Compton wavelength and

$$\lambda=(2\pi)^{-2}\ln(1/\gamma\kappa^2 s_0). \quad (12)$$

We note that considering s_0 small seems to imply that λ is a positive constant.

A similar calculation for the charge symmetric pseudoscalar case yields similar results except for the slight modification introduced by treating ϕ and J as vectors in isotopic spin space.

Although one would also want to examine real particle interactions in some detail, the form of Eq. (11) does suggest a starting point for a phenomenological investigation involving nonlinear meson theory. Such investigations are under consideration.[6,7]

I wish to thank Professor J. Schwinger for suggesting the application of these methods to a slowly varying meson field and for his many stimulating and informative discussions.

[1] P. T. Matthews, Phil. Mag. 41, 185 (1950).
[2] A. Salam, Phys. Rev. 82, 217 (1951).
[3] J. Schwinger, Phys. Rev. 82, 664 (1951).
[4] See reference 3, Eqs. (2.11) and (2.12).
[5] See reference 3, Sec. II.
[6] L. I. Schiff, Phys. Rev. 84, 1 (1951).
[7] B. J. Malenka, thesis, Harvard University (1951).

A Search for Double Beta-Decay in Palladium*

ROLF G. WINTER
Western Reserve University, Cleveland, Ohio
(Received December 20, 1951)

WITH the emission of a 2.98 Mev[1] beta-ray, ${}_{47}Ag^{110}$ decays directly into the ground state of ${}_{48}Cd^{110}$, while no decay of ${}_{47}Ag^{110}$ into ${}_{46}Pd^{110}$ has been found.[2] Therefore, it is probable that not much less than 2.5 Mev is available as kinetic energy for the transition

$${}_{46}Pd^{110}\to{}_{48}Cd^{110}+2\ \text{beta}^-.$$

Also,

$${}_{46}Pd^{108}\to{}_{48}Cd^{108}+2\ \text{beta}^-$$

is a possible transition. However, until recently-raised questions[3,4] regarding the decay of ${}_{47}Ag^{108}$ are answered, the available energy for this process cannot be estimated.

248.5 g of natural palladium, which contains 26.7 percent of ${}_{46}Pd^{108}$ and 13.5 percent of ${}_{46}Pd^{110}$, were installed in a Wilson cloud chamber and 10,097 acceptable photographs were taken. One photograph showed the tracks of two electrons, one with kinetic energy between 0.8 and 1.1 Mev, the other with kinetic energy between 1.4 and 212 Mev, emerging from the same point in the palladium. This picture has the expected appearance of a double beta-decay; however, this event could easily have been produced by a cosmic gamma-ray. It is quite possible that one gamma-ray ejected two electrons while passing through the palladium, or that one gamma-ray emitted electron collided with another electron before leaving the foil. In fact, the expected number of such occurrences in this experiment is about 0.6.

The sensitive time of the chamber was found to be 0.14 second. Using a conservative estimate of the geometry, one obtains a lower limit of 1.1×10^{18} years for the half-life of ${}_{46}Pd^{108}$, and a lower limit of 0.6×10^{18} years for the half-life of ${}_{46}Pd^{110}$.

For 2.5 Mev available kinetic energy, the Majorana-neutrino tensor or pseudovector theory[5] gives 3×10^{18} years, the process involving the emission of two Dirac neutrinos[5] gives 2×10^{21} years, and the first-order process suggested by the author[7,8] gives 9×10^{20} years in the allowed approximation.

I should like to express my thanks to Professor E. C. Creutz for numerous helpful discussions, and to Mr. R. Leamer for his able assistance.

* This work was done at the Carnegie Institute of Technology and was supported by the AEC.
[1] K. Siegbahn, Phys. Rev. 77, 233 (1950).
[2] M. Deutsch, Phys. Rev. 72, 527 (1947).
[3] R. Naidu and R. E. Siday, Proc. Phys. Soc. (London) 48, 332 (1936).
[4] M. Goodrich and E. C. Campbell, Bull. Am. Phys. Soc. 26, No. 7, 8 (1951).
[5] W. H. Furry, Phys. Rev. 54, 56 (1938).
[6] M. Goeppert-Mayer, Phys. Rev. 48, 512 (1935).
[7] R. G. Winter (unpublished doctoral thesis, Carnegie Institute of Technology, 1951).
[8] R. G. Winter, Phys. Rev. 83, 1070 (1951).

Measurement on the *I*, *F*, and *A* Lines of Thorium by a New Method

H. CRAIG
Department of Physics, Birbeck College, University of London, London, England
(Received December 26, 1951)

A NEW method for the measurement of β-ray energies has been used with the deposit from radioactive thorium. It is an adaptation suggested by R. E. Siday of the lens type spectrometer and is capable of very high accuracy in both the absolute and comparative measurements of the specific momenta of β-ray lines.

The method consists in the recording on a photographic plate of the line image of a line source. The angular rotation of the image with respect to the object can be found by producing a second image on the plate with the lens current reversed. For the absolute determination of the specific momentum, only this angle, the lens current, and the effective number of turns need be known, and in this respect Dietrich[1] has demonstrated the possibilities of the method in a pilot experiment, in which he obtained an accuracy of 1 in 700. For comparative determinations of momentum, only the angle and the lens current are required. Further details will be published shortly.

Comparison has been made between the *I* and *F* lines of thorium-*C*. The ratio between their $(H\rho)$'s was found to be 1.26317 $\pm$0.00012, where the estimated probable error of 1 part in 10,000 is very conservative. This ratio agrees exactly with that found by Lindström[2] with a semicircular focuser. The absolute energies can be found, as pointed out by Siegbahn,[3] by making use of the difference in binding energy between the *K* and L_1 shells of element 83. Assuming this difference to be 74,128$\pm$10 electron volts,[4] the velocity of light to be 299,793.1$\pm$0.25 km per second,[5] and the ratio e/m to be 1.75890$\pm$0.00005 abs. emu per g,[6] one obtains the specific momenta of *F* and *I* lines as 1388.5$\pm$0.3 and 1753.9 $\pm$0.4 gauss cm, respectively. The $(H\rho)$ value of the *A* line, by ratio to the *F* line, has been found to be 533.66$\pm$0.12 gauss cm.

Thanks are due the Department of Scientific and Industrial Research for a grant supporting this work.

[1] C. F. Dietrich, thesis, London (1951).
[2] G. Lindström, Phys. Rev. **83**, 465 (1951).
[3] K. Siegbahn, Arkiv Mat. Astron. Fysik **28B**, No. 6 (1941).
[4] Private communication from Mlle. Y. Cauchois.
[5] E. Bergstrand, Nature **163**, 338 (1949); Arkiv Fysik **2**, 119 (1950).
[6] Thomas, Driscoll, and Hipple, Phys. Rev. **78**, 787 (1950).

Use of HD for Experiments on the Proton-Deuteron Magnetic Moment Ratio

NORMAN F. RAMSEY
Harvard University, Cambridge, Massachusetts
(Received December 26, 1951)

IN the recent high precision experiments by Lindström,[1] Smaller,[2,3] Yasaitis,[2] and Anderson[2] on the ratio of the proton magnetic moment to that of the deuteron, a dominant limitation to the final accuracy of the experiment has been the uncertainty[2] as to the difference of the magnetic shielding correction for molecules containing hydrogen and deuterium. As discussed by Smaller[2,3] and Newell,[4] the large difference in the masses of hydrogen and deuterium gives rise to a difference in the zero-point vibration amplitude and consequently to a difference in the magnetic shielding even in molecules which are identical except for the interchange of deuterium and hydrogen. Since no one has yet been able to calculate the dependence of the shielding upon internuclear spacing, it has been impossible to determine with sufficient precision the dependence of the shielding upon the zero-point vibration amplitudes.

It is the purpose of this note merely to point out that this uncertainty can be overcome in future experiments on the proton-deuteron magnetic moment ratio by observing both the proton and the deuteron resonance in the molecule HD. In this molecule the modification of the magnetic shielding by the zero-point vibration is the same for both the proton and deuteron measurements. Experiments with HD should not be appreciably more difficult than some of the past experiments. HD can be obtained in high purity.[5] Furthermore HD is as convenient to handle as either H_2 or D_2, and some of the most accurate of the past experiments[3] have been with these gaseous molecules.

[1] G. Lindström, Phys. Rev. **78**, 817 (1950).
[2] Smaller, Yasaitis, and Anderson, Phys. Rev. **81**, 896 (1951).
[3] B. Smaller, Phys. Rev. **83**, 812 (1951).
[4] G. F. Newell, Phys. Rev. **80**, 476 (1950).
[5] Fookson, Pomerantz, and Rich, Science **112**, 748 (1950).

A Determination of the Nuclear Magnetic Moment of Co^{60}, Using the Method of Nuclear Alignment

B. BLEANEY, J. M. DANIELS,* M. A. GRACE,† H. HALBAN, N. KURTI, AND F. N. H. ROBINSON*
Clarendon Laboratory, Oxford, England
(Received December 26, 1951)

WE have in an earlier publication[1] described preliminary results of an experiment to align Co^{60} nuclei. The alignment was detected and measured by observation of the anisotropic polar diagram of γ-radiation from a 70-μcurie source, which was a single crystal with the composition (1% Co, 12% Cu, 87% Zn) $SO_4 \cdot Rb_2SO_4 \cdot 6H_2O$. This was cooled by adiabatic demagnetization to approximately 0.010°K when, as explained by Bleaney,[2] the crystalline interactions cause an alignment of the cobalt nuclei relative to the crystal axes. The alignment effect found by us has recently been confirmed by Gorter, Poppema, Steenland, and Beun,[3] who now also use the Bleaney method applied to a diluted cobalt Tutton salt. No conclusive results were obtained in previous Leiden attempts[4,5] relying on the Gorter-Rose[6,7] method or on the antiferromagnetism of a concentrated cobalt Tutton salt, an experiment announced by Gorter at the Oxford Conference on Low Temperature Physics (1951),[5] and since carried out in Leiden.

In the past two months we have performed further experiments, and the statistical accuracy of the results has been increased. Also the determination of temperatures was improved; first by correcting for a spurious magnetic effect caused by the cryostat (which made the T^* values quoted in our previous publication too high), and secondly, by accounting theoretically for the deviations from Curie's law. The observed temperatures reached after demagnetization now agree with those calculated from the known splittings of the ground state of the Co^{++} and Cu^{++} ions. The shape of the polar diagram as a function of temperature is in very close agreement with that predicted by Steenberg,[8] except at the lowest temperatures where, however, the theoretical $T-T^*$ relationship used is of doubtful validity. If $F(K_1)$ and $F(K_2)$ are respectively the γ-ray intensities along the K_1 and K_2 axes of the Co^{++} ions, a parameter of anisotropy can be defined as $F(K_2)/F(K_1)$. We observed, for example, that at 0.020$\pm$0.002°K the value of this parameter is 1.25$\pm$0.02; the value observed at the lowest temperatures was 1.45.

The anisotropy of the γ-radiation depends on temperature through the Boltzmann factor $\exp(\mu H/kTI)$, where μ and I are respectively the magnetic moment and spin of Co^{60}. H is the effective magnetic field acting on the nucleus; its magnitude can be calculated from measurements of the hyperfine splitting of the paramagnetic resonance spectrum of Co^{59} in this salt,[9] and from the known magnetic moment of Co^{59}. Thus, it is possible to deduce from the experimental data a value for the magnetic moment of Co^{60}, provided that the spin is known. Assuming that $I=5$, which Deutsch and Scharff-Goldhaber[10] suggest is the probable value, we obtain for the magnetic moment of Co^{60} the value 3.0$\pm$0.5 nuclear magnetons. The sign of the magnetic moment

cannot be obtained from this experiment. We hope, however, to carry out experiments on the polarization of γ-rays emitted from polarized (as opposed to aligned) nuclei, which, among other things, should give the sign of the magnetic moment.

We wish to express our thanks to Professor F. E. Simon for his continued interest and encouragement and to Mr. K. D. Bowers for carrying out the paramagnetic resonance measurements on the stable cobalt isotope.

* Nuffield research fellow.
† I.C.I. research fellow.
[1] Daniels, Grace, and Robinson, Nature **168**, 780 (1951).
[2] B. Bleaney, Proc. Phys. Soc. (London) **A64**, 315 (1951); Phil. Mag. **42**, 441 (1951).
[3] Gorter, Poppema, Steenland, and Beun, Leiden Communications **287b** (1951).
[4] Gorter, de Klerk, Poppema, Steenland, and de Vries, Physica **15**, 679 (1949); O. J. Poppema, Helv. Phys. Acta **23**, Suppl. III, 187 (1950).
[5] C. J. Gorter, Proceedings of the International Conference on Low Temperature Physics, Oxford, 1951, p. 158.
[6] C. J. Gorter, Ceremonies Langevin-Perrin, Les Phenomenes Cryomagnetiques, Paris, 1948; Physica **14**, 504 (1948).
[7] M. E. Rose, Phys. Rev. **75**, 213 (1949).
[8] N. R. Steenberg, unpublished.
[9] K. D. Bowers, unpublished.
[10] M. Deutsch and G. Scharff-Goldhaber, Phys. Rev. **83**, 1059 (1951).

Comparison of Total Photoneutron Yield from 160- and 320-Mev Bremsstrahlung

LAWRENCE W. JONES AND KENT M. TERWILLIGER
Radiation Laboratory, Department of Physics, University of California, Berkeley, California
(Received December 28, 1951)

THAT an appreciable fraction of the photoneutrons produced by a high energy (320-Mev) bremsstrahlung might be the result of quanta of energy greater than 150 Mev was pointed out by Eyges[1] on analysis of high energy[2,3] and lower energy[4] absolute photoneutron production cross sections and of transition curves.[2,5,6] Eyges proposes that the nuclear absorption cross section for photons has a resonance maximum in the region of 15 to 20 Mev, then falls almost to zero and rises once again somewhere above 100 Mev. The results of the present experiment bear out the essential validity of this theory.

In this experiment, the total photoneutron yield measurements previously reported[3] for the 320-Mev bremsstrahlung from the Berkeley synchrotron were repeated at 160 Mev maximum energy for nine elements. Full energy (320-Mev) measurements were also made on these nine elements at the same time as a check. The experimental arrangement used was very similar to that previously described.[3] Neutrons were counted at 90° to the beam direction with a boron trifluoride proportional counter in a "long counter" geometry of paraffin. The pulses from the counter were clipped to 0.5-microseconds pulse length.

The ionization chamber beam monitor was calibrated at both energies for equivalent numbers of low energy quanta by two methods. The first was the induced 10-minute half-life β^+ activity in copper foils because of the $Cu^{63}(\gamma, n)Cu^{62}$ reaction as used by Sagane.[7] The second was the photodisintegration of deuterium as determined by direct neutron counting from water and heavy water targets. Both of these reactions are presumably sensitive only to quanta below 50 Mev. The deuterium yield was 6.5 percent higher from 160-Mev bremsstrahlung than the copper yield for equal copper and deuterium yields at 320 Mev. The average of the deuterium and copper results was used.

Table I gives the ratios of total photoneutron yields for equivalent $Cu^{63}(\gamma, n)$ and $D(\gamma, n)$ reaction yields (i.e., for the same number of quanta below 30 Mev) from 320-Mev bremsstrahlung and 160-Mev bremsstrahlung. The probable counting errors of these ratios are less than 3 percent in every case except carbon (error 4 percent). The relative yields at 320 Mev checked within statistics the previously reported values.[3] Although the beam-pulse length at half-energy was only 20 microseconds, no neutron pile-up occurred in the counter because of the long average diffusion time (about 200 microseconds) of neutrons in the paraffin of the "long counter." Neutron pile-up and counts resulting from scattered gamma-rays or electrons were checked for, both by increasing the counter voltage by 100 volts and by reducing the beam intensity by a factor of four. In both cases the counts per unit beam were the same within statistics, indicating negligible contribution from either effect.

TABLE I. Ratios of total photoneutron yields.

Element	Be	C	Al	Fe	Cu	Mo	Ta	W	Pb
Yield at 320 Mev / Yield at 160 Mev	1.21	1.18	1.48	1.23	1.28	1.30	1.28	1.33	1.30

If the calibration methods described can be assumed to normalize the beam to equal numbers of quanta between 0 and 30 Mev for full and half energy beams, the shapes of the bremsstrahlung spectra at these energies indicate that only quanta of greater than 140 Mev energy could account for the 30 percent increase in yield actually observed.

[1] L. Eyges, Bull. Am. Phys. Soc. **26**, No. 8, 5 (1951).
[2] Terwilliger, Jones, and Jarmie, Phys. Rev. **82**, 820 (1951).
[3] D. W. Kerst and G. A. Price, Phys. Rev. **79**, 725 (1950).
[4] G. A. Price and D. W. Kerst, Phys. Rev. **77**, 806 (1950).
[5] Karl Strauch, Phys. Rev. **81**, 973 (1951).
[6] L. Eyges, Phys. Rev. **81**, 981 (1951).
[7] R. Sagane, Phys. Rev. **83**, 174 (1951).

Effect of Intrinsic Moment of Electron on Spectroscopic Isotope Shift*

G. BREIT AND W. W. CLENDENIN
Yale University, New Haven, Connecticut
(Received December 26, 1951)

IT is pointed out below that the intrinsic moment of the electron[1-3] has a non-negligible effect on the spectroscopic isotope shift. In a central electric field, according to the third paper listed in reference 1 the first order effect of the magnetic moment μ_s on the energy of an s electron is

$$\langle H''' \rangle = -\langle \mu_s \rho_2 (\mathcal{E}\sigma) \rangle = 2\mu_s \int_0^\infty f g \mathcal{E}_r r^2 dr, \quad (1)$$

where $\mathcal{E}$ is the electric field, $\mathcal{E}_r$ its radial component, ρ_2, σ the usual Dirac matrices and f, g are the radial functions defined in reference 1; r is the distance from the center of the nucleus. Calculations were made for a model in which the charge Ze is distributed with density proportional to r^{n-3} in $r<a$. The change in the electrostatic potential energy caused by the finiteness of the nucleus is referred to as δV, changes in $\langle \delta V \rangle$, $\langle H''' \rangle$ caused by change $\delta' a$ for fixed n by $\delta' \langle \delta V \rangle$, $\delta' \langle H''' \rangle$, respectively. The ratio to the volume effect[4] is

$$\mathfrak{R} = \delta' \langle H''' \rangle / \delta' \langle \delta V \rangle = -\gamma(2\rho+1)(2\rho+n+1)(e^3/mc^2)/[4\pi a(2\rho+n)], \quad (2)$$

where

$$\gamma = Z\alpha, \quad \rho = (1-\gamma^2)^{\frac{1}{2}}, \quad (3)$$

and α is the fine structure constant. In Eq. (2) the electronic wave function is approximated by the first nonvanishing power of r in f and g for a Coulomb field and[3] $\mu_s \cong -(\alpha/2\pi)(eh/2mc)$. For Pb^{208}, with $a = 0.5A^{\frac{1}{3}}10^{-13}$ cm,

$$\mathfrak{R} = -0.050. \quad (4)$$

The interaction of Eq. (1) is related to that invoked by Foldy[5] for the electron-neutron force.[6] It may be noted that in the non-relativistic approximation,

$$H''' \cong -(h\mu_s/2mc)\,\mathrm{div}\,\mathcal{E}, \quad (5)$$

and for this, values about 10 times those of Eq. (4) result if one calculates with relativistic wave functions. The parameter $2\mu_s/(e\alpha) = -e^2/(2\pi amc^2) \cong -1/20$. The ratio $f/g \cong -\gamma/2$ is ~ -0.3 for

Pb^{208}. The latter factor is nearly compensated by the fact that for V a change in a produces appreciable potential changes only well inside the nucleus, while $\mathcal{E}_r r^3$ is largest at the nuclear surface where fg is largest.

* Assisted by the joint program of the AEC and ONR.

[1] G. Breit, Phys. Rev. **72**, 984 (1947); **73**, 1410 (1948); **74**, 656 (1948). Equation (1) of present note is a rearrangement of Eqs. (1.4), (2.5), (2.6) of the last reference.

[2] P. Kusch and H. M. Foley, Phys. Rev. **72**, 1256 (1947); H. M. Foley and P. Kusch, Phys. Rev. **73**, 412 (1948).

[3] Julian Schwinger, Phys. Rev. **73**, 415 (1948); **76**, 790 (1949).

[4] J. E. Rosenthal and G. Breit, Phys. Rev. **41**, 459 (1932); G. Breit, Phys. Rev. **42**, 348 (1932).

[5] L. L. Foldy, Phys. Rev. **83**, 688 (1951); G. Breit, Proc. Natl. Acad. (to be published). The term containing $\mathrm{div}\,\mathcal{E}$ is explained without the use of the canonical transformation of Foldy and Wouthuysen.

[6] Rainwater, Rabi, and Havens, Phys. Rev. **72**, 634 (1947); **75**, 1295 (1949); E. Fermi and L. Marshall, Phys. Rev. **72**, 1139 (1947).

Ferromagnetic Resonance in Single Crystals of Cobalt-Zinc Ferrite

TOSHIHIKO OKAMURA AND YŪZŌ KOJIMA
Research Institute for Scientific Measurements, Sendai, Japan
(Received November 26, 1951)

WE succeeded in growing single crystals of Co-Zn ferrite, and its ferromagnetic resonance was observed at 9310 Mc from room temperature to the Curie temperature.

Single crystals of the ferrite were prepared as follows: 6.7 g Fe_2O_3, 1.9 g CoO, 1.4 g ZnO, and 12 g borax were mixed, kept at 1320°C for 3 hours in a platinum crucible, cooled at a rate of 1°C/min until 1150°C, and then the current was turned off.

A crystal used in the present experiment was a beautiful octahedral crystal, about 1 mm^3 in volume. The Curie point of this crystal was observed from the resonance experiments at *ca* 340°C. Moreover, from Guillaud's Curie temperature data[1] for various compositions of Co-Zn ferrites, our crystal seems to have the composition $Co_{0.7}Zn_{0.3}Fe_2O_4$.

A crystal was cut at the (100) plane into two pyramid-type specimens, and one of them was mounted at the bottom of the resonant cavity so as to make the (100) plane consistent with the direction of both the rf magnetic field and the dc magnetic field.

The experimental procedure and method were given in previous papers.[2,3]

Resonance fields and line half-widths from room temperature to *ca* 300°C were observed, and the results of measurements made with the [110] and [100] directions respectively parallel to the dc static field are shown in Fig. 1.

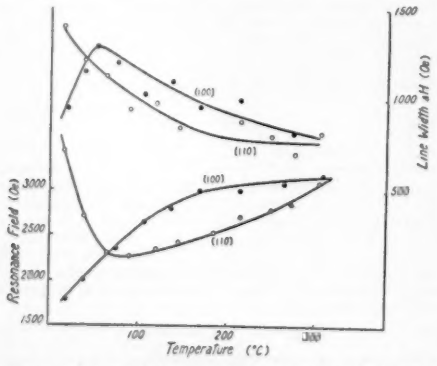

FIG. 1. Variation of the resonance field and the line half-width with temperature for the [110] and [100] directions in a single crystal of $Co_{0.7}Zn_{0.3}Fe_2O_4$.

The curves of resonance field *vs* temperature for these two directions cross at *ca* 70°C, and the line width for the [100] direction has a maximum value near this temperature.

Sintered polycrystalline specimens of the same composition were used to determine the demagnetizing factor N and magnetic saturation values M_s of the single crystal. Namely, resonance experiments were performed from room temperature to the Curie point for various specimens (a sphere 2 mm in diameter; a disk 0.25 mm in thickness and 3.12 mm in diameter; and a pyramid form whose base was 1 mm along the edges).

A second peak at lower magnetic field was always observed in the case of the experiment with polycrystalline specimens from *ca* 70°C to 100°C, as we had previously reported in the experiment with Mn-Zn single crystals,[4] and this "double peak" seems to have also an intimate relation with the phenomena in which the anisotropy energy K_1 changes its sign.

The demagnetizing factor N and the saturation magnetization M_s at each temperature were calculated from the resonance fields of polycrystalline specimens, and substituting these values in Kittel's resonance formula,[5] K_1 and g of the single crystal were determined for each temperature as shown in Table I in the fourth

TABLE I. Crystalline anisotropy energy K_1 and g-factors, as functions of temperature.

Temp. °C	g_p	M_s gauss	$K_1 \times 10^6$ ergs/cm³	g
20	2.07	516	2.36	1.91*
40	2.10	450	1.34	1.92*
60	2.11	381	0.16	1.96*
80	2.12	338	−0.21	2.06
120	2.15	269	−0.41	2.12
160	2.16	203	−0.34	2.12
200	2.17	134	−0.21	2.17
240	2.18	61	−0.07	2.16
286	2.19	8	−0.01	2.15

and the last column, respectively. The g-factors of the single crystal near room temperature could not be determined with sufficient accuracy because of a considerable increase in the value of K/M_s and NM_s in Kittel's formula, so these values are marked with asterisks.

In Table I g-factors obtained from the experiment with a spherical polycrystalline specimen, whose diameter is 2 mm, are also included in the second column, g_p. The values of g and g_p at high temperatures coincide satisfactorily with one another within the limits of error.

Experiments at a wavelength of 1.2 cm are being planned.

Details of the present experiment will be published in Science Reports of the Research Institute of Tohoku University.

The writers wish to express their thanks to Miss Kōko Takahashi for her assistance during the course of the experiment.

[1] C. Guillaud and H. Crevaux, Compt. rend. **230**, 1459 (1950).
[2] Okamura, Torizuka, and Kojima, Sci. Repts. Research Inst. Tohoku University **2**, 663 (1950).
[3] Okamura, Torizuka, and Kojima, Sci. Repts. Research Inst. Tohoku University **3**, 209 (1951).
[4] Okamura, Kojima, and Torizuka, details to be published in Sci. Repts. Research Inst. Tohoku University.
[5] C. Kittel, Phys. Rev. **73**, 155 (1948).

Low Energy γ-Transitions in Some Rare Earth Isotopes*

J. W. MIHELICH AND E. L. CHURCH
Brookhaven National Laboratory, Upton, New York
(Received January 3, 1952)

SEVERAL of the rare earths, when activated by neutron capture, decay by β-emission followed by an internally converted γ-transition of about 100 kev energy. In most cases, these energies have been well determined previously.[1] In order to obtain relative intensities of conversion lines and assign transition

TABLE I. Energies, intensities, and multipole assignments.

Converting (and parent) nucleus	Electron energy (kev) and shell		Energy sum (kev)	Rel. int.	Lifetime (sec)	Multipole order	$(K/L)_{exp}$	$(K/L)_{empirical}$[a]
$_{61}Pm_{82}^{147}$ (Nd^{147} 11 days)	46.21	K	91.40	6.4	$<5\times10^{-7}$[b]	($M1$) or ($M1+E2$)	6.4 ± 2.0	7.7 ($M1$)
	84.34	L_I	91.77	1.0			6.6 ± 1.5[c]	0.5 ($E2$)
	90.12	M_I	91.78					
	91.79	N_V	91.90					
			$\gamma=91.8$					
$_{67}Ho_{98}^{165}$ (Dy^{165} 2.5 hr)	39.34	K	94.95	6.4	$<3\times10^{-9}$[d]	($M1$) or ($M1+E2$)	5.9 ± 2.0	7.6 ($M1$)
	85.79	L_I	95.19	1.0				0.3 ($E2$)
	86.97	L_{III}	95.05	<0.2				
	92.99	M_I	95.12					
	94.92	N_V	95.08					
			$\gamma=95.1$					
$_{68}Er_{92}^{166}$ (Ho^{166} 27 hr)	23.00	K	80.47	0.13	1.7×10^{-9}[e]	($E2$)	$0.07^{+0}_{-0.02}$	7.5 ($M1$)
	70.99	L_I	80.74	<0.1				0.14 ($E2$)
	71.51	L_{II}	80.78	0.72				
	72.42	L_{III}	80.78	1.00				
	78.88	M_{III}	80.70	0.64				
	80.42	N_{III}	80.74	0.20				
			$\gamma=80.7$					
$_{70}Yb_{100}^{170}$ (Tm^{170} 127 days)	23.00	K	84.31	0.29	1.6×10^{-9}[d]	($E2$)	$0.16^{+0.2}_{-0.02}$	7.5 ($M1$)
	74.28	L_I	84.77	<0.1			0.145[d]	0.145 ($E2$)
	74.86	L_{II}	84.84	0.83				
	75.91	L_{III}	84.86	1.00				
	82.90	M_{III}	84.85	0.67				
	84.58	N_{III}	84.93	0.20				
			$\gamma=84.8$					
$_{72}Hf_{104}^{176}$ (Lu^{176} 3.7 hr)[f]	23.09	K	88.46	0.24	$<10^{-9}$[f]	($E2$)	$0.14^{+0.2}_{-0.02}$	7.5 ($M1$)
	78.12	L_{II}	88.87	0.71				0.14 ($E2$)
	79.33	L_{III}	88.90	1.00				
	86.78	M_{III}	88.89	0.84				
	88.40	N_{III}	88.79	0.23				
			$\gamma=88.9$					

[a] See reference 6.
[b] W. S. Emmerich and J. D. Kurbatov, Phys. Rev. **83**, 40 (1951).
[c] E. Kondaiah, Phys. Rev. **81**, 1056 (1951).
[d] See reference 1.
[e] F. K. McGowan, Phys. Rev. **81**, 1056 (1951).
[f] Scharff-Goldhaber, der Mateosian, and Mihelich, Bull. Am. Phys. Soc. **26**, No. 6, 38 (1951).

multipolarities, the conversion electron spectra of some of these isotopes have been re-examined using permanent magnet 180° photographic β-spectrographs. Relative line intensities were obtained by photometric densitometry, corrections being made for film sensitivity as a function of electron energy by the use of an experimentally determined extrapolation[3] of Cranberg and Halpern's curve for low energies.[3] Although sources were of about 1.0 mg/cm^2 thickness, areas of the lines, uncorrected for source absorption and weighted by the radius were used as a measure of the conversion line intensity. In other experiments[3] this has proved to be fairly reliable. Our magnetic fields were calibrated using the energies of the I^{131} γ-rays as determined by Lind *et al.*,[4] and appropriate Xe critical absorption energies interpolated from the x-ray data of Siegbahn.[5] The magnetic fields were extrapolated for radii corresponding to energies below 45 kev. This may account for the fact that the K sum energies are consistently lower than the L sum energies.

Internal conversion spectra of the γ-transitions following the β-decay of Nd^{147}, Dy^{165}, Ho^{166}, Tm^{170}, and Lu^{176m} were examined. Table I lists the energy and intensity data obtained as well as published lifetimes and empirical K/L ratios. Intensities are normalized to the most intense L line of each spectrum.

It is apparent that these spectra arise from different types of nuclear transitions. The transitions following the decay of Nd^{147} and Dy^{165} occur in odd-even nuclei. They have comparatively high K/L ratios and one predominant L conversion line. Lifetime and K/L ratio considerations[6] predict the multipolarity of both transitions to be $M1$ or ($M1+E2$) mixtures.

The transitions following the decay of Ho^{166}, Tm^{170}, and Lu^{176m} occur in even-even nuclei, and should therefore, as a rule, be of $E2$ multipole order.[6] This is in agreement with the lifetimes and the low K/L ratios ($\sim$0.15). Here the L conversion lines consist of intense L_{II} and L_{III} groups and a weak L_I group. Experimental L subshell conversion data should be of assistance in assigning multipole orders.[7]

It is interesting to note that, to within ±0.2 kev, the energies of the three $E2$ transitions vary linearly with atomic number. More data are needed to determine the significance of this observation.

Our thanks are due Dr. M. Goldhaber for his constructive criticism.

* Research carried out under contract with the AEC.

[1] *Nuclear Data*, National Bureau of Standards Circular No. 499 (1951).
[2] J. W. Mihelich (to be published).
[3] L. Cranberg and J. Halpern, Rev. Sci. Instr. **20**, 641 (1949).
[4] Lind, Brown, Klein, Muller, and DuMond, Phys. Rev. **75**, 1544 (1949).
[5] M. Siegbahn, *Spektroskopie der Roentgenstrahlen* (Julius Springer, Berlin, 1931).
[6] M. Goldhaber and A. W. Sunyar, Phys. Rev. **83**, 906 (1951).
[7] J. W. Mihelich and E. L. Church, Bull. Am. Phys. Soc. **26**, No. 6, 37 (1951).

Theory of Cooperative Phenomena

GÉRARD FOURNET
Office National d'Etudes de Recherches Aéronautiques, Châtillon s/Bagneux, Seine, France
(Received December 31, 1951)

IN a recent paper Kikuchi[1] has given a new theory of cooperative phenomena. We would like to call attention to the theory of order disorder transformations in binary alloys A_nB_m developed by Yvon[2] in France and in particular to compare his results with those of Kikuchi. The simplifying hypotheses are the same as those of the other theories. The only energy function that is necessary to consider is

$$W(r)=W_{AA}(r)+W_{BB}(r)-2W_{AB}(r), \tag{1}$$

where $W_{AA}(r)$ refers to the mutual potential energy of two A atoms separated by a distance r. Yvon assumes that $W(r_p)$ (hereafter designated by W_p) decreases rapidly with r_p, where r_p refers to the distance between pth neighbors. The probability $n_{1,A}(\mathbf{x}_i)$ of finding one A atom at the site defined by $\mathbf{x}_i$ and the probability $n_{2,AA}(\mathbf{x}_i,\mathbf{x}_j)$ of finding simultaneously one A atom at $\mathbf{x}_i$ and one A atom at $\mathbf{x}_j$ are expressed in the form of a series. By considering several terms, results as precise as are desired can be obtained. When we assume only W_1 nonzero and consider only two terms in the expansion for n_1 and one term for n_2, we obtain the classical approximation[2,3] of Bethe, Fowler, and Guggenheim and Takagi. We will show with an example that three of four terms suffice to reproduce exactly the results of the best approximations. In addition to its theoretical rigor the theory of Yvon has also the advantage of utilizing terms A_q (in calculating n_1) and B_q (in calculating n_2) which are independent of the lattice. The calculation of a limited number of terms (work now in progress) will permit treating nearly every case. One can also take into account further energies W_2, $W_3\cdots$ which can play important roles, as witness the case of β-brass.[4]

For comparison of the theories of Yvon and Kikuchi we have calculated the configurational energy above the critical temperature for a simple cubic lattice where there are 50 percent A atoms (or spin $+$) and 50 percent B atoms (or spin $-$). The configurational energy (only W_1 nonzero) is given by

$$E=\tfrac{1}{2}\cdot M\cdot 6\cdot n_{2,AA}(r_1)\cdot W_1,$$

where M refers to the total number of sites and $n_{2,AA}(r_1)$, the value of $n_{2,AA}(\mathbf{x}_i,\mathbf{x}_j)$ for $(\mathbf{x}_i-\mathbf{x}_j)=r_1$. The theory of Yvon gives for n_2

$$\log n_2=\log B_2+\Sigma\log B_3+\Sigma\log B_4+\cdots, \tag{2}$$

where B_4, for example, refers to the terms using groups of 4 sites. We must consider only groups where closure is obtained with only nearest neighbor interactions. In the simple cubic lattice the first terms are given in Fig. 1.

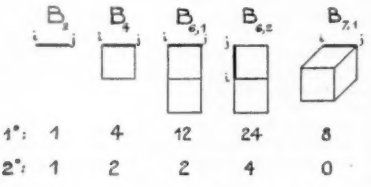

FIG. 1. 1°: Number of terms for simple cubic lattice. 2°: Number of terms for two-dimensional square lattice.

In order to conform with the notation of Kikuchi we must write [see Eq. (1)]

$$W_1=-\epsilon+(-\epsilon)-2(+\epsilon)=-4\epsilon \quad \text{and} \quad K=\epsilon/kT.$$

Then, from Eq. (2),

$$n_{2,AA}(r_1)=B_2B_4{}^4B_{6,1}{}^{12}B_{6,2}{}^{24}B_{7,1}{}^8,$$

one obtains

$$-E/(M\epsilon)=3K+11K^3+(542/5)K^5+\cdots,$$

identical to the result (D7.6) that Kikuchi reported from more complicated calculations than those given in his paper. We point out that if we make the approximation

$$n_{2,AA}(r_1)=B_2B_4{}^4B_{6,1}{}^{12}B_{6,2}{}^{24},$$

we find

$$-E/(M\epsilon)=3K+11K^3+(422/5)K^5+\cdots,$$

the expression (D7.3) obtained by Kikuchi from the calculations in his paper.

Since the B_q do not depend on the lattice under consideration, we can use the values already calculated to obtain immediate results for the two-dimensional square lattice. We have, in fact, for this lattice on the one hand,

$$E=\tfrac{1}{2}\cdot M\cdot 4\cdot n_{2,AA}(r_1)\cdot W_1,$$

and on the other,

$$n_{2,AA}(r_1)=B_2B_4{}^2B_{6,1}{}^2B_{6,2}{}^4B_{7,1}{}^0,$$

from which

$$-E/(2M\epsilon)=K+(5/3)K^3+(32/15)K^5+\cdots. \tag{3}$$

In the treatment of Kikuchi[1] for the same lattice the configurational energy in the disordered state is

$$E=2M\epsilon(4y_2-1)=2M\epsilon(H^{-3}-H^3)/(6-H^3-H^{-3}),$$

an expression that furnishes a development that is identical to (3). We know also that the result of the variational method[5] (identical with that of Kikuchi) contains only three exact terms in the development of the free energy for high temperatures [see (97), reference 5].

I thank Professor Guinier for some discussions and Dr. Walker for the translation of the manuscript.

[1] R. Kikuchi, Phys. Rev. **81**, 988 (1951).
[2] J. Yvon, Cahiers phys. **28**, 1 (1945).
[3] G. Fournet (to be published).
[4] G. Fournet, Compt. rend. **232**, 155 (1951).
[5] H. A. Kramers and G. H. Wannier, Phys. Rev. **60**, 252, 263 (1941).

Color Centers and Thermoluminescence in Alkali Halides

J. SHARMA
Khaira Laboratory of Physics, University College of Science, Calcutta, India
(Received December 31, 1951)

IN our study of thermoluminescence of alkali halides excited and colored by cathode-ray bombardment at -184°C, we have found that the coloration is closely associated with trapping centers. Some of the thermoluminescent traps give out peak emissions at temperatures exactly corresponding with those at which the color centers disappear. Thus, it appears that when F-centers are thermally destroyed they also directly or indirectly give out emissions. In the present work the rate of heating has been maintained fairly high, about 10–12°C/sec. However, no measurement of the absorption spectrum has yet been made here, and the production of color centers has been judged from visual coloration of the samples taken in finely powdered form. The failure of earlier workers to notice the effect may be a result of their working with single crystals where the rate of heating was low.

Potassium iodide powder (E. Merck, reagent type, melted and recrystallized in vacuum) is found to give four thermoluminescence peaks at 110–120, 158, 176, and 235°K. Of these the relative heights of the first three peaks depend slightly on the thermal history of the powder, but the trap at 235°K remains undisturbed (see Fig. 1). Under cathode-ray bombardment the sample becomes

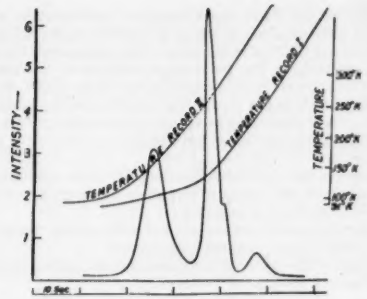

FIG. 1. Thermoluminescence curve of potassium iodide starting from liquid oxygen temperature, after excitation by cathode-rays at 10 kv for five minutes. The temperature record No. I corresponds to the thermoluminescence curve. The dotted part of temperature record No. II gives the temperature range at which coloration disappears on heating from 91°K after bombardment.

bluish green in color, presumably as a result of strong *F*-center absorption in the red region. It has been found that if the sample after bombardment is heated from liquid oxygen temperature, the coloration suddenly disappears at about 235°K, which is also the maximum glow temperature of the last luminescent trap. The present case is similar to that observed by Pringsheim[1] in the case of LiF, at −135°C, where an absorption band at 3200A disappears with strong emission in the blue region. Further, it has been seen here that the most favorable temperature for the bluish green coloration of potassium iodide is about 200°K, and this is also the temperature at which bombardment and subsequent thermoluminescence gives large amount of stored energy from the trap released at 235°K. If the heating is begun from 200°K after bleaching the coloration with visible light, the output of the peak decreases. On the other hand, if irradiation with visible light is done at liquid oxygen temperature, then the shallow traps are reduced in relative intensity while the trap with maximum glow at 235°K is enhanced (see Fig. 2). This suggests the destruction of shallow traps while the one at 235°K increases in population.

In accordance with the observation of Pringsheim,[2] it has been found that the weak coloration produced at room temperature is more stable than that produced at liquid oxygen temperature. When colored by bombardment at room temperature, it disappears at about 160°C, and here too it is associated with a faint luminescence.

Similar phenomena have been observed in potassium chloride. On bombardment at liquid oxygen temperature it gets colored pink.[3] On heating, the color disappears in two stages, at about 200°K and 520°K. At first the pink color disappears, leaving a magenta coloration which dies out at the higher temperature. Both colors are destroyed with strong luminescence peaks. When cathode-ray bombardment is done at about room temperature, only the latter coloration is produced.

In sodium chloride considerable bombardment at liquid oxygen temperature produced a greenish yellow color. On heating, at about 165°K it became dark brown and this color disappeared at about 500°K. Both the colors give strong emissions when they are thermally destroyed. The emission in NaCl in the latter case is so strong that even in a normally illuminated room its blue light could be easily seen. In another experiment, the sample was bombarded at room temperature and left for eighteen hours. On heating the color again disappeared, with strong emission in the blue region.

Since *F*-centers are most easily and copiously produced, it appears that their destruction is intimately connected with a high temperature strong emission peak.

The author is thankful to Professor S. N. Bose, Khaira Professor of Physics, University College of Science, Calcutta, for his guidance and helpful interest in the work.

[1] P. Pringsheim and P. Yuster, Phys. Rev. **77**, 90 (1950).
[2] Delbeco, Pringsheim, and Yuster, J. Chem. Phys. **19**, 574 (1951).
[3] H. N. Bose, Proc. Phys. Soc. (London) (to be published).

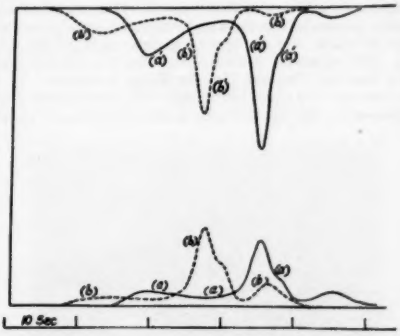

FIG. 2. The lower curves give the thermoluminescence records in which the sample (KI) after bombardment was irradiated with (a) total light and (b) red light from an Fe-arc. Obviously it shows quenching of shallow traps and enhancement of the last 235°K trap. The upper curves are simultaneous records for comparison from the portion of the sample which was protected from the arc light.

Temperature Dependence of the Line Half-Width of Ferromagnetic Resonance in Single Crystals of Zinc-Manganese Ferrite

TOSHIHIKO OKAMURA, YŪZŌ KOJIMA, AND YOSIHARU TORIZUKA
Research Institute for Scientific Measurements, Sendai, Japan
(Received October 29, 1951)

SINGLE crystals of nickel ferrite[1] and zinc manganese ferrite[2] were prepared by Galt, Yager, and others, and the *g*-factor, line half-width, anisotropy constant, and other physical properties were determined precisely at room temperature. According to their experimental results on the width of the resonance line at the

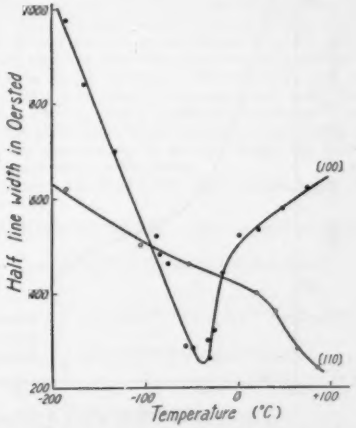

FIG. 1. Temperature dependence of the line half-width for a single crystal of $MnO ZnO 2Fe_2O_3$.

frequency of 24,160 Mc, the variations in ΔH with crystallographic direction were not large enough to be significant.[3] Recently, we have also succeeded in preparing by almost the same method[1,3] single crystals whose composition is approximately $ZnOMnO2Fe_2O_3$. The resulting crystals formed regular octahedra, whose size was 0.6~0.8 mm on the edge. A cone was cut out whose base plane is (100) and ferromagnetic resonance measurements were made at a wavelength of 3.22 cm, with the [110] and [100] directions respectively parallel to the static field. From the experimental data, the line half-widths with crystallographic direction were determined at various temperatures, and considerable difference was found between the [100] and [110] directions.

The experimental procedure and method were given in previous papers.[3,4]

The half-widths were observed from liquid nitrogen temperature to the Curie point *ca* 110°C. All the measurements were made while warming the crystal from the temperature of liquid nitrogen at the rate of 0.5° per minute. The results obtained are shown graphically in Fig. 1; the ordinate gives the half-width in oersteds, and the abscissa gives the temperature in degrees centigrade; open circles denote the [110] direction, and solid circles the [100] direction. For the [100] direction, ΔH decreases rapidly with rising temperature from −185°C up to *ca* −40°C; then it increases abruptly and afterwards increases slowly. On the other hand, in the case of the [110] direction, ΔH always decreases continuously with rising temperature and finally vanishes near the Curie point.

The experiment was repeated on the other single crystal having the same composition, and the same tendency was always observed in the same temperature range.

Thus, it was confirmed that the value of ΔH depends considerably on crystallographic direction and the variation of ΔH with temperature is quite different for different crystallographic directions. At room temperature, the value of ΔH is large compared to the result of Galt and his co-workers;[2] the reason for this seems to depend on the crystalline imperfection and the form of the specimen.

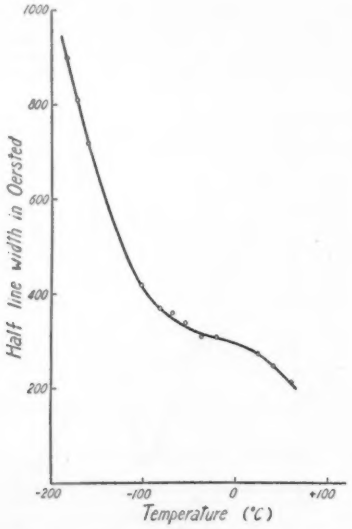

FIG. 2. Temperature dependence of the line half-width for a polycrystalline specimen of $MnOZnO2Fe_2O_3$.

Next, we performed also a resonance experiment on a disk-formed polycrystalline specimen of $ZnOMnOFe_2O_3$, 4.5 mm in diameter and 0.22 mm in thickness, at low temperature and at the same wavelength. The temperature variation of the line half-width is shown in Fig. 2; in the range −95°C to −115°C in which the half-width begins to increase rapidly, double peaks were observed in the resonance curves, which are similar to those found recently by the authors in $MnOFe_2O_3$[5] and $NiOFe_2O_3$[6] at low temperature.

Therefore, the occurrence of double peaks seems to be intimately connected with the change of crystalline anisotropy of the sample at low temperature, as expected.

Experiments on a thin-disk-formed and a sphere-formed specimen of the single crystal are being planned.

Details of this work will be published in the Science Reports of the Research Institute of Tohoku University.

[1] Galt, Mathias, and Remeika, Phys. Rev. **79**, 391 (1950).
[2] Galt, Yager, Remeika, and Merritt, Phys. Rev. **81**, 470 (1951); Yager, Merritt, and Guilland, Phys. Rev. **81**, 477 (1951).
[3] Okamura, Torizuka, and Kojima, Sci. Repts. Research Inst. Tohoku University **2**, 663 (1950).
[4] Okamura, Torizuka, and Kojima, Sci. Repts. Research Inst. Tohoku University **3**, 209 (1951).
[5] T. Okamura and Y. Torizuka, Phys. Rev. **83**, 847 (1951).
[6] T. Okamura, Nature **168**, 162 (1951); T. Okamura and Y. Torizuka, Sci. Repts. Research Inst. Tohoku University **3**, 219 (1951).

A Steady State Transient Technique in Nuclear Resonance

R. GABILLARD
Laboratoire de Radioélectricité, Université de Paris, Paris, France
(Received December 26, 1951)

THIS title heads two recent Letters to the Editor of this Review.[1] The authors do not seem to have noticed that some previous articles have already described the same effect and given its full theory.[2,3] We wish to draw attention to the fact that this phenomenon was discovered by the late Dr. Gooden.[4] We do not intend to review our previous theory, but will only give its new development concerning the measurement of T_2 in liquids in the presence of field inhomogeneities larger than the mean value of the intramolecular field.

When T_2 is larger than about 10^{-2} sec a well-known transient phenomenon is observed.[2,3] The decay of the oscillations (Fig. 1) is determined by phase shifts produced by both the molecular field h and the inhomogeneities $\delta = H_s - H_0$ of the magnetic field.

After resonance, the molecular field produces a phase shift $\varphi(t) = \int_0^t \gamma h(t)dt$, and we have to integrate over all the values of φ. These values are distributed according to a Gaussian probability function. The fact that the decay is described by the function $\exp(-t/T_2)$ and not by $\exp(-t^2/T_2)$ as it seems at first, is produced by the fact that $\langle\varphi^2\rangle_{h\delta}$ is related to $\langle h^2\rangle_{h\delta}$ not by $\langle\varphi^2\rangle_{h\delta}$

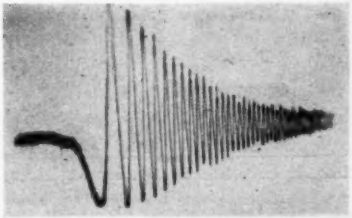

FIG. 1. Decay of oscillations for a Gaussian distribution of field inhomogeneities.

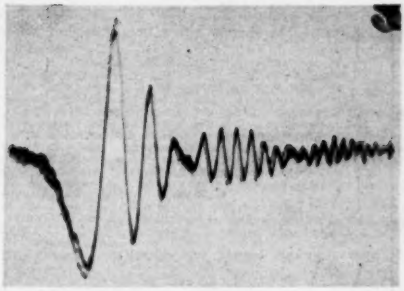

FIG. 2. Decay of oscillations for a "square" distribution of field inhomogeneities.

$=\gamma^2\langle h^2\rangle_{Av}t^2$ but by $\langle\varphi^2\rangle_{Av}=\gamma^2\langle h^2\rangle_{Av}t$ according to the well-known solution of the Gaussian random walk problem.

Field inhomogeneities produce an extra phase shift $\varphi(\delta)=\gamma\delta t$. In order to obtain the whole signal we have to integrate over all values of δ. An extra decay of the oscillations follows, described by the Fourier transform $F(t)$ of the distribution function $\psi(\delta)$ of δ over the sample. The envelope amplitude of the signal is the product,

$$A=\exp(-t/T_2)F(t).$$

Discrimination between the two effects is possible for special forms of $F(t)$.

There are two cases of particular interest:

I. We assume that $F(t)$ is a uniformly decreasing function of time. For example, this is the case when $\psi(\delta)$ is a bell-shaped function or a damped oscillation function. Then the signal aspect is that given in Fig. 1 and it is not possible to obtain from its decay curve a measure of T_2 if $F(t)$ is an unknown function. But if $F(t)$ is a periodic function of time, it is possible to draw information about $F(t)$ from the position of successive zeros. This is the case when $\psi(\delta)$ is a pulse-like function, and the study of signal decay is a convenient way to measure T_2.

For instance, when $\psi(\delta)=1/\Delta$ if $|\delta|\leqslant\Delta$ and $\psi(\delta)=0$ for $|\delta|>\Delta$, then

$$F(t)=\sin\Delta t/\Delta t,$$

and the signal is represented on Fig. 2. Measurement of the first zero time t gives the value of Δ from $\Delta t=\pi$. Then the amplitude ratio at successive maxima, which is only determined by T_2 and Δ, provides a measure of T_2. We obtain

$$T_2=\frac{3\pi}{2}\Big/\Delta\log\left(\frac{2}{3\pi}\frac{e_1}{e_2}\right).$$

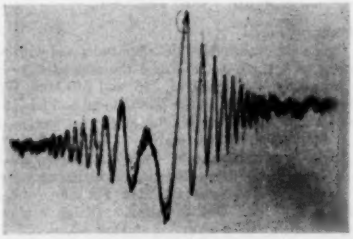

FIG. 3. Preresonance signal for $T_2>T_0$.

II. It is clear that $F(t)=\int_{-\infty}^{+\infty}\psi(\delta)\cos\gamma\delta t\,d\delta$ is an even function. On the other hand, $F(t)$ must be a periodic function of time t with a period T_0 (half-period of the modulating field). From these two properties it follows that

$$F(T_0-t)=F(t).$$

In the presence of very large inhomogeneities, $F(t)$ drops rapidly to zero in a time $\tau\ll T_2$ and increases again at time before the next resonance according to the even properties of $F(t)$.

Then:

(A) If $T_2<T_0$, the factor $\exp[(T_0-\tau)/T_2]$ is practically zero and there is no observable signal before resonance (Fig. 1 and Fig. 2).

(B) But if $T_2>T_0$, then $\exp[(T_0-\tau)/T_2]$ is an important factor and we can observe a signal before resonance, as seen in Fig. 3. The ratio of the signal amplitudes, e_1 after resonance and e_2 before resonance, is

$$\frac{e_1}{e_2}=\exp\left(\frac{T_0-t}{T_2}\right)\frac{F(T_0-t)}{\exp(t/T_2)F(t)},$$

and if $t\to 0$ (observations of signal near resonance) we get

$$T_2=T_0\log(e_2/e_1).$$

A limit to this method is set by random magnetic field fluctuations produced by the magnet power supplies. These fluctuations produce phase shifts strictly identical to those produced by molecular fields. These phase shifts introduce extra decays which are not generally even functions of time and are not eliminated like δ by the previous method. In our apparatus this limit occurs for $T_2>0.1$ sec.

Use of a permanent magnet would probably allow the measurement of times $T_2>0.1$ sec, but it is probable that the inhomogeneous magnetic field will set a new limit here.

[1] Bradford, Clay, and Strick, Phys. Rev. **84**, 157 (1951); Strick, Bradford, Clay, and Craft, Phys. Rev. **84**, 363 (1951).
[2] R. Gabillard, Compt. rend. **232**, 324 (1951).
[3] R. Gabillard, Compt. rend. **232**, 1477, 1551 (1951).
[4] J. S. Gooden, Nature **165**, 1015 (1950).

High Energy Nucleon-Deuteron Scattering*

P. B. DAITCH AND J. B. FRENCH
University of Rochester, Rochester, New York
(Received December 31, 1951)

WE consider the relationship between high energy nucleon-deuteron scattering and elementary nucleon-nucleon scattering. We find that one may, for the case of central potentials of arbitrary exchange character, write the nucleon-deuteron differential cross section in terms of the elementary cross sections. Except for a term which is important only in the backward direction, the reduction is simple and enables one to examine easily the arbitrariness caused by the fact that nucleon-nucleon scattering measurements do not give singlet and triplet cross sections separately nor the phases.

The quartet and doublet Born approximation matrix elements are given by[1]

$$M_q=(3\pi/m)(U_q+L_q+D_q),\quad M_d=(3\pi/m)(U_d+L_d+D_d),\quad (1)$$

and

$$d\sigma/d\omega=\tfrac{3}{4}|U_q+L_q+D_q|^2+\tfrac{1}{4}|U_d+L_d+D_d|^2,\quad (2)$$

where

$$U=(m/3\pi)\int\int\chi^*\varphi^*(S)e^{-i\mathbf{k}\cdot\mathbf{X}}V^U(1,3)e^{i\mathbf{k}_0\cdot\mathbf{X}}\varphi(S)\chi d\mathbf{X}d\mathbf{S},$$

$$L=(m/3\pi)\int\int\chi^*\varphi^*(S)e^{-i\mathbf{k}\cdot\mathbf{X}}(1-T_{23})V^L(2,3)\times e^{i\mathbf{k}_0\cdot\mathbf{X}}\varphi(S)\chi d\mathbf{X}d\mathbf{S},\quad (3)$$

$$D=(m/3\pi)\int\int\chi^*\varphi^*(S)e^{-i\mathbf{k}\cdot\mathbf{X}}T_{23}V^U(1,3)\times e^{i\mathbf{k}_0\cdot\mathbf{X}}\varphi(S)\chi d\mathbf{X}d\mathbf{S}.$$

Here the index 3 refers to the incident nucleon; 1, 2 are particles in the deuteron with 2 and 3 referring to like nucleons; χ is a 3-particle quartet or doublet spin wave function; $\varphi(S)$ is the deuteron space wave function with $\mathbf{S}=\mathbf{r}_1-\mathbf{r}_2$; $\mathbf{X}$ is the coordinate of the incident nucleon with respect to the deuteron center of mass; $\mathbf{k}_0$, $\mathbf{k}$ are the nucleon incident and final momenta ($k^2=k_0^2=8mE_0/9$, where E_0 is the incident lab energy); T is the total exchange operator; V^U and V^L are unlike and like particle potentials; and m = nucleon mass.

In U we transform variables by $\mathbf{X}=-\frac{2}{3}\boldsymbol{\rho}-\frac{1}{3}\boldsymbol{\zeta}$, $\mathbf{S}=\frac{1}{2}\boldsymbol{\rho}-\boldsymbol{\zeta}$. Then

$$U=(m/3\pi)\int\int\chi^*\varphi^*(|\boldsymbol{\zeta}-\tfrac{1}{2}\boldsymbol{\rho}|)\exp[i\mathbf{k}\cdot(\tfrac{2}{3}\boldsymbol{\rho}+\tfrac{1}{3}\boldsymbol{\zeta})]V^U(\rho)\times\exp[-i\mathbf{k}_0\cdot(\tfrac{2}{3}\boldsymbol{\rho}+\tfrac{1}{3}\boldsymbol{\zeta})]\varphi(|\boldsymbol{\zeta}-\tfrac{1}{2}\boldsymbol{\rho}|)\chi d\boldsymbol{\rho}d\boldsymbol{\zeta}. \quad (4)$$

For the nonspace exchange part of V^U, a translation of $\boldsymbol{\zeta}$ leads to a separated integral. For the space exchange part we approximate[2] $\chi^*(|\boldsymbol{\zeta}+\frac{1}{2}\boldsymbol{\rho}|)\chi(|\boldsymbol{\zeta}-\frac{1}{2}\boldsymbol{\rho}|)$ by $|\chi(\zeta)|^2$ and once again get separation. The result is

$$U\simeq(m/3\pi)S^2(\Delta\mathbf{k})\int\chi^*\exp[-i(\tfrac{2}{3}\mathbf{k}-\tfrac{1}{3}\mathbf{k}_0)\cdot\boldsymbol{\rho}]V^U(\rho)\times\exp[i(\tfrac{2}{3}\mathbf{k}_0-\tfrac{1}{3}\mathbf{k})\cdot\boldsymbol{\rho}]\chi d\boldsymbol{\rho}, \quad (5)$$

where $S(\Delta\mathbf{k})$ is the deuteron form factor[1] and $\mathbf{k}=\mathbf{k}-\mathbf{k}_0$. Since V^U is independent of particle 2, we eliminate the spin functions of 2 by expanding χ in terms of the singlet and triplet spin states for particles 1, 3. The integral then appears as a matrix element for $n-p$ scattering. Specifically we have

$$\begin{aligned}U_q&=(4/3)S^2(\Delta\mathbf{k})\,{}^{(3)}f(\epsilon,\psi),\\ U_d&=\tfrac{1}{3}S^2(\Delta\mathbf{k})[{}^{(3)}f(\epsilon,\psi)+3\,{}^{(1)}f(\epsilon,\psi)],\end{aligned} \quad (6)$$

where ${}^{(3)}f(\epsilon,\psi)$, ${}^{(1)}f(\epsilon,\psi)$ are the triplet and singlet $n-p$ scattering amplitudes ($d\sigma^{n,p}=\frac{1}{4}|{}^{(3)}f|^2+\frac{1}{4}|{}^{(1)}f|^2$) for a lab energy ϵ and cm scattering angle ψ. The quantities ϵ and ψ are given in terms of E_0 and θ (the nucleon deuteron c.m. scattering angle) by

$$\epsilon=E_0(25-7\cos\theta)/18, \quad \cos\psi=(-7+25\cos\theta)/(25-7\cos\theta). \quad (7)$$

An exactly similar treatment gives L in terms of like particle scattering. Except at backward angles, U and L dominate the scattering and therefore nucleon deuteron scattering is correlated in energy and angle by (7). The energy ratio increases with angle from unity at 0° to 1.8 at 180°. ψ differs little from θ.

D, however, involves the three particles in an essential fashion and cannot be reduced in the same way. It may be simply evaluated if one uses the Serber $n-p$ potential and leads then to $D_q=-2D_d=-(m/3\pi)I_3$, where I_3 is given by Chew.[1] On the other hand, by using the deuteron Fourier transform

$$\bar{\varphi}(p)=(2\pi)^{-\frac{1}{2}}\int\varphi(\mathbf{S})e^{i\mathbf{p}\cdot\mathbf{S}}d\mathbf{S},$$

we may write D in terms of the $n-p$ triplet scattering as

$$D_q=-2D_d=-(4/3)\varphi(|\mathbf{k}+\tfrac{1}{2}\mathbf{k}_0|)\int{}^{(3)}f(\epsilon',\psi')\bar{\varphi}^*(\mathbf{p})d\mathbf{p}, \quad (8)$$

where ${}^{(3)}f(\epsilon',\psi')$ is as defined previously the triplet $n-p$ scattering amplitude for $\mathbf{K}_0$ going to $\mathbf{K}_1$, where ϵ' and ψ' are determined by the equations

$$2K^2=2K_0^2=p^2+(\tfrac{1}{2}\mathbf{k}+\mathbf{k}_0)^2, \quad \mathbf{K}\cdot\mathbf{K}_0=\mathbf{p}\cdot(\tfrac{1}{2}\mathbf{k}+\mathbf{k}_0). \quad (9)$$

The nucleon-deuteron cross section now appears in the form

$$d\sigma/d\omega(E_0,\theta)=\tfrac{2}{3}|(4/3)S^2(\Delta\mathbf{k})({}^{(3)}f+{}^{(3)}g)+D_q|^2+\tfrac{1}{3}|\tfrac{1}{3}S^2(\Delta\mathbf{k})({}^{(3)}f+3\,{}^{(1)}f+{}^{(3)}g+3\,{}^{(1)}g)+D_d|^2, \quad (10)$$

where the f's and g's are unlike and like particle scattering amplitudes for ϵ, ψ as given by (7).

We note that since the $n-p$ and $p-p$ measurements do not determine the singlet and triplet amplitudes separately nor the relative phases, the scattering measurements allow a great deal of arbitrariness in calculating nucleon-deuteron scattering. For example, with 240-Mev protons at 20° one can easily vary the calculated $p-d$ cross section by a factor 20 by choosing various decompositions of the nucleon-nucleon cross sections. It seems reasonable, however, to determine the f's on the basis of the Serber $n-p$ interaction. Then we have that the signs are the same and

$$|{}^{(1)}f|^2=\eta^2|{}^{(3)}f|^2=[4\eta^2/(3+\eta^2)]d\sigma^{n,p}/d\omega, \quad (\eta=0.686). \quad (11)$$

Within the framework of central forces the only simple choice which can lead to an angular and energy independent $p-p$ cross section is

$${}^{(3)}g=0, \quad |{}^{(1)}g|^2=4d\sigma^{p,p}/d\omega, \quad (12)$$

with arbitrary phase of ${}^{(1)}g$.

With these determinations of the amplitudes and with relative phase of ${}^{(1)}g$ as ±1, we plot in Fig. 1 the calculated $p-d$ cross sections for proton energies of 95, 146, and 240 Mev. We have taken the $p-p$ cross section to be 5 mb/sterad and have used an empirical formula for the $n-p$ differential cross section. D was evaluated by numerically integrating (8): this gives a result little different from that given by Chew's I_3. Shown also in the figure are the available data.[3] The two calculated curves enclose the data except in the backward direction. The source of disagreement here is not clear. The backward scattering is a function mainly of low energy $n-p$ scattering and low momentum Fourier components of the deuteron. For example, at 95 Mev the main contribution is from ϵ between 20 and 150 Mev and p less than

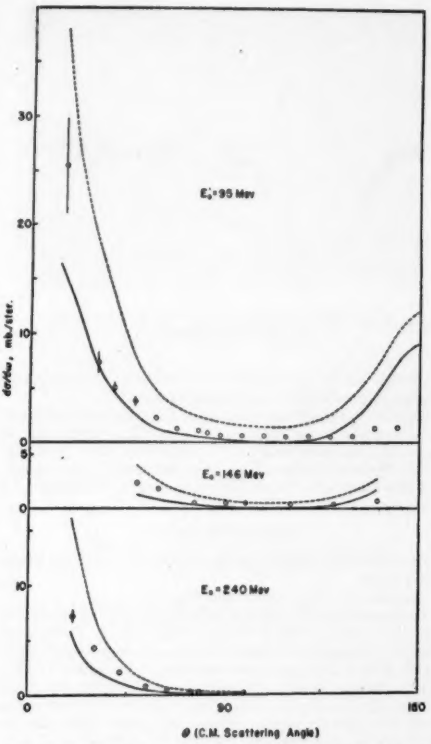

FIG. 1. Comparison of theoretical and experimental proton-deuteron elastic scattering cross section. Dashed and solid curves ar: for $p-p$ and $n-p$ amplitudes interfering constructively (${}^{(1)}g=+1$) and destructively (${}^{(1)}g=-1$), respectively. Sources of experimental data are listed in reference 3.

three times its average value in the deuteron. It seems possible that the backward peak would be reduced by the inclusion of tensor forces.[4]

* Assisted in part by the AEC.
[1] G. F. Chew, Phys. Rev. **74**, 809 (1948); R. L. Gluckstern and H. A. Bethe, Phys. Rev. **81**, 761 (1951).
[2] This approximation was checked by calculating the exact and approximate expressions using a Yukawa well and various energies and angles in the range of interest. At 90 Mev the agreement was everywhere within 10 percent; for large angles with higher energies the agreement is rather worse but since the exchange parts of U and L are dominant only for intermediate angles the approximation is satisfactory. We wish to thank Mr. T. A. Auerbach for making available to us his numerical evaluations for the exact integrals.
[3] M. O. Stern, University of California Radiation Laboratory Report No. 1440 (1951) (95-Mev data); Cassels, Stafford, and Pickavance, Nature **168**, 556 (1951) (146-Mev data); R. D. Schamberger, Phys. Rev. **83**, 1276 (1951) (240-Mev data).
[4] Horie, Tamura, and Yoshida, Prog. Theoret. Phys. **6**, 623 (1951).

Some Polystyrene Solid Solutions as Scintillation Counters*

THOMAS CARLSON AND W. S. KOSKI
Department of Chemistry, Johns Hopkins University, Baltimore, Maryland
(Received December 26, 1951)

THE scintillation efficiency and the spectral emission of a number of polystyrene solid solutions have been investigated. The method of preparing the solid solutions and the experimental procedure used in obtaining the data is similar to what has been reported previously.[1] A 5819 photomultiplier tube was used for the counting experiments. Co^{60} was used as a γ-ray source. A commercial x-ray machine was used as a source for the emission-spectra studies. The solid solutions compared were plastic disks containing 2 percent by weight of the phosphor in styrene, which were then polymerized by a 50-50 benzoyl peroxide-tricresyl phosphate catalyst. The results are summarized in Fig. 1 which gives the relative counting rates as a function of discriminator bias and in Table I where the peaks of the emission bands are recorded. It is interesting to compare these results with those obtained with the single crystals of the corresponding phosphors.[2] It will be noted that the relative order is not always the same. A notable exception is diphenylacetylene. In the crystalline state this material compares favorably with stilbene whereas in the solid solution its performance is much poorer. Since the emission bands of the solid solution and of the crystal are located in approximately the same spectral region, a poorer counting rate cannot be ascribed to a shifting away from the region of more favorable spectral response of the 5819 photomultiplier tube.

TABLE I. Wavelengths of emission bands of various 2 percent phosphor-plastic systems excited by x-rays.

Material	Wavelength (A)
stilbene	3760, 3600
diphenylbutadiene	4040
diphenylhexatriene	4200
diphenylacetylene	3720
diphenyldiacetylene	4610
anthracene	4475, 4235
diphenylethane	~3200
terphenyl	3620, 3480

Polystyrene-diphenylhexatriene solid solutions gave poor performances as counters. The large spectral shift toward the blue (1000A), plus the fact that there was a considerable amount of difficulty in realizing the polymerization of the solution, indicated that there probably was a chemical reaction between phosphor and catalyst or styrene with an interruption to the conjugation of the polyene chain. The corresponding system with diphenyloctatetraene failed to polymerize satisfactorily even after prolonged heating so it is not included in these results.

We wish to acknowledge our indebtedness to Professor J. D. H. Donnay and Professor R. Maddin for the use of their x-ray machines.

* This work was performed under the auspices of the AEC.
[1] W. S. Koski, Phys. Rev. **82**, 230 (1951).
[2] W. S. Koski and C. O. Thomas, J. Chem. Phys. **19**, 1286 (1951).

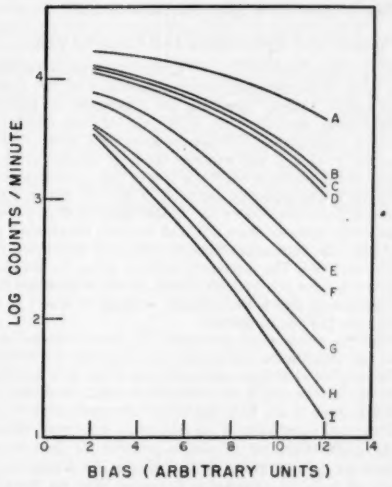

FIG. 1. Discriminator curves for some phosphor-plastic combinations: *A*—terphenyl; *B*—diphenylbutadiene; *C*—anthracene, *D*—stilbene; *E*—diphenyldiacetylene; *F*—biphenyl; *G*—diphenylacetylene; *H*—diphenylethane; *I*—polystyrene (plain).

Absence of Secondary Maxima in the Transition Curve for Electronic Showers

R. MAZE
Laboratoire École Normale Supérieure, Paris, France
(Received November 13, 1951)

IN a recent letter Tsai-Chü[1] tentatively explained the existence of a secondary maximum of the Rossi curve obtained by a counter arrangement very similar to that of Bothe and Thurin.[2]

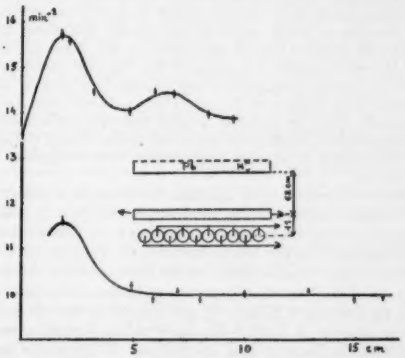

FIG. 1. Rossi curves for lead.

This experiment, the result of which was previously published,[1] does not show any maximum at 15 cm Pb or more, but indicates a small maximum at 7 cm.

I have repeated the experiment as described[2] and have reached the conclusion that this maximum at 7 cm Pb was due to statistical or other fluctuations, and should not be considered. As an effect like the one mentioned by Tsai-Chü could be more or less obliterated by a very important background of oblique rays, I placed another counter tray directly below the absorbent and measured the fivefold coincidences in order to make sure that the radiation really comes from the lead. The results were also negative.

The first curve of Fig. 1 is the same one which we have previously published. It was obtained with two crossed trays of 12 thin glass counters each with fourfold coincidences. The second curve was obtained with two trays of 10 counters instead of 12 (this explains the difference of ordinates). The measurements were carefully checked, and the precision of each point is 1 percent. The 8 percent ratio of fourfold to fivefold coincidences shows that the radiation emerging from the lead is responsible for only 27 percent of the observed counting rate. This explains the small amplitude of the first, well-known maximum.

[1] Tsai-Chü, Phys. Rev. **83**, 867 (1951).
[2] W. Bothe and H. Thurin, Phys. Rev. **79**, 544 (1950).
[3] R. Maze and Tsai-Chü, Compt. rend. **232**, 224 (1951).

The β-Decay of Radium E and the Pseudoscalar Interaction*

A. G. Petschek and R. E. Marshak
University of Rochester, Rochester, New York
(Received October 25, 1951)

THE selection rules associated with the five forms of β interaction[1] imply that the only type of transition which can reveal the presence of the pseudoscalar (P) interaction is a 0→0 yes transition. The contribution of the P interaction to all other types of transitions will be two orders of "forbiddenness" smaller than the contribution from the tensor (T) or axial vector (A) interaction which must be present. Examination of the list of radioactive nuclei[2] shows that one of the most promising candidates for a 0→0 yes transition is RaE, provided that its β spectrum is simple.[3] If we assume, as in the past, that the β spectrum of RaE is simple, then the forbidden shape which is observed[4] can be explained on the assumption that the spin change is 2 units and that the transition does not involve a parity change. The recent successes of the shell model make it desirable to reexamine this theoretical fit since the RaE nucleus, with its 83 protons and 127 neutrons, is ideally suited for shell model predictions. The shell model predicts[5] that the extra proton is $h_{9/2}$, $f_{7/2}$ or $p_{3/2}$ and that the extra neutron is $i_{11/2}$, $g_{9/2}$ or $d_{5/2}$. The shell model prediction is therefore unequivocal that the parity of RaE is odd although the prediction for the spin is not as clearcut (spin 2 or 0 is favored). Since the parity of the final even-even nucleus must be even, the β-ray transition in RaE must involve a parity change, and the previous fit with no parity change must be regarded as an accident.

We have attempted to fit the RaE β-spectrum by assuming a parity change and considering spin changes from 0 to 2; a spin change larger than 2 is excluded by the lifetime. All possible linear combinations of the five interaction forms (S, V, T, A, P) were examined except those excluded by the Fierz condition,[6] namely (SV) and (TA). The forbidden correction factors were calculated using the formulas of Konopinski and Uhlenbeck[6] and the interference formulas of Smith.[7] The finite radius corrections were taken from the paper by Rose and Holmes.[8] No corrections were applied for screening by the atomic electrons; these are said to be

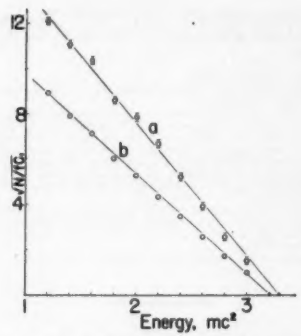

FIG. 1. Kurie plots of the RaE spectrum for (TP) mixture of interactions (a) $W_0=3.29$, $\Gamma=12.8$; (b) $W_0=3.20$, $\Gamma=13.8$.

small.[9] Since the chief feature of the correction factor needed to explain the spectrum of RaE is the large ratio ρ (about 2.6) of its value at low energies ($W=1.2\ mc^2$) to its value at high energies ($W=3.0$), it is possible to eliminate all but one of the linear combinations (TP) either by inspection or by maximizing the theoretical ρ.

The details are as follows: $\Delta J=2$, yes gives rise to a unique correction factor on either the T or A theories, which do not interfere; ρ turns out to be 0.7 which is almost a factor 4 too small. $\Delta J=1$, yes allows the following four linear combinations: (ST), (SA), (VT), (VA). For (ST) and (VA), the maximum value of ρ is less than 1.5 and for the other two combinations less than 1.3. These ratios are still too low by a factor of 2. $\Delta J=0$, yes allows the linear combinations (AP) and (TP); the A interaction alone allows the maximum value 1.2 for ρ whereas T alone allows 0.9. The linear combination (AP) does not fare any better; however, for the linear combination (TP) the maximum value of ρ is 3.6, and hence this theory has been subjected to further scrutiny.

The correction factor for the linear combination (TP) corresponding to $\Delta J=0$ yes is, in the notation of Smith:

$$C_{1(T+P)}=(M_0+\tfrac{1}{3}KN_0+\tfrac{1}{9}K^2L_0)+2\Gamma(N_0+\tfrac{1}{3}KL_0)+\Gamma^2L_0, \quad (1)$$

where $\Gamma=-i\lambda_P\int\beta\gamma_5/\lambda_T(\int\beta\sigma\cdot\mathbf{r})^*$ is taken to be real.[10] The large ratios occur where the nearly constant functions M_0, N_0 and L_0 almost cancel, thereby enhancing the importance of accurate values of these functions. Thus, an error in the finite radius corrections of approximately 0.1 percent leads to an error of up to 25 percent in $C_{1(T+P)}$ and explains the large theoretical errors assigned to the points in the Kurie plot of Fig. 1, corresponding to $\Gamma=12.8$ in the correction factor C_1 of Eq. (1). Figure 1 also contains a Kurie plot drawn for an end point of $W_0=3.2\ mc^2$, instead of the accepted $W_0=3.29$, and $\Gamma=13.8$; the required ρ is now 1.9 and the maximum attainable with other mixtures is 1.55 for (ST) or (VA). The theoretical errors in curve (b) are about half those in curve (a); for both curves, the errors are larger than the experimental errors. Reducing the endpoint to $W_0=3.15\ mc^2$ destroys the (TP) fit completely.

Within the errors noted previously, the linear combination of tensor and pseudoscalar interactions corresponding to $\Gamma=13\pm1$, can be regarded as giving a satisfactory fit of the RaE spectrum. Moreover, it is the only linear combination which can explain the forbidden shape of the RaE spectrum if the spectrum is simple and if the parity prediction of the shell model is accepted. Subject to this qualification, our calculation provides the first clearcut evidence for an admixture of the pseudoscalar interaction to explain all β-ray phenomena. It is evident that the 0→0 yes transition which is indicated for RaE cannot decide whether the S or V interaction must also be added to the (TP) combination.

We are indebted to Mrs. Petschek for assistance with the numerical calculations.

* This work was supported by the AEC.

[1] See E. J. Konopinski, Revs. Modern Phys. **15**, 209 (1943).

[2] Mayer, Moszkowski, and Nordheim, Argonne National Laboratory Report 4626 (1951); see also A. G. Petschek, Rochester Report 3035 (1951).

[3] Zavel'ski, Umarov, and Matushevski [J. Exptl. Theor. Physiks (U.S.S.R.) **19**, 1136 (1949), reported in Brookhaven Guide to Russian Scientific Periodical Literature **3**, 147 (1950)] have claimed that a very weak γ-ray (with an intensity of 0.1 percent) accompanies the β-decay of RaE; this claim, however, has not been substantiated by any of the numerous experimentalists who have studied RaE.

[4] Compare Flammersfeld, Z. Physik **112**, 727 (1939); G. J. Neary, Proc. Roy. Soc. (London) **A175**, 71 (1940) and most recently L. M. Langer and H. C. Price, Jr., Phys. Rev. **76**, 461 (1949) and R. Morrissey and C. S. Wu, Phys. Rev. **75**, 1288 (1949).

[5] Compare M. Fierz, Z. Physik **104**, 553 (1936), and the recent work on the β-decay of H^3 and He^6. We have not applied the de Groot condition [S. R. de Groot and H. A. Tolhoek, Physica **16**, 456 (1950)] because there is no experimental evidence to support it.

[6] E. J. Konopinski and G. E. Uhlenbeck, Phys. Rev. **60**, 308 (1941).

[7] A. M. Smith, Phys. Rev. **82**, 955 (1951).

[8] M. E. Rose and D. K. Holmes, Oak Ridge National Laboratory Report 1022 (1951); see also Phys. Rev. **83**, 190 (1951). We are indebted to Dr. Rose for correspondence concerning these calculations.

[9] J. R. Reitz, Phys. Rev. **77**, 10 (1950) and R. H. Good, Jr., Thesis, University of Michigan (1951).

[10] L. C. Biedenharn and M. E. Rose, Phys. Rev. **83**, 459 (1951).

Relaxation Effects in Ferromagnetic Resonance*

N. Bloembergen and R. W. Damon
Cruft Laboratory, Harvard University, Cambridge, Massachusetts
(Received November 1, 1951)

BY investigating the ferromagnetic resonance effect at high levels of microwave power, the saturation of the electronic spin system has been observed. This experiment, analogous to the saturation effect extensively studied in the nuclear and electronic paramagnetic resonance,[1] provides a means of determining the spin-lattice relaxation time, T_1, which is the characteristic time describing the transfer of energy from the spin system to the crystal lattice. The word "saturation," as used here, denotes a heating-up of the spin system, and so is used in a different way than is customary in connection with ferromagnetism.

Two methods are used for observing saturation. The first is a measurement of the decrease in the imaginary part of the permeability, μ'', as the microwave magnetic field strength, H_1, is increased. There should be a concomitant decrease in M_z, the component of magnetization along the static field, and this is the basis of the second method. The change in M_z is observed by pulsing the microwave field and observing the video voltage induced in a pick-up coil with its axis along the static field. This voltage is proportional to M_0-M_z, where M_0 is the total magnetization, and M_z is the steady-state value of the component of magnetization along the static field when the microwave field is on.

The samples used were single crystals of nickel ferrite,[2] made into spheres of about 0.5-mm diameter. Microwave power was supplied to the rectangular cavity by a magnetron, operating at 9000 Mc/sec. This generated 1-μsec pulses with a repetition rate

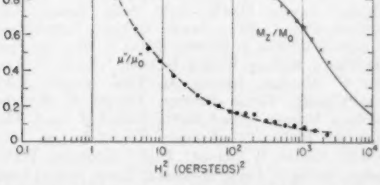

FIG. 1. Normalized curves for μ'' and M_z *vs* microwave field strength. The static field was set to the peak of the ferromagnetic resonance (2800 oersteds) along the [110] crystallographic direction.

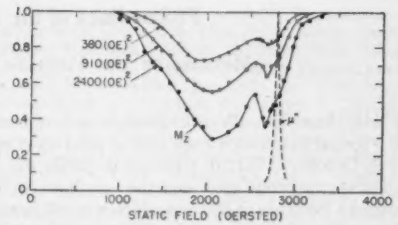

FIG. 2. Normalized results for M_z *vs* H_0 along a [110] axis, H_1^2 being a parameter. The dashed curve is the normalized resonance for μ'' at small values of H_1^2.

of 500 pps. The influence of repetition rate was shown to be negligible, indicating that the over-all heating of the sample was negligible.

From the classical equation of motion[1] for an assembly of magnetic spins, one expects that at resonance μ'' should decrease in proportion to M_z. This is not confirmed by the experimental data shown in Fig. 1. The value for the spin-lattice relaxation time derived from the M_z-curve is $T_1=3\times10^{-8}$ sec.

The dependence of μ'' and M_z on the static field, H_0, is shown in Fig. 2. The changes in M_z occurred over a broad range of H_0, but no effect was observed for field strengths greater than that at which the narrow resonance for μ'' occurs. A second sample gave essentially the same results. Crystalline anisotropy shifted both the μ''- and M_z-curves a few hundred gauss when the sample was rotated, but had no other effect.

The unexpected results clearly show that the spins cannot be treated as a single system with a macroscopic equation of motion for the magnetization vector. On the basis of the spin-wave model, the microwave field creates only spin-waves of very long wavelength. There are only a limited number of these states, and when they are nearly filled, a decrease of μ'' is observed, although the total magnetization has hardly changed. Polder noted that the direct interaction of these long spin-waves with the lattice is weak ($T_1\sim10^{-3}$ sec).[3] It is proposed that the energy of the long spin-waves is transferred to shorter spin-waves, and the rate of this process determines the saturation for μ''.

The transitions at still higher microwave power cause a change in the total magnetization M_z. These transitions, occurring mostly at lower static fields than the regular resonance, represent a breakdown of the selection rule that only spin-waves of zero wave number can be created. Theory and experiment indicate that the presence of lattice imperfections is important for these transitions. In a way which is not understood at present, the quanta absorbed in these processes are readily communicated to the whole spin system. In the steady saturated state the total number of quanta absorbed per unit time is balanced by the number of quanta transferred from the spin system to the lattice, which is equal to the number of spins divided by the relaxation time. In this way a value $T_1=3\times10^{-8}$ sec is obtained. This general argument is independent of any particular model. The spin-wave model is essentially a zero-temperature approximation and is, strictly, not applicable to these experiments where the spins are brought to a very high temperature. Other theoretical treatments[4] also make the approximation that the ferromagnetic spins are not highly excited, and are therefore not very helpful in this case.

The measurements will be extended over a range of temperatures to obtain more information about the relaxation process.

* This work was supported by the ONR.

[1] F. Bloch, Phys. Rev. **70**, 460 (1946); Bloembergen, Purcell, and Pound, Phys. Rev. **73**, 679 (1948); C. Kittel, Phys. Rev. **73**, 155 (1948); C. P. Slichter, thesis, Harvard University (1949).

[2] Supplied through the courtesy of Bell Telephone Laboratories, Murray Hill, New Jersey.

[3] D. Polder, Phil. Mag. **40**, 99 (1949); C. Kittel (private communication).

[4] J. H. Van Vleck, Phys. Rev. **78**, 266 (1950).

Proceedings of the American Physical Society

Minutes of the Meeting at Chicago, October 24–27, 1951

THE American Physical Society is not accustomed to taking a back seat at joint meetings; but in October, 1951, in Chicago it gladly did so, according the front seat and the spotlight to the American Institute of Physics which was celebrating its vigintennial. For several years our conventions at New York and at Washington have systematically been the largest assemblies of physicists that ever took place anywhere: but now we yield the palm to the Institute, which amassed no fewer than 3500 registrations, gathered 3000 people into the Civic Opera House during Thursday October 25, and assembled 850 at the banquet on Thursday evening. Fourteen hundred and fifty-eight of the registrants admitted to membership in our Society; it is to be presumed that many others conceded the fact by omission from their registration cards. A description of these affairs is published in *Physics Today*. The office of the Society is not displeased by the fact that, for once, the work of administering the meetings fell on other shoulders than those of its own deputies, and the University of Chicago got a well-deserved vacation from its annual stint of playing host to us. The Secretary publishes his personal gratitude to Mr. Wallace Waterfall and Miss Ruth Bryans for supervising the publication of the Chicago *Bulletin* and to Messrs. R. M. Bozorth, G. E. Moore, Gerald Oster, E. O. Salant, A. L. Schawlow, and R. L. Serber for distributing the papers into sessions.

The program of the meeting is republished here exactly as it stood in the Bulletin, with a subsequent page of errata. As it makes clear, the meetings of our Society were held on Wednesday afternoon (October 24) and on Friday and Saturday. Those held on Thursday are also listed here, but the credit for these belongs to the Institute.

The Council of the Society met on Friday evening. It elected to Fellowship Seymour Bernstein, S. K. Haynes, C. G. Shull, and J. A. Van den Akker, and to Membership three hundred and thirteen candidates whose names are appended. G. B. Pegram and C. C. Lauritsen were nominated for three-year terms to the Governing Board of the American Institute of Physics; K. K. Darrow and H. H. Nielsen were appointed to the United States National Committee of the International Union of Pure and Applied Physics. Preliminary steps were taken toward an elevation of dues, page charge (for articles in *The Physical Review*), and subscription rate of *The Physical Review* to nonmembers of the Society. This is necessitated by the continuing expansion of *The Physical Review* and rise in the unit costs of publication, which have already been reflected in a serious deficit incurred by the Society in its 1951 operations.

Elected to Membership: Abraham Abramowitz, Hans Aeppli, Pierre R. Aigrain, Heinz Albers-Schoenberg, Kurt Alder, Gentaro Araki, James S. Arthur, William R. Atkinson, Stanley Backer, Leo L. Baggerly, Silvio J. Balestrini, David A. Barge, Robert L. Barringer, Alexander Basil, Chester F. Bass, Theodore Baurer, Robert L. Becker, Stewart Becker, Arthur Beiser, Frank P. Beitel, Jr., Martin Berger, Martin J. Berger, Arthur I. Berman, Virgil J. Barry, Jr., Satyendra K. Bhattacherjee, Hans Bichsel, Frank E. Bjorkland, Nicolaas Bloembergen, Mortimer C. Bloom, Louis P. Bolgiano, Jr., Jose V. Bonet, S.J., Joseph R. Bookee, Robert S. Bradford, William T. Brahmstedt, Carter D. Broyles, Charles E. Buchwald, Lauren H. Bullis, James L. Burkhardt, Clyde R. Burnett, Antonio E. P. Cabral, Ilse R. Callomon, Richard H. Capps, John G. Carver, Harvey Casson, Victoria G. Castro, Chia-hua Chang, Raymond M. Chang, Russell H. Christian, Morton L. E. Chwalow, Edward N. Clarke, Harold E. Clearman, Joseph Cohen, James A. Collinson, A. Allen Comstock, Claude E. Cooke, Jr., C. Dewey Cooper, John J. Corrigan, Jerry A. Cowen, James L. Cox, Glenn A. Crosby, Frances R. Culver, James B. Cumming, Sperry E. Darden, Jr., Henry C. Daubert, Jr., Paul O. Davey, Abram Davis, William E. Deeds, Clive O. De Long, Jr., Robert L. Doan, Douglas J. Donahue, William R. Drake, James A. Dreesen, Victor W. Drexelius, James E. Drummond, Lawrence Dunkelman, Jerome Eckerman, Walter F. Edgell, Donald A. Edwards, Samuel F. Edwards, David F. Eggers, Henry Ehrenreich, Yehuda Eisenberg, Charles Ekstein, Bruce V. English, Walter Shaffer Ernst, Jr., Daryl D. Errett, Harold P. Eubank, George E. Evans, Robert G. Evans, William H. Evans, James E. Faulkner, Ralph Feder, George Feher, Joseph Feinstein, Robert L. Feldmann, Seymour I. Finkel, George W. Ford, Roberto I. M. G. Forneris, John David Fox, Wilfred D. Francis, Eli H. Freedman, William F. Fry, Hiroshi Fuknda, John W. Gardner, Isadore L. Gelles, Mervin H. Gilbert, Edward W. Girard, Allen N. Goland, Jose Goldemberg, Myron L. Good, James M. Goode, Shigeo Goto, Gordon R. Gottloeb, William H. Gust, Melvin N. Hack, Jay E. Hammel, Richard W. Hannum, Donald F. Hansen, Francis H. Harlow, Jr., William H. Harwood, William B. Hawkins, Jr., Miles V. V. Hayes, George E. Hays, Richard I. C. Hede, Richard M. Hedges, Ernst Heer, Robert Herr, Earl W. Hessee, Kenneth A. Hoagland, David S. Hoffman, Jack M. Hollander, Charles W. Hoover, Jr., Arnold Honig, Nahmin Horwitz, Yu-Chang Hsieh, Edward J. Huibregtse, Floyd B. Humphrey, William H. Hyslop, George J. Igo, Takehiko Ishizu, Theodore Jarvis, Louis R. Jauneau, David Jeffries, Robert G. Johnson, William Bruce Johnson, Friedrich A. Kaempffer, George Dewitt Kahl, Selig Kainer, Susumu Kamefuchi, Evan O. Kane, Arnold M. Karo, Rokuo Kawabe, Heiji Kawai, William J. Kearns, David T. Keating, Frederic Keffer, Paul J. Kellogg, William H. Kelly, Vincent P. Kenney, Arthur K. Kerman, Maung M. Kha, Ryoichi Kikuchi, Ki-ichi Kimura, Vivian Kramer, Donald E. Kreinheder, Theodore J. Krieger, John A. Kurtz, Robert H. Land, Thomas W. Layton, Richard D. Leamer, Robert J. Lee, Jack R. Leibowitz, Andrew W. Lennert, Paul J. Leurgans, Walter F. Leverton, Irving E. Levy, Sheldon L. Levy, Robert Lindsay, David E. Little, John T. Lund, Jr., William G. Machell, Robert P. MacKenzie, Robert J. Mackin, Jr., Karl G.

Malmfors, Donald E. Maxwell, John E. May, Jr., Endre A. Mayer, Carlyle D. McKay, Jack McLain, William D. McCoy, William H. Meiklejohn, Eric E. Metzger, Norman J. Meyer, Aubrey B. Mickelwait, Vaden W. Miles, James W. Miller, Leston W. Miller, Frederick E. Mills, Robert G. Mills, Yang L. Ming, San-ichiro Mizushima, Alvie O. Mooneyham, Jr., Donald P. Moore, Peter G. Moore, Bernard Mozer, Lyman Mower, Thomas R. Munson, John L. Need, Ronald G. Newburgh, William J. Noble, Koreichi Ogata, Walter T. Ogier, Raymond S. Ogrinc, Mladen Paic, Lowell S. Pelfrey, James R. Peterson, Thomas E. Petriken, Sebastian Pietropinto, Sergio P. Porto, Francisco E. Prats, Harold R. Raemer, Ernest C. Ray, W. Thornton Read, Jr., Howard L. Recht, Kenneth B. Rhodes, James W. Riggs, Jr., Hugh G. Robinson, Myron Robinson, Charles E. Roland, William S. Rothwell, Virginia V. Royden, Walter Rosenzweig, Sidney Ross, Benjamin Roth, James J. Ruddick, S.J., Klaus Ruedenberg, Lauren J. Rueger, Veikko R. Saari, Mendel Sachs, Harvey G. Safren, Kermit L. Sandefur, Aaron P. Sanders, Frederick L. Scarf, Henry F. Schaf, Jr., Edwin J. Scheibner, Lloyd E. Schilberg, Aurel M. Seifert, Duane C. Sewell, Robert L. Shacklett, Charles B. Shaw, Jr., Sol Skolnik, Bowen E. Simmons, W. Eugene Sinner, Edward F. Smiley, II, Francis F. Skiba, Donald C. Smith, Lyman A. Smith, Richard K. Smyth, Frank T. Solmitz, Hal L. Sowers, M. Lynn Stevenson, Donald H. Stork, Roger A. Strehlow, Seiichi Sueoka, Herbert J. Sukenik, Ivan Supek, Robert M. Sweet, Shuji Takagi, Hideo Takaki, John G. V. Taylor, Donald J. Tendam, Lee C. Teng, Carl D. Thurmond, Jay Todd, Jr., Carl Tatsuo Tomizuka, Frank M. Trantham, Jr., Jacques P. Trembley, Kenneth R. Trigger, George H. Trilling, Hiroomi Umezawa, Minoru Umezawa, Victor A. J. van Lint, James F. Vedder, Alfred R. Vernon, Frederick LeRoy Voelz, Paul F. Wacker, Wilhelm Walcher, LeRoy Walters, Jr., Joe W. Warmuth, William D. Warters, Monroe S. Wechsler, George H. Weiss, Gottfried K. Wehner, LeRoy Dougherty Weld, James A. Weinman, John R. Welty, James A. Whalen, Marian N. Whitehead, Tracy F. Wichmann, Charles H. Wilcox, Lee R. Wilcox, J. Norton Wilson, Robert N. Wilson, John A. Winfrey, Murray M. Winn, Henry H. Woodbury, Ervin C. Woodward, Jr., Sadaaki Yanagawa, Donald E. Young, Tom J. Ypsilantis, Theodore Zang, Harold W. Zeoli, and Sigurd Zienau.

KARL K. DARROW, *Secretary*
American Physical Society
Columbia University
New York 27, N. Y.

Errata Pertaining to Papers C1, C11, E11, H2, H12, I1, I6, I9, I10, I11, P1, and SP1

C1, by R. E. Fox, W. M. Hickam, T. Kjeldaas, Jr., and D. J. Grove. In line 16, $V_R+\Delta_R$ should read $V_R+\Delta V_R$.

C11, by Gilbert W. King. A footnote should be added, reading "This work was sponsored by the ONR under Contract No. N6-onr-228, T. O. II, Project NR 033 243."

E11, by Robert S. Livingston. In line 19, assembyl should read assembly.

H2, by M. M. Block, S. Passman, and W. W. Havens, Jr. In Table I, the results for D and Pb should read:

$2.9\pm1.2\times10^{-28}$ cm^2 sterad^{-1} $1.1\pm0.9\times10^{-28}$ cm^2 sterad^{-1}
$15\pm3.7\times10^{-28}$ cm^2 sterad^{-1} $3.5\pm1.7\times10^{-28}$ cm^2 sterad^{-1}

H12, by S. B. Treiman. In the last sentence, 20 and 600 8-cm^{-2} should read 200 and 600 g-cm^{-2}.

I1, by Peter Havas. Footnote 2 should read H. Steinwedel, S.-B Heidelberger Akad. Wiss., . . . instead of H. Steinwedel and S.-B Heidelberger, Akad. Wiss., ...

I6, by E. J. Schremp. In line 13, and should read an. In line 17, varities should read varieties.

I9, by Frederik J. Belinfante. In line 11, $\mathfrak{a}=\mathfrak{A}-\mathbf{U}_{\text{II}}$ should read $\mathfrak{a}=\mathfrak{A}-\mathbf{U}_{\perp}$. In line 16, $\mathfrak{E}=\mathfrak{E}_{\perp}+\mathbf{E}_{\text{II}}$ should read $\mathbf{E}=\mathfrak{E}+\mathbf{E}_{\text{II}}$.

I10, by Jerome Rothstein. In lines 8 and 9, measurement or observation of objects to grouping them in classes should read measurement or observation of objects leads to grouping them in classes. In reference 1, Phys. Rev. **82**, 322 (A) (1951) should read Science **114**, 171 (1951).

I11, by B. Liebowitz. In the formula for α $\left[1+\frac{4e}{Nm}\left(\frac{3}{2G}\right)\right]^{\frac{1}{2}}$ should read $\left[1+\frac{4e}{Nm}\left(\frac{3}{2G}\right)^{2}\right]^{\frac{1}{2}}$.

P1, by Donald H. Jacobs, Michael May, and Seymour Scholnick. The name of Michael May should be deleted from the list of authors.

SP1, by Frederik Belinfante. In lines 13 and 14, $\mathfrak{M}x(x')$ should read $\mathfrak{M}(x')$. In line 15, $\mathfrak{E}=\mathbf{D}-4\pi\mathbf{P}$ should read $\mathbf{E}=\mathbf{D}-4\pi\mathbf{P}$.

PROGRAMME

WEDNESDAY AFTERNOON AT 2:00

Morrison, Roosevelt Room

(R. S. MULLIKEN presiding)

Programme of the Division of Chemical Physics

AA1. Some Contributions to the Theory of Molecular Structure. JOHN E. LENNARD-JONES, *Cambridge University.* (45 min.)

AA2. The Photochemistry of Condensed Systems as Illustrated by the Optical Sensitization of the Photographic Emulsion. W. WEST, *Kodak Research Laboratories.* (45 min.)

AA3. The Theory of the Critical Point. BRUNO H. ZIMM, *General Electric Research Laboratories.* (45 min.)

THURSDAY MORNING AT 9:30

Chicago Civic Opera House

(GEORGE R. HARRISON presiding)

Joint Symposium on Physics Today with the Member Societies of the American Institute of Physics

The Nucleus. ENRICO FERMI, *University of Chicago.*
The Atom. E. U. CONDON, *Corning Glass Works.*
The Solid State. J. C. SLATER, *Massachusetts Institute of Technology.*

THURSDAY AFTERNOON AT 2:00

Chicago Civic Opera House

(GEORGE R. HARRISON presiding)

Joint Symposium on Physics Today (continued)

Acoustics. HARVEY FLETCHER, *Columbia University.*
Optics. EDWIN H. LAND, *Polaroid Corporation.*
Physics as Science and Art. K. K. DARROW, *Bell Telephone Laboratories.*

THURSDAY EVENING AT 7:30

Hotel Sherman, Grand Ballroom

(PAUL E. KLOPSTEG presiding)

Joint Banquet with the Member Societies of the American Institute of Physics

(Title to be announced). KARL T. COMPTON, *Chairman of the Corporation, Massachusetts Institute of Technology.*
(Title to be announced). THE HONORABLE BRIEN MCMAHON, *U. S. Senator from Connecticut.*

FRIDAY MORNING AT 9:30

Sherman, Louis XVI Room

(S. K. ALLISON presiding)

Nuclear Scattering

A1. The Theory of Neutron Scattering by Gases. N. K. POPE AND G. FELDMAN, *Chalk River Laboratory.*—The calculation of the differential cross section for neutron scattering by gas molecules requires summations over all the initial and final states of the molecule. For rigid molecules with infinite mass and infinite moment of inertia, the cross section can be reduced to a simple form analogous to that used in the scattering of x-rays.[1] However, even when allowance is made for the vibration of the nuclei,[1] the simplified expression gives a poor representation of the experimental cross sections for molecules such as H_2 and CH_4. A better approximation to the cross section has been obtained as an expansion in powers of two parameters, *viz.*, the ratio of the neutron mass to the molecular mass, and the ratio of the energy of the first excited rotational state to the energy of the incident neutron. Differential cross sections have been calculated for diatomic and spherical top molecules and have been compared with experimental results.

[1] N. K. Pope, Royal Society of Canada, June meeting, 1951, Paper 75.

A2. Scattering by Bound Particles with Short-Range Interaction Force. H. EKSTEIN, *Illinois Institute of Technology.*—For forces which are large over a small distance, Born's approximation is unsatisfactory. An alternative expansion is obtained by transforming the scattering equations so that the interaction potential is eliminated and replaced by a matrix α which describes the scattering by a *fixed* particle, in a manner analogous to that used in the discussion of multiple scattering by fixed centers.[1] The rigorous equation so obtained can be solved by iteration. The first approximation is formally the same as Born's first approximation, with α replacing the interaction potential between incident particle and scattering particles, but the higher approximations are different; in particular, they are convergent for the limiting case of point scatterers, where the second Born approximation diverges. For this particular case of point scatterers, the first approximation is identical with the result obtained by Fermi for the scattering of neutrons by bound protons.

[1] H. Eckstein, Phys. Rev. **83**, 721 (1951).

A3. Regular Meson Type Potentials in Proton-Proton Scattering.* R. D. HATCHER AND H. E. HART,† *New York University.*—Results of low energy proton-proton scattering using a meson potential give a mass for the π-meson[1] (316 times the mass of the electron) which is larger than that observed experimentally (275 m). Calculations show that a modification of the potential used will give results agreeing with the lower value. The potential used has the form $V=(1-e^{-x})(1/x-Ce^{-2x}/x)mc^2$ where C is a pure number parameter, and x is mc^2r/e^2. This potential has in addition the property of being everywhere finite. Alternate forms of these meson type potentials will be considered. Perturbation calculations which show the effect of the nuclear distance coulomb modification on the hydrogen atom and other applications will be discussed.

* This work was supported by the ONR.
† On leave of absence, Board of Education, New York City.
[1] G. Breit and R. D. Hatcher, Phys. Rev. **78**, 110 (1950).

A4. Total Cross Sections of Carbon and Hydrogen for 14-Mev Neutrons.* H. L. POSS, E. O. SALANT, AND L. C. L. YUAN, *Brookhaven National Laboratory.*—Carbon and hydrogen total cross sections for 14-Mev neutrons[1] were redetermined to a probable error of 1 percent. Thick zirconium-tritium targets were bombarded by 400-kev deuterons of Department of Terrestrial Magnetism's electrostatic generator. Neutrons were detected by a terphenyl-xylene scintillation counter, efficiency 5 percent.[2] They were monitored by counting the alpha-particles from the reaction. Source to detector distance: 40 in.; scatterer diameter: 1 in., so that only 0.2 percent of incident neutrons were scattered into detector for the thickest scatterer. Counting rate was about 2000/min. Neutron background of 6 percent was determined with 13-in. copper cylinder in neutron beam. A least-squares analysis of the transmission of six thicknesses each of carbon and polyethylene (40 to 85 percent transmission) gives the following total cross sections: $\sigma_C=1.279\pm0.004$ b, $\sigma_A=0.689\pm0.005$ b for an effective neutron energy evaluated to be 14.08 ± 0.05 Mev.[3]

* Research carried out under the auspices of the AEC.
[1] E. O. Salant and N. F. Ramsey, Phys. Rev. **57**, 1075 (1940). Ageno, Amaldi, Bocchiarelli, and Trabacchi, Phys. Rev. **71**, 20 (1947). W. Sleator, Phys. Rev. **72**, 207 (1947).
[2] Falk, Poss, and Yuan, Phys. Rev. **83**, 176 (1951).
[3] G. Snow, following abstract.

A5. Analysis of 14-Mev $n-p$ Scattering.* GEORGE SNOW, *Brookhaven National Laboratory.*—The total S-wave $n-p$ scattering cross section can be written[1]

$$\sigma^{(s)}_{\text{total}}=\sigma_{\text{triplet}}+\sigma_{\text{singlet}}$$
$$=\frac{3\pi}{[k^2+(\alpha_t-\frac{1}{2}\rho_{0t}k^2)^2]}+\frac{\pi}{[k^2+(\alpha_s-\frac{1}{2}\rho_{0s}k^2)^2]}. \quad (1)$$

α_t, r_{0t}, and α_s are determined from low energy data. Hence $\sigma^{(s)}_{\text{total}}$ is a function of unknown effective singlet range, r_{0s}, for an assumed well shape, if neutron energy is known. The neutron energy distribution from the $D-T$ reaction used above[2] has been calculated. 95 percent of the neutrons have relativistic kinetic energies between 13.88 and 14.23 Mev, and $[\langle(1/En)\rangle]^{-1}=14.08\pm0.05$ Mev. From experimental $n-p$ cross section[2] and Eq. (1), r_{0s} has been obtained for three choices of potential well shape; square (S), exponential (E), and Yukawa (Y). Exact S-wave phase shifts have also been calculated and resultant small corrections to $\sigma^{(s)}$ of Eq. (1) have been made. Results are $r_{0s}=2.23\pm0.25(S)$, $r_{0s}=2.28\pm0.33(E)$, $r_{0s}=2.29\pm0.40(Y)$.

* Research carried out under the auspices of the AEC.
[1] J. M. Blatt and J. D. Jackson, Phys. Rev. **76**, 18 (1949).
[2] Poss, Salant, and Yuan, preceding abstract.

A6. The Scattering of 30-Mev Alpha-Particles by Helium.* E. GRAVES,† *Massachusetts Institute of Technology.*—The angular distribution of elastic scattering of 30-Mev alpha-particles by helium has been measured using the emergent beam of the MIT cyclotron. The distribution has structure with broad maxima in the regions of $\theta'=53°$ and 90° in the center-of-mass system and minima at $\theta'=40°$ and 70° and rises strongly forward of $\theta'=40°$. Scattered alpha-particles were detected with a triple proportional counter, which could be rotated within a 2-foot diameter scattering chamber filled with helium. The absolute differential cross section was measured by comparison with the scattering from an Au foil target to be $(2.8\pm1.4)\times10^{-26}$ cm²/steradian at $\theta'=83.3°$. It has been suggested that the maxima and minima appear indicative of a well-defined diffraction of the DeBroglie wave amplitude associated with the motion of the alpha-particles by the interaction potential between them.

* This work has been assisted in part by the joint program of the ONR and AEC.
† Major, USA, assigned as student at MIT.

A7. Classification of Levels in Al^{28}.* L. J. KOESTER,†‡ *University of Wisconsin.*—A phase shift analysis[1] of the elastic scattering of protons by Mg^{24} has been completed. This work has yielded information regarding the angular momentum and parity quantum numbers of levels observed in Al^{28}. In the region of bombarding energies between 0.4 and 3.4 Mev, the general trend of the differential scattering cross section is well fitted by a combination of the effects of potential scattering (including coulomb) and of the three observed broad resonances. The parities, relative to Mg^{24}, of most of the narrow resonances are determined. A twofold ambiguity remains in their angular momentum quantum numbers because the experimental resolution was not sufficient to give the true maximum cross sections of the very narrow peaks. These excited states of Al^{28} are considered from the viewpoint of the shell model of the nucleus.

* Work supported by the AEC and the Wisconsin Alumni Research Foundation.
† AEC Predoctoral Fellow.
‡ Now at University of Illinois, Urbana, Illinois.
[1] Koester, Goldberg, Kaufmann, Mooring, and Saxon, Phys. Rev. **83**, 219(A) (1951).

A8. Precision Scattering Project.* JAMES S. ARTHUR, A. J. ALLEN, R. S. BENDER, R. L. ELY, H. J. HAUSMAN, L. A. PAGE, AND E. M. REILLEY, *University of Pittsburgh.*—A description is given of the performance of the apparatus for the Precision Scattering Project at the University of Pittsburgh. The scattering chamber is located in a subterranean room built in the hillside adjacent to the cyclotron. An 8-foot wall serves as shielding between the cyclotron and scattering room. A 6-ton focusing electromagnet directs the beam from the 47-inch cyclotron into the underground room through the shielding. A 40° uniform field, magnetic analyzer provides a beam of 0.5 microampere of 8-Mev protons with energy spread ±10 kev through $\frac{1}{8}$th inch analyzing slits. A similar magnet can be rotated about the target to analyze charged product particles of nuclear reactions at angles from 0° to 150°. Trimming and calibrating the magnets were achieved using polonium alpha-particles (values reproducible with a probable error in momentum of ±0.04 percent). The magnetic fields are electronically regulated and measured by the nuclear magnetic resonance method to better than 1 part in 5000.

* Work done in the Sarah Mellon Scaife Radiation Laboratory and assisted by the joint program of the ONR and AEC.

A9. Energy Levels in Al^{27}. E. M. REILLEY, A. J. ALLEN, J. S. ARTHUR, R. S. BENDER, R. L. ELY, AND H. J. HAUSMAN, *University of Pittsburgh.**—Twenty-two energy levels in Al^{27} have been found by the magnetic analysis of inelastically scattered protons at 90° from thin targets of aluminum. An analyzed beam of 8.0-Mev protons was utilized for the bombardment. Tentative values for the levels found are 0.810, 0.985, 2.253, 2.571, 3.041, 3.377, 3.727, 3.931, 4.008, 4.108, 4.288, 4.464, 4.568, 4.638, 4.864, 4.988, 5.110, 5.212, 5.352, 5.496, 5.560, and 5.615 Mev. A broad alpha-particle group from the $Al^{27}(p, d)Mg^{26}$ reaction corresponding to an excited state of Mg^{26} was also observed and is believed to be complex.

* Work done in the Sarah Mellon Scaife Radiation Laboratory and assisted by the joint program of the ONR and AEC.

A10. Inelastic Scattering of Protons from Nickel.* RALPH ELY, JR., A. J. ALLEN, J. S. ARTHUR, R. S. BENDER, H. J. HAUSMAN, AND E. M. REILLEY, *University of Pittsburgh.*—Using the equipment developed for the Precision Scattering Project at the University of Pittsburgh, inelastic scattering of 8-Mev protons from a thin nickel target has been observed at 90°. The sixteen energy levels obtained for natural nickel are 1.338, 1.475, 2.185, 2.497, 2.660, 2.812, 2.945, 3.083, 3.162, 3.227, 3.308, 3.465, 3.567, 3.642, 3.824, 3.943 Mev. At present, only the three levels 1.338, 1.475, 2.497 Mev can be assigned to nickel 60 from comparison with beta-decay of cobalt 60.

* Work done in the Sarah Mellon Scaife Radiation Laboratory and assisted by the joint program of the ONR and AEC.

A11. Total Cross Sections of Heavy Nuclei for Fast Neutrons.* D. W. MILLER,† R. E. FIELDS, AND C. K. BOCKELMAN, *University of Wisconsin.*—The total cross sections of twenty-three heavy nuclei from iron to bismuth were determined as a function of neutron energy. Monoenergetic neutrons in the energy range from 0.02 to 3.2 Mev were obtained by bombardment of thin lithium or Zr-T targets with protons from the electrostatic generator. Total cross sections of the closed-shell nuclei strontium, yttrium, barium, lanthanum, cerium, and praseodymium were measured at intervals of 0.02 Mev from 0.02 Mev to 1.4 Mev, and at about 0.15-Mev intervals from 1.4 Mev to 3.2 Mev. Using somewhat wider point separations, niobium and molybdenum were investigated from 0.1 Mev to 3.2 Mev. In addition, earlier results obtained at Wisconsin below 1.4 Mev for fifteen other heavy nuclei were extended to 3.2 Mev using about 0.15-Mev spacing between points. A broad maximum occurs in the total cross sections of the heavier elements. This maximum appears to move to higher neutron energies with increasing mass number.

* Work supported by the AEC and the Wisconsin Alumni Research Foundation.
† AEC Predoctoral Fellow.

A12. The Calculation of High Energy Scattering Cross Sections Using Variational Methods.* DAVID S. SAXON, *National Bureau of Standards* AND E. GERJUOY, *University of Southern California.*—High energy elastic scattering by a square well and by a Yukawa potential have been calculated using variational methods.[1] The actual application of these methods depends, of course, upon the evaluation of rather intricate integrals involving products of trial functions and the Green's function. For a trial function which consists of a plane wave with a suitably modified wave number in the interior of the scattering potential, the integrals can be evaluated in closed form, at least for forward scattering, and hence a rather simple expression can be obtained for the total cross section. The results are strikingly better than the Born approximation as indicated by comparison with exact calculations. As an example, for neutron-proton square well scattering, the variational results are within a few percent of the exact results of Camac and Bethe[2] over the energy range from 20 to 80 Mev. The extension to the case of exchange forces will be discussed.

* The preparation of this paper was sponsored (in part) by the ONR.
[1] J. Schwinger, hectographed notes on nuclear physics, Harvard (1947).
[2] M. Camac and H. A. Bethe, Phys. Rev. **73**, 191 (1948).

FRIDAY MORNING AT 9:30

Sherman, West Room

(N. S. GINGRICH presiding)

Electron Physics

B1. The Effect of the Thermal Velocity Distribution upon the Behavior of Diodes at Microwave Frequencies. P. PARZEN, *Federal Telecommunication Laboratories, Inc.*—Hahn[1] has shown that it is possible to account for the effect of the thermal velocity distribution on the dc properties of diodes by including a pressure term in the equation of motion. It is possible to

extend this method to higher frequencies and thereby compute the ac impedance and noise fluctuations of diodes. The results obtained by this method will be compared to those of Llewellyn[2] and Rack.[3] One of the fundamental results is that the process being classified as low or high frequency depends upon whether the frequency is much smaller or much larger than the plasma frequency at the virtual cathode.

[1] W. C. Hahn, Proc. Inst. Radio Engrs. 36, No. 9, 1115 (September, 1948).
[2] F. B. Llewellyn, *Electron Inertia Effects* (Cambridge University Press).
[3] A. J. Rack, Bell System Tech. J. 17, No. 4, 592 (October, 1938).

B2. On the Influence of Field on Temperature Saturated Emission from Semiconducting Cathodes. K. LEHOVEC, *Signal Corps Engineering Laboratories.*—The negative charge induced on a semiconducting cathode by an applied field may spread over a layer of many lattice spacings thickness. The corresponding potential may amount to several tenths of a volt, modifying the work function of the cathode. The voltage V across the space charge layer was calculated as function of applied field F for the case of positively and negatively charged surface states, respectively, and for full, or partial, or weak ionization of surface states, assuming quasithermal equilibrium conditions and an n-type semiconductor with weakly ionized donors. Under certain conditions the slope of the Schottky-lines may reach values as high as $dV/dF \approx kT/[e(F)]$, which is for $F \approx 100$ volt/cm and $T \approx 1000°K$ nearly two orders of magnitude larger than the slope calculated from deformation of image force potential by applied field.* Thus, the deformation of space charge potential may explain the large "Schottky"-slopes occasionally observed on oxide-coated cathodes, and constitutes an alternative explanation to that based on patch effects.

* W. Schottky, Physik Z. 15, 872 (1914).

B3. A Retarding Potential Method of Measuring the Electrical Conductivity of Oxide Coated Cathodes.* I. L. SPARKS,† *University of Missouri.*—A retarding potential method has been used to study the electrical conductivity of BaO-coated cathodes. This method, which involves a determination of the voltage drop across the coating as thermionic emission is being drawn from the coating, permits conductivity measurements without the use of probes. In a similar method used by Young and Eisenstein[1] it was assumed that the Schottky lowering of the potential barrier at the surface of the cathode was negligible compared with the voltage drop across the coating and that the method was applicable for a wide range of anode voltages. In the study reported here a method is developed which does not involve these assumptions. This method can be used for coatings whose thermionic emission to conductivity ratio is greater than 0.5 volt/cm. Advantages and disadvantages of the method will be given. It is found the slope of the retarding potential curve is less than the expected value, $-e/kT$. A possible explanation of this is given.

* This work supported in part by the ONR.
† Now at Eastern Illinois State College.
[1] A. Eisenstein and J. R. Young, Phys. Rev. 75, 347(A) (1949).

B4. A Study of Evaporated Films of BaO using Electron Diffraction Techniques.* PAUL RUSSELL, *University of Missouri.*—Electron diffraction techniques have been used previously to study compounds in continuously pumped vacuum systems at pressures of the order of 10^{-9} mm. Since thermionically active films of BaO are stable only at much lower pressures, an all-glass, sealed-off diffraction tube was developed which operates at less than 10^{-9} mm. This tube resembles an elongated cathode ray tube using magnetic focusing and deflection. A spectroscopically pure polished Ni sample is set at grazing incidence to the electron beam, about halfway between the gun and the screen. This sample may be heated to elevated temperatures. Above the sample is a Pt evaporator which contains the source of BaO. A movable Ta anode is inserted between the sample and evaporator for thermionic emission measurements. The diffraction pattern appears on a fluorescent screen and is recorded photographically. The diffraction patterns indicate (1) considerable preferred orientation of the first few monolayers laid down on Ni at 800°K, (2) a marked reduction in thermionic emission and change in pattern after heat treatment up to 1200°K, and (3) reduction in preferred orientation for thicker deposits.

* This work supported in part by the ONR.

B5. Microwave Propagation Through an Electronic Space-Charge in a Magnetic Field.* JAMES R. HOOPER, JR.,† *Harvard University.*—A linearly polarized electromagnetic wave traveling through an electronic space-charge in the presence of a magnetic field, parallel to the direction of propagation, is considered. Since the electronic motion is essentially circular about the magnetic lines of force, it is convenient to resolve the linearly polarized wave into two oppositely rotating circular components. The effect of the electron motion may be treated as a contribution to the apparent dielectric constant of the region, which will be different for each sense of circular polarization. Although high vacuum conditions are assumed, damping effects must be considered for magnetic fields near the cyclotron value because the resonant circular electron motion decreases the mean time between collisions with residual gas molecules. In particular, the case of a wave guide terminated in a space-charge is considered. The reflection coefficient is calculated for each sense of circular polarization, and the plane-polarized components reflected parallel to and normal to the incident polarization are calculated by recombining the reflected circular components. Experimental results for a resonant cavity terminated in an electronic space-charge will be presented.

* This research was supported jointly by the ONR and the Signa Corps under ONR Contract N5ori-76, T.O.I.
† Now at Case Institute of Technology, Cleveland, Ohio.

B6. Liquid-Filled Ionization Chambers. M. A. VAN DILLA,* *Massachusetts Institute of Technology.*—The present experimental work deals with the measurement of the energy dissipation of x-rays and gamma-rays by means of the ionization produced in insulating liquids. The liquid chosen was decane, and a collecting field of about 1000 volts per cm was used. Ions, not electrons, are collected since the electrons produced quickly attach to form negative ions. This means that initial recombination plays an important role and prevents saturation from being achieved. At the field strength used the ion current collection was about 5 percent of the ion production. Even so, the current collection per unit energy flux from a decane-filled ion chamber is 25 to 30 times more than that observed in an ion chamber of identical volume filled with a gas at standard temperature and pressure. Experiments on the variation of initial recombination with the quantum energy of the incident photons showed that Jaffe's theory of columnar recombination was inapplicable, and supported Lea's theory of cluster recombination. The variation of ion current collection with radiation intensity, polarizaing voltage and temperature was also measured, and comparisons with theory were made.

* Present address: Department of Physics, University of Utah, Salt Lake City, Utah.

B7. Photoelectric Thresholds in Photon Counters Containing Electronegative Quenching Gases. H. FRIEDMAN, T. CHUBB, AND D. A. PATTERSON, *U. S. Naval Research Labora-*

tory.—The spectral response of counter tubes to extreme ultraviolet light was measured with the aid of a vacuum monochromator. Observations were limited by the use of LiF windows to wavelengths above about 1050A. The admixture of small amounts of any strongly electronegative gases invariably produced a marked shift of the threshold toward the ultraviolet. Traces of chlorine, bromine, and halogenated hydrocarbons increased photoelectric threshold energies to roughly twice the values of the cathode surfaces in vacuum. Since, in counters containing halogen gases, the ionization potential of none of the gas ions exceeds twice the work function of the cathode, spurious counts due to positive ion neutralization at the cathode surface are largely absent.

B8. Drift Velocity of Electrons in Pure Gases.* D. D. ERRETT† AND F. F. RIEKE, *Purdue University.*—A pulse method for measuring the drift velocity of electrons in gases, described in a previous abstract,[1] has been improved and the apparatus modified so as to permit measurements on gases of high purity. The accuracy is estimated to be 3 percent for the smaller velocities; the errors become somewhat greater for velocities above 4×10^6 cm/sec. Measurements have been made on argon, helium, hydrogen, nitrogen, carbon dioxide, and water vapor. For each gas studied, the velocity proved to be uniquely determined by E/p, the ratio of field strength to pressure (expressed throughout in units of volts/cm/mm Hg). For helium and argon, comparison is made with the drift velocities calculated by Harriet Allen.[2] For helium, the agreement is excellent over the entire range of the calculations ($E/p<4$). For argon, the agreement is close for $E/p<2.5$; at higher field strengths the theoretical values rise above the experimental, presumably because of neglect of inelastic collisions. Rigorous calculations exist for only these two gases. Comparison with previously published measurements shows fairly good concordance of results for He, H_2, N_2, and CO_2. Existing data on water vapor is scanty and in poor agreement with the new results. In the course of measurements on argon, a delayed emission of electrons was observed at the larger values of E/p; this effect is attributed to indirect ionization through the agency of metastable atoms. Evidence was obtained that in water vapor the attachment of electrons to form negative ions is small for $E/p<10$, strong for E/p between 10 and 16, and somewhat less at higher values.

* Assisted by the ONR and AEC.
† Present address: North American Aviation, Inc., Downey, California.
[1] F. F. Rieke and D. Errett, Phys. Rev. **75**, 346(A) (1949).
[2] H. W. Allen, Phys. Rev. **52**, 707 (1937).

B9. Drift Velocity of Electrons in Gas Mixtures.* F. F. RIEKE AND D. D. ERRETT,† *Purdue University.*—The drift velocity of electrons has been measured as a function of E/p in 12 different argon-hydrogen, argon-nitrogen, and argon-carbon dioxide mixtures by the method described in an accompanying abstract.[1] The gas pressures ranged from 100 mm to 10 mm, and measurements were made to $E/p=20$. As is well known, addition of relatively small amounts of a multi-atomic gas to argon can result in a large increase in the drift velocity. For example, with $E/p=1$ the drift velocity in pure argon is 0.38 cm/μsec, in 0.01 H_2−0.99A it is 1.0 cm/μsec, in 0.01N_2−0.99A it is 2.3 cm/μsec, and in 0.01 CO_2−0.99A it is 1.9 cm/μsec. Families of curves are given to show the dependence of drift velocity on gas composition. The relation of the results to the theory of mixtures developed by Townsend and Bailey[2] is discussed.

* Assisted by the ONR and AEC.
† Present address: North American Aviation, Inc., Downey, California.
[1] D. D. Errett and F. F. Rieke, preceding abstract.
[2] Townsend and Bailey, Phil. Mag. **44**, 1033 (1922).

B10. Influence of Irradiation on the Characteristic of a Glow Discharge in Pure Rare Gases. K. W. MEISSNER AND W. F. MILLER, *Purdue University.*—Irradiation of the positive column of a glow discharge in pure rare gases by the radiation from a second discharge tube containing the same gas influences the $V-I$ characteristic of the irradiated glow discharge, shifting it to higher voltage for the same value of current. This effect was described for neon and helium by Meissner and Pierson[1] and new experiments show the same effect with the other rare gases argon, krypton, and xenon. The effect is explained by the presence of metastable atoms. Irradiation by strongly absorbed radiation diminishes the concentration of metastable atoms, removing them as sources of secondary ionization.—In the case of helium it was possible by filtering to study the irradiation effect of the two mainly absorbed lines 10830A and 20851A separately. The whole effect is practically caused by 20851A. This can be understood by considering the possible transitions involved.

[1] K. W. Meissner and R. M. Pierson, Proc. Indiana Acad. Sci. for 1949, **59**, 269 (1950).

B11. The Electric Current between Flashes of the Intermittent Glow Discharge in H_2. HERMAN RITOW, *Northwestern University.*—Measured frequencies in intermittent glow discharges indicate an effective capacity exceeding that ordinarily associated with the circuit. In an effort to evaluate this excess capacity at various pressures, measurements were made of the supply current, the starting and extinction potentials, the period of intermittence, and the external capacity. Graphical analyses of the data indicate that between luminous flashes, a leakage current ("dark current") flows between the electrodes. The average value of this current is constant when the supply current is constant. When the pressure is high the net dark current is in the same direction as the supply. When the pressure is less than that corresponding to the Paschen P×D minimum, it is opposite in direction to the supply current. At very low pressures the returning dark current may be many times the supply, while at very high pressures it may be a large fraction, half or more, of the supply current. Large electrode areas and separations increased the volume of the ionized gas and hence the charge many times over the values usually used in discharge experiments.

B12. Spectroscopic Investigations of Pulsed Gas Discharges.* W. R. ATKINSON, R. G. FOWLER, L. W. MARKS, AND G. W. CHARLES, *University of Oklahoma.*—Pulsed discharges in hydrogen, expanding as fronts into side tubes, were previously† shown to exhibit broadening of the Balmer lines, and intense continua. High resolution spectra show line contours appropriate to Stark broadening. Ion concentrations have therefore been calculated from this broadening by Holtzmark's theory. Maximum values of as much as 10^{17} ions per cc are observed. The magnitude of the maximum is proportional to the initial gas density, and its location is always at some point *in the side tube.* The maximum occurs at an instant in time independent of gas density and firing potential. The continuum beyond the last observable Balmer series member is shown to be of nonmolecular origin by experiments with water vapor. The level of excitation in the fronts is so high that O IV and C IV are observable. Total intensity measurements on H_β as a function of ion concentration have shown the intensity varies as the square of the concentration. This, together with the magnitudes of the observed concentrations, which frequently amount to half the original particle density in the tube, is strongly indicative of radiative recombination.

* Project supported by the ONR.
† R. G. Fowler, *et al.*, Phys. Rev. **82**, 879 (1951).

FRIDAY MORNING AT 9:30

Sherman, Grey Room

(J. E. MAYER presiding)

Chemical Physics

C1. Direct Measurement of Ionization Probability and Appearance Potential Using a Mass Spectrometer. R. E. FOX, W. M. HICKAM, T. KJELDAAS, JR., AND D. J. GROVE. *Westinghouse Research Laboratories.*—A retarding potential V_R is applied to one of the plates so that the low energy electrons are removed from the distribution. By measuring the change in the electron and ion currents when V_R is changed by ΔV_R, one may obtain the ionization probability as a function of the electron accelerating potential V_i, for electrons monoenergetic within ΔV_R. To remove the ions it is necessary to have a field in the ionization chamber. This field and the electron current is given a pulsed time dependence, so that when electrons are moving through the ionization chamber it constitutes a field free region. Space charge is minimized by using a small electron current. The value of V_i for vanishing ion current difference when added to $V_R+\Delta_R$ yields the true appearance potential. Contact potential between the filament and the ionization chamber does not influence this value. Preliminary measurements on a number of gases yielded appearance potentials within 0.1 volt of the spectroscopic value. Circuit improvements are being made in order to obtain increased accuracy.

C2. Van der Waals Forces in Magnetic Fields.* HENRY MARGENAU AND D. E. HARRISON, *Yale University.*—Formulas are worked out for the dispersion forces between molecules satisfying Hund's case *b*, the assumption being that these molecules interact in different magnetic states. In earlier publications, a simplifying average is taken over all magnetic states. This procedure is legitimate for most applications of the theory of Van der Waals forces, but not to the broadening of spectral lines absorbed or emitted in a magnetic field, which has recently been observed with great accuracy by microwave techniques. The work reported here consists mainly in a collection and combination of known matrix elements of the diatomic molecule and results in formulas of considerable complexity. Their numerical evaluation was carried out for O_2. We then inquired whether there is a correlation between the strength of these forces in different magnetic states and the width of lines originating from these states, these widths having been measured by Beringer and Castle.[1] The answer is negative and suggests complications with which the present (second order) theory cannot deal.

* Supported by the ONR.
[1] R. Beringer and J. G. Castle, Phys. Rev. **81**, 82 (1951).

C3. Calculations of the Diamagnetic Susceptibility of N_2. J. V. BONET AND A. V. BUSHKOVITCH, *Saint Louis University.*—The only straightforward quantum-mechanical calculation of the diamagnetic susceptibility of gases carried out so far appears to be that for H_2 by Van Vleck and Frank. We have attempted to calculate the diamagnetic term in the susceptibility of N_2 using a combination of the Fermi-Thomas method as applied to homonuclear molecules by Hund, and the Slater atomic orbital method. The Fermi-Thomas charge distribution is used in the region from the center of the molecule to a distance of 2 angstroms, where this approximation may be expected to be good. From 2 angstroms out, where spherical symmetry may be expected to be a good approximation, Slater atomic orbitals for silicon (double the charge of N_2) are used. The result is 2.3 times the observed value, part of the excess being probably due to the small paramagnetic term. This is a substantial improvement over the straight Fermi-Thomas method which was found, by Sommerfeld, to give ten times the observed result in the case of monatomic gases. The chief cause of the discrepancy is undoubtedly the neglect of the exchange effect in the Fermi-Thomas method. Calculations using the Fermi-Thomas-Dirac equation (with exchange) are in progress. The methods used can be extended to other homonuclear molecules.

C4. Excitation and De-Excitation of the Vibrational Motion of Hydrogen Molecules by Slow Hydrogen Atoms. E. BAUER, *National Research Laboratories.*—An interaction potential between a hydrogen molecule and a hydrogen atom based on one between a hydrogen molecule and an electric charge[1] is used. The cross section is calculated by using the Born approximation and corrected by multiplying it by the square of the ratio of exact to sine wave matrix element of the same process in one dimension.[2] The cross section for de-excitation of the first vibration state, σ_{10}, is obtained from the excitation cross section by using the principle of detailed balance. At gas kinetic energies σ_{10} is of the order 10^{-19} cm^2, so that one in 10^3–10^4 collisions produces de-excitation. The probability of recombination of two hydrogen atoms in a three-body collision in which the two atoms are de-excited from the vibrational continuum to a discrete state of the hydrogen molecule near the continuum is also estimated.

[1] T. Y. Wu, Phys. Rev. **71**, 111 (1947).
[2] E. Bauer, Phys. Rev. (to be published).

C5. Raman and Infrared Spectral Data, Force Constants, and Thermodynamic Properties for Dibromodichloromethane. ABRAM DAVIS, FORREST F. CLEVELAND, AND ARNOLD G. MEISTER, *Illinois Institute of Technology.*—Raman displacements, semiquantitative relative intensities, and precise depolarization factors were obtained for liquid CBr_2Cl_2. The infrared wave numbers for both liquid and gaseous CBr_2Cl_2, in the region 400 to 4000 cm^{-1}, also have been determined, using a Beckman IR-2 (KBr optics) spectrometer. Present values for these spectral data were compared with the results of the two previous investigators in order to decide upon the most probable values of the fundamentals. The values adopted for these were 154, 175, 230, 242, 262, 380, 684, 734, and 770 cm^{-1}, which agree very well with those of Delwaulle and Francois (1942), but differ considerably with those given by L. Lecomte, Volkringer, and Tchakirian (1937). The Wilson *FG* matrix method was used to calculate wave numbers corresponding to the vibrational frequencies, using force constants taken from CBr_4, CBr_3Cl, $CBrCl_3$, and CCl_4. Modification of these force constants led to calculated wave numbers which were within 1 cm^{-1} of the observed values. The observed fundamentals were then used to calculate heat content, free energy, entropy, and heat capacity for 12 temperatures from 100° to 1000°K to a rigid rotator harmonic oscillator approximation.

C6. Decomposition of Di-*t*-butyl Peroxide and Kinetics of the Gas Phase Reactions of *t*-butoxy Radicals in the Presence of Ethylenimine. DAVID H. VOLMAN AND ROBERT K. BRINTON, *University of California at Davis.*—The reaction of di-*t*-butyl peroxide with ethylenimine has been studied between 129° and 154°C. The *t*-butoxy radicals formed by the rupture of the O—O bond of the peroxide are postulated to enter into the

following reactions: decomposition into acetone and methyl radical, recombination of two methyl radicals to form ethane, abstraction of an H atom from the imine by methyl radical to form methane, and abstraction of an H atom from the imine by *t*-butoxy radical to form *t*-butyl alcohol. For the unimolecular decomposition of the peroxide into *t*-butoxy radicals an activation energy of 37.6 kcal per mole and a frequency factor of 3.5×10^{15}/sec are obtained. The capture of imine H atom by methyl radical is found to have an activation energy of 4.8 kcal/mole and a frequency factor of 4.5×10^{10} cc/mole/sec. The activation energy for the thermal decomposition of *t*-butoxy radical into acetone and a methyl radical is about 17 kcal/mole.

C7. Infrared Absorption by Asymmetrical Spectral Lines.* GILBERT N. PLASS AND DOUGLAS WARNER, *The Johns Hopkins University.*—Many recent theoretical investigations have studied the shape of pressure broadened spectral lines. Lindholm has shown that with Van der Waals forces the lines are asymmetrical, at low pressures the absorption coefficient, k, varying as $(\nu-\nu_0)^{-3/2}$ and $(\nu-\nu_0)^{-7/2}$ in the red and violet wings respectively. We have calculated the fractional absorption coefficient, A, for a single asymmetrical line and for a band with asymmetrical lines of equal spacing and intensity. The results are particularly simple for a single line. If k varies as $(\nu-\nu_0)^{-n}$ in the wings of a line, than A is proportional to $(Sa\alpha)^{1/n}$. This is the usual square root law for the Lorentz shape ($n=2$). For the Lindholm shape, A is the sum of two terms with appropriate values of n. The results which will be discussed show that the possible asymmetry of the line can be observed by measurements of A. In bands such as 15μ CO_2 and 50μ H_2O the continuous background from the wings of a few strong lines makes an appreciable contribution to the absorption, which is considerably different over wide frequency intervals for symmetrical and asymmetrical lines.

* This work supported by the ONR.

C8. Computation of Infrared Intensities. FRANK MATOSSI, *Naval Ordnance Laboratory.*—Numerical values for the effective charges (defined as $d\mu/dr$, μ = dipole moment, r = atomic distance) of vibrating molecules have been obtained experimentally from intensity measurements.[1] These values can be calculated theoretically from a classical model of the molecular dipole which considers the effect of induced atomic dipoles. The observed effective charges are obtained if the atomic polarizabilities α are assumed to be dependent on the atomic distance. $d\alpha/dr$ as determined from $d\mu/dr$ is in qualitative agreement with values obtained previously from Raman effect data. The results are given for the molecules CO, NO, CO_2, CS_2, OCS.

[1] For instance, D. Z. Robinson, J. Chem. Phys. **19**, 881 (1951).

C9. Theory of Dielectric Dispersion. MARIUS COHN, *University of Illinois.*—The Debye theory of dielectric dispersion[1] for polar substances considers a material in an applied oscillating electric field whose frequency is much lower than any resonant frequencies of the molecules involved. Only the contribution to the electric polarization from molecular reorientations is considered to be damped, while that due to molecular distortions is not. As a consequence a plot of the imaginary *vs* the real part of the dielectric constant always results in a semicircle with center of the real axis. Experimental curves for many substances, however, deviate significantly from this semicircular locus.[2] It is shown in this paper that even a single additional damping term could account for most of the deviations. While it was not possible to make accurate calculations, estimates indicate that sufficient damping may exist in some of the molecular distortions.

[1] P. Debye, *Polar Molecules* (Chemical Catalog Company, Inc., 1929, or Dover Publications, New York, 1945), especially Chapter V.
[2] D. W. Davidson and R. H. Cole, J. Chem. Phys. **18**, 1417 (1950).

C10. Proton Magnetic Resonance Absorption and Water Content of Biological Materials.* T. M. SHAW, R. H. ELSKEN, AND C. H. KUNSMAN, *Western Regional Research Laboratory.*—Earlier work showed that magnetic absorption by protons may be used to measure water content over the range encountered in natural and dehydrated biological materials.[1] A linear relation was found between height of the proton absorption line and water content for typical vegetable tissues. Recent work in the low moisture region has shown departures from linearity for some materials, for example apple tissue and starch. A recording radiofrequency spectrometer was used, together with a 4600 gauss permanent magnet modulated by one gauss. The lines observed at 25°C for a number of proteins and carbohydrates containing 5 to 20 percent water are similar and consist of a line 0.7 gauss wide superimposed symmetrically on a line about 9 gauss wide.

* Investigations under Research and Marketing Act, Bureau of Agricultural and Industrial Chemistry, Agricultural Research Administration, U. S. Department of Agriculture.
[1] T. M. Shaw and R. H. Elsken, J. Chem. Phys. **18**, 1113 (1950).

C11. Biased Random Walks in Classical, Statistical, and Quantum Mechanics. GILBERT W. KING, *Arthur D. Little, Inc., and Research Laboratory of Electronics, Massachusetts Institute of Technology.*—The distribution of random walks biased in one direction is governed by a Fokker-Planck equation with a linear term in $\partial/\partial x$. For example, if the bias is $1\pm\Delta x/x$, the radial diffusion or Schroedinger's equation results. If the bias depends not on location, but history, no linear terms appear. The controlling equation is parabolic with a diffusion coefficient a function of the conditional probabilities of the Markoff process. If in one dimension the probability of "persistence of velocity" is α, the coefficient is $\alpha/1-\alpha$ times that for the isotropic case. The proof for walks in one or more dimensions depends on classifying particles by their history and finding the condition for solution of the simultaneous difference equations. Random configurations of polymer chains are under a bias, forbidding particles to re-enter a point they have just left, in a tetrahedral lattice. The distribution is strictly Gaussian, the coefficient being twice that for isotropic diffusion. Even steric effects, in particular excluded volume, leave the distribution Gaussian. The "diffusion" coefficient is a scalar function of the fraction of walks of N steps permitted when excluded volume is taken into account over a range n, provided, as n, $N\to\infty$, $n\ll N$.

C12. An Apparatus for Creep and Low Frequency Dynamic Studies on Polymers.* T. E. MORRISSON AND T. W. DEWITT, *Mellon Institute.*—An apparatus is described for the measurement in torsion of the low frequency (0.001 to 1 cycle per second) dynamic properties of solid polymers. Data may be obtained from the decay of free vibrations or from the response to a sinusoidal driving force. In the latter case the phase angle between stress and strain is obtained by a method similar to that used by Ké[1] in studying metals. A low frequency sine-wave generator is briefly described. Provision is also made for measurements of creep under constant torque. The treatment of data, and calibration and operating characteristics of the instrument, is discussed. The use of the instrument is illustrated with data on a sample of high molecular weight polyisobutylene.

* This work was supported by the Office of Rubber Reserve of the Reconstruction Finance Corporation, Washington, D. C.
[1] T'ing-Sui Ké and Marc Ross, Rev. Sci. Instr. **20**, 795 (1949).

C13. Measurements of Components of Stress Produced by Shearing Strain. E. H. FREI,* *Weizmann Institute of Science.*—If certain solutions of high polymers are sheared between concentric cylinders, they tend to climb up the inner cylinder. It has been assumed that shearing strain not only produces shearing stress but also tensions.[1] An instrument, similar to

a Couette viscosimeter, has been built in order to distinguish between the various components of stress. The pressure on the inner cylinder is measured while measuring simultaneously the shearing stress in the conventional way. Using cylinders with different diameters it is possible to evaluate the components of stress in simple cases. A latex solution is found to show strong components depending on the curvature of flow that probably result from a three-dimensional network of molecules.[3] This makes a resolution of the components with this instrument alone impossible. After the network is destroyed by continuous shear the behavior of the substance becomes simpler and the components can be evaluated.

* At present at Institute for Advanced Study, Princeton, New Jersey.
[1] K. Weissenberg, Nature **159**, 310 (1947); R. S. Rivlin, Proc. Roy. Soc. (London) **A193**, 260 (1948); T. G. Oldroyd, Proc. Roy. Soc. (London) **A200**, 523 (1950); M. Reiner, Quart. Appl. Math. **8**, 341 (1951).
[2] E. H. Frei and A. Katchalsky, (to be published).

FRIDAY MORNING AT 9:30

Sherman, Crystal Room

(A. W. LAWSON presiding)

Metals

D1. Solid-State Diffusion in Cylindrical Geometry. DAVID D. VAN HORN, *Knolls Atomic Power Laboratory.**—As a result of restrictions as to the size and type of diffusion specimen imposed by the natures of the systems to be studied, it has been necessary to develop techniques for the determination of diffusion constants from small cylindrical diffusion couples. Solutions of the diffusion equations in cylindrical geometry will be discussed, with particular regard for the analysis of sources of error in the measurements, and for comparisons with the solutions in linear geometry. Cylindrical specimens one-half inch long and of the order of 0.10 in. in diameter have been prepared by electroplating. A method has been developed for determining the diffusion penetration curves of such specimens by cathodic sputtering (to be presented in the succeeding paper). Experimental results will be shown for the diffusion of copper into nickel.

* The Knolls Atomic Power Laboratory is operated by the General Electric Company for the AEC. The work reported here was carried out under contract No. W-31-109 Eng-52.

D2. Cathodic Sputtering as a Sectioning Method in Diffusion Studies. THOMAS F. FISHER, *Knolls Atomic Power Laboratory.**—A cathodic sputtering method for the removal and collection of uniform surface layers from small cylinders is described. The system used consists of a cylindrical anode one inch in diameter and one inch long. The cathodes were cylinders of the order of 0.10-in. diameter and 0.5-in. long placed axially inside the hollow anode. Using krypton gas at 100 microns pressure and a potential of 2400 volts, the sputtering current was one milliampere. Under these conditions, one mil layers uniform to better than 0.05 mil could be removed from the cathode in approximately 24 hours. Pure metals, single phase alloys, and two phase alloys were studied. In all cases it was found that satisfactory uniform layers could be removed and that the composition of the collected metal agreed closely with that of the original alloys. This method is particularly suited for the study of diffusion in radioactive materials.

* The Knolls Atomic Power Laboratory is operated by the General Electric Company for the AEC. The work reported here was carried out under contract No. W-31-109 Eng-52.

D3. Experimental Evidence for the Vacancy Mechanism for Diffusion in Metals and Alloys.* FOSTER C. NIX AND FRANK E. JAUMOT, JR.,† *University of Pennsylvania.*—The diffusion of cobalt in cobalt-aluminum alloys of compositions near the 50–50 atomic percent composition was investigated in an attempt to test the vacancy mechanism of diffusion. These alloys have the property of containing a large number of vacancies in excess of the vacancies normally present in a lattice due to thermal excitations. The experimental technique used consisted essentially of computing the diffusion coefficients from the decrease in activity of radioactive Co^{60} due to the penetration of this isotope into the alloys. The value of the absorption coefficient of Co-Al alloys for the complex spectrum of Co^{60} required by the mathematical analysis was measured using powdered metal techniques. The results of diffusion of cobalt into cobalt-aluminum alloys of five different compositions, at temperatures of 1050°C, 1150°C, and 1250°C were obtained. The activation energy for the process was computed for each concentration. The data indicate that the diffusion coefficient has a minimum value at the ideal composition and rises sharply on the aluminum-rich side. Thus, the vacancy mechanism is indicated as the predominant mechanism in diffusion in substitutional alloys.

* This work was supported by the ONR.
† This paper is based on part of a thesis submitted by Frank E. Jaumot, Jr., in partial fulfillment of the requirements for the degree of Ph.D. at the University of Pennsylvania.

D4. X-Ray Study of Lattice Imperfections. P. H. MILLER, JR., *University of Pennsylvania.* In a spherical crystallite with the central scattering center missing from a simple cubic lattice shifts in the position of the diffraction maxima occur, as well as changes in the density and linear dimensions. The fractional changes are, respectively:

$$\frac{\Delta d}{d} = -8.4\frac{x}{M^3}$$

$$\frac{\Delta \rho}{\rho} = -\left(\frac{6}{\pi}+24x\right)\frac{1}{M^3}$$

$$\frac{\Delta l}{l} = +\frac{8x+2/\pi}{M^3},$$

where x is the fraction of an interatomic distance the nearest neighbors of the missing atom move outward, and M is the number of atoms along a diameter of the sphere. If x is positive, the crystallite becomes larger but the lattice constant apparently decreases. When these results are applied to the NiAl system one finds that the 46 atomic percent Ni alloy contains some Al atoms at Ni sites and a much smaller number of Ni vacancies than estimated by Bradley and Taylor.[1] Application of these equations to order disorder phenomena and Schottky and Frenkel defects will be discussed.

[1] A. J. Bradley and A. Taylor, Proc. Roy. Soc. (London) **159**, 56 (1937).

D5. An Electron Microscope and Diffraction study of the Aging of Evaporated Metal Films.* E. J. SCHEIBNER, *Illinois Institute of Technology.*—An electron diffraction study was made of the aging of thin metal films of aluminum, silver, and

gold on silicon monoxide substrates by transmission and on quartz crystals by reflection. The effect of aging, accelerated by heating, is determined for each film by an investigation of the resulting diffraction pattern and corresponding micrograph. It was found that a growth in grain size occurred in the films and that aluminum films developed a [111] fiber structure after aging. Successive stages in the aggregation of silver and gold films are illustrated in their electron micrographs, while those of the aluminum films indicate their high resistance to aggregation. A modification of the diffraction specimen holder of the RCA type emu electron microscope permitted the insertion of an entire quartz crystal into the microscope column. With this adaptation it was possible to obtain reflection patterns from the films without destroying the crystals. A comparison between the properties of the metal films is made after examination of the results obtained from the diffraction patterns and micrographs.

* This research was supported by U. S. Army Contract under Signal Corps Project. The work was done at the State Engineering Experiment Station of Georgia Institute of Technology, Atlanta, Georgia.

D6. Tracer Method for Measurement of Evaporated Bi Film Thicknesses.* JOHN J. ANTAL AND A. H. WEBER, *Saint Louis University*.—A simple method for the measurement of very thin films prepared by evaporation in a vacuum through determination of the activity of an included tracer is given. A comparison of the activity of the film of unknown thickness to that of a standard of known mass gives the mass of the unknown film. The area of the unknown film is then measured with a planimeter and its thickness is computed. Because of the relative character of the measurements, the natural decay of the tracer is automatically accounted for. High accuracy in the range 1 to 100A, continuous calibration, and nondestruction of the specimen recommend this method. Bi^{210} was used successfully as a tracer in Bi films in the present experiments, with less than 4 percent error and a range in thickness of 1 to 300A. Two types of activity which occurred in the Bi^{210} standards are explained by a variation in the structure of the films determined by electron diffraction.

* Supported by a Research Corporation grant

D7. Temperature Dependence of Internal Friction at 44 kc.* W. B. NOWAK, *Massachusetts Institute of Technology*.—The internal friction of Al has been measured at 44 kc as a function of temperature for various amounts of cold work. The Al, 99.99+ percent pure, was in the form of resonant rods with an average grain diameter of 1.7 mm. Measurements were made from 300°K to 65°K and for compressional strains up to 1.35 percent. For the Al, and for annealed 99.5 percent Be (0.45 mm grain size), a broad low temperature maximum in the Q^{-1} *versus* temperature curve has been found in qualitative agreement with the literature. Upon cold working, the Q^{-1} of Al at 300°K increased and the magnitude of the low temperature peak relative to 300°K increased. Cold work also produced a temperature shift of the maximum from 143°K to 110°K. The existence of a minimum in the Q^{-1} of Al near 300°K is shown[2] and it is also shown that freshly annealed Al "ages," or anneals further, at 300°K. The apparatus will be described and a tentative explanation of the "aging" and of the low temperature peak will be put forth in terms of "pinned-down" dislocations and a possible relaxation effect.

* Sponsored by AEC. contract.
[1] P. G. Bordoni, Ricerca sci. (August, 1949), p. 851.
[2] J. Pittenger, Phys. Rev. **83**, 889 (1951).

D8. Effect of Plastic Deformation on Anelastic Properties of Alpha-Brass.* JOHN KAUFFMAN AND DAVID LAZARUS, *University of Illinois*.—Measurements have been made over a considerable temperature range of the effect of plastic deformation on the relaxation due to stress induced preferred orientation of Zn atoms[1] in 70–30 alpha-brass. Data were taken with large-grained polycrystalline wire specimens of 1 mm diameter, using a torsion pendulum. In a range of temperature above room temperature, plastically deformed specimens show a shorter relaxation time than annealed specimens. With increasing temperature, the effect disappears, and, in some cases, shows a reversal. The data are considered in terms of the vacancy mechanism for atomic diffusion. An excess number of vacancies is produced as a result of cold work and contributes to the diffusion process. These vacancies rapidly equilibrate at temperatures of the order of 220°C.

* Supported in part by the AEC.
[1] C. Zener, Phys. Rev. **71**, 34 (1947); T. S. Kê, J. Appl. Phys. **19**, 205 (1948).

D9. Temperature Dependence of the Resistivity of Deuteron Irradiated and Annealed Molybdenum.* BURTON RANDOLPH,† *Purdue University*.—The temperature dependence of the resistivity of molybdenum has been investigated for unannealed, annealed, and deuteron-irradiated samples between room temperature and 1.2°K. The resistivity at room temperature shows only a slight change upon annealing (a decrease of 3 percent) but somewhat more after bombardment (an increase of 4 percent). However, by extending the measurements to the helium range it has been found that the residual resistivity (constant from 12°K to 1.2°K) is twice as great in the unannealed sample than in the annealed, and three times greater in the bombarded sample. The specimens were cooled during bombardment with 10-Mev deuterons so that the actual temperature during bombardment was never higher than −100°C. By heating in hydrogen the irradiation effects can be healed out. The annealing process, as well as the behavior of the irradiated material as compared with cold-worked material, will be discussed.

* Supported by the AEC.
† To be introduced by K. Lark-Horovitz.

D10. Statistical Theory of Properties of Solid Solutions. R. SMOLUCHOWSKI, *Carnegie Institute of Technology*.—Properties of binary solid solutions are considered from the point of view of the fluctuation of local composition in the crystalline lattice. These variations influence the properties of the alloys by varying the corresponding local concentration of electrons. A simple general statistical method is given for calculating properties of random and ordered solid solutions. The basic group in a face-centered cubic lattice consists of an atom and its nearest neighbors. In a body-centered cubic atom and its nearest and second nearest neighbors which are only 15 percent further away. The theory is applied to saturation magnetization magnetostriction, thermoelectric power electrical resistance, and its temperature coefficient and other properties in various alloys. Satisfactory agreement with experiment is obtained.

D11. Thermal Conductivity of Metals. P. H. SIDLES AND G. C. DANIELSON, *Iowa State College*.—A new method of measuring thermal diffusivity and, hence, thermal conductivity of metals is suggested. Like the methods of King[1] and Starr,[2] this method uses a heat source, whose temperature varies sinusoidally, located at one end of an effectively infinite rod. Unlike these methods, only one period of the heat wave is required to eliminate the unknown coefficient determining the heat lost by radiation, since both velocity and amplitude decrement of the heat wave are measured. The new method is faster in taking data and simpler incomputation. The thermoelectric potentials from two thermojunctions are amplified and plotted on a Brown "Electronic" recorder, thus giving a permanent record of all necessary data for computing the thermal diffusivity. Results for different metals at room temperature and at elevated temperatures will be given.

[1] R. W. King, Phys. Rev. **6**, 437 (1915).
[2] C. Starr, Rev. Sci. Instr. **8**, 61 (1937).

D12. Optical Properties of Sodium Tungsten Bronze. G. C. DANIELSON AND E. CHIVERS, *Iowa State College.*—With the addition of sodium the insulator WO_3 acquires electrical properties corresponding to a metal with a concentration of free electrons in the conduction band equal to the concentration of sodium atoms.[1] These free electrons must also explain the change in color from blue to red to yellow with increasing sodium content. The color changes might be caused either by selective reflection, as suggested by the classical theory of Zener and successfully applied by Jaffe[2] to solutions of alkali metals in ammonia, or by internal photoelectric absorption, as suggested by Mott and Jones for copper and brass. Single crystals of the red and yellow "bronzes" have been grown large enough for us to measure the optical constants by polarimetric methods. For red or yellow light the optical constants have normal values as predicted by the classical theory of metals. For yellow crystals using blue light and for red crystals using green or blue light the absorption coefficient (nk) becomes anomalously large. This suggests that the color of these crystals is caused by internal photoelectric absorption rather than by selective reflection.

[1] Huibregtse, Barker, and Danielson, Phys. Rev. (to be published).
[2] H. Jaffe, Phys. Rev. 58, 207 (1940).

D13. Design of Extensometer for Creep Studies.* R. PIZZAROT† AND B. GOSSICK, *Purdue University.*—The extensometer incorporates automatic and remote operation for irradiation studies over a wide range of extensions (10 percent→10^{-3} percent). The creep specimen is mechanically coupled to a metal core within a mutual inductance bridge. The amount of deformation of the creep specimen determines the position of the core and thus the amount of bridge unbalance. The output of the bridge is electronically amplified and rectified. A recording milliammeter connected to the output of the rectifying stage records the creep rate. The tolerances of mutual inductance bridges being never perfect, a residual voltage always remains which is 90° out of phase with that produced by displacements of the core. By making a composite core of juxtaposed laminations of steel and copper, one can empirically obtain a core which produces output voltages in quadrature with those of a steel core. When two such bridges are connected together the null may be reduced to the order of the noise level of the amplifier to which the bridge system is connected. On our most sensitive scale, full-scale deflection corresponds to 1160A displacement of the metal core with a noise level corresponding to 40.6A. Creep curves with commercial copper wire will be presented.

* Supported by the AEC.
† To be introduced by K. Lark-Horovitz.

FRIDAY MORNING AT 9:30

Morrison, Mural Room

(A. O. NIER presiding)

Nuclear Instrumentation

E1. Resolution of Fast Neutron Energy Measurements using Proton Recoils from a Thin Radiator.* BEN R. GOSSICK,† *Purdue University.*—The general equation for analyzing counting data is

$$N(E)=\frac{8(g+1)M}{\pi g^2 S\zeta_1\zeta_2\zeta_3\zeta_4 ER(E)\sigma(E)},$$

where $N(E)$ represents the number of neutrons emitted per second per Mev from an isotropic point source. E is the energy of the protons, $R(E)$ the total range in the radiator material, $\sigma(E)$ the scattering cross section of hydrogen. ζ_1, ζ_2, ζ_3, and ζ_4 are fractional errors in energy due to uncertainties in (1) the beginning of the range, (2) the end of the range, (3) the angle of the incident neutron, and (4) the angle of the recoil proton respectively. s represents the hydrogen density of the radiator, n the counting rate, and g is given by Geiger's law $R(E)=KE^{g/2}$. By maximizing the counting rate at constant total error, the possible resolving power can be setimated. A well-designed spectrometer of this type will yield a total error of from 5 to 15 percent with source intensities in the commonly available range $3\cdot10^3<N(E)<10^7$.

* This work was done at Oak Ridge National Laboratory, Oak Ridge, Tennessee.
† To be introduced by K. Lark-Horovitz.

E2. A Crystal Spectrometer for Neutrons. L. B. BORST* AND V. L. SAILOR, *Brookhaven National Laboratory.*—A crystal spectrometer of the type described by Zinn[1] has been constructed for use with the Brookhaven reactor. A beryllium crystal[2] has been found to be exceptionally good as a neutron monochromator giving unusually strong Bragg reflections while having a double-crystal rocking curve of only 5 minutes width. The high intensity permits the use of planes of high Miller indices, which greatly enhances the resolution of the instrument. For example the $(12\bar{3}0)$ set of planes have a grating space of only 0.747 a.u., which give a first-order reflection for 1-ev neutrons at an angle of 11°. Using this set of planes preliminary cross-section curves have been obtained for In, Ir, Rh, and Au in the range from 1 ev to 10 ev. With a collimated beam of 10 minutes divergence the resolution is high enough to permit the observation of the natural widths of most resonances lying below 2.5 ev. At present more careful data are being taken on several resonances to obtain accurate values of the resonance integrals.

* Now at the University of Utah, Salt Lake City, Utah.
[1] W. H. Zinn, Phys. Rev. 71, 752 (1947).
[2] Two excellent single crystals of beryllium were generously furnished by Professor A. R. Kaufman of the Division of Industrial Cooperation at MIT.

E3. Scintillation Neutron Detector.* WILLIAM BERNSTEIN AND A. W. SCHARDT, *Brookhaven National Laboratory.*—Lithium iodide crystals have been grown with up to 0.5 percent by weight of TlI as activator. The activated melt forms an opaque, brown, polycrystalline mass if cooled rapidly. Single crystals $\frac{1}{2}$-in. diameter and $\frac{3}{4}$-in. high have been grown with parts which are clear and white. Excess thallium was found at the crystal boundaries. The crystals were tested with thermal neutrons from a spectrometer. All activated crystals gave pulses well above noise whereas no scintillations were detected from unactivated crystals. A single line with a full width at half-maximum of 25 percent was obtained with under-activated crystals. The pulse height corresponded to that produced by 50–100 kev gamma-rays on Harshaw NaI-Tl. Crystals grown with an excess of activator showed one line equivalent to 100–170 kev on NaI-Tl. A continuous distribution of pulses was found above the line with a cutoff at 450-kev NaI-Tl equivalent. One crystal shows a second peak near the upper cutoff which is about 15 percent wide.

All pulses are stopped by interposing cadmium between the crystal and neutron source.

* Work performed under the auspices of the AEC.

E4. Performance of 5819 Photomultipliers in Scintillation Spectrometers.* A. W. SCHARDT AND WILLIAM BERNSTEIN, *Brookhaven National Laboratory.*—Three dozen 5819 photomultipliers[1] have been tested for resolution with a ½-in. cube NaI-Tl crystal permanently mounted in an aluminized reflector with a quartz window.[2] The full width at half-maximum of the photoline of 670 kev quanta varied between 9 and 16 percent with most tubes around 12 percent. For 22 kev the extremes are 35 to 60 percent with most tubes near 45 percent. An attempt was made to correlate these results with some of the photomultiplier characteristics such as quantum efficiency, gain, uniformity, noise, dynode voltages, and electron collection efficiency. If the voltage between photocathode and first dynode is above 200 volts no quantitative correlation could be found. However, tubes with high cathode sensitivity have in general a better resolution.

* Work performed under the auspices of the AEC.
[1] We are indebted to R. W. Engstrom of RCA, Lancaster, for the loan of some selected tubes.
[2] A. W. Schardt and W. Bernstein, "Resolution of scintillation spectrometer," Rev. Sci. Instr. (to be published).

E5. Monitor for Natural Radioactivity in the Atmosphere.* M. H. WILKENING, *New Mexico Institute of Mining and Technology.*—A monitor for studying the decay products of radon and thoron found in the atmosphere is described. A point-to-plane type of electrostatic precipitator is used to collect samples of particulate matter from the atmosphere and deposit them on a moving metallic tape. The activity associated with the collected material can be measured either with a scintillation counter for detection of the alpha-activity or with an end-window Geiger counter for detection of the beta-activity. A count rate meter and strip-chart recorder are used to give a permanent register of the activity. A kymograph type of synchronous motor and set of reduction gears is used as a driving mechanism for the collecting tape. By varying the speed, the monitor's response can be set to emphasize either the short-lived (3.05 min) RaA, the radon products RaA through RaC″ (effective half-life about 40 min), or the long-lived, low level ThB (10.6 hr) activity. Under normal monitoring conditions which favor the radon products, counting rates varying from about 50 to 200 counts per minute above background are obtained. The instrument is planned for use in correlating atmospheric radioactivity with fluctuating aerosol concentrations and varying meteorological conditions.

* Research supported by funds from the ONR.

E6. A Combination Cloud-Ion Chamber using Cylindrical Geometry.* FIELDING BROWN, R. R. RAU, AND GEORGE T. REYNOLDS, *Princeton University.*—Following general principles previously reported,[1,2] a cloud-ion chamber using cylindrical geometry has been constructed and is in operation. The chamber contains three concentric electrodes: ¼-in. diameter steel, $3\frac{3}{32}$-in. o.d. by $\frac{3}{32}$-in. thick glass, and $8\frac{1}{4}$-in. o.d. by ¼-in. thick glass. The outer glass electrodes are coated with a transparent and electrically conducting coating to permit cloud-chamber illumination and also make ion chamber action possible. The outermost electrode serves as the chamber wall and the intermediate cylinder (collecting electrode) is at +1400 volts. This permits electron collection throughout the entire chamber volume. Thus heavily ionizing events, such as stars, which are produced in the approximately 5 liters of chamber gas, are photographed and the size and shape of associated ion chamber pulses can be recorded. Typical events will be shown.

* Supported by the joint program of the AEC and ONR.
[1] M. J. Cohen, Phys. Rev. **75**, 1329 (1949).
[2] Lewis, Brown, Seevers, and Hones, Rev. Sci. Instr. **22**, 259 (1951).

E7. Scattering of Light from Small Drops. RICHARD L. LANDER AND C. E. NIELSEN, *Ohio State University.*—Small drops were produced in a continuous cloud chamber, and the angular distribution of light scattered from them was studied over the range of angles from 28° to 147°. The detecting system was a phototube circuit and galvanometer. Values of intensity obtained with no drops present, but with other conditions unchanged, were subtracted from the values observed with drops in the chamber in order to obtain the intensity of light scattered from the drops alone. Data obtained by photographic methods exist for the range 20° to 100°.[1] The present results agree well with these data, but the observed intensities at angles between 100° and 147° are considerably greater than had been speculated. The ratio of the intensity at 140° to that at 40° is about 5:7 for drops of radius 1.4×10^{-3} cm. The speculated ratio is about 1:15. For drops of radius 4.8×10^{-4} cm the ratio is 1:8, indicating that the angular distribution depends strongly upon the drop size.

[1] J. G. Wilson, *The Principles of Cloud Chamber Technique* (Cambridge University Press, London, 1951).

E8. Special Techniques For Processing Thick Nuclear Emulsions. BERTRAM STILLER, MAURICE M. SHAPIRO, AND FRANCIS W. O'DELL, *Naval Research Laboratory.*—A modified procedure for uniform development of 400μ ultrasensitive emulsions by the temperature-cycling method[1] is described. A favorable ratio of minimum grain density to background is obtained by warm, "dry" development with amidol for ≈20 min at 23°C. Dry development also reduces the incidence of surface deposits of colloidal Ag. A pre-wiping technique further inhibits these deposits while avoiding the risk of distortion from wiping the wet swollen emulsion. We have confirmed[1] that swelling is markedly reduced by fixing and washing at 5°C. Clearing time for 400μ emulsions is thereby extended <30 percent. The tendency of thick emulsions, once dried, to strip from their base is prevented by (a) immersion in a plasticizing solution, (b) application of a protective coating, and (c) storage and use in a constant-humidity environment. "Eradication" and resensitization of 400μ Ilford G5 emulsions is achieved by a 7-day exposure to a moisture-saturated atmosphere at 35°C, followed by drying.[2] A stack of emulsions without glass support provides a large sensitive volume in which tracks can be readily followed from one layer to the next.[3] The lateral swelling (≈25 percent) which has heretofore discouraged the use of such emulsions is prevented by a special method of mounting and processing them, based on a suggestion by C. Waller of Ilford, Ltd.

[1] Dilworth, Occhialini, and Vermaesen, Bull. centre phys. nucleaire Bruxelles No. 13a; Bonetti *et al.*, *ibid.*, No. 13b.
[2] M. Wiener and H. Yagoda, Rev. Sci. Instr. **21**, 39 (1950).
[3] P. Demers, Phys. Rev. **78**, 320 (1950).

E9. A Combination Crossed-Field and Time-of-Flight Mass Spectrometer. J. A. HIPPLE AND H. SOMMER, *National Bureau of Standards.*—A crossed-field mass spectrometer in which the ions take a trochoidal path having multiple cycles has been modified to permit accurate timing with a high frequency voltage for a time-of-flight of the ions of n complete cycles. The operation is based on the fact that the time for one complete cycle is given by the cyclotron frequency condition. The entering ions pass between two parallel wires placed on the focal plane where a sinusoidal voltage deflects the ions in the direction of the magnetic field causing them to miss the final exit slit unless they pass between the wires when the rf voltage is near zero. After n complete cycles those ions which were not deflected by the first pair of electrodes pass through a similar pair of electrodes connected to the same source of rf voltage and will not be deflected if the frequency is a multiple of half the cyclotron resonant frequency. The ions not deflected by the two pairs of electrodes are able to pass through a final slit to the ion collector, and the current is measured with a

dc amplifier or multiplier. The advantages over other schemes based on the cyclotron frequency condition will be discussed.

E10. The University of Kansas Van de Graaff Generator.* L. W. SEAGONDOLLAR, R. K. SMITH, W. R. ALEXANDER, AND J. W. TEENER.—This generator was designed to fit into an ordinary laboratory room 50 ft×25 ft×10 ft so as to leave maximum space for target and detecting assemblies. It follows the Herb design and is contained in a steel pressure tank 16 feet long and 6 feet in diameter. The steel tank is mounted on concrete piers. The removable head of the tank is mounted on a heavy rolling cart and all generator components are mounted on the head. The generator is rolled out of the tank for maintenance or repair. The seven-foot accelerator tube has six-inch i.d. electrode spinnings. Electron loading makes the present voltage limit two million volts. Stable operation occurs up to and including the $Li^7(p, n)$ threshold. A Zinn type ion source is used. Stability is obtained by corona current control using a 25-degree electrostatic analyzer on the mass-2 beam. Further comment will be made on the design of the generator and operational characteristics will be discussed.

* Supported in part by the ONR.

E11. The Oak Ridge 86-in. Cyclotron. ROBERT S. LIVINGSTON, *Oak Ridge National Laboratory*.—During the spring of 1951 an 86-in. fixed frequency proton cyclotron has been placed in successful operation. The energy reached by the protons exceeds 20 Mev as determined by the frequency and the geometry, and also by the $C^{12}(p, pn)C^{11}$ reaction. The protons at terminal energy are more than 2 percent relativistic. This has been made possible by the use of optimized magnetic shimming and increased radiofrequency voltage between the dees. Internal currents of hundreds of microamperes above 20 Mev have been observed. Beam measurements have been made by probes equipped with electron traps and by calorimetry techniques. Several unique features of the mechanical design of the cyclotron are (1) horizontal magnetic field with the median plane vertical; (2) insulated, negatively-biased dees to provide satisfactory operation with a self-excited, grounded-grid oscillator; (3) heavily water-cooled dees suspended vertically; (4) demountable dee-assembyl with provision for rapid replacement in case of failure or need for revised experimental facilities; (5) suppression of radioactivity induced in dees by use of appropriate lining; (6) high pumping speed system with resulting fast pump-down time; (7) targets which will withstand 10 kw of beam without deterioration; (8) bayonet-type vacuum seal for rapid removal of target heads; (9) ion source removable through a vacuum lock.

E12. Operating Current and Energy of the M.I.T. Linear Electron Accelerators.* M. LABITT, R. J. DEBS, I. HALPERN, AND P. T. DEMOS, *Massachusetts Institute of Technology*.—The M.I.T. Linear accelerator is one of the standing wave type.[1] It is 21 feet long and is powered by tunable magnetrons which are operated in pulses two microseconds long at 120 cps. The accelerator is currently being used at a maximum energy of about 17 Mev with average currents of several microamperes. The energy spread of the electrons within a single pulse is from 2 to 4 Mev, and there is an additional energy "jitter" of about ½ Mev from pulse to pulse. The accelerator beam is probably less than $\frac{1}{16}$ in. in diameter, but moves about within an area of diameter ½ in. in successive pulses. Although the adjustment of the accelerator controls for maximum energy and best beam definition is fairly critical, it has been found that, once adjusted, the properties of the accelerator beam will remain unchanged for several hours at a time. The electron beam leaves the accelerator through a thin aluminum window, emerging into a well-shielded target room. The beam has been used both directly and to produce x-rays. So far, the main use of the accelerator has been for photonuclear experiments.

* This work was assisted by the joint program of the ONR and AEC and is described in more detail in the M.I.T.-L.N.S.E. Technical Report No. 50 by P. T. Demos.

[1] See J. C. Slater, Revs. Modern Phys. 20, 473 (1948).

FRIDAY AFTERNOON AT 2:00

Sherman, West Room

(J. H. VAN VLECK presiding)

Magnetism; Low Temperatures

F1. Ferromagnetic Domain Structure of Single Crystals and Bicrystals of Nickel.* URSULA M. MARTIUS, K. V. GOW, AND BRUCE CHALMERS, *University of Toronto*.—Single crystals and bicrystals of nickel, with predetermined orientation, have been grown by the methods of Chalmers and Gow. The following range of orientation was studied: Crystals which contained two (111) directions in the plane of the surface, and small deviations from this orientation; crystal with a single (111) direction in the plane of the surface and specimens with a (100) plane as the crystal surface, hence containing no direction of easy magnetization in the plane of the surface. The colloid technique was used to study the domain structure on the carefully electropolished crystal surfaces. The general features of the domain structures are in agreement with the predictions of the theory. The patterns on nickel are very sensitive to small differences in crystallographic orientation. Two effects have been observed in the proximity of small angle crystal boundaries. Changes in domain spacing and new substructures can result directly from the small differences in crystal orientation; also, curvature of the Bloch wall has been found in many patterns. The curvature is attributed to lattice strains associated with the crystal boundaries.

* Martius, Gow, and Chalmers, Phys. Rev. 82, 106 (1951).

F2. Effect of Stress on the Curvature of Domain Boundaries. H. J. WILLIAMS AND R. M. BOZORTH, *Bell Telephone Laboratories*.—Most domain boundaries are plane surfaces, which have been observed as straight lines on magnetic domain patterns. Some curvature has been noted,[1] especially in nickel, which has a high magnetostriction and a moderately low crystal anisotropy. Photographs of domain patterns now show large curvature near regions that have been plastically deformed. Plastic deformation of other materials, including a silicon-iron alloy, causes marked changes in their domain patterns, and a variety of these will be shown. The attempt has been made to study experimentally the relation between stress and curvature in material having a simple stress distribution. Often the patterns are quite complex.

[1] H. J. Williams and J. G. Walker, Phys. Rev. 83, 634 (1951).

F3. Strain Induced Curvature of Bloch Walls in Silicon Iron. L. J. DIJKSTRA AND U. MARTIUS, *Ontario Research Foundation.*—In a study of the ferromagnetic domain patterns in a large-grained silicon iron, special attention has been directed to the effect of stress especially in the vicinity of grain boundaries. It has been observed that increasing stress causes a sequence of changes in the pattern, commencing with a reorientation of the domains and subsequent splitting up into narrower domains by a process which appears to nucleate at the boundaries. Considerable local curvature of the domain walls is inherent in this splitting process. On the other hand, marked curvature of the Bloch walls can also be observed in regions where plastic deformation has caused the lattice to become curved; in such cases, curvature of the lattice has been confirmed by x-ray diffraction.

F4. Magnetically Induced Ultrasonic Velocity Changes in Polycrystalline Nickel.* S. J. JOHNSON, *Andersen Laboratories,* AND T. F. ROGERS,** *Cambridge Research Center.*—Measurements on the changes of ultrasonic velocity in pure polycrystalline nickel rods induced by the application of magnetic fields[1] have been continued. Large diameter rods are used in order to provide high D/λ ratios in the 1- to 10-megacycle region. Velocity changes have been noted for both compressional and shear waves with magnetic fields either along or transverse to the rod axis. Such changes, attributable to the ΔE effect,[1,2] show a marked decrease with increasing frequency; representative compressional saturation values of 3 percent and 0.8 percent are obtained at 1 and 5 megacycles, respectively. Comparison with published data for single nickel crystals[2,3] shows general agreement as to the nature and magnitude of the effects noted, but the polycrystalline saturation values are appreciably smaller.

* Supported by the Air Force Cambridge Research Center.
** Now at the Massachusetts Institute of Technology.
[1] T. F. Rogers and S. J. Johnson, J. App. Phys. **21**, 1061 (1950).
[2] Mason, McSkimin, and Bozorth, Phys. Rev. **83**, 220(A) (1951).
[3] W. P. Mason, Phys. Rev. **82**, 715 (1951).

F5. Approximate Treatment of Order-Disorder Transitions in the Triangular Ising Lattice. L. D. FOSDICK AND H. M. JAMES, *Purdue University.*—The approximation method previously applied to the treatment of the order-disorder transition in the square Ising array in two dimensions[1] has been applied to the triangular lattice, with similar results. Attention is fixed on a central dipole surrounded by a hexagon of dipoles. Two order parameters represent the tendency of coupling to other dipoles to produce short-range and long-range order of the dipoles under consideration; two consistency relations serve to fix these parameters as functions of the temperature and coupling energy. The Curie temperature indicated by this method is about 10 percent higher than the known exact value, being close to the value obtained by the quite different method of Kikuchi.[2] Our method indicates a finite jump in the specific heat at the Curie point, but a considerably larger one than that given by Kikuchi's method; it therefore appears that the present method permits more accurate description of the system near the Curie point.

[1] H. M. James and L. D. Fosdick, Phys. Rev. **81**, 312(A) (1951). Erratum: The method gives a finite discontinuity in the specific heat of a square lattice, not an infinite one as reported there.
[2] R. Kikuchi, Phys. Rev. **81**, 988 (1951).

F6. Statistics of the Three-Dimensional Ferromagnet. B. MARTIN,* D. TER HAAR,† and V. A. JOHNSON, *Purdue University.*—The variational method of Kramers and Wannier has been applied to the three-dimensional ferromagnet.[1] A cubic Ising model with interaction of only nearest neighbors has been used. Denote by J the interaction energy corresponding to the difference between the state in which neighboring spins are parallel and that in which they are antiparallel. The partition function is

$$f = \Sigma_{\mu=\pm 1} \exp(K \Sigma_{\mu\mu'}),$$

where $K = J/2kT$ and the summation is extended over all spins in the crystal. The partition function is approximated through two reductions, each of which leads to an eigenvalue problem which is treated by the Ritz method. The configurational energy and specific heat are calculated from the appropriate derivatives of the partition function. A series solution for f was derived earlier. Now a numerical solution has been obtained for small k, and corresponding numerical values of specific heat and energy have been calculated. The numerical and series values agree well, with the difference increasing with K.

* Now at Owen-Illinois Glass Company, Toledo, Ohio.
† Now at University of St. Andrews, Scotland.
[1] See D. ter Haar and B. Martin, Phys. Rev. **77**, 721(L) (1950) for the series solution and additional references.

F7. An Approximate Quantum Theory of the Antiferromagnetic Ground State. P. W. ANDERSON, *Bell Telephone Laboratories.*—Klein and Smith[1] have shown that a careful treatment of the zero-point energy in the Heller-Kramers[2] semiclassical theory of ferromagnetic spin waves leads one to quite exact results for various properties, particularly the energy, of the ferromagnetic ground state as well as of the low excited states. This is the result of the fact that the Kramers-Heller treatment is basically a purely quantum-mechanical approximation valid to order $1/S$. (S is the spin quantum number of the atoms in the ferromagnet.) A similar treatment of the antiferromagnet, for which the ground state is not known, has been carried out, based on Hulthén's[3] spin-wave treatment of the antiferromagnetic lattice. Results are obtained valid to order $1/S$ for the energy and for the long-range order in the ground state of the simple cubic and plane lattices. For the linear chain the method shows that the zero-point energy of the spin waves is alone adequate to destroy long-range order, a result which agrees with the exact treatment of Hulthén.[4] Nonetheless, a surprisingly close estimate of the energy is obtained in this case.

[1] Klein and Smith, Phys. Rev. **80**, 1111 (1950).
[2] Heller and Kramers, Proc. Amst. Acad. Sci. **37**, 378 (1934).
[3] L. Hulthén ,Proc. Amst. Acad. Sci. **39**, 190 (1936).
[4] L. Hulthén ,Ark. für Mat., Astron. o. Fys. **26a**, 11 (1938). See also H. Bethe, Z. Physik **71**, 205 (1931).

F8. On Generalizations of the Weiss Molecular Field Theory of Antiferromagnetism.* J. SAMUEL SMART, *U. S. Naval Ordnance Laboratory.*—The usual Weiss molecular field treatment of ferromagnetism and antiferromagnetism considers only interactions between nearest neighbors. Recent work of Néel[1] and Anderson[2] has indicated the importance of considering second nearest neighbor interactions as well. If both interactions are included and are allowed to be either ferromagnetic or antiferromagnetic, there are four possibilities as indicated in Table I. The calculations of Néel and Anderson

TABLE I.

	I	II	III	IV
Nearest neighbor	f	a	a	f
Second nearest neighbor	f	a	f	a

(Case II) have been extended to Cases III and IV for b.c.c. and f.c.c. lattices. For Case III, the material is antiferromagnetic with ordering of the first kind for all values of γ_2/γ_1, where γ_1 and γ_2 are the molecular field coefficients for first and second nearest neighbor interactions, respectively. For Case IV, the material is ferromagnetic for small γ_2/γ_1 and antiferromagnetic with ordering of the second kind for large γ_2/γ_1. The relation of these results to the experimental data on antiferromagnetic compounds will be discussed.

* Supported in part by ONR.
[1] L. Néel, Ann. phys. **3**, 137 (1948).
[2] P. Anderson, Phys. Rev. **79**, 705 (1951).

F9. The Magnetic Susceptibility of Zinc at Liquid Nitrogen Temperatures. J. W. McClure,* *Northwestern University.*—Measurements were made of the difference between the susceptibilities parallel and perpendicular to the hexagonal axis of zinc, employing a torsion method. The specimen was a single crystal of New Jersey Superpure zinc, weighing about 0.7 gram. The susceptibility parallel to the hexagonal axis was found to be field dependent in the region investigated, 54°K to 85°K and 2.7 to 9.7 kilogauss. The order of magnitude of the variations was 0.01×10^{-6}. While definite maxima and minima were observed, the range of measurements was not large enough to determine if the susceptibility as a function of field strength oscillates as in the de Haas-van Alphen effect.[1,2] Measurements were also made on a zinc specimen containing 0.016 atomic percent copper. These results differed from those for pure zinc by order of experimental error, about 0.001×10^{-6}.

* Now at the University of Chicago, Chicago, Illinois.
[1] J. A. Marcus, Phys. Rev. **76**, 413, 621 (1949).
[2] S. Sydoriak and J. Robinson, Phys. Rev. **75**, 118 (1949).

F10. Specific Heats of Several Metals and Semiconductors between 1.8 and 4.2°K.* I. Estermann and S. A. Friedberg,** *Carnegie Institute of Technology.*—Specific heats of very pure samples of magnesium, titanium, zirconium, and germanium and an impure sample of germanium† have been measured between 1.8 and 4.2°K. In each case, C_v can be resolved into an electronic contribution, γT, and a lattice contribution, $464.5(T/\theta)^3$. From the γ-values, the density of states at the Fermi level, $N(E_0)/n_a$, and the effective mass ratio, m^*/m, of the conduction electrons have been calculated. These quantities and the values of γ and θ are given in Table I.

Table I.

Sample	θ	$\gamma\times10^4$	$N(E_0)/n_a$ levels/atom/ev	m^*/m
Mg	342	3.25	0.289	1.33
Ti	290	8.29	0.736	3.26
Zr	265	6.92	0.615	2.24
Cr	400	3.74	0.332	2.88
Ge (pure)	278	0.00	...	...
Ge (impure)	286	1.29	0.115	7.39

* Assisted by the ONR.
** Westinghouse Graduate Fellow in Physics during the course of much of this work.
† A p-type sample, degenerate at these temperatures and containing 3.7×10^{19} holes/cm³.

F11. Some Observations on the Superconductive Transition in Pure Metals.* W. F. Love, *University of Pennsylvania.*—Mendelssohn and MacDonald[1] have reported that with properly prepared samples the superconductive transition in a longitudinal magnetic field is continuous, reversible, and spread over a considerable range of magnetic field strengths. Several specimens of pure Sn, In, and Tl have been prepared in 50μ bore capillaries, using a variety of methods of attaching current and potential leads. In all cases, the transition is continuous in increasing field strengths. In decreasing fields, considerable hysteresis develops and the transition to the normal state occurs in a single discontinuous step in most cases, and in fields considerably below that which resistance first began to appear in increasing fields. One specimen of indium returned to the normal state in several discrete steps, probably due to the existence of several crystallites, since another specimen prepared in the same manner showed a single drop. These results support the earlier measurements of de Haas and Voogd.[2]

* Supported by the AEC.
[1] Mendelssohn and MacDonald, Proc. Roy. Soc. (London) **A200**, 66 (1949).
[2] De Haas and Voogd, Leid. Comm., No. 191d.

F12. Meissner Effect in Alloys of In-Tl and Sn-Bi.* E. Callen, W. F. Love, and F. C. Nix, *University of Pennsylvania.*—The Meissner effect in single crystal spherical specimens of In-Tl alloys has been measured by the magnetic method of Shoenberg.[1] For concentrations up to 10 atmos percent Tl the frozen in flux is small and the magnetic properties like those of pure superconducting metals, as has been previously reported.[2] For higher concentrations of Tl increasing deviations are observed, especially as regards the breadth of the magnetic transition. The frozen in flux shows a maximum at compositions in the region of the transformation (cubic to tetragonal) occuring in this system. In the intermediate state, the diamagnetic moment of specimens of high Tl content is very sensitive to the small mechanical disturbances caused by the measuring technique. In increasing fields, the moment decreases with successive displacements of the sample, while in decreasing fields, it increases. In both cases, a final equilibrium value is attained after sufficient mechanical agitation. A considerable amount of the frozen in flux can be destroyed in this manner. Preliminary studies on a Sn plus 5 atmos percent Bi alloy show that the frozen in flux can be reduced to 20 percent by annealing a sufficiently long time.

* Supported by the AEC.
[1] Shoenberg, Proc. Roy. Soc. (London) **A175**, 49 (1950).
[2] J. W. Stout and L. Guttman, Phys. Rev. **79**, 396 (1950).

F13. The Melting Curve of He³. D. W. Osborne, B. M. Abraham, and B. Weinstock, *Argonne National Laboratory.*—Measurements of the melting pressure of He³ have been made by the blocked capillary technique from 1.51°K to 0.16°K. The data between 1.09°K and 0.16°K were obtained by surrounding the cupro-nickel capillary with iron ammonium alum, which was cooled by adiabatic demagnetization. In order to facilitate thermal contact between the small tube and the salt, copper vanes were soldered to the capillary, and the salt chamber was filled with He⁴ to a pressure of 1 atmos at 77°K. From 1.51°K to 0.5°K the melting pressure follows the equation $P=26.8+13.17^3$ atmos, but below 0.5°K the experimentally determined pressure rapidly approaches a constant value of 29.3 atmos. Further experiments are needed to determine whether the horizontal portion of the observed melting curve is to be attributed to poor thermal contact between the capillary and the salt below 0.5°K or to a transition in the liquid near 0.5°K. Regardless of this question it seems clear that the liquid is the stable condensed phase of He³ at 0°K.

Friday Afternoon at 2:00

Sherman, Crystal Room

(J. R. Platt presiding)

Spectroscopy—Radio Frequencies to X-Rays

G1. On a Multiple Scattering Theory of the Grating and the Wood Anomalies.* Vic Twersky, *Mathematics Research Group, New York University.*—The wave scattered by a grating of cylinders (or bosses on a perfectly conducting or rigid plane) is obtained as an infinite sum of "orders of scattering." The first order is the usual single scattering approximation,

while the higher orders include sums of products of single cylinder scattering coefficients and Schlömilch series involving Hankel functions of spacing. For $a \ll \lambda/2\pi \ll b, r$ (radius-a, spacing-b, distance-r) all orders are summed explicitly on neglecting end effects and certain "resonance wavelengths" discovered. These correspond to optimal simultaneous fulfilment of the physical conditions that the magnitudes of all orders be maxima and that either successive orders be in phase to reinforce, or out of phase to partially annul the first. These "maximal effects" should appear as bright and dark bands (overlaying the usual continuous spectra observed with broad-band radiation) at wavelengths somewhat longer than those having principal maxima in the grating's plane (Rayleigh's values), with intensities ranging from say 25–0.28 times the single scattered values, widths roughly proportional to λ^2, and character determined by material, polarization, and angle of incidence. These are not the usual ghosts that haunt the grating but are rather close kin of the skeletons in its closet discovered by Wood in 1902.

* Research supported in part by the Geophysical Research Directorate of the Air Force.

G2. The Arc Spectrum of Germanium. KENNETH L. ANDREW AND K. W. MEISSNER, *Purdue University.*—Despite earlier investigations of the germanium arc spectrum by Gartlein,[1] Rao,[2] and Kiess[3] many combinations and many predicted terms are still missing. A reinvestigation of the spectrum was, therefore, justified. A quartz arc lamp employing pure germanium electrodes covered with pure germanium dioxide was developed and yielded about 150 new lines between 10 460A and 4735A. This source produces very sharp lines. Wavelength measurements with a 30-foot concave grating and a Perot-Fabry interferometer resulted in the following contributions to the term analysis: (1) Kiess' terms arising from the $4s^24p5p$-configuration were verified and the missing $5p^1P_1$-term was found. (2) Three terms attributed by Kiess to the $4s^24p6p$-configuration have been confirmed and six of the missing seven terms of this configuration established. (3) Many of the new lines were identified as combinations between the even $5p$-terms and known odd terms found by Gartlein and Rao. (4) New odd and even terms were found.

[1] C. W. Gartlein, Phys. Rev. **31**, 782 (1928).
[2] K. R. Rao, Proc. Roy. Soc. (London) **A124**, 465 (1929).
[3] C. C. Kiess, J. Research Natl. Bur. Standards **24**, 1, RP 1266 (1940).

G3. Long Forbidden $s-ns$ Series in RbI. J. E. MACK, *University of Wisconsin.*—The forbidden lines previously interpreted[1,2] as $s-(n-3)f$ must be reinterpreted as $s-ns$. The high f-terms cannot be resolved from their neighbors with higher l-values. Thus, there occur in a 28-meter absorption path in rubidium the absorption lines (attributable to fields from neighboring atoms) $6s^2S_{\frac{1}{2}}-ns^2S_{\frac{1}{2}}$, where n runs from 32 to 52 or possibly 53.

[1] H. R. Kratz and J. E. Mack, Phys. Rev. **76**, 173(A) (1949).
[2] J. E. Mack, Phys. Rev. **77**, 745(A) (1950).

G4. K-Excitation Potentials of the Elements. G. L. ROGOSA, *Florida State University.*—Tables of the K-excitation potentials or the K-absorption limits of the elements are easily available, but practically all of these tables suffer from two defects: (1) a confusion of the relationship of the Siegbahn x-unit to the angstrom; (2) the use of old inaccurate data. The values of the excitation potentials are particularly important in the calibration of highly stabilized, high voltage x-ray power supplies and in the precise measurement of gamma-ray energies by internal conversion experiments, especially with the improvements in the magnetic field measurements.[1] The preparation of a table of excitation potentials in absolute volts is proceeding by careful investigation of the available literature and the use of the necessary fundamental constants as given by DuMond.[2] Particular use is made of the tables by Cauchois and Hulubei.[3] The criteria for the selection of particular values will be discussed and copies of the tables will be made available.

[1] Walter I. Brown, Phys. Rev. **83**, 271 (1951).
[2] J. W. M. DuMond and E. R. Cohen, Phys. Rev. **82**, 555 (1951).
[3] Y. Cauchois and H. Hulubei, *Longuers D'Onde des Emissions X et des Discontinuités D'Absorption X.*

G5. The Nuclear Spin of Cl^{38} from the Microwave Spectrum of $C^{13}H_3Cl^{38}$. D. A. GILBERT, *State University of Iowa.*—The early work of Wu and Feldman[1] on the β-spectrum of $Cl^{38} \rightarrow A^{38}$ was interpreted to require a spin change $\Delta I = 3$ and hence the spin of Cl^{38} to be 3; however, in a more recent paper[2] Wu and Feldman point out that a unique value of ΔI cannot be obtained from this β-spectrum. The microwave spectrum of $Cl^{36}CN$, as measured by Townes and Aamodt,[3] would require spin 2. The present work shows clearly that the spin is 2. In this experiment a study was made of the $J=0\rightarrow1$ rotational transitions of $C^{13}H_3Cl^{38}$. The observed hyperfine pattern is shown to fit best with the theoretical pattern for $I=2$. The magnitude of the frequency separations gives the value -15.6 ± 0.6 mc for the quadrupole coupling constant, eqQ, and $-0.0164\pm0.0008\times10^{-24}$ cm^2 for the nuclear electric quadrupole moment, Q. This work was supported by the ONR.

[1] C. S. Wu and L. Feldman, Phys. Rev. **76**, 693 (1949).
[2] C. S. Wu and L. Feldman, Phys. Rev. **82**, 457 (1951).
[3] C. H. Townes and L. C. Aamodt, Phys. Rev. **76**, 691 (1949).

G6. The Nuclear Moment and Hyperfine Structure Anomaly of K^{40}.* JOSEPH T. EISINGER AND BENJAMIN BEDERSON, *Massachusetts Institute of Technology.*—An atomic beam method was used to measure the following quantities: $g_I(K^{40})/g_I(K^{39}) = -1.2434\pm0.0003$, $\mu_I(K^{40}) = -1.2965\pm0.0004$ nm, $\Delta\nu(K^{40}) = 1285.790\pm0.007$ Mc/sec. A mass spectrometer was used to separate the K beam into its isotopes, K^{40} being detected by an electron multiplier. The transitions were observed at high fields, the line widths being 3 kc/sec at about 150 Mc/sec. According to Bohr and Weisskopf[1] the hfs, calculated on a point dipole assumption, must be corrected by a factor $1+\epsilon$ where ϵ depends on the structure of the nucleus. The present experimental data yield $\Delta = \epsilon(K^{39}) - \epsilon(K^{40}) = [\Delta\nu(K^{39})/\Delta\nu(K^{40})][g_I(K^{40})/g_I(K^{39})](9/4) - 1 = (0.46\pm0.03)$ percent. Different nuclear models for K^{40} were used to obtain theoretical values for Δ. Satisfactory agreement can most readily be obtained when the asymmetrical nuclear model proposed by Bohr[2] as a refinement of the Bohr-Weisskopf theory is used.[3]

* This work was supported in part by the Signal Corps, the Air Materiel Command, and the ONR.

[1] A. Bohr and V. F. Weisskopf, Phys. Rev. **77**, 94 (1950).
[2] Aage Bohr, Phys. Rev. **81**, 331 (1951).
[3] Aage Bohr, private communication.

G7. Quadrupole Moment of the Electron Distribution in the Hydrogen Molecule.* N. J. HARRICK, R. G. BARNES, AND P. J. BRAY, *Harvard University.*—Measurements on the Harvard molecular beam apparatus, making use of a long homogeneous magnet and the Ramsey separated rf technique, have been made on transitions $m_J=0$, $m_J=-1\rightarrow0$, and $m_J=0$, $m_J=0\rightarrow+1$ in H_2. From these measurements the rotational magnetic moment and dependence of the diamagnetic susceptibility on the orientation of the molecules' rotational angular momentum have been calculated to be $\mu_R = 0.88287\ 0.00008$ nm and $\xi_{+1} - \xi_0 = -(3.86\pm0.20)\times10^{-31}$. From the former, the contribution of the high frequency terms to the susceptibility per molecule of H_2 is determined to be $\xi_{HF} = 1.5115\pm0.0002\times10^{-31}$. The quadrupole moment relative to the internuclear axis is

$$Q_e = -20(mc^2/e^2)[(\xi_{+1} - \xi_0) - \tfrac{1}{2}\xi_{HF}]^{\frac{1}{2}} = (0.339\pm0.014)\times10^{-16}\ \text{cm}^2.$$

This compares favorably with the theoretically computed[1] value of $Q_e = 0.31\pm10^{-16}$ cm^2. Improved values of spin-spin

and spin-rotational magnetic interaction constants have been obtained for both H_2 and D_2. From the spin-spin constant for H_2 a value of the internuclear distance has been calculated.

* This work was partially supported by the joint program of the ONR and AEC.
[1] N. F. Ramsey, Phys. Rev. **78**, 221 (1950).

G8. Sign Determination for Molecular Magnetic Moments.* C. K. JEN, J. W. B. BARGHAUSEN, AND R. W. STANLEY, *The Johns Hopkins University.*—The sign of the molecular magnetic moment can be determined by noting the asymmetry of the microwave Zeeman pattern due to a circularly polarized wave.[1] Circular polarization is produced from initial linear polarization by a mica phase-shifter or a squeezed section of wave guide. The absorption cell, formed by a short section of round wave guide, is placed in the center of a solenoid, which furnishes a steady magnetic field up to about 2500 oersteds. It has been found that either the $\Delta M=+1$ or the $\Delta M=-1$ Zeeman transitions can be completely suppressed by using the circularly polarized wave with a definite sense of rotation relative to the direction of the magnetic field. The signs of the rotational magnetic moments of ammonia and water molecules have both been found to be positive, in agreement with current concepts.

* Supported by Bureau of Ordnance, U. S. Navy, under Contract NOrd-7386.
[1] An earlier work has been done by J. R. Eshach, MIT thesis, December, 1950.

G9. Pressure-Broadening of Absorption Lines.* STANLEY BLOOM AND HENRY MARGENAU, *Yale University.*—Elementary perturbation theory is used to derive a formula for the intensity distribution of a pressure-broadened absorption line. To obtain a correct result it is necessary to calculate the probability of collision-induced transitions, not between the states of an isolated molecule as is customary, but between the unsharp energy states which characterize the molecule by virtue of its collisions with others. Unless the statistical matrix is taken diagonal the intensity distribution is of apparently meaningless complexity. Our result is similar to that obtained by Anderson[1] for emission lines, but it contains an anti-resonant term. Complete reduction to Anderson's formula occurs under two conditions: 1. The broad lines are sufficiently far apart to escape overlapping when broadened. 2. The absorbed light has a random distribution of phases, over which an average can be taken. Our method does not, however, seem to produce the correct numerical factor needed for detailed balancing between absorption and emission at all frequencies.

* Supported by the ONR.
[1] P. W. Anderson, Phys. Rev. **76**, 647 (1949) (Eq. (2)).

G10. Further Studies of *l*-Type Doubling Transitions in HCN and DCN.* THOMAS L. WEATHERLY, EDWARD R. MANRING, AND DUDLEY WILLIAMS, *Department of Physics and Astronomy, The Ohio State University.*—Absorption lines caused by direct transitions between *l*-type doubling levels have been observed for $J=9$, 10, and 11 for HCN and $J=10$, 11, and 12 for DCN. The observed frequencies $\Delta\nu$ and the resulting q-values defined by $q=\Delta\nu/J(J+1)$ are listed in Table I. The values of q calculated from Nielsen's expression[1]

TABLE I. *l*-type doubling transitions in HCN and DCN.

Molecule	Rotational level J	Observed frequency (mc/sec)	q-value (mc/sec)
HCN	9	20,181.39±.15	224.23*8*
HCN	10	24,660.40±.10	224.18*5*
HCN	11	29,585.12±.20	224.13*0*
DCN	10	20,454.58±.15	185.95*1*
DCN	11	24,539.20±.10	185.90*3*
DCN	12	28,992.55±.20	185.85*0*

are $q=226.2$ mc/sec for HCN and $q=183.6$ mc/sec for DCN. Thus the observed q-value for HCN is slightly lower than the calculated value, and the observed q-value for DCN is slightly higher than the calculated value. The q-values obtained from the observed spectra show a slight decrease with increasing J.

* This work was done in connection with Contract AF 19(122)-13 between Air Force Cambridge Research Center and The Ohio State University Research Foundation.
[1] H. H. Nielsen, Phys. Rev. **78**, 296 (1950).

G11. The Microwave Spectrum of a Slightly Aspherical Top—the Structure and Dipole Moment of Sulfuryl Fluoride.* ROBERT M. FRISTROM,† *Harvard University.*—The microwave spectrum of the slightly aspherical rotor, sulfuryl fluoride, has been investigated. Seven lines were found in the twenty- to thirty-thousand-megacycle region. Six of these lines were assigned to $J=1\rightarrow2$ and $2\rightarrow3$ rotational transitions of the molecule $S^{32}O_2F_2$ and the other to the $1_{11}\rightarrow2_{12}$ transition of $S^{34}O_2F_2$. These lines can be fitted to within the limits of experimental error (0.002 percent) with the following reciprocal moments of inertia:

$a_{32}=5139.77$ mc $\quad a_{34}=5139.77$ mc
$b_{32}=5077.81$ mc $\quad b_{34}=5073.10$ mc
$c_{32}=5057.22$ mc $\quad c_{34}=5052.51$ mc.

Structural parameters were determined from these moments and the assumption of C_{2v} symmetry. The latter was confirmed by intensity measurements.

S−O 1.370±0.01A $\quad$ S−F 1.570±0.01A
O−S−O angle 129°38′±30′ $\quad$ F−S−F angle 92°47′±30′.

The S−O distance differs by −0.06A from the published electron diffraction value. Measurements on stark lobes of the three $1\rightarrow2$ transitions of $S^{32}O_2F_2$ gave a quantitative check of the assignment and a value of 0.228 Debye unit for the dipole moment.

* This work was supported by the Navy Department through the ONR under Task Order V.
† Present address: The Johns Hopkins University, Applied Physics Laboratory, Silver Spring, Maryland.

G12. Microwave Spectrum and Structure of Ozone.* RICHARD H. HUGHES.—A study has been made of the rotational spectrum of ozone between 8000 and 43,000 mc. The $2_{0,2}\rightarrow1_{1,1}$ line was found at 42,833 mc and the $3_{1,3}\rightarrow4_{0,4}$ at 11,073 mc. Using the frequencies of these lines and values of the asymmetry parameter δ between 0.01596 and 0.01600, moments of inertia were calculated which have been used to predict correctly the frequencies of seven other strong lines of J's between 9 and 23 to within ±200 mc. Calculations have not been made to account for two other observed lines of medium intensity and four of weak intensity. The calculated Stark effects of the two low J lines are consistent with the observed. Because of zero point vibrations, three moments of inertia slightly inconsistent with a planar structure are obtained. Assuming a planar structure, and taking the moments of inertia two at a time, the following range of values were obtained for the parameters of an isosceles triangle: the length of the two equal sides = 1.276−1.279A°; the apex angle = 116.5 −117.0°. The bond distance agrees well with that given by electron diffraction† but the angle differs considerably from the electron diffraction value of 127±3°. The dipole moment is 0.65±0.05 Debye.

* The early phase of this work was supported in part by the ONR when the author was in the Chemistry Department at Harvard University.
† W. Shand and R. A. Spurr, J. Am. Chem. Soc. **65**, 179–81 (1943).

G13. Microwave Absorption Spectrum of H_2O_2. J. T. MASSEY AND D. R. BIANCO, *The Johns Hopkins University.**—Utilizing an experimental sampling technique developed for the purpose, four absorption lines of the hydrogen peroxide molecule have been found at frequencies of approximately

14,830, 22,050, 27,638, and 35,912 mc. Using a dc field with a small 100 kc ac field superimposed, the Stark effect of the four lines has been studied and it has been found that all of the lines exhibit a quadratic Stark effect. It has been possible to completely resolve the Stark components of the first three of the four lines. There is considerable evidence that the H_2O_2 molecule has a nonplanar structure[1,2] and should possibly exhibit torsional oscillation.[3,4] The method outlined by Koehler and Dennison[5] is being applied to this model and calculations are also being made on a planar model in an attempt to correlate the observed microwave spectrum with the molecular structure.

* This work was supported by the U. S. Navy, Bureau of Ordnance under Contract NOrd-7386.
[1] W. G. Penney and W. B. B. M. Sutherland, J. Chem. Phys. **2**, 492 (1934).
[2] Lu, Hughes, and Giguère, J. Am. Chem. Soc. **63**, 1507 (1941).
[3] L. R. Zumwalt and P. A. Giguère, J. Chem. Phys. **9**, 458 (1941).
[4] P. A. Giguère, J. Chem. Phys. **18**, 88 (1950).
[5] J. S. Koehler and D. M. Dennison, Phys. Rev. **57**, 1006 (1940).

FRIDAY AFTERNOON AT 2:00

Sherman, Louis XVI Room

(ENRICO FERMI presiding)

Mesons and Cosmic Rays

H1. The Interaction of Charged π-Mesons with the Deuteron. W. B. CHESTON,* *University of Rochester.*—Calculations on the interaction of a charged meson of positive energy with the deuteron have been carried out in the conventional weak-coupling pseudoscalar theory for both direct and gradient couplings. The nucleon-nucleon interaction has been treated phenomenologically and the "impulse" approximation[1] employed. The processes considered were radiative absorption, charge-exchange scattering, and elastic and inelastic scattering; the nonradiative absorption results have already been published.[2] The ratio {σ nonradiative/σ radiative} in the pseudoscalar theory is essentially constant over a meson energy interval 0–25 Mev in contrast to the pseudovector theory. The differential cross section for charge-exchange scattering has a minimum in the forward direction, but otherwise mirrors the behavior of the charge-exchange scattering from a single nucleon target.[3] The elastic and inelastic scattering differential cross sections are peaked in the forward direction for direct coupling and at right angles for gradient coupling. For both types of coupling, the energy dependence of the total cross section is similar to the dependence of the single nucleon cross section.[3]

* Present address: Washington University, St. Louis, Missouri.
[1] G. Chew, Phys. Rev. **80**, 196 (1950).
[2] W. Cheston, Phys. Rev. **83**, 1118 (1951).
[3] Ashkin, Simon, and Marshak, Prog. Theor. Phys. **5**, 634 (1950).

H2. Charged π Meson Production in D and Pb at 90° from a 381-Mev Proton Beam.* M. M. BLOCK, S. PASSMAN, AND W. W. HAVENS, JR., *Columbia University.*—The differential cross sections for the production of charged π-mesons in D and Pb at (90±5)° from a 381-Mev proton beam have been obtained. Nuclear emulsions imbedded in tapered copper absorbers are exposed to mesons produced by bombardment of targets by the internal circulating proton beam of the Nevis cyclotron. The irradiation geometry we have previously described has been modified to provide better energy resolution. The deuterium cross section was obtained by using a deuterated paraffin target and subtracting the known carbon cross section. The absolute cross sections were obtained by monitoring the C^{11} activity production in the target or in a polyethylene foil. Preliminary results are shown in Table I.

TABLE I.

Element	90°π^+ cross section, integrated over meson energy	90°π^- cross section integrated over meson energy
D	$(2.8\pm1.2)\times10^{-28}$ cm²-ster^{-1}	$(2.5\pm2.0)\times10^{-28}$ cm²-ster^{-1}
Pb	$(11.7\pm4.5)\times10^{-28}$ cm²-ster^{-1}	$(4.0\pm3.0)\times10^{-28}$ cm²-ster^{-1}

Theoretical calculations for the production of π^+ mesons in a heavy element have been extended to include deuterium. Comparison of the calculations with experiment and the implications as to nuclear forces will be discussed.

* This work was supported by the joint program of the ONR and AEC.

H3. Interactions of Pi-Mesons in Carbon.* H. BYFIELD, J. KESSLER, AND L. LEDERMAN, *Columbia University.*—The scatterings and absorptions of pi-mesons (62±10 Mev) in carbon were studied in a 16-in. cloud chamber. Momenta of mesons incident upon and scattered from a single 2 g/cm² carbon plate were determined with a precision of about 10 percent. A total of about 500 nuclear events produced by both π^+ and π^- mesons consisted of elastic scatterings, inelastic scatterings[1] and stars with two to zero prongs. The latter (apparent stoppings) were restricted to a central fraction of the illuminated region to minimize confusion with out-scatterings. An angular distribution for elastic scattering of the π^- mesons is obtained which is strongly peaked forward, drops to a plateau of 5 mb/sterad at 60° and rises to 9 mb/sterad for backward scattering. We find

$$\int_{10°}^{180°} \sigma_{\text{elas}}(\theta)d\Omega = 204\pm18 \text{ mb}.$$

These results are in agreement with those obtained from counter studies.[2] The inelastic ($\Delta E>15$ Mev) angular distribution has a valley centered about 90°, probably because of the thickness of carbon plate and has a total cross section of 39±8 mb. The total absorption cross section (excluding elastic scatters <60°) is 244±20 mb. Fast protons ($E>40$ Mev) are observed in 11 percent of the stars. The total cross sections for π^+ interactions are very similar and these results will be detailed.

* Assisted by the joint program of the ONR and AEC.
[1] Bernardini, Booth, Lederman, and Tinlot, Phys. Rev. **82**, 105 (1951).
[2] Isaacs, Sachs, and Steinberger, this meeting.

H4. Elastic Scattering of Negative Pions in Carbon.* P. ISAACS, A. SACHS, AND J. STEINBERGER, *Columbia University.*—The elastic scattering of 62- and 90-Mev negative pions in carbon has been measured. Mesons defined in a two-counter telescope are scattered in a carbon plate and detected in two scintillation counters, with sufficient absorber between the counters to accept mesons only with energy greater than 56 and 79 Mev, respectively, for the two incident beams. Angular distributions for both beams show (a) Coulomb scattering at small angles with a gradual transition to diffraction scattering between 10 and 15 degrees, (b) a broad minimum in the 90-degree region with a differential cross

section of about 2×10^{-27} cm²/steradian, and (c) a slight rise in cross section for backward angles. For incident mesons of 90 ± 5 Mev, the integrated elastic cross sections are $2.4\pm.3\times10^{-25}$ cm² between 15 and 180 degrees and $2.2\pm.3\times10^{-25}$ cm² between 70 and 180 degrees, compared to the inelastic cross section of $3.08\pm.13\times10^{-25}$ cm². The 62-Mev results are in agreement with those of cloud-chamber experiments performed in this laboratory.[1]

* Research assisted by the ONR and AEC.
[1] Byfield, Kessler, and Lederman, Bull. Am. Phys. Soc. 26, No. 6, Abstract H2 (1951) (this meeting).

H5. Lifetime of the Pi-Meson.* L. LEDERMAN, H. BYFIELD, AND J. KESSLER, *Columbia University*.—The decay-in-flight of 62-Mev pi-mesons in the gas of a 16-in. magnet cloud chamber has yielded[1] a value for the lifetime of the negative pi-meson. This value has been improved by increased statistics and better knowledge of beam impurities. The best present value is $2.85\pm.25\times10^{-8}$ sec. The lifetime of the positive pi-meson has been determined in a similar manner. The π^+ beam is obtained simply by reversing the field of the cyclotron magnet, the cloud-chamber location remaining fixed. The scanning and geometrical corrections were carried out in the same way as for the negatives.[1] Electron contamination is obtained from scattering plate data and electronic experiments and is taken as <2 percent. The mu meson contamination is assumed the same as in the π^- beam. With these assumptions, the ratio of π^+ to π^- lifetimes is: $\tau^+/\tau^-=1.01\pm0.11$.

* Assisted by the joint program of the ONR and AEC.
[1] Lederman, Booth, Byfield, and Kessler, Phys. Rev. 83, 685 (1951).

H6. A Photographic Study of $\pi\rightarrow\mu\rightarrow\beta$-Decay.* H. J. BRAMSON, A. M. SEIFERT, AND W. W. HAVENS, JR., *Columbia University*.—Work previously reported[1] on the β-spectrum from μ-meson decay and on the search for anomalous μ-meson ranges from $\pi\rightarrow\mu$ is being continued. To date, some 1500 $\pi\rightarrow\mu$-decays have been observed where the μ-meson ends in emulsion 0.6 mm or 1 mm thick. Since a nearly monoenergetic monodirectional acceptance of π-mesons is achieved by suitable collimation,[2] mesons can be identified as π or μ before the apparent decay with an uncertainty of no more than one part in 10^3. A search was made for decay ranges shorter than 450 microns. One such event has been found: where the μ-meson has a range of 235 microns. Multiple scattering measurements of the β-tracks to determine their energy are in progress. Current data yield substantially the same spectrum presented earlier,[1] indicating a finite cut-off at the high energy end. The results of increased statistics will be presented.

* This research is being assisted by the joint program of the ONR and AEC.
[1] H. J. Bramson and W. W. Havens, Jr., Phys. Rev. 83, 861 (1951).
[2] H. Friedman and L. J. Rainwater, Phys. Rev. 81, 644 (1951).

H7. Annihilation Radiation from μ^+ Mesons. M. H. JOHNSON, *Naval Research Laboratory*.—The scheme $\mu^++\epsilon^-\rightarrow A\rightarrow2\gamma$ represents annihilation of a μ^+ meson through the intermediate state A. As intermediate states for which the transformation of rest mass to radiation is allowed, consider the three possibilities: $A_1=\epsilon^++\epsilon^-$; $A_2=\mu^++\mu^-$; and $A_3=\pi^0$. Radiation theory in the first two cases and the experimental π^0 lifetime in the third approximately determine transition matrix elements from A to the final state. The absence of experimental evidence for the transformations $\mu^+\rightarrow\epsilon^++\gamma$, $\mu\rightarrow\epsilon^-+\gamma$ and $\pi^0\rightarrow\mu^++\epsilon^-$, serve to set approximate upper limits on the transition matrix elements from A to the initial state. An upper limit to the annihilation rates in all three cases of 10^{-7} sec^{-1} can be so established for an electron density 10^{24} cm^{-3}, in comparison to the observed decay rate 10^8 sec^{-1}.

H8. Relative Pair Production Cross Section in the Region 50 to 300 Mev.* C. R. EMIGH, *University of Illinois*.—A cloud-chamber survey has been made of pairs produced in Al, Ag, and Au foils by an x-ray beam from the 300-Mev betatron. Two foils were placed parallel and spaced 14 cm apart in the chamber to intercept the same x-ray beam. The ratio of pairs produced in one foil to those produced in the other was determined. All possible combinations and relative positions of the foils were used during the experiment. Preliminary results of 36,000 pairs analyzed to date give for the pair-production cross section of Au to Al the values of $.89\pm.02$ for 50 to 100 Mev, $.85\pm.03$ for 100 to 150 Mev, $.89\pm.04$ for 150 to 200 Mev, and $.78\pm.1$ for 200 to 300 Mev. The ratio of Ag to Al is $.94\pm.02$ for 50 to 100 Mev, $.92\pm.03$ for 100 to 150 Mev, $.91\pm.04$ for 150 to 200 Mev, and $.84\pm.09$ for 200 to 300 Mev. The ratios are low compared with the Bethe-Heitler theory, approximately 6 percent for Au to Al and 3 percent for Ag to Al.

* Assisted by the joint program of the ONR and AEC.

H9. Penetrating Showers under Hydrogen and Heavier Elements Observed in a Cloud Chamber at Sea Level.* A. B. WEAVER AND MARCEL SCHEIN, *University of Chicago*.—Local penetrating showers produced by ionizing and nonionizing radiation in various materials above a cloud chamber were studied. The chamber was located at sea level and was operated in a field of 9270 gauss. The materials placed above the chamber to generate the penetrating showers were: (1) liquid hydrogen averaging 2 g/cm²; (2) paraffin, 40 g/cm²; (3) carbon, 57.3 g/cm²; (4) aluminum, 92.5 g/cm²; and (5) lead, 168 g/cm². Some of the events observed and the information obtained concerning nucleon-nucleon collisions will be discussed.

* Assisted by the joint program of the ONR and AEC.

H10. A Study of Penetrating Showers Produced in Be, Carbon, and Lead at Sea Level. L. GRODZINS, G. DEL CASTILLO, AND W. Y. CHANG, *Purdue University*.—The equipment used for the 11 months investigation was a counter controlled cylindrical cloud chamber (12 in. diam, 8 in. deep) as previously reported.[1] Three plates, the upper two of Be, 4.8 g/cm² each, and the lowest of Pb, 17 g/cm², were placed inside the chamber for the full 11 months. 43 g/cm² of C was placed above the chamber for the first 6 months and 43 g/cm² of Pb placed there for the remaining 5. Defining a penetrating particle as one which passes through the 17 g/cm² Pb plate without multiplication and without scattering through more than 20°, the results for the multiplicity of charged particles in the first gas space below the origin of the shower can be summarized as follows (in each shower at least one particle penetrates 110 g/cm² Pb below the chamber).

No. of parts/shower		2	3	4	5	6	7	8	9	10	15	av. mult.
No. of showers observed	Be	45	12	3	1	2						2.5
	C	52	21	3	5	1	1				1	2.8
	Pb	47	15	3	2	2	1	1	1	1		2.8

The multiplicity distribution in each element is generally compatible with the theory of multiple production by primary nucleons of a few Bev energy.

[1] G. Del Castillo and W. Y. Chang, Phys. Rev. 81, 323 (1951).

H11. Two Cosmic-Ray Decreases Associated with the Geomagnetic Storms and Sunspot Activity of May and June, 1951.* R. L. CHASSON, *University of California*.—Continuous records of the total and hard (20-cm lead absorber) sea-level cosmic-ray intensity have been made in Berkeley, starting November, 1950. The apparatus consists of four geometrically identical wide-angle triple-coincidence counter telescopes, two for each radiation component. Correlations between intensity fluctuations and atmospheric and geomagnetic disturbances

have been made. A considerable intensity decrease started on May 23, 1951, followed on May 25 by a magnetic storm. The intensity then slowly returned to its pre-storm value. The May 23 decrease coincided with the disappearance around the West limb of the giant sunspot group Mt. Wilson 10662 (May 9–May 23). A larger, more persistent intensity decrease started June 11, 1951. A magnetic storm occurred June 17, in the middle of the period of the large intensity decrease. The passage across the disk of the giant sunspot group Mt. Wilson 10692 (June 12–June 25) coincided with the period of the latter decrease. Such a pre-storm decrease of intensity has been noted previously,[1] also in conjunction with unusual sunspot activity and accompanying geomagnetic disturbances.

* Work performed under auspices of the Joint program of the ONR and AEC.

[1] A. Duperier and M. McCaig, Nature **157**, 477 (1946).

H12. Analysis of the Nucleonic Component Using Neutron Latitude Variations.* S. B. TREIMAN,† *University of Chicago.*—A function, $S_A(N, x)$, is defined which gives the rate of production of neutrons per gram of air at depth x arising from a unit vertical flux of primary cosmic ray particles of atomic weight A and momentum to charge ratio N. Using the Simpson[1] neutron latitude curve for 312 g-cm^{-2}, and the Winckler[2] primary spectrum, a geomagnetic analysis gives the function $S(N, x) = \Sigma_A f_A(N) S_A(N, x)$, where $f_A(N)$ is the fraction of primaries of atomic weight A. It is found that $S(N, x)$ is almost independent of N for N between 10 and at least 13.6 Bev/c. From available data[3] it appears that the $f_A(N)$ are almost independent of N in this range. It is then shown, assuming high energy collisions behave like single nucleon-nucleon interactions, that the $S_A(N, x)$ are, for all A, almost independent of energy for primary nucleon energies between 4 and at least 12.7 Bev, and for x at least between 20 and 600 8-cm^{-2}.

* Assisted in part by the Office of Air Research, USAF.
† Predoctoral Fellow.
[1] J. A. Simpson, Jr., Phys. Rev. **76**, 569 (1949); Phys. Rev. (to be published).
[2] Winckler, Stix, Dwight, and Sabin, Phys. Rev. **79**, 656 (1950).
[3] B. Peters, *Progress in Cosmic Ray Physics* (North Holland Publishing Company, Amsterdam)(to be published).

H13. Experiments on the Solar-Produced Component of the Cosmic Radiations.* J. A. SIMPSON, W. FONGER, AND L. WILCOX, *University of Chicago.*—Time-dependent changes of the primary cosmic-ray radiations have been investigated in the low and intermediate energy range by measuring the neutron intensity of the nucleonic component. Continuous observations were made simultaneously at several latitudes and altitudes and the momentum distributions of the changes were investigated in high altitude aircraft operating between 40° and 69°N. Twenty-seven day periodic recurrences of increased primary intensity have been found and associated with large disturbed regions on the sun. Hence, they coincide with a 27-day solar spin. These regions are identified by the observation of solar radio noise bursts and by visual flare effects. During the first half of 1951, differences of intensity within 30 days became as large as the order of 10 percent at sea level. The increases were observed simultaneously at all recording stations. Some local regions in the sun persisted for at least three solar rotation periods and were accompanied by increased primary radiation. It is shown that these increases are neither a result of geo-dipole magnetic field changes nor dependent on the properties of the atmosphere. Changes of intensity of primaries with momenta >5(Bev/c) have been observed. It is shown that these appreciable increases of primary cosmic-ray intensity are associated with local regions on the sun.

* Assisted in part by the Office of Air Research, USAF.

H14. Heavy Metal Cosmic Ray Primaries. HERMAN YAGODA, *National Institutes of Health.*—Microscopic examination of 2-mm thick emulsion castings exposed in the stratosphere at elevations reaching 110,000 ft provides evidence for a group of heavy primaries of $Z>26$. In a preliminary report[1] an exceptionally heavy track was identified as of charge 49 ± 3 on the basis of thin-down length. Scanning at low power for heavy primaries ($Z\geq6$) whose tracks terminate in the emulsion indicates that at atmospheric depths of 7 to 15 g.cm^{-2} heavy metal nuclei ($Z>34$) have an abundance about 0.3 that of the Fe-Co-Ni group. These tracks are characterized by dense cylinders of secondary ionization up to 30 microns diameter and pronounced thin down lengths of 500 ±100 microns. The flux of heavy metal nuclei is rapidly attenuated in traversing the upper atmosphere, as the examination of an equal volume of emulsion flown at 80,000 ft failed to reveal tracks heavier than $Z=26$. One event shows the fragmentation of a heavy metal nucleus into a narrow angle beam comprised of Fe$+$2Ne$+$Be$+$He$+$H nuclei which indicates a charge on the incident particle of 53 ± 6. The method has been checked on an event showing the breakdown of an iron nucleus (identified by delta-ray count) into O$+$Be$+$Li $+$11H particles. The presence of heavy metal nuclei is this indicated both by the ionization along their tracks and charge conservation in nuclear interactions.

[1] H. Yagoda, Phys. Rev. **80**, 753 (1950).

FRIDAY AFTERNOON AT 2:00

Sherman, Grey Room

(G. WENTZEL presiding)

General Physics—Theoretical

I1. Classical Meson Theory and Action at a Distance. PETER HAVAS, *Lehigh University.*—A theory of action at a distance was developed recently for particles interacting through neutral meson fields.[1,2] This work has now been extended to charged fields in the classical counterpart of the charge symmetrical theory of Kemmer. The field theoretical equations of motion, found recently for retarded interaction through vector meson fields,[3] contain integrals over the past and entire motion for the retarded and half-retarded, half-advanced interaction, respectively. As in the neutral theory we omit them from the postulated equations of motion of action at a distance. A variational principle is developed for these new equations with symmetric interaction; the equations of motion, of the variation of charge and of the fields of the "adjunct" field theory are derivable from it. An energy-momentum tensor and a charge-current vector guaranteeing detailed conservation laws are defined. The application of the Wheeler-Feynman method to the equations of both theories is discussed. Analogous results are obtained for scalar mesons.

[1] P. Havas, Phys. Rev. (to be published) (vector and scalar mesons).
[2] H. Kanazawa, Prog. Theor. Phys. **5**, 1050 (1950); H. Steinwedel and S.-B. Heidelberger, Akad. Wiss., math.-naturwiss. Kl., 281 (1950) (vector mesons).
[3] K. J. Le Conteur, Proc. Cambridge Phil. Soc. **45**, 429 (1949).

I2. The Contribution of Interaction Moments to Nuclear Magnetic Moments. MARC ROSS, *University of Wisconsin.*—The spin-antisymmetric interaction moment[1,2] can contribute to the static magnetic dipole moments of nuclei and to magnetic transitions in nuclear isomers and in the two- and three-body systems. This interaction moment is determined from the three-body moment anomaly and may be considered to represent a modification of neutron intrinsic moment due to the proximity of protons, and vice versa. The contribution to the magnetic moments of nuclei has been calculated, using wave functions prescribed by M. G. Mayer's spin-orbit coupling model. A very simple expression for the moment is found. For odd proton nuclei the resulting contribution is roughly $+\frac{1}{2}$ n.m. for $j=l+\frac{1}{2}$ and $-\frac{1}{2}$ n.m. for $j=l-\frac{1}{2}$; and the same with opposite sign for odd neutron nuclei. Thus the spin-antisymmetric contribution is small, and of such a sign as to increase the magnitudes of theoretically predicted moments. The results suggest that if interaction effects lead to important modifications of nuclear moments these may only show up in the heavy nuclei.

[1] N. Austern, Phys. Rev. **81**, 307(A) (1951).
[2] R. G. Sachs and N. Austern, Phys. Rev. **81**, 705, 710 (1951).

I3. Covariant Theory of Damping. J. C. PIRENNE,* *National Research Council, Canada.*—The covariant construction of the S-matrix in the Cayley form in terms of a hermitian operator K, will be compared with previous non covariant formulations of Heitler and Pauli. New general formulas for K will be presented, connecting Gupta's and Miyazima's results.[1,2] The nth order approximation of K and S are closely related, and K is generally expressed in terms of the anti-hermitian parts of the S_p of order $p \leqslant n$.

* Associate Fellow of the "Fonds National de la Recherche Scientifique," Bruxelles, Belgique.
[1] S. Gupta, Proc. Cambridge Phil. Soc. **47**, 454 (1951).
[2] Miyazima, Prog. Theor. Phys. **5**, 152 (1950).

I4. On the Thermodynamics of Fields. A. E. SCHEIDEGGER AND C. D. MCKAY, *Queen's University.*—In connection with our recent investigations on quantum statistics of Fields,[1] some further results have been obtained. Firstly, one expects that the formalism for constructing the thermodynamic functions of vacuum fields breaks down if the fields are treated classically. This is explicitly shown to be the case. Secondly, it has been observed that the thermodynamic functions of the relativistic fields do not yield the thermodynamic functions of the nonrelativistic fields if c approaches infinity. It is shown that this is the result of the presence of the rest mass of the particles in the hamiltonian. A subtraction procedure to subtract this rest mass has been developed and it is shown that the latter introduces a new parameter into the thermodynamic functions which is very similar to the temperature. Thirdly, it is of some interest to calculate the fluctuations of the thermodynamic variables around their expectation values. Thus expressions for the vacuum fluctuations of quantized fields have been obtained.

[1] A. E. Scheidegger and C. D. McKay, Phys. Rev. **83**, 125 (1951).

I5. On an Extension of the Classical Infinitesimal Group of Canonical Transformations.—D. C. RIVIER,* *National Research Council, Canada.*—By introducing a generalization of the classical poisson bracket of two functions of canonical variables, it is possible to extend the infinitesimal group of canonical transformations. The generalized poisson bracket satisfies all the main identities of the usual poisson bracket, chiefly the jacobi identity. This is a necessary condition for the generalized set of transformations to form an infinitesimal continuous group. The main difference between the new and the usual poisson bracket is that the new one involves derivatives of order higher than the first. The set of generalized infinitesimal transformations may be put in a one-one correspondence with the infinitesimal group of unitary transformations of quantum mechanics, in such a way that correspondence between generalized poisson bracket and commutators is valid generally. This gives a different approach to the problem of correspondence between classical and quantum mechanics.

* Postdoctoral Fellow of the "Commission Suisse des Bourses de Mathematiques et de Physique."

I6. On the Geometry of the Group-Space of the Proper Lorentz Group. E. J. SCHREMP, *Naval Research Laboratory.*—The group-space of the proper Lorentz group possesses a complex 3-dimensional projective representation P_3 (or 4-dimensional affine representation S_4) whose geometry is determined by the algebra of complex quaternions, and whose homogeneous (or nonhomogeneous) coordinates are the coordinates (q^0, q^1, q^2, q^3) of a general complex quaternion q.[1] In S_4, which is a form of "spin-space," there are embedded two conjugate systems of imprimitivity of varieties of four real dimensions. These systems furnish two alternative representations of the tangent space to space-time, each having (in the terminology of projective relativity) and imaginary "index." The *external motions* induced in either system by the transformations of the corresponding parameter group comprise the proper Lorentz and imaginary gauge transformations. The *internal motions* simultaneously induced in the varities of the given system comprise certain real Euclidean rotations and real gauge transformations. Physically, the space P_3 (or S_4) may be identified with the relativistic phase space (i.e., external momentum space and internal configuration space) of a single non-localizable elementary particle. The abovementioned geometrical motions then serve to describe the physical motions of the particle's distribution in phase.

[1] See E. J. Schremp, *On the Interpretation of the Parameters of the Proper Lorentz Group*, Proceedings of the 1950 International Congress of Mathematicians, Cambridge, Massachusetts (to be published).

I7. A Remark on the Fundamental Reversibility and the Phenomenological Irreversibility. SATOSI WATANABE, *Wayne University.*—It is obvious that "irreversibility of observation" in the sense of von Neumann's theory,[1] is the essential element that enables us to deduce irreversible conclusions from the reversible theoretical scheme of quantum physics. Born's new "quantum-theoretical deduction"[2] of the H-theorem, which does not refer to observations, is shown to be no exception to this general remark. The problem then concerns how and where this irreversibility of observation should be introduced in the process of deduction to obtain results in forms as conformable as possible to the phenomenological theory. Some fundamental postulates and practical prescriptions will be given, rationalizing the deduction of irreversible results, such as the H-theorem, the "retarded" potential,[3] etc., from the reversible basic laws.

[1] J. von Neumann, Math. Grundl. d. Quantenm. Berlin, 1932.
[2] M. Born, Ann. Inst. Henri Poincaré **11**, 1 (1949).
[3] S. Watanabe, Phys. Rev. (to be published).

I8. Do Coulomb Fields Signal Faster than Light? D. I. CAPLAN AND F. J. BELINFANTE, *Purdue University.*—The coulomb field $\mathbf{E}_{\text{II}} = -\nabla V = -\nabla\Phi_{\text{ret}} - \partial\mathbf{A}_{\text{ret}}/c\partial t$ acts instantaneously by $V(\mathbf{x}, t) = \int d^3x' \rho(\mathbf{x}', t)/r$. The retardation effects of Φ_{ret} and $\mathbf{A}_{\text{ret}}$ cancel each other because of the supposed analytical character of the charge and current distributions in deterministic field theory. Measure at P the field $\mathbf{E}_{\text{II}}$ of an electron instantaneously at T, which traversed the past light cone from P at R, and was scattered at S between R and T. Φ_{ret} and $\mathbf{A}_{\text{ret}}$ would be useful for calculating $\mathbf{E}_{\text{II}}(P)$ only if at R we could predict outcome of deterministically predetermined scattering. *Quantum mechanically*, we might break the analytical behavior of the expectation values by "reduction" of the wave function after S. If we often measure simultaneously $\mathbf{E}_{\text{II}}(P)$ and scattered electron position at T, then

$\langle \mathbf{E}_{\text{II}}(P)\rangle_{\Psi} = \langle -\nabla\Phi_{\text{rot}} - \partial\mathbf{A}_{\text{rotII}}/c\partial t\rangle_{\Psi}$ unless we select *a posteriori* those cases for which the electron is found at T in a definite position T', for which selected cases $\langle \mathbf{E}_{\text{II}}(P)\rangle_{\Psi} = \langle -\nabla V_{T'}\rangle_{\Psi}$. Conversely, a measured $\mathbf{E}_{\text{II}}(P)$ may give more probability for electron to be at T' than, say, T''; but it gives no unmistakenly certain instantaneous signal at P of electron position at T.

I9. Gauge-Independent Quantized Bopp Theory. FREDERIK J. BELINFANTE, *Purdue University.*—The unperturbed energy of Bopp's electrodynamics is $\mathcal{H}_0 = \mathcal{H}_{\text{maxwell}} - \mathcal{H}_{\text{Proca}} + \mathcal{H}_{\text{matter}} - \mathcal{H}_{\text{vacuum}}$. In interaction representation we quantize Bopp's unperturbed field using opposite-to-usual sign for the neutral-Proca-field commutators. The interaction with matter is $W = W_{\text{maxwell}} - W_{\text{Proca}}$. We choose for W_{maxwell} the interaction operator of gauge-independent quantum electrodynamics. As this separates the coulomb field, it is convenient to do the same in W_{Proca}. Thence $W = (\mathbf{E}_{\text{II}}\cdot\mathfrak{e}/4\pi) - \mathfrak{j}\cdot\mathfrak{a}$, where $\mathbf{E}_{\text{II}}(\mathfrak{x}) = -\nabla\int d^3\mathfrak{x}'\rho(\mathfrak{x}')/r$, $\mathfrak{j} = e\colon\psi^\dagger\alpha\psi\colon$, $\mathfrak{e} = \mathfrak{E} - \mathfrak{F}$, $\mathfrak{a} = \mathfrak{A} - \mathfrak{U}_{\text{II}}$, if $\mathfrak{E}$, $\mathfrak{B}$ $(=\text{curl}\mathfrak{A})$ is the transverse maxwell field, and $\mathfrak{F}$, $\mathfrak{G}$ $(=\text{curl}\mathfrak{U})$ is the Proca field (with potential four-vector $\mathbf{U}$, Y). The integrability (covariance) of the generalized Schrödinger equation with W is shown. In Heisenberg representation, $\mathfrak{B}$ forms a tensor with $\mathfrak{E} = \mathfrak{E} + \mathbf{E}_{\text{II}}$, and $\mathfrak{G}$ with $\mathbf{F} = \mathfrak{F} + \mathbf{E}_{\text{II}}$, and Bopp's interactions appear in the field equations for $\mathbf{E}$, $\mathfrak{B}$, $\mathbf{F}$, $\mathfrak{G}$, $\mathbf{U}$, Y. We make the expectation value of the energy positive definite by imposing the new covariant auxiliary condition for Proca as for maxwell field: $\mathfrak{E}^{(+)}\Phi = \mathfrak{A}^{(+)}\Phi = \mathfrak{F}^{(-)}\Phi = \mathbf{U}^{(-)}\Phi = 0$, with $\mathfrak{E}$, $\mathfrak{A}$, $\mathfrak{F}$, $\mathbf{U}$ in interaction representation and the state vector Φ in Heisenberg representation. The expectation values of the fields are then retarded maxwell and Proca fields as discussed by Bopp.[1]

[1] F. Bopp, Ann. Physik **38**, 345 (1940); **42**, 575 (1943).

I10. Information, Logic, and Physics. JEROME ROTHSTEIN, *Evans Signal Laboratory.*—Relativity made it clear that no geometry has *a priori* validity for physics but rather that world geometry is a physical theory whose truth resides in successfully coordinating experience. We assert the same for all mathematics and logic. Logic can be formulated via the calculus of classes (sets, ensembles). Its empirical justification stems from the fact that measurement or observation of objects to grouping them in classes satisfying relations isomorphic to those of the calculus of sets. Classification involves choice from a number of alternatives, i.e., acquiring information or measuring.[1] Conventional logic is inapplicable when classifications cannot be made (operationally undefined) or when set algebraic relations are violated. Quantum logics of Reichenbach, and von Neumann and Birkhoff, correspond, respectively, to these cases; complementarity retains conventional logic by excluding features generating these cases. Such non-Aristotelian logics may be useful for unmeasurables (e.g., virtual processes, certain divergencies, Einsteinian completion of quantum theory) and for other sciences.

[1] J. Rothstein, Phys. Rev. **82**, 322(A) (1951).

I11. A Relation between Planck's Constant and the Gravitational Constant (to be read by title). B. LIEBOWITZ, *New York.*—As a basis for a different approach to atomic theory I have proposed[1] an atomic model comprising electromagnetic wave fields associated with the nucleus and its circumnuclear electrons. The existence of such wave fields depends on inhomogeneity of space around the nucleus. This inhomogeneity concept stems from the Einstein effect, hence a theory based on it must involve the gravitational constant G, at least implicitly. But eventually such theory must involve h, hence a relation between h and G is expected. By purely dimensional and numerical procedure one easily finds

$$G \cong 3\pi e^3/2[mN\alpha(1+\alpha)]^2,$$

or

$$\alpha \cong \frac{1}{2}\left\{\left[1+\frac{4e}{Nm}\left(\frac{3\pi}{2G}\right)\right]^{\frac{1}{2}} - 1\right\},$$

where $\alpha = 2\pi e^2/hc$, mN is "atomic weight" of electron, etc. Calculating α, hence h, from $G = 6.673\times10^{-8}$,[2] using atomic data of December, 1950, h comes out about 0.05 percent low. Aside from uncertainties in G, this discrepancy could conceivably be partly the result of differences between macroscopic values of atomic constants (e.g., deflection) and microscopic values (e.g., spectroscopic) arising from this inhomogeneity.

[1] B. Leibowitz, Phys. Rev. **64**, 294 (1943); *ibid.* **66**, 343 (1944).
[2] Bur. Standards RP, 1480 (1942).

FRIDAY AFTERNOON AT 2:00

Morrison, Mural Room

(J. C. BOYCE presiding)

Invited Papers. Topics in Nuclear Physics.

J1. Evidence for Strong Spin Orbit Coupling from the Low States of Light Nuclei. R. K. ADAIR, *University of Wisconsin.* (30 min.)

J2. Recent Experiments in Neutron Physics: Neutron-Proton Capture Cross Section; Neutron-Electron Interaction; Total Cross Sections in the Kev Region; Capture Gamma-Rays. BERNARD HAMERMESH, *Argonne National Laboratory.* (30 min.)

J3. Systematics of Isomer Energy Levels. R. D. HILL, *University of Illinois.* (20 min.)

J4. Beta Spectra. LAWRENCE M. LANGER, *University of California, Los Alamos Scientific Laboratory.* (30 min.)

SATURDAY MORNING AT 9:00

Sherman, Crystal Room

(K. LARK-HOROVITZ presiding)

Semiconductors, I

K1. Quantum Theory of the Internal Field in an Idealized Crystal.* D. L. DEXTER AND W. R. HELLER, *University of Illinois.*—The quantum-mechanical polarizability of an idealized crystal is calculated by the semiclassical method. The excited states which contribute are exciton states as deduced from the crystal model first discussed by Frenkel[1] and result from the transition dipole-dipole interactions of excited atoms.[2] A generalization of the Lorentz "local field" emerges naturally. Corrections to the Lorentz value for the polarizability of an atom within the crystal, $\alpha_a/[1-(4\pi n_0/3)\alpha_a]$, where α_a is the polarizability of an isolated atom, arise from three main sources: (1) exchange effects, (2) higher order terms in the atomic interactions than dipole-dipole terms, and (3) the existence of more than one excited state to which the atom can make virtual transitions. A brief discussion is given of these corrections, which are important in real crystals; it is shown that caution must be exercised in obtaining meaningful oscillator strengths from absorption data, and, in particular, that the local field correction differs for different energy levels.

* Research supported by the ONR.
[1] J. Frenkel, Phys. Rev. **37**, 17, 1276 (1931); Physik. Z. Sowjetunion **9**, 158 (1936).
[2] W. R. Heller and A. Marcus, Phys. Rev. (to be published). See also Phys. Rev. **82**, 315 (1951).

K2. Electronic States in Crystals under Large Over-All Perturbations.* PAULA FEUER AND HUBERT M. JAMES, *Purdue University.*—Solutions of the three-dimensional Schroedinger equation are considered for a periodic potential modified by a perturbing potential. A method of Slater[1] has been modified and used to develop the theory of large over-all perturbations, such that the energy lies close to one permitted band in one region of the crystal and close to a second permitted band in another. The solution of the perturbed periodic Schroedinger equation is expressed as $\psi=\sum_k\{\phi_1(r_k)a_1(r-r_k)+\phi_2(r_k)a_2(r-r_k)\}$, where $a_1(r-r_k)$ and $a_2(r-r_k)$ are functions localized about the Kth atom of the crystal, appropriate to the first and second permitted bands, respectively. Difference equations are derived for the coefficients ϕ_1 and ϕ_2. The theory has been applied to a one-dimensional crystal in a uniform electric field, using the narrow band approximation; an expression has been obtained for the probability for an electron to cross a forbidden energy band.

* Work supported in part by the Signal Corps.
[1] J. C. Slater, Phys. Rev. **76**, 1592 (1949).

K3. Experimentally Derived Configurational Coordinate Curves. CLIFFORD C. KLICK, *Naval Research Laboratory.*—If it is assumed that the configurational coordinate curves of the ground and excited states of a system are parabolas and that under these conditions the system can be treated as a quantized harmonic oscillator, the constants necessary to describe both curves may be determined from experiment. Seven optical measurements which can be applied are: wavelengths of the absorption and emission peaks, band width of the absorption and emission bands at low temperatures, relative change in band width with temperature of the absorption and emission bands, and variation with temperature of luminescence efficiency or decay constant. For systems in which the effective mass of the vibrating system in both its ground and excited state is unknown, six experiments determine both the curves and the unknown masses. If the mass is assumed, four experiments suffice. The latter case is illustrated by computations on thallium-activated potassium chloride and the results compared with the curves computed theoretically by Williams.[1]

[1] F. E. Williams, J. Chem. Phys. **19**, 457 (1951).

K4. Pulse-Heating of Bulk Semiconductors.* J. HIRSCH† and R. B. MCQUISTAN, *Purdue University.*—The pulse heating method by Ehrenberg and Hirsch[1] to obtain resistance-temperature characteristics of semiconducting films at heating rates up to 5000°C/sec has been adapted for the study of bulk specimens of semiconducting materials. A heating current of rectified, unfiltered ac is passed through the specimen. During the intervals when the heating current is interrupted a constant, nonheating "measuring" current is passed through the specimen and the potential developed between two probes is applied to the vertical deflection plates of a cathode-ray tube via a direct coupled amplifier. The resistance thermometer, a transparent gold film on 0.001-in. mica, is cemented to the sample with mica as electrical insulator between sample and gold film. The voltage developed by a constant measuring current across the gold film is applied to the vertical deflection plates during the periods when heating current flows. A typical pulse-heating record for an N-type Ge sample will be shown (heating pulse 0.2 sec, horizontal sweep frequency 3 c/sec). A $\log\rho$ *vs* $1/T$ graph can be obtained by a "static method" in a few minutes.

* Supported by Signal Corps Contract W36-039-SC-38151.
† To be introduced by K. Lark-Horovitz.
[1] J. Hirsch, Ph.D. thesis, University of London (1950) (Proc. Phys. Soc. (London) **64**, 700 (1951)).

K5. The Effect of Certain Group IV Oxides on the Permittivity and Loss Tangent of Barium Titanate. GRAHAM W. MARKS AND LESTER A. MONSON, *U. S. Navy Electronics Laboratory.*—Respective mixtures of barium titanate and the dioxides of silicon, titanium, zirconium, cerium, and thorium were prepared in from 0.5 to 50 mole percentages of the latter. Chemically pure materials were used. The powders were pressed and air-fired for one to two hours at 1200 to 1360°C. After silvering, the ceramics were placed in a constant temperature oven and the permittivity and loss tangent determined over the range from 30° to 170°C at a frequency of 1000 cycles. The densities were measured at room temperature. Values of the permittivity were then corrected for the porosity of the ceramics. The Curie point of pure barium titanate is 127.8 ±0.2°C and is lowered by all of the oxides except silica which raises it. The permittivity is also lowered. Calculations of the permittivities of these ceramics from the relationship, $\ln\epsilon=v_1\ln\epsilon_1-v_2\ln\epsilon_2$ (in which ϵ is the permittivity of the mixture, ϵ_1 and ϵ_2 that of the respective pure constituents, and v_1 and v_2 the respective volume fractions) did not, in general, yield values which corresponded to those determined experimentally.

K6. Isotope Effect in RbD_2PO_4. B. T. MATTHIAS, *Bell Telephone Laboratories.*—Crystals of a tetragonal modification of RbD_2PO_4 were grown and the dielectric constant parallel to the c-axis was determined as a function of temperature. RbD_2PO_4 becomes ferroelectric below 218°K which is about 5° higher than the Curie point of KD_2PO_4 at 213°K. The Curie points of KH_2PO_4 and RbH_2PO_4 are at 123°K, and 147°K, respectively. It is interesting to note that the higher the critical temperature of a ferroelectric transition, the smaller

the influence of isotopic change, which may reflect the increasing importance of kT *vs* the zero point energy. Rochelle salt[1] (shift of upper Curie temperature from 297°K to 308°K) furnishes another instance.

[1] A. N. Holden and W. P. Mason, Phys. Rev. **57**, 54 (1939).

K7. Optical and Electrical Behavior of Lanarkite. L. M. ROTH, K. W. MEISSNER, AND K. LARK-HOROVITZ, *Purdue University.*—Photoconductive oxidized PbS films show* on the surface (electron diffraction pattern) lanarkite ($PbO \cdot PbSO_4$) whereas the bulk of the material (x-ray diffraction pattern) consists of PbS. Using single crystals of lanarkite mounted between a quartz plate and an aluminum sheet with a very small slit, the optical transparency in the visible and ultraviolet, as well as in the near infrared, has been determined. An unpolished single crystal and a thinner polished single crystal were used. The polished crystal showed continuous absorption at wavelengths below 3020A and the unpolished below 3400A. This corresponds to an absorption edge of about 3.6 electron volts. The absorption in the infrared, tested by M. Becker, with the same equipment used for the testing of the lead sulfide cells themselves, showed that lanarkite shows no absorption up to about 5μ. Lanarkite itself is an insulator and no photoconductive properties in the material were detected with the same illumination with which lead sulfide films show photoconductive response.

* Daughty, Lark-Horovitz, Roth, and Shapiro, Phys. Rev. **79**, 203(A) (1950).

K8. Magnetoresistive Effect in Impurity Semiconductors.* W. J. WHITESELL, II, AND V. A. JOHNSON, *Purdue University.*—A number of investigations have demonstrated the dependence of the resistivity of semiconductors upon magnetic field. The theoretical treatment of this effect due to Harding[1] is based upon the Lorentz solution of the Boltzmann equation and involves the assumption that the mean-free-path of the conduction electrons is independent of their energies. Actually these electrons are subject to various scattering mechanisms, especially lattice scattering with an energy-independent mean-free-path and Rutherford scattering with a mean-free-path proportional to the square of energy. The integrals giving the dependence of ρ upon H have been evaluated on the basis that $1/l = 1/l_L + 1/l_I$. In this way the dependence of $\Delta\rho/\rho_0$ on H has been found as the proportion of impurity scattering rises from 0 to 100 percent. There is a general tendency for the quantity $\Delta\rho/\rho_0$ divided by H^2 to increase with increasing proportion of impurity scattering. When compared with experimental data for typical germanium samples,[2] the theoretical curve is much too low at room temperature, but gives increasingly better fit as the temperature decreases.

* Supported in part by Signal Corps Contract.
[1] J. W. Harding, Proc. Roy. Soc. (London) **A140**, 205 (1933).
[2] J. W. Cleland, M. S. thesis, Purdue University, 1949; I. Estermann and A. Foner, Phys. Rev. **79**, 365 (1950).

K9. Comparison of the Adiabatic and Isothermal Hall Effects.* V. A. JOHNSON AND F. L. SHIPLEY, *Purdue University.*—The interpretation of observed Hall effect data involves the question of whether the conditions of the experiment are those assumed in the derivation of the theoretical expression. One usually employs the isothermal Hall coefficient, derived on the assumption that the transverse electric current, the longitudinal and transverse temperature gradients are zero. Another theoretical expression is the adiabatic Hall coefficient, based on zero values of transverse electric and thermal currents and longitudinal temperature gradient. Both of these expressions depend upon the nature of the scattering encountered by conduction electrons. The difference between the adiabatic and isothermal Hall coefficients has been evaluated as a function of the ratio of the resistivity due to impurity ion (Rutherford) scattering to the total resistivity. This difference increases with increasing impurity scattering, but is only a few thousandths percent for a high thermal conductivity semiconductor in the temperature range such that conduction electron density is almost independent of temperature. However, this difference increases at low temperatures due to the more rapid change of carrier density with temperature; a similar effect occurs at high temperatures due to the production of intrinsic carriers. Differences arising from existing temperature gradients in the nonisothermal, nonadiabatic case have been considered.

*Supported by a Signal Corps Contract.

SATURDAY MORNING AT 9:00

Sherman, Grey Room

(MARIA GOEPPERT-MAYER presiding)

Nuclear Physics: Miscellaneous Topics

L1. Absolute Backscattering Coefficients for Positrons and Electrons. HOWARD H. SELIGER, *National Bureau of Standards.*—Backscattering coefficients for isotropic sources of Na^{22} positrons and P^{32} electrons have been measured for backing materials ranging from carbon to lead using 4π absolute beta-counters.[1] In these experiments the source and backing were placed inside the sensitive volume of the counter so that all backscattered particles were detected. Although the ratio of electron to positron backscattering is always greater than 1 as reported previously,[2] the individual values obtained with the 4π counter differ considerably for both electrons and positrons from those obtained in the original experiment, where only a small solid angle ($\sim\frac{1}{4}\pi$) was subtended by a G-M counter at 90° to the face of the backing. Further experiments with both electrons and positrons indicate a marked anisotropy in the angular distribution of the backscattered radiation, with a maximum for high Z and a minimum for low Z, at 90° to the plane of the backing. In addition, the backscattered radiation becomes more energetic at smaller angles with the backing. Experimental details and a qualitative explanation of these results will be presented.

[1] H. H. Seliger and L. Cavallo, J. Research Natl. Bur. Standards **47**, 41 (1951).
[2] H. H. Seliger, Phys. Rev. **78**, 491 (1950).

L2. Measurements of the Relative Transmission of Beta-Particles Through Geiger-Müller Counter Windows.* CHIA-HUA CHANG AND C. SHARP COOK, *Washington University.*—The measurements of the relative transmission of beta-particles through Geiger-Müller counter windows has been reported at previous meetings of the American Physical Society.[1] The work since then has been concentrated on the relative transmission of negatrons and positrons through windows of two electrically different materials. An aluminum

foil of thickness 7.2 mg/cm² and a mica sheet of thickness 5.9 mg/cm² have been used for these investigations. The radioactive sources employed are Cu^{61} for positrons and P^{32} for negatrons. It has been found that the aluminum window has almost the same transmission curve for both positrons and negatrons except for a slight deviation in its lower energy region, which might be explained as having been caused by a possible instrumental distortion. However, the mica window gives a distinctly smaller transmission for positrons than for negatrons throughout the entire energy range studied. This makes it appear that the transmission curve for nonconducting G-M tube windows may be different for positrons than for negatrons. A possible explanation for this phenomenon will be presented.

* Assisted by the joint program of the ONR and AEC.
[1] C. H. Chang and C. S. Cook, Phys. Rev. 83, 872 (1951); also Phys. Rev. 79, 244 (1950).

L3. Ranges of High Energy Electrons in Water. J. OVADIA, J. W. BEATTIE, AND J. S. LAUGHLIN, *University of Illinois.*—A betatron was used to produce an external electron beam continuously variable from 5 to 22 Mev. Well-collimated beams of different cross-sectional areas were incident on a water chamber. The distribution of ionization in the water was measured with a small ion chamber (0.381 cm³) whose position was varied by remote control. Typical ionization distributions as a function of electron energy will be presented. These distributions can be converted into essentially number of electrons *versus* range plots by correcting for the specific ionization of the electrons as a function of energy.[1] The extrapolated ranges from these plots should correspond to the "practical maximum range" defined by Bleuler and Zünti.[2,3] The variation of these experimental extrapolated ranges with energy in water has been compared with the predicted maximum theoretical ranges.[4,5] The calculated ranges which include density effects agree more closely with our experimental values.

[1] R. B. Brode, Rev. Modern Phys. **11**, 222 (1939).
[2] E. Bleuler and W. Zünti, Phys. Acta **19**, 375 (1946).
[3] F. L. Hereford and C. P. Swann, Phys. Rev. **78**, 727 (1950).
[4] E. Fermi, Phys. Rev. **57**, 485 (1940).
[5] O. Halpern and H. Hall, Phys. Rev. **73**, 477 (1948).

L4. The Energy Loss of Monoenergetic Electrons in Carbon and Water. JOHN I. LODGE AND FRANK L. HEREFORD, *University of Virginia.*—A number of experiments[1] have confirmed the Halpern-Hall and Wick calculations of the polarization reduction in ionization and energy loss of charged particles traversing condensed media. These two calculations differ somewhat, particularly in the predicted magnitude of the polarization effect in carbon. Previous measurements[2] of the stopping power of carbon relative to that of water (S_{H_2O}/S_C) for 1–10 Mev electrons favored the Halpern-Hall results. This measurement has been repeated with significant improvements in experimental technique. In particular the beta-spectrum of P^{32} magnetically analyzed to provide a homogeneous, gamma-free beam of electrons was employed, and the C and H_2O sample thicknesses were determined with greater precision. As in the previous work,[3] multiple and backscattering effects were essentially eliminated through choice of equal sample thicknesses as measured in radiation lengths. The influence of these effects was investigated experimentally. A typical result for 0.75-Mev electrons yields $S_{H_2O}/S_C = 1.12 \pm 0.02$ in best agreement with the Wick result.

[1] W. L. Whittemore and J. C. Street, Phys. Rev. **76**, 1786 (1949); E. Pickup and L. Voyvodic, Phys. Rev. **80**, 89 (1950).
[2] F. L. Hereford, Phys. Rev. **74**, 574 (1948).

L5. Calorimetric Determination of the Roentgen for 400-kv X-Rays. J. S. LAUGHLIN, J. W. BEATTIE, AND J. OVADIA, *University of Illinois.*—The unit of ionization, the roentgen, has customarily been employed to measure the output of x-ray generators. The conversion of this ionization unit into actual energy flux for experiments is difficult, since this requires an accurate knowledge of the spectral distribution in addition to other factors related to the absorption of the x-rays in various media. In order to measure the energy flux directly an improved version of the calorimetric method employed for 22.5-Mev x-rays[1,2] has been applied to a 400-kv self-rectifying x-ray generator with an inherent filtration of 1.75 mm copper. This calorimeter employed thermistors as temperature sensitive elements. Its construction and calibration will be described. For 400-kv x-rays the energy flux was measured as 2800±60 ergs/cm²-roentgen. Comparison with theoretical calculations will be made.

[1] J. S. Laughlin and J. W. Beattie, Phys. Rev. **83**, 231(A) (1951).
[2] J. S. Laughlin and J. W. Beattie, Rev. Sci. Instr. **22**, 572 (1951).

L6. Calorimetric Calibration of a Secondary Standard for 150–317 Mev Bremsstrahlung.* P. D. EDWARDS, *University of Illinois.*—A secondary standard, 4-in. diameter, parallel plate ionization chamber consisting of a 0.016-in. Al center foil separated by 0.052-in. air gaps from 0.25-in. Cu front and back plates and adopted for use with a Victoreen M-70 electrometer has been calibrated calorimetrically. Absolute calibration was performed with an improved Pb block calorimeter of a type previously used[1] except that the temperature sensitive elements were changed to thermistors after the method of Laughlin. Five-minute irradiations were used with a maximum of 33 milliwatts emerging from the 0.5 in. diameter collimator. With present knowledge of corrections to be applied, the results are accurate to 4 percent.

Mev	ergs/esu per cm air (NTP)
317	6400
300	6600
250	5510
200	4930
150	4720

* Assisted by the joint program of the ONR and AEC.
[1] E. L. Piper and G. H. Price, Phys. Rev. **81**, 309 (1951).

L7. The "Effective" Atomic Numbers of Materials for Various γ-Ray Interactions.* G. J. HINE,** *Massachusetts Institute of Technology.*—The "effective" atomic number of a material composed of several elements cannot be expressed by a single number. For each of the different processes by which γ-rays can interact with matter, the various atomic numbers in the material have to be weighted differently. The "effective" atomic number for photoelectric absorption of γ-rays follows as $Z_{\text{photoel.}} = (\Sigma_i p_i Z_i^{3.1})^{1/3.1}$. If only light elements with an atomic number $2 \geq Z \geq 20$ are involved, p_i is the fraction by weight of each element present in the material. The "effective" atomic number for pair production is given by $Z_{\text{pair}} = \Sigma_i p_i Z_i$. Finally, it will be shown that an "effective" atomic number for the backscattering of secondary electrons emmitted from a material under γ-irradiation can be defined as $Z_{\text{backsc.}} = \pi_i (Z_i+1)^{p_i} - 1$. For a medium composed of several elements, $Z_{\text{backsc.}}$ is always smaller than Z_{pair}. Experimental results will be presented for the relative intensity of backscattered secondary electrons produced by the Co^{60} γ-rays in materials of known and unknown composition; for bones a value of $Z_{\text{backsc.}} = 11.5 \pm 0.5$ has been determined.

* Assisted by the joint program of the ONR and AEC.
** Special Research Fellow of the National Cancer Institute, Bethesda, Maryland.

L8. The Neutrons from the Disintegration of the Separated Isotopes of Silicon by Deuterons.* C. E. MANDEVILLE, C. P. SWANN, AND S. D. CHATTERJEE,† *Bartol Research Foundation of the Franklin Institute.*—Thick targets of the oxides of the separated isotopes of silicon have been irradiated by deuterons of energy 1.4 Mev, supplied by the Bartol Van de

Graaff statitron. The resulting neutron spectra have been observed by recording recoil protons, knocked on in the forward direction in Eastman NTA plates. Q-values obtained at zero and ninety degrees with the incident deuterons are as follows:

Reaction:	Q-values (Mev)
$Si^{29}(D,n)P^{29}$	0.29
$Si^{29}(D,n)P^{30}$	3.27, 2.52, 1.81, 1.27
$Si^{30}(D,n)P^{31}$	4.92, 4.59, 3.73, 2.70, 1.51

The estimated probable error in all Q-values is ± 0.04 Mev.

* Assisted by the joint program of the ONR and the AEC.
† Calcutta, India. Guest physicist, Bartol Research Foundation, 1951.

L9. The Angular Distribution of Prompt Neutrons in the Fission of Pu^{239}. J. S. FRASER, *Chalk River Laboratory.*—Collimated fission fragments from a 200 $\mu g/cm^2$ layer of Pu^{239} exposed to slow neutrons from the thermal column of the N.R.X. pile were detected and identified in energy in a gridded ionization chamber. Coincident prompt fast neutrons in a given direction were counted by proton recoils in a fixed electron collecting chamber filled with methane. The fission chamber was rotated to set the collimator at various angles to the direction of the fast neutron chamber. Angular distributions of the fast neutrons relative to the collimated fission fragments are presented. For curve (a) only the light fragments were selected; for curve (b) all fragments were allowed. Curve (a) yields a ratio $N(0°)/(180°) = 1.72 \pm 0.06$. Assuming for analysis the same energy distribution of the neutrons in the frame of reference of a fragment as for U^{235} fission, it appears that the light fragment emits about 30 percent more neutrons than the heavy. Curve (b) gives $N(0°)/N(180°) = 0.992 \pm 0.020$ which checks the experimental technique. It also gives $N(0°)/N(90°) = 4.35 \pm 0.15$. Observations at 0° and 180° to the light fragment as a function of fragment kinetic energy indicate a lower average of this energy in the most probable neutron emitting mode than in the most probable splitting.

L10. New Medium Mass α-Emitters.* K.-H. SUN, F. A. PECJAK, AND B. JENNINGS, *Westinghouse Research Laboratories* AND A. J. ALLEN, *University of Pittsburgh.*—A general consideration of nuclear shell configulrations and α-emitting systematics of heavy nuclei[1] (near $Z = 82$ and $N = 126$) led previously to the discovery of severa new α-emitters in the lanthanide rare earth region[2,3] ($N = 82$). We have now extended the work to the region of other closed shell nuclei of lower masses ($N = 50$) and found two new α-emitters by bombarding $_{44}$Ru with a 30-Mev α-beam. Their half-lives were found to be ~4 min and ~4 hr. In addition, another new α-emitter with a ~8-hr half-life was also observed when $_{78}$Pt, an element having isotopes low in neutron content, was bombarded by a 30-Mev α-beam. This should be grouped with the α-emitters obtained by bombarding $_{79}$Au and $_{80}$Hg with 200-Mev protons.[3] Work is being continued in obtaining better values for half-lives and in searching for more new α-emitters by extending the technique of α-bombardments to elements in the other closed shell regions (Ca, Ni, Sn, etc.) and to those having isotopes with low neutron content (Hg, Os, W, Hf, Dy, Pd, etc.).

* Assisted by the joint program of the ONR and AEC.
[1] Perlman, Ghiroso, and Seaborg, Phys. Rev. **77**, 26 (1950); also a much earlier work of W. Heisenberg, Report du VII^{me} Congres Solvay (1934).
[2] Thompson, Ghiroso, Rasmussen, and Seaborg, Phys. Rev. **76**, 1406 (1949); Rasmussen, Reynolds, Thompson, and Ghiorso, Phys. Rev. **80**, 475 (1950).
[3] Sun, Pecjak, Jennings, Allen, and Nechaj, Phys. Rev. **82**, 772 (1951).

L11. On the Fine Structure of the Alpha-Particles of Po^{210}. S. DE BENEDETTI AND G. H. MINTON, *Carnegie Institute of Technology.*—The well-established gamma-radiation from Po^{210} must be accompanied by a weak group of low energy alpha-particles which had not yet been detected despite of several attempts to study the fine structure of this isotope.[1] A coincidence method has been applied to the investigation of this problem. A source of Po was located in a liquid scintillant and the distribution in pulse height of the alpha-particles was studied. In this way the height corresponding to the main alpha-group was determined. Subsequently we studied the height of the alpha-pulses in coincidence (resolving time 3×10^{-8} sec) with the gamma-rays detected by means of another thick scintillation counter. A clear shift of the position of the peak was observed, corresponding to the known energy of the gamma-rays. An attempt was made to determine the half-life of the excited state for which an upper limit of 10^{-9} sec was found. At present some experiments for the study of the alpha-gamma angular correlation are under way.

[1] W. Y. Chang, Phys. Rev. **69**, 60 (1946). W. G. Wadey, Phys. Rev. **74** 1846 (1948).

L12. Atomic Masses of Titanium, Vanadium, and Chromium.* T. L. COLLINS, A. O. NIER, AND W. H. JOHNSON, JR., *University of Minnesota.*—In a recent communication[1] we reported on the packing fractions of elements from sulfur to scandium as measured with a double focusing mass spectrometer. This study has now been extended to include all of the isotopes of titanium and chromium and the abundant isotope of vanadium. Measurements were made by doublet comparisons with hydrocarbon fragments. Using $H^1 = 1.008146 \pm 3$ and $C^{12} = 12.003842 \pm 4$, we find the following packing fractions: Ti^{46}, 7.18 ± 0.01; Ti^{47}, 7.09 ± 0.02; Ti^{48}, 7.68 ± 0.01; Ti^{49}, 7.43 ± 0.01; Ti^{50}, 7.85 ± 0.01; V^{51}, 7.74 ± 0.01; Cr^{50}, 7.58 ± 0.01; Cr^{52}, 8.26 ± 0.02; Cr^{53}, 7.98 ± 0.02; Cr^{54}, 8.09 ± 0.04. Results for iron and nickel will also be given.

* Supported by joint program of the ONR and AEC.
[1] Collins, Nier, and Johnson, Phys. Rev. **83**, 228(A) (1951).

L13. Atomic Masses of Xenon, Iodine, and Some Isotopes of Tin.* R. E. HALSTED, *University of Minnesota.*—The double-focusing mass spectrometer previously described[1] has been used to measure the masses of xenon, iodine, and some isotopes of tin by the doublet method, comparisons being made with hydrocarbon fragments. Using $H^1 = 1.008146 \pm 3$ and $C^{12} = 12.003842 \pm 4$, the following packing fractions ($\times 10^4$, all negative) were obtained:

Xe^{136}, 3.64 ± 0.01;	Xe^{134}, 3.88 ± 0.02;	Xe^{132}, 4.08 ± 0.01;
Xe^{131}, 4.06 ± 0.05;	Xe^{130}, 4.25;†	Xe^{129}, 4.18 ± 0.02;
Xe^{128}, 4.34 ± 0.01;	Xe^{126}, 4.38 ± 0.02;	Xe^{124}, 4.36 ± 0.02;
I^{127}, 4.30;†	Sn^{124}, 4.45 ± 0.02;	Sn^{122}, 4.71 ± 0.03;
Sn^{120}, 4.95 ± 0.03;	Sn^{119}, 4.94 ± 0.02;	Sn^{118}, 5.10 ± 0.03;
Sn^{117}, 5.09 ± 0.02;	Sn^{116}, 5.25;†	Sn^{114}, 5.20 ± 0.03.

Comparisons will be made with existing nuclear reaction and mass spectrographic data.

* Supported by joint program of the ONR and AEC.
[1] A. O. Nier and T. R. Roberts, Phys. Rev. **81**, 507 (1951).
† Tentative value.

SATURDAY MORNING AT 9:00

Sherman, West Room

(DONALD W. KERST presiding)

Gamma-Rays

M1. Gamma-Gamma-Coincidence Absorption and Angular Correlation of I^{131}. DANIEL SCHIFF, *University of Illinois.**—The gamma-rays emitted in the decay of I^{131} were investigated with sodium iodide scintillation counters. Absorption of the gamma-gamma-coincidences showed that at least 85 percent of these coincidences occur between the 80-kev and 284-kev lines. The coincidences remaining with thick absorbers, not accounted for by the 284-kev line and apparently caused by a harder component, were shown by critical absorption not to be connected with the 80-kev line. They are probably coincidences with the bremsstrahlung due to the beta-rays emitted by I^{131}. We conclude that the 638-kev line does not go to the 80 kev level as previously reported,[1,2] but leads to the ground state of Xe^{131}. Angular correlation measurements showed the coincidences between the 80-kev and 284-kev gammas to be isotropic within 3 percent. Assuming pure radiation, this characterizes the spin of the 80-kev level as $\frac{1}{2}$. However, the existence of interference due to a mixture of radiations may cause the correlation to vanish even if the spin of the 80-kev level is not $\frac{1}{2}$.

* Supported in part by the joint program of the ONR and AEC.
[1] Kern, Mitchell, and Zaffarano, Phys. Rev. **76**, 94 (1949).
[2] Bell, Cassidy, and Kelley, Phys. Rev. **82**, 103 (1951).

M2. Gamma-Gamma Coincidences in "Cs^{137}" and Fe^{59}. FRANZ R. METZGER, *Department of Physics, University of Illinois.**—Using sodium iodide scintillation counters, we have investigated several sources which, according to the presently accepted decay schemes, should not exhibit any gamma-gamma coincidences. Be^{7} was found to be free of such coincidences. However, in Cs^{137} as well as in Fe^{59} sources we found an appreciable number of gamma-gamma coincidences. In Cs^{137} sources, the coincidences are the result of Cs^{134} (2.3 years half-life) formed in a second-order reaction. In our source, obtained from Oak Ridge, the Cs^{134} activity was about two percent of the total activity. This amount of Cs^{134} is of the order of magnitude expected from known cross sections and the flux density of the pile. Measurements at different discriminator settings showed that in Fe^{59} the gamma-gamma coincidences occur between a 200-kev gamma-ray and a one-Mev radiation. A line corresponding to a 195 ± 10-kev gamma-ray was consequently found in a scintillation spectrometer. The 200-kev radiation is very likely the transition between the 1.3- and 1.1-Mev levels in Co^{59}. It occurs in 2.5 percent of all the Fe^{59} disintegrations.

* Supported in part by the joint program of the ONR and AEC.

M3. Angular Correlation of Rh^{106}. J. J. KRAUSHAAR, *Brookhaven National Laboratory.**—The spectrum of Rh^{106} has been analyzed by a NaI scintillation spectrometer. The energies and relative intensities of the five main gamma-rays have been determined and agree well with the values reported in the previous abstract. The partial decay scheme, consistent with the beta- and gamma-ray intensities, has been investigated in order to explain the discrepancy between the measured angular correlation[1] and the calculated one for a 0–2–0 quadrupole-quadrupole transition. The effect of the 1.04–0.51-Mev gamma-ray cascade in competition with the 0.62–51 cascade is to lessen the expected values of $\epsilon(\theta)$ for a 0–2–0 transition in proportion to the intensity, relative efficiency of the counters, and values of $\epsilon(\theta)$ for the competing cascade. The contribution of the 1.04–0.51 transition is not enough with these considerations to explain the discrepancy. It may be that a loss of memory in the angular correlation of the 0–2–0 transition is involved. The correlation of the higher energy cascade has been roughly determined by differential and integral discrimination.

* Under contract with the AEC.
[1] E. L. Brady and M. Deutsch, Phys. Rev. **78**, 5 (1950).

M4. Angular Correlation Between Inelastically Scattered Protons and Gamma-Rays from the 1.4-Mev Level in Mg^{24}.* H. E. GOVE AND A. HEDGRAN,† *Massachusetts Institute of Technology.*—A 7.8-Mev proton beam from the MIT cyclotron was used to bombard a thin isotopic magnesium target. Coincidences between inelastic protons from the 1.4-Mev level in Mg^{24} and the corresponding gamma-rays were measured as a function of proton angle for two gamma-ray angles (protons, gamma-rays and beam co-planar). The experimental equipment employed has been described previously,[1] the only modification being the NaI gamma-counter. For the case in which the gamma-counter makes an angle of $-90°$ to the incident beam the angular correlation exhibits a rather pronounced maximum for a proton angle of $+90°$ (protons and gamma-rays emitted back to back). For a gamma-angle of $-30°$ no large variation in correlation occurs. The angular distribution of the inelastic protons has also been measured and indicates the presence of angular momentum terms as high as three. The possibility of using such measurements as an independent check of previously measured spins of excited states and for predicting unknown spins will be suggested.

* This work was assisted in part by the joint program of the ONR and AEC.
† On leave from the Nobel Institute for Physics, Stockholm, Sweden.
[1] Boyer, Gove, Harvey, Deutsch, and Livingston, Rev. Sci. Instr. **22**, 311 (1951).

M5. Capture γ-Rays from Protons on N^{14}. C. H. JOHNSON, C. D. MOAK, AND G. P. ROBINSON, *Oak Ridge National Laboratory.*—The γ-ray spectrum has been observed for the resonant capture of protons by N^{14}. A thick TaN target was bombarded with 280-kev protons from the Cockcroft-Walton generator. Gamma-rays resulting from the capture of protons at the 277-kev[1] resonance entered a large NaI (Th) crystal at 0° to the proton beam. Scintillations produced in the crystal were detected by a type 5819 photomultiplier. Pulses from the photomultiplier were amplified with a linear amplifier and studied with a one-channel differential discriminator. Gamma-rays from Cs^{137} and Na^{22} served to calibrate the pulse heights in terms of energy. The resulting capture γ-ray spectrum shows six groups. The energies of these six γ-rays can be arranged to give the total excitation energy in O^{15} (7.61 Mev) only if there are three intermediate levels in O^{15} giving rise to three cascade processes of two γ-rays each. These three pairs of γ-ray energies are 0.75 and 7.0 Mev, 1.38 and 6.4 Mev, and 2.38 and 5.3 Mev. In each case the addition to 7.61 Mev is considered within experimental error.

[1] R. Tangen, Kgl. Norske Videnskab. Selskab, Skr. No. 1 (1946).

M6. Photodisintegration Thresholds of Beryllium and Deuterium.* J. C. NOYES,† J. E. VAN HOOMISSEN,‡ W. C. MILLER, AND B. WALDMAN, *University of Notre Dame.*—A 90-degree, two-foot radius, electrostatic analyzer has been used to measure the energy of the electrons from our electrostatic generator. This measurement depends on the machining

of the deflecting plates, the positioning of the components of the analyzer, and the determination of the deflecting voltage. The total error contributed by these factors is less than 0.1 percent. The entrance and exit slits were adjusted to give a resolution of 2 kev. X-rays produced in a thick gold target by the electron beam emerging from the analyzer disintegrated the beryllium and deuterium. The neutrons were detected by a BF_3 counter, and the x-rays were monitored by a G-M counter. The neutron yields at various electron energies up to 30 kev above the thresholds were extrapolated to zero. The neutron binding energies of beryllium and deuterium are 1.664 ± 0.002 Mev and 2.231 ± 0.003 Mev, respectively.

* Supported in part by the joint program of the ONR and AEC.
† AEC Predoctoral Fellow, now at Boeing Airplane Company, Seattle, Washington.
‡ Now at Sandia Base, Albuquerque, New Mexico.

M7. Cu(γ, d):(γ, p) Ratio.* WARREN H. SMITH, *Iowa State College.*—The relative abundance of photodeuterons from copper was determined by magnetic curvature and range measurements. 65-Mev bremsstrahlung struck an 18-mil copper foil in a 12-inch helium-filled cloud-chamber, situated in a 3470-gauss field and viewed stereoscopically. Tracks of length at least 8 cm ending in the illuminated region were measured. The mean magnetic rigidity, in an interval 4 to 14 cm from the end, was obtained for 70 tracks. Tracks of measurable length different from 14 cm thus required correction (<12 percent). The expected rigidity for protons and deuterons of such range is known from the gas stopping power (calibrated by Po α's). The expected spread from scattering is calculated. The data indicate the appearance of both masses, with respective $H\rho$ distributions separated by approximately twice their individual half-widths. The observed d/p ratio 0.5 ± 0.15 (for equal range and solid angle intervals) provides an independent check of high photodeuteron abundance.[1]

* Work was performed at the Ames Laboratory of the AEC.
[1] P. R. Byerly, Jr., and W. E. Stephens, Phys. Rev. **83**, 54 (1951).

M8. Photoprotons from Bismuth. M. ELAINE TOMS AND WILLIAM E. STEPHENS, *University of Pennsylvania.**—The high energy photoprotons from some medium weight elements[1] have seemed to show an angular variation which suggests that they were produced by a direct photoprocess. To check if this mechanism were present in heavy nuclei, for which the coulomb barrier would suppress lower energy evaporated photoprotons, we have looked for photoprotons from a one-mil foil of bismuth irradiated with x-rays from a 24-Mev betatron and recorded in nuclear emulsions. The photoproton yield observed is about 3×10^4 protons/mole/r, which is smaller than the anisotropic protons observed in Rh, Ag, and Cu.[1] This yield is of the order of magnitude of or somewhat smaller than the yield calculated with reasonable assumptions on the Weisskopf-Ewing model. The photoproton energy distribution has a peak near 11 Mev, somewhat higher than that calculated on this model. The angular distribution seems isotropic, within the rather poor statistical uncertainties of 20 percent. Thus we find no evidence for any direct photoeffect for protons from bismuth in this energy range.

* Supported by the Air Research and Development Command and the joint program of the AEC and ONR.
[1] Curtis, Hornbostel, Lee, and Salant, Phys. Rev. **77**, 290(L) (1950); B. C. Diven and G. M. Almy, Phys. Rev. **80**, 407 (1950); P. R. Byerly and W. E. Stephens, Phys. Rev. **83**, 54 (1951).

M9. Angular Distribution of Photofission Fragments from Thorium.* E. J. WINHOLD, P. T. DEMOS, AND I. HALPERN, *Massachusetts Institute of Technology.*—A 16-Mev x-ray beam from the M.I.T. Linear Accelerator has been used to produce fission in a thorium target. The fission fragments were collected on aluminum foils arranged about the target in such a way as to pick up the fragments emitted in various directions. After exposures to the beam for times ranging from 6 to 180 minutes, the foils were counted with Geiger counters for periods up to several days. The ratio of the activity observed at 90° to that observed at 0° to the x-ray beam seems to be independent of both the duration of the exposure and the time of the measurement after the exposure. When account is taken of the angular resolution of the foil arrangement, and if the distribution of the activity is assumed to follow an $a+b\sin^2\theta$ relationship, then $b/a=0.25\pm0.08$.

* This work was assisted by the joint program of the ONR and AEC.

M10. Photofission of Uranium.* ROGER E. ANDERSON AND ROBERT B. DUFFIELD, *University of Illinois.*—The threshold for photofission of U^{238} has been measured by a catcher technique and found to be 5.2 ± 0.1 Mev. This is in disagreement with the value of 7.0 Mev predicted by the liquid drop model[1] but in agreement with an earlier experimental result obtained by a different method.[2] The cross sections for photofission of U^{238} and for the total photoneutron production from U^{238} have been determined up to 23 Mev. Both cross sections show maxima at approximately 15 Mev and decrease to small values at 23 Mev. This result is in agreement with the model proposed for photonuclear reactions by Goldhaber and Teller.[3] There is a sharp break in the photofission yield curve at 5.9 Mev, the threshold of the $U^{238}(\gamma, n)$ reaction.

* Assisted by the joint program of the ONR and AEC.
[1] S. Frankel and N. Metropolis, Phys. Rev. **72**, 914 (1947).
[2] Koch, McElhinney, and Gasteiger, Phys. Rev. **77**, 329 (1950).
[3] M. Goldhaber and E. Teller, Phys. Rev. **74**, 1046 (1948).

M11. Gamma-Ray Absorption Coefficients in the 5–10-Mev Energy Range.* E. S. ROSENBLUM, E. F. SHRADER, AND R. M. WARNER, *Case Institute of Technology.*—Gamma-ray absorption coefficients in lead and uranium are being investigated using radiation from the Case betatron. Collimation limits the beam to about a 0.6-degree cone; errors due to radiation scattered in the absorber are negligible. The radiation is analyzed with a magnetic pair spectrometer and a detection system consisting of stilbene crystals and RCA 5819 photomultipliers, providing an energy resolution of about 10 percent at 10 Mev and 15 percent at 5 Mev. A fast coincidence circuit, described previously,[1] having a resolving time of 5×10^{-9} second, gives a background of less than one percent of the counting rate when no absorber is in the beam. Preliminary measurement of the absorption coefficient in Pb at 10 Mev gives a value of 0.56 cm^{-1}, indicating that the correction to the theory at 10 Mev is of the same order of magnitude as that found by other investigators at higher energies. Results for Pb and U at 5 and 10 Mev will be presented.

* Work supported by the AEC.
[1] E. F. Shrader, Rev. Sci. Instr. **21**, 883 (1950).

SATURDAY MORNING AT 9:30

Sherman, Louis XVI Room

(J. H. VAN VLECK presiding)

Invited Papers

N1. UNESCO and International Cooperation in the Physics Sciences. RONALD FRASER, *International Council of Scientific Unions.* (20 min.)

N2. Photoelastic Analysis of Ultrasonic Waves. E. A. HIEDEMANN, *Michigan State College.* (30 min.)

N3. Recent Experiments with the University of Michigan Shock Tube. OTTO LAPORTE, *University of Michigan.* (30 min.)

N4. The Interaction of π-Mesons with Protons. HERBERT L. ANDERSON, *University of Chicago.* (30 min.)

SATURDAY AFTERNOON AT 2:00

Sherman, Crystal Room

(JOHN BARDEEN presiding)

Semiconductors, II

O1. Energy Levels in KCl. L. G. PARRATT AND E. L. JOSSEM, *Cornell University.**—Evidence is presented for the existence of discrete filled "ionization" levels below the filled $3p$ band of potassium and of chlorine in crystalline KCl in the immediate locale of a $1s$ vacancy. This evidence comes from observed shapes, widths, and energy positions of component lines in the $K\beta$ x-ray emission spectra. These lines were recorded with the newly constructed focusing crystal spectrometer previously described.[1] Also, evidence is presented for local discrete empty "excitation" levels below the ionization continuum. This evidence comes from an interpretation of the x-ray absorption spectra in the region of the K edge of potassium and of chlorine as recorded by Trischka.[2] Based upon these measurements and tentative interpretations, an energy level diagram for KCl is proposed to account for the component x-ray emission and absorption lines, and the enigmas of (1) the experimentally narrow β_1 line (0.92 ev full width at half-maximum for potassium and 0.67 ev for chlorine), (2) the unexplained component lines accompanying β_1, and (3) the absorption maxima and minima are tentatively resolved.

* Supported in part by the ONR.
[1] E. L. Jossem and L. G. Parratt, Phys. Rev. **79**, 210 (1950).
[2] J. W. Trischka, Phys. Rev. **67**, 318 (1945).

O2. Anionic Self-Diffusion and Electrical Conduction in Sodium Bromide. H. W. SCHAMP, JR.*—The diffusion coefficient of the radioactive bromide ion in sodium bromide was measured by evaporating a thin layer of sodium bromide containing the radioactive bromide ion onto one face of a single crystal of the compound, heating this exposed specimen for a definite length of time (360°C–688°C), cooling it, and then sectioning it to determine the distribution of radioactivity within the crystal. Above 450°C the results of the direct measurement of the diffusion coefficient are quantitative and can be expressed as $D_{\mathrm{Br}}=50\exp(-2.02/kT)$ cm²/sec. It is shown that below this temperature the actual coefficient is certainly lower than the measured value. The diffusion coefficient calculated from conductivity can be expressed as $D_{\mathrm{con}}=4.36\exp(-1.66/kT)$ at high temperatures and as $D_{\mathrm{con}}=6\times10^{-6}\exp(-0.80/kT)$ at low temperatures. The ratio $D_{\mathrm{Br}}/D_{\mathrm{con}}=11.5\exp(-0.36/kT)$ is taken as a measure of the transport numbers in the range of temperatures from 500°C to 700°C. It is shown that at low temperatures the diffusion coefficient directly measured is at least 30 to 40 times smaller than the coefficient calculated from conductivity, and it is concluded that the existence of pairs is unlikely.

* AEC Predoctoral Fellow.

O3. The Effect of Pressure on the Position of the *F*-band in Alkali Halides. E. BURSTEIN, J. J. OBERLY, AND J. W. DAVISSON, *Naval Research Laboratory.*—The effect of hydrostatic pressure on the position of the F-band in NaCl, KCl, and KI has been investigated up to 2000 atmospheres. The measured shifts in the position of the F-band, like those due to temperature changes, are found to be larger than the values calculated from the known dependence of the position of the F-band on the lattice constant of the various alkali halides. Further, the ratio $\Delta E_{\mathrm{obs}}/\Delta E_{\mathrm{calc}}$ increases in the order KI<KCl<NaCl. In terms of the "particle-in-a-box" model for the F-center[1] the discrepancy between experimental and calculated values may be attributed to the fact that the trapped electron exerts a considerably smaller repulsion on its neighbors than the halogen ion it replaces, so that the neighboring alkali metal ions which make up the walls of the box in which the electron is trapped are displaced from their normal position in the lattice toward the electron. Preliminary calculations based on these considerations show that, other factors being equal, the shift in the F-band should increase with decreasing compressibility of the host crystal in agreement with the experimental results.

[1] E. Burstein and J. J. Overly, "Optical properties of F-centers at liquid helium temperatures," Low Temperature Symposium, National Bureau of Standards (1951).

O4. Rectification Effects in Diamond. G. W. CURL AND G. C. DANIELSON, *Iowa State College.*—Point contact rectification has been observed both in counting and in photoconducting diamonds. The counting rate and the photoconducting current are usually greatest when the probe is the positive electrode, but the degree of rectification varies greatly with different diamonds. In the case of photoconductivity, the rectification effect has been investigated by applying an alternating potential to a circuit consisting of a diamond and a capacitor in series. The direct current potential appearing on the capacitor is measured by an electrometer circuit. The de-

pendence of this direct current potential upon the magnitude and frequency of the applied potential will be shown.

O5. Infrared Absorption of Nucleon-Bombarded Silicon. I.* M. BECKER, H. Y. FAN, AND K. LARK-HOROVITZ, *Purdue University*.—Recent investigations show that the absorption in silicon, beyond 1.1 micron, rises again toward longer wavelengths and is smaller the higher the resistivity. It has also been found that the resistivity of both *n*- and *p*-type silicon increases upon irradiation with high energy nucleons. We have therefore investigated the infrared absorption of silicon bombarded by neutrons in the Oak Ridge reactor and by 10-Mev deuterons in the Purdue cyclotron. The effects of the bombardment by neutrons and deuterons are similar and are the same for *n* and *p*-type samples: (a) A new[1] narrow absorption band appears at 1.75 microns. It sharpens with decreasing temperature, the half-width at 100°K is about 0.6 of that at room temperature. Its peak shifts toward shorter wavelength with decreasing temperature and is moved to 1.65 microns at 100°K. (b) Except for the new band the longer wavelength absorption is reduced to very small values. (c) The absorption edge, shows an apparent shift toward longer wavelengths. A shift over 0.05 micron has been observed. Both *n*- and *p*-type samples have reached resistivities of the order 10^3 ohm-cm due the bombardments.

* Supported by a Signal Corps Contract.
[1] Lark-Horovitz, Becker, Davis, and Fan, Phys. Rev. **78**, 334(A) (1950).

O6. Infrared Absorption of Nucleon-Bombarded Silicon. II.* H. Y. FAN, *Purdue University*.—The reduction of long wavelength absorption to very small values is convincing evidence for ascribing the long wavelength absorption to free carriers. The new absorption band at 1.75 microns fits the usual expression of line broadening. As it sharpens with decreasing temperature, $\int \mu(\nu) d\nu$ for the band remains nearly constant. Therefore, this band may be due to electron transitions between discrete energy levels in the energy gap. The increase of resistivity of both *N* and *P*-type materials indicate that both[1] hole traps *A* and electron traps *B* are introduced by the bombardment. The new absorption band is due to excitations from *A* to higher discrete levels *A'* and/or due to excitations from lower discrete levels *B'* to *B*. From the high resistivities reached due to the bombardments and from the position of the new band the energies of these levels can be estimated. The apparent shift of the fundamental absorption edge seems to indicate that imperfections of the lattice introduced by bombardment give rise to changes in band to band excitation.

* Supported by a Signal Corps Contract.
[1] Reading Report, July, 1951, and Cleland, Crawford, Jr., Lark-Horovitz, Pigg, and Young, Jr., Phys. Rev. **83**, 312 (1951).

O7. Atomic Heat of Silicon and Germanium at Very Low Temperatures.* P. H. KEESOM AND NORMAN PEARLMAN, *Purdue University*.—The atomic heat of Si has been measured between 1–100°K and of Ge between 1–80°K. Between 1 and 4°K for Si: $C_v = 6.5\times10^{-4}T^3 + 3.1\times10^{-5}T$ joules/degree mole and for Ge: $C_v = 3.87\times10^{-4}T^3 + 2.6\times10^{-5}T$ joules/degree mole. Assuming the linear term in T is due to a source other than the lattice vibrations, the Debye temperature is constant below 4°K and is Si: 668 degrees, Ge: 369 degrees. Both θ_D curves show a minimum, 32 percent below the T^3-region value, at $T = 40$°K (Si) and $T = 22$°K (Ge). The two θ_D curves can be brought to coincidence below the minimum if the two axes (θ_D and T) for Si are reduced by 1.8. The linear term in C_v is not yet understood. It seems doubtful that it is due to the free electron gas, which is responsible for the similar term in metals. Hall measurements indicate that the number of carriers is a hundred times less than is necessary to explain this term.

* Sponsored by Signal Corp Contract W36-039-SC-38151.

O8. Pressure Dependence of Zener Current in Germanium. K. B. MCAFEE, W. SHOCKLEY, AND M. SPARKS, *Bell Telephone Laboratories*.—The dependence of Zener current[1] upon pressure in $p-n$ junctions in germanium has been observed and compared with theory and other measured values of the change of energy gap with pressure, Since the probability of penetration of the energy gap f depends exponentially upon the effective mass m, the field strength E, and the energy gap ϵ_G, terms involving the volume dilation, as well as the pressure dependence of ϵ_G, the dielectric constant κ, and the effective mass m, are involved in the comparison. An independent method has been used to determine the extent to which a change of the dielectric constant with pressure influenced the result. This consists of a measurement of the change in capacity of the $p-n$ junction at a constant reverse bias as pressure is applied. The pressures employed range from 0 to 200 atmospheres. In this region $(d\ \ln i/d\Delta)_V$, the current change per unit current per unit dilation, is about 300. This assumes a value for $d\Delta/dp$ of 1.34×10^{-6}/atmos calculated from measurements of the elastic constants of germanium. The value of $(d\ \ln i/d\Delta)$ is constant for two decades of current as the voltage V is increased, dropping off considerably for higher currents sufficient to produce some heating.

[1] McAfee, Ryder, Shockley, and Sparks, Phys. Rev. **83**, 650 (1951).

O9. Evidence of Hole Traps in Ge Produced by Fast Neutron Bombardment. J. H. CRAWFORD, JR., J. W. CLELAND, K. LARK-HOROVITZ, J. C. PIGG, AND F. W. YOUNG, JR., *Oak Ridge National Laboratory*.—Prior to the work reported here there was no direct experimental evidence of hole traps (donors) being produced in Ge by nucleon bombardment,[1] although their presence might be expected by analogy from the behavior of *P*-type Si whose resistance increases monotonically with bombardment. It has now been shown experimentally that there is a certain limiting hole concentration $(n_h)_{\text{limit}}$ above which fast neutron bombardment of *P*-type Ge causes a decrease in conductivity due to the trapping of conducting holes. $(n_h)_{\text{limit}}$ proves to be temperature dependent. At 55°C $(n_h)_{\text{limit}} \sim 5\times10^{17}$ cm^{-3} while at −78°C its value is less than 4×10^{16} cm^{-3}. Several exposures of *P*-type samples with appropriate hole concentrations made at −78°C and 55°C successively during the same bombardment show that the conductivity decreases at the low temperature and increases at the high temperature. These findings are in good qualitative agreement with a model proposed by Lehman and James[2] in which they consider that both electron traps and hole traps associated with bombardment produced defects are introduced in equal concentrations below the middle of the forbidden energy band.

[1] Cleland, Crawford, Lark-Horovitz, Pigg, and Young, Phys. Rev. **83**, 312 (1951).
[2] K. Lark-Horovitz, Appendix II (Lehman and James), International Conference on Semiconductors, Reading, 1950; G. W. Lehman, Phys. Rev. **81**, 321 (1951).

O10. Calculation of the Specific Heat of Ge.* YÜ-CHANG HSIEH, *Purdue University*.—The specific heat of Ge has been calculated from its elastic constants[1] (as measured at B.T.L.).[2] Since the values of the elastic constants satisfy approximately the condition for consideration of first neighbors only, i.e., $4C_{11}(C_{11}-C_{44}) = (C_{11}+C_{12})^2$, only the four nearest neighbors are considered in the calculation. 174 frequencies of vibration are calculated and an approximate frequency spectrum is derived. The specific heat calculated agrees with the unpublished experimental date of Parkinson[3] within about 10 percent in the range 20°K to 150°K; below 20°K using discrete frequencies the theoretical values calculated check fairly well with the experimental results of Parkinson[3] and of Keesom and Pearlman,[4] down to 10°K.

* Supported by Signal Corps Contract.
[1] H. M. J. Smith, Trans. Roy. Soc. (London) **241**, 105 (1948).
[2] J. Bardeen and W. Shockley, Phys. Rev. **50**, 72 (1950).
[3] Parkinson, Ph.D. thesis, Oxford, 1948; Keesom and Pearlman, Signal Corps Report (W36-039-SC-32020, August, 1951).

O11. An Automatic Multirange Recording Device for Measuring Varying Potentials. J. C. PIGG, *Oak Ridge National Laboratory.*—In measurements of the changing electrical properties of semiconductors during neutron bombardment in the nuclear reactor, it is desirable to use automatic recording methods whenever possible. A device has been constructed and is currently being used which fulfills the requirements of the semiconductors under consideration. The components are a 0–3-mv 12-point Brown Electronic recorder with a four-deck 12-point selector switch ganged to the Brown input selector switch, a system of limit switches which activate appropriate stepping relays for automatic circuit changes, a system of scale indication, a vibrating reed electrometer for high resistance measurements, and constant current, constant voltage, and variable power supplies. By means of the limit switches and relays proper scale and circuit changes can be made to keep the data within the range of the recorder and provide a linear plot for changes up to twelve orders of magnitude. Each major component is connected to a needle plug terminal board so that any circuit within the range of the available components can be readily employed. By means of the selector switch ganged with the recorder input switch the external circuit can be changed for each point. This instrument is currently being used to measure resistivity of Ge, Si, and Cu_2O during neutron bombardment, and can also be used to measure static characteristics of semiconductor circuit components.

SATURDAY AFTERNOON AT 2:00

Sherman, Grey Room

(F. W. LOOMIS presiding)

General Physics

P1. Development of Ultra Compact, Ultra High Speed Digital Computers, II. DONALD H. JACOBS, MICHAEL MAY, AND SEYMOUR SCHOLNICK, *The Jacobs Instrument Company.*—In continuation of a program[1] of the development of all-electronic, all-parallel digital computers, a second special-purpose machine has been developed and constructed. This computer, called JAINCOMP-B, is an advanced development of the previously described JAINCOMP-A. It is a 24-digit binary machine in which two 24-digit numbers are added in eight microseconds. Inputs come from registers of switches or punch cards and results are displayed on banks of neon lamps. A magnetic core storage system[2] of 2–4-microsecond access time is used. The computer carries out automatically a program of trigonometric ray tracing, and has several alternate programs (paraxial rays, extra-axial rays, etc.). The computer is small ($16\frac{1}{2}\times21\frac{1}{2}\times30$ inches), light (110 lbs), and simple (300 subminiature tubes). Faults can be located very rapidly with a system of signal lights, and faulty circuits can be replaced instantly because all circuitry is constructed on unitized plug-in subassemblies, of which there are 500. The computer is aircooled via a system of internal ducts. A single type of low cost tube is used throughout, and no selection of tubes is required. No high precision components are employed. The machine computes a program of 171 steps in 0.24 sec.

[1] D. H. Jacobs and M. May, Phys. Rev. **82**, 325(A) (1951).
[2] D. H. Jacobs and M. May, Phys. Rev. **83**, 243(A) (1951).

P2. A Stabilized Synchronous Amplifier. R. G. NUCKOLLS AND L. J. RUEGER, *National Bureau of Standards.*—Synchronous or lock-in amplifiers are known[1,2] to suffer from lack of stability, linearity, and, in addition, from shift of both zero and sensitivity with background noise level. A design was needed in the National Bureau of Standards microwave spectroscopy project with the quantitative, stable performance characteristic of well-designed inverse feedbacks amplifiers. A design using two identical stabilized amplifiers has been used 8 months with negligible short or long term shift of both zero and sensitivity. The voltage wave form in one amplifier is the sum of the reference and input signals; the other wave form is the difference. The difference in *average peak* values is selected by two crystal rectifiers and measures the synchronous component of the input. The circuit has a linear dynamic voltage range greater than 60 db, restricted at the low end by noise and circuit asymmetry and at the upper limit by overloading of the particular crystals used. Alternately, the difference of some property other than average peak voltage; such as rms or average power might be selected with equal or superior results.

[1] W. C. Michels and M. L. Curtis, Rev. Sci. Instr. **12**, 444 (1941).
[2] N. A. Schuster, Rev. Sci. Instr. **22**, 254 (1951).

P3. A Critical-Flow Pneumatic Hygrometer. W. A. WILDHACK, T. A. PERLS, AND J. W. HAYES, *National Bureau of Standards.*—The theory of pneumatic instruments based on critical flow[1] has been adapted to a continuous-flow device to measure humidity. For truly critical flow, the mass discharged through a nozzle must be independent of downstream pressure and proportional to upstream pressure. These conditions are only realized at Reynolds numbers greater than 6000 ± 1000. The critical-flow "bridge" incorporates four nozzles, all operating at Reynolds numbers greater than 7000. The nozzles have long expansion cones (2° total angle) and reach critical flow at a pressure ratio of 0.82 ± 0.02. An impedance causing a pressure drop up to 200 mm Hg may be inserted between nozzles without any change in flow. A calcium-sulfate desiccator removes over 99.9 percent of the moisture from one arm of the bridge and the change in mass flow is measured by the difference in absolute pressure at the entrance to the downstream nozzle. The theoretical calibration of the device involves only pressure and temperature measurements and no experimental proportionality factors. This theoretical calibration agrees with measurements made on standard humidity apparatus to within an uncertainty of ±0.5 percent relative humidity.

[1] W. A. Wildhack, Rev. Sci. Instr. **21**, 25 (1950).

P4. Distribution of Potential in an Electrically Excited Excited Nonhomogeneous Medium. LACHLAN GILCHRIST, *University of Toronto.*—Electric and electromagnetic excitation are applied to the Earth's crust, a nonhomogeneous approximately layered medium in order to obtain evidence for the location of inhomogeneities or anomalies, measured potentials are incorporated in a formula which is applicable only to a homogeneous medium. For example, for a steady state

$$V=\frac{i\rho}{2\pi}\left(\frac{1}{a}-\frac{1}{b}-\frac{1}{L-a}+\frac{1}{L-b}\right)$$

is used, since there is no unique formula applicable to a non-homogeneous medium; L = distance between source and sink; a, b = the distances of the potential probes from the source; i = current; ρ = resistivity. To minimize or eliminate experimental evidence of "spurious" anomalies the following are essentially necessary. 1. The "stake resistances" at the source and at the sink should be equalized. These are dependent largely on bowls of fifty-feet radius adjacent to and including the center of symmetry of the source and sink and may be measured readily. For numerous typical set-ups the values have been calculated. If it is not convenient to equalize the "stake resistances," they should be measured for correctional purposes, in locating "true" anomalies. 2. The centers of symmetry must be located to evaluate L, a and b. This may be done geometrically or analytically if the distribution of potential within the bowls is determined experimentally. Illustrations are presented from field explorations of the locations of anomalies embedded in extensive earth materials from which they differed in average resistivity.

P5. Propagation of Short Radio Waves Well beyond the Horizon. THOMAS J. CARROLL, *National Bureau of Standards.*—For wavelengths shorter than about 6 meters, radio field strengths well beyond the horizon from high power transmitters have been consistently measured to be many orders of magnitude greater than the fields calculated for a so-called "standard" refracting atmosphere, even when conditions of superrefraction in the atmosphere are known not be be present. A very simple calculation of the fields internally reflected by the "standard" troposphere, following the method of Bremmer as used in the troposphere by Feinstein, agrees remarkably well with measurements at 50 Mc and 3300 Mc. The breakdown of "standard refraction" theory is attributed provisionally to the error in the assumption of linearly decreasing index of refraction to indefinitely great heights. If constant unit index is assumed above 10 km, a bilinear model results, which has been extensively treated theoretically by Furry and others. The bilinear model of "standard" refraction explains the reduced attenuation rate of fields at several horizon distances as higher order modes becoming dominant. Theory and experiment are gradually coming into agreement that the formerly predicted high attenuation rates for vhf and microwaves beyond the horizon are quite erroneous.

P6. Electromagnetic Field Measurements in the Plane of a Circular Aperture. ROBERT E. HOUSTON AND ROBERT H. NOBLE, *Michigan State College.*—The short wavelengths of microwaves have been used by Andrews[1] to study the diffraction pattern of circular apertures in a plane conducting screen. His data did not show the expected rise at the edge of the aperture probably because his detector was of necessity not small compared with the wavelength. Bethe[2] has shown that the expression for the field contains a term proportional to $(a^2-r^2)^{-\frac{1}{2}}$, where a is the radius of the circular aperture. This experiment used 600-megacycle radiation and a detector about 1/25 wavelength. Fields were measured in the plane of apertures with diameters ranging from twice to one-fourth wavelength. A rapid rise in field was noted at the edge of each. The aperture with diameter one-half wavelength showed the greatest transmission per unit area.

[1] C. L. Andrews, J. Appl. Phys. **21**, 761 (1950).
[2] H. A. Bethe, Phys. Rev. **66**, 163 (1944).

P7. Velocities of Ionized Air Shocks near Detonating Explosives. J. SAVITT AND R. H. STRESAU, JR., *U. S. Naval Ordnance Laboratory.*—Measurements of shock velocities in the immediate vicinity of small charges of explosives have been made using a vacuum thermocouple type timer.* The ionized air of the shock was used to start and stop the timing circuit when the shock front reached the charged probes. The distances and times involved varied from about 0.025 to about 0.400 inch and from about 0.10 to about 2.00 microseconds. The air shocks were produced by the detonation of various samples of highly confined primary and high explosives varying in weight up to about one gram and in loading density up to about 95 percent of crystal density. The air shock velocity was found to be dependent upon the distance from the detonation, the composition of the explosive, its weight, and its geometry; but independent of the loading density. Some of the probe problems will be discussed and some of the results of the measurements of ionized air shock velocities presented.

* R. H. Stresau, Phys. Rev. **76**, 880 (1949).

P8. Synchronized Rotating Mirror System.* RICHARD G. FOWLER AND ROBERT J. LEE, *University of Oklahoma.*—A synchronized rotating mirror system has been constructed as an improved means of observing previously described phenomena.[1] These phenomena involve the appearance of moving luminosity in a side tube joined at right angles to a regular discharge tube. Rotating mirror investigations of this luminosity were previously conducted with a system depending on chance for photographic register. The new mirror system is photoelectrically synchronized to record each discharge of the tube. The system consists of a rotating concave mirror, and an infrared projector and photocell circuit which trip a thyratron, thus discharging a condenser through a relay to close a vacuum switch and fire the tube just as the mirror is in axial position. To eliminate aberration, the arrangement requires that the image fall on a film only 6 cm wide at a distance of 115 cm with 30-rps mirror speed. Excellent reproducibility of register and mirrorgram detail has been obtained.

* Project supported by the ONR.
[1] Fowler, Goldstein, and Clotfelter, Phys. Rev. **82**, 879 (1951).

Post-Deadline Papers, If Any

SATURDAY AFTERNOON AT 2:00

Sherman, Louis XVI Room

(ALLEN C. G. MITCHELL presiding)

Beta-Decay, Nuclear Isomerism, etc.

Q1. Empirical Analysis of Nuclear Shell Effects in β-Energetics.[1] C. D. CORYELL, R. A. BRIGHTSEN,[2] AND A. C. PAPPAS,[3] *Massachusetts Institute of Technology.*—An analysis of available decay data for nuclides of odd A ($A>50$) indicates that the total energy E_β for β-decay or electron capture is given reasonably satisfactorily by the Weizsäcker-Bohr-

Wheeler term $B_A[|Z-Z_A|-0.5]$ in any region not affected by neutron or proton shell edges. The reduction in neutron or proton binding energies associated with the crossing of a shell edge leads to displacements ΔZ_A in the Z_A curve, upward for neutron crossings and downward for proton crossings. Empirically identified shifts in the well-defined Z_A curves indicate the following values $|B_A \Delta Z_A|$ in Mev for the discontinuities in neutron and proton binding energies at the shell populations of 28, 50, 82, and 126: 1.0 and 1.2, 2.2 and 1.7, 1.7 and 1.3, and 1.1 (neutrons only). This procedure has been used to establish limits on the energy effects of possible subshells at other nucleon numbers such as 34, 40, 64, and 100. It can also be extended to give better interpolations among atomic masses.

[1] Supported in part by the AEC.
[2] Presently at Westinghouse Atomic Power Division, Pittsburgh.
[3] Fellow of the Norwegian Council of Scientific and Industrial Research.

Q2. Atomic Binding Energy Considerations in Negative Beta-Decay.* H. M. SCHWARTZ, *University of Arkansas.*—The extreme low end of negative beta-spectra is sensitive to the mode of utilization of the excess atomic binding energy liberated in the increase of nuclear charge during the decay process. In the case of the heavy nuclides, a measurable cutoff is to be expected in the lower end of the spectrum corresponding to this excess binding energy, if this energy is carried away by the beta-particle *subsequent* to its appearance in the nuclear decay process.[2] Such a cutoff does not, however, follow from an application of conventional time-dependent perturbation theory to the combined system of nucleus, lepton field, and atomic electrons, subject to Fermi and coulomb couplings. There seems, as yet, to exist no clear-cut experimental evidence regarding this question, although it is hoped that pertinent data from proportional counter measurements now in progress will be available in the near future.

[1] This work is supported in part by the AEC.
[2] Edwards, Damon, and Schwartz, Phys. Rev. **82**, 333(A) (1951). The following additional reference has come to our attention recently: L. Goldstein, J. phys. et radium **8**, 235 and 316 (1937).

Q3. The *K*-Auger Yield for Ba. C. D. BROYLES* AND S. K. HAYNES, *Vanderbilt University.*—Measurements of the Auger yield for elements of $Z>40$ are few and tend on the whole to give larger yields than predicted by the approximate theory of Massey and Burhop. We have made a careful comparison in a lens spectrometer of the intensity of the *K*-Auger lines with the intensity of the *K*-conversion line from the isomeric state of Ba^{137}. The source ($\sim$.01 mg cm^{-2}) was vacuum evaporated onto a copper on Formvar film of about .075 mg cm^{-2} total weight. The counter window was less than .018 mg cm^{-2} Nylon supported on Lectromesh with a transmission limit of about 3 kev. Because the forbidden Kurie plot curved sharply upward below 40 kev, the base line under the Auger peaks was slightly uncertain. A preliminary minimum value for the Auger yield of Ba is 0.129 ± 0.01 compared to a value of 0.15 predicted by Massey and Burhop.[1] The origin of the excess electrons below 40 kev will be discussed.

* AEC Predoctoral Fellow.
[1] H. S. S. Massey and E. H. S. Burhop, Proc. Roy. Soc. (London) **153**, 681 (1936).

Q4. Proposed Methods for Determining *K*-Capture Partial Lifetimes.* A. J. SAUR AND H. M. SCHWARTZ, *University of Arkansas.*—Because of the peculiar difficulties in obtaining precise measurements, only a few reliable values for *K*-capture partial lifetimes are known. These measurements have been made by ingenious methods applicable to only a small number of nuclides. From information obtained at this and other laboratories, we have designed a proportional counter arrangement for such studies which should be applicable to a fairly large family of nuclides, as determined by a careful study of known physical and chemical properties of such nuclides. The proportional counter is so designed as to resolve with relatively high accuracy pulses due to Auger electrons emitted in *K*-capture from the weaker pulses due to the less ionizing *X*, unconverted gamma, and hard positron radiation. Limits to the precision obtainable are imposed by the as yet insufficiently studied surface effects in proportional counters as well as by inadequate present knowledge of *K*-shell fluorescence yields for higher *Z* elements. Two other methods, involving, respectively, cloud-chamber and hot-atom chemistry techniques, will be discussed.

* This work is supported in part by the AEC.

Q5. Beta-Spectra of Ce^{144} and Pr^{144}. FRED T. PORTER AND C. SHARP COOK, *Washington University.**—Electron spectra from thin sources of chemically purified Ce^{144} have been observed in the 180° uniform field magnetic spectrometer. Ce^{144} (275-day) decays to Pr^{144} (17-min) which decays to stable Nd^{144}. The highest energy beta-group, which is believed to be associated with the decay of Pr^{144}, has an end-point energy, according to the *F-K* plot, of 2.97 ± 0.02 Mev. The *F-K* plot exhibits a straight line back to approximately 450 kev where a small deviation occurs. A large deviation occurs at about 310 kev. The latter groups can be fitted into a decay scheme consistent with observed gamma-radiations attributed to Ce^{144}. From the linearity of the high energy *F-K* plot and the absence of gamma-radiation of sufficient intensity to follow all disintegrations of Pr^{144}, it appears that the most probable mode of decay of Pr^{144} is by beta-emission to the ground state of Nd^{144}.

* Assisted by the joint program of the ONR and AEC.

Q6. Relative Internal Conversion in the *L* Subshells.* J. W. MIHELICH AND E. L. CHURCH, *Brookhaven National Laboratory.*—An experimental survey is being made of the relative intensity of L_I, L_{II}, and L_{III} conversion lines of certain low energy γ-rays originating in nuclei of medium atomic number. Data have been obtained for the following multipole orders: *M*1, *M*1+*E*2, *E*2, and *M*4. Semicircular photographic spectrographs are being employed. The results can be summarized as follows. Multipole order assignments are taken from Goldhaber and Sunyar.[1] (1) *M*1 transitions are *L* converted in the L_I shell predominantly. This is in accord with the observation that experimental K/L_{total} ratios for magnetic dipole transitions are not in disagreement with the ratio of the following theoretical values: the *K*-shell conversion coefficients of Reitz[2] and the L_I shell coefficients of Gellman, Griffith, and Stanley.[3] (2) *E*2 transitions are *L* converted in the L_{II} and L_{III} shells primarily, L_I conversion being appreciably less. (3) It seems that relative mixtures of *M*1 and *E*2 may be determinable from L_{II}/L_I or L_{III}/L_I ratios. (4) *M*4 transitions are *L* converted in primarily the L_I and L_{III} shells. This trend with increasing magnetic multipole order is in agreement with the approximate theory of Tralli and Lowen.[4]

* Research performed under auspices of the AEC.
[1] M. Goldhaber and A. W. Sunyar, Phys. Rev. **83**, 906 (1951).
[2] J. R. Reitz, Phys. Rev. **77**, 10 (1950).
[3] Gellman, Griffith, and Stanley, Phys. Rev. **80**, 866 (1950).
[4] N. Tralli and I. S. Lowen, Phys. Rev. **76**, 1541 (1949).

Q7. 514-kev Energy Level of Rubidium 85. W. S. EMMERICH AND J. D. KURBATOV, *Ohio State University.*—The de-excitation of the 514 ± 3-kev energy level appearing in orbital electron capture of strontium 85, half-life 65 days, has been studied.[1] A permanent magnet spectrograph, a lens spectrometer, and coincidence absorption techniques were used. The internal conversion of the gamma-ray was found to be 7×10^{-3} and the *K* to *L* conversion ratio is 13. Coincidences could not be detected between x-rays and gamma-rays. This shows that the 514-kev excitation level in Rb is metastable. A search was made for radiation corresponding in energy to

levels known to exist from the disintegration of Kr 85. In the region from 120 to 200 kev such radiation is absent to the limit of 0.75 percent of the total activity.[2]

[1] M. Ter-Pogossian and F. T. Porter, Phys. Rev. **81**, 1057 (1951).
[2] L. Cheng and J. D. Kurbatov, Phys. Rev. **79**, 237 (1950).

Q8. Isomerism of Sr^{85}. A. W. SUNYAR, J. W. MIHELICH, G. SCHARFF-GOLDHABER, M. DEUTSCH,* AND M. GOLDHABER, *Brookhaven National Laboratory.*†—Sr^{85m} (70 min) decays via a two-step isomeric transition and a cross-over transition to the ground state, and by K capture (~16 percent) to a 150-kev excited state of Rb^{85}. The lifetime determining step is a highly converted $E3$ transition of ~6 kev which is followed by an $M1$ transition of ~220 kev. The $M4$ cross-over transition of ~226 kev has been observed in a 180° magnetic spectrograph. The conversion coefficient for the 220-kev transition is obtained by comparison of gamma-ray and conversion electron intensities for the 150-kev and 220-kev transitions. Conversion electrons from the 6-kev transition have been observed in a flow proportional counter and an ion chamber. The main isomeric transition proceeds as follows:

$$p\ 1/2 \xrightarrow{6\ \text{kev}} 7/2+ \xrightarrow{220\ \text{kev}} g\ 9/2.$$

The 7/2+ state involves coupling of 7 odd neutrons in g 9/2 orbits as previously noted for several isomeric transitions. The intensities of the $M4$ cross-over transition agrees with that expected from the semi-empirical formula of Goldhaber and Sunyar.[1] The ground state of Sr^{85} ($65d$) decays by K-capture to an excited state of 510 kev, for which a half-life of (0.9±0.2) μsec has been established. A decay scheme consistent with shell theoretical predictions and experimental evidence for the decay of Kr^{85}, Rb^{85}, and Sr^{85} will be discussed.

* Permanent address: Massachusetts Institute of Technology.
† Research performed under the auspices of the AEC.
[1] M. Goldhaber and A. W. Sunyar, Phys. Rev. **83**, 906 (1951).

Q9. Disintegration Scheme of Lu^{176m}. G. SCHARFF-GOLDHABER, E. DER MATEOSIAN, AND J. W. MIHELICH, *Brookhaven National Laboratory.*—Lu^{176m} is known[1] to decay with a half-life of 3.7 hr, emitting beta-particles of 1.0- to 1.2-Mev maximum energy, whereas the ground state of Lu^{176} has a beta-spectrum with a maximum energy of 0.2 to 0.4 Mev and a half-life of 2.4×10^{10} yr. A search was therefore made, with a sensitive scintillation spectrometer, for a γ-ray of 0.6–1 Mev due to an isomeric transition of Lu^{176m}. No such γ-ray was observed, indicating that the spin difference between ground state and excited state is at least 5. However, a strongly converted (89.0±0.5) kev γ-ray was found in the 3.7-hr Lu isomer following the β-ray (1.1 Mev) with <1-μsec delay, with a K/L ratio of 0.10±0.06, indicating an $E2$ transition. The spin and parity of the first excited state in Hf^{176} are thus 2+, in agreement with a rule for even-even nuclei recently pointed out by Goldhaber and Sunyar.[2] Beta-rays of 1.2 Mev going directly to the ground state of Hf^{176} were also found. Spin and parity of Lu^{176m} are assigned as 1+.

[1] K. Way *et al.*, Natl. Bur. Standards (U. S.) Circ. 499.
[2] M. Goldhaber and A. W. Sunyar, Phys. Rev. **83**, 906 (1951).

Q10. The Radioactive Decay of Te^{125m}. P. AXEL AND J. C. BOWE,* *University of Illinois.*†—The branching ratios for each of the two transitions in Te^{125m} were determined by experiments which used a thin-lens beta-ray spectrometer, a NaI crystal scintillation spectrometer, and two proportional counters in coincidence. The unconverted 110-kev gamma-ray from the first transition was observed and its K conversion coefficient was measured as 160±20. For the second transition, the following branching was obtained: K conversion = 0.80 ±0.06, L conversion = 0.11±0.03, M conversion = 0.02, and the unconverted gamma-ray = 0.07±0.02. These data are consistent with the suggested level assignment[1] of $_{1/2}$, $d_{3/2}$, and $_{11/2}$. They further indicate that the second transition is predominantly magnetic dipole. A comparison of these results with existent theoretical internal conversion calculations will be given.

* Now at Argonne National Laboratory, Chicago, Illinois.
† Assisted by the joint program of the ONR and AEC.
[1] J. C. Bowe and G. S. Goldhaber, Phys. Rev. **76**, 437 (1949).

Q11. The Second Transition in the Decay of Sn^{119m}. J. C. BOWE* AND P. AXEL, *University of Illinois.*†—The photons from the second transition of the 250-day isomer[1] of Sn^{119} were detected in coincidence with x-rays from the first transition by using two proportional counters. These photons have an energy of 23.8±0.6 kev. Since In x-rays (24.2 kev) and Sn x-rays (25.2 kev) were present, the gamma-rays could be distinguished only by coincidence measurements. The fraction of the unconverted gamma-rays was found to be 0.13 ±0.03. This corresponds to a total conversion of 7.3±1.7. The experimental evidence favors an assignment of magnetic dipole to this transition.

* Now at Argonne National Laboratory, Chicago, Illinois.
† Assisted by joint program of the ONR and AEC.
[1] J. W. Mihelich and R. D. Hill, Phys. Rev. **79**, 781 (1950).

Q12. The Decay of Rh^{106}. DAVID E. ALBURGER, *Brookhaven National Laboratory.**—$Ru^{106}-Rh^{106}$ beta-rays with end points 3.53±0.01 Mev (68 percent), 3.1±0.1 Mev (11 percent), 2.44±0.07 Mev (12 percent), and 2.0±0.1 Mev (3 percent) have been observed using a lens spectrometer. Gamma-rays are also present with energies of 0.513, 0.624, 0.87, 1.045, and 1.55 Mev and relative intensities of 1:0.53: 0.03:0.08:0.025, respectively, as measured by photoelectric conversion. There is evidence for a gamma of 2.9 Mev. The 0.513- and 0.624-Mev lines are internally converted with K intensities of 7.5×10^{-4} and 2.3×10^{-4} relative to total beta-radiation. At 1.6 percent resolution the 0.513-Mev transition K and L conversion lines are separated and have a ratio of 7.8±1. Using the recent analysis of K/L ratios by Goldhaber and Sunyar, one can conclude that this transition is an electric quadrupole; from relative conversion intensity the 0.624-Mev line must also be $E2$. The results are consistent with beta-decay to states in Pd^{106} at zero, 0.513, 1.137, and 1.55 Mev. The 0.87- and possible 2.9-Mev gamma-rays and excess beta-rays are apparently associated with weakly excited higher states. From this scheme the K-conversion coefficients of the 0.513- and 0.624-Mev gammas are $(3.5\pm1)\times10^{-3}$ and $(2.1\pm1)\times10^{-3}$, both consistent with $E2$.

* Under contract with the AEC.

Q13. A Clarification of the Radioactivity of Nd^{151} and Pm^{151}. W. C. RUTLEDGE,* J. M. CORK,† AND S. B. BURSON, *Argonne National Laboratory.*‡—Enriched Nd^{150} was activated in the Argonne reactor. The internal conversion electrons and photoelectrons from a lead radiator were investigated in a permanent magnet-type beta-spectrograph. Gamma-rays of 85.4 and 117.1 kev, decaying with a half-life of 12 min, show work-function differences of prometheum. Apparently they follow emission of the 1.93-Mev beta-ray, which is thus assigned to Nd^{151}. Absorption measurements show prometheum K-x-rays and another gamma-ray of 895 kev. This 12-min activity proves to be the parent of a 27.5-hr beta-ray of 1.1 Mev in Pm^{151}. (This is the usual case where the half-lives of members of a chain with odd mass numbers increase successively down the chain.) Associated gamma-rays of 64.7, 65.8, 69.6, 99.9, 116.2, 105.0 (or 144.0), 163.1, 168.0, 177.0, 208.3, 231.9, 239.9, 275.2, and 340.1 kev are characterized by samarium work function differences. Absorption measurements also show a weak 615-kev gamma-ray. These data and coincidence measurements make it possible to propose a decay scheme.

* Phoenix Project Fellow, University of Michigan.
† University of Michigan.
‡ Supported in part by the joint program of the ONR and AEC.

Q14. Mass Designation of the 51.5 Min-Tc Isomer.* HEINRICH A. MEDICUS AND HARRY T. EASTERDAY, *University of California.*—By proton bombardment of molybdenum of natural isotopic composition about a dozen Tc activities are produced which, with a few exceptions, could all be ascribed to specific isotopes. One exception is the Tc isomer of 51.5-min half-life and 34.4-kev transition energy[1] which is relatively difficult to detect due to its low energy and because it is masked by the 52.5-min positron emitter, Tc^{94}. By bombardment of enriched Mo isotopes with protons of 9.5-Mev energy in the 60-in. cyclotron and then by using a lens spectrometer to compare the intensity of the L-line of the isomer with characteristic conversion lines of the known isotopes, it could be proved that this isomer belongs to Tc^{96} whose ground state has a half-life of 104 hours. This isomer was also produced by 4-Mev protons from the Berkeley electrostatic generator on natural molybdenum. This also confirms the previous results[1] that the isomer is not connected with the positron emitter Tc^{95} since the (p, n) threshold to produce the latter activity requires a proton energy of 5.1 Mev.

* This work was supported by the AEC.
[1] Medicus, Preiswerk, and Scherrer, Helv. Phys. Acta **23**, 299 (1950).

SATURDAY AFTERNOON AT 2:00

Sherman, West Room

(H. MARGENAU presiding)

Joint Symposium of the American Physical Society and the Philosophy of Science Association

R1. Inductive Logic and Science. R. CARNAP, *University of Chicago.* (45 min.)
R2. Philosophical Interpretations of Modern Physics. P. FRANK, *Harvard University.* (45 min.)
R3. Quantum Measurement as an Amplifying Process. W. M. ELSASSER, *University of Utah.* (45 min.)

SUPPLEMENTARY PROGRAMME

SP1. Phenomenological Theory of Lamb Shift.* FREDERIK J. BELINFANTE, *Purdue University.*—Ignoring self-interactions one can explain the Lamb shift and anomalous magnetic moments of electrons and protons by introducing appropriate interactions between these particles and photons. Using methods of gauge-independent quantum electrodynamics we take in the generalized Schrödinger equation for these particles the interaction operator $W=\mathbf{D}_{II}{}^2/8\pi-\mathbf{D}_{II}\cdot\mathbf{P}-\mathbf{D}_{II}\cdot\mathfrak{E}/4\pi-\mathfrak{E}\cdot\mathbf{P}+2\pi\mathbf{P}^2-\mathfrak{A}\cdot\mathbf{j}-\mathfrak{B}\cdot\mathbf{M}+\frac{1}{2}C(\mathbf{j}^2-\rho^2)$, where $\mathfrak{E}$, $\mathfrak{B}$ = transverse electromagnetic field; $\mathfrak{A}(\mathbf{x}, t)=\int d^3\mathbf{x}'\ \mathrm{curl}'\mathfrak{B}(\mathbf{x}', t)/4\pi r$; $\mathbf{D}_{II}(\mathbf{x}, t)=-\nabla\int d^3\mathbf{x}'\rho(\mathbf{x}', t)/r$; $\rho=e(:\psi_P{}^\dagger\psi_P:-:\psi_e{}^\dagger\psi_e:)$; $\mathbf{j}=e(:\psi_P{}^\dagger\boldsymbol{\alpha}\psi_P:-:\psi_e{}^\dagger\boldsymbol{\alpha}\psi_e:)$; $\mathbf{P}=f_P:\psi_P{}^\dagger\boldsymbol{\gamma}\psi_P:+f_e:\psi_e{}^\dagger\boldsymbol{\gamma}\psi_e:$; $\mathbf{M}=f_P:\psi_P{}^\dagger\boldsymbol{\sigma}\psi_P:+f_e:\psi_e{}^\dagger\boldsymbol{\beta}\boldsymbol{\sigma}\psi_e:$; $\boldsymbol{\gamma}=-i\beta\boldsymbol{\alpha}$. The integrability of $ih\delta\Psi[\sigma]=\int d^3\mathbf{x}'\delta t\times(\mathbf{x}')W(\mathbf{x}', \sigma)\Psi[\sigma]$ is proved for flat σ. We put $\mathbf{D}=\mathfrak{E}+\mathbf{D}_{II}$, $\mathbf{H}=\mathfrak{B}-4\pi\mathbf{M}$, $\mathfrak{E}=\mathbf{D}-4\pi\mathbf{P}$. In Heisenberg representation then $\mathbf{D}$, $\mathbf{H}$ and $\mathbf{E}$, $\mathfrak{B}$ are tensors satisfying with ρ, j the phenomenological maxwell equations. The energy density is $(\mathbf{E}^2+\mathfrak{B}^2)/8\pi+\frac{1}{2}C(\mathbf{j}^2-\rho^2)+\Sigma_{e,P}\Re\{\psi^\dagger(mc^2\beta-ihc\boldsymbol{\alpha}\cdot\nabla)\psi\}-\mathfrak{A}\cdot\mathbf{j}-\mathfrak{B}\cdot\mathbf{M}$ and the momentum density $=\mathbf{E}\times\mathfrak{B}/4\pi c+\Sigma_{e,P}\Re\{\psi^\dagger(h/i)\nabla\psi+\frac{1}{2}\times\mathrm{curl}(\psi^\dagger\hbar\boldsymbol{\sigma}\psi)\}-\rho\mathfrak{A}/c-\mathfrak{B}\times\mathbf{P}/c$. The experimentally observed magnetic moments are obtained by choosing $f_P=+0.000976\mu_B$ and $f_e=-0.00119\mu_B$, and a Lamb shift $\delta E_{2s\frac{1}{2}}-\delta E_{2p\frac{1}{2}}=1062$ Mc is obtained by choosing $C=1.062\times10^{-22}$ cm³. This Lamb shift then depends on atomic number and quantum numbers by $\delta E_{nlj}=\{|f_e/\mu_B|(-1)^{l-j+\frac{1}{2}}(j+\frac{1}{2})^{-1}(l+\frac{1}{2})^{-1}+(2C/\pi)(m_ec/\hbar)^2\times\delta_{l,0}\}\times Z^4\alpha^2\ \mathrm{Ry}/n^3$, in good agreement with Bethe's formula.

* To be given at the end of Session I if time permits.

SP2. Clustering of Ions.*† HENRY MARGENAU AND STANLEY BLOOM, *Yale University.*—Kinetic theory is employed in investigating the extent to which polarizable molecules attach themselves to slowly moving ions in a gas, the underlying picture being that commonly used in deriving the barometer formula, i.e., the aggregation of molecules in a constant field of force. An intermolecular potential energy of the form $-\mathrm{KR}^{-4}$ for $r\gtrsim r_0$ but ∞ for $r\lesssim r_0$, leads to a very great tendency for cluster formation of r_0 is taken to be the (Van der Waals) distance of closest approach. This potential, however, packs most of the clustered molecules into the sharp crevasse near r_0 and therefore falsifies the result. When the cusp is removed and a more adequate potential of the form $cR^{-12}-\mathrm{KR}^{-4}$ is chosen, the tendency to aggregate is seen to vanish, except in the case of Li^+, which remains a strong clustering agent. Our analysis treats the neutral molecules as points and therefore ignores all steric effects. These would reduce clustering still further and are therefore uninteresting except in unusual cases.

* Supported by the ONR.
† To be given at the end of Session B if time permits.

Author Index to Papers Presented at the Chicago Meeting

Adair, R. K.—J1
Alburger, David E.—Q12
Anderson, Herbert L.—N4
Anderson, P. W.—F7
Anderson, Roger E. and Robert B. Duffield—M10
Andrew, Kenneth L. and K. W. Meissner—G2
Antal, John J. and A. H. Weber—D6
Arthur James S., A. J. Allen, R. S. Bender, R. L. Ely, H. J. Hausman, L. A. Page, and E. M. Reilley—A8
Atkinson, W. R., R. G. Fowler, L. W. Marks, and G. W. Charles—B12
Axel, P. and J. C. Bowe—Q10
Bauer, E.—C4
Becker, M., H. Y. Fan, and K. Lark-Horovitz—O5
Belinfante, Frederik J.—I9, SP1
Bernstein, William and A. W. Schardt—E3
Block, M. M., S. Passman, and W. W. Havens, Jr.—H2
Bloom, Stanley and Henry Margenau—G9
Bonet, J. V. and A. V. Bushkovitch—C3
Borst, L. B. and V. L. Sailor—E2
Bowe, J. C. and P. Axel—Q11
Bramson, H. J., A. M. Seifert, and W. W. Havens, Jr.—H6
Brown, Fielding, R. R. Rau, and George T. Reynolds—E6
Broyles, C. D. and S. K. Haynes—Q3
Burstein, E., J. J. Oberly, and J. W. Davisson—O3
Byfield, H., J. Kessler, and L. Lederman—H3
Callen, E., W. F. Love, and F. C. Nix—F12
Caplan, D. I. and F. J. Belinfante—I8
Carnap, R.—R1
Carroll, Thomas J.—P5
Chang, Chia-hua and C. Sharp Cook—L2
Chasson, R. L.—H11
Cheston, W. B.—H1
Cohn, Marius—C9
Collins, T. L., A. O. Nier, and W. H. Johnson, Jr.—L12
Coryell, C. D., R. A. Brightsen, and A. C. Pappas—Q1
Crawford, J. H., Jr., J. W. Cleland, K. Lark-Horovitz, J. C. Pigg, and F. W. Young, Jr.—O9
Curl, G. W. and G. C. Danielson—O4
Danielson, G. C. and E. Chivers—D12
Davis, Abram, Forrest F. Cleveland, and Arnold G. Meister—C5
De Benedetti, S. and G. H. Minton—L11
Dexter, D. L. and W. R. Heller—K1
Dijkstra, L. J. and U. Martius—F3
Edwards, P. D.—L6
Eisinger, Joseph T. and Benjamin Bederson—G6
Ekstein, H.—A2
Elsasser, W. M.—R3
Ely, Ralph, Jr., A. J. Allen, J. S. Arthur, R. S. Bender, H. J. Hausman, and E. M. Reilley—A10
Emigh, C. R.—H8
Emmerich, W. S. and J. D. Kurbatov—Q7
Errett, D. D. and F. F. Rieke—B8
Estermann, I. and S. A. Friedberg—F10
Fan, H. Y.—O6
Feuer, Paula and Hubert M. James—K2
Fisher, Thomas F.—D2
Fosdick, L. D. and H. M. James—F5
Fowler, Richard G. and Robert J. Lee—P8
Fox, R. E., W. M. Hickam, T. Kjeldaas, Jr., and D. J. Grove—C1
Frank, P.—R2
Fraser, J. S.—L9
Fraser, Ronald—N1
Frei, E. H.—C13
Friedman, H., T. Chubb, and D. A. Patterson—B7
Fristrom, Robert M.—G11
Gilbert, D. A.—G5
Gilchrist, Lachlan—P4
Gossick, Ben R.—E1
Gove, H. E. and A. Hedgran—M4
Graves, E.—A6
Grodzins, L., G. Del Castillo, and W. Y. Chang—H10
Halsted, R. E.—L13
Hamermesh, Bernard—J2
Harrick, N. J., R. G. Barnes, and P. J. Bray—G7
Hatcher, R. D. and H. E. Hart—A3
Havas, Peter—I1
Hiedemann, E. A.—N2
Hill, R. D.—J3
Hine, G. J.—L7
Hipple, J. A. and H. Sommer—E9
Hirsch, J. and R. B. McQuistan—K4
Hooper, James R., Jr.—B5
Houston, Robert E. and Robert H. Noble—P6
Hsieh, Yü-Chang—O10
Hughes, Richard H.—G12
Isaacs, P., A. Sachs, and J. Steinberger—H4
Jacobs, Donald H., Michael May, and Seymour Scholnick—P1
Jen, C. K., J. W. B. Barghausen, and R. W. Stanley—G8
Johnson, C. H., D. C. Moak, and G. P. Robinson—M5
Johnson, M. H.—H7
Johnson, S. J. and T. F. Rogers—F4
Johnson, V. A. and F. L. Shipley—K9
Kauffman, John and David Lazarus—D8
Keesom, P. H. and Norman Pearlman—O7
King, Gilbert W.—C11
Klick, Clifford C.—K3
Koester, L. J.—A7
Kraushaar, J. J.—M3
Labitt, M., R. J. Debs, I. Halpern, and P. T. Demos—E12
Lander, Richard L. and C. E. Nielsen—E7
Langer, Lawrence M.—J4
Laporte, Otto—N3
Laughlin, J. S., J. W. Beattie, and J. Ovadia—L5
Lederman, L., H. Byfield, and J. Kessler—H5
Lehovec, K.—B2
Lennard-Jones, John E.—AA1
Liebowitz, B.—I11
Livingston, Robert S.—E11
Lodge, John I. and Frank L. Hereford—L4
Love, W. F.—F11
Mack, J. E.—G3
Mandeville, C. E., C. P. Swann, and S. D. Chatterjee—L8
Margenau, Henry and Stanley Bloom—SP2
Margenau, Henry and D. E. Harrison—C2
Marks, Graham W. and Lester A. Monson—K5
Martin, B., D. ter Haar, and V. A. Johnson—F6
Martius, Ursula M., K. V. Gow, and Bruce Chalmers—F1
Massey, J. T. and D. R. Bianco—G13
Matossi, Frank—C8
Matthias, B. T.—K6
McAfee, K. B., W. Shockley, and M. Sparks—O8
McClure, J. W.—F9
Medicus, Heinrich A. and Harry T. Easterday—Q14
Meissner, K. W. and W. F. Miller—B10
Metzger, Franz R.—M2
Mihelich, J. W. and E. L. Church—Q6
Miller, D. W., R. E. Fields, and C. K. Bockelman—A11
Miller, P. H., Jr.—D4
Morrisson, T. E. and T. W. DeWitt—C12
Nix, Foster C. and Frank E. Jaumot, Jr.—D3
Nowak, W. B.—D7
Noyes, J. C., J. E. Van Hoomissen, W. C. Miller, and B. Waldman—M6
Nukolls, R. G. and L. J. Rueger—P2

Osborne, D. W., B. M. Abraham, and B. Weinstock—F13
Ovadia, J., J. W. Beattie, and J. S. Laughlin—L3
Parratt, L. G. and E. L. Jossem—O1
Parzen, P.—B1
Pigg, J. C.—O11
Pirenne, J. C.—I3
Pizzaro, R. and B. Gossick—D13
Plass, Gilbert N. and Douglass Warner—C7
Pope, N. K. and G. Feldman—A1
Porter, Fred T. and C. Sharp Cook—Q5
Poss, H. L., E. O. Salant, and L. C. L. Yuan—A4
Randolph, Burton—D9
Reilley, E. M., A. J. Allen, J. S. Arthur, R. S. Bender, R. L. Ely, and H. J. Hausman—A9
Rieke, F. F. and D. D. Errett—B9
Rivier, D. C.—I5
Ritow, Herman—B11
Rogosa, G. L.—G4
Rosenblum, E. S., E. F. Shrader, and R. M. Warner—M11
Ross, Marc—I2
Roth, L. M., K. W. Meissner, and K. Lark-Horovitz—K7
Rothstein, Jerome—I10
Russell, Paul—B4
Rutledge, W. C., J. M. Cork, and S. B. Burson—Q13
Saur, A. J. and H. M. Schwartz—Q4
Savitt, J. and R. H. Stresau, Jr.—P7
Saxon, David S. and E. Gerjuoy—A12
Schamp, H. W., Jr.—O2
Schardt, A. W. and William Bernstein—E4
Scharff-Goldhaber, G., E. der Mateosian, and J. W. Mihelich—Q9
Scheibner, E. J.—D5
Scheidegger, A. E. and C. D. McKay—I4
Schiff, Daniel—M1
Schremp, E. J.—I6
Schwartz, H. M.—Q2
Seagondollar, L. W., R. K. Smith, W. R. Alexander, and J. W. Teener—E10
Seliger, Howard H.—L1
Shaw, T. M., R. H. Elsken, and C. H. Kunsman—C10
Sidles, P. H. and G. C. Danielson—D11
Simpson, J. A., W. Fonger, and L. Wilcox—H13
Smart, J. Samuel—F8
Smith, Warren H.—M7
Smoluchowski, R.—D10
Snow, George—A5
Sparks, I. L.—B3
Stiller, Bertram, Maurice M. Shapiro, and Francis W. O'Dell—E8
Sun, K.-H., F. A. Pecjak, B. Jennings, and A. J. Allen—L10
Sunyar, A. W., J. W. Mihelich, G. Scharff-Goldhaber, M. Deutsch, and M. Goldhaber—Q8
Toms, M. Elaine and William E. Stephens—M8
Treiman, S. B.—H12
Twersky, Vic—G1
Van Dilla, M. A.—B6
Van Horn, David D.—D1
Volman, David H. and Robert K. Brinton—C6
Watanabe, Satosi—I7
Weatherly, Thomas L., Edward R. Manring, and Dudley Williams—G10
Weaver, A. B. and Marcel Schein—H9
West, W.—AA2
Whitesell, W. J., II, and V. A. Johnson—K8
Wildhack, W. A., T. A. Perls, and J. W. Hayes—P3
Wilkening, M. H.—E5
Winhold, E. J., P. T. Demos, and I. Halpern—M9
Williams, H. J. and R. M. Bozorth—F2
Yagoda, Herman—H14
Zimm, Bruno H.—AA3

Proceedings of the American Physical Society

Minutes of the 1951 Thanksgiving Meeting at Houston, Texas

THE 309th meeting of the American Physical Society, being the 1951 Thanksgiving meeting, was held at Houston, Texas, in the buildings of the Rice Institute, on Friday, November 30, and Saturday, December 1, 1951. This was the second time in four years that we enjoyed the opportunity of convening at Houston; the transposition of the Thanksgiving meeting from its normal habitat was rendered easy by the facts that in 1947 a Chicago meeting was held in December and in 1951 a Chicago meeting was held in October. The meeting was one of our "small" ones: in the universal opinion of those who attend them, the small meetings are much pleasanter than the big ones. There were 223 registrants, and the banquet was attended by 163 people. Simultaneous sessions could not be avoided except on the Friday morning, but were held to a minimum. Contributed papers numbered sixty-three. Invited papers ranged over a wide variety of topics, with concentrations on cryogenics because it is cultivated at Rice Institute, on nuclear physics for the same reason, and on cosmic rays because of the peculiar aliveness of this field. The pleasures of the meeting were largely due to the hospitality of the Rice Institute, in which connection special thanks are extended to C. W. Heaps (Chairman of the Local Committee), W. V. Houston and T. W. Bonner; and to the amenity of the climate, the temperatures being consistently from 70 to 80 degrees Fahrenheit higher than they were at the next previous Thanksgiving meeting. Nobody on this occasion presided in overcoat, hat, and gloves.

The banquet of the Society was held on the Friday evening in the Rice Institute Commons, and the after-dinner speakers were W. V. Houston and K. K. Darrow.

The Council met on the Saturday afternoon. Two candidates were elected to Fellowship in the Society and 138 to Membership: their names are appended. As the first steps toward balancing the budget of the Society, now sadly out of balance, the page-charge on articles in *Physical Review* was lifted from $8 to $12, and the subscription-rate of *Physical Review* to nonmembers of the Society was raised from $25 to $30. The latter change will go into effect on July 1, 1952, the former as soon as the necessary formalities can be completed. Further steps will be announced at the business meeting which the Society will have held in New York before these minutes appear.

Elected to Fellowship at the Houston meeting: William Vick Smith and B. Vodar.

Elected to Membership at the Houston meeting: Siddhi Sadhan Swarup Agarwala, Don M. Alstadt, Miguel Awschalom, James C. Axtell, Sidney W. Benson, Stephan Berko, Sarmukh S. Brar, Robert J. Breen, James G. Brennan, Ernest G. Brock, Reinhard Budde, Robert O. Clark, William S. Coakley, Robert J. Collier, Jerry P. Conner, Earl C. Cooper, George A. Coulter, Cecil F. Dam, Donald W. Davidson, James M. Davidson III, Harold L. Davis, Egilda DeAmicis, Leonard M. Diana, Leonard Allan Dietz, Russell J. Donnelly, Lawrence Dresner, Robert M. Eisberg, Saul Epstein, Noel H. Ethridge, John W. Faust, Jr., William H. Fletcher, Acey L. Floyd, Jr., Herbert D. Friedlander, Thomas Fulton, Francis C. Gilbert, Frederick H. Giles, Peter C. Giles, Marvin D. Girardeau, Jr., Robert G. Glasser, Kurt Gottfried, Leonard P. Grady, Frank A. Grant, Donald W. Green, Ernest J. Hannig, Jr., Marvin Hass, Richard A. Haubrich, Jr., William M. Hickam, Robert L. Hickok, Jr., Robert C. Hirt, Edward W. Hones, Jr., Adelore L. Houde, Frederick L. Hunter, Clyde A. Hutchison, Jr., Ralph J. Jaccodine, Bernard Jouvet, Jack H. Kahn, Richard J. Kandel, Bela Karlovitz, Leonard I. Katzin, Ronald H. Kay, Margaret G. Kivelson, Philipp H. Klein, John E. Klingensmith, CSC, Arthur W. Knudsen, Ryogo Kubo, Perry W. Kuhns, Keith J. Laidler, Edwin N. Lassettre, Herbert R. Lawrence, Sidney Levine, Charles Lindenmeier, John I. Lodge, Frank J. Loeffler, Juan Manuel Lozano, Gustav D. Magnuson, Koichi Mano, Andre J. Martin, Osman K. Mawardi, Robert G. McAllen, William R. McDonell, Hugh McManus, Francisco M. Medina, Robert L. Miller, Edmund A. Milne, Jan M. Minkowski, John W. Morfitt, James Nicol, Gordon A. Noble, William O. Nobles, Perry Okey, Ascher Opler, Gordon D. Patterson, Robert M. Petrie, Frank E. Pretzel, Richard Grayson Quynn, Clarence S. Rainwater, Cyril Reid, Elias Reisman, William H. Robinson, Fred Rosebury, Arthur H. Rosenfeld, Thomas F. Ruane, Robert J. Rubin, Norman Rudnick, Homer W. Schamp, Jr., Paul Seligmann, Robert G. Shulman, Henry S. Sicinski, William G. Simeral, Raymond M. Smith, Warren H. Smith, Norman H. Spear, Aldenlee Spell, William E. Standring, Jr., George S. Stanford, Thomas R. Stengle, Charles B. Stewart, Robert A. Swanson, Langthorne Sykes, George W. Tautfest, William J. Taylor, Irwin Tessman, Richard W. Thickens, George C. Towe, Charles E. Treanor, John V. Vanden Bossche, Douglas M. Van Patter, Thomas E. Van Zandt, Richard F. Wallis, Matt W. Webb, George W. Wheland, Walter H. Wessel, Charles I. Whitman, John H. Wise, Scott E. Wood, Lee A. Young, Robert A. Young, and Saleh S. Younis.

Karl K. Darrow, *Secretary*
American Physical Society
Columbia University
New York 27, New York

Errata Pertaining to Papers G12 and H12

G12, by W. O. Milligan and Harry B. Whitehurst. Instead of "adsorbents," read "adsorbates" for the last word in the first sentence.

H12, by Enos E. Witmer. Instead of "m_μ" read "m u" at two places.

PROGRAMME

FRIDAY MORNING AT 10:00

Physics Amphitheatre

(G. B. PEGRAM presiding)

Greetings from the President of Rice Institute.

Response by the President of the American Physical Society.

Invited Papers in Nuclear Physics

A1. Research at Rice Institute Using 14-Mev Monoenergetic Neutrons. T. W. BONNER, *Rice Institute.* (40 min.)

A2. Experiments on Light Nuclei and on Atomic Beams. S. K. ALLISON, *University of Chicago.* (30 min.)

A3. Nuclear Shell Structure. E. FEENBERG, *Washington University.* (40 min.)

A4. High Energy Electron and X-Ray Beams from the 80-Mev Synchrotron. H. C. POLLOCK, *General Electric Company.* (20 min.)

FRIDAY AFTERNOON AT 2:15

Chemistry Lecture Hall

(C. W. HEAPS presiding).

Invited Papers

B1. Vibrational Spectra of Fluorinated Hydrocarbons. J. RUD NIELSEN, *University of Oklahoma.* (30 min.)

B2. Recent Results with the Curved-Crystal Gamma-Ray Spectrometer. D. E. MULLER, *California Institute of Technology.*

Optics and general physics

B3. The Emission Spectra of Nitrogen Bombarded by High Energy Protons. R. J. SHALEK AND T. W. BONNER, *Rice Institute,* AND L. M. BRANSCOMB, *Harvard University.*—The spectra of nitrogen produced from its bombardment with protons from a Van de Graaff accelerator have been photographed in the region 2500–5000A with a quartz spectrograph. The prominent members of the second positive system of nitrogen and also the (0,0) band of the first negative system of singly ionized nitrogen appear. Spectra have been obtained when protons passed through air at a pressure of 15 cm of mercury; also at lower pressures of 4.0, 1.7, and 0.8 cm of mercury.

B4. Cathodoluminescence of Commercial Oxide Coated Cathodes. ARTHUR G. ROUSE, *St. Louis University,* AND JOHN B. DRAHMANN, *Seattle University.*—Flat cathodes were bombarded with an unfocused electron beam and the luminescence was studied spectrographically and with a photomultiplier. The temperature of the cathode was varied from −140°C to +50°C. The photomultiplier showed a maximum at −125°C in an $L-T$ curve. $L-V$ curves agreed with the law $L=kV^n$ with a possible increase in n at −140°C. The spectrograms showed various peaks and a visible phosphorescence was observed at low temperatures.

B5. A Point Focusing Monochromator for Low Angle X-Ray Diffraction. L. SHENFIL, W. E. DANIELSON, AND J. W. M. DUMOND, *California Institute of Technology.*—An anastigmatic point focus of monochromatic ($CuK\alpha_1$) radiation is achieved by means of two successive reflections from two cylindrically bent quartz crystals whose focal circles are mutually perpendicular. The sample is placed between the second crystal and the point focus, and the scattered beam is detected by means of a photographic film placed at the point focus at right angles to the undeviated beam. The diffraction patterns of a sample without large scale lattice structure appear as rings about the primary point focus and the interpretation of these is much simpler than in the case of a line-focused primary beam. Features as close as 6 minutes in angular measure from the primary beam can be resolved. The background fog without sample is roughly estimated as less than 1/5000 as intense as the primary beam at ten minute scattering angle. Diffraction rings out to the 20th order have been obtained with particles of Dow Latex 580 G lot 3584 (dry) and preliminary measurements of eleven rings from five different exposures yield a computed mean diameter 2692±3A (value and precision subject to slight revisions with further work).

B6. Infrared and Raman Spectra and Calculated Thermodynamical Properties of CH_3-CH_2F and CH_3-CHF_2.* D. C. SMITH AND R. A. SAUNDERS, *Naval Research Laboratory,* AND J. RUD NIELSEN AND E. E. FERGUSON, *University of Oklahoma.*—The infrared absorption spectra of ethyl fluoride and 1,1-difluoroethane have been studied in the region 2–38μ for the compounds in the gaseous state and in the region 2–22μ for the liquids. Prisms of LiF, NaCl, KBr, and KRS-5 were employed. The Raman spectra of both compounds in the liquid state have been obtained with a three-prism glass

spectrograph of linear dispersion 15A/mm at 4358A. Depolarization ratios were determined for the stronger bands. The Raman spectrum of 1,1-difluoroethane was also obtained for the gaseous state. A complete assignment of fundamentals is proposed for each molecule and used for detailed interpretation of the spectra and for the calculation of thermodynamical functions over the temperature range 298–600°K and at the boiling point.

* Supported by the ONR and AEC.

B7. Infrared and Raman Spectra and Calculated Thermodynamical Properties of $CF_2=CHCl$.* J. RUD NIELSEN AND C. Y. LIANG, *University of Oklahoma*, AND D. C. SMITH, *Naval Research Laboratory*.—The infrared absorption spectra of gaseous and liquid 1,1-difluoro-2-chloroethylene have been obtained in the regions 2–22μ and 2–38μ, respectively, with the aid of LiF, NaCl, KBr, and KRS-5 prisms. The Raman spectrum of the compound in the liquid state has been photographed with a three-prism glass spectrograph of linear dispersion 15A/mm at 4358A. Relative intensities and depolarization ratios were determined for all but the weakest Raman bands. A complete assignment of fundamental vibration frequencies is given, the spectra are interpreted in detail, and thermodynamical functions are calculated for the temperature range 298–600°K.

* Supported by the AEC.

B8. Beer's Law Generalized and Applied to the Herzberg Continuum in Oxygen Gas. R. M. LANGER, *HI COG, Scientific Research Division*.—The large deviations from Beer's law in various continuous absorption spectra of O_α may be interpreted in terms of the weakening of selection rules when molecules react with light while undergoing collision. None of the published empirical formulas for the pressure dependence of the absorption coefficient are satisfactory even though some fit the data over a fivefold range of pressure. If the physical mechanism here favored is used to work out a generalization of Beer's law the result is a power series instead of the usual expression containing one term or irrational exponents. In the case of the Herzberg continuum, ($2000<\lambda<2400$A) which is of special significance in atmospheric physics, (N_2 molecules are comparable with O_2 in collision effectiveness) two terms are required and suffice to represent the data over a pressure range from 0.2 to 100 atmospheres. The formula is thus not only sounder than the others but is much wider in scope and range of applicability. For the case of room temperature Oxygen gas absorption at $\lambda=2150$A the decimal absorption coefficient α is $\alpha=7.1\times10^{-5}fp/p_0(1+1.25p/p_0)$ cm^{-1}, where f is the mole fraction of O_2 and p/p_0 is the total pressure in atmospheres. The constants change only slightly in the wavelength range $2000<\lambda<2400$A. These considerations are applied to rocket observations and atmospheric ozone theory.

B9. The Effect of Recent Mass Measurements on the Faraday. H. SOMMER, D. N. CRAIG, J. I. HOFFMAN, AND J. A. HIPPLE, *National Bureau of Standards*.—Recently we have reported in two parallel communications the measurement of the faraday by an electrochemical method using sodium oxalate and a physical method using the omegatron. These independent results agreed beautifully on the basis of the atomic and isotopic weights recommended at that time; we would like to point out that this agreement no longer obtains when one uses the mass spectroscopic values that have been reported since the publication of our earlier communications. The new value for the mass of H^1 raises the omegatron result by 18 ppm and the new value for Na^{23} lowers the sodium oxalate result by a greater amount. This resultant disagreement of approximately one part in 10,000 far exceeds the estimated probable errors of the two experiments.

B10. The Application of the Laplace Transformation and a Mechanical Harmonic Synthesizer in the Analysis of Electric Circuits. HERBERT D. SCHWETMAN, *Baylor University*, AND S. LEROY BROWN, *University of Texas*.—The purpose of this research was to demonstrate the applicability of a mechanical harmonic synthesizer to the solution of the operational equation related to the analysis of electric circuits. Specifically, the machine has been used to determine the roots of the polynomial in s (the derivative operator) found in the denominator of the equation $i_k=E_k(s)/D(s)$. In order to achieve this purpose, the mesh currents of several electric circuits, in which the numerical values of the circuit elements were known, were computed by use of the laplace transformation method in conjunction with the mechanical harmonic synthesizer. In designing a circuit to demonstrate a specified method, it was observed that the character of the roots of the polynomials could be predicted by use of the facts which follow: 1. For every mesh that consists of R–C elements or R–L elements there is one real root. 2. For every mesh that consists of R–L–C elements there are: a. At least one real root when $R/2>(L/C)^{\frac{1}{2}}$; b. Two real roots when $R/2=(L/C)^{\frac{1}{2}}$; c. Two conjugate complex roots when $R/2<(L/C)^{\frac{1}{2}}$ where R, L, and C are the effective values of the resistance, inductance, and capacitance of the elements in the mesh.

B11. Thermal Coefficients Applying to Deflection of Springs. RALPH W. MANN, *Humble Oil & Refining Company*.—For isoelastic materials (iron-nickel alloys) a critical examination shows that other constants in addition to the thermoelastic coefficient of Young's modulus contribute to the changes of flexural deflection with temperature under constant load. Timoshenko[1] has developed a formula $\delta=(PL^3/bh^3E)[(1-\mu^2)/(1-k\mu^2)]$ where δ = deflection, P = load, L = length, b = breadth, h = thickness, E = Young's modulus, μ = Poisson's ratio, and k is a factor involving the breadth, thickness, and curvature of the spring. Changing to dimensional form, differentiating with respect to temperature T, and simplifying, we obtain

$$\frac{1}{\delta}\frac{d\delta}{dT}=-\frac{1}{E}\frac{dE}{dT}-\frac{1}{L}\frac{dL}{dT}-\frac{2(1-k)\mu^2}{1-\mu^2}\frac{1}{\mu}\frac{d\mu}{dT}.$$

These terms, in order and considered with positive signs, are the deflection coefficient of the spring, the thermal coefficient of Young's modulus, the coefficient of thermal expansion, and a factor times the thermal coefficient of Poisson's ratio. A similar formula applies to torsional deflection.

[1] G. Timoshenko, Mech. Eng. 45, 259 (1923).

FRIDAY AFTERNOON AT 2:15

Physics Amphitheatre

(W. V. HOUSTON presiding)

Invited Papers in Cryogenics and Biophysics

C1. Results from Low Temperature Studies at Rice Institute. C. F. SQUIRE, *Rice Institute.* (30 min.)

C2. Experimental Investigations of Liquid Mixtures of Helium 3 and Helium 4. HENRY SOMMERS, *Los Alamos Scientific Laboratory.* (30 min.)

C3. Experiments on Second Sound in Liquid Helium II. J. R. PELLAM, *National Bureau of Standards.* (30 min.)

C4. Recent Work in the Biophysics Laboratory at Tulane University. ROBERT NIESET, *Tulane University.*

FRIDAY AFTERNOON AT 2:15

Physics Laboratory 210

(T. W. BONNER presiding)

Nuclear physics

D1. Tracer Studies on Alligator Weed Using 2,4-D-C^{14}. KARLEM RIESS, T. T. EARLE, AND JOHN HIDALGO, *Tulane University.*—A study of 2,4-D (2,4-dichlorophenoxyacetic acid) labeled with carbon-14 in alligator weed (*Alternanthera philoxeroides* (Mart). Griseb.) was undertaken to determine the distribution, the rate and mode of transport of this herbicide with the plant. It was found that the distribution was somewhat uneven, more going up than down, at a rate of approximately 4.3 centimeters per hour. The mode of travel was through the vascular bundles and the epidermal tissue of the plant. Manual maceration and extraction of 2,4-D with ethyl alcohol proved the best method of sample preparation. The addition of a wetting agent, Tween 20, did not increase the rate of travel or distance traveled, but did affect the quantity of 2,4-D absorbed by the plant. This work was part of a project to control aquatic pests in the navigable inland waterways of the South.

D2. Preparation of Thin Zirconium Tritium Targets.* J. P. CONNER AND J. R. SMITH, *Rice Institute.*—In the preparation of very thin tritium by evaporation of zirconium metal and absorption of tritium into it as described previously,[1] considerable difficulty was encountered when targets with zirconium films about 10 micrograms/cm^2 were desired. Improvements in technique necessary for making these very thin targets will be discussed. Targets have been prepared on tungsten, aluminum and beryllium blanks with tritium-zirconium atomic ratios as high as 1–1½.

* This work assisted by the AEC program.

[1] A. B. Lillie and J. P. Conner, Rev. Sci. Instr. **22**, 210–211 (1951).

D3. An 800-kc Cockroft-Walton Generator. WM. A. ROBBA,* *A & M College of Texas.* (Introduced by J. G. Potter.)—The generator was constructed to provide a stable source of 100 μamp at 120 kv and to explore the feasibility of constructing similar units operable at much higher voltages, realizing the gains in efficiency, regulation, compactness and economy inherent in rf supplies. A small driver feeds a two stage push-pull power amplifier, which in turn is coupled to a 13-stage multiplier stack through a step-up transformer. The stack condensers are 0.035 μf at 10,000 v, and the rectifiers are 1 B 3 tubes with the filaments heated by rf. 180 watts are required by the power amplifier for the indicated output. Tube failures limited the voltages obtained. At higher frequencies the large stray capacitance of the rectifier condenser stack prevented an effective match for the step-up transformer. It is concluded that greatly increased voltages will be obtained when rectifier tubes and condensers of better design, now available, are employed.

* Now student at Oak Ridge School of Reactor Technology.

D4. Differential Cross Section of $H^3(d,p)T^3$ at Low Energy.* CHARLES F. COOK AND J. RICHARD SMITH, *Rice Institute.*—Measurements of the 90° differential cross section of the reaction $H^3(d,p)T^3$ are being investigated using a Cockroft Walton Particle Accelerator, over the range of 40–180 kev deuteron energy. Protons are counted with a proportional counter. Thin deuterium targets are prepared by evaporation of heavy paraffin on polished target blanks in high vacuum. Target thicknesses are accurately determined by evaporating heavier quantities of paraffin on blanks and weighing to approximately 1 percent accuracy, then extrapolating to the range of interest. Targets ranged from 5–10 micrograms per cm^2 which corresponds to a few kev thickness at 100-kev deuteron energy.

* This work was assisted by the AEC program.

D5. The Disintegration of Lithium by Deuteron Bombardment. L. M. BAGGETT* AND S. J. BAME, JR.,* *Rice Institute.*—Thin target excitation curves for $Li^7(d,n)$, $Li^6(d,n)$, and $Li^7(d,p)$ reactions are presented. The neutron data were taken at 90 degrees to the deuteron beam using a BF_3 filled proportional counter in the long geometry. Resonances were observed in the $Li^6(d,n)$ reaction at 0.41 and at 2.12 Mev; in the $Li^7(d,n)$ reaction at 0.68, 0.98, and 2.1 Mev; and in the $Li^7(d,p)$ reaction at 0.75, 1.00, and 1.4 Mev. These resonances correspond to excited states in Be^8 at 22.58 and 23.68 Mev and in Be^9 at 17.22, 17.45, 17.80, and 18.3 Mev. The cross sections of the resonances observed in the $Li^6(d,)$ reaction were 9 and 41 millibarns/steradian; those for the $Li^7(d,n)$ reaction were 39, 43, and 58 millibarns/steradian; and those for the $Li^7(d,p)$ reaction were 0.230, 0.235, and 0.255 barn.

* Now at the Los Alamos Scientific Laboratory.

D6. $p-\gamma$ Angular Correlation in the Reaction $Li^6(d,p)Li^7$* at Low Energy. W. H. BURKE AND J. R. RISSER, *Rice Institute.*—At low bombarding energies (375 kev) the experimental cross section of the $Li^6(d,p)Li^7$ reaction when corrected for

barrier penetration gives indication of a broad resonance level in Be^8.[1] In the hope of throwing light on the character of this Be^8 state, the angular correlation of protons and the 480-kev gammas from Li^7* was measured using coincidence equipment with resolving time of 0.08 μsec and with energy selection for the gamma-radiation. $p-\gamma$ coincidences were found to be independent of the angle between the direction of emission of proton and gamma-ray to within 10 percent, the present statistical accuracy of the measurements. 500-kev deuterons were used, since at this energy the yield is almost entirely due to the Be^8 level. This work was assisted by the joint program of the ONR and AEC.

[1] W. Whaling and T. W. Bonner, Phys. Rev. 79, 258 (1950).

D7. Angular Correlation Studies of $(d; p, \gamma)$ Processes of the Target Nuclei Li^6, B^{10}, and O^{16}. G. C. PHILLIPS,* N. P. HEYDENBURG, D. B. COWIE. *Carnegie Institution of Washington.*—The angular correlation of $(d; p, \gamma)$ reactions have been investigated for the target nuclei Li^6, B^{10}, and O^{16}. Medium thin targets were bombarded by monoenergetic deuterons accelerated by the pressure electrostatic generator. The energy of the deuterons was 1.0 Mev for the Li^6 target, 1.81 Mev for the B^{10} target, and 1.70 and 2.04 Mev for the oxygen target. The enriched Li^6 and B^{10} isotopes were supplied by the Isotopes Division, AEC, Oak Ridge. The angular correlations were obtained by observing proton-gamma-ray coincidences with apparatus having a time resolution of 10^{-8} sec. The angular correlation functions observed were all isotropic within the statistical errors. The absence of correlations will be discussed. For Li^6 and B^{10} isotropy is perhaps explicable, but the isotropy for O^{16} was not expected.

* Fellow of the Carnegie Institution of Washington, on leave from the Rice Institute, Houston, Texas.

D8. Evidence for Stripping in the $B^{10}(d,n)C^{11}$ Reaction at Low Deuteron Energies. J. R. RISSER AND W. H. BURKE, *Rice Institute.*—The theory of stripping[1] predicts preferential forward emission of the uncaptured nucleon when a deuteron reaction proceeds by stripping rather than by formation of a compound nucleus. While apparently the effect of potential barrier has not been evaluated in the theory, it would seem reasonable that the forward emission might persist to low bombarding energies. We have observed pronounced forward emission with peaks in the region 35°–40° for the neutrons from $B^{10}(d,n)C^{11}$ reaction for bombarding energies from 0.8 to 1.6 Mev, the peaks occurring at approximately the same angle for all energies. In order to explain this effect in compound nucleus formation, deuteron angular momenta with l of at least 2 would be required. The fact that the effect persists to deuteron energy as low as about 1 Mev is interpreted as evidence that the reaction proceeds at least in part by stripping. This work was assisted by the joint program of the ONR and AEC.

[1] S. T. Butler, Proceedings of the Harwell Conference (1950).

D9. Inelastic Scattering of Protons from Light Nuclei. N. P. HEYDENBURG, G. C. PHILLIPS,* AND DEAN B. COWIE, *Carnegie Institution of Washington.*—An investigation was made of inelastic scattering of 7.4-Mev protons at 90° from the following thin foil targets: Be^9, C^{13}, C^{12} (47 percent) CaF_2, Ni, Al, and Na, and from the following gas targets: Normal BF_3, enriched $B^{10}F_3$ (96 percent), N_2, O_2, CH_4, and Ne. The following energy levels in Mev were observed: Be^9 2.57; B^{10} 2.34; B^{11} 2.06; C^{12} 4.20; N^{14} 2.35, 3.95; O^{16} none; F^{19} 1.53, 3.83; Ne 1.44, 4.36; Na^{23} 3.67; Al 1.02, 2.30, 2.89, 3.32, 4.48; and Ni 1.44. The scattered protons were observed using double coincidence proportional counters. Ranges and energies were determined with calibrated aluminum foils.

* Research Fellow, Carnegie Institution of Washington.

D10. A Study of the 1435-kev Resonance of Carbon Bombarded by Deuterons. K. FAMULARO, L. C. THOMPSON, AND T. W. BONNER, *Rice Institute.*—The yield of the $C^{13}(d,n)N^{13}$ reaction as a function of bombarding energy has been investigated in the region of $E_d = 1435$ kev. Previous experiments failed to detect a resonance for neutron production at this energy, although a narrow resonance was observed there for gamma and proton production in the competing reactions. An improved method of observation involving a larger solid angle of the detector and a greater efficiency of counting was used to search for a neutron resonance. A weak resonance with a width of about 6 kev was observed at the same energy (1435) as that shown by the competing reactions. An anomaly in the elastic scattering cross section for deuterons scattered by carbon has been observed in this same range of bombarding energy, through the use of a magnetic analyzer.

D11. Neutron Yields from the Nuclear Photoeffect. J. S. LEVINGER, *Louisiana State University,* AND H. A. BETHE, *Cornell University.*—The yields of neutrons produced in photonuclear reactions by 300-Mev bremstrahlung[1,2] *appear* to increase more rapidly with atomic number than the neutron yields predicted from theory.[3] We analyze the yields for elements from copper to uranium in terms of multiplicity of neutron production, approximating the neutron multiplicity n as proportional to the photon energy W: i.e., $n = W/E$. E, the average energy expended per neutron emitted, is calculated from the compound nucleus model. E is about equal to $\frac{1}{7}$ the neutron binding energy, thus decreasing with increasing Z. (We calculate how much E is increased above this value for low Z due to proton competition; it is presumably decreased for uranium by photofission.) The experimental yields give an integrated photonuclear cross section equal to 0.14 (NZ/A) Mev-barns. (The yield for uranium is 35 percent high.) This integrated cross section has the correct form as, but a somewhat higher absolute value than, the theoretical result[3] of 0.060 $(NZ/A)(1+0.8x)$, where x is the fraction of exchange force.

[1] D. W. Kerst and G. A. Price, Phys. Rev. 79, 725 (1950).
[2] Terwilliger, Jones, and Jarmie, Phys. Rev. 82, 820 (1951).
[3] J. S. Levinger and H. A. Bethe, Phys. Rev. 78, 115 (1950).

D12. On the Radioactivity of Ag^{108}. MAX GOODRICH,* *Louisiana State University,* AND EDWARD C. CAMPBELL, *Oak Ridge National Laboratory.*—Most nuclear tables list no gamma-rays in the activity of 2.3-min Ag^{108} and give 2.8 Mev as the beta-ray end point. Recent measurements on this isotope made at Oak Ridge National Laboratory with a scintillation spectrometer have shown gamma-rays of 0.61 ±0.02 Mev, 0.42±0.02 Mev, and 0.19±0.02 Mev to be present in relative numbers ~4:1:1. The beta-ray end point was found to be 1.49±0.05 Mev with no higher energy beta-ray present to more than a few percent of the total. Coincidence experiments indicated that the gamma-rays are not in cascade with the beta-ray. An examination of the x-ray spectrum, made with a proportional counter, showed the energy of the x-rays to be lower than the K x-rays of Ag. Ag^{108} is then presumed to decay both by K-capture to excited levels of the Pd^{108} nucleus and by beta-decay to the ground state of Cd^{108}. The branching ratio is roughly $(N_\beta/N_K) = 2$.

* Research participant of the Oak Ridge Institute of Nuclear Studies.

D13. Delayed γ-Emission from Decay of C^{15}. EMMETT L. HUDSPETH AND WILLIAM B. ROSE, *University of Texas,** AND N. P. HEYDENBURG, *Carnegie Institution of Washington.*—Intense γ-radiation has been observed in the decay of C^{15}, which was produced by deuteron bombardment at 1.8 Mev of a $BaCO_3$ target in the C.I.W. statitron. The $BaCO_3$ was obtained from Oak Ridge and had a carbon isotopic ratio of 4.77 percent C^{14}. The decrease in intensity of the γ-radiation

showed the same 2.4-second half-life as the β-decay[1] of C^{15}. Coincidence absorption data show that the energy of the most prominent γ-radiation is approximately 5.5 Mev, corresponding to the first excited level of N^{15}. An attempt was made to perform $\beta-\gamma$ coincidence measurements with Geiger counters, but the high background counts from other radioactive elements and the relatively low concentration of C^{14} in our target made this impossible. We plan to do this under more favorable conditions with crystal counters. The β-emission of C^{15} and the excitation curve for its production have been studied in more detail.

* Assisted by the AEC.
[1] Hudspeth, Swann, and Heydenburg, Phys. Rev. **80**, 643 (1950).

D14. Neutrons from the Deuteron Bombardment of F^{19}. J. W. BUTLER, *Naval Research Laboratory.*—A survey has been made for neutron thresholds in the reaction $F^{19}(d,n)Ne^{20}$ using similar techniques to those previously described.[1] No thresholds have been observed between 0.5 and 2 Mev although an indication of a level at 11.5 Mev is reported[2] in Ne^{20}, which should give a threshold at about 0.8 Mev. A further search for thresholds is being made using a modified technique. The excitation function at 0° for the reaction has been made using a flat response detector. The function increased smoothly from 0.5 to 2 Mev and was similar in appearance to the curve obtained with the threshold counter.

[1] T. W. Bonner and J. W. Butler, Phys. Rev. **83**, 1091 (1951).
[2] James Terrell and G. C. Phillips, Phys. Rev. **83**, 703 (1951).

FRIDAY EVENING AT 7:00

Rice Institute Commons

(C. C. LAURITSEN presiding)

Banquet of the American Physical Society

After-dinner speakers: W. V. Houston and M. S. Vallarta

SATURDAY MORNING AT 10:00

Chemistry Lecture Hall

(C. F. SQUIRE presiding)

Cryogenics; Geophysics

E1. The Resistance Variation of MnSe at Low Temperatures. JOHN SCALES AND C. W. HEAPS, *Rice Institute.*—MnSe has been found[1] to have an antiferromagnetic Curie temperature at about −110°C. Recent experiments indicate that this material may go through phase transitions as its temperature is lowered. Lindsay has detected[2] three phases between 0°C and −190°C, and two of these phases appear to be antiferromagnetic. We have measured the electrical resistance of various samples of MnSe and found that the temperature-resistance curves show anomalies. A hysteresis effect is observed which may be associated with a time lag of the phase changes. Three different slopes of the resistance curve during three different temperature ranges are interpreted as being due to the successive appearances of three different phases. A possible resistance change caused by the appearance of antiferromagnetism has not been detected. If it exists it is masked in this material by the phase changes.

[1] C. F. Squire, Phys. Rev. **56**, 922 (1939).
[2] Robert Lindsay, Phys. Rev. **84**, 569 (1951).

E2. Abiabatic Thermal Changes in Barium Titanate Ceramic and Strontium Titanate Ceramic at Low Temperatures. R. W. SCHMITT AND R. T. SWIM, *Rice Institute.*—The adiabatic thermal changes at 4°K in barium titanate ceramic show a heating effect whether the electric field is applied or removed. An interpretation of these results is that the polarization process is thermodynamically irreversible. The large temperature dependence of the dielectric constant at 4°K may be understood as a result of the thermodynamically irreversible polarization. Quantitative results are given as to the temperature rise as a function of electric field strength and as a function of temperature. The results of similar measurements on strontium titanate ceramic, whose dielectric constant has a different temperature dependence from that of $BaTiO_3$, are also discussed.

E3. Studies of Superconductivity with a Torsion Pendulum. ARTHUR L. LATHROP, *Rice Institute.*—The torsion pendulum consists of a tungsten wire fiber to which is attached a tin sphere. Damping and period measurements have been made on this system in different magnetic fields and at different temperatures. Measurements of this sort enable one to measure the different steady state and transient torques that operate on the system when the tin is in the normal and in the superconducting state.

E4. Temperature Dependence of Electrical Conductivity. W. V. HOUSTON, *Rice Institute.*—Recent measurements of the electrical conductivity of pure metals over a wide range of temperature have made possible an evaluation of the theories. General considerations indicate, that the resistance will be proportional to T at high temperatures and will approach proportionality to T^5 at very low temperatures. The behavior at intermediate temperatures depends more on details of the electron scattering process and varies from metal to metal. Two effects have been considered. In 1929 a parameter was introduced to describe the angular dependence of the scattering by an individual ion. Proper selection of this parameter and θ permits rather satisfactory description of the resistances of sodium and lithium as reported by MacDonald and Mendelssohn. The necessary value of θ, however, is not the one to be expected on the basis of the elastic constants. Consideration of the normal vibrations of a crystal shows that the division into longitudinal and transverse waves is valid only for long wavelengths. For short wavelengths most vibrations have longitudinal components. An approximate method of taking

them into account gives a good description of the observations with reasonable values of the characteristic temperatures.

E5. Experimental Laboratory Studies of Elastic Wave Propagation. W. L. ROEVER, *Shell Oil Company.*—A technique is described which is analogous to the method used in seismic exploration and which is applied to model acoustic systems set up in the laboratory. A spark is used to generate transient elastic waves and piezoelectric or other detectors are used to convert the resulting pressures or displacements to voltages. These are amplified and displayed as a function of time on a cathode-ray tube where they are photographed. A two-layer system consisting of a layer of water over a layer of concrete was studied. The experimental dispersion curves are compared with the theoretical curves for normal mode propagation as given by Press and Ewing[1] for a liquid layer over a semi-infinite solid. (Longitudinal and transverse wave velocities of solid larger than longitudinal velocity of liquid.) The constants were adjusted to fit measured values for concrete. The results are in good agreement and we believe are the first experimental results to be compared with the theory at frequencies less than the frequency of the Airy phase.

[1] F. Press and M. Ewing, Trans. Am. Geophysical Union, Vol. 29, No. 2, April, 1948.

E6. On the Propagation of Rayleigh Waves on the Surface of a Visco-Elastic Solid. C. W. HORTON, *University of Texas.*—Scholte[1] has shown that a wave can be propagated over the surface of a visco-elastic solid and that this wave reduces to the well-known Rayleigh wave when the viscosity of the solid approaches zero. The cubic equation which governs this wave has been solved for the case of a poisson solid ($\lambda=\mu$). The behavior can be characterized by a dimensionless parameter $\delta=\omega\eta/\mu$ where ω is the angular frequency, η is the coefficient of viscosity, and μ is the shear modulus. For the range of physical parameters of interest in seismology and seismic prospecting δ is less than 0.1 and the modification of the classical Rayleigh motion is very slight. The presence of internal friction changes the difference in phase angle between the vertical and horizontal displacements from $\pi/2$ to $\pi/2 - 0.1014\delta$ for small δ. The ratio between the vertical and horizontal maximum displacements remains equal to 1.468 independently of the value of δ. The wave motion has an attenuation factor of $2.908\delta/\lambda_0$ where λ_0 is the wavelength of the Rayleigh wave in the same medium in the absence of internal friction.

[1] J. G. Scholte, Physica 13, 245 (1947).

E7. Wave Propagation Ducts in Geophysics. Lynn G. HOWELL, *Humble Oil and Refining Company.*—The occurrence of ducts in propagating both elastic and electromagnetic waves is pointed out along with their similarities. The dispersive propagation of longitudinal elastic waves was observed in a duct-layer over the Hawkinsville Salt Dome in the Gulf Coast region of Texas. Also, an example of the dispersion of Rayleigh waves produced by layering is given. In general, with Rayleigh waves the high frequency branch of the dispersion curve has not been observed in land areas; however, there is some evidence that this branch does exist in a particular Gulf Coast area. Atmospheric ducts for microwaves are found over the Gulf of Mexico with the summer season being the optimum period. During the winter season the meteorological conditions are more variable.

Invited Paper

E8. Elastic Constants of Rocks at High Pressures and Temperatures. D. S. HUGHES, *University of Texas.* (25 min.)

SATURDAY MORNING AT 10:00

Physics Amphitheatre

(C. C. LAURITSEN presiding)

Invited Papers on Cosmic-Ray Phenomena

F1. Recent Research in Cosmic Radiation and Radio Waves Emitted by the Sun. M. S. VALLARTA, *Universidad de México.* (25 min.)

F2. Multiple Meson Production at Extremely High Energies. M. F. KAPLON, *University of Rochester.* (30 min.)

F3. Report on *V*-particles. C. D. ANDERSON, *California Institute of Technology.* (40 min.)

Post-Deadline Papers, If Any

SATURDAY AFTERNOON AT 1:30

Physics Amphitheatre

(C. P. BONER presiding)

Invited Paper

G1. Crystal Counters. K. G. MCKAY, *Bell Telephone Laboratories.*

Solid and Liquid States

G2. Dipole Lattice in the Spherical Model.* MELVIN LAX, *Syracuse University.*—The statistical mechanical treatment of a lattice of classical dipoles, electric or magnetic, has been intractable because of the restriction of fixed length of the dipoles. The spherical model consists in replacing the above stringent restriction by the weaker restriction that the sum of

the squares of the dipole vectors have the correct value, thus permitting some, but not much, fluctuation from the correct situation. The spherical method has previously been applied by T. H. Berlin and J. S. Thomsen (ONR report, 1950) to the dipole lattice problem including the appropriate tensor coupling but only nearest-neighbor interactions. The present paper reports a generalization of the previous work to include interactions between all neighbors. The evaluation of the partition sum in the presence of long-range forces requires care because some of the eigenvalues depend on the shape of the specimen. A formula has been derived, however, for the susceptibility, in which the shape dependence of the specimen is explicitly shown to cancel. Qualitative agreement is found with the nearest-neighbor calculation: At sufficiently low temperatures, for purely dipole-dipole interactions, an antiferroelectric transition is observed for three-dimensional crystals, but not in one or two dimensions.

* This work has been supported in part by the ONR.

G3. Modification Functions in the Fourier Inversion of Diffraction Data. JÜRG WASER, *Rice Institute.*—The reduced intensity function $I(s)$ describing essentially the diffraction of particles or waves by scattering matter can be fourier inverted to yield a radial distribution function

$$D(r)/r = \text{const} \int_0^\infty I(s) \sin sr ds.$$

If $I(s)$ be modified by multiplication with a suitable function $M(s)$ the result of inversion of $I(s)M(s)$ is

$$D'(r)/r = \text{const} \int_{-\infty}^{+\infty} T(u-r)D(u)/u du,$$

which represents the folding of the original $D(r)/r$ with the cosine transform $T(r)$ of $M(s)$

$$T(r) = \text{const} \int_0^\infty M(s) \cos sr ds.$$

Of special interest are functions $M_f(s)$ which are zero for $s \geq s_0$. It is found that the functions $T(r)$ related to such $M_f(s)$'s must be of the form

$$T(r) = \Sigma_n a_n J_{2n+\frac{1}{2}}(s_0 r)/(s_0 r)^{\frac{1}{2}},$$

where the J's are bessel functions. The properties of these functions will be discussed in relation to the shape of the peaks of $D(r)/r$, and illustrated by examples. An analogous theorem holds for the fourier and Patterson analyses of scattering information from crystals.

G4. Experimental Studies on Quartz Resonators. K. S. VAN DYKE AND W. F. PALMER, *Wesleyan University.**—Progress along two lines is reported. (1) The Q's of small rings cut from natural quartz have been pushed up into the millions. A Z-cut ring 1¼ inches in diameter vibrating in circumferential longitudinal compression at 160 Kc attains a Q of 3.2×10^6 in vacuum. Of particular interest are the several-fold progressive increase to this value during three months of baking at 125°C, the rapid absorption of atmospheric water vapor and the retention of the latter until baking is renewed. Q's of 2×10^6 hold for a 2.1 mc thickness-shear resonance of a thin BT-cut plate ($5.2\times5.2\times0.26$ cm). (2) Studies of the distribution of strain throughout square AT- and BT-cut thickness-shear resonators have been extended to include rectangular and circular plates, still using partial plating and electrical impedance measurements as the surveying tools. The decrease of amplitude from the center outward in the circular plates is not symmetrical to the plane of the shear but shows a preference for certain directions inclined to this plane. In the circular plate, particularly, very minor irregularities of boundary seem to have considerable effect on the distribution pattern.

* This work was supported by contract with the U. S. Signal Corps.

G5. The Antiferromagnetic Structure of Manganese Dioxide by Neutron Diffraction. R. A. ERICKSON,* *Oak Ridge National Laboratory.*—Neutron diffraction patterns from MnO_2 have been obtained at several temperatures between 20 and 300°K. The room temperature pattern consists of the superposition of coherent nuclear peaks on a background of characteristic paramagnetic diffuse scattering. At 20°K the magnetic scattering is almost completely coherent as indicated by the small magnetic diffuse scattering and the presence of several super-lattice magnetic reflections. The positions and intensities of these peaks are accounted for with an antiferromagnetic model having unit cell dimensions twice those of the chemical cell. In this model the magnetic moments are normal to the tetragonal axis in antiparallel rows along each of the crystal axes. The body centered and lattice corner moments thus form two antiferromagnetic sublattices. From the powder diffraction pattern alone it is not possible to assign unique alignment directions within the base plane to the moments of either sublattice. However, this model is entirely consistent with the single crystal susceptibility measurements of Bizette and Tsai[1] if the moments in one sublattice are normal to those in the second.

* Graduate Fellow of the Oak Ridge Institute of Nuclear Studies, now at the University of Tennessee.

[1] Bizette and Tsai, *Colloque sur les phénomènes cryomagnétiques* (Perrin-Langevin, 1948).

G6. Electrical Properties of Rutile Single Crystals.* L. F. CONNELL† AND R. L. SEALE, *University of Texas.*—Electrical properties of single crystals of reduced synthetic rutile have been studied with emphasis upon applicability as a semiconductor. The principal type of conduction has been verified and the density and mobility of carriers estimated. Other dc measurements included tests on point rectification, bulk resistivity, and barrier-layer potential for a number of samples carried in steps from a normal, fully-oxidized condition to a highly reduced state. Consistent rectification ratios did not exceed 10:1. Bulk resistivity in any given degree of reduction appeared ohmic; barrier-layer effects agreed well with predictions of the Mott-Schottky theory for extrinsic semiconductors. Ac measurements included tests on capacitance and loss-factor for samples over the range of reduction at frequencies up to 50 kc using a General Radio 716 capacitance bridge in a parallel-resistance method. The total capacitance showed anomalous dispersion of the apparent dielectric constant over the frequency range. A satisfactory equivalent circuit has been found, as tested by plotting the series resistance and reactance in the complex plane. The high capacitances were shown to be due to the high barrier potential, with the controllable bulk resistance of the rutile shunting its low bulk capacitance.

* The work described was done at Defense Research Laboratory under the sponsorship of the Bureau of Ordnance, Navy Department.
† Now at North Texas State College, Denton, Texas.

G7. The Time Rate of Transformation of α-Monoclinic Selenium into Hexagonal as a Function of the Temperature. JOHN MURPHY AND ARTHUR E. LOCKENVITZ, *University of Texas.*—α-Monoclinic selenium prepared by precipitation from a solution of selenium in carbon bisulfide was used as the dielectric between the plates of an aluminum plate condenser. Above about 90°C α-monoclinic selenium transforms into hexagonal via an intermediate form, probably β-monoclinic. The transformation at a fixed temperature can be followed with time by measuring the capacity of the condenser containing the selenium. The data from capacity measurements fit the laws $dN_1/dt = -\lambda_1 N_1$ and $dN_2/dt = -\lambda_2 N_2$ where N_1 and N_2 are the number of molecules of the α- and β-forms, respectively, and λ_1 and λ_2 are different functions of the temperature. It is assumed that form α transforms to form β which in turn transforms to the stable hexagonal form. λ_1 and λ_2 appear

to be some exponentially increasing functions of the temperature.

G8. The Time Rate of Transformation of Amorphous Selenium into Another Form as a Function of Temperature. ARTHUR E. LOCKENVITZ AND KENNETH H. RIBE, *University of Texas.*—Amorphous selenium precipitated from a dilute HCl solution of selenious acid was used as the dielectric between an aluminum plate condenser whose capacity was measured at 3 megacycles with a General Radio 821A twin *T* bridge. Above 25°C amorphous selenium transforms to another form, probably α-monoclinic, with a resultant change in dielectric constant and capacity of the condenser. The time rate of change of capacity at constant temperature in the region between 20°C and 50°C increased with temperature. $\text{Log}(1-\Delta c/\Delta c_f)$ plotted against time gives essentially a straight line within the limits of experimental error, the slope of the straight lines being greater at higher temperatures. Δc and Δc_f are the change in capacity at time t and infinity, respectively. This suggests the law of transformation to be $\Delta c = \Delta c_f \exp(-\lambda t)$ where λ is a function of the temperature. It is hoped that the form of $\lambda = F(T)$ can be determined.

G9. Investigations on the Debye-Frenkel Theory of Ultrasonic Absorption. P. A. HUDSON* AND M. EISNER, *A & M College of Texas.*—The Debye-Frenkel theory postulates the existence of molecular rearrangements to account for the anomolies observed in the absorption of ultrasonic waves in liquids. An attempt was made to study the effect of these rearrangements by comparing the absorption in isomeric liquids and by inducing rearrangements by compression. Allyl alcohol and acetone were selected for the isomeric study and ethyl ether was used in studying the pressure dependence. The absorption coefficients, measured at 3.5 mc by a pulse echo technique, were 0.0087 cm^{-1} for allyl alcohol and 0.0053 cm^{-1} for acetone. Comparing these values with those predicted by the classical Stokes-Kirchoff theory reveals that the more highly associated liquid, allyl alcohol, shows an absorption closer to the classical value than does acetone. This is in qualitative agreement with the prediction of the Debye-Frenkel theory. The experiments on ethyl ether failed to reveal a significant pressure dependence for the absorption for pressures up to 2 atmospheres.

* Now at the National Bureau of Standards, Washington, D. C.

G10. On the Supercooling of Water. B. LUYET, *St. Louis University.**—Investigations on the possibility of solidifying water in the vitreous state† led to the following observations on some of the conditions in which water can be kept liquid at subzero temperatures. Droplets of water were projected with an atomizer onto a piece of glass 0.15 mm thick, and the latter, held by forceps mounted on a rotating arm, was swung into a cooling bath of petroleum ether and, after a minute, it was swung back into the focal plane of a polarizing microscope, between crossed nicols. The diameter of the drops on the glass varied from 0.1 to 1.5 mm. Despite the jarring, supercooling below −20°C was quite common, and several cases of supercooling below −30° were recorded; the smaller droplets were more frequently supercooled at the lower temperatures than the larger ones. But numerous apparent inconsistencies in the effect of the factors studied—temperature, size of the drops, cooling velocity, jarring, specimen of water used, even average time for the assumed chance formation of the nuclei—indicate that some fundamental factors causing the spontaneous crystallization of supercooled liquids are still unknown.

* With the assistance of G. Gardner.
† Work supported by Research Corporation.

G11. On Polarization in Electrolyte Solutions.* JOHN A. RIDER AND GEORGE JAFFÉ, *Louisiana State University.*—At the last Washington meeting one of the authors reported on a theory of polarization which, originally designed for crystals, can be made applicable to electrolytes by a generalization of the boundary conditions. Measurements to test the theory were performed in an ac bridge arrangement with a modified Jones bridge. The cell used was designed to bring out the characteristics of polarization, and was very different from the usually employed forms. It was in the shape of a plate condenser with guard ring, having relatively large surface and small (though variable) plate distance. The main difficulty which had to be overcome consisted in the enormous size of the capacitances which had to be balanced (up to 150 microfarads). The final measurements are in quantitative agreement with the theory as to the dependence of conductance and capacitance on concentration of the solutions, plate distance, and frequency. However, in order to explain the large capacitances, it is necessary to assume the presence of a group of ions (hydrated ions?) which have about 100 times smaller mobilities than ordinary electrolytic ions.

* Work supported by the ONR.

G12. Diamagnetic Properties of Adsorbed Gases. W. O. MILLIGAN AND HARRY B. WHITEHURST,* *Rice Institute.*—Adsorption isotherms have been obtained at 25°C on a silica gel, using water, *n*-propyl alcohol, acetic acid, salicylaldyde, and *n*-heptane as the adsorbents. At each point on the isotherms, the magnetic susceptibility of the adsorption complex was measured, using the Faraday method. At high pressures, near saturation, the observed dimagnetic susceptibilities correspond to the susceptibility of the bulk liquid. At low pressures corresponding to less than a monolayer, the susceptibility differed for the bulk liquid except for *n*-heptane. An increase in the diamagnetic susceptibility was observed for water and *n*-propyl alcohol, and a decrease for acetic acid and salicylaldehyde.

* Now at Owens-Corning Fiberglas Corporation, Newark, Ohio.

G13. Structural Constants of ClO_2. J. B. COON, *A & M College of Texas.*—Recent,[1] improved electron diffraction data for ClO_2, ($S'' = 1.491 \pm 0.014$A, $2\theta'' = 116.5° \pm 2.5°$), when compared with spectral data gives for the first time a check on the ground electronic state of ClO_2. Published work[2] shows that the rotational structure of the violet absorption spectrum of ClO_2 yields the following data: First difference between the $\Delta_1 F$'s interpreted as $2\bar{B}'' = 0.612 \pm 0.003$ cm^{-1}. Second difference between sub-bands interpreted as $2(\Delta A - \Delta\bar{B}) = -1.188$ cm^{-1}. Second difference in J structure interpreted as $2\Delta\bar{B} = -0.0615$ cm^{-1}. The three constants $2\bar{B}''$, S'', $2\theta''$ are dependent, and their experimental values given above are consistent within experimental error giving agreement between spectral data and electron diffraction data. In view of the electron diffraction results, the best values for S'' and $2\theta''$ exactly consistent with the above value of $2\bar{B}''$ are ($S'' = 1.484$A and $2\theta'' = 115.3°$). A preliminary result from some unpublished work by E. Ortiz and the author on the vibrational frequencies and their isotope shifts is $2\theta'' = 114.4°$. Starting with the above exactly consistent model and using the constants $2(\Delta A - \Delta\bar{B})$ and $2\Delta\bar{B}$, which determine the change in the moments of inertia, the bond distance and the angle of the excited electronic state may be determined: ($S' = 1.648$A and $2\theta' = 104°$). The sum of Pauling's single bond covalent radii for Cl and O gives $S' = 1.65$A.

[1] J. D. Dunitz and K. H. Hedberg, J. Am. Chem. Soc. 72, 3108 (1950).
[2] Jesse B. Coon, J. Chem. Phys. 14, 665 (1946).

G14. Reduction of Temperature Coefficient of Magnetic Moment for a Bar Magnet. R. W. LONG AND I. A. ROBERTSON, *Houston* (introduced by C. W. Heaps).—An arrangement of a magnetic shunt to sheath a cylindrical magnet has resulted in greatly improved magnetic stability. A bar magnet of 925 cgs

units magnetic moment, $\frac{1}{16}$ inch diameter and 2½ inches long was stabilized normally. Variations of its magnetic moment with temperature over a range of 10°C to 35°C were measured. The same magnet then was temperature compensated. Comparisons of data over the identical temperature ranges showed at least 25 times smaller variations. This can be further improved. Such magnets are of great interest in magnetic observatory work.

SATURDAY AFTERNOON AT 2:00

Physics Laboratory 210

(C. D. ANDERSON presiding)

Nuclear Physics; Cosmic Rays; Theoretical Physics

H1. Production and Detection of Circularly Polarized Gamma-Rays. OTTO HALPERN, *University of Southern California.*—It has been shown before[1] that capture of a polarized neutron by a nucleus followed by emission of a single quantum may lead to polarized products. The gamma-ray emitted in the direction of the neutron spin will sometimes be circularly polarized. Among several possible analyzers a special Compton effect[2] appears to be useful and simple. The cross section for backward scattering of moderately hard quanta depends strongly on the polarization of the scattering electron; it almost vanishes for one spin state and obtains therefore almost twice the value of the cross section for unpolarized electrons for the second spin state. Even if the scatterer is unpolarized the electron scattered forward is almost totally polarized which can be ascertained by a single Coulomb scattering experiment. A scatterer with polarized electrons is formed, e.g., by magnetized iron which contains about 24 unpolarized and 2 polarized electrons. The differential scattering cross section for the Compton process envisaged will therefore vary depending on the state of magnetization between 24 and 28 times the value obtaining for a single unpolarized electron. Other arrangements will be discussed.

[1] O. Halpern, Phys. Rev. **82**, 753 (1951).
[2] O. Halpern, Nature, 168 (1951).

H2. A Quadrature Method for Computing Neutron Distributions in Two Dimensions.* E. LEIGH SECREST,** *M.I.T.*—An iterative method has been developed, which, when combined with a quadrature approximation, leads to an approximate solution of the transport equation governing the scattering and absorption of multiply scattered neutrons. An integral relation for the distribution function was set up in a form suitable for iterative solution. To facilitate performance of the iterations, the assumption was made that the neutron distribution at a given point in space can be represented by flow along a finite number of streamlines (the quadrature approximation). The method was used to determine the effect of introducing a void in the form of a slit into a semi-infinite scattering medium (either capturing, or noncapturing, infinite or finite). Satisfactory results were indicated in boundary regions after a few iterations providing several quadrature directions were used for calculation of the iterative integrals. In regions distant to the slit a *small* number of *directions* combined with a *large* number of iterations was found satisfactory. Although the investigation was made primarily for the one-velocity transport equation, a procedure is indicated whereby energy dependence of the distribution can be included to some extent.

* Part of a thesis submitted to the Department of Physics of the Massachusetts Institute of Technology, in partial fulfillment of the requirements for the degree of Ph.D., supported by AEC Predoctoral Fellowship.
** Now Assistant Professor of Physics at North Texas State College, Denton, Texas.

H3. On the Diffusion of Thermal Neutrons. GEORGE JAFFÉ, *Louisiana State University.*—Considerable work has been performed on the theory of neutron diffusion within the last decade. However, as far as the author is aware, all theories start from a *linear* integral equation (the so-called "transport equation"), which neglects the motion of the moderator molecules. This can be included by starting from the original Boltzmann equation which is of the *second order* in the unknowns. The author has shown[1] how the Boltzmann equation can be transformed so as to represent the changes in a progressing beam. In this form it can be integrated for the case of thermal neutrons. It is necessary only to assume that the distribution of the moderator atoms is maxwellian, and that of the neutrons "almost maxwellian," i.e., given by the product of a maxwellian factor into a series progressing with general harmonics. If that is done, the problem is reduced to a set of differential equations which the author has established and solved in a very general way in his theory of the anisotropic radiation field as early as 1922. Thereby the results of this theory become immediately applicable to the diffusion of thermal neutrons.

[1] G. Jaffé, Ann. Physik **6**, 195 (1930).

H4. The Magnetic Moments of Nuclei. H. A. WILSON, *Rice Institute.*—On Dirac's theory an electron, with spin $s=\frac{1}{2}$, has a magnetic moment $2(s(s+1))^{\frac{1}{2}}he/4\pi m_e c$. We may therefore suppose that a nucleus with charge Ze and mass Am will have a magnetic moment $2(s(s+1))^{\frac{1}{2}}hZe/4\pi Amc$, where s is integral or half-odd integral. Dividing this by $he/4\pi m_p c$, where m_p is the mass of a proton gives $2(s(s+1))^{\frac{1}{2}}Zm_p/Am$. If the nucleus is rotating with spin I it will also have a magnetic moment $(I(I+1))^{\frac{1}{2}}Zm_p/Am$. The resultant magnetic moment is then $(j(j+1))^{\frac{1}{2}}gZm_p/Am$, where g is Lande's factor and j is the nuclear spin.

H5. On the Anomalous Magnetic Moments of Nucleons. FERNANDO E. PRIETO C.,* *Universidad de México.*—Using the neutral, charged, and symmetrical pseudoscalar theories of meson, and a combination of Dyson's, Feynman's, and Schwinger's computation methods, the electromagnetic and mesic corrections to the anomalous magnetic moments of nucleons have been calculated. It was found that only the symmetrical theory gives corrections to both the proton and the neutron moments. Adjusting the coupling constant to obtain the experimental value of the neutron moment, a value is obtained for the proton moment which is about 60 times smaller than the experimental one. The introduction of the electromagnetic correction does not improve these results because it is too small compared with the mesic correction.

* Instituto de Física de la Universidad Nacional de México and Instituto Nacional de la Investigación Científica.

H6. The Energy Spectrum of Primary Cosmic Radiation as Determined from Neutron Intensities.* M. S. VALLARTA, *Universidad de México.*—Using the neutron intensity measurements of J. A. Simpson and assuming that there is proportionality between number of neutrons measured and number of primary protons, the energy spectrum of the primary proton component of cosmic radiation can be determined by standard methods. If the spectrum is written in the form $n=K/E^{\gamma}$ (n=number of primary protons and E=energy), the analysis shows that γ increases from the value 1.175 in the low energy range (1.3 to 4.3 Bev) to 1.815 in the medium energy range (4.3 to 14 Bev). This is in agreement with results derived from measurements on charged secondary particles at balloon and rocket altitudes.

* Research done under the auspices of Instituto Nacional de la Investigación Científica, México, D. F.

H7. Time Dependent Description of Resonance Reactions.* MARCOS MOSHINSKY, *Universidad de México.*—It is known that cross sections for resonance scattering and reaction, can be derived from appropriate boundary conditions[1] connecting the stationary wave functions and their normal derivatives at the nuclear surface. An extension of these boundary conditions to time dependent states has been achieved with the help of a description of resonance reactions in Fock space.[2] We make use of these boundary conditions to obtain a time dependent description for the process of single level elastic scattering. With the help of an appropriate generalization of the concept of hankel transform, an explicit form is obtained for the time dependent wave function representing the scattering process, and the only parameters present in the wave function are the poles of the scattering matrix. A discussion of the asymptotic behavior of this wave function when $t\rightarrow\infty$, shows that a causal description of the process of scattering can only be obtained if the poles of the scattering matrix are in the lower half-plane of the wave number k, or on the imaginary axis.[3] Extensions of this time dependent description to the case of many level scattering, and to nuclear resonance reactions, will be discussed.

* This work is supported by the Instituto Nacional de la Investigación Científica.
[1] E. P. Wigner, Phys. Rev. **70**, 606 (1946).
[2] M. Moshinsky, Phys. Rev. **81**, 347 (1951).
[3] W. Schützer and J. Tiomno, Phys. Rev. **83**, 249 (1951).

H8. Fourth-Order Effects in Vacuum Polarization.* JUAN DE OYARZABAL, *Universidad Nacional de México.*—The covariant S matrix formalism of Dyson[1] has been applied to the calculation of the fourth order effects in the polarization of vacuum by an electromagnetic field. Explicit form for the function $A^{e'}(x)$, the external electromagnetic field modified by the interaction with the pair field, is given to order α^2.

* This work was performed under the auspices of the Instituto Nacional de la Investigación Cientfica of Mexico City.
[1] F. J. Dyson, Phys. Rev. **75**, 486, 1736 (1949).

H9. The Classical Quantum Electrodynamics of Interacting Fields. M. DRESDEN AND H. DEAN BROWN, *University of Kansas.*—The customary technique employed in problems in field theory is a perturbation calculus, a development in powers of the coupling parameter. In many instances this development is not appropriate and other development schemes have been constructed as in the strong-coupling theories. However, the description of the intermediate coupling case, as well as the variation of the physical characteristics with the coupling parameter, are not too transparent in these schemes. To investigate these points, an elementary example has been studied in some detail. The system chosen consists of two interacting neutral scalar fields, both fields possessing quanta of finite rest mass. The lagrangian density of the system has the form

$$L=-\frac{\hbar c}{2k_1}\left[\left(\frac{\partial\psi_1}{\partial x_\mu}\right)^2+k_1^2\psi_1^2\right]-\frac{\hbar c}{2k_2}\left[\left(\frac{\partial\psi_2}{\partial x_\mu}\right)^2+k_2^2\psi_2^2\right]-\tfrac{1}{2}g(\psi_1+\psi_2)^2.$$

The coupling term is slightly different from the more usual $g\psi_1\psi_2$ this form is essential for the discussion if arbitrary large values of g are allowed. This problem can be solved exactly for all g, with the help of a canonical transformation, which separates the hamiltonian of the system into the hamiltonian of four uncoupled fields.

H10. The Positional Correlations in Interacting Fields. H. DEAN BROWN AND M. DRESDEN, *University of Kansas.*—The use of the uncoupling canonical transformation allows the explicit calculation of energies and wave functionals in the problem of two interacting fields. Since the calculation methods utilized are noncovariant one encounters the usual divergencies. The dependence of the energy—even in the ground state of the system—on the coupling parameter, is rather complicated. It is for instance not true—except in the limit of very weak coupling—that this energy splits up additively in terms which represent the energy of the separate fields and the interaction energy respectively. In many treatments one of the fields is considered as static, then the application of a perturbation procedure enables one to obtain an expression for the potential energy between the sources of the static field. In the present discussion neither field was treated in the static approximation, it has not appeared possible to separate the energy in field energy and interaction energy, or in static and nonstatic parts. It would seem quite difficult to attribute an unambiguous significance to potential energy in this situation. It can be shown, that the quantity $\langle\psi_1(x_1)\psi_2(x_2)\rangle_{Av}$ the positional correlation function, exhibits some of the characteristics of a classical interaction energy.

H11. Scattering of Strongly Coupled Pseudovector Mesons. MELVIN EISNER, *A. & M. College of Texas.*—The differential scattering cross section for the scattering of strongly coupled pseudovector mesons by nucleons has been calculated. Successive canonical transformations are used to reduce the hamiltonian to a simple form, resembling the pseudoscalar hamiltonian. The differential cross section for mesons of momentum k_0 is

$$\sigma(\theta)=a^2/4\cdot(k_0/\omega_0)^4\cdot[(g^2-\mu^2f^2)/(2\mu^2f^2+g^2)]^2\cdot(1-\cos^2\theta),$$

where g and f are coupling constants and a is the "half-width" of the nucleon density distribution function. The nucleon recoil has been neglected and no distinction has been made between elastic and inelastic scattering. The cross section is of the order of 10^{-28} cm^2 for a choice of 10^{-14} cm for a, and selection of f and g compatible with the condition for strong coupling.

H12. Nuclear Masses as Integral Multiples of a Natural Unit of Mass. ENOS E. WITMER, *University of Pennsylvania.*—Some time ago the writer proposed the hypothesis that the masses of those nuclei not subject to beta-decay are integral multiples of a natural unit of mass for nuclei and elementary particles. This unit was designated the *prout* and it was taken to be one-eleventh of the rest mass of the negative electron. Recently important new tables[1,2] of nuclear masses and reaction energies have appeared. Taking the mass of the proton to be 20 197 prouts, the nucleus of O^{16} is found to have

320 629 prouts. Hence 1 prout = 0.0000498 882260 mμ = 46.4523 kev. With this value of the prout the data of references 1 and 2 are in good agreement with our hypothesis. Our computed values of the isotopic masses of H^1, H^2, and C^{12} are 1.008 1413, 2.014 7360, and 12.003 8045 mμ respectively. Also most nuclei up to O^{16} that are subject to beta decay conform to the integral rule stated here, but not the neutron. Five of the nuclear masses in prouts up to O^{16} are divisible by 11.

[1] Li, Whaling, Fowler, and Lauritsen, Phys. Rev. **83**, 512 (1951).
[2] Heinz Ewald, Z. Naturforsch. **6a**, 293 (1951).

Saturday Afternoon at 4:30

Cohen House

Tea offered by Rice Institute to members of the Society and to guests

Author Index to Papers Presented at the Houston Meeting

Allison, S. K.—A2
Anderson, C. D.—F3
Baggett, L. M. and S. J. Bame, Jr.—D5
Bonner, T. W.—A1
Brown, H. Dean and M. Dresden—H10
Burke, W. H. and J. R. Risser—D6
Butler, J. W.—D14
Connell, L. F. and R. S. Seale—G6
Conner, J. P. and J. R. Smith—D2
Cook, Charles F. and J. Richard Smith—D4
Coon, J. B.—G13
Dresden, M. and H. Dean Brown—H9
Eisner, Melvin—H11
Erickson, R. A.—G5
Famularo, K., L. C. Thompson, and T. W. Bonner—D10
Feenberg, E.—A3
Goodrich, Max and Edward C. Campbell—D12
Halpern, Otto—H1
Heydenburg, N. P., G. C. Phillips, and Dean B. Cowie—D9
Horton, C. W.—E6
Houston, W. V.—E4
Howell, Lynn G.—E7
Hudson, P. A. and M. Eisner—G9
Hudspeth, Emmett L., William B. Rose, and N. P. Heydenburg—D13
Hughes, D. S.—E8
Jaffé, George—H3
Kaplon, M. F.—F2
Langer, R. M.—B8
Lathrop, Arthur L.—E3
Lax, Melvin—G2
Levinger, J. S. and H. A. Bethe—D11
Lockenvitz, Arthur E. and Kenneth H. Ribe—G8
Long, R. W. and I. A. Robertson—G14
Luyet, B.—G10
Mann, Ralph W.—B11
McKay, K. G.—G1
Milligan, W. O. and Harry B. Whitehurst—G12
Moshinsky, Marcos—H7
Muller, D. E.—B2
Murphy, John and Arthur E. Lockenvitz—G7
Nielsen, J. Rud—B1
Nielsen, J. Rud, C. Y. Liang, and D. C. Smith—B7
Nieset, Robert—C4
Oyarzabal, Juan de—H8
Pellam, J. R.—C3
Phillips, G. C., N. P. Heydenburg, and D. B. Cowie—D7
Pollock, H. C.—A4
Prieto, C., Fernando E.—H5
Rider, John A. and George Jaffe—G11
Riess, Karlem, T. T. Earle, and John Hidalgo—D1
Risser, J. R. and W. H. Burke—D8
Robba, Wm. A.—D3
Roever, W. L.—E5
Rouse, Arthur G. and John B. Drahmann—B4
Scales, John and C. W. Heaps—E1
Schmitt, R. W. and R. T. Swim—E2
Schwetman, Herbert D. and S. Leroy Brown—B10
Secrest, E. Leigh—H2
Shalek, R. J., T. W. Bonner, and L. M. Branscomb—B3
Shenfil, L., W. E. Danielson, and J. W. M. DuMond—B5
Smith, D. C., R. A. Saunders, J. Rud Nielsen, and E. E. Ferguson—B6
Sommer, H., D. N. Craig, J. I. Hoffman, and J. A. Hipple—B9
Sommers, Henry—C2
Squire, C. F.—C1
Vallarta, M. S.—F1, H6
Van Dyke, K. S. and W. F. Palmer—G4
Waser, Jürg—G3
Wilson, H. A.—H4
Witmer, Enos E.—H12

Proceedings of the American Physical Society

Minutes of the Meeting at Berkeley, California, December 27–29, 1951

THE 310th meeting of the American Physical Society was held at Berkeley, California, on Thursday, Friday, and Saturday, December 27, 28, and 29, 1951. The actual registrations came to 431, with many of those attending having come from considerable distances. In view of the bad weather prior to and during the meetings, this large attendance was surprising. The programme was the largest in the history of the West Coast, with one hundred and twenty-five contributed papers, nine invited papers, and three post-deadline papers. Dr. Robert F. Christy was unable to be present because of illness, and his time was given to Dr. Erwin W. Müller, Chief of the Kaiser-Wilhelm-Institut of Berlin and Professor at the Free University of West Berlin, who gave a very interesting description of his important work on point projection microscopes.

The local arrangements were unusually effective, with the new Le Conte Hall Annex providing a perfect setting for the meetings. Professors Birge, White, and the capable office staff of the Department of Physics took care of arrangements and most of the running of the meeting. The Thursday and Friday afternoon sessions had been arranged so as to allow a short recess before the sessions for invited papers. This allowed the Berkeley people to arrange for about thirty minutes of coffee and tea, very refreshing and pleasant interludes. Almost 200 were served each day. Arrangements had also been made for trips to the Radiation Laboratory. The Society is indebted to Dr. Cooksey for arranging these trips. We are also greatly indebted to the Berkeley Chamber of Commerce for providing us with badges and literature concerning Berkeley and the Bay region.

The first West Coast meeting of our Division of Electron Physics was a successful and well-attended one, adding considerably to the success of one of the best meetings ever held on the West Coast.

Many of our members received the Bulletin for this meeting just before, during, or even after the meeting. Such delays are inevitable when the Bulletin is mailed during the Christmas rush. The only ways to avoid them are (a) to transfer the winter meeting on the West Coast to some other time than the holiday week, and (b) to increase by two or possibly three weeks the interval between deadline and meeting. Any member who feels strongly for or against either of these changes is asked to notify the Local Secretary for the Pacific Coast.

J. Kaplan
Local Secretary for the Pacific Coast
University of California
Los Angeles 24, California

Errata Pertaining to Papers B7, D6, K5, Q11, and Q13

B7, by Kenneth James Harker. The next to the last sentence should read: When two or more eigenfunctions have the same L and S the method still yields all eigenfunctions possible.

D6, by W. D. Perkins and M. Kent Wilson. In line 8, $\nu_1(A_g) = 1342$ should read $\nu_1(A_g) = 1334$. In line 9, $\nu_6(A_u) = 70$ should read $\nu_6(A_u) = ??$.

K5, by W. D. Knight. In line 19, two orders of magnitude greater than . . . should read twice as great as . . . .

Q11, by Arthur L. Bennett, Ivar Highberg, Ernest Barkofsky, and Lucien M. Biberman. The title of the abstract should read: The Aeroballistics Laboratory of the U. S. Naval Ordnance Test Station.

Q13, by W. C. Barber, G. E. Becker, and E. L. Chu. A footnote should be added reading: Assisted by the joint program of the ONR and AEC.

PROGRAMME

THURSDAY MORNING AT 10:00

Room 310, Le Conte Hall

(L. B. LOEB presiding)

Meeting of the Division of Electron Physics

Forty minutes will be allowed for presentation and ten minutes for the discussion of each paper.

A1. Space Charge Phenomena in High Density Electron Beams. M. CHODOROW, *Stanford University.*

A2. Ejection of Electrons by Ion Impact. H. D. HAGSTRUM, *Bell Telephone Laboratories.*

A3. Field Emission; a Comparison between Theory and Experiment Including Pulsed Emission at Large Densities. W. P. DYKE, *Linfield College.*

THURSDAY AFTERNOON AT 1:30

Room 4, Le Conte Hall

(W. M. POWELL presiding)

B1. Anisotropy Energy in a Cubic Lattice of Spin Dipoles. JACK R. TESSMAN, *University of California, Berkeley.*—Classically there is no anisotropy energy in a saturated cubic lattice of spin dipoles. However, as has been pointed out by Kittel,[1] anisotropy arises quantum mechanically from the requirement that, for each dipole, S_x, $S_y \neq 0$ even for maximum polarization in the z-direction. The spin-wave method as developed by Heller and Kramers[2] and by Klein and Smith,[3] and applied by them to ferromagnetic exchange interactions, is here applied to paramagnetic dipole interactions for which the interaction energy is given by

$$H_{ij} = J[\mathbf{S}_i \cdot \mathbf{S}_j - 3(\mathbf{S}_i \cdot \mathbf{r})(\mathbf{S}_j \cdot \mathbf{r})/r^2].$$

The simplifying assumption is made of nearest neighbor interactions only. Expressions are obtained for the anisotropy energy for a plane square lattice and for a cubic space lattice.

[1] C. Kittel, Phys. Rev. **82**, 965 (1951).
[2] G. Heller and H. A. Kramers, Proc. Roy. Acad. Sci. (Amsterdam) **37**, 378 (1934).
[3] M. J. Klein and R. S. Smith, Phys. Rev. **80**, 1111 (1950).

B2. Elastic Scattering of 190-Mev Deuterons by Protons.* MARTIN O. STERN, *University of California, Berkeley.*—Experiments on elastic scattering of the 184-inch cyclotron's 190-Mev deuterons reported earlier[1,2] while in progress, have been completed. Differential scattering cross sections between 15° and 170° in the center of mass have been measured by the polyethylene-carbon subtraction method in stilbene scintillation counters feeding fast amplifiers. The range 40° to 160° was covered by observation of coincidences between the deuteron and its partner proton. The intervals 15° to 45° and 150° to 170° were covered with a single crystal preceded by aluminum absorber. The change in hydrogen effect with varying absorber was observed. An elastic scattering cross section between 10° and 180° of $(29 \pm 3) \cdot 10^{-27}$ cm² was obtained. Agreement with the theory of Chew[3] is excellent for the range 50° to 120°. At smaller angles the observed effect is about 0.7 of the calculated one; in the "pick-up" region near 180° a peak is found which is a factor of five lower than that theoretically predicted.

* Assisted by the AEC.
[1] A. L. Bloom and M. O. Stern, Phys. Rev. **81**, 660 (1951).
[2] M. O. Stern and A. L. Bloom, Phys. Rev. **83**, 178 (1951).
[3] G. F. Chew, Phys. Rev. **74**, 809 (1948).

B3. Inelastic and Total Scattering of 190-Mev Deuterons by Protons.* ARNOLD L. BLOOM,† *University of California, Berkeley.*—Total and differential inelastic cross sections for $d-p$ scattering have been measured at the 184-in. cyclotron, using stilbene counter techniques similar to those used for elastic $d-p$ scattering.[1] The total cross section was obtained by measuring the differential cross section for scattering of charged particles and integrating over all solid angles; since any $d-p$ collision scatters two charged particles, the integral is twice the total cross section. This method gives $\sigma = (92 \pm 7) \times 10^{-27}$ cm², Rutherford scattering excluded. Inelastic collisions in which both protons suffer large changes of momentum were examined by measuring coincidences between protons. The angles between scattered protons have a narrow distribution near 90° in the laboratory system; the differential cross sections $\sigma(\Phi)$ for scattering one of the protons through an angle Φ are about one-third the corresponding free $p-p$ cross sections at comparable momenta.[2]

* This work was performed under the auspices of the AEC.
† Now at Varian Associates, San Carlos, California.
[1] M. Stern and A. Bloom, Phys. Rev. **83**, 178 (1951).
[2] Birge, Kruse, and Ramsey, Phys. Rev. **83**, 274 (1951).

B4. Locating Buried Radioactive Sources. J. D. GRAVES AND RICHARD I. CONDIT, *Broadview Research and Development, Burlingame, California.*—Expressions have been obtained for the nuclear radiation intensity above the surface of the ground (assumed plane) from buried point sources of cobalt 60. The optimum procedure for expeditiously locating such sources from large distances by detecting their gamma-radiation depends chiefly upon the depth of burial and is expressed in terms of the angle between the detector-source line and the ground surface. This optimum angle is 0 degrees for sources on the surface, 30 degrees for sources at a depth of about 8 cm, 60 degrees for sources at about 100 cm, and approaches 90 degrees for sources at very great depths. Thus, the maximum radiation intensity at any given large distance parallel to the ground from a source buried a finite depth occurs above the surface, and accordingly the search for buried radioactive materials is best attempted with detectors at elevated positions. About the elevation of maximum intensity, the intensity decreases more rapidly with decreasing elevation than with increasing elevation. Where actual field conditions in-

volve extended sources and nonplanar topography, the advantages of elevated detection are even more pronounced. These results have important applications in the search procedures for radioactive ores, contamination, and tracers.

B5. Isotope Effects in the Decarboxylation of Malonic Acids. PETER E. YANKWICH, EDWARD C. STIVERS, AND ROBERT F. NYSTROM, *Department of Chemistry and Radiocarbon Laboratory, University of Illinois, Urbana.*—Malonic and bromomalonic acids carboxyl-labeled with carbon fourteen have been decarboxylated at their melting points. Effluent carbon dioxide and carbon dioxide obtained from combustion of the resulting acetic acid were subjected to radioactivity and isotope-ratio determination. The intramolecular isotope effects for carbon thirteen and fourteen were calculated from the results of these determinations.

For malonic acid, both the carbon thirteen and carbon fourteen effects are in agreement with earlier work,[1-3] but the agreement for carbon fourteen is not complete.[4] For bromomalonic acid, the carbon thirteen effect agrees with that predicted,[5] but the carbon fourteen effect disagrees both with the prediction and with previous observation.[3]

[1] Jacob Bigeleisen and Lewis Friedman, J. Chem. Phys. **17**, 998 (1949).
[2] Lindsay, Bourns, and Thode, Can. J. Chem. **29**, 192 (1951).
[3] Peter E. Yankwich and Melvin Calvin, J. Chem. Phys. **17**, 109 (1949).
[4] Arthur Roe and Max Hellmann, J. Chem. Phys. **19**, 660 (1951).
[5] Jacob Bigeleisen, J. Chem. Phys. **17**, 425 (1949).

B6. Pulse Analysis with the Aid of a Mechanical Synthesizer-Analyzer. S. LEROY BROWN, *University of Texas.*—The method of utilizing a mechanical harmonic synthesizer to perform harmonic analysis[1] has been modified so that the harmonic content of a pulse may be readily determined. The amplitudes of the fifteen sine components of the synthesizer are set to the values of fifteen equispaced ordinates of a short pulse. For example, if the pulse is considered to be 1/48th of its repetition period, a few hundred sine components may be evaluated from a single trace made by the machine as its fundamental turns through not more than 90°. Similarly, a few hundred cosine components are evaluated from a second trace with the cosine components of the machine set to the values of the equispaced ordinates of the pulse. The sine and cosine components of shorter and shorter pulses, of the same shape, may be evaluated from these two original traces. By suitable change of scale, these curves represent the sine and cosine Fourier transforms of the pulse; i.e., they represent the continuous spectrum of the pulse. Since both sine and cosine components are found, the phase angles as well as the amplitudes are determined.

[1] S. Leroy Brown, J. Franklin Inst. **228**, 675 (1939).

B7. LSM_LM_S Eigenfunctions of an Atom. KENNETH JAMES HARKER, *University of California, Los Angeles.* (*Introduced by E. Lee Kinsey.*)—Gray and Wills[1] have described a method for finding the LSM_LM_S[2] eigenfunctions of an atom whose outer shell contains n equivalent electrons with angular momentum l, n and l arbitrary. A more direct method using group theory is introduced here to solve the same problem. One starts from a single electron basis with a central field only. An electrostatic interaction perturbation is next introduced. The products of single electron orbital wave functions are transformed to a new basis according to the complete reduction of the direct product of the rotation group: $D_l \times D_l \times D_l \times \cdots = \Sigma D_L$. Likewise, the products of single electron spin functions are transformed to a new basis according to the reduction: $D_{\frac{1}{2}} \times D_{\frac{1}{2}} \times D_{\frac{1}{2}} \times \cdots = \Sigma D_S$. The products of these reduced spin and orbital functions transform as $D_L \times D_S$. The latter products are then made antisymmetric by a straightforward process. If no antisymmetric function transforming like $D_L \times D_S$ exists, the answer is zero. The method also provides automatically for accidental degeneracy. The method has been successfully applied to the d^3 and f^3 configurations.

[1] N. M. Gray and L. A. Wills, Phys. Rev. **38**, 248 (1931).
[2] E. U. Condon and G. H. Shortley, *Theory of Atomic Spectra* (Cambridge University Press, London, 1935), Section 58.

THURSDAY AFTERNOON AT 1:30

Room 1, Le Conte Hall

(A. C. HELMHOLZ presiding)

C1. Aluminum-24, A Delayed Heavy-Particle Emitter. ANN C. BIRGE, *Radiation Laboratory, Department of Physics, University of California, Berkeley.*—The beam of the 32-Mev linear accelerator was run through a proportional counter and into its Mg wall. A delayed heavy-particle activity was observed with a half-life of 2.3 ± 0.2 sec, and threshold of 15.4 ± 0.3 Mev. By a consideration of the energy available, it can be shown that the only possible heavy-particle emitter that can be formed with this threshold energy from a stable Mg isotope is Al^{24}. The reaction is $Mg^{24}(p, n)Al^{24}$. The mass of Al^{24} calculated from the threshold energy is 24.0075. As in the other delayed alpha-particle emitters reported previously by Alvarez,[1] the observed life-time is that of the beta-decay that precedes the heavy particle. The energy available in this case would allow either a proton or alpha-particle to be emitted, but there is more energy available for the latter.

[1] L. W. Alvarez, Phys. Rev. **80**, 519 (1950).

C2. Interpretation of Photonuclear Experiments. L. EYGES, *University of California, Berkeley.*—An analysis of the experiments to date on photonuclear reactions suggests the following picture for heavy nuclei ($Z \gtrsim 50$). The emission of particles (mainly neutrons) is governed by the statistical model. The photon total absorption cross section drops off rapidly above about 20 Mev and begins to rise again near the threshold for meson production. In the experiments on total neutron yields with 330-Mev bremsstrahlung[1] there are as many neutrons produced by photons with energies above the meson threshold as by photons with lower energies. The integrated total cross sections for Z_n^{64}, Sb, and Ta^{181} can be evaluated and by comparison with the Levinger-Bethe formula[2] lead to values of 0.5, 0.4, and 0.7, respectively, for the fraction of exchange force in the $n-p$ interaction.

[1] Terwilliger, Jones, and Jarmie, Phys. Rev. **82**, 820 (1951); D. W. Kerst and G. A. Price, Phys. Rev. **79**, 725 (1950).
[2] J. S. Levinger and H. A. Bethe, Phys. Rev. **78**, 115 (1950).

C3. Photodissociation of Deuteron by High Energy Gamma-Rays. SEISHI KIKUCHI, *University of California, Berkeley.*—An analysis was made on proton tracks found in the photographic emulsion, which had been exposed by S. White to secondary particles from a deuterium gas target bombarded by high energy synchrotron gamma-rays of maximum energy of about 320 Mev to investigate photomesons from deuterons. The energy spectra of protons at the emission angles of 45, 90, and 135 degrees were obtained. In each case it shows a fairly sharp cutoff at the energies 190, 140, and

95 Mev, respectively. These energies correspond to the energy of the proton expected, if it were produced by the splitting of a deuteron into a proton and a neutron by the absorption of a photon of energy 320 Mev. The angular distribution of protons shows a fairly strong forward asymmetry. The cross section per photon for the photodisintegration increases steeply with the increasing photon energy above the meson threshold. The absolute value of the cross section is of the order of magnitude of the meson production cross section. The author's thanks are due S. White for placing the plates at his disposal.

C4. Some Differential Analyzer Methods for Orbit Problems in the Cyclotron. BAYARD RANKIN, JOHN KILLEEN, AND WALTER H. BARKAS. *University of California, Berkeley.*—The equations of motion for a charged particle in a magnetic field have been solved previously in some special cases.[1] These solutions almost always lead to numerical methods. However, the median and vertical plane motion for any axially symmetric field can be obtained quickly on a differential analyzer after transforming the equations by a few simple devices. Only resets on the integrands are required for each set of initial conditions, and an orbit can be drawn every five minutes. The horizontal motion is solvable on an analyzer of six integrators and three input tables. It is necessary simply to introduce the variable $\lambda=\dot{\varphi}+eH/mc$ in the equation $t=\int r\dot{\varphi}d[\int\lambda dt]$ and effect a transformation which leaves the relativistic mass independent of the initial conditions without changing the momentum. The vertical motion is handled similarly but demands more integrators. An approximation to the vector potential is necessary. Of special interest are the paths of 30–100-Mev π-mesons which are produced in a target at a radius of 80 inches in the 184-inch cyclotron. 200 of these have been obtained on a selsyn-driven analyzer by using the methods described. Various focusing points have been examined at seven different energies.

[1] E.g., Norman D. Coggeshell and Morris Muskat, Phys. Rev. **66**, 187 (1944), and Walter H. Barkas, Phys. Rev. **78**, 90A (1950).

C5. Influence of Well Shape on the Pickup Process in Deuterium. IRA L. KARP, *University of California, Berkeley.*—Calculations of the pickup process at high energies in deuterium,[1] carried out in Born approximation with an approximate deuteron wave function, exceed the experimental values for 90-Mev incident nucleons by a factor of roughly three to five.[2] In an effort to account for this discrepancy the momentum distribution of the deuteron has been recalculated using exponential and square wells fitted to the low energy data. The results are negative, i.e., all three distributions lie within a few percent of each other for 90-Mev incident nucleons (although at higher energies the Chew distribution lies well above the other two). It is probable that in the calculation of the pickup process the Born approximation must be especially poor. On the one hand, the pickup process depends on high momentum components in the deuteron wave function and on correspondingly small separation of the deuteron particles, and, on the other hand, the use of the Born approximation implies that the deuteron particles are far enough apart so that in the scattering by one particle the interaction with the other can be neglected. An estimate of the correction for this interaction is being made.

[1] G. F. Chew, Phys. Rev. **74**, 809 (1948).
[2] M. O. Stern, University of California Thesis (UCRL-1440).

C6. A Generalization of the WKB Method to Radial Wave Equations. R. H. GOOD, JR., *University of California, Berkeley.*—The usual radial WKB approximations are based on the exponential function, perhaps because of the linearity of the equations. Instead one may use the function which arises in solving the corresponding free particle problem. This insures that the approximation will give the exact result in the free particle problem and consequently that it will be useful at high energy. This point of view may be applied uniformly to the radial Dirac equation, the radial Schrödinger equation, and the one-dimensional Schrödinger equation. In the last case the familiar WKB approximation is the result. In this treatment of the radial equations connection formulas are not required. Also the eigenvalue condition arises from a comparison of asymptotic developments in such a way that one would expect the approximate eigenvalues to be close to the correct ones. In predicting the wave functions themselves the approximation is poor near the turning points. For a Coulomb potential the approximation reproduces the Bohr and Sommerfeld-Dirac formulas for the energy levels precisely. It also gives good results for the amplitude and phase of the nonrelativistic unbound Coulomb wave functions at infinity. It is expected that the method will have application in high energy radially symmetric scattering problems.

C7. Radiative Corrections to the Distribution of Nuclear Recoils from Electron Scattering. L. I. SCHIFF, *Stanford University.**—The scattering of fast electrons by nuclei can be investigated experimentally by measuring the distribution of the recoil nuclei with respect to their angle and energy. Only momentum transfers large in comparison with mc are significant if the recoil nucleus is to be detectable. If both recoil angle and energy can be measured, a comparison can be made with the Mott-Rutherford formula corrected for nuclear size and for the emission of low energy photons. If only the recoil angle can be measured, a correction for the emission of higher energy photons must also be applied. This effect has been estimated on the basis of the Bethe-Heitler formula, and is correct within a factor in a logarithm that is so chosen that the low energy photon cutoff cancels between low and high energy photon corrections. The calculation shows that for large momentum transfers, the photon tends to emerge close to the direction of either the incident or the scattered electron. The analogous result in pair production is that either the electron or the positron tends to emerge close to the direction of the incident photon when the momentum transfer is large.

* Assisted by the joint program of the ONR and AEC; a fuller account of this work will be published as a Microwave Laboratory report.

THURSDAY AFTERNOON AT 1:30

Room 3, Le Conte Hall

(F. A. JENKINS presiding)

D1. Electronic States of Molecular Crystals. N. W. BLAKE,* D. S. MCCLURE, AND H. WINSTON,† *University of California, Berkeley.*—It has been found possible to classify electronic levels of molecular crystals as "scatterer" or "absorber" levels (Peierls[1]), by studying emission and absorption spectra at low temperatures, and the emission lifetime as a function of temperature. Scatterers have narrow emission and absorption bands because of the κ (electronic wave number) selection

rule, whereas absorbers have broad bands because κ is not quantized. In case the lowest allowed κ level of a scatterer is above the lowest forbidden K level, a long-lived temperature dependent emission should be observed (trapping). Mixed crystals of scatterers should display the emission spectra of both components, while for absorbers, only the component having the state of lowest energy will emit. These and other criteria have shown that the 3130A state of naphthalene is a good scatterer, the 3500A state of phenanthrene is closer to scatterer than absorber and the 4000A state of anthracene is an absorber.

* Now at Columbia University, Department of Chemistry.
† Now at U.C.L.A., Department of Chemistry.
[1] R. Peierls, Ann. Physik **405**, 905 (1932).

D2. A Vibrational Analysis of the Fluorescence of Naphthalene Vapor. O. SCHNEPP AND D. S. MCCLURE, *University of California, Berkeley.*—The fluorescence spectrum of naphthalene vapor has been photographed and found, under suitable conditions, to consist of a number of discrete bands. Thirty-nine bands were measured and a vibrational analysis was carried out making use of assignments of infrared and Raman fundamentals. The analysis indicates that the transition observed is forbidden by symmetry and made weakly allowed by a molecular vibration of frequency 478 cm^{-1} belonging to the representation b_{2u}. This indicates that the wave function of the lowest excited singlet state of naphthalene belongs to the irreducible representation A_g or B_{1g} of the point group D_{2h}.

D3. Unusual Dispersion Aspects of Gypsum in the Near Infrared. R. M. VANDERBERG, *University of California, Los Angeles.* (Introduced by J. W. Ellis.)—When a beam of infrared radiation is sent through a gypsum crystal section placed between crossed polarizers, no orientation is found at which extinction occurs for all wavelengths. This phenomenon results from a dispersion of the bisectrices, which has been known in the visible as a rotation of these axes of about one degree. In the near infrared this rotation increases to about 50° at 2.5μ. An anomaly occurs near 2.0μ, which is the region of an absorption band produced by the water of crystallization. The wave plate maxima spacings shown in the infrared spectrum depart markedly from the formula $\delta\lambda = (-\lambda^2/t\Delta\mu)\delta n$, derived on the assumption of constant $\Delta\mu$, as the wavelength increases beyond 2.0μ. This demonstrates a large dispersion of the birefringence.

D4. Structure of the 3μ-Band of $NaBr \cdot 2H_2O$. D. S. WEBBER AND A. N. BAKER, JR., *University of California, Los Angeles.*—The 3μ absorption band of $NaBr \cdot 2H_2O$ was re-investigated with the same spectrometer used by Lyon and Kinsey.[1] The use of very thin single crystals, instead of the polycrystalline films previously studied, and some refinements of the instrument, reducing zero-drift and background radiation, revealed details of the structure not heretofore observed. The band shows four distinct components. The component at 3478 cm^{-1} is assigned to the fundamental asymmetric vibration of the water molecule, ν_3. The components of 3420 cm^{-1} and 3551 cm^{-1} are assigned to the fundamental symmetric vibration mode, ν_1, split by the crystalline field. This is in excellent agreement with the results of Nayar[2] in a study of the Raman effect. Since ν_3 is primarily infrared active, and ν_1 is primarily Raman active, most of the absorption of the band as a whole is caused by ν_3. The fourth component, at 3239 cm^{-1}, is assigned as previously to a polymer effect.

[1] W. Lyon and E. L. Kinsey, Phys. Rev. **61**, 482 (1942).
[2] P. G. N. Nayar, Proc. Indian Acad. Sci. **A8**, 479 (1938).

D5. Rotational Temperatures of OH in Several Flames. H. P. BROIDA, *National Bureau of Standards.*—Spectroscopic scans have been made using a high resolution grating monochromator with photoelectric detection through the various regions of several oxygen flames with the object of determining the contribution from each region to the intensity measurements. Hydrogen, acetylene, methane, and propane were used with variations of fuel to oxygen ratio from one-half to twice that necessary for stoichiometric mixture. The OH rotational temperatures have been measured as a function of position in each flame. The constancy of measured temperature for different fuel to oxygen mixtures with the same fuel and the higher than adiabatic temperature suggests a lack of thermal equilibrium in the inner cone. In the hot gases above the reaction zone evidence of rotational and electronic equilibrium is found. The concentration of thermally produced OH in the hot gases at atmospheric pressure is so large in oxygen flames near stoichiometric mixtures that it is difficult to use the emission from this radical for studies of the reaction zone.

D6. The Vibrational Spectrum of Dinitrogen Tetroxide. W. D. PERKINS AND M. KENT WILSON, *Harvard University.*—The infrared spectrum of dinitrogen tetroxide has been investigated between 240 cm^{-1} and 5000 cm^{-1} with confirmation of the previously reported bands. Two hitherto unobserved bands[1] have been found at 430 cm^{-1} and 684 cm^{-1} and shown by their temperature dependence to belong to dinitrogen tetroxide and not to nitrogen dioxide. From these data, together with existing Raman data,[2] it has been possible to assign the frequencies to normal modes as follows: $\nu_1(A_g) = 1342$, $\nu_2(A_g) = 811$, $\nu_3(A_g) = 265$, $\nu_4(A_u) = 70$, $\nu_5(B_{1g}) = 1722$, $\nu_6(B_{1g}) = 500$, $\nu_7(B_{1u}) = 684$, $\nu_8(B_{2g}) = (1133)$, $\nu_9(B_{2u}) = 1747$, $\nu_{10}(B_{2u}) = 430$, $\nu_{11}(B_{3u}) = 1260$, and $\nu_{12}(B_{3u}) = 748$. The frequency ν_8 was calculated from a valence-type potential function. A consideration based on selection rules, together with a comparison of the Raman spectra of the liquid and the solid, indicates a planar, ethylene-type configuration in agreement with the structure proposed from x-ray diffraction measurements.[3]

[1] G. B. B. M. Sutherland, Proc. Roy. Soc. (London) **A141**, 342 (1933).
[2] J. D. S. Goulden and D. J. Millen, J. Chem. Soc. 2620 (1950).
[3] J. S. Broadley and J. M. Robertson, Nature **164**, 915 (1949).

D7. The Spectrum of Nd^{+++} in Crystals. ROBERT A. SATTEN, *University of California, Los Angeles.*—The tentative identification of transitions from the ground state to various quartet states of f^3 electrons is made possible partly on the basis of consistency among the following: (a) the expected relative positions of the electrostatic interaction energy terms; (b) extrapolation from identified terms of other rare earths; (c) empirical term diagrams, drawn for most of the groups of absorption lines between 9000 and 3500A in solid $Nd(BrO_3)_3 \cdot 9H_2O$ at room and liquid N_2 temperatures, which aid in determining J by the crystal splitting; and (d) a value of the single-electron Lande interval factor[1] $\zeta_{4f} = 900$ cm^{-1} which yields fair agreement among predicted and observed positions of certain intense groups of lines as well as with values of ζ_{4f} found by extrapolation from other rare earths. Terms assigned to observed groups of lines with various degrees of probability are $^4I_{13/2}$; $^4F_{3/2,5/2,7/2,9/2}$; $^4G_{5/2,7/2,9/2,11/2}$; and^4 $D_{1/2}$. The latter term was calculated in intermediate coupling. The empirical term diagrams (c) yield the splitting of the levels of the free Nd^{+++} ion in the crystal field. The $^4I_{9/2}$ ground state is split into five levels at 0, 115, 184, 363, and 382 cm^{-1}.

[1] Condon and Shortley, *The Theory of Atomic Spectra* (Cambridge University Press, London, 1935).

D8. Relations between the Vibrational Intensities of Isotopic Molecules. J. C. DECIUS, *Department of Chemistry, Oregon State College.*—In some unpublished work, Crawford[1] has shown that there exist some very simple relations be-

tween the integrated intensities, A_k, of isotopic molecules. These relations have the form $\Sigma_k A_k/\lambda_k = \Sigma_k A_k^*/\lambda_k^*$, where $\lambda_k = 4\pi^2\nu_k^2$, ν_k is a fundamental vibration frequency, the summation is extended over a single symmetry species, and the starred quantities refer to an isotopically substituted molecule. These relations are, however, restricted to the case in which the species in question is *not* one in which a component of rotation occurs. In the general case, where the species of the fundamentals may be the same as that of a rotation, the foregoing formula must be replaced by $\Sigma_k(A_k/\lambda_k) = \Sigma_k(A_k^*/\lambda_k^*) + \Phi$, in which Φ is a function of the mass changes, $\Delta m_\alpha = m_\alpha^* - m_\alpha$; the moments of inertia; the equilibrium geometry of the molecule; μ_x^0, μ_y^0, μ_z^0 the components of the dipole moment, and the corresponding dipole derivatives, $[(\partial\mu x)/(\partial Qk)]_0$, etc.; and of certain force constants. Symmetry may be used advantageously to simplify the function Φ. Moreover, Φ vanishes when the molecule has no permanent dipole moment.

[1] B. L. Crawford, Jr. (private communication).

THURSDAY AFTERNOON AT 3:30

Room 310, Le Conte Hall

(F. A. JENKINS presiding)

Invited Papers

E1. Molecular and Atomic Spectra Associated with the Solid State. J. W. ELLIS, *University of California, Los Angeles.* (45 min.)

E2. Absorption Spectra of Simple Radicals in Thermal Equilibrium. K. WIELAND, *University of Zurich.* (30 min.)

FRIDAY MORNING AT 9:00

Room 4, Le Conte Hall

(E. M. MCMILLAN presiding)

F1. Neutron Spectrum from $B^{10}(\alpha, n)N^{13}$, N^{13*}. MARGUERITE ROGERS, F. K. ODENCRANTZ, AND G. J. PLAIN, USNOTS, *Inyokern.*—The neutron spectrum from separated B^{10} bombarded by polonium particles was recorded on Eastman HTA film. The tracks of recoil protons in the forward direction were measured by a B-and-L microscope using a filar micrometer eyepiece at total magnification 1000. Recoil proton groups at 0.90, 0.96, 1.01, 1.13, 1.27, and 1.32 Mev were observed. A total of 1000 tracks were measured.

F2. High Energy Electron-Electron Scattering. CHARLES E. VIOLET, F. C. GILBERT, ROBERT W. DEUTSCH AND WALTER H. BARKAS. *University of California, Berkeley.*—Eradicated electron sensitive nuclear emulsions were exposed to 200-Mev electrons obtained by magnetic analysis of pairs converted in the synchrotron beam. By following primary electron tracks in the emulsion, 427 electron-electron scattering events were recorded in which the scattered electron of lower energy, or knock-on electron, had an energy greater than 30 kev. The knock-on energy was determined by measuring either the range or the angle between the knock-on and primary tracks. The observed absolute differential cross section, as a function of knock-on energy, was found to be consistent with Møller's theoretical cross section. At this primary energy, a sufficient number of events of large fractional energy transfer could not be observed to detect exchange, spin, and retardation effects, and actually only the classical relativistic theory was verified. Two pairs initiated by primary electrons and two cases in which primary electrons vanished in the emulsion were also observed in 102.6 cm of track. No heavy particle events were observed.

F3. Physical Measurements on Nuclear Photographic Emulsion. A. J. OLIVER AND WALTER H. BARKAS, *University of California, Berkeley.*—Calculations of the stopping power of nuclear photographic emulsion and of the volume of emulsion at the time of exposure may be made with more accuracy if the dependence of density and thickness upon relative humidity were known in more detail than is available in published specifications. A device has been developed for measuring the expansion of emulsion with measured increases of relative humidity, both for unprocessed and for processed plates. The measurement of thickness without distorting soft emulsion at relative humidities from 10 percent to 90 percent was the primary contribution of this work. A second project was the measurement of average thickness and weight for the derivation of a density *vs* relative humidity relationship. A third measurement was a check of the refractive indices of emulsion and of the immersion oil employed, so that depth measurements with the microscope are calibrated properly. Measured shrinkage factors were found to vary between 1.8 and 3, depending on humidity conditions. The emulsion measured was Ilford type C-2, and the processing included fixing and hardening in Kodak Acid Fixer. A chart has been worked out to be employed in determining thickness at exposure, given final thickness and the relative humidities before and after processing.

F4. Electron Pickup by Fast C^{12} Nuclei in Emulsion. PETER C. GILES AND WALTER H. BARKAS. *University of California, Berkeley.*—C^{12} particles, accelerated in the 60-inch cyclotron to about 120 Mev, were detected by D-1 nuclear emulsion plates which were subsequently developed in D_{19} developer. Measurements were taken of the gap density,[1] as a function of the residual range, on 223 particle tracks. It was noticed that the gap density passed through a minimum at a residual range of about 35 microns, where it is assumed that electron pickup begins. By comparing points on the terminal side of the electron pickup point with points on the initial side of the pickup point of equal gap density, the charge on the

particle was estimated as a function of the residual range. It was assumed that the rate of energy loss may be determined from $dE/dR = Z^2 f(V)$, where $f(V)$ is determined from proton data, E is the particle energy, R the residual range, and Z the instantaneous value of the charge carried by the ion.

[1] P. E. Hodgson, Phil. Mag. 41, 725 (1950); also Bowker, Green, and Barkas, Phys. Rev. 81, 649 (1951).

F5. Detection of Azimuthal Polarization in Double N–P Scattering at 150 Mev.* L. F. WOUTERS, *University of California, Berkeley.*—In order to circumvent the accidental background in the double scattering experiment, the first scattering is performed inside the 184-inch cyclotron tank. LiD and LiH targets are compared in order to obtain the D-neutron contribution to the polarization caused by the $p-n$ interaction. The second scattering is performed as an orthodox $n-p$ scattering experiment by paraffin-carbon difference, in the well-collimated neutron beam emerging outside the cyclotron shielding. Four scintillation counter telescopes are arranged in an azimuthal array observing the second scatterer. Each telescope consists of two photomultiplier-liquid phosphor units; these are operated from a pulsed H.V. source which is keyed in synchronism with the cyclotron beam pulse. Using selected 1P28 photomultipliers, the counter behavior is indistinguishable from normal dc operation, when using 100 microsecond keying pulses at 2 to 2.4 kv. Five to ten volt signal pulses are obtained from incident protons, and these are mixed in a current-biased crystal diode coincidence circuit. The system shows an over-all resolution time of 5×10^{-9} sec. This work was performed under the auspices of the AEC.

* D. Swanson and L. F. Wouters, Phys. Rev. (to be published).

F6. Fast Protons from 270-Mev N–D Scattering.* W. HESS, J. B. CLADIS, AND J. HADLEY, *University of California, Berkeley.*—The differential cross section for production of high energy protons in N–D scattering, using the 270-Mev neutron beam of the 184-inch cyclotron, has been measured at scattering angles between 4° and 58°. For normalization, yields of protons from N–P scattering were measured at each scattering angle. In all cases, only protons have a cut-off energy of 200-Mev $\cos^2\Phi$ were accepted by the counter system. In addition, through the use of a magnetic analyzer, energy distributions of the N–D protons were measured at 4° and at 22.5°. The energy distributions closely resembled, in shape, the energy distributions of N–P protons at the same angles, confirming the similarity in nature of collisions of high energy neutrons with free protons and with protons bound in deuterium. Total yield of protons above the cut-off energy is lower for N–D than for N–P collisions; however, the ratio of the two being about 0.7 at all angles observed. Effects of the exclusion principle, of the internal momentum distribution of the deuteron, and of the difference in average potential energy between the dineutron and the deuteron will be discussed as possible courses of the lowering of the N–D proton yield below that from N–P scattering.

* This work was performed under the auspices of the AEC.

F7. Nuclear Cross Sections for High Energy Neutrons and Protons. R. JASTROW AND J. E. ROBERTS, *University of California, Berkeley.*—An earlier study[1] of nuclear cross sections for neutrons at energies up to 270 Mev has been continued. We find that it is desirable to modify the customary assumption on the density of nuclear matter in order to account for the neutron cross sections over the full energy range from 14 Mev to 270 Mev. As usual, we take the density of nucleons in the nucleus to be uniform within a region whose radius increases roughly as $A^{\frac{1}{3}}$. However, outside this core a diffuse region is assumed in which the nucleon density falls off in a distance of the order of the range of nuclear forces. In the light elements the diffuse region is comparable with the core of constant density, while small compared with this core in the heavy elements. At moderately low energies, of the order of 25 Mev, the diffuse tail is relatively opaque. The increase in total cross section resulting from the tail is greater, relatively, for the light elements than for the heavy elements, and brings the calculated neutron cross sections into better agreement with the observed values at energies between 14 Mev and 40 Mev. At the same time the presence of the diffuse region destroys the diffraction pattern in the elastic cross sections of the light elements while only blurring slightly the diffraction patterns of the heavy elements. This result is also fn agreement with recently reported experimental results.[2]

[1] R. Jastrow, Phys. Rev. 82, 261 (1951).
[2] Richardson, Ball, Leith, and Moyer, Phys. Rev. 83, 859 (1951).

FRIDAY MORNING AT 9:00

Room 1, Le Conte Hall

(E. O. LAWRENCE presiding)

G1. Mechanism of Fission. GLENN T. SEABORG, *Department of Chemistry and Radiation Laboratory, University of California, Berkeley.*—An empirical correlation of the known data on spontaneous fission seems to point to an important effect of the nuclear type (or radius) on the rate. A plot of the logarithm of the "half-life" *versus* the fissionability parameter, Z^2/A (or Z^2/r^3), indicates that on the average the spontaneous fission rate is greater or an even-even nuclide than one with an odd number of nucleons. Extrapolation of the straight line representing the even-even nuclei to theregion of instantaneous rate (10^{-20} seconds) of spontaneous fission gives the expected value of about 47 for Z^2/A. The higher rates may result from the higher zero point energy of the modes of vibration which lead to fission associated with even-even nuclei because of their expected smaller radii. Similar considerations may be useful in interpreting the results of slow neutron and photofission. Thus the small fission cross section of Cm^{242} and relatively high photofission thresholds of U^{235}, U^{233}, and Pu^{239} may be associated with the odd nucleon intermediate nuclei, in contrast to the large fission cross sections of U^{234}, U^{232}, and Pu^{240} and the relatively low photofission threshold of U^{238} all represented by even-even intermediates.

G2. Alpha-Activity in Bi^{209} as Detected with Nuclear Emulsions. DEAN C. DUNLAVEY AND GLENN T. SEABORG, *Department of Chemistry and Radiation Laboratory, University of California, Berkeley.*—Alpha-emission of particle energy about 4.85 Mev has been observed in the bismuth fraction produced by the bombardment of lead with 60-Mev protons in the 184-inch cyclotron. The observed alpha-decay has a half-life approximating 12 hours. Correlation with the accompanying decay of the other radiation as measured with a Geiger counter[1] and with the alpha-systematics indicates the emitting isotope to be Bi^{209} with a partial alpha-half-life of 2×10^{4} years. Following chemical separation, the carrier free bismuth was placed in a solution of pH about 4 and, for time

intervals appropriately spaced following bombardment, impregnated into freshly eradicated Ilford C-2 nuclear emulsion plates. The associated gamma-conversion electron activity determined the maximum concentration of bismuth which could be tolerated by the emulsion without producing excessive fogging. Aliquots equal to those placed in the emulsion were counted in a windowless proportional counter to enable association of the alpha-abundance found in the emulsion with the number of known over-all disintegrations. The alpha/K branching ratio was found effectively constant and reproducible at about 10^{-7} over a series of experiments.

[1] H. M. Neumann and I. Perlman, Phys. Rev. **78**, 191 (1950).

G3. Complex Alpha-Structure of the Heavy Elements. Frank Asaro, Fred L. Reynolds, and I. Perlman, *Department of Chemistry and Radiation Laboratory, University of California, Berkeley.*—A study of complex alpha-energy spectra was undertaken in the hope that a correlation with alpha-systematics might promote a better understanding of nuclear states and their influence on the alpha-decay process. A 75-cm radius of curvature 60° symmetrical analyzer with photographic plate detection of alpha-particles was used for the energy discrimination. The complex alpha-particle energy spectrum of Cm^{242} comprises two groups: one at 6.110 ± 0.003 Mev, 73 ± 1 percent abundant; and one group 45.9 ± 1.0 kev lower in energy, 27 ± 1 percent abundant. The complex alpha-particle energy spectrum of Am^{241} comprises six groups: 5.544 Mev, 0.23 ± 0.06 percent abundant; 5.533 Mev, 0.34 ± 0.06 percent abundant; 5.502 Mev, 0.21 ± 0.02 percent abundant; 5.475 Mev, 84.2 percent abundant; 5.433 Mev, 13.6 ± 1.4 percent abundant; 5.378 Mev, 1.4 ± 0.2 percent abundant. The identification of the experimentally observed alpha-groups with the alpha-emission spectra of the indicated nuclides is conclusively proved by the constancy of the respective energy differences and abundance ratios over wide ranges of sample activity prepared from different sources of material. In every case studied of even-even nuclei all groups lie very close to the alpha-systematic half-life *vs* energy curves for even-even nuclides.

G4. Isomeric States of Bi^{210}. Harris B. Levy and I. Perlman, *Department of Chemistry and Radiation Laboratory, University of California, Berkeley.*—In 1950 Neumann, Howland, and Perlman[1] reported finding a possible isomer of RaE. Bismuth was irradiated at high neutron flux to produce Bi^{210}. After the RaE had decayed out, a residual long-lived alpha-activity was found in the bismuth fraction. This alpha-activity was assigned to Bi^{210} on the basis of experiments in which the Tl^{206} daughter was milked out. The alpha-particle energy was determined at that time to be 5.03 ± 0.05 Mev, indicating that it was an excited state of RaE. Recently some of this bismuth fraction was electromagnetically separated, and the mass fractions 208, 209, and 210 were examined. The increase in the specific activity of the 210 mass fraction and the corresponding decrease in the specific activity of the 208 and 209 mass fractions confirmed the assignment of the alpha-activity to Bi^{210}. The energy of the alpha-particle was redetermined to be 4.93 ± 0.02 Mev. The disintegration energy is therefore 5.03 ± 0.02 Mev. Comparison with the latest calculated alpha-disintegration energy of RaE, 5.06 Mev, leaves considerable doubt as to whether the long-lived alpha-emitter or RaE is the ground state of Bi^{210}.

[1] Neumann, Howland, Jr., and Perlman, Phys. Rev. **77**, 720 (1950).

G5. On the Semiempirical Correlation of Alpha-Decay Rates. J. O. Rasmussen, *Department of Chemistry and Radiation Laboratory, University of California, Berkeley.*—The decay rate data for the even-even type nuclides of the heavy region can be well correlated by a "many body" formula based on the experimental value of the "effective nuclear radius for alpha-particles" of Th^{232}. The experimental value $r=10.27\cdot10^{-13}$ cm was determined by Jungermann[1] from the alpha-induced fission cross section excitation function on Th^{232}. The simple decay rate expression used is of the form $\lambda=fP$ where λ is the decay constant in sec^{-1}, f is the hypothetical "decay constant without barrier," and P is the penetration factor, calculated by the WKB approximation. The experimental decay data for 27 different even-even type alpha-emitters were used to calculate f. Excluding only the four nuclides with 126 or less neutrons, the average of $\log f$ is 18.84 ± 0.15. It is pointed out that f is very nearly equal to D/h, where D is the average level spacing for the ground states of the alpha-emitters as deduced from the energy spacing of alpha-fine structure groups. The orbital electron screening correction to the alpha-decay energy is also discussed.

[1] J. Jungermann, Phys. Rev. **79**, 640 (1950).

G6. L X-Rays and Low Energy Gamma-Radiation in the Decay of Am^{241}. C. I. Browne and I. Perlman, *Department of Chemistry and Radiation Laboratory, University of California, Berkeley.*—The L x-rays and low energy gamma-rays given off following the alpha-decay of Am^{241} have been studied on a 10-inch bent crystal x-ray spectrometer. Eight gamma-rays have been observed in the spectral region 12–85 kev, with energies ranging from 14.23 ± 0.06 to 59.78 ± 0.02 kev. The $L\alpha_2$, $L\alpha_1$, $L\eta$, $L\beta_3$, $L\beta_4$, $L\beta_1$, $L\gamma_1$, and $L\gamma_6$ x-rays of neptunium from gamma-ray internal conversion have been observed. They were identified by comparing the observed energies with extrapolations of the Moseley relationship and assuming the identities, the agreement in energy was close. Estimates of relative intensity have been made on both the gamma- and x-radiation, and lead to the conclusion that the ratio of vacancies produced in the L shell by internal conversion is $L_I:L_{II}:L_{III}=6:5:2$. A partial decay scheme is suggested and a number of the gamma-ray transitions are shown to be in good agreement with known spacings from alpha-particle complex structure.

G7. Alpha-Radioactivity in Elements below Lead. S. G. Thompson, J. O. Rasmussen, and A. Ghiorso, *Department of Chemistry and Radiation Laboratory, University of California, Berkeley.*—In a continuation of the survey for alpha-activity among cyclotron-produced, neutron deficient isotopes of the medium heavy elements, alpha-activity was found in a number of rare earth nuclides with atomic number greater than 62 (samarium). Element assignments were usually made by chemical separations and the mass numbers of several were assigned either by mass spectrographic determination or by means of excitation functions. Alpha-radioactivity caused by traces of heavy element ($Z>82$) contamination even in the purest samples was nearly always produced and discrimination by means of alpha-energy determination or by chemical separations was necessary. Alpha-energies in the rare earths ranged from 2.7 Mev in long-lived Gd^{160} to 4.2 Mev in a 7-minute dysprosium isotope. The alpha-emitting rare earth isotopes are of neutron number 84 or greater and their instability toward alpha-decay is interpreted as being caused by the influence of 82 neutrons.

G8. The Production and Assignment of Ra^{230} and Ac^{230}. William A. Jenkins and Glenn T. Seaborg, *Department of Chemistry and Radiation Laboratory, University of California, Berkeley.*—The bombardment of thorium metal with 180-Mev deuterons in the 184-inch cyclotron, followed by extensive chemistry, has demonstrated the presence of a new isotope of radium. This isotope proved to decay by beta-particle emission with a half-life of one hour and is best assigned to Ra^{230}. Attempts to milk the actinium daughter were unsuccessful and consequently the upper limit of the actinium half-life is set at one minute. The beta-particle energies were measured by

Feather analysis of aluminum absorption curves and by Fermi analysis of a beta-particle spectrograph plot which indicated two beta-distributions with maxima at 2.2 and 1.2 Mev. From the disintegration energies predicted by closed decay energy cycles, it seems most probable that the 1.2-Mev beta is associated with the one-hour decay of Ra^{230} and the 2.2-Mev beta, with Ac^{230}. This assignment was strengthened by the recent discovery by Harvey and Depocas[1] of a 67-minute activity which they assigned to Ac^{229}. This half-life of Ac^{229} has been recently confirmed by the reaction $Ra^{226}(\alpha, p)Ac^{229}$ in this laboratory.

[1] B. G. Harvey (private communication, September, 1951).

FRIDAY MORNING AT 9:00

Room 3, Le Conte Hall

(J. KAPLAN presiding)

H1. Postive Ion Energies in a Point-to-Plane Corona. MARK SCHINDLER AND G. L. WEISSLER, *University of Southern California*.—In a negative point-to-plane corona the energies with which positive ions strike the point electrode are of interest. In order to obtain an estimate of these energies an experiment was undertaken using as a corona point the junction of a thermocouple which had been shaped to conform with previously used electrode configurations.[1] Pure N_2 was used to avoid pulsating corona currents such as Trichel pulses in air, and the thermocouple deflections were noted for various corona currents at three N_2-pressures. These deflections were correlated in a separate calibration of the corona thermocouple with the amount of power from a small heater element necessary to produce the observed deflections. Heat energy losses resulting from conduction, radiation, and convection were taken into account, and energy transfer from positive ions to neutral N_2 molecules in the neighborhood of the point considered. The ion energies were thus estimated to be of the order of 100 ev.

[1] G. L. Weissler, Phys. Rev. 63, 96 (1943).

H2. Electrical Fields in the Crooke's Dark Space of Low Pressure Glow Discharges by Electron Beam Probes. ROBERT P. STEIN, *University of California, Berkeley*.*—An electron beam probe of 10^4 volts and up was made to traverse the Crooke's dark space of 3-cm diameter glow discharges in air and N_2 at from 2×10^{-2} to 1.5×10^{-1} mm pressure, both at various distances from the cathode in the dark space as well as at other points in the glow discharge. The deflections of the beam were calibrated by known fields and thus registered the fields existing. Fields ranging from 400 volts/cm down to 2 volts/cm could be measured. The curves obtained as functions of pressure and current were reproducible and clean cut. Superficially the curves generally confirm the form of variation observed once by Aston with a linear fall in the abnormal region tending to concave upward as the normal region is approached. The data obtained and their interpretation will be presented.

* Supported by the ONR.

H3. Spray Electrification of Liquid Drops. E. E. DODD, *University of California, Berkeley*.*—A determination of the simultaneous size and charge of individual liquid spray drops has been made by the Hopper and Laby method. The statistical ion fluctuation charging theory of Natanson[1] is found to hold for nonconducting liquids in the investigated drop diameter range of about 2 to 30 microns, i.e., the charging probability is Gaussian with the average charge zero and the mean square charge proportional to the drop volume. Contact effects render the charging probability of clean mercury asymmetric, the average charge being positive and increasing with drop size.

* Supported in part by Research Corporation and ONR funds.
[1] G. L. Natanson, Doklady Akad. Nauk. 53, 113 (1946).

H4. Positive Wire Corona Mechanisms in Hydrogen and Argon. EUGENE J. LAUER, *University of California, Berkeley*.* —Mechanisms in the corona discharge from a fine platinum wire at a positive potential along the axis of a hollow nickel cylinder have been investigated by using the oscilloscope to analyze the pulses caused by α-particles passed through the low field region parallel to the wire. The most important secondary electron generating mechanism in the hydrogen discharge is the photoelectric effect at the cathode. γ_p the secondary coefficient for the photoelectric effect has values from 70×10^{-5} at 100-mm to 5×10^{-5} at 650-mm pressure. γ_i for the hydrogen ions at the cathode is less than 10^{-4}. The mobility of the positive hydrogen ions is 13.4 ($\pm$0.4) cm^2/volts $\times$sec at 760 mm and 20°C. γ_i for the argon positive ions is about 9×10^{-4} extrapolated to zero pressure and decreases with increasing pressure. The photon γ_p is less than 1/10 the ion γ_i. Most of the ions are A_2^+ with a mobility of 1.94 ($\pm$0.08) cm^2/volt$\times$sec.

* Supported by the ONR.

H5. Some Experiments Confirming the Existence of Electrical Phenomena during the Freezing of Dilute Aqueous Solutions. MARVIN E. BACKMAN, *U. S. Naval Ordnance Test Station, Inyokern*.—Workman and Reynolds[1] have reported the discovery of an electrical effect accompanying the freezing of dilute aqueous solutions. This effect has been confirmed for several solutions by a simple experimental method. During the orderly freezing of dilute aqueous solutions of ionic solutes a potential is developed across the ice-water interface. A plot of the potential *versus* time is characteristic of the solute and concentration used.

[1] E. J. Workman and S. E. Reynolds, Phys. Rev. 78, 254 (1950).

H6. Further Measurements of Electron Drift Velocities in a Grid Ionization Chamber. W. N. ENGLISH, *Pacific Naval Laboratory, Esquimalt, B.C.*.*—The method used to obtain electron drift velocities in argon-CO_2 mixtures and in methane, in the low X/p range 0.05 to 0.5 volt per cm mm Hg, has been described.[1] Data have now been obtained for neon, krypton, and xenon with CO_2, for argon and krypton with CH_4, and for argon with N_2. Two interesting features have been noted. The first is a maximum in the drift velocity which moves up in X/p as the amount of polyatomic gas is increased. This maximum is tentatively identified with the maximum in the Ramsauer free path. The second is a marked variation in the shape of this maximum with the particular polyatomic gas used. This seems to indicate a surprising sensitivity to the arrangement of the molecular energy levels which are responsible for "moderating" the electrons.

* The measurements were made in the Chalk River Laboratory, in large part by O. W. Schwer.
[1] W. N. English, Phys. Rev. 83, A389 (1951).

H7. On the Theory of Condensation of Gases. R. J. RIDDELL, JR., *University of California, Berkeley.*—The problem of treating the condensation of a gas is intimately related to the asymptotic behavior of the virial coefficients in the equation of state. According to Mayer,[1] the virial coefficients, for a gas in which the intermolecular forces are additive, are obtained as the sum of "irreducible integrals," in which the integrands may be conveniently represented by linear graphs of i points and k lines of a certain type which will be called "stars." Thus the problem of obtaining the virial coefficients is separated into two parts: (a) to find the number of stars of a particular type (a purely combinatorial problem), and (b) to calculate the value of the integral associated with them. The first problem was studied in detail and an exact equation for the generating function of the number of stars was obtained. This may be solved asymptotically in i and k. The first approximation gives the result that all graphs are stars. The evaluation of the integrals for rigid spheres was also investigated but with little success. The asymptotic contributions to the virial coefficient for $k=i$ and $k=i+1$ were obtained.

[1] Mayer and Mayer, *Statistical Mechanics*, Chapter 13.

FRIDAY MORNING AT 11:00

Room 310, Le Conte Hall

(E. O. LAWRENCE presiding)

Invited Papers

I1. Radioactivity of the Heaviest Elements. I. PERLMAN, *University of California, Berkeley.* (30 min.)

I2. The Fine Structure of Hydrogen. WILLIS E. LAMB, *Stanford University.* (30 min.)

FRIDAY AFTERNOON AT 1:30

Room 1, Le Conte Hall

(R. T. BIRGE presiding)

J1. The Decay of Ag^{105} and Ag^{106}. RAYMOND W. HAYWARD, *National Bureau of Standards.*—Using a magnetic lens and a scintillation spectrometer, studies were made on the K-capture activities of Ag^{105} and Ag^{106} which were produced by (α, n) and $(\alpha, 2n)$ reactions on rhodium and by (d, n) and $(d, 2n)$ reactions on palladium using the Department of Terrestrial Magnetism sixty-inch cyclotron. Conversion and photoelectron peaks were found corresponding to nineteen different transitions. By following the decay rate of each peak over a period of three months the isotopic assignment of each transition was made. The observed transition energies in Ag^{105} are 62, 112, 154, 180, 281, 321, 343, 393, and 444 kev and in Ag^{106} the energies are 222, 399, 409, 511, 620, 717, 815, 1040, 1220, and 1550 kev with a probable error of approximately one percent. Gamma-gamma coincidences were observed in both isotopes and also specifically coincidences between the 62- and 281-kev gamma-rays of Ag^{105} were measured with a scintillation spectrometer coincidence detector. The K and L conversion ratios were determined for the stronger radiations. The 511-, 620-, 1040-, and 1550-kev gamma-rays are among those observed by Alburger[1] in the decay of Rh^{106}. Decay schemes based on experimental information and on shell model considerations will be proposed for both Ag^{105} and Ag^{106}.

[1] David E. Alburger, Bull. Am. Phys. Soc. 26, No. 6, 38 (1951).

J2. Measurement of Gamma-Rays in the Reaction $C^{13}(p, \gamma)N^{14}$.* H. H. WOODBURY, R. B. DAY AND A. V. TOLLESTRUP, *Kellogg Radiation Laboratory, California Institute of Technology.*—A NaI scintillation spectrometer has been used to study the γ-rays produced at various resonances[1] in the reaction $C^{13}(p, \gamma)N^{14}$. The target, which was 20-kev thick at 1.7 Mev, was composed of carbon enriched to 60 percent C^{13} deposited on a tantalum backing. Preliminary results on the energies of the stronger γ-rays are summarized in Table I, where E_R is the proton bombarding energy at resonance and E_x is the excitation energy of the compound nucleus, N^{14}. Further efforts are being pointed toward improving the precision of these measurements as well as measuring the energies of several weak γ-rays that occur. Coincidence experiments are also being carried out to aid in determining the decay scheme.

TABLE I.

E_R(Mev)	E_γ(Mev)	E_x(Mev)
0.55	1.6, 2.3, 4.1, 8.0	8.05
1.16	1.6, 2.3, 4.0, 4.6	8.62
1.25	8.7	8.70
1.76	9.2	9.18
2.1	4.5, 5.0	9.49

* This work was assisted by the joint program of the ONR and AEC.

[1] Seagrave, Day, and Perry, Jr., Phys. Rev. 81, 661 (1951).

J3. A New Gamma-Ray from $C^{13}+p$.* A. V. TOLLESTRUP, R. B. DAY, AND H. H. WOODBURY, *Kellogg Radiation Laboratory, California Institute of Technology.*—The γ-radiation from the reaction $C^{13}+p$ has been investigated with a NaI scintillation spectrometer. A new γ-ray has been observed in addition to the 2.4- and 3.5-Mev γ-rays produced at the 0.46- and 1.70-Mev resonances, respectively. Its assignment to the C^{13} reaction was made by comparing the yield from thin targets of normal carbon with a thin carbon target enriched to 60 percent C^{13}. This γ-ray has been observed for proton bombarding energies from 1.2 to 2.5 Mev. Preliminary estimates indicate that the yield does not vary by more than a factor of five in this region. Within the experimental error of ± 4 per-

cent the γ-ray energy is given by $E\gamma = 0.92\,(E_p - 0.46)$ Mev. Since no 2.4-Mev γ-radiation is found with this γ-ray we conclude that it occurs in a transition to the 2.4-Mev state of N^{13}, which subsequently decays into a proton and C^{12}.

* This work was assisted by the joint program of the ONR and AEC.

J4. Investigation of the Reaction $B^{11}(p, \lambda)C^{12}$.* TORBEN HUUS AND ROBERT B. DAY, *Kellogg Radiation Laboratory, California Institute of Technology.*—The excitation curve for the reaction $B^{11}(p, \gamma)C^{12}$ has been investigated by means of a NaI scintillation counter in the region of proton bombarding energies from 0.14 Mev to 2.7 Mev. Besides the well-known resonance at 0.162 Mev, two other resonances were found, one at 0.67 Mev with $\Gamma = 0.31$ Mev, and another at 1.37 Mev with $\Gamma = 1.15$ Mev. An estimate of the cross sections is given in Table I. The γ-ray energies were obtained from the pulse

TABLE I.

E_p in Mev	ϵ in 10^{-29} cm²	E_γ in Mev		
0.162	1.1	4.45	11.6	
0.67	0.4	4.44	12.0	16.4
1.37	0.4	4.45	12.7	16.9

height spectrum by comparison with the 2.62-Mev ThC'' γ-ray. They confirm the existence of a cascade transition through the well-known level in C^{12} at 4.45 Mev. The cascade transition was found to be resonant only at the two lower resonances, and the ground-state transition only at the 1.37 Mev resonance, but in none of the cases can a small amount of the alternative transition be completely excluded. The results are consistent with the interpretation that the two broad resonances are an inverted doublet formed by s-wave protons.

* Assisted by the joint program of the ONR and AEC.

J5. Elastic Scattering of Li^7+p and $C^{13}+p$. WILLIAM D. WARTERS AND EDMUND A. MILNE, *Kellogg Radiation Laboratory, California Institute of Technology.*—A double focusing magnetic proton spectrometer[1] has been so mounted as to permit observations over a continuous range of scattering angles from 0 to 160 degrees. A fluxmeter and current control system have also been built, allowing spectrometer settings accurate to well within 0.1 percent. This equipment is being used to study the elastic scattering of protons from Li^7 and C^{13}. Data have been taken for Li^7 near the 440-kev resonance at 50, 70, 90, 145, and 160 degrees in the center-of-mass system. The cross sections at 90 and 145 degrees agree with previous results from this laboratory.[2] Analysis of the data is currently in progress. Data have been taken for C^{13} near the 456-kev resonance at every 10 degrees from 40 to 160 degrees. Preliminary analysis, confirming the previous work,[3] indicates that the 456-kev level is probably a $^2S_{\frac{1}{2}}$ state in N^{14}.

* Assisted by the joint program of the ONR and AEC.
[1] Snyder, Ruben, Fowler, and Lauritsen, Rev. Sci. Instr. 21, 852 (1950).
[2] Brown, Snyder, Fowler, and Lauritsen, Phys. Rev. 82, 159 (1951).
[3] G. Goldhaber and R. M. Williamson, Phys. Rev. 82, 495 (1951).

J6. Cross Section of the $D(d, p)H^3$ Reaction.* W. A. WENZEL AND WARD WHALING, *Kellogg Radiation Laboratory, California, Institute of Technology.*—The cross section of the $D(d, p)H^3$ reaction has been determined over the deuteron energy range 25–550 kev from the yield of protons from a thick target of D_2O ice and the stopping cross section of ice given in the previous abstract. The angular distribution over the deuteron energy range 200–550 kev was obtained from measurements of the yield of protons from a thin ice target at 10° intervals between 80° and 170° in the laboratory. At lower energies the asymmetry factor[1] $Y(\theta) = Y(90°)[1 + (0.175 + 0.0031\ E_{kev})\cos^2\theta]$ was used to calculate the total cross section from the observed yields at $150_{lab}°$. The total cross section is given in Table I. The 16-inch double focusing mag-

TABLE I.

E_p(kev)	25	50	100	200	300	400	500
σ(barns)	$6.4\ 10^{-4}$	$4.3\ 10^{-3}$	$1.7\ 10^{-3}$	$3.3\ 10^{-3}$	$4.7\ 10^{-3}$	$5.7\ 10^{-3}$	$6.5\ 10^{-3}$

netic analyzer was used to measure the cross section at energies above 200 kev by observation of both protons and tritons. Values obtained by this method fall below the values given in the table by at most 20 percent.

* Assisted by the joint program of the ONR and AEC.
[1] Bretscher, French, and Seidl, Phys. Rev. 73, 815 (1948).

J7. The Stopping Cross Section of Ice.* WARD WHALING AND W. A. WENZEL, *Kellogg Radiation Laboratory, California Institute of Technology.*—The stopping cross section $\epsilon = (1/N)dE/dx$ for protons in D_2O ice has been measured over the proton energy range 50–550 kev. The 16-inch double-focusing magnetic analyzer was used to determine the energy E_P of protons scattered at $\theta_{LAB} = 90°$ from a clean Cu target and then the change of energy ΔE_P of the scattered protons when a thin (≈ 5 kev) layer of ice was condensed on the surface of the copper. Relative values of ϵ as a function of proton energy are calculated from the variation of ΔE_P with E_P. Absolute values of ϵ were determined from the yield of protons scattered from the 0 in the ice, which is a known[1] function of ϵ and the scattering cross section for protons on oxygen. Taking this scattering cross section as given by the Rutherford formula we have determined ϵ in terms of the thick target yield over the energy range 250–500 kev. Using these results and the relative values we find the following values for the stopping cross section. Evidence that the scattering

E_P(kev)	20	50	100	200	300	400	500
$\epsilon(10^{-15}$ ev-cm²)	19	25	26	22	17	14	12

from 0 should be described by the Rutherford formula will be presented.

* This work was assisted by the joint program of the ONR and AEC.
[1] Snyder, Rubin, Fowler, and Lauritsen, Rev. Sci. Instr. 21, 866 (1950).

J8. Low-Lying Levels in Be^7 and B^{10}.* ROBERT B. DAY AND TORBEN HUUS, *Kellogg Radiation Laboratory, California Institute of Technology.*—The γ-radiation produced by bombarding B^{10} with protons has been investigated with a NaI scintillation spectrometer in a search for low energy levels in Be^7 that are excited by the reaction $B^{10}(p, \alpha)Be^7$.* In the region below 1 Mev we find γ-rays of the following energies: 178 ± 10 kev, 432 ± 2 kev, and 718 ± 5 kev. The energy of the first is rendered somewhat uncertain by the presence of a nearby γ-ray that is produced in the tantalum target backing, but its energy and intensity are consistent with the interpretation that it is Compton scattering of the 432-kev γ-ray from the surroundings. The second γ-ray is from a well-known level in Be^7, while the third is probably produced by inelastic scattering in B^{10}. Excitation curves for the last two γ-rays have also been investigated up to bombarding energies of 2.7 Mev. The 432-kev radiation has a single broad resonance at 1.52 Mev. The cross section $(4\pi \cdot \sigma_{90°})$ for the 718-kev radiation increases monotonically from $5 \cdot 10^{-4}$ barns at 1.52 Mev to 0.02 barn at 2.65 Mev.

* Assisted by the joint program of the ONR and AEC.

FRIDAY AFTERNOON AT 1:30

Room 4, Le Conte Hall

(F. BLOCH presiding)

K1. On the g Factor of Metallic Na.* Y. YAFET, *University of California, Berkeley.*—The spectroscopic splitting factor that one would observe in a microwave experiment on solid Na is calculated. On account of the strong coupling between electronic spins, it is assumed that in most of the transitions only the component of the total spin along the applied field changes. Correlation effects do not play a role in such transitions and the one-particle approximation may be used. The conduction electrons at the top of the Fermi band are practically free ($m^*=1.069$),[1] so that one expects a g close to g_{spin}. Departures from this value will arise, because of spin-orbit and spin-nuclear effects. The latter is found to be comparable to the first one only at temperatures low enough to have a large nuclear alignment, $\sim 1°$K. The spin-orbit effect has been treated as a perturbation and the resulting inhomogeneous equation solved numerically to the first order by a development of the Bardeen method.[2] The angular momentum is quenched as long as spin-orbit interaction is not taken into account. The admixture caused by spin-orbit interaction is mainly from a p term and depends on the angle θ_0 between the propagation vector and the applied field, resulting in $\Delta g=-3.7\times 10^{-4}\sin^2\theta_0$. The corresponding broadening is of the same order of magnitude as the relaxation line width.[3]

* Assisted by the ONR.
[1] J. Bardeen, J. Chem. Phys. **6**, 367 (1938).
[2] A. W. Overhauser, thesis, University of California.

K2. Spin-Echo Measurements of Nuclear Spin-Spin Coupling.*,† E. L. HAHN‡ AND D. E. MAXWELL, *Stanford University.*—Molecules which contain nuclear magnetic moments as close, nonequivalent neighbors exhibit the spin-echo envelope modulation effect.[1] Resonant H and F^{19} nuclei indicate on the echo envelope (1) a frequency δ, proportional to the dc magnetic field H_0, which corresponds to the chemical shift between like nuclear species, and (2) a second frequency J, which is independent of H_0. Echo measurements for two protons in liquid dichloroacetaldehyde (CCl_2HCHO) give $J/2\pi=2.8$ cps and $\delta/2\pi=104$ cps. The envelope shape is predicted if the Hamiltonian operator

$$\mathcal{H}=-\hbar[\gamma\sigma_{1z}(H_0+h_1)+\gamma\sigma_{2z}(H_0+h_2)+J/4\bar{\sigma}_1\cdot\bar{\sigma}_2]$$

is chosen to describe the system. h_1 and h_2 are absolute chemical shifts in gauss of nuclei 1 and 2, respectively, and $\delta=\gamma(h_1-h_2)$. The possibility that J has its origin in the magnetic coupling of spin-to-spin via electrons has been considered.[2]

* Supported in part by the ONR.
† Independent work on this coupling effect has been done by McNeil, Slichter, and Gutowsky at the University of Illinois.
‡ National Research Council Post-doctoral Fellow.
[1] E. L. Hahn, Phys. Rev. **80**, 580 (1950).
[2] Suggested independently by Gutowsky, McCall, and Slichter, Phys. Rev. **84** (in press). E. M. Purcell and N. F. Ramsey (private communication) have calculated J for the HD molecule on the basis of a spin-electron-spin coupling mechanism which can account for large values of J.

K3. Nuclear Magnetic Resonance Absorption in Glycine. T. M. SHAW, R. H. ELSKEN, AND K. J. PALMER, *Western Regional Research Laboratory,* Albany, California.*—The magnetic resonance absorption of protons in a polycrystalline specimen of glycine has been observed in a magnetic field of approximately 4600 gauss for temperatures ranging from 25°C to −160°C. The line width of the resonance[1] is found to undergo a transition centered near −70°C. For temperatures above the transition (25° to −65°C) the observed line width is 9.5±0.5 gauss. For temperatures below the transition (−80°C to −160°C) the observed line width is 16.6±1 gauss. Calculations of the theoretical second moment of the absorption line for a rigid lattice yield a value of about 44 gauss[2] if a $H_3N^+CH_2COO^-$ (zwitter-ion) configuration[3] is assumed (the actual value depends upon the assumed position of the third proton on nitrogen) and a value about one-half as large for the uncharged form (NH_2CH_2COOH). Experimental values of the second moment compare favorably with the theoretical value for the zwitter-ion configuration.

* Bureau of Agricultural and Industrial Chemistry, Agricultural Research Administration, U. S. Department of Agriculture. Report of a study made under the Research and Marketing Act of 1946.
[1] H. S. Gutowsky and G. E. Pake, J. Chem. Phys. **16**, 1164 (1948).
[2] G. Albrecht and R. B. Corey, J. Am. Chem. Soc. **61**, 1087 (1939).

K4. Nuclear Magnetic Resonance in Metallic Rb and Cs. D. F. ABELL AND W. D. KNIGHT, *University of California, Berkeley.*—A check on the validity of the formula[1] for the shift of nuclear magnetic resonance absorption frequencies in metals should be found in the consistency of experimental results in simple metals. We report here the results for Rb and Cs, and compare them with previously published values for Li and Na. General agreement is good, although reliable independent values for χ_p and $\langle|\psi_p(0)|^2\rangle_{Av}/|\psi_a(0)|^2$ are not available, except perhaps for Na. The measured values of $\Delta H/H$ are 0.02, 0.1, 0.6, and 1 percent, respectively, for Li*, Na, Rb, and Cs, at room temperature of about 25°C. The product of χ_p and the ratio of wave functions above, evaluated in terms of formula (1), reference 1, is a smoothly decreasing function of atomic number, following very closely a plot of Pauli's formula for χ_p. The significance of this is not clear, in view of the wide range of independent theoretical and experimental values for χ_p.

[1] Townes, Herring, and Knight, Phys. Rev. **77**, 852 (1950).
* The value given in reference 1 is incorrect.

K5. Properties of Transition Metals V and Nb by Nuclear Magnetic Resonance. W. D. KNIGHT, *University of California, Berkeley.*—The magnetic properties and the electronic structures in the transition metals are of considerable interest.[1,2] We report here concerning line shifts and line widths of nuclear magnetic resonance absorption signals in V* and Nb metals. The products $\chi_p\langle|\psi_p(0)|^2\rangle_{Av}/|\psi_a(0)|^2$, evaluated in terms of the line shifts, are 0.38×10^{-6} and 0.22×10^{-6} cgs/gm for V and Nb, respectively. Assuming a spin susceptibility χ_p given by Pauli's formula for one s-electron per atom, the ratios of the wave functions as above are 2.5 and 2.2. This is in general agreement with the idea of contraction of the s-wave functions when free atoms condense to the metallic state. These values are only approximate, since formula (1), reference 1 in preceding abstract, includes hyperfine structure interval factors for atomic s-states, and these are not known very accurately. The line widths between points of maximum slope are 16 gauss and 12 gauss for V and Nb. These are about two orders of magnitude greater than would be expected to result from simply nuclear magnetic dipolar coupling, and are probably caused by quadrupolar coupling with the crystalline field and to anisotropy of the line shift because of lattice strains at the powder particle surfaces.

* Measurements on V made by the author at Brookhaven National Laboratory under the auspices of the AEC.
[1] C. Zener, Phys. Rev. **81**, 441 (1951).
[2] Hume-Rothery, Irving, and Williams, Proc. Roy. Soc. (London) **A208**, 431 (1951).

K6. Theory of the Nuclear Quadrupole Interaction of Nb^{93} in $KNbO_3$.* M. H. COHEN, *University of California, Berkeley.*†—Optical hyperfine structure measurements have shown that the spin of Nb^{93} is 9/2 but have failed to show any

quadrupole coupling, $KNbO_3$, a ferroelectric, has a twinned orthorhombic structure at room temperature. At 220°C a transition to tetragonal symmetry occurs. The electric field-gradient tensor is axially symmetric in a crystal of tetragonal symmetry but not in one of orthorhombic symmetry. A crude estimate of the gradient of the local field was made from the measured values of the maturation polarization and the lattice distortion. An approximate value of the quadrupole moment was taken from Townes' empirical plot. Combined these yield an estimated order of magnitude of 1 mc for the Stark splitting in the crystalline field. Second-order perturbation calculations of the energy levels for spin 9/2 in a strong magnetic field have been carried out for an axially symmetric field gradient and for an unsymmetric field gradient.

* Assisted in part by the ONR.
† AEC predoctoral fellow.

K7. Chemical Effects in Nuclear Induction. J. T. ARNOLD, *Stanford University.* (Introduced by F. Bloch.)—Using a carefully shimmed magnet and small samples, we have been able to resolve nuclear induction signals having a separation of approximately two milligauss in 7600 gauss. This degree of resolution has facilitated the observation of temperature and dilution dependence of the absolute chemical shifts of the OH groups of methyl and ethyl alcohols[1] and a slight splitting of hydrogen and fluorine signals in certain chemical compounds.[2] The absolute chemical shift of the OH group of ethyl alcohol was measured as a function of temperature in the interval, 150°K to 350°K.[3] Dilution experiments were made with chloroform and carbon tetrachloride. Two of the lines of ethyl alcohol and numerous lines of fluorine-substituted compounds show multiplicity under slow passage observation. In the case of ethyl alcohol, to within the limit of resolution, the CH_3 line consists of three, and the CH_2 line of four components.[4] The multiplet splitting of the fluorine lines is about ten times that of the hydrogen lines.

[1] J. T. Arnold and M. E. Packard (to be published in J. Chem. Phys.).
[2] M. E. Packard and J. T. Arnold, Phys. Rev. **83**, 210(A) (1951).
[3] Two possible explanations have been proposed by N. F. Ramsey and U. Liddel in a letter to be published in the J. Chem. Phys.
[4] A rule from which these numbers of components could have been expected has been given by H. S. Gutowsky and D. W. McCall, Phys. Rev. **82**, 748 (1951). It is also in agreement with the phenomenological theory of E. L. Hahn.

FRIDAY AFTERNOON AT 3:30

Room 310, Le Conte Hall

(R. T. BIRGE presiding)

Invited Papers

L1. Energy Loss of Fast Particles. ROBERT F. CHRISTY, *California Institute of Technology.* (30 min.)
L2. High Energy Proton-Deutron Scattering. OWEN CHAMBERLAIN, *University of California, Berkeley.* (30 min.)

SATURDAY MORNING AT 9:00

Room 1, Le Conte Hall

(H. E. WHITE presiding)

M1. Design and Operation of a High Geometry Electrostatic Time-of-Flight Mass Spectrograph. WILLIAM E. GLENN, *Department of Electrical Engineering and Radiation Laboratory, University of California, Berkeley.*—A mass spectrograph has been designed and constructed which measures e/m by measuring the time-of-flight of ions that have been accelerated and bunched by electrostatic fields. This instrument is similar to the Smyth and Wilson "Isotron." It has been able to collect about 30 percent of the ions formed of a given isotope. The resolution is such that the width of the intensity *versus* mass peaks is $\frac{3}{4}$ of a mass unit wide at 1 percent of the maximum intensity for all masses. The stability and linearity of the mass calibration is accurate to less than 1/10 of a mass unit. Experimental determinations of the geometry, resolution, and calibration were made with rubidium, cesium, and thallium. Methods of detection include the use of an electron multiplier and vibrating reed electrometer. Methods of eliminating the direct, neutral beam and ions of the wrong transit time have been devised. The instrument can be used for the isolation of individual artificially produced radioactive isotopes and some preliminary experiments of this type have been performed.

M2. Microscopy by Reconstructed Wave-fronts. HUSSEIN M. A. EL-SUM AND PAUL KIRKPATRICK, *Stanford University.*—Holograms produced by the method of Gabor[1] produce good reconstructions even when the illuminating radiation is far from monochromatic. White light may be used successfully, even with panchromatic film. This result is evidence of the great relative importance of the low order fringes. A hologram of a collection of object features not lying in the same plane normal to the illuminating beam admits of reconstruction so that any desired plane of the distributed object may be brought into focus. Examples are presented. Holograms may be produced with x-rays and reconstructed with visible light. A hologram made from a published x-ray diffraction pattern by Kellstrom yielded a good reconstruction corresponding to the published description of the object. Methods have been developed for getting rid of nearly all of the hologram noise resulting from dirt, defects in glass parts, and optical non-uniformity of the photographic film base.

[1] D. Gabor, Proc. Phys. Soc. (London) **B114**, 449 (1951).

M3. Use of Successive Diffractions to Double or Quadruple the Resolving Power of a Grating. F. A. JENKINS AND L. W. ALVAREZ, *University of California, Berkeley.*—The

availability of blazed gratings suggests the possibility of reflecting the light back to the grating one or more times to obtain increased dispersion and resolving power. One method utilizes a plane mirror which is placed in a parallel beam from the grating.[1] Greater intensity for a given dispersion was obtained thereby, but no increase in resolving power. By using two mutually perpendicular plane mirrors as a reflex combination in the focal plane of a concave grating, an arrangement similar to that suggested by Walsh[2] for prism monochromators, we have succeeded in doubling the resolving power hitherto obtainable with this grating. Spectra of Hg and I_2 corresponding to the fourth order of a 30,000 line/in grating were photographed, whereas only the second order of the same wavelength is observable in single diffraction. The astigmatism is annulled in an even number of diffractions, yielding a saving in intensity. Since it can be shown that the width of the line is not increased in successive diffractions, the resolving power is proportional to the dispersion and to the number of diffractions.

[1] E. Hulthén and E. Lind, *Arkiv Fysik*, **2**, 253 (1950).
[2] A. Walsh, *Nature* **167**, 810 (1951).

M4. Resolution and Sensitivity of Microwave Spectrographs.* H. R. JOHNSON, *Research Laboratory of Electronics, Massachusetts Institute of Technology.*—Obtaining narrow lines in microwave spectroscopy is important, since it determines whether or not fine structure can be resolved and the accuracy with which it can be measured. Sensitivity determines whether or not weak lines can be observed at all. We have used a Stark modulation spectrograph in our laboratory for over a year; in *K*-band it yields line half-widths at half intensity of 50 kc/sec and has a limiting sensitivity of 10^{-9} cm^{-1} with a Stark cell 1 m long and a 5-sec time constant. The factors responsible for this line width will be discussed, and an equation from which the ultimate sensitivity of our Stark spectrographs can be predicted will be presented. This discussion will include the effect of detector crystal noise and Stark modulation frequency. It will be shown that for most purposes a Stark modulation frequency of about 6 kc/sec is optimum, and that the generally accepted expression for optimum cell length is incorrect for our spectrographs. The optimum length is greater by a calculable factor that is typically about 5 or 10.

* This work has been supported in part by the Signal Corps, the Air Materiel Command, and the ONR.

M5. The Reflection of X-Rays and the X-Ray Microscope. L. M. RIESER, JR., *Stanford University.*—A large number of accurate measurements on the reflection of x-rays from evaporated films have recently been made, stimulated in part by the development of the x-ray microscope. Applications of some of these results to this instrument are discussed. Among the important features of a satisfactory reflector for x-rays are small particle size to reduce scattering and relation of absorption to refractive index. Results of measurements at $\lambda = 1.54$A and $\lambda = 2.28$A indicate that beryllium, aluminum, nickel, gold, and perhaps iridium are suitable reflectors when deposited on glass, while chromium, copper, and silver are not. Silver, used so frequently in the early version of this instrument, has little to recommend it other than ease of evaporation. Knowledge of the ratio of reflected to incident intensity becomes increasingly important in the design of the compound microscope described in paper M7. In this instrument the x-rays appearing in the final image undergo four reflections, emphasizing the importance of a reflector, such as glass or aluminum to insure uniform distribution across the field and sufficient total intensity. Mere striving for high critical angle in the choice of x-ray mirrors is not sufficient.

M6. The Structure and Stability of Thin Evaporated Metallic Films. MARSDEN S. BLOIS, JR., *Stanford University.*—The dependence of the structure and stability of thin (10A–1000A) evaporated metallic films upon the nature of the metal, nature of the substrate, and the evaporation parameters has been investigated using electron microscopy, the optical absorption spectra, and density measurements. The absorption spectra of thin (~10A) silver films was found to depend upon the particle sizes of these particulate deposits, and the absorption maximum characterizes them in a convenient manner. The change of structure undergone by these films as the evaporation parameters are varied, is thus indicated by gross color changes of the films. These structural changes are also observed with the electron microscope. The densities of a series of silver and copper films were measured using a thickness determination given by a Tolansky multiple beam interferometer, the mass being determined directly with a semimicro balance. The plot of density *vs* thickness gives evidence for the strong migration of these metals in the early stages of film formation while the outer layers to be deposited form on top of the underlying metal to build up an apparently normal solid structure with the result that for thick films the density asymptotically approaches that of the bulk metal.

M7. The Compound X-Ray Microscope. H. H. PATTEE, JR., *Stanford University.* (Introduced by Paul Kirkpatrick.)—A simple x-ray microscope using a pair of crossed concave mirrors has been described by Kirkpatrick and Baez.[1] Limitations on resolution, speed, and width-of-field are discussed. A method is described for designing a compound x-ray microscope using two pairs of crossed mirrors giving great improvement over the simple system in resolution, speed, and width-of-field. Mirrors must be aspherical surfaces, with extremely precise contours and smooth metallic coating to realize optimum theoretical performance. Multiple-beam interferometry allows determination of average contours of mirrors to about ±10A. Smoothness of metallic coats may be observed by electron microphotographs of replicas. A compound x-ray microscope has been constructed using only spherical mirrors. This has several advantages over a simple system using spheres, but will not approach the capabilities of an aspherical compound system. A technique for producing extremely small, intense, focused beams of x-rays at a known location on a specimen is being developed. This would allow microdiffraction and microabsorption measurements to be made on volumes of the order of 10^{-15} cm^3.

[1] P. Kirkpatrick and A. V. Baez, J. Opt. Soc. Am. **38**, 766 (1948).

M8. Acceleration of Multiply Charged Nuclei.* CORNELIUS A. TOBIAS, *University of California, Berkeley.*—A method is proposed for cyclotron acceleration of nuclei ${}_zA$ to high energies without limitation in their atomic number z. A low voltage external ion source is used in which an intense beam of ions with low multiplicity of charge, e.g., ${}_zA^{(++)}$ is made. These ions are "preaccelerated" in a linear accelerator to a velocity which is somewhat higher than the velocity of the *K*-electrons of ${}_zA$. Only those ions remain usable which retain their charge (++) during the entire preacceleration, without electron exchange. If the gas pressure of the accelerator is low enough a large fraction of ${}_zA^{(++)}$ is retained and can be injected in a frequency modulated cyclotron tangentially to a cyclotron orbit for ${}_zA^{(++)}$. When the cyclotron orbit is reached, the ions ${}_zA^{(++)}$ are passed through the edge of a thin metal foil which strips them of all their electrons, forming ${}_zA^{(++)}$. If the ions arrive in proper phase, they will be accelerated in the cyclotron without much further loss because of electron exchange. A similar preaccelerator can be used for tangential injection of the stripped ions ${}_zA^{(++)}$ in the bevatron.

* This work was supported by the AEC.

M9. Relative Spectral Sensitivity Calibration of Electron Multiplier Phototubes in the 2500A–3500A Region. E. H. GILMORE AND R. H. KNIPE,* *U. S. Naval Ordnance Test Station, Inyokern.*—The utility of the electron multiplier

phototube is enhanced in certain studies if its relative spectral sensitivity curve can be determined. The 1P-28 type extends the useful spectral range to about 2200A in the ultraviolet; however, relative spectral sensitivity determinations at wavelengths shorter than 3500A are in general considerably more difficult than those at longer wavelengths. The authors have calibrated some of these tubes by a comparison of the phototube response with that of a thermopile. Two methods of accomplishing the required nonselective attenuation have been employed: the standard method of increasing the separation of the source from the monochromator used, and a method whereby the attenuation is accomplished by use of a diffusely reflecting surface. In general the standard deviation from the mean curve obtained is less than eight percent. Calibration by the use of the diffuse reflector proved to be the more rapid method of the two, and is, in the opinion of the authors, freer of pitfalls.

* Now at Duke University.

M10. Precision Measurement of Uniformity of Materials by Gamma-Ray Transmission.* JOHN N. HARRIS AND ARTHUR I. BERMAN, *Los Alamos Scientific Laboratory.*—The uniformity of the product of thickness and density (i.e., mass per unit area) of materials of constant mass absorption coefficient is determined by measurements of the variation in gamma-ray transmission. The radiation is detected with a scintillation detector and vibrating-reed electrometer. For a given incident intensity, maximum sensitivity is attained when a source is chosen which emits gamma-rays whose mean free path in the material under investigation equals the thickness. This optimum condition for cobalt-60 radiation obtains for thicknesses of 3, 1, and ½-in. of Al, Fe, and U, respectively; using a 1-curie source, variations of 0.01 percent in the uniformity of plates of these thicknesses have been measured. The method may be applied also to the scanning of curved surfaces and extended materials where the source and detector cannot permanently be fixed with respect to each other. For this latter case, the problem of compensating for the effect of source-detector misalignment is considered.

* Work performed under the auspices of the AEC.

M11. Ion Trajectories in the Omegatron. CLIFFORD E. BERRY, *Consolidated Engineering Corporation.*—The Omegatron is a mass spectrometer in which an alternating electric field acts normal to a uniform magnetic field.[1] Ions having a cyclotron resonant frequency equal to the frequency of the applied electric field travel in unbounded spiral orbits. Ions out of resonance pursue bounded orbits.

For a strictly two-dimensional system, the equations of motion are readily solved to give the ion trajectories. The general solutions including both arbitrary phase angle and initial velocity vector will be given. From these solutions, the resolving power and path length are readily derived, and, in addition, the following conclusions can be drawn: (a) The phase angle between the time of origin of an ion and the exciting voltage has only a minor effect on the path length. (b) At any given time, all resonant ions lie within a narrow band on a rotating radial spoke. (c) At any given time, all nonresonant ions of a given mass lie within a narrow band about a circle intersecting the origin and rotating about the origin. That diameter of this circle which passes through the origin is always normal to the radial spoke of the resonant ions.

[1] Sommer, Thomas, and Hipple, Phys. Rev. **82**, 697 (1951).

M12. Effect of Chemical Structure on Stopping Powers for High Energy Protons. T. J. THOMPSON. *University of California, Berkeley.*—The stopping power of various organic compounds relative to copper is being measured for protons of mean energy 270 Mev. The compounds selected consist of C, H, N, O, and Cl in various combinations so that possible structural effects on the stopping power may be observed. The sample thickness is selected so as to reduce the energy of the beam from 340 Mev to approximately 200 Mev. The remainder of the proton range is dissipated in copper absorbers of variable thickness. Ionization chambers before and behind the absorber column are used to obtain Bragg curves of absorber thickness *vs* relative ionization in the usual manner. It is known that the stopping power of a compound is very nearly an additive function of the stopping power of the elements making up the compound. The relative stopping power at 270 Mev, while not strictly additive, is, in the case tested, additive within the accuracy of most nuclear experiments. There appears to be, however, a measurable deviation from additivity. Preliminary results, which must be further verified, indicate that unsaturated compounds (e.g., benzene) have slightly higher stopping power than would a mixture of graphite and saturated compound (e.g., cyclohexane) of the same atomic constitution. Details will be discussed. Experiments with other compounds and solutions and the liquid gases are being carried out.

SATURDAY MORNING AT 9:00

Room 4, Le Conte Hall

(R. T. BIRGE presiding)

N1. Theory of the Angular Width of Cerenkov Radiation from a Particle Undergoing Multiple Scattering. K. G. DEDRICK, *Stanford University.*—A theoretical formula is being developed to describe the Cerenkov radiation from a fast particle traveling through a substance consisting of screened Coulomb potential centers. The procedure is to calculate the radiation from a series of short connected segments with angles between them corresponding to single scattering. This expression is then averaged over the single scattering angles to obtain the distribution of radiated power in terms of the viewing angle. It will contain contributions due both to the average change in direction of the scattered particles, and to the partial incoherence of the radiation from the individual path segments.

N2. Cerenkov Radiation from Positrons. T. C. WILFONG, JR., AND J. E. HENDERSON, *University of Washington.*—Preliminary results indicate that Cerenkov radiation has been obtained using positrons from copper 64 and zinc 63, both of which were prepared in the University of Washington Cyclotron. Intensity considerations required the design of equipment in which a large fraction of the positrons emitted from a broad source are focused by a magnetic field upon a special Lucite target. Shields serve to eliminate any electrons that might be present. In addition two nearly symmetrical lucite paraboloids of revolution with the target at their joint apex serve to gather the radiation over a large solid angle. One paraboloid collects radiation in the direction of motion of the positron and the other collects radiation going in the opposite

direction. Asymmetry between the radiation in the two directions is taken as indication that Cerenkov radiation exists. Gamma-rays were distinguished from the Cerenkov radiation by thin obstacles over portions of the films used to detect the radiation. Although no intensity measurements have been made as yet, our results indicate that the efficiency of production is approximately the same as that of ordinary electrons.

N3. A New Type Cerenkov Counter.* ROBERT W. BIRGE, *University of California, Berkeley.*—A new type Cerenkov counter has been built that uses ideas similar to those suggested by I. A. Getting.[1] In our counter the center portion is cut out to reduce the amount of light due to scintillations. Previous tests of Getting's counter by R. H. Dicke[2] were not conclusive, mainly because of the lack of a fast coincidence circuit to eliminate phototube noise. However, the recent experiments by John Marshall[3] indicate that a Cerenkov counter can be made to work. The counter to be described was tested in coincidence with a stilbene crystal using a circuit with a resolving time of about 10^{-9} seconds, developed by Lee Neher at the Radiation Laboratory. Transition curves were taken using the gamma-rays from π^0-meson decay in the target of the 184-inch cyclotron. Evidence will be given to show that Cerenkov radiation from the resulting electrons can be detected with reasonable efficiency.

* This work was performed under the auspices of the AEC.
[1] I. A. Getting, Phys. Rev. **71**, 123(L) (1947).
[2] R. H. Dicke, Phys. Rev. **71**, 737(L) (1947).
[3] J. Marshall, Phys. Rev. **81**, 275(L) (1951).

N4. High Energy Photoprotons from Carbon.* J. W. ROSE AND W. S. GILBERT. *University of California, Berkeley.*—A study is being made of the high energy protons ejected from carbon by the 322-Mev bremsstrahlung of the Berkeley synchrotron. The protons are detected by means of a counter telescope consisting of three liquid scintillators each viewed by two or three 1P21 photomultiplier tubes connected in parallel. The protons are required to stop in the second counter, and pulse-height analysis in the first counter is used to differentiate between protons and mesons. $d\sigma/d\Omega$ per equivalent quantum, Q, has been measured at 90° in the lab. Preliminary results indicate a variation with energy of $1/E^{2.8}$ from 85 Mev to 200 Mev.

* This experiment was performed under the auspices of the AEC.

N5. Photodisintegration of the Deuteron. W. S. GILBERT AND J. W. ROSE. *University of California, Berkeley.*—Photons of a maximum energy of 312±15 Mev in the "spread-out" bremsstrahlung beam of the Berkeley electron synchrotron have been used to disintegrate deuterium. The gas was bombarded in a high pressure, low temperature target at a pressure of 136 atmospheres and at a temperature of 77°K. The protons from the $D(\gamma, n)p$ reaction were detected by the scintillation counter telescope system described in the preceding abstract. Since the photoeffect, in the absence of meson production, is a two-body problem, knowledge of a proton's energy and angle in the laboratory system uniquely determines the energy of the x-ray responsible for the disintegration. Using this fact, absolute values of $d\sigma/d\Omega$ at several angles were determined for x-ray energies of 200 Mev and 250 Mev in the center-of-mass system, and total cross sections were determined for these energies. $\sigma_t(200\text{ Mev}) = (9.5\pm30\text{ percent}) \times 10^{-29}$ cm^2 and $\sigma_t(250\text{ Mev}) = (13\pm40\text{ percent}) \times 10^{-29}$ cm^2. The indicated probable errors are based on counting statistics alone and give an indication of the limits on the relative cross sections. The absolute cross sections may be in error by as much as a factor of 2. These cross sections are far greater than any smooth extrapolation based on the calculated cross sections at lower energies[1,2,3] could yield. One therefore concludes that above the meson threshold, the cross section rises sharply with increasing energy.

[1] J. F. Marshall and E. Guth, Phys. Rev. **76**, 1881 (1949).
[2] L. I. Schiff, Phys. Rev. **78**, 734 (1950).
[3] J. F. Marshall and E. Guth, Phys. Rev. **78**, 739 (1950).

N6. Internal Momentum Distributions from Scattering Experiments. J. B. CLADIS, W. HESS, AND B. J. MOYER. *University of California, Berkeley.*—The mean free path in nuclear material and the de Broglie wavelength of a 340-Mev proton are such that a single collision with a nucleon of a light nucleus is expected when the proton is scattered. Thus, at scattering angles greater than about 25°, where interference terms are small, the proton energy spectra reflect the momentum distribution of the nucleons in the target nucleus. An expression for the spectra as a function of momentum distribution and scattering angle has been given by Wolff.[1] Energy spectra of protons scattered from H, D, and C have been obtained at scattering angles of 30° and 40°. These spectra are obtained by deflecting the protons by a magnetic field into channels defined by proportional counters and a bank of 35 Geiger-counters. Spectra calculated by inserting the theoretical momentum distribution for the deuteron and the gaussian distribution[2] for carbon into Wolff's formulas fit the data fairly well at both angles. The Chew-Goldberger distribution contains too many high momentum components.

[1] P. A. Wolff, UCRL-1410.
[2] E. M. Henley and G. H. Huddlestone, Phys. Rev. **82**, 754 (1951).

N7. Nuclear Momentum Distributions. PETER A. WOLFF. *University of California, Berkeley.*—Using the impulse approximation, a formula has been obtained which gives the energy distributions, at several angles, of fast protons that have been scattered from nuclei. The formula involves an integral over the nuclear momentum distribution and can, therefore, be used to extract information about this distribution from experimental data on scattering. The fitting of the experimental curves is most sensitive to the high momentum components in the nuclear wave function; in particular, it will be shown that long tailed momentum distributions such as that proposed by Chew and Goldberger[1] are not suitable, whereas a Gaussian with average energy of about 25 Mev fits the data well at several angles of scattering. The final theoretical energy distributions contain corrections, calculated by the Monte Carlo method, for the effects of multiple scattering of the proton within the nucleus. These distributions will be compared with those obtained by Cladis[2] experimentally and a discussion will be given of the error inherent in the method, which is estimated to be about five percent for protons of 340 Mev.

[1] G. F. Chew and M. L. Goldberger, Phys. Rev. **77**, 470 (1950).
[2] Previous abstract.

N8. The Long-Lived Phosphorescence of Potassium Iodide-Thallium Iodide. BERNARD SMALLER AND EUGENE AVERY, *Argonne National Laboratory, Chicago.*—The long-lived phosphorescent decay of KI–Tl$^{\text{II}}$ has been investigated using Co^{60} gamma-rays as the stimulating agent.

Analyses of the complete decay curve for the temperature range 255–360°K permits resolution into several exponential decay periods ranging from 1–10^4 sec. Determination of the frequency factors, s, and activation energies, ΔH, for the various trapping levels gave agreement with the absolute rate

TABLE I.

Trap No.	Log$s$	ΔH(ev)	$\sigma \times 10^{17}$ cm^2
1	12.81	0.92	1.8
2	11.83	0.84	1.7
3	11.25	0.76	2.4
4	10.01	0.65	1.0

theory[1] which predicts for the decay time, τ

$$1/\tau = (kT/h)\exp(\Delta S/R)\exp(-\Delta H/RT) = se^{-\Delta H/RT}.$$

Discrepancies exist, however, with the glow curve phenomenon, previously reported,[2] which may be attributed to the low capture cross sections calculated for the process. The various constants of the reaction are given in Table I.

[1] Glasstone, Laidler, and Eyring, *The Theory of Rate Processes* (McGraw-Hill Book Co., Inc., New York, 1941).
[2] Smaller, May, and Freedman, Phys. Rev. **79**, 940 (1950).

N9. New Technique for the Determination of Photonuclear Cross Sections.* LESTER L. NEWKIRK, *Iowa State College.*—A new technique for measuring photonuclear cross sections has been developed and applied to the $Cu^{63}(\gamma, n)Cu^{62}$ and $C^{13}(\gamma, n)C^{11}$ reactions up to 60 Mev. The results are in good agreement with other results obtained by different methods. Radioactivity is used to monitor the synchrotron beam. A mechanical "oscillator" slides a test sample and an identical monitor sample alternately into the beam. As the oscillator moves to and fro, the electron energy of the synchrotron is switched back and forth between two values. From one run to another the monitor sample is irradiated at the same electron energy, but the test sample is irradiated at various energies. Since conditions of irradiation and counting are always the same, any random or long time changes in beam intensity will show up in the monitor sample activity. The required photon distribution was determined by obtaining with the oscillator an activation curve for the $Ag^{107}(\gamma, n)Ag^{106}$ reaction, whose cross section is known[1] the results were then applied to the bremsstrahlung spectra of presumed known shape.

* Work was performed at the Ames Laboratory of the AEC.
[1] B. C. Diven and G. M. Almy, Phys. Rev. **80**, 407 (1950).

N10. Recent Developments with the Mass Synchrometer.* LINCOLN G. SMITH, *Brookhaven National Laboratory.*—Recent work on an instrument for comparing accurately the cyclotron frequencies or periods of ions of nearly equal mass and thus measuring their mass differences will be described. As originally arranged[1,2] this device has yielded higher resolution than most conventional mass spectrometers and required less critical alignment of component parts. However intensity obtainable for given resolution is materially lower because of a much lower duty cycle and greater loss of ions per unit path over the longer path used. In recent modifications the velocities of ions are modulated at 180° from the source in a short rf field rather than one pulsed at a considerably lower rate. Moreover, ions make only two or possibly a few more rotations between source and detector. Thus intensity for given resolution is quite comparable with that of conventional instruments. In fact, with the detector just behind or below the source rather than between it and the modulator, materially larger intensity may be obtainable. It appears, however, that obtaining it requires use of a square wave rather than a sinusoidal modulating field. Comparison of this instrument with others for measuring cyclotron frequencies or periods and with deflection-type spectrometers will be discussed.

* Research carried out under contract with AEC.
[1] L. G. Smith, Rev. Sci. Instr. **22**, 115 (1951).
[2] L. G. Smith, Phys. Rev. **81**, 295(A) (1951).

N11. Slow Neutron Crystal Spectrometer. R. G. ALLEN, C. P. STANFORD, T. E. STEPHENSON, AND S. BERNSTEIN, *Oak Ridge National Laboratory.*—The use of a crystal spectrometer as a source of monoenergetic neutrons has been, in general, limited to the region of energies greater than about .03 electron volts because of the presence of higher-order reflections from the crystal. However, by making use of the total reflection properties of mirrors for neutrons incident at very small glancing angles, order-free reflections from the crystal have been obtained and the useful range of a crystal spectrometer extended to around .005 electron volts. In practice, the lower energy limit of usefulness is determined only by the intensity available in this energy range. With this arrangement total neutron cross section measurements as a function of energy have been made for the strong capturing substances, gold, indium and silver in the region between .02 to .005 electron volt. Total cross section measurements of the strong scatterers nickel and nickel oxide have also been made in this energy region. Values for the coherent scattering cross sections were obtained from the heights of the discontinuities in the total cross section at wavelengths satisfying the Bragg law for ninety degree glancing angles for the various sets of crystalline planes. Detailed results for these substances will be given and compared to results of other observers obtained by the use of other techniques.

N12. The University of Washington 60-in. Cyclotron. F. K. DONNELLY, H. J. ENGEBRETSON, J. E. HENDERSON, T. J. MORGAN, F. H. SCHMIDT, AND J. F. STREIB, *University of Washington.*—Successful operation of a new conventional type cyclotron has recently been achieved. Internal D and H_1 beams $>100\mu a$ are obtained with 100-kv peak dee to ground at ~60-kw input. An rf deflector will be installed shortly. Although patterned after the Berkeley 60-in. cyclotron, the instrument has several new features. The grounded grid oscillator uses one ML 354 triode, 75-kw plate dissipation. The plate is at dc ground; hence, no insulated water supply is required. A 2-kw frequency doubler "booster" oscillator drives the main oscillator over the low voltage tank discharge. The system is extremely stable and will "ride-thru" almost continuous sparking. Bake-out time is short. The tube is cathode-biased and no constant current network is required. Although the machined gasket surfaces of the aluminum alloy vacuum chamber included several welded areas, the structure was vacuum tight at first test. The chamber is joined to cylindrical dee stem tanks by a single transition section, below which is located a 20-in. diffusion pump. The electrical terminations of the dee stems (spiders) are adjustable from outside the vacuum. The cyclotron is housed in a 40-ft-diameter room built into a natural ravine for earth shielding. An opening leads through a shielded passage; the deflected beam will be utilized in a low background laboratory. Generous assistance was given by staff, graduate students, and technical personnel.

* Jointly supported by the University of Washington, the ONR and the AEC.

N13. The Determination of the Height and the Diurnal Variation of the Night Airglow.* EDWARD V. ASHBURN, *U. S. Naval Ordnance Test Station, Inyokern.*—A critical analysis has been made of the method given by Roach and Pettit[1] for determining the intensity, height, and diurnal variation of the night airglow. In particular, this method, involving separation of the airglow from the total light of the night sky, has been put in analytical form. The analysis indicates in general that their evaluation of the intensity of the airglow can be appreciably improved by more rigorous techniques. It also indicates that the large scale features of the relative diurnal variation of the 5577A airglow as obtained by Roach and Pettit are essentially correct, although it suggests the desirability of additional data in support of their hypothesis of the semifixed isophot pattern. Their two techniques for determining the height of 5577A airglow yield, as they stated, results whose accuracy is relatively low.

* ONR Project NR 082-045 (in part).
[1] F. E. Roach, and Helen Pettit, Geophys. Research (September, 1951).

SATURDAY MORNING AT 9:00

Room 3, Le Conte Hall

(V. F. LENZEN presiding)

O1. Considerations of the Elastic Constants of Copper.* J. A. BRINKMAN, *North American Aviation, Inc., Downey, California.*—The potential used by Fuchs[1] in calculating the elastic constants for copper does not satisfy the condition required on the forces to maintain lattice stability:

$$12\frac{\partial W}{\partial r}\bigg|_{r=r_0}+6\frac{\partial W}{\partial r}\bigg|_{r=\sqrt{2}r_0}+24\frac{\partial W}{\partial r}\bigg|_{r=\sqrt{3}r_0}+12\frac{\partial W}{\partial r}\bigg|_{r=3r_0}+\cdots=0.$$

This condition demands that $\partial W/\partial r|_{r=r_0}=0$, if only nearest neighbor interactions are important. However, this derivative must have a nonzero value to explain the observed elastic constants. Hence, $\partial W/\partial r|_{r=\sqrt{2}r_0}$ must be of the same order of magnitude and opposite sign. Thus, the contribution from next nearest neighbors is not negligible when compared with the first derivative term resulting from nearest neighbors. An attempt has been made to satisfy the foregoing stability condition as well as the observed elastic constants by using a Morse potential to explain the compressibility, and a modification of this potential to explain the two shear elastic constants. The necessity for this modification arises from the dependence of compressibility on volume forces, while the shear constants are independent of volume forces.

* This work is based upon studies conducted for the Atomic Energy Commission under Contract AT-11-1-GEN-8.
[1] K. Fuchs, Proc. Roy. Soc. (London) **A151**, 622 (1936).

O2. A Theoretical and Experimental Investigation of High Temperature Graphitization.* W. P. EATHERLY, *North American Aviation, Inc., Downey, California.*—The high temperature graphitization process has been studied using samples of index rod, a gas-baked petroleum coke. The various electrical and magnetic properties change only slightly at temperatures below 1800°C, which variations are attributable to the binder material. In the range from 1800° to 2700°C rapid changes occur, coupled with growth in crystallite size and the evaporation of impurity atoms. The electrical conductivity, magneto-resistance, and magnetic susceptibility increase monotonically, but both the Hall coefficient and thermoelectric power pass through sharp maxima. The thermal conductivity shows a much more gradual increase which extends over the entire temperature range investigated. Employing the band energies calculated from the tight-binding approximation,[1] analytic expressions can be computed for the various electronic phenomena. These expressions agree qualitatively with the experimental data, and indicate that the electric and magnetic changes induced by graphitization are due primarily to the freeing of electrons trapped by crystal defects and impurities. The mean free path of the conduction electrons is limited by scattering from crystallite boundaries and defects rather than from lattice oscillations. The data and theory both indicate the unusual electronic characteristics of graphite are caused by the prominent action of a Brillouin zone boundary.

* Work performed under AEC contract.
[1] P. R. Wallace, Phys. Rev. **71**, 622 (1947).

O3. Magnetic Susceptibility of Polycrystalline Anisotropic Materials, and Observations on Artificial Graphites.* J. D. MCCLELLAND AND J. J. DONOGHUE, *North American Aviation Inc., Downey, California.*—A study of the anomalous diamagnetism of graphite provides a sensitive index of the role of the Fermi energy, of interest in the theory of conduction phenomena. However, the extreme anisotropy of graphite makes single observations on a specimen have a questionable significance. An invariant measure was therefore sought, and found in the sum of any three mutually perpendicular susceptibilities observed on the same cubical specimen, termed the "total" susceptibility. An experimental verification of the invariance is presented for polycrystalline artificial graphites of differing anisotropy. The "total" susceptibility of artificial graphites is -21.0×10^{-6} per g, only ten percent less than natural graphite. The method has been applied to observe the growth of the dimagnetism of carbon during graphitization. Index rod carbon was raised to successively higher temperatures up to 2800°C for two minute periods, and the room-temperature susceptibility determined between anneals. The results indicate the removal of impurities below 2000°C, and a steady growth in dimagnetism as crystallite perfection and growth proceeds.

* Work performed under AEC contract.

O4. Deformation and Fracturing of Thick-Walled Steel Cylinders under Explosive Attack. JOHN PEARSON AND JOHN S. RINEHART, *Michelson Laboratory, U. S. Naval Ordnance Test Station, Inyokern.*—Tests have been conducted on annealed heavy-walled cylinders of low carbon (1020) steel internally loaded by explosive charges. The purpose of these tests was to obtain basic information on the manner and type of fracturing and plastic flow obtained by extremely high pressures acting for short durations. It was observed that all of the cylinders tended to fracture in long fragments in the same basic pattern, but with variations because of wall thickness and manner of loading. Experimental results indicate that the radial cleavage type of fracture is initiated within the cylinder wall and propagated to the surface, while the shear type fracture associated with the inner portion of the cylinder wall appears as an independent energy relieving process. Microstructure analysis of the cylinder fragments shows a definite relationship between the type of fracture and the amount of distortion of the grain boundary. Considerable shock twinning is present in the cylinder fragments, and the grain structure near the inner surface shows severe distortion and flow. Strain measurements indicate that considerable plastic strain occurs during the explosive loading and cleavage fractures were always observed to occur in association with considerable plastic deformation.

O5. Some Tensile Fractures Generated in Metals by Impulsive Compressional Loading. JOHN S. RINEHART AND JOHN PEARSON, *Michelson Laboratory, U. S. Naval Ordnance Test Station, Inyokern.*—One aspect of the part that high intensity stress waves play in the fracturing of metal cylinders subjected to internal explosive loading has been studied. It has been found that tensile type fractures will result from the interference of reflected tensile stress waves whenever the resulting tensile stress exceeds the critical normal fracture stress of the material. The magnitude of this resulting tensile stress and its location within the body are largely dependent on the geometry of the metal-explosive system. Stress wave velocities have been measured for low-carbon steel, brass, copper, lead and aluminum alloy from the geometry of fracture. These velocities are in reasonably good agreement with accepted values for the velocities of dilatational waves in these metals.

O6. The Measurement of Young's Modulus and Internal Friction in Metal Specimens Suitable for Uniform Cyclotron Irradiation.* F. E. BOWMAN AND M. TARPINIAN, *North American Aviation, Inc., Downey, California.*—Theoretical considerations suggest that a study of the effects of cyclotron irradiation upon the elastic constants of metals should lead to further understanding of the nature of radiation damage. A technique has been developed for obtaining Young's modulus on samples that are suitable for such irradiations. Cyclotron characteristics enforce stringent limitations upon specimen size. Through necessity for uniform irradiation the specimen diameter is limited to about 0.005 inch by the particle range. The dimensions of the cyclotron beam fix a specimen length of about one-half inch. In order to meet these requirements, an apparatus was developed that employs the specimen as a vibrating cantilever beam. The beam modulates a light that falls on a photocell. The signal is impressed on a scaler, and thus the characteristic frequency of the sample is determined to about one part in one thousand. From this frequency the modulus can be computed. By photographing an oscilloscope pattern of the photocell signal as the vibration excitation is interrupted, a free decay curve is obtained and an internal friction value determined.

* This work is based upon studies conducted for the AEC under Contract AT-11-1-GEN-8.

O7. Interactions of Shock Waves in Air with Three-Dimensional Surfaces, I. RICHARD I. CONDIT, *Broadview Research and Development, Burlingame, California.*—Existing information on the interaction of shock waves in air with rigid surfaces has been largely limited to one- or two-dimensional surfaces. Extension to three-dimensional surfaces seems promising with an experimental procedure which records in sequence the positions of the leading edge of the region of interaction of shock wave and surface. These contours of interaction are photographed in a direction normal to the general orientation of the surface with the source of the shock waves between the motion picture camera and the test surface. The test surface must have an indicator coating which is deformed or altered by the passing shock wave in a manner that will allow photographic registration. Examples of such indicators will be given. The time sequence of photographs allows the determination of shock wave velocities and peak pressures at the surface. Thus at any point on the surface, the influence of the shape of the surface on the peak pressure can be evaluated. The results are most readily analyzed when the surfaces only suffer gradual changes in shape—as with natural topography. The procedure is equally adaptable to studies of full-scale explosions or accurate small-scale model shots.

O8. Growth of Single Crystals of Tantalum and Their Surface Structure. M. H. NICHOLS,*† *California Institute of Technology.*—Single crystals of tantalum of centimeter length have been grown in tantalum wire by a moving temperature gradient technique.[1] Qualitative examination of the thermionic electron projection tube pattern shows it to be identical with that of tungsten single crystals.[1] This is another indication that the anisotropy of thermionic emission from these metals is a surface rather than a volume effect.[2] The tantalum crystals so grown exhibited a plateau-like surface structure normal to the (110) direction extending approximately 2 degrees of arc around the wire either side of the (110) direction after approximately 4½-hours vacuum heating at 2500°K. After this amount of heating, a plateau-like structure normal to the (100) direction was just visible with a microscope magnification of 100. After sufficient vacuum heating to evaporate approximately 5 percent of the wire diameter, the plateau normal to the (110) direction extended over 10 degrees of arc, and the plateau normal to the (100) direction extended over approximately 5 degrees of arc.

* This work was sponsored by the ONR.
† Now at the University of Michigan.
[1] M. H. Nichols, Phys. Rev. **57**, 297 (1940).
[2] C. Herring and M. H. Nichols, Revs. Modern Phys. **21**, 185 (1949).

O9. One-Dimensional Flow with Mass Addition. EDWARD W. PRICE, *U. S. Naval Ordnance Test Station, Inyokern.*—Analysis has been made of flow in a straight channel with mass addition along the channel corresponding to the case of a typical solid propellant rocket motor. One-dimensional, steady-state, adiabatic flow with chemical equilibrium and constant stagnation enthalpy was assumed. It was found that, when the mass addition was a known function of the variables of state of the stream (as is the case in a rocket motor), the entire (one-dimensional) flow field could be computed for any given upstream pressure using conventional numerical methods. When the discharge characteristic of the rocket nozzle was known, the upstream pressure (and hence the flow field) could be specified as a function of two variables, one depending on the mass addition function and one depending on the ratio of the nozzle throat area to the flow channel area. When this area ratio is $\geqq 1$, the flow reaches sonic speed at the downstream end of the channel, and the flow field in the straight channel is dependent only on the mass addition function. In the event that the gas composition is unchanging in the stream, the form of solution of the flow problem is independent of upstream pressure.

O10. Time-Resolved Spectroscopy of the Incandescence Associated with Ultraspeed Pellets. EARLE B. MAYFIELD, *Michelson Laboratory, U. S. Naval Ordnance Test Station, Inyokern.*—Improved time-resolved spectra of the luminous trails associated with 5 km/sec ultraspeed pellets[1] have been obtained and reduced. Improved optical instrumentation was used, including an O'Brien drum spectrograph with a writing speed of 0.1 mm/sec and provided with a millisecond timer. Quantitative studies of the spectra indicate that about 90 percent of the emitted light can be identified with the atomic lines of the metals and the molecular bands of their oxides. Very little of the superimposed continuous spectra can be attributed to ballistic or air shock. Pellets have been fired into a chamber that contained gases at reduced pressures. The effect of gas pressure on the time-resolved spectra has been determined.

[1] Allen, Rinehart, and White, Phys. Rev. **83**, 889 (1951).

O11. Transient Waves through Steel Produced by Impulsive Loading.* WILLIAM A. ALLEN AND CLYDE L. MCCRARY, *Michelson Laboratory, U. S. Naval Ordnance Test Station, Inyokern.*—The transient behavior of a thick circular plate deforming under explosive attack has been investigated. An experimental technique, based upon the principle of the optical lever, has been used to measure surface oscillations as small as 10μ in amplitude. A long focal-length sweeping-image camer with a writing speed of 3 mm/μ sec was used to obtain time resolution as short as 0.1 μsec. Measured particle velocities on the free surface indicate the presence of elastic and plastic waves. Particle velocities determined by this method are not inconsistent with reported values.[1] Measured transit-times of the waves through the steel plate confirm reported values.[2] For most of the plates tested, permanent strain developed within 20 μsec. The permanent strain of each recovered plate was found to a limiting configuration of the transient deformation.

* Work supported by Armament Branch, ONR.
[1] J. S. Rinehart, J. Appl. Phys. **22**, 555 (1951).
[2] Pack, Evans, and James, Proc. Phys. Soc. (London) **60**, 1 (1948).

O12. Successive Approximations in a Theory for Critical Stability of Fluids. H. L. MORRISON, *U. S. Naval Ordnance Test Station, Inyokern.*—The theory[1] for conditions of critical mechanical stability of fluids at nonconstant temperature in porous media involves the solution of two simultaneous differential equations in mixed variables: w, the vertical component of flow velocity; and θ, the alteration of temperature distribution by incipient flow. In starting the solution by the method of Picard, w has been taken $w_1 = w_m \sin \pi z/D$ (in the notation of reference 1), and from the predominantly-θ equation a first approximation, θ_1, to θ has been obtained by quadratures. At this juncture, the w-equation has been used (by numerical integration) to solve the critical stability problem in two ways: (a) directly, and (b) after multiplication[1] by the spatial derivative of temperature. It has been found that the latter calculation produces numbers in better general accord with experiment than the former. This conclusion is interpreted to mean that a much better w_1 can be had, of the general nature of $\exp(-\varphi z/D) \sin \pi z/D$; detailed examinations of solutions of approximate differential equations bear this out.

[1] Morrison, Rogers, Jr., and Schilberg, J. Appl. Phys. (1951, in press).

O13. Variational Approach to a Theory for Critical Stability of a Fluid. F. T. ROGERS, JR., *U. S. Naval Ordnance Test Station, Inyokern.*—In reference 1 are derived two simultaneous linear differential equations in mixed variables and nonconstant coefficients, which, with suitable boundary conditions, define the thermal environment at critical stability of a fluid (heated from below) in a porous medium. For the special case ($\varphi = 0$) of an environment linear in the vertical spatial variable and independent of the other two, we have established that these equations are the Euler-Lagrange conditions that $\int_0^D [(-\beta_\varepsilon/k^2) \exp(\nu \beta_\varepsilon z)(w'^2 + A w^2) + A\lambda(\theta'^2 + A\theta^2) - (2A\lambda\beta_\varepsilon/k^2)\theta w'] dz$ assume an extreme value with respect to "weak" variations, and furthermore, that for w and θ eigenfunctions and for β_ε eigenvalues of the problem, this extremum is zero. Notation here is precisely that of reference 1. It has not as yet proved feasible accurately to extend these relationships to the case of $\varphi > 0$, though approximate relationships can be devised for $\varphi > 0$ with an accuracy decreasing with increasing φ.

[1] Rogers and Morrison, Proc. Fourth Annual Heat Transfer and Fluid Dynamics Inst. (Stanford, 1951), p. 45.

SATURDAY AFTERNOON AT 2:00

Room 1, Le Conte Hall

(J. KAPLAN presiding)

P1. Electrodynamics as a Basis for Special Relativity. ARTHUR E. RUARK, *Institute for Cooperative Research, The Johns Hopkins University.*—The Lorentz transformation is usually derived from the symmetry of the physical experiences of two observers on inertial frames, and the assumption that both observers obtain the same value of c, no matter how the source is moving. Suppose we replace the second postulate by the statement that the Maxwell equations and the Lorentz force are valid for the "resting" observer. We can discuss a simple clock,—a negative charge, rotating around a heavy positive charge in a plane perpendicular to the X axis. Setting this system into uniform motion, it becomes the clock of the moving observer. The resting observer can use the retarded potentials to discuss its behavior. A few lines suffice, to derive the mass increase and the decrease of angular velocity which occur when the clock is set into motion. The expansion of times associated with a moving body, the constancy of light velocity for the moving observer, the Lorentz contraction of a moving body, and the Lorentz transformation follow in order, with ease. This attack makes these matters so readily understandable, on the basis of retardation of electrical forces, that it appears to possess didactic value.

P2. The Surface Ionization of Lanthanum. JOHN H. REYNOLDS, *University of California, Berkeley.*—A modified ion source of the surface type has been constructed in which the ionizing surface is a bare tungsten ribbon which intercepts 1.5 percent of the neutral vapor from a secondary tungsten ribbon located in the plane of the first defining slit. The secondary filament is coated with the solid sample under investigation, in this case La_2O_3. Accelerated ions from the bare filament are analyzed with a 60° sector mass spectrometer by standard techniques. The stability of the source is adequate. Thus for a fixed secondary-filament voltage setting, the emission is a reproducible function of the ionizing-filament voltage setting over periods of several hours. For source pressures of 10^{-7} mm or less, it is found that the character of the ion emission differs significantly from that observed from La_2O_3 using a conventional surface ionization source in that a strong La^+ component is present, sometimes without competing LaO^+ emission. Reasons for this will be discussed. For pure La^+ emission, the variation with surface temperature of the ion current, i, is in good agreement with that predicted by the Saha-Langmuir equation, namely, $d \ln i/d(1/T) = -(e/k)(V_i - V_w)$, where V_i is the ionization potential of lanthanum and V_w is the work function of the ionizing surface.

P3. Photomesons from Deuterium. R. STEPHEN WHITE, MARK J. JAKOBSON, AND ALVIN G. SCHULZ. *University of California, Berkeley.*—Hydrogen and deuterium gases have been bombarded in a high pressure, low temperature target by photons from the Berkeley synchrotron to produce charged mesons. The π_+-mesons were detected by trans-stilbene scintillation crystals using $\pi\mu$, $\pi\beta$, and $\pi\mu\beta$ coincidence detection, and both π^+ and π^- mesons were detected with nuclear emulsions. At angles to the beam direction of 135±16°, 90±16°, and 45±16° the ratios of the number of π^- to π^+ mesons were 1.21±0.17, 1.07±0.13, and 0.96±0.11, respectively. No variation of the ratio with meson energy, within statistics, was observed. Absolute values for the π^+-meson energy distribution

TABLE I.

45±16°		90±16°		135±19°	
$\left[\frac{d^2\sigma(\bar{\theta}, \bar{E}_\pi)}{dE_\pi d\Omega}\right]_D \Big/ \left[\frac{d^2\sigma(\bar{\theta}, \bar{E}_\pi)}{dE_\pi d\Omega}\right]_H = \frac{D}{H}$	$\bar{E}_\pi$(Mev)	$\frac{D}{H}$	$\bar{E}_\pi$(Mev)	$\frac{D}{H}$	$\bar{E}_\pi$(Mev)
0.84±0.17	43	1.04±0.31	42	0.81±0.10	42
0.86±0.13	57	0.75±0.08	55	0.80±0.07	56
0.78±0.14	87	0.78±0.11	70	0.60±0.15	76
···	···	0.68±0.05	75	···	···
···	···	0.58±0.09	94	···	···
$\left[\frac{d\sigma(\bar{\theta})}{d\Omega}\right]_D \Big/ \left[\frac{d\sigma(\bar{\theta})}{d\Omega}\right]_H$	0.81±0.10	0.75±0.05		0.80±0.06	
$[\bar{\sigma}T]_D/[\bar{\sigma}T]_H$	0.78±0.03				

functions from hydrogen and deuterium in cm², per proton, per equivalent quantum, per Mev, per steradian have been measured, and the differential and total cross sections have been obtained by integrating over energy and angle, respectively. The ratios of the cross sections in the lab system from deuterium and hydrogen at each of the detection angles are given in Table I. Errors given are standard deviations resulting from statistics only. The statistics of the data are not sufficient to compute the proton spin-flip probability from the theory of Chew and Lewis.

P4. Capture of μ^- Mesons in Nuclear Emulsions. D. F. Sherman, Harry H. Heckman, and Walter H. Barkas. *University of California, Berkeley.*—The behavior of μ^- mesons produced in the cyclotron has been investigated to verify deductions from cosmic-ray studies. A beam of μ^- mesons has been obtained inside the 184-inch cyclotron by bombarding a Be target with the proton beam. Because many of the π-mesons so produced disintegrate near the target, the target region acts as a diffuse source of μ-mesons. A channel was constructed to select a beam of negative mesons of momentum 130 ± 3 Mev/c. An absorber which stops the π-mesons of momentum up to 140 Mev/c was placed in this beam, and an Ilford C-2 emulsion in a wedge absorber was placed behind it to detect μ^- mesons which penetrated the absorber. μ^- mesons were found ending in the plate with a density of about 4000 per cc in the energy interval 54 to 70 Mev. About 6 percent of these form one prong stars of low energy. This agrees with results of George and Evans.[1] An additional 35 percent show evidence of nuclear capture in the form of two pronglets, each about a micron long, or a "blob" at the end of the track.

[1] E. P. George and J. Evans, Proc. Phys. Soc. (London) **A44**, 193 (1951).

P5. Scattering of Negative π-mesons in Aluminum, Copper, and Lead. Harry H. Heckman and Walter H. Barkas. *University of California, Berkeley.*—A new technique is being used to measure nuclear scattering cross sections of π^--mesons as they traverse a semi-infinite scatterer. A stripped nuclear emulsion is embedded in the scatterer, exposed to an incident beam of 50_{-8}^{+16} Mev π^--mesons, and scanned. Most of the mesons stop at the expected distance from the absorber edge as determined from the range-energy relation. A few mesons are found at smaller depths of penetration and are attributed to large angle scattering. Mesons traveling opposite (90°–180°) to the direction of the incident beam are attributed to nuclear scattering and are used in the cross section calculation. The assumptions in this calculation are: (a) spherically symmetric nuclear scattering, and (b) nuclear scattering cross section independent of meson energy from 30–60 Mev. There is no geometrical correction factor, i.e., the cross section is proportional to the ratio of the backward flux to incident flux, both of which are observed in the same strip of emulsion. The analysis does not distinguish between elastic and inelastic scattering. The total (elastic and inelastic) nuclear scattering cross section for π^--mesons in the energy interval 40_{-10}^{+30} Mev is being studied for Al, Cu, and Pb. A preliminary value for Cu is 560 ± 160 mb.

P6. Photo Production of Negative Pions from Deuterium. R. E. LeLevier, *University of California, Berkeley.*—The meson energy spectrum for fixed recoil angles of meson and proton in photo-π^- production from deuterium was calculated using the impulse approximation[1] and a phenomenological spin dependent interaction.[2] The spectrum is peaked near the unique energy which results at given free neutron production angles. The main portion of the spectrum is essentially given by $\phi_0^2(\mathbf{k})$ where $\phi_0(\mathbf{k})$ is the Fourier transform of the deuteron wave function, and $\mathbf{k}$ is the momentum of the original proton in the deuteron. For a given meson energy the conservation laws determine $\mathbf{k}$. If the final protons are in a singlet spin state there is a sharp rise in the spectrum at the maximum possible meson energy. This is because of a large increase in the phase-space factor and the ^1S proton-proton interaction. The experimental ratio of the height of the "spike" to that of the central peak would provide a measure of the spin-flip process, since there is no spike if the final protons are in a spin triplet state.

[1] G. Chew, Phys. Rev. **80**, 196 (1950).
[2] M. Lax and H. Feshbach, Phys. Rev. **81**, 189 (1951).

P7. Range Straggle of μ^+-Mesons. F. M. Smith, W. Birnbaum, and W. H. Barkas, *University of California, Berkeley.*—The present study is being conducted on the monoenergetic μ^+-mesons arising from decay of π^+-mesons stopping in photographic emulsion. In 200-micron emulsion ~17 percent of these μ's will lose all of their kinetic energy in the film. The track lengths of those μ-mesons which visibly stop are measured with regard to *total* range. The shrinkage factor of the processed film has been determined in order to find the proper depth component of the range. Preliminary results on the range distribution of 260 tracks are in good agreement with the predictions of straggling theory: The standard deviation of the range is found to be 4.4 percent, and the distribution is not inconsistent with an assumption of normality. Recent reports[1–3] indicate the existence of μ-tracks of very short range. Although some of these might conceivably lie within the tail of the distribution, others are too far out to be included and presumably must be attributed to another process.

[1] W. H. Barkas, Phys. Rev. **83**, 236(T) (1951); also U.C.R.L., 1285.
[2] W. F. Fry, Phys. Rev. **83**, 1268 (1951).
[3] E. Gross (private communication).

P8. Analysis of Neutral Meson Gamma-Ray Spectra from Carbon. W. E. Crandall, K. Crowe, B. J. Moyer, W. K. H. Panofsky, R. Phillips, and D. Walker, *University of California, Berkeley.*—The gamma-ray spectra for angles of observation of 0°, 47°, 90°, 133°, and 180° from carbon targets bombarded by 345-Mev protons have been measured with a multi channel pair spectrometer,[1] and the spectrum obtained by averaging over all angles is compared with the expected spectrum arising from the decay of a neutral pion into two gamma-rays. Uncertainties in the low energy portion of the spectrum make a precise assessment of the symmetry properties difficult, but the contribution to the spectrum from nonneutral pion decay radiation does not need to be more than 2 percent of the observed radiation. If it is assumed that only decay of neutral pions contributes to the radiation observed, then the energy distribution of the neutron pion is derivable from the spectrum. The spectra for lower energy proton bombardments have been measured for two supplementary angles of view of the target and, based on the observed angular dependence of the spectra for 345-Mev protons, the excitation function for neutral pion production is deduced.

[1] Aamodt, Hadley, and Panofsky, Phys. Rev. **81**, 565 (1951).

P9. The Photoproduction of Negative Mesons from Deuterium. Richard Madey, Kenneth C. Bandtel, and Wilson J. Frank, *University of California, Berkeley.*—Evidence will be presented for the observation of the photomeson production process $\gamma+n\rightarrow\pi^-+p$. The photon source is the 322-Mev bremsstrahlung of the Berkeley synchrotron. Pion-proton coincidences were observed at pion laboratory angles of 90° and 120°. Correlated proton angles are predicted from the conservation laws for the photoproduction of a pion from a free neutron at rest. The predicted pairs of correlated meson and proton angles remain very nearly the same over all photon energies in the region of interest. Furthermore, the upper energy limit of the bremsstrahlung spectrum restricts the protons to an angular region in the forward direction within less than about sixty degrees from the beam direction. The

effect of the loose binding of the neutron in deuterium imparts a calculable smearing of the angle and energy correlations. When the angle of the proton telescope is varied to seven degrees on either side of the associated correlation angles, the difference in the counting rates between heavy water and ordinary water shows a well-defined peak at the predicted proton angles of 31.5° and 20°.

P10. Angular Distribution of π^+-Mesons Produced in $P-P$ Collisions.* MARIAN WHITEHEAD AND CHAIM RICHMAN. *University of California, Berkeley.*—The energy spectra of π^+-mesons produced by 341-Mev protons striking H' have previously been measured at 0°, 18°, and 60° [1,2] to the proton beam. In order to determine the angular distribution of the mesons more accurately a careful measurement of the production at 35° has been made. As at 0° and 60° the hydrogen cross section was found by taking a polyethylene carbon difference. The mesons were separated from the proton beam by a magnetic field and were detected at the end of their range, by nuclear emulsions embedded in an aluminum absorber. The characteristic peak, which is assumed caused by the reaction $p+p\rightarrow\pi^++d$,[3] is observed at a meson energy of 48 Mev with a width at half-maximum of 4 Mev. The finite width is the result of the beam's energy variation and the resolution of the detector. Previously the angular distribution in the center-of-mass system was assumed to be of the form $d\sigma/d\Omega = a(b+\cos^2\theta_{cm})$, and values of the constants were calculated from the 0° and 60° data.[4] These data in conjunction with the present results enable one to fix the constants with greater precision.

* This work was sponsored by the AEC.
[1] Cartwright, Richman, Whitehead, and Wilcox, Phys. Rev. **78**, 823 (1950), and Phys. Rev. **81**, 652 (1951).
[2] V. Z. Peterson, Phys. Rev. **79**, 407 (1950), and Peterson, Iloff, and Sherman, Phys. Rev. **81**, 647 (1951).
[3] Crawford, Crowe, and Stevenson, Phys. Rev. **82**, 97 (1951).
[4] Marian Whitehead and Chaim Richman, Phys. Rev. **83**, 855 (1951).

P11. The Production of Photo-mesons from Helium. MARK J. JAKOBSON, ALVIN G. SCHULZ, AND R. STEPHEN WHITE, *University of California, Berkeley.*—A study has been made of the mesons produced from helium and hydrogen by bombarding a low temperature, high pressure target with the 318±10-Mev bremsstrahlung beam of the Berkeley synchrotron. π^+-mesons were detected by scintillation counters, using $\pi-\mu$, $\pi-\beta$, and $\pi-\mu-\beta$ delayed coincidence detection. Ilford C-2, 200μ nuclear emulsions were used to obtain the π^-/π^+ ratio. Measurements were made at angles of 45°, 90° and 135° to the photon beam direction. The minimum energy detected was about 27 Mev resulting principally from the energy loss of the mesons in the target walls. The mean values of the minus-plus ratio from helium at 45°, 90°, and 135° are: .99±.15, 1.09±.14, and 1.00±.12, respectively. Differential and total cross sections for π^+-production were evaluated extrapolating from the minimum energy detected to zero meson energy. The results are presented in Table I (not corrected for nuclear absorption in the absorbers).

TABLE I.

Gas	$\frac{d\sigma(\theta)}{d}$ cm² (steradian)⁻¹	(equivalent quantum)⁻¹ (proton)⁻¹		σ cm² (equivalent quantum)⁻¹ (proton)⁻¹
	45°±16°	90°±19°	135°±20°	
Helium	2.5±0.2×10⁻³⁰	4.0±0.3×10⁻³⁰	3.2±0.2×10⁻³⁰	4.1±0.2×10⁻²⁷
Hydrogen	5.5±0.5×10⁻³⁰	7.4±0.5×10⁻³⁰	5.4±0.4×10⁻³⁰	7.8±0.4×10⁻³⁰
Ratio $\frac{\text{Helium}}{\text{Hydrogen}}$	0.45±0.06	0.54±0.05	0.59±0.06	0.53±0.04

P12. Nonlinear Pseudoscalar Meson Theory. E. M. HENLEY, *Stanford University.*—A nonlinear term has been introduced into the usual meson wave equation in order to account for nuclear saturation and shell structure.[1] Experimental evidence from meson production, absorption, and scattering favors a pseudoscalar meson with pseudovector coupling, rather than the scalar meson previously investigated. A study has been undertaken to determine the effect of a nonlinearity which corresponds to a point-contact repulsion[1] on such a neutral meson field, making use of classical field theory. For an isolated nucleon, at rest, a particular angular dependence is chosen for the meson field, similar to that for the linear case, so that separation of the angular part of the wave equation becomes possible. The total source strength is found for this case. A variation principle for an arbitrary source is also investigated, together with various nuclear models. It is hoped to carry this analysis further, to the case of charged mesons and more realistic nuclear models than the simple ones chosen to date.

[1] L. I. Schiff, Phys. Rev. **84**, 1 (1951).

P13. Classical Meson Fields. I. D. FOX AND JAMES R. WILSON, *University of California, Berkeley.*—Dirac[1] derived an equation of motion for a point electron in a classical electromagnetic field by equating the flux of field energy-momentum leaving the particle to the rate of change of the particle's energy-momentum. The usual divergence associated with the field of a classical point electron was identified as a relativistically invariant mass renormalization term. A similar procedure was used by Bhabha[2] in treating the problem of the point nucleon in a classical neutral vector meson field, and by T. D. Lee[3] for the case of the neutral scalar field. The method has been extended by the present authors to the treatment of the symmetric and charged scalar fields. The equation of motion of the nucleon was developed as described previously. In addition, conservation of charge was used to derive the equation of motion of the isotopic spin. Both the neutral and the symmetric scalar theories were applied to scattering problems.

[1] P. A. M. Dirac, Proc. Roy. Soc. (London) **A167**, 148 (1938).
[2] H. J. Bhabha, Proc. Roy. Soc. (London) **A172**, 384 (1939).
[3] Private communication.

SATURDAY AFTERNOON AT 2:00

Room 4, Le Conte Hall

(W. B. FRETTER presiding)

Q1. The Latitude Effect of Cosmic Rays between Geomagnetic Latitudes 54° and 88°N.* H. V. NEHER, VINCENT Z. PETERSON, AND EDWARD A. STERN, *California Institute of Technology, Pasadena.*—In the summer of 1951, balloon flights with ionization chambers were made, from shipboard going north from Boston, and from Thule, Greenland. The four flights from shipboard were made at geomagnetic latitudes, λ_m, 55°, 57.5°, 62.5°, and 67.5°N. These flights as well as five of those at Thule (λ_m=88°N) were made simultaneously with similar flights at Bismarck, N. D. The data show that the daily

fluctuations at high altitudes occur simultaneously at these widely separated places and further that these fluctuations are larger than the total latitude effect between Bismarck and Thule. An examination of the records of the magnetic field of the earth both from Mt. Wilson and the Danish station at Thule, shows that, during the times flights were made, there was no appreciable magnetic disturbance.

* Supported in part by the joint program of the ONR and the AEC.

Q2. The Mean Free Path of the High Energy Nuclear Component.* ROBERT R. BROWN, *University of California, Berkeley.*—The mean free path of the charged particles that produce penetrating showers has been measured in carbon, sulfur and iron. The measurements were carried out at Lake Sabrina, California (2765 m). A hodoscope arrangement similar to that of Walker, Walker, and Greisen[1] was used. In order to reduce the background due to the extra nuclear interactions of mu-mesons a producing layer of 50 gm/cm² of graphite was used. Events in which one charged particle entered and three or more charged particles left, the graphite producing layer were recorded as a function of the absorber thickness. Analysis of the data obtained gives mean free paths in carbon, sulfur and iron of 65 ± 5, 76 ± 7, and 115 ± 12 gm/cm², respectively. The results are consistent with collision mean-free paths determined by the nuclear geometric cross section.

* Assisted by the joint program of the ONR and the AEC.
[1] Walker, Walker, and Greisen, Phys. Rev. **80**, 546 (1950).

Q3. Angular Distribution of the Decay Tracks of Neutral *V*-Particles.* W. B. FRETTER AND M. M. MAY, *University of California, Berkeley.*—An investigation was carried out into the angular distribution of the decay tracks of neutral *V*-particles.[1] The angles θ_1, θ_2 which the decay tracks make with the proposed path of the *V*-particle (line drawn from the apex of the *V* to the probable initial event) were measured. Only cases where the coplanarity of the three paths could be established were considered (27 out of 35). Under a two particle decay scheme, there are two independent variables once mass values are assumed. From θ_1 and θ_2 were calculated, on the one hand, the ionizations of the daughter particles, and, on the other, the angle ϕ^* which their momenta in the rest system of the V^0-particle make with the velocity of the V^0-particle. Assuming two decay processes:[2] $V^0\rightarrow p+\pi^-$, V^0 mass = 2350 e.m., $V^0\rightarrow\pi_+ +\pi^-$, V^0 mass = 800 e.m., fair agreement was obtained with the observed ionizations and with a sine distribution function for ϕ^*. Three or four anomalous cases were noted.

* Assisted by the joint program of the ONR and the AEC.
[1] W. B. Fretter, Phys. Rev. **83**, 1053 (1951).
[2] Armenteros, Barker, Butler, and Cachon, "The Properties of Neutral V-Particles," to be published, Phil. Mag., October, 1951.

Q4. A Cloud-Chamber Study of Penetrating Showers in Light and Heavy Elements.* W. D. WALKER,† N. M. DULLER, and J. D. SORRELLS,‡ *Rice Institute.*—Penetrating showers were studied using a large rectangular cloud chamber containing carbon and lead plates. The chamber was operated in conjunction with an extensive hodoscope placed beneath it. The apparatus was operated during the summer of 1951 at Echo Lake, Colorado. Star production (i.e., elastic scatterings) by primary particles capable of producing penetrating showers was investigated. There were extremely few pictures of particles that produced a star in the chamber and also a penetrating shower detected in the hodoscope. It is concluded that the elastic scattering cross section for high energy primaries is very small compared to the geometric cross section, as would be expected from Fermi's statistical theory. A comparison has been made between penetrating showers starting in carbon, lead, paraffin, and iron. The rate of showers, per mean-free path of generating material, with n penetrating secondaries appears to be almost the same for light and heavy elements with n ranging from 2 to 20 particles.

* Supported in part by grants from the Research Corporation and R.E.S.A.
† Presently on leave of absence at the University of California, Berkeley.
‡ Now at California Institute of Technology.

Q5. Zenith Angle Effects for Cosmic-Ray Protons and Mesons.* C. E. MILLER, J. E. HENDERSON, GERALD GARRISON, AND WAYNE SANDSTROM, *University of Washington.*—A magnetic cloud chamber has been used to determine the distribution in momentum of those charged particles stopping in fifteen cm of lead absorber as a function of zenith angle. Observations were made at an altitude of 3.3 km for vertical incidence and for angles of 45° east and west. The method gives the intensity of low energy mesons (momentum below 400 mev/c) and, because of nuclear reactions in the absorber, the intensity of protons to 2.5 bev/c. For these low energy mesons the intensity is found to decrease by a factor of three in going from the vertical to 45° east or west. Within statistics, no change in the positive to negative ratio is found. The decrease in intensity at 3.3 km in going from zero to 45° zenith angle is the same as that found for vertical observation in going from this altitude to sea level. This one would expect from the effective atmospheric depths involved. For low energy protons the intensity also decreases by three from zero to 45° at the altitude 3.3 km which is not at all the same as the factor of about twenty between vertical observations at this altitude and at sea level. For higher energy protons (momentum above 1 bev/c) a pronounced east-west asymmetry is found. Observations are still continuing.

* Supported in part by the ONR.

Q6. Energy Loss of Cosmic-Ray μ-Mesons.* ROBERT HOFSTADTER AND ALVIN M. HUDSON, *Department of Physics and Microwave Laboratory, Stanford University.*—A triple-coincidence telescope, consisting of three NaI(Tl) crystals, has been used to measure the energy loss of μ-mesons in the cosmic rays at sea level. Six inches of lead above the telescope absorbed most of the soft component and three inches of lead between the middle and lower crystals absorbed slow mesons. The middle crystal, of thickness two inches, has been viewed by an RCA C7157 photomultiplier. Energy loss calibration was obtained by measuring the well-resolved gamma-ray lines in the C^{12*} (4.4 Mev) spectrum and the gamma lines of the thorium spectrum. The observed curve is presented in the form of a 70-channel differential energy loss spectrum and shows a sharp peak close to 27.5 Mev. The theoretical energy loss distribution has been computed on the basis of Landau's straggling theory with the Bethe-Bloch energy loss formula and the cosmic ray μ-meson spectrum.[1] The experimental curve is slightly narrower than the theoretical curve. The possible significance of these results will be discussed.

* Aided by the Joint Program of the ONR and AEC.
[1] B. Rossi, Revs. Modern Phys. **20**, 537 (1948).

Q7. Protons and Mesons at 9000 Feet.* A. Z. ROSEN, *University of California, Berkeley.*—An apparatus[1] consisting of three cloud chambers arranged so as to measure the angular deviation of a particle in a magnetic field and its range in Cu has been operated during the summer of 1951 at 9000 ft. Data were obtained on the spectra of single protons and mesons having ranges between 34.1 g/cm² and 117.8 g/cm² of Cu after having traversed from 0 g/cm² to 345 g/cm² of Pb-absorber over the apparatus. The use of a tray of counters above the Pb-absorber to operate a neon light in coincidence with the triggering telescope, made possible the counting of protons originating from neutral particles incident on the absorber, and also allowed some estimate of the neutron intensity to

be made. The absolute differential intensities of the protons will be detailed and also the intensities relative to those for the mesons which are corrected for reduction in acceptance angle because of the large angular deviation of the mesons in the magnetic field. The results will be compared to those obtained at sea level with the same apparatus.

* This work has been assisted by the joint program of the ONR and AEC.
[1] R. B. Brode, Revs. Modern Phys. **21**, 37 (1949).

Q8. Penetrating Cosmic-Ray Showers in Water.* GEORGE W. ROLLOSSON,† *University of New Mexico, Albuquerque.*—Penetrating showers produced locally by neutral radiation were studied using counter techniques. The collision length in water of the neutral, penetrating, shower-producing component was found to be (98 ± 13) g/cm^2. A comparison of this collision length with that obtained by others in carbon[1] and aluminum[2] seems to indicate that the hydrogen nuclei in water have a rather small cross section for the production of penetrating showers by neutral radiation. Measurements taken at two elevations show the absorption length in air of the neutral, penetrating, shower-producing component to be (115 ± 19) g/cm^2.

* Supported in part by a grant from the Research Corporation.
† Now at Sandia Corporation, Albuquerque, New Mexico.
[1] Walker, Walker, and Greisen, Phys. Rev. **80**, 546 (1950).
[2] E. P. George and A. C. Jason, Proc. Phys. Soc. (London) **A63**, 1081 (1950).

Q9. Knock-On Secondaries from Penetrating Particles in Carbon. JOHN R. GREEN, *University of New Mexico.*—Cloud-chamber pictures obtained to investigate penetrating showers produced in carbon* have been re-examined for knock-on particles accompanying individual penetrating particles (mostly mu-mesons) emerging from carbon plates. The probability that a penetrating particle leaving a one-inch carbon plate will be accompanied by a knock-on is about ten percent. The angular distribution of secondaries relative to the parent particles is approximated by $\cos^n\theta$, with n between 2 and 3. Ten percent of the secondaries scatter noticeably in the one-half inch of gas between plates and have energies below 1 Mev. Eighty percent traverse the gas without scattering but cannot penetrate the following one-inch carbon plate; these have energies of a few Mev. The remaining ten percent traverse one or more carbon plates. One to two percent produce additional ionizing particles in the carbon plates or in the one-half inch lead plates that identified the penetrating particles; these particles possess energies of 100 Mev or higher. The general behaviour of the secondaries is consistent with that expected of electrons. Agreement was found between observations at sea level and at 12,000 feet.

* The pictures were obtained while the author was at the University of California, Berkeley, with the Cosmic Ray Group on a project supported in part by the ONR and AEC. See Phys. Rev. **80**, 832 (1950).

Q10. Absorption Cross Sections for 19.5-Mev Quanta.* ARTHUR I. BERMAN, *Los Alamos Scientific Laboratory.*—Total cross sections for 19 elements, from hydrogen to uranium, were found by a photonuclear detector method[1] which measured the C^{11} activity induced by betatron bremsstrahlung. The penetration of the radiation (maximum energy, 20.4 Mev) through the absorbers was detected by the $C^{12}(\gamma, n)C^{11}$ reaction (threshold, 18.7 Mev) in polyethylene. The use of high counting rates and dual monitor-detector Geiger counters, which completely or partially canceled errors due to timing, intensity fluctuations, and uncertainty in counter, resolving-time theory, reduced most random probable errors to approximately 0.4 percent. Systematic errors added about 0.4 percent to this. The narrow band width permitted a determination of the proportion of counts due to secondary effects. If the approximate high-energy validity of the Klein-Nishina Compton cross section (verified here to within 7 percent) is assumed, together with recent photonuclear data, then the theoretical (essentially Bethe-Heitler formula including screening) and experimental pair cross sections are related by $(\sigma_t-\sigma_a)/\sigma_t=(1.6\pm0.2)\times10^{-5}Z^2$.

* Work performed under the auspices of the AEC.
[1] G. D. Adams, Phys. Rev. **74**, 1707 (1948).

Q11. The Aerobaillistics Laboratory of the U. S. ARTHUR L. BENNETT, IVAR HIGHBERG, ERNEST BARKOFSKY, AND LUCIEN M. BIBERMAN, *Naval Ordnance Test Station, Inyokern.*—The U.S.N.O.T.S. is completing a facility for the accurate experimental evaluation of the parameters (such as lift, overturning moment, and drag) required for the prediction of the behavior of a new projectile design. The Laboratory is an enclosed range for the measurement of the trajectory of models in free flight. Since safe extrapolation to full scale requires that the model exceed the critical Reynolds number, the range is designed for models at least 3 inches in diameter. The configuration to be studied is projected through the range by a suitable gun. The laboratory building is 480 ft long, 40 ft wide, and 30 ft high; a clear radius of 10 ft about the trajectory is provided to avoid wall interference at velocities near Mach 1. The position and orientation of the model is recorded photographically at frequent intervals by multiple photographs taken by pairs of cameras at 20 ft spacing. The microsecond flash lamps, which provide the light for the photographs, are precisely timed by a submultiple of the frequency of a crystal clock. Measurement of the photographs provides the position and orientation (hence yaw) of the model at known time intervals. From these data the aerodynamic and ballistic characteristics of the model are determined. Auxiliary equipment for shadowgraph, schlieren, and interferometer photographs will be added as needed for study of flow about the models. Photographs of the building and the instruments are presented and the operating technique described.

Q12. The Differential Cross Section for the Scattering of 9.5-Mev Protons from Helium. T. M. PUTNAM, *University of California, Berkeley.*—The angular distribution of 9.5-Mev protons scattered from helium nuclei has been measured with photographic emulsions. The 20-Mev molecular hydrogen beam from the 60-in. cyclotron in Crocker Laboratory was the source of protons. The scattering chamber was the nuclear multiplate camera of Allred, *et al.*, developed at Los Alamos.[1] Forty angles from 10° to 172.5° were measured. The scattered particles passed through a two-slit collimating system which, together with the beam collimation system, determined the scattering volume. The geometry was such that the angle of the nuclear plate with the slit axis did not enter into the solid angle determination. Approximately 2500 tracks were counted at each angle using suitable acceptance criteria to establish the identity of the scattered particles. The construction of the multiplate camera was such that the relative accuracy for a group of points from a given run is expected to be within the counting statistics. An absolute standard error to be assigned to the data is five percent for the angular range of 10° to 25° and 2.9 percent for the range of 25° to 172.5°.

[1] Allred, Rosen, Tallmadge, and Williams, Rev. Sci. Instr. **22**, 191 (1951).

Q13. Electron-Electron Scattering at 6.1 Mev. W. C. BARBER, G. E. BECKER, AND E. L. CHU, *Stanford University.*—The absolute differential cross section for the scattering of 6.1-Mev electrons by the electrons in a beryllium foil has been measured at 90° and 109° in the cm system. Electrons from a linear accelerator were first magnetically analyzed and then collimated to form the incident beam. Electron-electron scattering events were detected by end-window Geiger counters in coincidence. The counter with the defining aperture was connected in coincidence (1) with a counter at the conjugate scattering-angle, lying in the plane determined by the incident beam and the scattering direction to the defining counter; and

(2) with another counter at the conjugate-angle but lying outside this plane, thus counting only accidental coincidences. The number of $e-e$ coincidences was then given by the difference between (1) and (2), with appreciable corrections arising from asymmetry in the background and from dead-time losses. These corrections required measurements of single and coincidence count rates with the scatterer in and out of the beam. The average result at each angle is somewhat lower than that predicted by the Møller theory, but the discrepancy is not greater than the present experimental uncertainty of the order of ± 10 percent. Possible systematic errors are being investigated.

SUPPLEMENTARY PROGRAMME

S1. Eigenfunctions and Landé Interval Factors for Terms of f^3 Electrons. Selection Rules Applicable to Rare Earth Bromates.* ROBERT A. SATTEN, *University of California, Los Angeles.*—The eigenfunctions corresponding to the Russell-Saunders terms of f^3 electrons were calculated by the method of Gray and Wills[1] as linear combinations of products of single-electron eigenfunctions. Also the Landé interval factors $\zeta(LS)$ for the various Russell-Saunders terms arising from f^3 electrons were computed in terms of the single-electron spin-orbit interaction[1] "parameter" ζ_{4f}. The diagonal sum rule was used to calculate all the $\zeta(LS)$ values whose LS values occur only once. To obtain the remaining ζ's, the Russell-Saunders eigenfunctions for LS values which occur twice were used. Selection rules were derived by the usual group theoretical means for electric and magnetic dipole as well as electric quadrupole radiation for an atom in an electric field of symmetry C_{3v}. These selection rules do not agree with the corresponding rules given by K. H. Hellwege.[2] The results apply to rare earth bromates. Thus it can be determined that the 8600A group of absorption lines in $Nd(BrO_3)_3 \cdot 9H_2O$, identified as a transition to $^4F_{3/2}$, cannot arise solely from electric dipole, or solely from magnetic dipole, or electric quadrupole radiation alone.

* To be given after Session D if time permits.

[1] Condon and Shortley, *The Theory of Atomic Spectra* (Cambridge University Press, London, England, 1935).

[2] K. H. Hellwege, Ann. Physik 4, 95 (1948).

Author Index to Papers Presented at the Berkeley Meeting

Abell, D. F. and W. D. Knight—K4
Allen, R. G., C. P. Stanford, T. E. Stephenson, and S. Bernstein—N11
Allen, William A. and Clyde L. McCrary—O11
Arnold, J. T.—K7
Asaro, Frank, Fred L. Reynolds, and I. Perlman—G3
Ashburn, Edward V.—N13
Backman, Marvin E.—H5
Barber, W. C., G. E. Becker, and E. L. Chu—Q13
Bennett, Arthur L., Ivar Highberg, Ernest Barkofsky, and Lucien M. Biberman—Q11
Berman, Arthur I.—Q10
Berry, Clifford E.—M11
Birge, Ann C.—C1
Birge, Robert W.—N3
Blake, N. W., D. S. McClure, and H. Winston—D1
Blois, Marsden S., Jr.—M6
Bloom, Arnold L.—B3
Bowman, F. E. and M. Tarpinian—O6
Brinkham, J. A.—O1
Broida, H. P.—D5
Brown, Robert R.—Q2
Brown, S. Leroy—B6
Browne, C. I. and I. Perlman—G6
Chamberlain, Owen—L2
Chodorow, M.—A1
Christy, Robert F.—L1
Cladis, J. B., W. Hess, and B. J. Moyer—N6
Cohen, M. H.—K6
Condit, Richard I.—O7
Crandall, W. E., K. Crowe, B. J. Moyer, W. K. H. Panofsky, R. Phillips, and D. Walker—P8
Day, Robert B. and Torben Huus—J8
Decius, J. C.—D8
Dedrick, K. G.—N1
Dodd, E. E.—H3
Donnelly, F. K., H. J. Engebretson, J. E. Henderson, T. J. Morgan, F. H. Schmidt, and J. F. Streib—N12
Dunlavey, Dean C. and Glenn T. Seaborg—G2
Dyke, W. P.—A3
Eatherly, W. P.—O2
El-Sum, Hussein M. A. and Paul Kirkpatrick—M2
English, W. N.—H6
Eyges, L.—C2
Fox, I. D. and James R. Wilson—P13
Fretter, W. B. and M. M. May—Q3
Gilbert, W. S. and J. W. Rose—N5
Giles, Peter C. and Walter H. Barkas—F4
Gilmore, E. H. and R. H. Knipe—M9
Glenn, William E.—M1
Good, R. H., Jr.—C6
Graves, J. D. and Richard I. Condit—B4
Green, John R.—Q9
Hagstrum, H. D.—A2
Hahn, E. L. and D. E. Maxwell—K2
Harker, Kenneth James—B7
Harris, John N. and Arthur I. Berman—M10
Hayward, Raymond W.—J1
Heckman, Harry H. and Walter H. Barkas—P5
Henley, E. M.—P12
Hess, W., J. B. Cladis, and J. Hadley—F6
Hofstadter, Robert and Alvin M. Hudson—Q6
Huus, Torben and Robert B. Day—J4
Jakobson, Mark J., Alvin G. Schulz, and R. Stephen White—P11
Jastrow, R. and J. E. Roberts—F7
Jenkins, F. A. and L. W. Alvarez—M3
Jenkins, William A. and Glenn T. Seaborg—G8
Johnson, H. R.—M4
Karp, Ira L.—C5
Kikuchi, Seishi—C3
Knight, W. D.—K5
Lamb, Willis, E.—I2
Lauer, Eugene J.—H4
LeLevier, R. E.—P6
Levy, Harris B. and I. Perlman—G4
Madey, Richard, Kenneth C. Bandtel, and Wilson J. Frank—P9
Mayfield, Earle B.—O10
McClelland, J. D. and J. J. Donoghue—O3
Miller, C. E., J. E. Henderson, Gerald Garrison, and Wayne Sandstrom—Q5
Morrison, H. L.—O12
Neher, H. V., Vincent Z. Peterson, and Edward A. Stern—Q1
Newkirk, Lester L.—N9
Nichols, M. H.—O8
Oliver, A. J. and Walter H. Barkas—F3
Pattee, H. H., Jr.—M7
Pearson, John and John S. Rinehart—O4
Perkins, W. D. and M. Kent Wilson—D6
Perlman, I.—I1
Price, Edward W.—O9
Putnam, T. M.—Q12
Rankin, Bayard, John Killeen, and Walter H. Barkas—C4
Rasmussen, J. O.—G5
Reynolds, John H.—P2
Riddell, R. J., Jr.—H7
Rieser, L. M., Jr.—M5
Rinehart, John S. and John Pearson—O5
Rogers, F. T., Jr.—O13
Rogers, Marguerite, F. K. Odencrantz, and G. J. Plain—F1
Rollosson, George W.—Q8
Rose, J. W. and W. S. Gilbert—N4
Rosen, A. Z.—Q7
Ruark, Arthur E.—P1
Satten, Robert A.—D7, S1
Schiff, L. I.—C7
Schindler, Mark and G. L. Weissler—H1
Schnepp, O. and D. S. McClure—D2
Seaborg, Glenn T.—G1
Shaw, T. M., R. H. Elsken, and K. J. Palmer—K3
Sherman, D. F., Harry H. Heckman, and Walter H. Barkas—P4
Smaller, Bernard and Eugene Avery—N8
Smith, F. M., W. Birnbaum, and W. H. Barkas—P7
Smith, Lincoln G.—N10
Stein, Robert P.—H2
Stern, Martin O.—B2
Tessman, Jack R.—B1
Thompson, S. G., J. O. Rasmussen, and A. Ghiorso—G7
Thompson, T. J.—M12
Tobias, Cornelius A.—M8
Tollestrup, A. V., R. B. Day, and H. H. Woodbury—J3
Vanderberg, R. M.—D3
Violet, Charles E., F. C. Gilbert, Robert W. Deutsch, and Walter H. Barkas—F2
Walker, W. D., N. M. Duller, and J. D. Sorrells—Q4
Warters, William D. and Edmund A. Milne—J5
Webber, D. S. and A. N. Baker, Jr.—D4
Wenzel, W. A. and Ward Whaling—J6
Whaling, Ward and W. A. Wenzel—J7
White, R. Stephen, Mark J. Jakobson, and Alvin G. Schulz—P3
Whitehead, Marian and Chaim Richman—P10
Wilfong, T. C., Jr., and J. E. Henderson—N2
Wolff, Peter A.—N7
Woodbury, H. H., R. B. Day, and A. V. Tollestrup—J2
Wouters, L. F.—F5
Yafet, Y.—K1
Yankwich, Peter E., Edward C. Stivers, and Robert F. Nystrom—B5

The Physical Review

Isomeric Proper-Field
Nuclear Scattering of Lighter Elements and
Disintegration of the Deuteron by the
. . . . . .
Nuclear Magnetic Moment of Cesium
Nuclear Spin Moment and Temperature of
. . . . . .
Neutron Scattering Lengths
Hyperfine Structure and Isotope Shift
Proton Recombination at 100 Mev
Genetic Relationships and Nuclear Types of
Neutron Yield from the Nuclear Photo
Reaction Be⁹(p, 2γ)Li⁸
(p, n) Reaction on Separated Isotopes of
Isotopic Magnetization in Alloys
Neutron Transmission Cross Sections
Proton Neutron Spectrum of Ra
Spin-Spin Relaxation in a Single Crystal
Absorption Curve of the Cosmic
Semiconductivity and Photoconductivity of
Multiple Scattering of Waves in
Masses of Lead and Bismuth
Divergence of Perturbation Theory in
Geometrical Optics and the Upper
Impulse Approximation
Classification of Energy Levels in
Point Transformations in Quantum
Further Calculations of Z-Ray
Motion of a Ferromagnetic
Ion Clustering
Letters to the Editor:
Anomalous
Diurnal Variations in
Scattering of 6.5-
Phenomena Associated with
Ionizations in Gases
Properties of Magnesium
Lateral Spread of Cosmic-Ray
Drift Mobility of Electrons in
Photoneutron Production in
. . . . . .
Photoneutron Production in
Hyperfine Structure in the
. . . . . .
Hyperfine Structure in the
Is There a Neutral π-Meson?
Auger Rediscussion of the
Comment on the "Quantum
Nonlinear Theory
Search for Double Beta
Measurements on the
Use of HD for
Determination of the
. . . . . .
Composition of Cold
. . . . . .
Effect of Isotopic Mixture of
Paramagnetic Resonance in
Low Energy γ-Ray
Theory of Cosmic
Color Centers and
Temperature Dependence of
Paradox
Steady-State
High Energy
Some Phenomena
Absence of Boundary
β-Decay of Sodium 24 and
Ionization Effects in
Proceedings of the American Physical
Minutes of the Meetings of
Minutes of the 109th
Minutes of the Meeting of